The El'gygytgyn impact structure, Siberia: Impactites from a mid-size impact structure in volcanic target rocks

Die El'gygytgyn-Impaktstruktur, Sibirien: Impaktite in einer mittelgroßen Impaktstruktur in vulkanischem Zielgestein

by

Dipl. Geogr. Ulli Raschke

Dissertation submitted to obtain the academic degree

Doctor rerum naturalium (Dr. rer. nat.)

presented to the Department of Earth Sciences,

Freie Universität Berlin

Berlin, January 2017

Freie Universität Berlin

museum für naturkunde berlin

I Declaration

Hiermit versichere ich, dass ich die vorliegende Arbeit selbstständig verfasst und keine anderen als die angegebenen Hilfsmittel benutzt habe. Die Stellen der Arbeit, die anderen Werken wörtlich oder inhaltlich entnommen wurden, sind durch entsprechende Angaben der Quellen kenntlich gemacht.

Diese Arbeit wurde in gleicher oder ähnlicher Form noch keiner Prüfungsbehörde vorgelegt.

Ulli Raschke, Berlin, im Januar 2017

Day of defense: 02/22/2017

Referees:

1. Univ. Prof. Dr. Wolf Uwe Reimold (Erstgutachter)

Museum für Naturkunde Berlin

Leibniz-Institut für Evolutions- und Biodiversitätsforschung

Invalidenstraße 43

10115 Berlin

and

Humboldt Universität zu Berlin

Unter den Linden 6

10099 Berlin

2. Univ. Prof. Dr. Harry Becker (Zweitgutachter)

Freie Universität zu Berlin

Institut für Geologische Wissenschaften

Malteser Straße 74-100

12249 Berlin

II Acknowledgments

First of all, I want to express my gratitude to my supervisor Prof. Dr. Wolf Uwe Reimold from the Museum für Naturkunde and Humboldt Universität zu Berlin. He supported me from the very first steps in this project. Together, we developed the idea to write a DFG proposal to contribute to the ICDP El'gygytgyn-drilling project. He has shown me the way of scientific work and he advised me in the procedure of publication of well-written papers. Without his help, I would never have been in Chukotka. This trip was not only a great experience of the Arctic environment that also allowed me to complete my PhD project with an additional wide range of samples from the crater, but it also led to an amazing change in my private life.

I also want to acknowledge PD Dr. Lutz Hecht from the FU Berlin and Museum für Naturkunde, Berlin. He has made a great contribution by listening when I told him about my problems and helping in finding solutions. It was a pleasure for me to discuss a lot of volcanic material with him. During his excursion to the Canary Islands, I discovered the fascination of volcanic rocks.

I am grateful to Prof. Dr. Harry Becker, who agreed to be my second referee from the Freie Universität, Berlin.

Special thanks go to Prof. Dr. Thomas Kenkmann, now University of Freiburg. He stimulated my interests in impact geology and he was a very good supervisor for my diploma thesis about the Lockne crater.

Since 2005, I have been working at the Museum für Naturkunde Berlin, at first as student assistant and later as PhD candidate. During this time, a network of friends and good colleagues has grown.

- Hans-Rudolf Knöfler has taught me the preparation of thin sections. This is an important skill for the work in geology and enabled me to analyze more than 300 thin sections.

- Dr. Ralf-Thomas Schmitt, curator of minerals, rocks and ores, was an invaluable advisor for the geochemical part of the publications. He supported me in geochemical systematics and he always had time for my questions and me.

- Patrice T. Zaag was also involved in this project as a student assistant, and he has become a friend of mine. He contributed to the expedition to the El'gygytgyn structure and significantly contributed to the new geological map of this structure.

• Peter Czaja helped me with the handling of the electron microprobe and we spend a few weeks together in this laboratory. Kirsten Born supported me very friendly during the work at the scanning electron microscope.

• Dr. Jörg Fritz has had an open mind for new ideas. We had plenty of nice scientific discussions. He introduced me to RAMAN spectroscopy.

• Hwa Ja Götz (photographer at MfN) made a number of high quality images of El'gygytgyn shatter cones. Friederike Schwarz and Elke Gerhardt-Mayer from the secretariat of the FB1 did a great job and helped me uncounted times with the rules and laws of bureaucracy.

In preparation of my PhD project, the curation of the impactite sequence of the ICDP El'gygytgyn drill core was mandatory. Prof. Dr. Christian Koeberl (University of Vienna), one of the principal investigators (PI), helped me to obtain access to this material and he supported me financially at that early time.

The following students carried out practicals within this project: Cornelia Kolzer, Paul Weber, Thomas Michalik, Daniel Werner and Dschamilja Marusha Wannek. They worked with the core scanner, made pictures of the drill cores, and prepared data for me. Sincere thanks are given to them.

It was a great pleasure for me to participate in the 2011 expedition to the El'gygytgyn crater structure. To all team members I want to express my warmest thanks: Dr. Georg Schwamborn (AWI Potsdam) and Dr. Grigori Federov (AARI St. Petersburg) for the organization of the expedition (starting with the general preparation and financing up to the successful access to the crater region, which required special skills and experience). Further thanks go to Maaret Sauerbrey (neé Kukkonen, University of Cologne) for plenty of nice photographs, which I partially used for a manuscript. Nikifor Ostanin (University of St. Petersburg) gave me support with access to the older Russian geological maps of the crater area.

Very special thanks go to Elena Aleksandrovna Raschke (neé Morozova), for the way in which she changed and enriched my life and has become the most important person for me. In addition, she helped me with the translation of a lot of Russian literature.

Dr. Olaf Juschus and Dr. Norbert Nowaczyk provided me with a huge number of samples from the crater region, which were very useful for planning the expedition and later for complementation of the sample sets.

Furthermore, I gratefully acknowledge the DFG, who funded the projects RE 528/10-1, 528/10-2 and 528/12-1, to Prof. Dr. Wolf Uwe Reimold and Dr. Ralf-Thomas Schmitt.

III Structure of this thesis

This PhD thesis is composed of five published, peer-reviewed articles, which each form a separate Chapter. In addition, there are the Chapters (1) “Introduction”, (7) “General Discussion”, and (8) “Conclusions”. The PhD candidate is the first author of four of these articles, and a co-author of the fifth article.

All publications are included in complete form and have not been condensed. The five Chapters have their own introduction, methodology, results, discussion, and conclusion sections. The references of all Chapters have been combined in one list to avoid a mass repetition and improve usability of this thesis. During incorporating the manuscripts into this work, the page numbers and the numbering of the headings as well as the position of tables and numbers in the text were adapted to a uniform layout. The listed figure captions were cut to only fill a line (table captions only two lines). The manuscripts used for this thesis are:

Chapter 2 (Article 1): Koeberl C., Pittarello L., Reimold W. U., **Raschke U.**, Brigham-Grette J., Melles M., and Minyuk P. 2013. El’gygytgyn impact crater, Chukotka, Arctic Russia: Impact cratering aspects of the 2009 ICDP drilling project. *Meteoritics and Planetary Science* 48:1108-1129, doi: 10.1111/maps.12146.

Chapter 3 (Article 2): Raschke U., Reimold W. U., Zaag P. T., Pittarello L., and Koeberl C. 2013a. Lithostratigraphy of the impactite and bedrock section in ICDP drill core D1c from the El’gygytgyn impact crater, Russia. *Meteoritics and Planetary Science* 48:1143-1159, doi: 10.1111/maps.12072.

Chapter 4 (Article 3): Raschke U., Schmitt R. T., and Reimold W. U. 2013b. Petrography and geochemistry of impactites and volcanic bedrock in the ICDP drill core D1c from lake El’gygytgyn, NE Russia. *Meteoritics and Planetary Science* 48:1251-1286, doi: 10.01111/maps12087.

Chapter 5 (Article 4): Raschke U., Zaag P. T., Schmitt R. T., and Reimold W. U. 2014. The 2011 expedition to the El’gygytgyn impact structure, Northeast Russia: Towards a new geological map for the crater area. *Meteoritics and Planetary Science* 49: 978-1006, doi: 10.1111/maps.12306.

Chapter 6 (Article 5): Raschke U., McDonald I., Schmitt R.T., Reimold W.U., Mader D., and Koeberl C. Geochemical studies of impact breccias and country rocks from the El’gygytgyn impact structure, Russia. *Meteoritics and Planetary Science* 50:1071-1088, doi: 10.1111/maps.12455.

IV Contribution of the author of this thesis to the published articles

In autumn 2009, the drill cores from the Lake El'gygytgyn ICDP (International Continental Scientific Drilling Program) project arrived in Germany. Since this time, the PhD candidate was involved with handling of the lowermost 200 m of this drill core (impactite section). He organized the transport from the University of Cologne to the Museum für Naturkunde, Berlin (MfN). After a short training course at the ICDP-GFZ Potsdam, he documented and catalogued the drill core material according to ICDP standard, using special core software (DIS), provided by the ICDP. Five students supported this work. The preliminary rock description and classification were entered into the ICDP webpage. In May 2010, an international sampling party was held at the MfN. U. Raschke organized this event and, later, the preparation (cutting and boxing) and shipment of more than 600 drill core samples to the members of the scientific consortium. The PhD candidate produced thirty percent of all thin sections (~ 300) himself. Hans Rudolf Knöfler (preparation laboratory) generated the remaining thin sections.

Besides this, ~200 samples were used for geochemical studies. The PhD candidate and Kathrin Krahn (technical assistant) prepared these samples and Dr. Ralf-Thomas Schmitt performed the XRF analyses and helped with the data interpretation.

The PhD candidate is the first author of four published articles, wrote the various text versions, and studied the literature. U. Raschke produced most of the figures and tables. The petrographic studies, inclusive of the lithological classification, drill core stratigraphy, and shock determination, were carried out by U. Raschke. Usually, the first author did more than 60% of the data discussion and interpretation. The proportion for each of the manuscripts is different and clearly depends on the scientific background of the PhD candidate. An estimation in percent is given for the chapters 2-6.

Furthermore, the PhD candidate was a member of the 2011 El'gygytgyn expedition and was responsible for the mapping and sampling of country rocks in the eastern half of the crater area, and, later, for creating the new geological map of this region.

Professor Dr. Wolf Uwe Reimold is the first supervisor and first referee of this thesis. He supported the PhD candidate in all aspects, especially the petrographic and geochemical interpretation of data, and in the publication process for the peer-reviewed articles. He is co-author of all manuscripts.

Chapter 2 (article 1): This manuscript gives an overview to the ICDP drilling campaign at Lake El'gygytgyn in 2008/09 and was written, in the majority, by Prof. Dr. Christian Koeberl. The part of the PhD candidate as co-author was to clarify the lithostratigraphy of the drill core and to give input to earlier versions of the article. In addition, he made a number of images available for this publication. The contribution of the PhD candidate to this manuscript is < 10 %.

Chapter 3 (article 2): The PhD candidate developed the initial lithostratigraphy for this drill core based on early petrographic and geochemical results. Therefore, the interpretation and discussion of the lithostratigraphy in this manuscript was done by U. Raschke with approximately 85% input. First scanning electron microscopic (SEM) and MicroRAMAN studies were supported by Kirsten Born (MfN) and Dr. Jörg Fritz (formerly employed at MfN). Furthermore, a first set of 35 samples was analyzed with XRF and INAA. The analyses were done by Dr. Ralf-Thomas Schmitt (MfN) and Dieter Mader (University of Vienna). Patrice T. Zaag (student research assistant in this project) created a figure and compiled all available data in preparation of a preliminary geological map of the El'gygytgyn crater (Fig. 3.3).

Chapter 4 (article 3): The PhD candidate prepared a large number of thin sections and analyzed approximately 150 of them by polarization microscopy for a detailed petrographic description of the drilled rocks, including determination of shock metamorphism (identification of planar deformation features (PDF), diaplectic glass, silica melt (lechatelierite), and planar fractures). Another focus was on the investigation of melt particles from all units of the drill core and from surficial country rock samples. This work was combined with the production of compositional backscattered electron (BSE) images and chemical analyses of different melt particles, using the Museum für Naturkunde electron microprobe (EMP). Technician Peter Czaja provided introduction to and support during microprobe analysis. Further analytics by SEM and MicroRAMAN were done, with individual support (see paragraph above). Dr. Ralf-Thomas Schmitt produced XRF data of the remaining ~90 core samples. Patrice T. Zaag counted and selected all clasts larger than 1 cm on the surface of the drill core (impactite sequence) for analysis of clast population and clast size distribution. The discussion of this manuscript is based on all these works, with an estimated input of 75% to the preparation of this manuscript by the PhD candidate.

Chapter 5 (article 4): U. Raschke and Patrice T. Zaag were participants in the 2011 Russian-German expedition to Lake El'gygytgyn. During 26 days in the field, they studied 43 outcrops and took samples along the entire eastern crater rim. The PhD candidate was partly involved in the preparation of high quality polished thin sections and compiled all available data of the regional geological setting from the literature. Elena Raschke helped with translation of Russian texts. Many figures and tables, as well as the supplementary material, were created or modified by U. Raschke. Patrice T. Zaag developed a Digital Elevation Model (DEM) for the geological map and intensively worked with ArcGIS. Dr. Ralf-Thomas Schmitt produced the XRF data of the samples from the crater rim and helped with the interpretation of the results. Prof. Dr. Wolf Uwe Reimold was the applicant for the successful DFG proposal RE 528/12-1 and helped with data interpretation and editing of this extraordinarily long paper (73 pages, including supplementary material). The contribution of the PhD candidate to this manuscript is about 70%.

Chapter 6 (article 5): The PhD candidate produced the main part of this paper, including the discussion. His contribution is estimated at 45 %. He created the figures 1-3, 7, and table 1. Dr. Ralf-Thomas Schmitt created figures 4, 5 and tables 2 and 5, which are based on our previous publications, and gave support with helpful discussion. Instrumental Neutron Activation Analysis (INAA) was carried out at the Department of Lithospheric Research, University of Vienna by Dr. Dieter Mader. Prof. Dr. Christian Koeberl (University of Vienna and Natural Historical Museum, Vienna) supported the interpretation of the results (of REE´s). The contents of PGE and Au were determined in Cardiff by Laser-Ablation-ICP-MS by Dr. Iain McDonald. Prof. Dr. Wolf Uwe Reimold checked the clarity and plausibility of data interpretation and the structure of this manuscript.

V Abstract

The El'gygytgyn crater in Chukotka (Russia) is one of the best-preserved complex impact structures, worldwide. At ca. 3.6 million years ago a projectile of probably chondritic composition hit into an at least several hundred-meter-thick sequence of different, predominantly felsic, volcanic rocks. These belong to the Upper Cretaceous Ochotsk Chukotka Volcanic Belt (OCVB). In addition to the dominant rhyolitic/rhyodacitic ignimbrites, there are also layers of andesitic to basaltic composition. Some time after crater formation (some thousand to fifty thousand years), a lake was established in the impact structure and accumulation of lake sediments started. The El'gygytgyn impact structure is not only a special crater in terms of its lithologies, but it provides with its undisturbed lacustrine sedimentation a great climate archive for the entire Quaternary era. These were also the main reasons for the deep drilling of the structure by the International Continental Scientific Drilling Program (ICDP) in 2009. Of the four drill holes achieved, borehole D1c is the deepest with ~520 m and yielded approximately 200 m of impact-related rocks from the flank of the collapsed central uplift. These rocks have been accurately examined during this thesis work, focusing on the lithostratigraphy, the distribution of shock effects within the drilled sequence, and on the development of suevitic breccias and impact-induced melt.

The drilled rocks can be divided into four units. The uppermost 12 meters (316-328 meters below lake floor = mblf) are reworked suevite and contain unshocked to strongly shocked clasts of various volcanic rocks (basalt to rhyolite). Furthermore, in this unit occurs the comparatively largest proportion of impact-generated melt as several centimeter large melt particles or tiny (<1 mm) glass spherules. The fine-grained matrix consists mainly of the same material as the lithic clasts and is enriched with finest-grained ash particles from the collapsed ejecta plume and with clay and fine sand from the post-impact sedimentary phase and the beginning of lake development at El'gygytgyn. The following 63 m (328-391 mblf) polymict breccia are free of lacustrine sediments and can be called suevite due to their content of small impact-generated melt particles, besides shocked mineral and lithic clasts. Into this unit, three meter-sized blocks of mainly unshocked rhyolitic ignimbrite were incorporated, probably during the deposition of suevite. In one of the blocks and in two other clasts of rhyodacitic ignimbrite, shatter cones have been found.

Next, in the footwall, an approximately 32 m (391-423 mblf) thick sequence of rhyolitic pyroclastites occurs. Here, several layers of volcanic deposits could be identified. At the top of this unit is a basaltic layer of approximately 1 m thickness that contains many deformed (sheared) minerals as well as the lowermost occurrence of shocked minerals and

glass shards, as well as fragments of the overlying suevite. The formation of this thin layer is considered the result of the likely turbulent emplacement of the suevite onto the crater floor, or, alternatively, as a mixed layer related to the modification stage of cratering. It follows a relatively uniform suite of about 94 m (until the end of the hole at ~517 mblf) of welded, rhyolitic/rhyodacitic ignimbrites, which show some lithological peculiarities and deformation. First, at the top, two exotic, mafic blocks with cataclastic grain size reduction and shear deformation effects occur. These blocks are extremely altered and enriched in a variety of trace elements in comparison to all other lithologies. This could reflect an enrichment due to post-impact, hydrothermal alteration. Second, there is a dike of polymict impact breccia in the lower part of this unit. Shock metamorphism in minerals was identified in the dike, but no impact-generated melt particles. Furthermore, it was resolved by geochemical studies that there is not a single ignimbrite, but there are two separate, very similar layers of rhyolitic/rhyodacitic ignimbrite. They are not shock deformed but are brecciated, i.e., they are crisscrossed by a multitude of fissures and cracks that dissect this previously massive rock. This part of the sub-crater basement was obviously strongly “tectonically” affected by the rise and collapse of the central uplift.

In summer 2011, it was possible to participate in a Russian-German expedition to the crater structure. During the nearly four-week field campaign, the eastern half of the crater rim was mapped and sampled, in some detail. The petrographic and geochemical results for the collected samples led to the generation of a new geological map of the impact structure, and the surface rocks could be compared with those of the drill core. It turned out that the rhyolitic ignimbrites not only dominate the crater floor, but they also constitute around two-thirds of the area around the crater. The presence of basaltic and intermediate rocks could be mapped and classified more accurately than before. In addition, meter sized blocks of impact melt breccia were sampled at the southeast lakeshore of El’gygytgyn.

In case of El’gygytgyn, it was a very important issue to find out the different characteristics of volcanic and impact melt particles. Impact melt occurs at surface as glass spherules, pebbles, and impact melt blocks. Samples of these were compared with those from the core (glass spherules, melt clasts from the suevitic units) and additionally with the volcanically produced, unshocked melts and glasses from the ignimbrites. There are two types of impact- generated melts; a pure glass and a melt mixed with strongly shocked lithic clasts (impact melt breccia). Geochemical studies revealed that the impact melt breccia is a mixture of mainly rhyolitic/rhyodacitic ignimbrite and rare basaltic andesite. That corresponds with the geochemical character of the suevite and upper bedrock sequence.

Glass spherules (200-500 µm) from the upper part of the drill core and the lake or river terraces have a glassy, siliceous margin and may contain some crystal inclusions or

microfragments (as quartz, feldspar or zeolithe). The rims of spherules are different in their chemical signatures (lower content of silicium) from those of the inclusions. Another type of spherule is filled by aluminosilicate melt that is partly crystallized. A clearly definable rim is lacking. All spherules were possibly produced within the ejecta plume, in analogy to the Bosumtwi crater, Ghana (Koeberl et al. 2007a).

Volcanic melt particles in the ignimbrites (bedrock and country rock) occur mainly as "fiamme" structures and are fine-grained crystallized. Volcanic glass shards only occur at a minor proportion. These melt particles can be easily distinguished from impact melt that represents - in contrast - translucent melt particles with or without shocked lithic clasts.

To constrain the composition of the projectile that formed the El'gygytgyn crater comprehensive geochemical studies were necessary in collaboration with researchers from the Universities of Cardiff and Vienna. Major and trace elements, including the Rare Earth Elements (REE) and Platinum Group Elements (PGE), were measured from samples of drill core material and country rocks. The suevitic breccias, especially the reworked suevite of the drill core, show a higher PGE content compared to all other lithologies. These elevated PGE contents are most likely the result of an admixture of a meteoritic component, probably of chondritic composition, which would be in good agreement with other studies on the same drill core. Nevertheless, the reworked suevite contains also a higher proportion of a mafic component, as indicated by the REE contents, in comparison to the suevite. The composition of this mafic component and its PGE content cannot clearly be determined, because of the possible contribution from chemically unusual mafic blocks to the chemical budget. Therefore, it is not possible at this stage to determine more precisely the nature of the meteoritic projectile.

As a result of this work, the following reconstruction of the impact event was achieved: A likely chondritic projectile hit the Earth 3.58 million years ago and created the impact crater in siliceous volcanic rocks. The rhyolitic rocks of the crater floor were only slightly tilted during the cratering event. Overlying andesites and basalts were found not only in the core, but also on the eastern rim of the crater. The lower part of the suevite is very poor in melt and includes a relatively homogeneous distribution of shocked minerals. This could be a result of an intensive mixing process (e.g., by a ground surge) inside the crater. The upper suevitic rocks (reworked suevite) were possibly deposited from the ejecta fallout and exhibit all stages of shock metamorphism, from unshocked to melt clasts and glass spherules. Finally, the finest ash particles were accumulated as top layer after the impactites. There is no evidence for the formation of a coherent melt sheet. In the hot and slow cooling crater area, a zone of hydrothermal activity was established for an, as yet unknown, time. Ultimately, the crater lake developed. Early sedimentation was interrupted by debris flows off the unstable

inner crater wall. Only after that, maybe a period as long as fifty thousand years, first deposits of pollen can be detected, as per the work of A. A. Andreev (pers. comm.).

VI Zusammenfassung

Der El'gygytgyn Krater in Tschukotka (Russland) ist eine der besterhaltenen komplexen Impaktstrukturen, weltweit. Vor ca. 3,6 Millionen Jahren traf ein kosmisches Projektil, mit wahrscheinlich chondritischer Zusammensetzung, auf eine mindestens mehrere hundert Meter mächtige Sequenz aus verschiedenen, überwiegend felsischen, vulkanischen Gesteinen. Diese gehören dem Oberkreide-zeitlichen Ochotsk-Chukotka Vulkangürtel (OCVB) an. Neben den dominierenden rhyolithisch/rhyodazitischen Ignimbriten gibt es auch Gesteinsschichten von andesitischer bis basaltischer Zusammensetzung. Einige Zeit nach dem Kratereinschlag (etwa einige tausend bis fünfzig-tausend Jahre) bildete sich ein Kratersee, und die Ablagerung lakustriner Sedimente begann. El'gygytgyn ist somit nicht nur ein besonderer Krater was seine Lithologien angeht, sondern er stellt mit seiner ungestörten Seesedimentation ein großartiges Klimaarchiv für das gesamte Quartär dar. Das waren auch die Hauptgründe für die Tiefbohrung in dieser Struktur, durchgeführt vom International Continental Scientific Drilling Program (ICDP), im Jahre 2009. Von den vier abgeteuften Bohrungen ist D1c mit rund 520 m die tiefste und sie erbrachte rund 200 m impaktbeeinflusste Gesteine von der Flanke des Zentralbergs. Diese Gesteine wurden im Rahmen dieser Dissertation genau und vielfältig untersucht - mit Schwerpunkt auf Lithostratigraphie, die Verteilung der Schockeffekte innerhalb der erbohrten Sequenz, und die Zusammensetzung und Entstehung von suevitischen Brekzien und impaktinduzierten Schmelzen.

Die erbohrten Gesteine lassen sich in vier Gesteinseinheiten untergliedern. Die obersten zwölf Meter (316-328 mblf = meters below lake floor) des Bohrkerns bestehen aus aufgearbeiteten suevitischen Brekzien (reworked suevite), die reich an ungeschockten bis hin zu extrem geschockten Klasten der verschiedenen vulkanischen Gesteine (Basalt bis Rhyolith) sind. Des Weiteren gibt es hier den größten Anteil an impaktinduzierter Schmelze, von mehrere Zentimeter großen Schmelzpartikeln bis zu winzigen (<1mm) Glaskügelchen. Die feinkörnige Matrix besteht überwiegend aus dem gleichen Material wie die Gesteinsklasten und ist angereichert mit feinen Aschepartikeln aus der kollabierten Glutwolke sowie mit feinen Tonen und Sanden aus der sedimentären, postimpakt Phase der Kraterbildung, der beginnenden Seebildung des El'gygytgyn. Die folgenden 63 m (328-391 mblf) polymikte Gesteinsbrekzie sind frei von lakustrinen Sedimenten und können durch ihr Vorkommen an kleinen Impaktschmelzpartikeln zusammen mit geschockten Mineral- und Gesteinsklasten als Suevit bezeichnet werden. Innerhalb dieser Einheit kommen drei metergroße Blöcke nahezu ungeschockten, rhyolithischen Gesteins vor, die während der

Suevitablagerung eingearbeitet worden sein müssen. In einem dieser Blöcke sowie in weiteren Gesteinsklasten wurden drei, mehrere Zentimeter große shatter cones (Strahlenkegel) gefunden.

Weiter, im Liegenden, gibt es eine ca. 32 m (391-423 mblf) mächtige Abfolge von rhyolithischen Ignimbriten. Hier konnten mehrere Lagen vulkanischer Ablagerungen identifiziert werden. Am oberen Ende dieser Einheit gibt es eine basaltische Lage von etwa 1 Meter Mächtigkeit, die viele gescherte Gesteins- und Mineralklasten enthält, das letzte (tiefste) Auftreten von geschockten Mineralen aufweist, und eine Vermischung mit Glasscherben und Fragmenten des überlagernden Suevites zeigt. Die Ausbildung dieser dünnen Lage kann als Resultat einer turbulenten Platznahme des Suevits am Kraterboden betrachtet werden, oder alternativ, als ein Vermischungshorizont, resultierend aus der Modifizierungsphase des Kraters. Es folgt ein relativ uniformer Bereich von ca. 94 m (bis zum Ende der Bohrung bei ~517 mblf) mit homogenen, rhyolithisch/rhyodazitischen Ignimbriten, der einige Einschaltungen und Störungen aufweist. Zum einen gibt es im oberen Bereich zwei exotische, mafische Blöcke, die kataklastische Korngrössenverkleinerung mit Scherung aufweisen. Diese Blöcke sind extrem alteriert und mit verschiedensten Spurenelementen angereichert, im Vergleich zu allen anderen Lithologien. Dies könnte während einer postimpakten, hydrothermalen Alteration geschehen sein. Zum anderen gibt es einen polymikten Gang (Impaktbrekzie) im unteren Teil dieser Einheit. Es konnten schockmetamorphe Änderungen in Mineralen diagnostiziert werden, jedoch nicht mit Sicherheit impaktinduzierte Schmelzpartikel. Weiterhin konnte geochemisch festgestellt werden, dass es sich nicht um einen einheitlichen Ignimbrit handelt, sondern dass es sich hierbei um zwei getrennte, aber sehr ähnliche Lagen von rhyolithisch/rhyodazitischen Ignimbriten handelt. Sie weisen keine schockmetamorphen Effekte auf, sind aber brekziert, d.h. mit einer Vielzahl von Klüften und Rissen durchzogen, die das massige Gestein z.T. fein zerlegen. Diese Region des Krateruntergrundes wurde offensichtlich durch den Aufstieg und den Kollaps des Zentralberges stark tektonisch beansprucht.

Im Sommer 2011 war es möglich, an einer russisch-deutschen Expedition zum Kratersee teilzunehmen. Während der knapp vierwöchigen Feldkampagne wurde die Osthälfte des Kraterrandes ausführlich kartiert und beprobt. Die petrographischen und geochemischen Ergebnisse der Gesteinsanalysen mündeten zum einen in eine neue, geologische Karte der Impaktsruktur und zum anderen konnten die oberflächlich anstehenden Gesteine mit denen des Bohrkerns verglichen werden. Dabei zeigte sich, dass nicht nur die rhyolithisch/rhyodazitischen Ignimbrite den erbohrten Krateruntergrund dominieren, sondern auch rund zwei Drittel des Kratersgebietes ausmachen. Das Vorhandensein von basaltischen und intermediären Gesteinen konnte genauer kartiert und klassifiziert werden. Sowohl im

Bohrkern (als Teil der suevitischen Brekzien), als auch am Kraterrand überlagern diese Gesteine die Ignimbrite. Darüber hinaus wurden auch metergroße Blöcke von Impaktschmelzbrekzie am südöstlichen Seeufer beprobt.

Im Falle von El'gygytgyn war die Unterscheidung von vulkanischen und impakschmelzhaltigen Gesteinen oder Klasten ein wichtiger Bestandteil der Arbeit. Impaktschmelze kommt oberflächlich als Glaskügelchen, Geröll und Blöcke von Schmelzbrekzie vor. Proben davon wurden mit denen aus dem Bohrkern (Glaskügelchen, Schmelzklasten vom Suevit) verglichen und dann in Bezug zu den ungeschockten, vulkanisch produzierten Schmelzen und Gläsern (v.a. der Ignimbrite des unteren Festgesteins) gesetzt. Zusammenfassend gibt es zwei Typen von impaktgenerierten Schmelzklasten, die an der Oberfläche gefunden wurden: Zum einen reine Gläser und zum anderen Schmelze gemischt mit stark geschockten Gesteinsklasten - Impaktschmelzbrekzie. Gerölle von Schmelze innerhalb der Seeablagerungen bestehen aus beiden Phasen, sowohl relativ reinen, schwarzen Gläsern, als auch bräunliche Impaktschmelzbrekzie. Weiterhin gibt es metergroße Blöcke, die ebenso beide Phasen von Schmelze beinhalten. Laut der geochemischen Untersuchung ist die Impaktschmelzbrekzie ein Gemisch aus vorwiegend rhyolithischem/rhyodazitischem Ignimbrit und wenig basaltischem Andesit. Die Zusammensetzung passt gut zu der des erbohrten Suevits und der oberen Festgesteinssequenz.

Die Glaskügelchen (200-500 µm groß) aus dem oberen Bereich des Bohrkerns und den See- bzw. Flussterrassen besitzen einerseits einen glasigen, silikatischen Rand und können hohl sein bzw. einige Kristalleinschlüsse oder Mikrofragmente von verschiedenen Mineralen, z. B. Quarz und Feldspat oder Zeolith, aufweisen. Der Rand der Kügelchen ist in seiner chemischen Signatur (geringerer Anteil an Silizium) unterscheidbar im Vergleich zu den Einschlüssen oder Mikrofragmenten. Ein anderer Typ von Kügelchen ist gefüllt mit aluminiumsilikatischer Schmelze, die teilweise kristallisiert ist. Ein klar definierbarer Rand fehlt bei diesen. Alle Kügelchen wurden wahrscheinlich in der Glutwolke gebildet (siehe Kapitel 3).

Ein weiteres Kriterium für die Unterscheidung von vulkanischer und impakt-produzierter Schmelze ist, dass die typische „Fiamme" Struktur des rhyolithischen/ rhyodazitischen Ignimbrites meistens feinkörnig kristallisiert ist, mit nur einem kleinen Gehalt an glasigen Scherben. Somit ist die vulkanische Schmelze leicht zu unterscheiden von impaktgenerierter Schmelze, die im Gegensatz dazu als durchsichtiges bis braun-schwarzes Glas, teilweise vermischt mit geschockten oder ungeschockten Gesteinsklasten, auftritt.

Zur Eingrenzung der Bestimmung des Projektils, das den El'gygytgyn Krater geformt hat, waren umfassende geochemische Untersuchungen notwendig, in Zusammenarbeit mit

Forschern der Universitäten Cardiff und Wien. Haupt- und Spurenelemente, inklusive der Seltenen Erden (REE) und Platingruppenelemente (PGE), wurden an Proben aus dem Bohkern und vom Kraterrand analysiert. Die suevitischen Brekzien, besonders der aufgearbeitete Suevit vom Bohrkern, zeigen einen höheren Anteil an PGE, verglichen mit allen anderen Gesteinseinheiten. Diese erhöhten PGE-Gehalte sind ein mögliches Ergebnis einer Anreicherung mit einer meteoritischen Komponente, möglicherweise von chondritischer Zusammensetzung. Dies würde gut zu anderen Studien des gleichen Bohrkerns passen. Nichtsdestotrotz, der aufgearbeitete Suevit beinhaltet auch eine höhere Anreicherung an mafischen Komponenten im Gegensatz zum Suevit, wie es der REE-Gehalt indiziert. Die Zusammensetzung dieses mafischen Anteils und sein PGE-Gehalt kann nicht genau bestimmt werden, da eine mögliche Anreicherung mit den chemisch ungewöhnlichen mafischen Blöcken zum Gesamthaushalt der Elemente beigetragen haben könnte. Daraus folgt, dass es zu diesem Zeitpunkt, mit den Ergebnissen dieser Arbeit, nicht möglich ist, die Art des meteoritischen Projektils zweifelsfrei bestimmen zu können.

Als Ergebnis dieser Arbeit kann folgende Rekonstruktion des Impaktereignisses erstellt werden: Ein wahrscheinlich chondritisches Projektil traf die Erde vor 3,58 Millionen Jahren und erschuf den Einschlagskrater in den hauptsächlich felsischen Vulkaniten. Dabei sind die rhyolithischen Gesteine des Krateruntergrundes relativ ortsnah verblieben (parautochthon) und während der Kraterbildung nur leicht verkippt worden. Die den Ignimbriten aufliegenden Andesite bzw. Basalte finden sich nicht nur im Bohrkern, sondern auch weitflächig am östlichen Kraterrand. Der untere Teil des Suevits ist sehr schmelzarm und beinhaltet eine relativ homogene Verteilung der geschockten Minerale. Dies könnte aus einem intensiven Mischungsprozess (z.B. einem basalen Gesteinsschuttstrom) innerhalb des Kraters resultieren. Der obere Teil des Suevits (reworked suevite) ist möglicherweise beim Niedergehen von Partikeln aus einer Glutwolke abgelagert worden und enthält Partikel in allen Stufen der Schockmetamorphose, von ungeschockt bis hin zu Schmelz/Glaskügelchen. Zum Schluss kamen feinste Aschepartikel zur Ablagerung als oberste Schicht auf der gerade entstandenen Kraterhohlform. Es gibt keinen Hinweis darauf, dass sich ein zusammenhängender Schmelzsee ausgebildet hatte. Das heiße und langsam abkühlende Kratergebiet etablierte wahrscheinlich eine Zone mit hydrothermaler Aktivität für eine unbekannt lange Zeit. Schließlich entwickelte sich der Kratersee. Erste Sedimentation wurde gestört von Gesteinsrutschungen vom instabilen, inneren Kraterrand. Erst danach, in einer Zeitspanne von einigen tausend bis zu fünfzigtausend Jahren, wurden erste Ablagerungen von Pollen aus der näheren und weiteren Umgebung sedimentiert.

VII Abbreviations and Units

a) Abbreviations

AARI	Arctic and Antarctic Research Institute, Sankt Petersburg
AWI	Alfred-Wegener-Institute, Potsdam
Am	Amphibole
Bt	Biotite
Cal	Calcite
Chl	Chlorite
EDX	Energy-dispersive X-ray spectroscopy
EMP	Electron microprobe
Fsp	Feldspar
GFZ	Deutsches GeoForschungsZentrum Potsdam
Hbl	Hornblende
INAA	Instrumental neutron activation analysis
LA-ICP-MS	Laser ablation inductively coupled plasma mass spectrometry
MfN	Museum für Naturkunde Berlin
mblb	meters below lake bottom
mblf	meters below lake floor
n.a.	Not analyzed
Ol	Olivine
PDF	Planar deformation features
PF	Planar Fractures
Pl	Plagioclase
Px	Pyroxene
Qtz	Quartz
SEM	Scanning electron microscope
T	Temperature
XRF	X-ray fluorescence spectroscopy
Zeo	Zeolite
Zrn	Zircon

b) Units

a	Year
°C	Degree Celsius
GPa	Gigapascal
km s^{-1}	Kilometer per second
kV	Kilovolt
Ma/Myr	Million Years
masl	Meters above sea level
µm	Micrometer
nm	Nanometer
ppb	Parts per billion
ppm	Parts per million
vol.%	Volume percent
wt.%	Weight percent

VIII List of Figures

Figure 1.1: Worldwide distribution of impact craters 6

Figure 1.2: Classification of impactites 9

Figure 1.3: Geological setting of impactites on Earth 11

Figure 1.4: Conditions of shock metamorphism and normal crustal metamorphism. 12

Figure 2.1: Extent of the Arctic sea ice in the summer of 2008 18

Figure 2.2 (a-c): Satellite image of the El'gygytgyn impact crater 20

Figure 2.3: Simplified geological map of the El'gygytgyn area 22

Figure 2.4 (a-c): Location and setting of the El'gygytgyn impact structure. 26

Figure 2.5: Aerial view of the campsite looking toward the western crater rim 27

Figure 2.6 (a, b): Aerial views of the field camp 27

Figure 2.7 (a, b): The modified GLAD 800 drill rig on a platform 28

Figure 2.8: Schematic cross section of the El'gygytgyn basin stratigraphy 30

Figure 2.9 (a, b): Core segments from the drilling project at the El'gygytgyn 32

Figure 2.10: Schematic representation of the simplified drill core litho-stratigraphy 34

Figure 2.11 (a-h): Interval 316.8-320 mblb 36

Figure 2.12 (a-h): Interval 320-328 mblb 37

Figure 2.13 (a-h): Interval 328-390 mblb 38

Figure 2.14 (a-h): Interval 390-423 mblb 39

Figure 2.15 (a-h): Interval 423-517 mblb 40

Figure 3.1: Schematic outline of the El'gygytgyn impact structure 47

Figure 3.2: Combined lithostratigraphic table of the Lake El'gygytgyn region 48

Figure 3.3: Simplified geological map 50

Figure 3.4: Stratigraphic column of the impactite sequence 55

Figure 3.5: Photographs of drill core 57

Figure 3.6: Microphotographs. 59

Figure 3.7: Photos of shatter cones in the suevite sequence 60

Figure 3.8: Microphotographs of thin section scans 64

Figure 4.1: Simplified geological sketch map of the El'gygytgyn impact structure 70

Figure 4.2: Stratigraphic column of the impactite sequence 72

Figure 4.3: Images of the lower bedrock unit 77

Figure 4.4: Upper bedrock 79

Figure 4.5 (a-e): Mafic blocks 81

Figure 4.6 (a-e): Photograph of a representative core box 83

Figure 4.7: Vesicle-rich impact glass particle 87

Figure 4.8: Reworked suevite. Complete core box No. 100 89

Figure 4.9: Reworked suevite. Two combined thin section images 91

Figure 4.10: Clast population 93

Figure 4.11: Variations of the SiO_2 (A), TiO_2 (B), Al_2O_3 (C), Fe_2O_3 (D) 97

Figure 4.12: Variations of Zr (A) and V (B) abundances versus depth 101

Figure 4.13: Total alkali-silica (TAS) plots after Cox et al. (1979) for target lithologies 101

Figure 4.14: Zr versus TiO_2 discrimination diagram (Leat and Thorpe 1986) 102

Figure 4.15: Harker diagrams 103

Figure 4.16: Total alkali-silica (TAS) plot after Cox et al. (1979) for the suevite 104

Figure 4.17: Harker diagrams 107

Figure 4.18: Harker diagrams 108

Figure 4.19: SiO_2/Al_2O_3 versus Fe_2O_3/K_2O discrimination diagram 109

Figure 5.1: Geographic location of the El'gygytgyn impact structure in NE Russia 127

Figure 5.2: Stratigraphic map of the El'gygytgyn crater area 131

Figure 5.3: Digital elevation model for the El'gygytgyn impact structure 132

Figure 5.4: Overview map showing all locations that were sampled 135

Figure 5.5: Total alkali-silica (TAS) plot after Le Maitre et al. (1989) 145

Figure 5.6: Geological map of the El'gygytgyn impact crater 153

Figure 5.7: SiO_2 versus alkali element abundance discrimination diagram 156

Figure 5.8: Harker diagrams 160

Figure S1: Aerial photograph of the north-eastern crater rim.....163

Figure S2 (a-e): Basalt a) Panoramic view over the south-eastern crater rim.....164

Figure S3 (a-c): Andesitic basalt.....165

Figure S4 (a-c): Rhyodacitic ignimbrite.....166

Figure S5 (a-f): Rhyolitic ignimbrite.....167

Figure S6 (a-e): Andesitic-dacitic tuff.....168

Figure S7 (a-k): Basaltic-andesitic tuff.....169

Figure S8 (a-f): Rhyodacitic tuff.....171

Figure S9 (a-e): Impact melt breccia.....172

Figure S10: This figure shows the complete new geological map of the El'gygytgyn.....173

Figure S11: Harker diagrams.....175

Figure 6.1: Geological map of the El'gygytgyn impact crater 196

Figure 6.2: Simplified NW-SE cross-section through the El'gygytgyn impact 198

Figure 6.3: Stratigraphic column of the ICDP drill core 199

Figure 6.4: Zr/TiO_2 versus Nb/Y diagram for classification of volcanic rocks..... 200

Figure 6.5: CI chondrite normalized REE plots 208

Figure 6.6: CI-normalized PGE plots..... 211

Figure 6.7: (a) Os vs. Ir, (b) Rh vs. Ir, and (c) Ru vs. Ir abundance plots 211

Figure 7.1: Stratigraphic columns for the impactite sequence 219

Figure 7.2: Left: Thin section from the reworked suevite at 318.24 mblf..... 225

Figure 7.3 (a-e): Impact melt breccia 231

IX List of Tables

Table 2.1: Penetration, drilling and core recovery at ICDP Sites 5011-1 and 5011-3 31

Table 4.1: Sample statistics for whole-rock chemical analysis 95

Table 4.2: Average chemical composition, standard deviation and range of rock compositions for the reworked suevite, suevite, upper and lower bedrock 100

Table 4.3: Average chemical composition and standard deviation for the suevite of the El'gygytgyn drill core D1c in comparison to the average target composition 118

Table S1: Whole rock chemical compositions of individual samples 121

Table 5.1: Compilation of different stratigraphic units of the northern OCVB 130

Table 5.2: Average chemical composition, standard deviation, and range of rock composition for the reworked suevite, suevite, upper and lower bedrock 143

Table 5.3: Percentage of the different target lithologies 154

Table 5.4: Average chemical composition and standard deviation for the suevite of the El'gygytgyn drill core D1c in comparison to average target compositions 157

Table S1: Locations and short lithological descriptions of surface samples 176

Table S2: Compilation of whole rock compositions of surface samples 190

Table 6.1: List of ICDP drill core samples for analytical studies 204

Table 6.2: Selected major and trace element abundances of samples 206

Table 6.3: Concentrations of platinum group elements and Au in impactites and target lithologies 207

Table 6.4: Compilation of the average REE contents 209

Table 6.5: Compilation of the average Cr, Co, and Ni contents 210

Table 6.6: Calculated average PGE composition 215

X Content

I Declaration I

II Acknowledgments II

III Structure of this thesis IV

IV Contribution of the author of this thesis to the published articles V

V Abstract VIII

VI Zusammenfassung XII

VII Abbreviations and Units XVI

a) Abbreviations XVI

b) Units XVII

VIII List of Figures XVIII

IX List of Tables XXI

X Content XXII

CHAPTER 1 1

1. INTRODUCTION 1

1.1 MOTIVATION AND GOALS 1

1.1.1 Motivation for this Project 1

1.1.2 Why Drilling at Lake El'gygytgyn 1

1.1.3. Drilling Project 2

1.1.4 Goals for this Project 3

1.2 IMPACT CRATERING 5

1.2.1 The Role of Impact Cratering 5

1.2.2 Formation of Terrestrial Impact Structures 5

1.2.3 The Impact Lithologies 8

1.2.3.1 The Formation of Suevite ("The Suevite Conundrum") 8

1.2.4 Recognition of an Impact Structure (Shock Metamorphic Effects) 12

1.2.4.1 Shatter Cones 12

1.2.4.2 Planar Microfractures - PF, PDF and More 13

1.2.4.3 Feather Features (FF) 14

1.2.4.4 Mosaicism 15

1.2.4.5 Diaplectic Glass and Ballenquartz 15

1.2.4.6 Silica Melt – Lechatelierite 16

1.2.4.7 High-Pressure Polymorphs 16

CHAPTER 2 17

EL'GYGYTGYN IMPACT CRATER, CHUKOTKA, ARCTIC RUSSIA: IMPACT CRATERING ASPECTS OF THE 2009 ICDP DRILLING PROJECT 17

2.1 ABSTRACT 17

2.2 INTRODUCTION 18

2.3 GEOLOGICAL SETTING OF THE EL'GYGYTGYN IMPACT STRUCTURE 19

2.4 RATIONALE FOR DRILLING PROJECT 22

2.5 DRILLING PROJECT AND OPERATIONS 24

2.6 SEDIMENT CORES 29

2.7 PERMAFROST CORE 31

2.8 IMPACTITE CORE 32

2.8.1 Impactite Drill Core Stratigraphy 32

2.8.1.1 Impact Melt Breccia 33

2.8.1.2 Intermediate Layer - Volcanic Sequence 35

2.8.1.3 Rhyodacitic Ignimbrite 35

2.9 RESULTS OF IMPACTITE STUDIES 41

2.10 CONCLUSIONS 44

CHAPTER 3 46

LITHOSTRATIGRAPHY OF THE IMPACTITE AND BEDROCK SECTION OF ICDP DRILL CORE D1C FROM THE EL'GYGYTGYN IMPACT CRATER, RUSSIA. 46

3.1 ABSTRACT 46

3.2 INTRODUCTION 47

3.3 GEOLOGICAL BACKGROUND 49

3.4 REGIONAL LITHOSTRATIGRAPHY 51

3.5 METHODS 52

3.6 LITHOLOGICAL UNITS 54

3.6.1 The Transition Zone (313.73-316.77 mblf) 56

3.6.2 The Reworked Suevite (316.77-328.00 mblf) 56

3.6.3 The Suevite (328.00-390.74 mblf) 59

3.6.4 The Upper Bedrock Unit (390.74-420.89 mblf) 61

3.6.5 The Lower Bedrock Unit (420.89–517.09 mblf) 63

3.7 DISCUSSION AND CONCLUSION 65

CHAPTER 4 68

PETROGRAPHY AND GEOCHEMISTRY OF IMPACTITES AND VOLCANIC BEDROCK IN THE ICDP DRILL CORE D1C FROM LAKE EL'GYGYTGYN, NE RUSSIA. 68

4.1 ABSTRACT 68

4.2 INTRODUCTION 69

4.3 SAMPLES AND METHODOLOGY 71

4.4 THE STRATIGRAPHY OF THE IMPACTITES BETWEEN 517.09 AND 316.77 MBLF DEPTH 74

4.5 RESULTS 75

4.5.1 Petrographic Analysis 75

4.5.1.1 The Lower Bedrock (517.09 to 420.89 mblf) 75

4.5.1.2 The Welded Ignimbrite 75

4.5.1.3 The Contact or Shear Zone Between the Two Subunits of Ignimbrite 76

4.5.1.4 The Ash Tuff Veins 78

4.5.1.5 Shock Metamorphism 78

4.5.1.6 The Upper Bedrock Unit (420.89 to 390.74 mblf) 78

4.5.1.7 The Mafic Blocks in the Lower and Upper Bedrock Units 80

4.5.1.8 The Polymict Impact Breccia Revealed as Suevite (390.74 to 328 mblf) ... 82

4.5.1.9 The Polymict Impact Breccia Dike (471.96–471.42 mblf) 84

4.5.1.10 Micro-Analysis of Melt Particles Within Suevite and Reworked Suevite 84

4.5.1.11 The Reworked Suevite Unit (approximately 328-316.77 mblf) 88

4.5.2 The Fractures 91

4.5.3 Analysis of the Clast Population and Its Grain-Size Variation Throughout the Impactite Section 92

4.5.4 Chemical Analysis of the D1c Lithologies 95

4.5.4.1 Chemistry of Felsic Target Lithologies 95

4.5.4.2 Compositions of Mafic Target Lithologies 99

4.5.4.3 Chemical Composition of Suevite and Polymict Impact Breccia Dike 103

4.5.4.4 Chemical Composition of the Reworked Suevite 105

4.6 DISCUSSION 109

4.6.1 Petrography of the Impact Rocks and Their Origin 109

4.6.1.1. The Lower Bedrock Unit (517.09 to 420.89 mblf) 109

4.6.1.2 The Upper Bedrock Unit (420.89 to 390.74 mblf) 111

4.6.1.3 The Massive Suevite Unit (390.74 to 328 mblf) 112

4.6.1.4 The Reworked Suevite Unit (Approximately 328-316.77 mblf) 113

4.6.1.5 Distribution of Shock Features Throughout the Impactites in D1c 115

4.6.1.6 Alteration 116

4.6.1.7 Chemical Composition of Impact Breccias and Target Rocks 116

4.7 CONCLUSIONS 118

SUPPLEMENTARY MATERIAL 120

CHAPTER 5 126

THE 2011 EXPEDITION TO THE EL'GYGYTGYN IMPACT STRUCTURE, NORTHEASTERN RUSSIA: TOWARD A NEW GEOLOGICAL MAP FOR THE CRATER AREA. 126

5.1 ABSTRACT 126

5.2 INTRODUCTION 126

5.2.1 Geological and Stratigraphic Background 128

5.2.2 Drilling Campaign 2008/09 134
5.2.3 The 2011 Expedition to El'gygytgyn Crater 136
5.3 METHODOLOGY 136
5.3.1 Preparation for the Expedition 136
5.3.2 Field Work and Sampling 137
5.3.3 Petrographic and Geochemical Analysis 138
5.3.4 Creating the Map 139
5.4 RESULTS 139
5.4.1 The Lithological Groups 139
5.4.1.1 Basalt 140
5.4.1.2 Basaltic Andesite 140
5.4.1.3 Andesite 141
5.4.1.4 Rhyodacitic Ignimbrite 142
5.4.1.5 Rhyolitic Ignimbrite 146
5.4.1.6 Andesitic-Dacitic Tuff 147
5.4.1.7 Basaltic-Andesitic Tuff 147
5.4.1.8 Rhyodacitic Tuff 149
5.4.1.9 Impact Melt Breccia 150
5.4.1.10 Quaternary Deposits 151
5.4.1.11 The New Map 151
5.5 DISCUSSION 153
5.5.1 Geological Setting of the El'gygytgyn Area 153
5.5.2 Distribution of Stratigraphic Formations 155
5.5.2.1 Pykarvaam Formation 155
5.5.2.2 Voron'in Formation 155
5.5.2.3 Koekvun' Formation 157
5.5.2.4 Ergyvaam Formation 158
5.5.2.5 Enmyvaam Formation 158

5.5.2.6 Paleogene 158

5.5.3 Comparison of Surface Volcanics with the Bedrock drilled by the ICDP Project 158

5.5.4 Tectonic Setting 159

5.6 CONCLUSIONS 161

5.7 SUPPLEMENTARY MATERIAL 163

CHAPTER 6 195

GEOCHEMICAL STUDIES OF IMPACT BRECCIAS AND COUNTRY ROCKS FROM THE EL'GYGYTGYN IMPACT STRUCTURE, RUSSIA. 195

6.1 ABSTRACT 195

6.2 INTRODUCTION AND GEOLOGICAL BACKGROUND 195

6.2.1 Impact and Volcanic Melt Rocks in the Crater Area and in the Drill Core 200

6.2.2 Previous Studies of Siderophile Elements, Platinum Group Elements, and Rare Earth Elements 202

6.3 SAMPLES AND ANALYTICAL METHODS 203

6.4 RESULTS 205

6.4.1 Composition of the drill core material and target rocks 205

6.4.2 Rare Earth Elements 205

6.4.3 Siderophile Elements 209

6.4.4 Platinum Group Element analysis – the Presence of a Meteoritic Component 210

6.5 DISCUSSION 212

6.6 CONCLUSIONS 216

CHAPTER 7 218

7. GENERAL DISCUSSION 218

7.1 OBTAINED DRILL CORE MATERIAL (IMPACTITES) AND ITS DIFFERENT STRATIGRAPHIC INTERPRETATIONS 218

7.2 THE NEW GEOLOGICAL MAP OF THE EL'GYGYTGYN IMPACT STRUCTURE 221

7.3 EMPLACEMENT OF BASAL IMPACT ROCKS 222

7.4 FORMATION OF THE SUEVITE 224

7.5 THE DISTRIBUTION OF SHOCK METAMORPHISM OVER THE ENTIRE LENGTH OF THE DRILL CORE 226

7.6 DISTINCTION OF IMPACT PRODUCED MELT AND VOLCANIC MELT 227

7.6.1 The Impact Produced Melt Volume in Drill Core D1c 228

7.6.2 Occurrences of Melt at El'gygytgyn Crater 229

7.6.2.1 Glass Bombs and Blocks of Impact Melt Breccia 229

7.6.2.2 Impact Melt of the Drill Core 232

7.6.2.3 Spherules 233

7.6.2.4 Volcanic Melt of the Crater Rim and from the drilled Rocks 233

7.7 IDENTIFICATION OF A METEORITIC COMPONENT 234

7.7.1 Siderophile Elements 234

7.7.2 Platinum Group Elements (PGE) and Rare Earth Elements (REE) 235

7.7.3 Mixing Calculations 237

7.8 WHAT DID THIS WORK ON THE EL'GYGYTGYN IMPACT CRATER YIELD WITH RESPECT TO OTHER CRATERS? 237

CHAPTER 8 239

CONCLUSIONS 239

REFERENCES 241

CHAPTER 1

1. INTRODUCTION

1.1 MOTIVATION AND GOALS

1.1.1 Motivation for this Project

I had my first contact with the El'gygytgyn impact structure in 2004. Dr. Olaf Juschus (then of HU Berlin, now at the Hochschule für Nachhaltige Entwicklung Eberswalde) made a presentation at the Humboldt Universität zu Berlin. He reported about the 2003 summer field trip to Lake El'gygytgyn that was focused on geophysical studies and sampling of water, plants, and rocks. I was excited about this expedition to the "end of the world". At this time, I was already interested in impact geology, and in the following years, I did my diploma thesis about the Lockne impact structure in Sweden. In 2007, El'gygytgyn came back into my focus and I participated in the "Lake El'gygytgyn workshop 2007" in Cologne (http://www-icdp.icdp-online.org/front_content.php?client=29&idcat=357&idart=2115&lang =28) in preparation of the planned ICDP drilling campaign 2008/09. Here, I forged links to the relevant international community. The idea was born to write a DFG proposal with focus on the investigation of the drilled impactites, including the possibility to prepare a PhD thesis. In 2009, Prof. Dr. W.U. Reimold (Museum für Naturkunde Berlin, MfN) submitted a proposal for this project - and it was successful. In spring 2010, I started with the work within the framework of this planned project. A few months before, I was already involved with the logistics and transport of the drilled material from the Universität zu Köln to the MfN. After that, I began with core curation according to the international ICDP standards.

1.1.2 Why Drilling at Lake El'gygytgyn

The International Continental Scientific Drilling Program (ICDP) was founded in 1996 by funding institutions of initially three nations (Germany, USA, and China). Since this time the ICDP has grown and actually, it consists now of 24 members (23 countries and UNESCO). The aim is the creation of a new international standard for scientific drilling, core curation, and sample handling. More information can be obtained here: www.icdp-online.org.

The following reasons gave the impetus for a multidisciplinary and multinational deep drilling project at Lake El'gygytgyn:

(1) *Paleoclimatology*: The 3.58 Ma (Layer 2000) old El'gygytgyn impact structure has never been glaciated during the entire Late Cenozoic and the lacustrine post-impact sedimentation remained undisturbed. This allowed obtaining full-length sediment core that yields a complete

climate archive for the past 3.6 Ma. This is unique for an area of this high latitude and very important for the interpretation of the global climate evolution (Melles et al. 2005). Another aspect for paleoclimate research is the evolution of the permafrost ecosystem e.g., `why and how the Arctic climate system evolved from a warm forested ecosystem into a cold permafrost ecosystem between 2 and 3 million years ago? ´ (Brigham-Grette et al. 2007).

(2) *Impact geology*: The El'gygytgyn impact structure (Chukotka, Arctic Russia) is the only known impact structure formed in mostly siliceous volcanic rocks. The crater is excavated in the outer zone of the Late Cretaceous Okhotsk-Chukotka Volcanic Belt (OCVB), composed of ~92% rhyolithic and rhyodacitic ignimbrites and ~8% basaltic-andesitic rocks as lavas, sills and tuffs (this work - Chapter 5). The predominant ignimbrites belong to the Pykarvaam Series (88.5 ± 1.7 Ma, Stone et al. 2007). Such a target composition is unique among the terrestrial impact structures, and thus provides a splendid opportunity to study shock metamorphism in felsic terrestrial volcanics. Shock metamorphosed target rocks and impact melt breccias occur surficial only as redeposited material in the terraces around lake El'gygytgyn. Drilling is the only possibility to receive exact information of the existence and prevalence of impact rocks, in general; and the progression of shock metamorphism, the geochemistry, and petrology of such impactites, in detail. The results have the potential for comparable studies with other impact structures on Earth and on other planets, with respect to such volcanic settings.

1.1.3. Drilling Project

The proposed drilling campaign included three drilling sites (Gebhardt et al. 2006):

- Borehole 5011-1 near the center of the lake, where debris flows off the crater rim were expected to be almost absent, and where an undisturbed record of paleoclimate data could be expected. The geographical position would correspond to the eastern flank of the stratigraphic uplift with a typical sequence of suevite and brecciated bedrock (as interpreted from gravimetric studies by Gebhardt et al. 2006).

- Borehole 5011-2 close to the shoreline of the lake in order to better understand the mechanisms of mass movement and the impact of paleoclimate change on permafrost evolution.

- Borehole 5011-3, a relatively shallow borehole into the western lake catchment, into the permafrost.

The drilling campaign started in November 2008 with a 142 m long sediment core that was retrieved from the permafrost soil at ICDP Site 5011-3 in the western lake catchment. Sediment cores followed from lake drilling at site 5011-1. The first two holes (1a

and 1b) provided nearly complete records of the uppermost 150 m of the sediments in central Lake El'gygytgyn. Borehole 1c intersected the transition zone between the lacustrine sediments and the impact rocks at around 316 mblf. The ~200 meters of the impactite sequence comprise a ~22 m zone (316-328 mblf) that contains a suevite with higher portions of impact melt particles and strongly shocked clasts and minerals, compared to the underlying suevite. This unit also shows intercalations with lake sediments and ash particles and is called "reworked suevite". Then follows a ~63 m (328-391 mblf) thick unit of melt-poor "suevite" and the sharp contact to the "upper bedrock" unit. These rocks (391-423 mblf) are pyroclastic flows (mainly ignimbrites) with a basaltic layer at the top and the deepest occurrence of shock metamorphism. The "lower bedrock" contains ~94 m of a uniform ignimbrite with two exotic mafic blocks at the top and a polymict breccia dike at 471 mblf. At 517.09 mblf the drill core 1c ends. Core recovery was 76% for the impactite sequence, on average (Melles et al. 2011; this work - Chapter 2).

1.1.4 Goals for this Project

The scientific goals of this PhD project were aimed at investigating the impactite sequence of drill core 1c that was sunk against the flank of the central uplift structure somewhat offset from the crater center. The following aspects were noted for this crater and provided strong interest for scientific pursuit that made this project highly interesting:

(1) Characterization and classification of the impactite sequence (with a creation of a litho-stratigraphy); (2) detailed petrographic (especially shock metamorphic) characterization of the litho-components; (3) lithological and chemical analysis of the components of these breccias in comparison with country rock types.

The research objectives for this work can be summarized as follows:

1. Lithological and shock metamorphic classification of volcanic rocks and impact breccia components. This includes detailed analysis and comparison of volcanic melts (in tuff and ignimbrite) with impact-generated melts (in the suevitic units).
2. Variation of shock metamorphic evidence over the entire length of the core with statistical analysis of their distribution – aiming at evidence to reconstruct the origin of materials occurring over the entire length of core.
3. Geochemical studies of Platinum Group Elements (PGE) to identify a meteoritic component within the impactites, and thus to identify the nature of the projectile that formed the El'gygytgyn impact structure.

4. Using this information for understanding of formation and emplacement of impact breccias.

5. Creation of a comprehensive geological map for the crater region, based on the results of the 2011 El'gygytgyn field trip.

In detail, the following objectives were to be pursued:

(a) Detailed multidisciplinary investigation of the uppermost transition zone (from 313.73-316.77 mblf) to post-impact sediments will provide essential insight into the final stages of crater fill formation - especially in comparison with recent drill core results from Chesapeake Bay (Gohn et al. 2008), Bosumtwi, Ghana (Koeberl et al. 2007a) and Ries Crater (the Enkingen drill core - Reimold et al. 2013). Crucial to this work is the question whether the uppermost impactites represent fallout from the ejecta plume or a mixture of fallout and material that never left the crater. This section of the El'gygytgyn drill core is also vital for the understanding of the immediate post-impact recovery of the environment and changeover from impact to post-impact sedimentation processes.

(b) The suevite sequence comprises components derived from different target rocks and that were shock deformed to various degrees. The existing crude shock classification for volcanic rocks by Gurov et al. (2005) should be tested and expanded. Shock attenuation in the underlying monomict impact breccias was to be analyzed and compared with other impact structures.

(c) A further objective for this project is the attempt to trace the nature of the meteoritic projectile that formed this impact structure. Comprehensive chemical analysis of target rock components and impact breccias is required to characterize the compositions of all lithological components. This step is necessary to be sure that the system analyzed does not contain any yet unsampled components. If this could be established, platinum group element analysis would be carried out on target rocks and impact breccia by instrumental neutron activation analysis and by Laser-Ablation-ICP-MS. If it is possible to establish a chemical (siderophile elements and PGE) signature for the meteoritic projectile, this would be followed by trying to establish projectile distribution throughout the impactite sequence, with special reference to the uppermost section of suevite, which might contain a component of late fallout from the ejecta plume.

(d) An extension of the PhD project became possible in 2011. There was the opportunity for participation in an expedition to the El'gygytgyn impact structure. With separate funding from the DFG (Re 528/12-1 to Prof. Dr. Wolf Uwe Reimold), it was possible to realize a field trip. U. Raschke and a student assistant (P. T. Zaag) collected country rock samples along the

eastern half of the crater rim. The results were an updated geological map of the crater and a comparison of country rocks with drilled impactites.

In conclusion, the proposed research was to provide a scientific framework for the understanding of the crater formation and shock distribution in a series of impact breccias, generated in siliceous volcanics. This aspect of impact research is not only original in the context of the study of the terrestrial impact crater record, but would also provide fundamental information to be applied when and where similar volcanics-based impact terrains will be investigated on planetary surfaces, e.g., on the surface of Mars.

1.2 IMPACT CRATERING

1.2.1 The Role of Impact Cratering

The origin and evolution of all solid bodies of our solar system is a result of impacts, collision and accretion of cosmic material (planetesimal) in the ancient solar nebular (e.g., French 1998, Melosh 1989). Thereby, "hypervelocity" or "bolide" impacts refer to the collision of two planetary bodies of (or close to) cosmic velocity. A shock wave with ultrasonic velocity is generated and propagates into the target and projectile. In general, impact structures are one of the dominant landforms on all terrestrial planets (French 1998). Today, there are approximately 190 impact structures confirmed on Earth (see Fig. 1.1). It is now widely accepted that the origin of the Moon is the result of a collision of a Mars-sized object with the Proto-Earth about 4.5 Ga ago (e.g., Canup and Asphaug 2001, Zhang et al. 2012). Shock waves, caused by impact processes, produce extreme conditions for shock pressures (>100 GPa) and temperatures, unique for the wide field of geology. Shock metamorphism characterizes the deformation effects in minerals caused by the passage of a shock wave through natural rocks. Shock metamorphism contains processes such as solid-state deformation, melting, and vaporization (e.g., Stöffler and Grieve 2007).

1.2.2 Formation of Terrestrial Impact Structures

The cratering process is very complex and many details are still uncertain, but the general process can be characterized by the following three stages (Melosh 1989, Stöffler and Grieve 2007, Reimold and Koeberl 2014):

1) Contact and compression: A moving projectile makes contact with the ground surface and penetrates the solid target rocks to approximately 1 - 2x its own diameter. It instantly releases its kinetic energy in form of a shock wave that travels through the target rocks and the projectile (back) in a radially outward moving shock front.

Figure 1.1: Worldwide distribution of impact craters. The El'gygytgyn impact structures is labeled with a yellow star. The newly confirmed Saqqar impact structure (Kenkmann et al. 2015) is added. Source: http://www.passc.net/ EarthImpactDatabase/ Worldmap.html, last access: 04/20/2017.

The energy transmitted into the target rocks is reduced rapidly, due to the increasing volume of rocks, which is passed by the hemispherically travelling shock wave, and additional energy is lost by heating, deformation, and acceleration of target rocks. Near the crater rim, the velocity of shock waves decreases to that of a regular elastic wave or seismic wave. The shock wave reaches the rear surface of the projectile and will be reflected back as a rarefaction (or release) wave. Now, the projectile is unloaded of energy, and this part of the process ends.

2) Excavation: The projectile is at the center of the surrounding, roughly hemispherical shock wave and its following release wave, which propagate through the target rocks. So, the target rocks become compressed and ejected to form a bowl-shaped transient crater. The up- and outwards-ejected (into the atmosphere) material forms an ejecta curtain and is deposited around the crater structure.

3) Modification: The transient cavity collapses by gravity, and due to mass movement from its outer flank inward. The crater structure becomes wider and shallow by inward moving landslides and slumping off the crater walls (along listric faults). At larger, complex craters, a central uplift rises up as a result of a combination of the gravity controlled processes of the inward directed flows and the elastic rebound of the crater floor. After the collapse of the central uplift the final crater form is established.

Impact craters on Earth can be described as nearly ‘circular rimmed depressions’ (Melosh 1989). According to Melosh (1989) and French (1998), three different types are distinguished:

Simple, bowl shaped craters, <2 to 4 kilometers in diameter on Earth, depending on target rock properties (e.g., for crystalline rocks ~4 km maximum and for sediments ~2 km.). Their geometries are similar but not identical to the transient crater in shape and dimension. A mixture of fallback ejecta, debris and slumped material from walls and rim fills these craters. This crater-fill breccia contains both unshocked and shocked rock fragments with a variable content of impact melt.

Complex craters display a different, more elaborate form with wall terraces, central peaks/uplifts, and comparatively flat floors. Responsible is the interaction between shock-wave effects, gravity and target rock properties. As a result, mass movements in all directions characterize the modification of large impact craters (up- and downwards as well as in- and outwards with regard to the center of the crater). The stratigraphic uplift is roughly one-fifth of the crater diameter (e.g., El’gygytgyn, Gebhardt et al. 2006).

Multiring basins, consisting of ‘multiple concentric uplifted rings and intervening down-faulted valleys’ (Spudis 1994). These largest planetary impact structures have a

diameter up to more than 1000 kilometer and were mostly created during an early period in the evolution of the planetary system (≥3.9 Ga) (French 1998).

1.2.3 The Impact Lithologies

Impactites are the rocks affected or produced by hypervelocity impact cratering processes (Stöffler and Grieve 2007). The varied types of impactites are produced at different stages of the event (1-3, see above) and at different locations (beneath, within and around the final crater) during the impact process (French 1998). This classification is applicable for single and multiple impacts on Earth, Mars, and Moon, and on planetary bodies of the asteroid belt. Main geological criteria for the distinction of impactites are the texture, strength of shock metamorphism, and lithological elements. The different types of impactites are arranged in the following diagram (Fig. 1.2) after Stöffler and Grieve (2007). The main category is the kind of distribution, proximal or distal; further distinguished are unshocked or shocked rocks - with or without melt content.

1.2.3.1 The Formation of Suevite ("The Suevite Conundrum")

The formation of suevite or suevitic breccia is still under debate, e.g., recently at the Bridging the Gap Conference in September 2015 in Freiburg (Stöffler 2015; Grieve et al. 2015). Thereby the focus was on the Ries impact crater, Germany. It is one of the best-studied complex impact structures on Earth. The distribution of suevite can be described as a heterogeneous accumulation of ejected material with the largest content of highly shocked minerals and clasts outside the crater rim, generally called outer or fallout suevite. The inner - or crater-fill - suevite shows a lesser abundance of highly shocked lithic clasts. Another fact is, in case of the Ries, that no coherent melt sheet was established. The melt content of inner and outer suevite is relatively comparable. After a model of Stöffler et al. (2013) and Artemieva et al. (2013) the collapse of the primary ejecta cloud (vapor plume) led to the formation of the "crater-fill suevite" within the crater. Possibly due to the high content of volatile elements in the target rocks (e.g., water-saturated Jurassic limestones) a coherent melt sheet was fragmented by huge phreatomagmatic-like explosions. This secondary formation of suevite is in accordance with the occurrence of impact melt agglomerates, which are restricted to small patchy areas (e.g., von Engelhardt 1997; Pohl et al. 2010; Reimold et al. 2011; Artemieva et al. 2013; Stöffler et al. 2013).

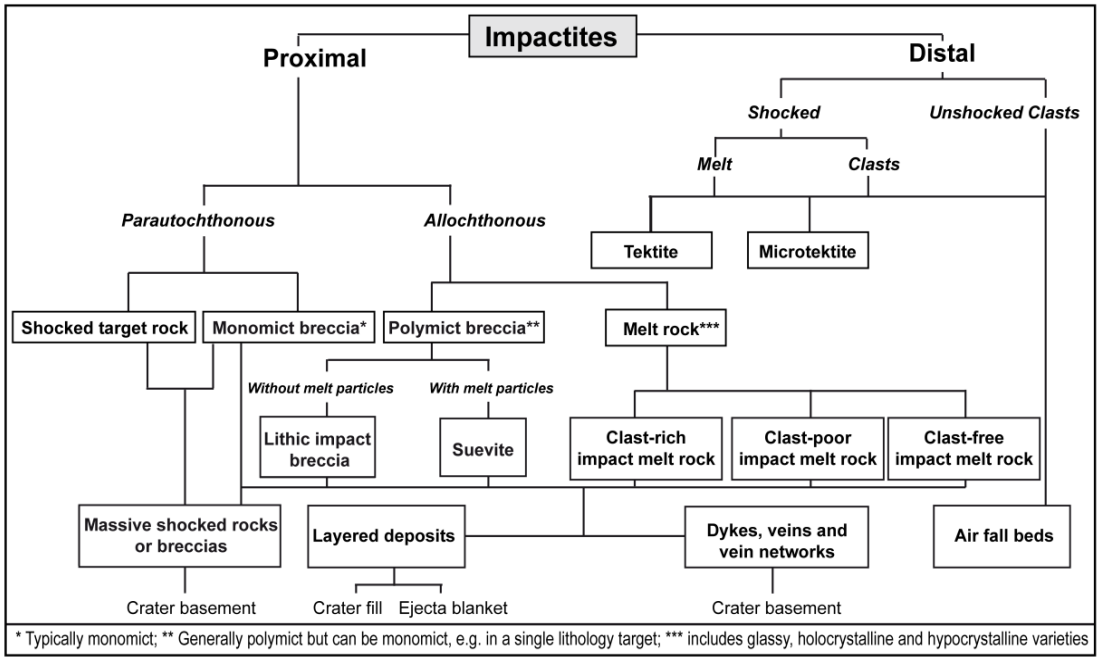

Figure 1.2: Classification of impactites from single impacts according to geological setting, composition, texture, and degree of shock metamorphism. Modified after Stöffler and Grieve (2007).

An alternative model by Osinski et al. (2008) considers the groundmass of the suevite, i.e., silicate glass, calcite, and clay minerals, as a series of impact-generated melts, which crystallized upon cooling. Therefore, the crater-fill suevite may have been accumulated as a melt sheet. An outward flow of impact-melted material, caused by the uplift movement of the central crater, could have formed the outer suevite (Osinski et al. 2004, 2008).

Some of the larger craters show a huge, almost horizontal, and coherent impact melt sheet (e.g., Popigai, Russia, see Masaitis 1998). The majority of all known craters on Earth contains lesser proportions of melt, maybe lenses or small patches of impact melt or impact melt breccias (for example the Ries crater, Germany; see Stöffler et al. 2013).

The uppermost layer of impactites has been considered as fallback breccia (Chapters 3, 4, and 5). Due to the frequent erosion of the uppermost part of impact structures, this lithology is very rarely exposed on surface, but it has been documented by drilling campaigns in impact structures (e.g., El'gygytgyn). Around and above the crater rim is the zone in which the ejecta curtain deposits its material as polymict impact breccia, with or without melt inclusions. A special feature is the mega-block zone, for example known from the Ries crater, Germany (Fig. 1.3). This material in the form of huge blocks of decameter size was accumulated near the crater rim and was generated during the collapse of the central uplift. In general, the distribution of ejecta, within and outside the crater depression, depends on the

impact angle of the projectile. Typical patterns of ejecta material can be observed at juvenile surfaces on Moon or Mars (French 1998).

The exact shape, size and modification of a crater depend upon multiple parameters, such as the physical properties of the target rocks, the gravity of the impacted body, and target topography, as well as the size, material, and velocity and direction (impact angle) of the projectile (e.g., Melosh 1989). Under a critical angle of ~12° the impactor forms an elliptical instead of a round crater (Bottke et al. 2000; Poelchau and Kenkmann 2008).

In former times, a lot of impact structures on Earth were identified as crypto-volcanic basins/holes or other circular structures (e.g., salt diapir). Their origin can be validated through investigations of meso- to macroscopic shatter cones, micro-deformation features in mineral grains (shock metamorphism), and the recognition of traces of the meteoritic projectile (as reviewed by, e.g., French and Koeberl, 2010). All collisions of extraterrestrial bodies with the Earth have the potential to create a catastrophic event for all life forms, regional or global - depending on their size and target material. Only one of the five global mass extinction events in the Phanerozoic has been related so far to a large meteorite impact: The Cretaceous-Paleogene boundary extinction event ~65.5 Ma ago to the Chicxulub impact (Gulf of Mexico) (e.g., Schulte et al., 2010). However, Richards et al. (2015) reveal a possible constrain of timing of this mass extinction not only to the Chicxulub impact event but rather to the Deccan continental flood basalt eruptions at about the same time. Seismic modeling suggests that the Chicxulub impact could have triggered volcanic eruptions worldwide. So, the ongoing volcanism in the Deccan region could have been increased due to a huge pulse of mantle plume-derived magma (for further information, see Richards et al. 2015).

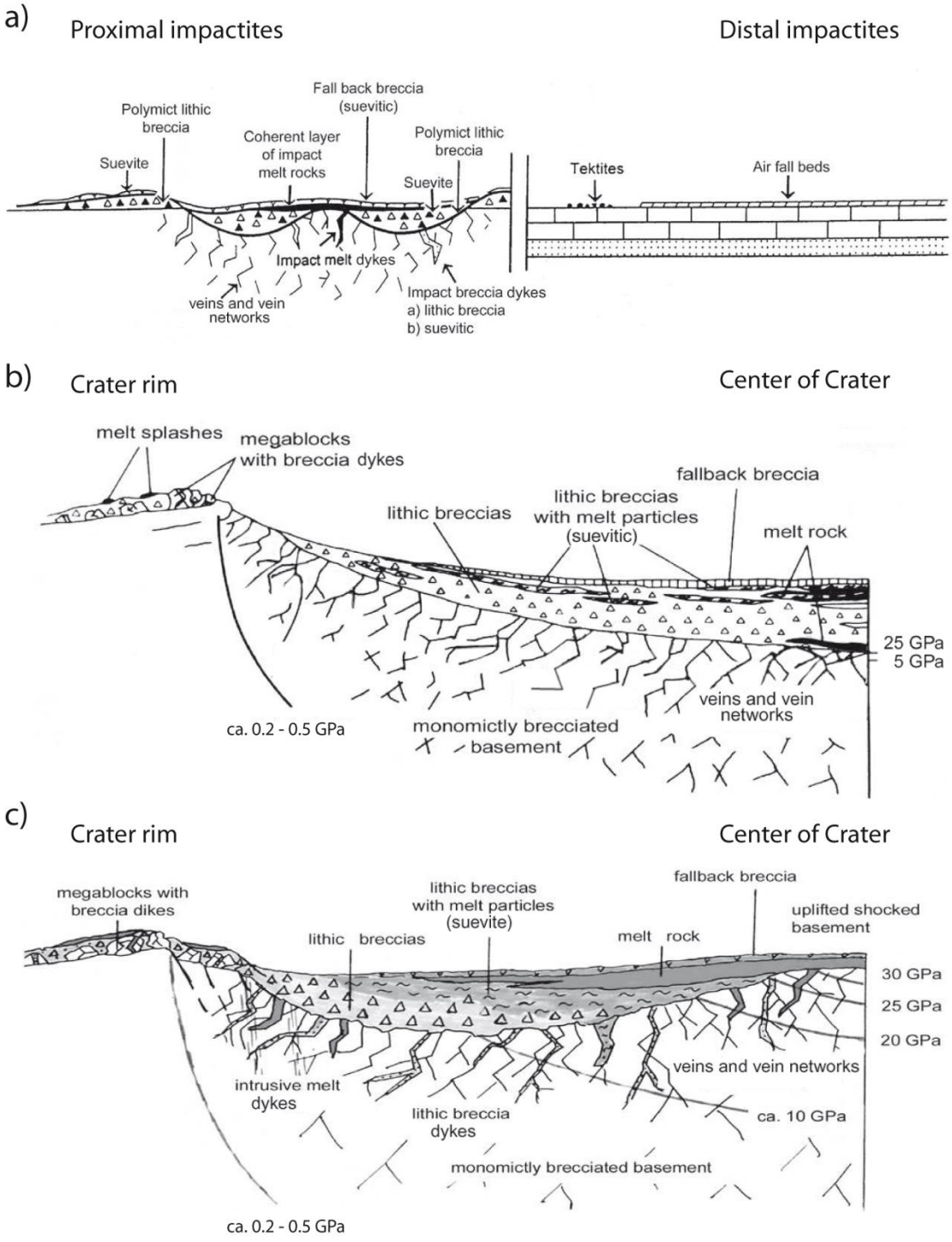

Figure 1.3: Geological setting of impactites on Earth: a) proximal and distal impactites, b) proximal impactites at a simple impact crater (diameter range on Earth: ~ 30 m to about 2-4 km); c) proximal impactites at a complex impact crater with central uplift (diameter range on Earth: ~ 5 km to 50-60 km); shock pressure isobars are shown in the parautochthonous crater basement. Modified after Stöffler and Grieve (2007).

1.2.4 Recognition of an Impact Structure (Shock Metamorphic Effects)

Shock metamorphic effects are the result of a shock wave that is "produced naturally only by hypervelocity impact of extraterrestrial objects" (French 1998). A shock wave is a compressional wave with material transport; in contrast, seismic waves are compressional waves without material transport (Stöffler and Grieve 2007). Certain shock deformation features have properties that make them useful for the identification of impact structures. They are unique, easy to recognize, occur over a wide pressure range, and they survive a long geological time period (French and Koeberl 2010). The exact determination of peak shock pressure in relation to shock features is the result of many theoretical studies, the analysis of nuclear bomb explosions, and of laboratory experiments over the last 7 decades. Figure 1.4 shows important shock metamorphic effects in relation to pressure and temperature.

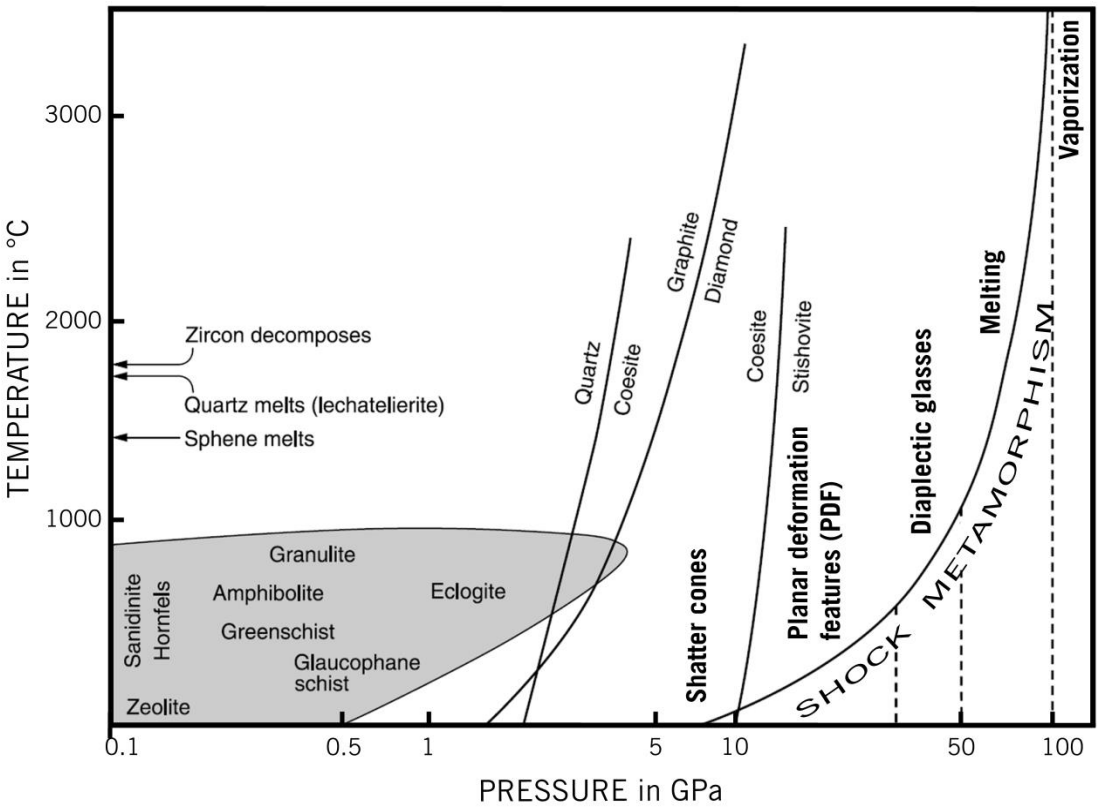

Figure 1.4: Conditions of shock metamorphism and normal crustal metamorphism combined in a temperature-pressure plot. The logarithmic x-axis displays pressure (in GPa). The linear y-axis shows the temperature. The grey-shaded region at lower left (P < 5 GPa, T < 1000°C) encloses the conventional facies for crustal metamorphism. Pressures of shock metamorphic conditions begin at a higher level, from < 2 GPa to > 100 GPa. Approximate formation conditions for specific shock effects (labeled) are indicated by vertical dashed lines: PDF (~7 - ~30 GPa), diaplectic glasses (~30 – 50 GPa), and melting (50 – 100 GPa). The exponential curve ("Shock metamorphism") indicates the approximate post-shock temperatures produced by specific shock pressures in granitic crystalline rocks. Adapted from French (1998).

1.2.4.1 Shatter Cones

Shatter cones are the only distinct meso- to macroscopic recognition criterion for meteorite impact structures (French 1998). Branca and Fraas (1905) were the first who described "Strahlenkegel" from the Steinheim impact basin, Germany. In 1947, Dietz described structures with a cup-and cone-like appearance and coined the term "shatter cones". They have a distinctive, curved morphology with striations (visible at the surface) and they describe a more or less round, partly conical geometry. Full shaped cones of 360° are very rare. The apex or the apical areal (a few millimeters to a few centimeters wide) is located at the top of the cone, where all striations run together. It has often a roundish to polygonal habit that is delimited by fractures (Baratoux and Reimold 2016; Hasch et al. 2016). The exact processes of formation of shatter cones are still unclear. General consensus is that a hemispheric shock wave, which propagates through the target rocks, is necessary for the creation of shatter cones. At critical places inside the rocks (e.g., a pre-impact fracture, joints or other locations for inhomogeneity) this wave induces a special, conical fracture system (Johnson and Talbot 1964, and Baratoux and Melosh 2003). The size of shatter cones can vary from smaller than 1 cm up to more than 12 m (Dietz 1968). Impact cratering experiments produced small-sized shatter cones (e.g., Roddy and Davis 1977; Kenkmann et al. 2012; Wilk and Kenkmann 2015a, 2015b, 2016). In onea case (Kenkmann et al. 2012), tiny shatter cones were produced with an impact velocity of ~7 km s^{-1} and peak shock pressures up to 70 GPa. The typical low-shock pressure regime for the formation of shatter cones ranges from approximately 2 GPa up to 10 GPa, but maybe as high as 30 GPa (French 1998) or possibly up to 30-45 GPa (Sharpton et al. 1996). They can form in any consolidated lithology, but are generally best developed in fine-grained lithologies, for example limestone or shale. A state of the art report about shatter cones and their formation is given in a 2016 special issue of MAPS (*Meteoritical and Planetary science* 51:1389-1551).

1.2.4.2 Planar Microfractures - PF, PDF and More

At the microscopic scale, a few distinct shock-metamorphic effects, especially planar structures, can be observed in rock-forming silicates. The peak shock levels given for the following microscopic shock effects are based on experiments with single crystals or samples of non-porous and dense material, essentially for temperatures below 250°C. In the case of dry and porous sandstone (e.g., from the Barringer crater, Arizona), the ranges of occurrence of many shock effects can be up to 4 times lower, due to the effect of crushing pores (more information in Kowitz et al. 2013a, b, and Kowitz et al. 2016).

Planar Fractures (PF) are not diagnostic shock effects by themselves, because there are similar features known from non-impact deformation (e.g., French 1998; French and Koeberl 2010; Reimold et al. 2013; Vasconcelos et al. 2013; and Gieré et al. 2015). However,

together with other shock features, especially PDF, they can be used for the constraint of peak shock pressure. According to Langenhorst and Deutsch (2012), PF are low-pressure (<10-20 GPa) shock effects, similar in appearance to cleavage. Quartz itself does not possess cleavage planes, so PF in quartz could be a good indication for impact deformation (Langenhorst and Deutsch 2012) – but one that needs to be confirmed by additional evidence. PF are planar open fissures, with typically 3-10 μm width, and they occur in sets of subparallel features at spacings of more than 20 μm (Stöffler and Langenhorst 1994) and up to 500 μm (French et al. 2004). PF are formed earlier than PDF and are not intersected by them (Poelchau and Kenkmann 2011; Zaag et al. 2016).

Planar Deformation Features (PDF) are the most used shock effects for recognizing new impact structures (e.g., French and Koeberl 2010). They occur as single or multiple sets of parallel, thin, closely-spaced planes/optical discontinuities, often resolvable by optical microscopy as thin lamellae or as planes with tiny vugs (decorated PDF). These decorated PDF are the result of the thermal annealing process subsequent to the formation of original PDF (Grieve et al. 1996). The lamellae are ≤2 μm wide and spaced at ~2 to 10 μm (Stöffler and Langenhorst 1994). PDF occur as single or as multiple sets in a single crystal - or grain - of quartz. On the basis of the different orientations of the sets to the long axis (c-axis) a system of shock peak pressures was established for quartz minerals in dense, quartzose rock and dense sandstones (see Stöffler and Langenhorst 1994). The estimated shock pressures by which PDF form range from ~8-35 GPa (Huffman and Reimold, 1996; French and Koeberl 2010, and references therein). When shock pressure exceeds 30-35 GPa, the crystal is converted to diaplectic quartz glass (Stöffler and Langenhorst 1994). The lower boundary for creation of PDF is assumed to be at 8-10 GPa as observed in shock recovery experiments (e.g., Huffmann and Reimold 1996). Kowitz et al. (2013a, 2013b, and 2016) stated that the formation of PDF starts at pressures of 10 GPa, according to shock recovery experiments for dry and porous sandstone. Finally, experiments with pre-heated discs of single quartz crystals showed that complete transformation to diaplectic glass is already reached at 26 GPa (Langenhorst and Deutsch, 1994). Furthermore, the direction of the shock wave in relation to the crystal lattice has an influence on the formation of planar shock effects. Quartz shocked parallel to the c-axis has higher density and refractivity than quartz shocked parallel to other directions, e.g., $\{10\bar{1}0\}$; for more information, see Langenhorst and Deutsch (1994).

1.2.4.3 Feather Features (FF)

Feather features (FF) are shock-induced elements (in quartz) that consist of a PF and a series of parallel lamellae that are said to typically emanate from one side of the PF with an angle >35° (French 2004; Poelchau and Kenkmann 2011; Zaag et al. 2016). These lamellae are straight to slightly curved and shorter than the fractures from which they originate.

According to these authors, it is possible with FF to determine the local sense of shearing in a sample and to constrain the orientation of the principal axis of maximum stress, which in turn can be used to determine the orientation of the shock wave. Thereby, it is possible to deduce differential stress field conditions for the formation of PF and PDF. They represent a low peak shock pressure <10 GPa (Poelchau and Kenkmann 2011). New investigation of feather features by Zaag et al. (2016) reaveled addional features. They studied thin sections of the ~250 Ma old Serra da Cangalha impact structure, Brazil. Their major outcomes are: i) 'Two-sided FF or truly "feather-like" FF'in that the feather features emenate from both sides of a planar fracture (PF). This phenomenon occurs very rarely and cannot be explained as a shear-induced mechanism (c.f. Poelchau and Kenkmann 2011). They favored the hypothesis 'that "arrowhead-like" FF occur as the result of oscillation of both subgrains in the course of scattering, refraction, and/or reflection of the shock wave.' ii) The FF can also emanate from curviplanar and curved fractures. This may be a result of a bifurcation process. For more information see Zaag et al. (2016).

1.2.4.4 Mosaicism

Mosaicism is an effect on a single crystal or grain. Crystal subdomains are differently oriented (French and Koeberl 2010). A patchwork extinction pattern is observed under the microscope with crossed polarizers (Stöffler and Langenhorst 1994). Mosaicism often appears together with PDF and represents a relatively moderate shock pressure range of ≥10 GPa.

1.2.4.5 Diaplectic Glass and Ballenquartz

Diaplectic glass is a shock-diagnostic feature and arises in quartz due to transformation into a quasi-amorphous state at shock pressures of about 30-35 GPa for non-porous, dense material (French and Koeberl 2010, Langenhorst and Deutsch 2012). Thereby the refractive indices and the birefringence decrease gradually and the quartz grain becomes isotropic. Notable is that Kowitz et al. (2013a, 2016) found diaplectic quartz glass at 5 GPa shock pressure in dry, porous sandstone by shock recovery experiments. The transformation to diaplectic glass is gradual over a wide range of shock pressure, beginning with the formation of PDF at 10-15 GPa. It ends with the complete change of a crystal to a glass-like phase at 30-35 GPa. The crystal lattices collapse completely to glass-like material - in the solid state - as a response to rapid shock compression. This gradual process involves a decrease of the refractive indices and densities of shocked quartz grains in proportion to increasing pressure (Langenhorst and Deutsch 2012).

The origin of the "ballen" texture is uncertain; it could develop during the cooling and/or recrystallization from shock-produced lechatelierite (fused silica glass) or diaplectic quartz glass (French and Koeberl 2010). Ferrière et al. (2010) observed that α-quartz ballen are the result of back-transformation of β-quartz and/or α-cristobalite with time. Between ~35

and 45-50 GPa, where mineral and then rock fusion will begin, diaplectic glass would transform during the cooling process into individual "ballen," consisting of single α-quartz crystals, all of the same optical orientation. But with a shock pressure >50 GPa lechatelierite (SiO_2 melt) shows ballen structure with different optical orientations that gradually transform into ballen with intragranular polycrystallinity (Grieve et al. 1996).

1.2.4.6 Silica Melt – Lechatelierite

SiO_2 melt or lechatelierite is a common shock barometric effect and is produced at an even higher degree of shock >50 GPa (Grieve et al. 1996, their Figure and Table 1). Generally, it is found in impact melt glasses or inclusions/schlieren and is the result from melting of highly shocked quartz, which was mixed into impact melt during the crater forming process (Grieve et al. 1996).

1.2.4.7 High-Pressure Polymorphs

The high-pressure shock wave can transform (together with the accompany heating) minerals into a higher density phase. Polymorphs are known from quartz and other (accessory) minerals such as zircon, or TiO_2 (French and Koeberl 2010). Typical high-pressure forms of quartz are stishovite and coesite. They both occur as finest-grained aggregates and are the result of a partial transformation of quartz. Stishovite is believed to crystallise during the shock compression phase (unstable > 400°C), whereas coesite is produced while pressure is released (unstable >1100°C), by transformation of a high-pressure phase in combination with a long pressure pulse in the order of > milliseconds (Stöffler 1971; Stöffler and Langenhorst 1994). Coesite occurs more in diaplectic glass than in PDF-rich quartz; whereas stishovite is found mostly in quartz with PDF (Stöffler 1971a). Coesite represents a shock pressure range of 30-60 GPa and Stishovite of 12-45 GPa (Stöffler and Langenhorst 1994). Coesite can also be generated under endogenic high static pressure conditions, and occur in kimberlite dikes or in subduction zones (French and Koeberl, 2010).

CHAPTER 2

EL'GYGYTGYN IMPACT CRATER, CHUKOTKA, ARCTIC RUSSIA: IMPACT CRATERING ASPECTS OF THE 2009 ICDP DRILLING PROJECT.

This Chapter was published as the following peer-reviewed article:

Koeberl C., Pittarello L., Reimold W. U., **Raschke U.**, Brigham-Grette J., Melles M., and Minyuk P. 2013. El'gygytgyn impact crater, Chukotka, Arctic Russia: Impact cratering aspects of the 2009 ICDP drilling project. *Meteoritics and Planetary Science* 48:1108-1129, http://dx.doi.org/10.1111/maps.12146

2.1 ABSTRACT

The El'gygytgyn impact structure in Chukotka, Arctic Russia, is the only impact crater currently known on Earth that was formed in mostly acid volcanic rocks (mainly of rhyolitic, with some andesitic and dacitic, compositions). In addition, because of its depth, it has provided an excellent sediment trap that records paleoclimatic information for the 3.6 Myr since its formation. For these two main reasons, because of the importance for impact and paleoclimate research, El'gygytgyn was the subject of an International Continental Scientific Drilling Program (ICDP) drilling project in 2009. During this project, which, due to its logistical and financial challenges, took almost a decade to come to fruition, a total of 642.3 m of drill core was recovered at two sites, from four holes. The obtained material included sedimentary and impactite rocks. In terms of impactites, which were recovered from 316.08 to 517.30 m depth below lake bottom (mblb), three main parts of that core segment were identified: from 316 to 390 mblb polymict lithic impact breccia, mostly suevite, with volcanic and impact melt clasts that locally contain shocked minerals, in a fine-grained clastic matrix; from 390 to 423 mblb, a brecciated sequence of volcanic rocks including both felsic and mafic (basalt) members; and from 423 to 517 mblb, a greenish rhyodacitic ignimbrite (mostly monomict breccia). The uppermost impactite (316-328 mblb) contains lacustrine sediment mixed with impact-affected components. Over the whole length of the impactite core, the abundance of shock features decreases rapidly from the top to the bottom of the studied core section. The distinction between original volcanic melt fragments and those that formed later as the result of the impact event posed major problems in the study of these rocks. The sequence that contains fairly unambiguous evidence of impact melt (which is not very abundant anyway, usually less than a few volume %) is only about 75 m thick. The reason for this rather thin fallback impactite sequence may be the location of the drill core on an elevated part of the central uplift. A general lack of large coherent melt bodies is evident, similar to

that found at the similarly sized Bosumtwi impact crater in Ghana that, however, was formed in a target composed of a thin layer of sediment above crystalline rocks.

Figure 2.1: Extent of the Arctic sea ice in the summer of 2008 (NASA Goddard Space Flight Center image). The location of the El'gygytgyn structure in the northeastern corner of Siberia, at the Chukotka Peninsula, is also shown. The crater is at a crucial place with respect to the Arctic ice cover, and the study of the lake sediments, which provide valuable information on the development of the climate in the area during the past approximately 3.5 Myr, was a major driving force for the drilling project.

2.2 INTRODUCTION

The El'gygytgyn impact structure is located in the far northeastern part of Russia centered at 67°30′ N and 172°05′ E), on the Chukotka peninsula (Fig. 2.1). El'gygytgyn consists of a circular depression with a rim diameter of about 18 km that is filled by a lake with a diameter of 12 km that is off-center with regard to the crater. The structure was discovered and described as a gigantic volcanic crater in 1933 (Obruchev 1957). The first suggestion that this structure might be of impact origin was made by Nekrasov and Raudonis (1963); these authors searched unsuccessfully for coesite in thin sections of volcanic rocks from the crater rim and, consequently, concluded that the "El'gygytgyn basin" had a tectonic and volcanic origin. Without any further evidence, this structure appeared in a list of probable terrestrial impact craters by Zotkin and Tsvetkov (1970). From a study of satellite imagery of the structure, Dietz and McHone (1976) suggested that El'gygytgyn might be the largest Quaternary impact crater preserved on Earth. Shortly afterward, Dietz (1977) suggested that El'gygytgyn might be the source crater of the Australasian tektites.

Gurov and co-authors visited the El'gygytgyn structure in 1977 and confirmed its impact origin after finding shock metamorphosed rocks and impact melt rock (Gurov et al.

1978; Gurov and Gurova 1979; Gurov et al. 1979a, b). Investigations of the El'gygytgyn crater by these researchers continued into the 1980s and 1990s (Gurov and Gurova 1991). Further work was performed by Feldman et al. (1981), who gave a short description of the geology of the crater and its target. Gurov and colleagues studied the main types of impact melt rocks and highly shocked volcanic rocks. A preliminary geophysical investigation of the crater was carried out by Dabizha and Feldman (1982). The geological structure of the crater rim was described by Gurov and Gurova (1983) and Gurov and Yamnichenko (1995); see also Gurov et al. (2007). Although the impact origin of the El'gygytgyn structure had been recognized and confirmed more than 20 years ago, an endogenic origin for this structure was once again proposed later by Belyi (1982, 1998). Nevertheless, the matter is firmly settled due to the unambiguous evidence for an impact origin in the form of shock metamorphic effects in the crater rocks.

First age determinations for the El'gygytgyn impact crater were obtained by fission track (4.52 ± 0.11 Ma; Storzer and Wagner 1979) and K-Ar dating (3.50 ± 0.50 Ma; Gurov et al. 1979a). These data quickly invalidated the suggestion of Dietz (1977) of El'gygytgyn as the source of the Australasian tektites (of 0.8 Ma age). More detailed fission track analyses resulted in an age for the crater of 3.45 ± 0.15 Ma (Komarov et al. 1983). Subsequently, Layer (2000) performed ^{40}Ar-^{39}Ar age dating of impact glasses and found an age of 3.58 ± 0.04 Ma for the impact event, in good agreement with some of the earlier results.

Here, we discuss the impact cratering-related aspects of a recent international and multidisciplinary scientific drilling project at El'gygytgyn that led to the recovery of a drill core through the lake sediments, impact breccia, and uplifted and brecciated bedrock near the crater center.

2.3 GEOLOGICAL SETTING OF THE EL'GYGYTGYN IMPACT STRUCTURE

Among the slightly more than 180 currently confirmed impact structures on Earth, there are just a few (Lonar, Logancha, Vista Alegre, Vargeão, and Cerro do Jarau) that formed within basaltic volcanic rock. However, a major aspect of the importance of El'gygytgyn is that it represents the only currently known impact structure formed in siliceous volcanic rocks, including tuffs. Thus, the impact melt rocks and target rocks provide an excellent opportunity to study shock metamorphism of silicic volcanic rocks. The shock-induced changes observed in porphyritic volcanic rocks from El'gygytgyn can be applied to a general classification of shock metamorphism of siliceous volcanic rocks.

At 18 km diameter, El'gygytgyn is a medium-sized impact structure. Even though the rim is partly eroded, especially in the southeastern part, the rim height is generally about 180

m above the lake level and 140 m above the surrounding area. An outer ring feature, on average 14 m high, occurs at about 1.75 crater radii from the center of the structure. A similar outer ring structure was noted at the Bosumtwi impact structure (e.g., Koeberl and Reimold [2005] and references therein), but the nature and origin of such features have yet to be explained. The El'gygytgyn crater is surrounded by a complex system of radial and concentric faults. The density of the faults decreases from the bottom of the rim to the rim crest and outside the crater to a distance of about 2.7 crater radii (Gurov et al. 2007).

The crater and its lake are shown in Figs. 2.2a and 2.2b. The lake that fills part of the crater interior has a maximum depth of about 170 m and is surrounded by a number of lacustrine terraces (cf. Gurov et al. 2007). Only minor remnants are preserved of the highest terraces that are about 80 and 60 m above the present day lake level. The widest terraces are 40 m above the current lake level and surround the lake on the west and northwest sides; the most modern terrace is 1-3 m above the current lake level, indicating severe changes in the water level with time. Even though many small creeks discharge into the lake, the only outlet is the Enmyvaam River, which cuts the crater rim in the southeast.

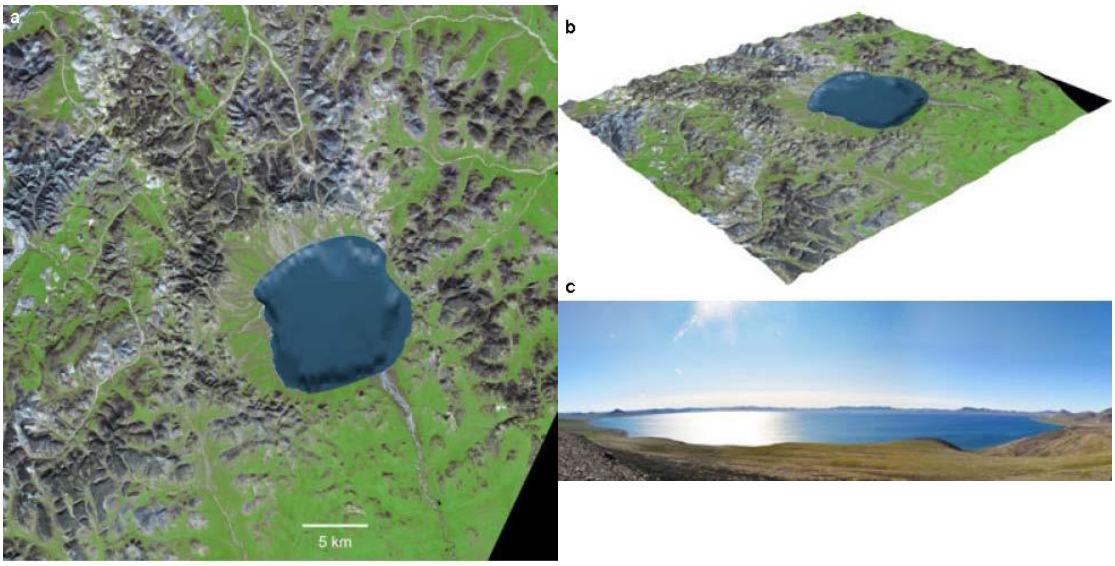

Figure 2.2 (a-c): a) Satellite image of the El'gygytgyn impact crater, Arctic Russia (NASA Aster image). The image shows the 12 km-diameter Lake El'gygytgyn, which is asymmetrically located with the 18 km-diameter impact crater. b) Perspective view of satellite image with digital elevation model (DEM); projection by M. Schiegl (Austrian Geological Survey), and DEM of Lake El'gygytgyn from digital elevation model data by M. Nolan (University of Alaska at Fairbanks) at: http://www.uaf.edu/water/faculty/nolan/lakee/data.htm (accessed 2009). c) Panoramic image of El'gygytgyn crater and lake; view from the northeast to the southeast (U. Raschke, July 2011).

A central peak is not exposed on the recent surface of the crater floor, nor is it evident in bathymetric data of the lake bottom. However, from gravity measurements, Dabizha and Feldman (1982) suggested the presence of an approximately 2 km wide central peak underneath postimpact sediments, and centered relative to the crater outline. Nolan et al.

(2003) suggested that the central uplift is centered within the outline of the lake, which, however, would offset the central uplift relative to the crater center. Seismic investigations during the preparation of the drilling project revealed the presence of a buried central uplift, not unlike the situation at the Bosumtwi impact structure in Ghana, with a diameter of approximately 2 km, and which is centered with respect to the crater rim rather than the lake outline (Gebhardt et al. 2006). According to these seismic measurements, the thickness of the sedimentary fill near the crater center (above and near the central uplift) is about 360-420 m. The sediments are underlain by units with distinctly higher seismic velocities that were interpreted as allochthonous breccia, 100-400 m thick (Gebhardt et al. 2006; Niessen et al. 2007).

In terms of regional geology, the crater is excavated in the outer zone of the Late Cretaceous Okhotsk-Chukotka Volcanic Belt (OCVB), mainly involving the so-called Pykarvaam Series (88.5 ± 1.7 Ma; Stone et al. 2009). Laser $^{40}Ar/^{39}Ar$ dating of the unshocked volcanic rocks in the crater yielded an age-range from 89.3 to 83.2 Ma (Layer 2000). The volcanic sequence includes lava, tuffs, and ignimbrites of rhyolitic to dacitic composition, which belong to the younger Voron´in and Koekvun' formations. Rarely, andesites and andesitic tuffs occur. The whole sequence is, in general, gently dipping at 6° to 10° to the east-southeast (Gurov and Koeberl 2004). Detailed field observations by Gurov and co-workers (Gurov and Koeberl 2004) in the 1990s allowed establishing a rough pre-impact stratigraphy. From the top to the bottom, it consists of approximately 250 m of rhyolitic ignimbrites, approximately 200 m of rhyolitic tuffs and lavas, approximately 70 m of andesitic tuffs and lavas, and approximately 100 m of rhyolitic to dacitic ash and welded tuffs. This sequence dominates in the southern, western, and northern part of the crater, whilst the southeastern and eastern parts of the crater mainly consist of dacitic and andesitic lavas. A basalt plateau, approximately 110 m in thickness, overlies the rhyolites and ignimbrites in the northeastern part of the crater rim (Gurov and Koeberl 2004). These basalts possibly belong to the Koekvun' volcanic suite, which is located above the Pykarvaam series in the volcanic sequence (83.1 ± 0.4 Ma; Stone et al. 2009).

The general geology at El'gygytgyn is summarized in Fig. 2.3. The most widespread lithology represents pyroclastic deposits of rhyolitic-dacitic composition (approximately 89% by volume). Occurrences of basaltic rock are limited to isolated patches. In terms of mineralogy, the general composition of the target is dominated by quartz clasts and grains, K-feldspar ($Or_{60–80}$), plagioclase ($An_{20–30}$), biotite, and rarely amphibole, embedded in a fine-grained clastic matrix with glass, quartz, and feldspar fragments. The fabric of the matrix ranges from glassy to fine-grained granular, occasionally with spherulites (Gurov et al. 2005).

The less abundant andesites and andesite tuffs occur only locally and contain fragments and clasts of andesine (An_{45} to An_{40}), clinopyroxene, and amphibole (Gurov and Koeberl 2004).

On the surface, impact melt rocks occur at El'gygytgyn mainly in the form of redeposited material on the lacustrine terraces. No actual outcrops of impact breccias have been found so far. The most probable origin of these rocks is from the ejecta blanket and fallback material that is now only present as eroded remnants and material that slumped off the rim. The impact melt rocks include aerodynamically shaped glass bombs and shock metamorphosed breccias. The glass bombs are generally fresh and do not display significant postimpact hydrothermal alteration or alteration due to weathering (Gurov and Koeberl 2004; Gurov et al. 2005).

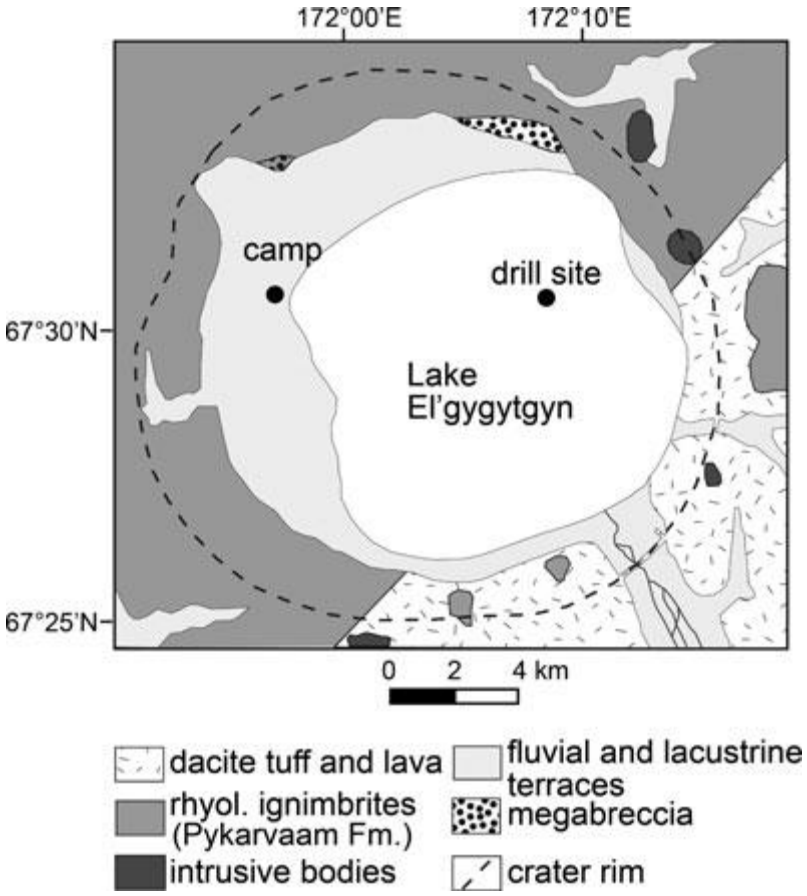

Figure 2.3: Simplified geological map of the El'gygytgyn area (modified after Gurov and Koeberl 2004; Gurov et al. 2005; and Stone et al. 2009). The figure also shows the location of the drill rig and the camp site for the ICDP project, and the two drilling locations (black dots).

2.4 RATIONALE FOR DRILLING PROJECT

Drilling allows obtaining information on the subsurface structure of impact craters, provides ground truth for geophysical studies, and delivers samples of rock types not exposed at the surface. For more than a decade, the International Continental Scientific Drilling

Program (ICDP) has supported projects to study impact craters (Koeberl and Milkereit 2007). The first ICDP study of an impact structure was at the subsurface Chicxulub impact crater, Mexico, from late 2001, which reached a depth of 1511 m and intersected 100 m of impact melt breccia and suevite. Between June and October 2004, the 10.5 km Bosumtwi crater, Ghana, was drilled with ICDP support. It is a well preserved complex impact structure with a pronounced rim and is almost completely filled by the 8 km diameter Lake Bosumtwi. This is a closed-basin lake that has wide paleoclimatic significance and allowed researchers to accumulate a detailed paleoenvironmental record. In terms of impact studies, Bosumtwi is one of the best preserved young complex craters known, and is the source crater of the Ivory Coast tektites. The drilling outcomes also allowed correlating all the geophysical studies, and provide material for geochemical and petrographic correlation studies between basement rocks and crater fill in comparison with tektites and ejected material. Sixteen different cores were drilled at six locations within the lake, to a maximum depth of 540 m. Borehole logging as well as vertical seismic profiling (to obtain 3-D images of the crater subsurface) were performed in the two deep boreholes. About 2.2 km of core material was obtained. This includes approximately 1.8 km of lake sediments and 0.4 km of impactites and fractured crater basement (in the deep crater moat, and on the central uplift). For details of the Bosumtwi drilling project, see Koeberl et al. (2007a). Chesapeake Bay, a much larger impact structure than Bosumtwi or El'gygytgyn, was drilled to a depth of almost 2 km in 2005–6; results of this drilling project are reported by, e.g., Gohn et al. (2008, 2009).

The El'gygytgyn impact crater is a unique study target for an ICDP project for two main reasons: (1) predrilling site surveys indicated that a full-length sediment core would yield a complete record of climate evolution for the past 3.6 Myr in an area of the high Arctic for which few paleoclimate data exist, and (2) it is the only known impact crater on Earth that has formed in acidic volcanic rocks, allowing the study of shock metamorphic effects in such target rocks and the geochemistry and petrology of "volcanic" impactites, and potential analog studies for other planets. These aspects clearly mark El'gygytgyn as a world-class research site. As at Bosumtwi, the deep basin that formed as a result of the impact event is an ideal location for the accumulation of lake sediments that carry paleoclimate information.

Its sedimentological aspect makes Lake El'gygytgyn unique in the terrestrial Arctic, especially because geomorphological evidence from the catchment has suggested that the crater was never completely glaciated throughout the Late Cenozoic. Two sediment cores retrieved from the deepest part of the lake in 1998 and 2003 revealed lacustrine basal ages of approximately 250 and 340 ka, respectively, and thus, represent the longest continuous climate records available at that time from the Arctic region. The continuous sedimentation confirmed the lack of glacial erosion, and the sediment composition underlined the sensitivity

of this lacustrine environment to reflect high-resolution climatic change on Milankovitch and sub-Milankovitch time scales (cf. Brigham-Grette et al. 2007).

Seismic investigation carried out during expeditions in 2000 and 2003 led to a depth-velocity model of brecciated bedrock overlain by a different breccia layer, in turn overlain by two lacustrine sedimentary units of up to 350 m thickness (e.g., Niessen et al. 2007). The upper well-stratified sediment unit appears undisturbed apart from intercalation with debris flows near the crater wall. Extrapolation of sedimentation rates obtained from earlier shallow cores indicated that the entire Quaternary and possibly beyond was expected to be represented in the 170 m thick upper unit; the lower unit, which was probably characterized by a higher sedimentation rate, covered the earlier postimpact history of the lake.

In terms of impact research, El'gygytgyn gains its importance by being the only currently known impact structure formed in siliceous volcanic rocks, as mentioned above. The shock-induced changes observed in porphyritic volcanic rocks from El'gygytgyn can be applied to a general classification of shock metamorphism of siliceous volcanic rocks (cf. Gurov et al. 2005). However, impactites exposed on the surface have been almost totally removed by erosion, and thus the deep drilling project provides a unique opportunity to study the crater-fill impactites in situ and determine their relations and succession. The goals of the project included, inter alia, obtaining information on the shock behavior of the volcanic target rocks, the nature and composition of the asteroid that formed the crater, and the abundance of impact melt rocks.

Main coring objectives included to obtain replicate cores of 630 m length to retrieve a continuous paleoclimate record from the deepest part of the lake and information about the underlying impact breccias and bedrock. Studies of the impact rocks offer the planetary community the opportunity to study a well preserved crater uniquely situated in igneous volcanic rocks. An additional shorter core was to be drilled into permafrost from the adjacent catchment to test ideas about Arctic permafrost history and sediment supply to the lake since the time of impact.

2.5 DRILLING PROJECT AND OPERATIONS

The El'gygytgyn drilling project took almost a decade from the first planning steps to execution. ICDP funded a workshop in Amherst MA, USA, in November of 2001 to stimulate scientific interests in deep drilling at Lake El'gygytgyn. A second workshop was held in March 2004 in Leipzig, Germany, to synthesize results from a 2003 expedition and discuss the possibilities for interdisciplinary research goals for drilling. After completion of presite surveys (cf. Melles et al. 2011), a pre-proposal was submitted to ICDP in January 2004,

outlining the status of our science and planning efforts. A review of that pre-proposal by the ICDP Science Advisory Group (SAG) was very encouraging, and thus a full proposal was submitted in January 2005, which was well received and was accepted for funding (partial funding covering some of the drilling operations only) in the summer of 2005. The following years were occupied by intense fundraising efforts, which were necessary due to the final cost of about US$10 million for the entire drilling operations, and by putting the required complex technical and logistical requirements (including permitting issues) of the project in place. Finally, movement of equipment began in 2008, permafrost drilling was performed at the end of 2008, and sediment and impactite core drilling at the center of the frozen lake commenced in February of 2009 and was completed in May 2009.

The descriptions of the actual drilling operations follow closely the report by Melles et al. (2011). Because of the remote location of the crater, and the lack of any infrastructure, the project involved a massive logistical undertaking. Figure 4 gives an impression of the routes and distances covered in getting equipment to the crater. During the summer of 2008, most of the technical equipment and field supplies were transported in 15 shipping containers from Salt Lake City, UT, USA, to Pevek, Russia, by ship first to Vladivostok and then on through the Bering Strait to Pevek (Fig. 2.4a). Two additional containers with equipment were sent from Germany to Vladivostok via the Trans-Siberian Railway. In Pevek, the combined cargo was loaded onto trucks that were then driven with bulldozer assistance across a distance of more than 350 km over winter roads cross country to the El'gygytgyn crater (Figs. 2.4b and 4c). At the shore of the frozen crater lake, a temporary winter camp was constructed that was designed for up to 36 persons (Fig. 2.5). The camp consisted of 12 insulated and heated sleeping huts, another hut equipped for medical care, one used as an office, a small canteen, a sauna, and two separate outhouses, built alongside a staging area regularly cleared of heavy snow by snow plows (Fig. 2.6a). Next to the office hut, a laboratory container was placed that was equipped for whole-core measurements of magnetic susceptibility. In addition, there was a reefer container in which the sediment cores were kept from freezing (as the ambient temperatures could reach 50°C) to prevent destruction of sedimentary structures; no such restrictions applied to the impactite cores. Other camp features included a generator building for electricity supply; storage places for vehicles, fuel, and containers; and a helicopter landing pad.

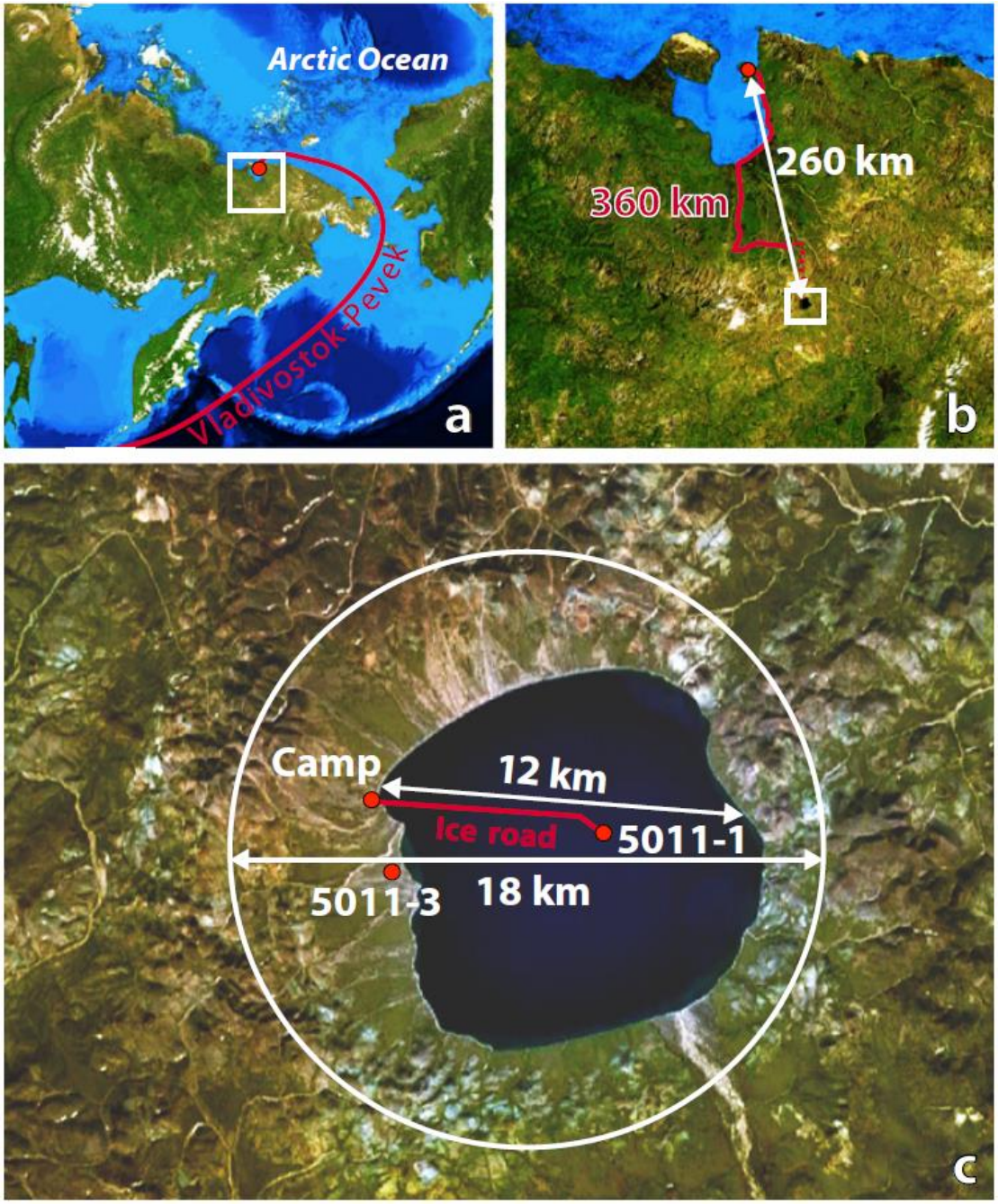

Figure 2.4: (a-c): Location and setting of the El'gygytgyn impact structure with respect to the logistics of the drilling project (modified from Melles et al. 2011). a) Location of the crater in central Chukotka, NE Russia, about 850 km west of the Bering Strait. The drill rig and all equipment arrived at the lake first by barge from Vladivostok along the indicated route. b) All equipment was transported to the site from the town of Pevek, a gold mining center located on the coast of the East Siberian Sea. Helicopters were used to transport scientists, food, and delicate equipment out to the drill site, whereas the 17 shipping containers with the drilling system were transported by truck. c) Satellite image with lake and crater diameter, the locations of ICDP Sites 5011-1 and 5011-3, and the outline of crater rim (white circle).

Figure 2.5: Aerial view of the campsite looking toward the western crater rim

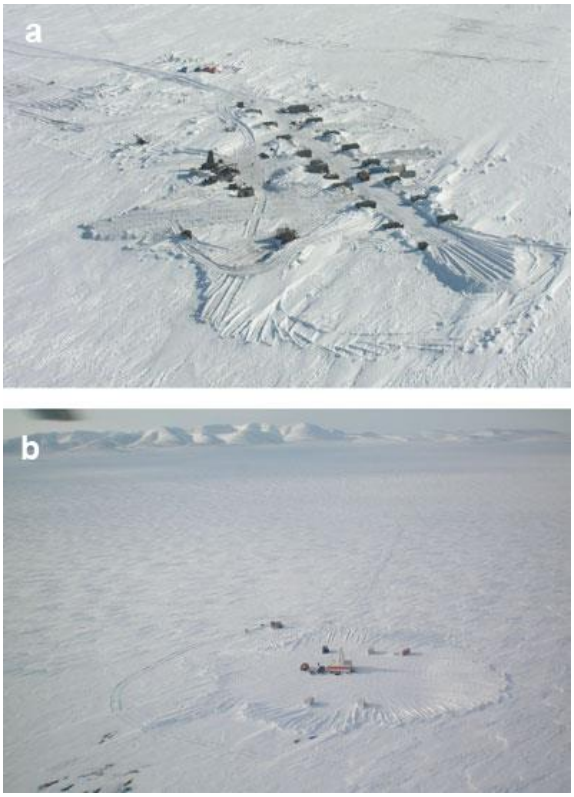

Figure 2.6: (a, b): Aerial views of (a) the field camp on the western shore of Lake El'gygytgyn and (b) the drilling platform on the ice pad at ICDP Site 5011-1, from Melles et al. (2011). The camp was designed for up to 36 people with facilities for maintaining two 12 h shifts. The ice pad was first cleared of snow and then artificially flooded with lake water to thicken and strengthen the ice to roughly 2 m. A gas-powered electrical generator fueled all operations. Crew changes along the 7 km ice road to the camp were accomplished by shuttle bus and Russian all-terrain vehicles ("vezdahut"). The ice road was flagged every 25 m for safe travel during whiteouts.

In total, the project completed one borehole into permafrost deposits in the western lake catchment (ICDP Site 5011-3) and three holes at 170 m water depth in the center of the lake (Site 5011-1). Permafrost drilling at Site 5011-3 was conducted from November 23 until December 12, 2008. Using a mining rig (SIF-650M) that was rented from and operated by a local drilling company (Chaun Mining Corp., Pevek), the crew reached a depth of 141.5 m with a recovery of 91%. After completion of the drilling, the borehole was permanently instrumented with a thermistor chain for future ground temperature monitoring as part of the Global Terrestrial Network for Permafrost (GTN-P) of the International Permafrost Association (IPA), hoping to improve the understanding of future permafrost behavior in the light of contemporary rapid climate change.

In January/February 2009, an ice road between the camp and Site 5011-1 on Lake El'gygytgyn was established based on ice conditions and marked by bamboo poles every 25 m for better orientation during heavy snow storms (Fig. 2.4c). Subsequently, an ice pad of 100 m diameter at the drill site was artificially thickened to 2.3 m by clearing the snow and pumping lake water onto the ice surface, to allow for lake drilling operations with a 100 ton drilling platform (Fig. 2.6b). Drilling was undertaken using a lake drilling system similar to the GLAD 800 system that had been employed at Bosumtwi (Koeberl et al. 2007a). The GLAD 800 system used in Russia

was developed and adapted for use under extreme cold conditions and was operated by the US consortium DOSECC (Drilling, Observation and Sampling of the Earths Continental Crust). It consists of a modified Christensen CS-14 diamond coring rig positioned on a mobile platform that was weather-protected by insulated walls and a tent on top of the 20 m high derrick (Fig. 2.7). The system was financed by the major funding agencies of the El'gygytgyn Drilling Project and was permanently imported into Russia, where it remains for further scientific drilling projects.

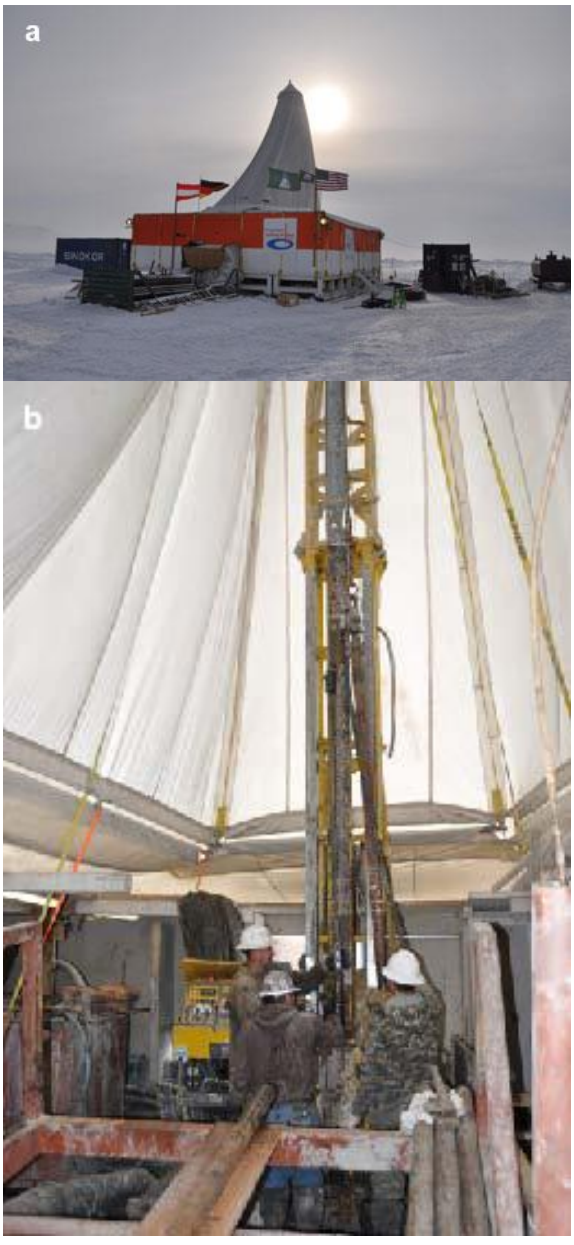

Figure 2.7: (a, b): a) The modified GLAD 800 drill rig on a platform contained within a tent to keep the interior above freezing, at ICDP Site 5011-1 at the center of the frozen Lake El'gygytgyn. b) The drill rig in operation within the tent.

Drilling at Site 5011-1 was conducted from February 16 until April 26, 2009. The drill plan included the use of casing anchored into the sediment to allow drilling to start at a field depth of 2.9 m below lake bottom (mblb). Holes 1A and 1B had to be abandoned after twist-offs at 147 and 112 mblb, respectively. In Hole 1A, the hydraulic piston corer (HPC) system was used down to 110 mblb, followed by the extended nose corer (EXC) below (details about equipment used are given in Harms et al. 2007). The recovery achieved with these tools was 92%. Similarly, drilling with the HPC down to 100 mblb and with EXC below provided a recovery rate of 98% in Hole 1B. Hole 1C was first drilled by HPC between 42 and 51 mblb, to recover gaps still existing in the core composite from Holes 1A and 1B, and was then continued from 100 mblb. Due to the loss of tools during the twist-offs, further drilling had to be performed with the so-called alien bit corer. The employment of this tool may at least partly explain a much lower recovery of the lake sediments in Hole 1C (recovery rate about 52%), although this could also be due to the higher concentration of gravel and sand in

these deeper lake sediments. The recovery increased to almost 100% again at a depth of 265 m, when the tool was changed to a hardrock bit corer (HBC), which has a smaller diameter than the tools employed above. The boundary between lake sediments and impact rocks was encountered at 315 mblb. Further drilling into the impact breccia and brecciated bedrock down to 517 mblb by HBC took place with an average recovery of 76%.

On-site processing of the cores recovered at Site 5011-1 involved magnetic susceptibility measurements with a multisensor core logger (MSCL, Geotek Ltd.) down to a depth of 380 mblb. Initial core descriptions were conducted based on macroscopic and microscopic investigations of the material contained in core catchers and cuttings (lake sediments), and on the cleaned core segments not cored with liners (impact rocks). Additionally, down-hole logging was carried out in the upper 394 m of Hole 1C by the ICDP Operational Support Group (OSG), employing a variety of slim hole wireline logging sondes. Despite disturbance of the electric and magnetic measurements in the upper part of the hole, due to both the presence of metal after the twist-offs at Holes 1A and 1B and some technical problems, these data provide important information on the in situ conditions in the hole (e.g., temperature, natural gamma ray, U, K, and Th contents) and permit depth correction of the individual core segments. The locations, depth, and schematic lithologies of the drill cores obtained in the drilling project, in comparison with a schematic cross section of the El'gygytgyn crater and lake, are shown in Fig. 2.8, and a summary of core depths and recovery is given in Table 2.1.

2.6 SEDIMENT CORES

This brief description follows Melles et al. (2011). Based on the whole-core magnetic susceptibility measurements on the drill cores from ICDP Site 5011-1, the field team was able to confirm that the core composite from Holes 1A to 1C provided nearly complete coverage of the uppermost 150 m of the sediment record in central Lake El'gygytgyn, and that the gap between the top of the drill cores and the sediment surface had been properly recovered by the upper part of a 16 m long sediment core (Lz1024) taken during an earlier site survey in 2003 (cf. Melles et al. 2011). The construction of a final composite core record was completed during core processing and subsampling, which began in September 2009 at the University of Cologne, Germany. The cores were first split lengthwise and both core halves were macroscopically described and documented by high resolution line scan images (MSCL CIS Logger, Geotek Ltd.). On one core half, color spectra and magnetic susceptibility were measured in 1 mm increments, followed by major and trace element analysis by X-ray fluorescence (XRF) analyses, using an ITRAX Core scanner (Cox Analytical Systems) and X-radiography in steps of 2.0 and 0.2 mm, respectively. Measurements of p-wave velocity

and gamma-ray density were then conducted in steps of 2 mm at the Alfred Wegener Institute in Bremerhaven, Germany, before the cores were continuously subsampled after return to Cologne for paleomagnetic and rock magnetic measurements. Subsequently, 2 cm thick slices were continuously sampled from the core composite, excluding deposits from mass

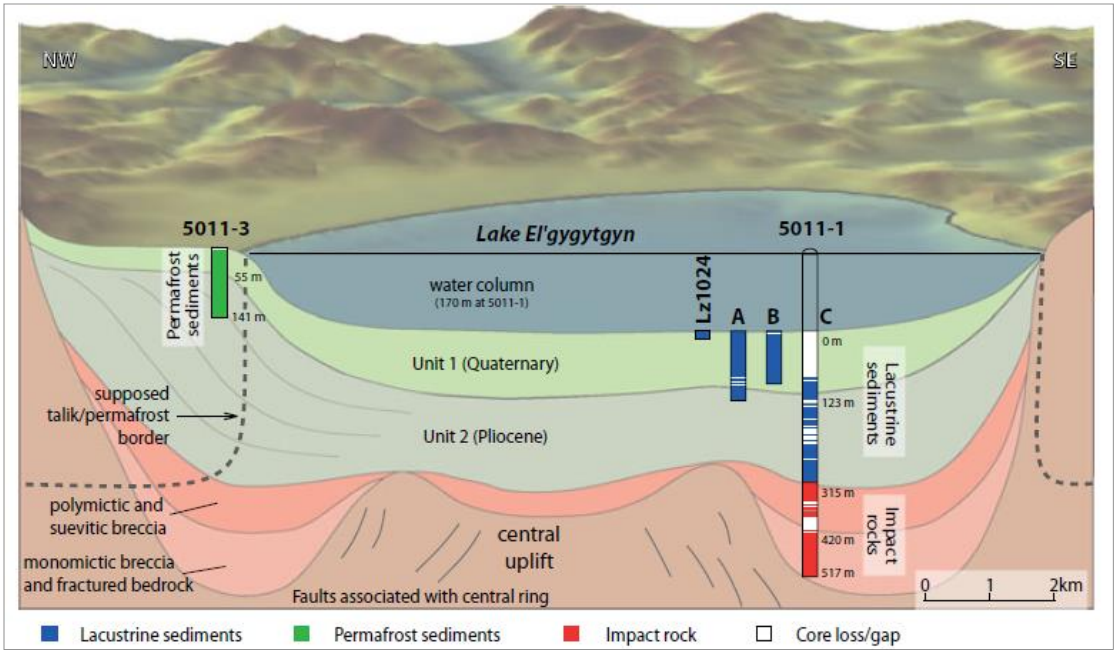

Figure 2.8: Schematic cross section of the El'gygytgyn basin stratigraphy showing the locations of ICDP Sites 5011-1 and 5011-3 (after Melles et al. 2011). At Site 5011-1, three holes (1A, 1B, and 1C) were drilled to replicate the Quaternary sections. Hole 1C further penetrated the remaining lacustrine sequence and then 200 m into the impact rock sequence. Lz1024 is a 16 m long pilot core taken in 2003 that overlaps between the lake sediment surface and the beginning of the drill cores 1A and 1B at Site 5011-1.

movement events, and split into eight aliquots of different sizes for additional biological and geochemical analyses. These aliquots, along with some irregular samples from replicate cores (e.g., for luminescence dating or tephra analyses), were subsequently sent to the sediment science team members responsible for specific studies. In addition, thin sections were prepared from representative sections of the cores to conduct microanalyses of the various lithologies identified during visual core descriptions. After the initial descriptions and sampling procedures have been completed, the remaining, untouched core halves will be shipped to the US National Lacustrine Core Repository (LacCore) at the University of Minnesota, USA, for long-term archiving.

Drilling was very successful because the 315 m-thick lake sediment succession was completely penetrated. The sediments do not seem to include hiatuses due to lake glaciation or desiccation, and their composition reflects the regional climatic and environmental history with great sensitivity.

Table 2.1: Penetration, drilling and core recovery at ICDP Sites 5011-1 and 5011-3 in the El'gygytgyn crater (all data given in field depth; from Melles et al. 2011).

Site	Hole	Type of material	Penetrated (mblb)	Drilled (m)	Recovered (m)	Recovery (%)
5011-1	1A	Lake sediment	146.6	143.7	132.0	92
	1B	Lake sediment	111.9	108.4	106.6	98
	1C	Total	517.3	431.5	273.8	63
		Lake sediment		225.3	116.1	52
		Impact rocks		207.5	157.4	76
5011-3		Permafrost deposits	141.5	141.5	129.9	91

Hence, the record for the first time provides comprehensive and widely time continuous insights into the evolution of the terrestrial Arctic since Pliocene times. This is particularly true for the lowermost 40 m and uppermost 150 m of the sequence, which were drilled with almost 100% recovery and likely reflect the initial lake stage during the Pliocene and the last approximately 2.9 Ma, respectively. Some first results of the investigations of the sediment cores in terms of paleoclimate studies have been published by Melles et al. (2012) and Brigham-Grette et al. (2013). In particular, the data show that around 3.5 million years ago, immediately after the impact event, summer temperatures at El'gygytgyn were approximately 8 °C warmer than today when pCO_2 was approximately 400 ppm. Multiproxy evidence suggests extreme warmth and polar amplification during the middle Pliocene, sudden stepped cooling events during the Pliocene-Pleistocene transition, and warmer than present Arctic summers until approximately 2.2 Ma, after the onset of Northern Hemispheric glaciation. The results presented by Brigham-Grette et al. (2013) indicate that Arctic cooling was insufficient to support large-scale ice sheets until the early Pleistocene.

2.7 PERMAFROST CORE

For permafrost research, in November–December 2008 a 142 m-long sediment core was retrieved from the permafrost deposits at ICDP Site 5011-3 in the western lake catchment by the local drilling company Chaun Mine Geological Company (CGE). The core penetrated coarse-grained, ice-rich alluvial sediments with variable contents of fine-grained material. The entire core was completely frozen when recovered. This confirmed modeling results that suggested that the unfrozen talik (a layer of year-round unfrozen ground that occurs in permafrost areas) alongside the lake descends with more or less a vertical boundary until the permafrost base is reached at a depth of a few hundred meters (Fig. 2.4). The permafrost cores

were described and photographically documented after recovery. They were kept frozen in the field and during transport to the ice laboratory (-30 °C) at the Alfred Wegener Institute in Bremerhaven (Germany). There, the cores were cleaned, the documentation was completed, and subsamples were taken from the sediment and ice for ongoing laboratory analyses. Results will be published elsewhere.

2.8 IMPACTITE CORE

Core D1c intersected the transition zone between the lacustrine sediments and the main impact breccia sequence at around 315 mblb. The impactite core, described below and the subject of the various papers in this volume, was recovered from 316.75 mblb to a depth of 517.09 mblb. The topmost part of the impactite core segment was recognized even in the field laboratory, immediately after drilling, as a likely suevite (Fig. 2.9). The core boxes were

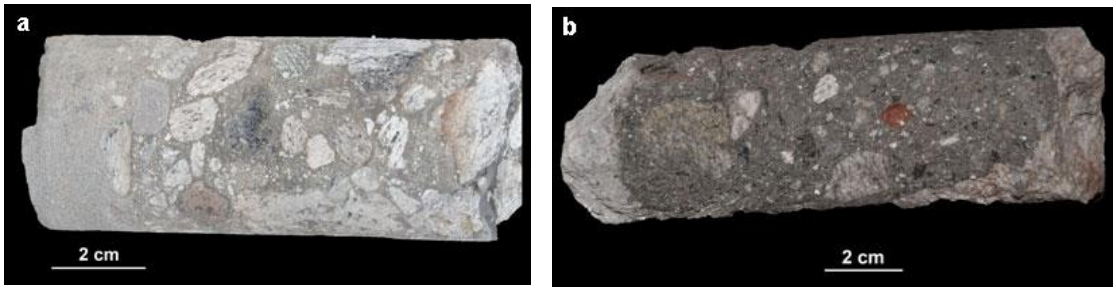

Figure 2.9: (a, b): Core segments from the drilling project at the El'gygytgyn impact crater, showing suevitic impact breccia, from (a) about 316 and (b) 319 m below the lake floor, just below the transition from the postimpact lake sediments. The glassy melt rock, which forms during the impact when some of the rock is heated to over 2000 °C, is the dark gray frothy inclusion in the center of the core segment. The cores were photographed by CK in the camp shortly after retrieval.

transported together with the sediment cores from Pevek to St. Petersburg and on to Germany. The impactite core boxes were moved in late 2009 to the Natural History Museum in Berlin, where they were opened, cleaned, photographed, and curated according to ICDP protocol (see Raschke et al. [2013a] for details). The sampling party for the impactite core took place at the Natural History Museum in Berlin on May 15 and 16, 2010. Subsequently, several hundred core samples were prepared and sent to research teams around the world.

2.8.1 Impactite Drill Core Stratigraphy

The following description is based on samples studied at the University of Vienna (cf. Pittarello et al. 2013) and differs slightly from complementary efforts by Raschke et al. (2013a) and Wittmann et al. (2013).

The studied drill core ranges from 316.80 m to approximately 517 mblb. The whole core can be divided into three main parts: (1) approximately 75 m of polymict lithic

breccia/suevite, intercalated with lacustrine sediments in the first 10 m, and containing large melt blocks (up to 40 cm) distributed throughout the profile; (2) approximately 30 m of different volcanic rocks, highly altered, varying from rhyolitic to basaltic lavas, tuffs, and ignimbrites; and (3) approximately 100 m of fractured, welded, rhyo-dacitic ignimbrite, including abundant so-called fiamme of pumice, and crosscut by a 50 cm-thick suevite dyke at the depth of 471.40 m. A summary of our lithological classification of the core is shown in Fig. 2.10.

2.8.1.1 Impact Melt Breccia

This unit can be divided into three subunits: the first two units (from the top) are characterized by the occurrence of lacustrine sediments in the matrix, alternating with impact melt clasts. The overall unit is quite altered, with open fractures, especially at the contact between the impact melt/volcanic blocks and the unconsolidated matrix, where drilling mud penetrated.

1. The interval between 316.8 and 320 mblb (Fig. 2.11) consists of lacustrine sediments intercalated with impact breccia and impact melt blocks. The lacustrine sediments include fine-grained (sand-size <2 mm) grains, which are equigranular, rounded to subrounded, with many being composed of glass fragments (cf. also Wittmann et al. 2013). In the drill core, lacustrine sediments showing parallel bedding are locally preserved and recognizable. The blocks of impact breccia (suevite, as confirmed by detailed petrographic studies, Pittarello et al. 2013; see also Raschke et al. 2013a) consist of a polymict breccia, with fragments of impact melt, volcanic rocks, and mineral grains in a fine-grained (lower than in the sediments) clastic/glassy matrix. Locally, sediments are mixed in with the matrix. Large impact melt blocks (up to 40 cm) also occur along the drill core. Such impact melt blocks have a variety of colors (from whitish to blackish), but are generally characterized by high porosity (vesiculation), and depending on color, they resemble either volcanic pumice or lava scoria.

2. The interval between 320 and 328 mblb (Fig. 2.12) is similar to the core section above, but it is marked by an obvious reduction in the lacustrine sediment contribution. The transition is gradual and occurs through a progressive decrease in thickness and abundance of the bedded sediments. A reddish polymict lithic breccia (suevite) progressively becomes the dominant lithology. Such a breccia includes abundant blackish angular melt fragments (up to 2 cm in size), clasts of greenish volcanic rocks, and mineral fragments, suspended in a reddish fine-grained matrix. The core section contains abundant impact melt blocks, similar in size and

-

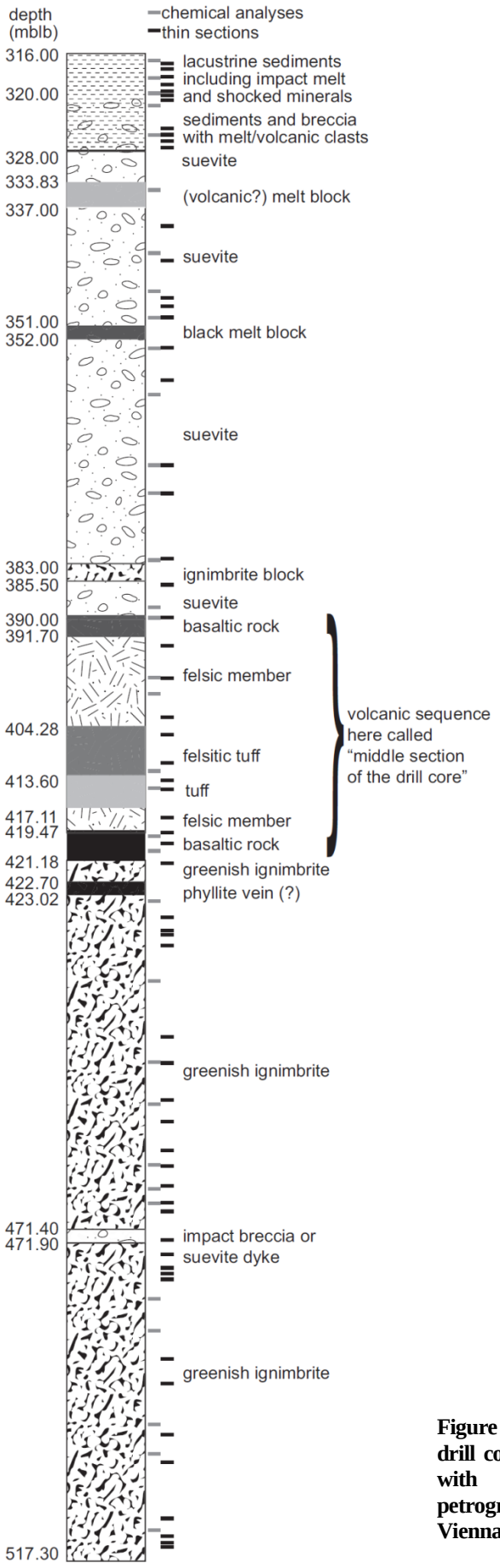

Figure 2.10: Schematic representation of the simplified drill core litho-stratigraphy (cf. Pittarello et al. 2013), with the samples selected for chemical and petrographic analyses performed at the University of Vienna.

characteristics to those described in the subunit above, but more frequently observed.

3. The interval between 328 and 390 mblb (Fig. 2.13) seems more homogenous in terms of lithology. The sediments are totally absent, as well as the impact melt blocks, whereas a reddish breccia dominates. The rock is weakly consolidated and all the samples have to be impregnated with epoxy before proceeding with the thin section preparation. The breccia is a polymict lithic impact breccia, which can locally be classified as suevite, because of the local occurrence of shocked minerals and impact melt (in fact that can be determined only by detailed petrography). The breccia consists of mineral, lithic, and melt fragments in a fine-grained reddish matrix. The melt fragments occur as angular blackish clasts and their sizes (from cm to mm) and abundance seem to decrease progressively through the subunit. Volcanic clasts, a few cm in size, occur in the drill core section.

2.8.1.2 Intermediate Layer - Volcanic Sequence

From 390 to 423 mblb, several volcanic formations follow (Fig. 2.14). The volcanic sequence is complex and the pervasive alteration makes the classification difficult. Although of similar appearance, the sequence includes subunits with different compositions (from felsic-rhyodacitic, SiO_2 70 wt% - to mafic-basalt, SiO_2 <50 wt%), as revealed by geochemical analysis. The felsic members are generally blackish to reddish in color, with locally recognizable fluidal fabric and porphyritic texture (mm-sized whitish grains). The mafic members are blackish to greenish in color, generally with fluidal fabric, containing abundant whitish grains (phenocrysts). Abundant fractures cut the core section, most of them are open, up to a few mm apart, but a relative displacement between blocks was not observed.

2.8.1.3 Rhyodacitic Ignimbrite

From 423 to 517 mblb, a single lithology dominates: a rhyodacitic ignimbrite (Fig. 2. 15). This ignimbrite includes abundant welded blackish pumice inclusions (called "fiamme" in volcanology, because of their elongated shape). The pumice particles can reach 20 cm in length and 3 cm in thickness. They are aligned, defining an apparent "foliation," which is determined by the compaction of the pyroclastic deposit. The flattened pumice particles show interfingering contacts with the host and chilled margins, marked by darker intensity of the matrix color and more abundant phenocrysts. The phenocrysts in the pumice particles consist of altered feldspar, whereas quartz is almost absent. The host contains abundant mm-sized whitish grains (quartz and feldspars) in a grayish glassy matrix. Some glass portions are preserved, are generally greenish in color (because of devitrification), and show perlitic fracturing. Locally, a greenish halo of probable glass surrounds the pumice particles. The unit is crosscut by abundant fractures and veins, generally concordant with the magmatic foliation,

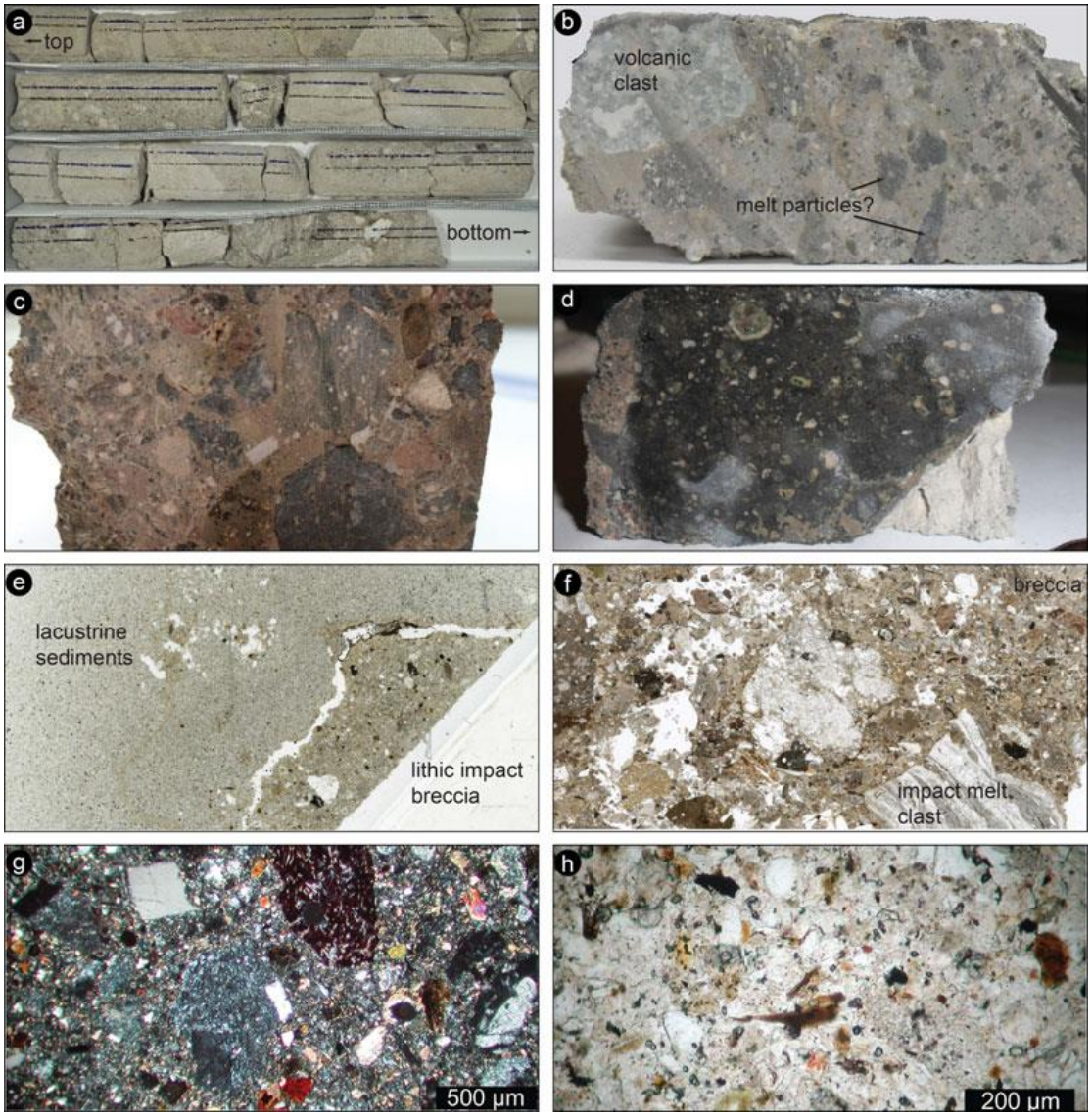

Figure 2.11 (a-h): Interval 316.8-320 mblb. a) Box containing the core run 98. The core width is 6 cm. The fine bedding in the lacustrine sediments as well as the impact melt blocks are recognizable (note: the blue and black lines on the core in this and all other core images were applied immediately after core retrieval to indicate the "up" position; with the blue line being on the right when facing up). b) Impact breccia, with possible impact melt (blackish in color) and probably volcanic rock clasts in a grayish matrix, mixed with lacustrine sediments. Sample width 6 cm. Sample 98Q4-W4-8 (317.8 mblb). c) Impact breccia, with poorly sorted clasts of volcanic rocks and impact melt in a reddish matrix. Sample 4 cm wide. Sample 98Q5-W11-15 (318 mblb). d) Impact melt clast, blackish in color and containing small whitish crystals. Sample 4 cm wide. Sample 98Q5-W24-27 (318.4 mblb). Wet surface to enhance the contrast. e) Contact between a fragment of impact breccia and the lacustrine sediments. The contact is open as a result of the sample preparation. Picture 3 cm wide. Thin section scan. Sample 99Q1-W17-19 (319.1 mblb). f) Impact breccia general aspect. Note the extensive porosity (white holes with irregular shape) and the variety of sizes and types of clasts, from impact melt fragments to unshocked volcanic rocks. Image width 3 cm. Thin section scan. Sample 98Q6-W7-11 (318.8 mblb). g) Impact breccia in an enlarged view. Volcanic rock fragments, variously shocked, are recognizable, as well as mineral fragments. Sample 99Q1W17-19 (319.1 mblb). Cross-polarized light microphotograph. h) The matrix of the impact breccia, including angular and rounded mineral fragments and melt particles (dark-brown in color). Sample 99Q1-W17-19 (319.1 mblb). Plane-polarized light microphotograph.

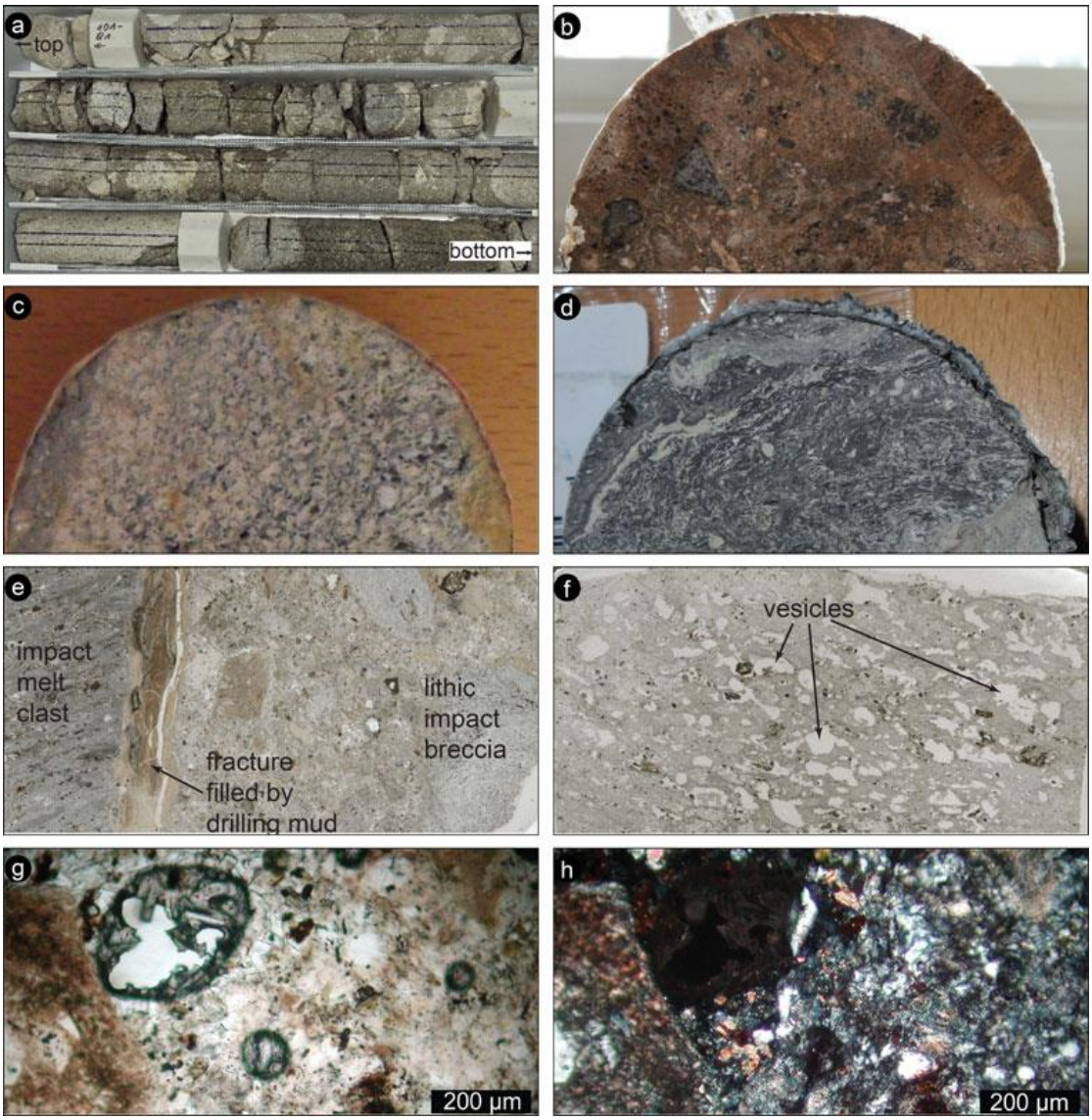

Figure 2.12 (a-h): Interval 320-328 mblb. a) Box containing core run 101 (approximately 319-321 mblb). The core width is 6 cm. The lacustrine sediment contribution is reduced in comparison with the core above, but the likely impact melt bodies dominate in this section. Whitish and blackish porous melt boulders, tens of cm long, are visible in the lower rows of the box. b) Sample of impact breccia, with poorly sorted clasts of volcanic rocks and impact melt clasts in a reddish matrix. Sample 6 cm wide. Sample 99Q5-W34-38 (321.3 mblb). c) Sample of likely volcanic rock, grayish in color, showing a layering and few whitish grains. Sample 6 cm wide. Sample 99Q5-W15-17 (321 mblb). d) Sample of impact melt clast, blackish in color and showing a definite internal flow fabric. At the right lower corner of the sample, the contact with the breccia is visible; breccia contains some lacustrine sediments. Sample 6 cm wide. Sample 101Q3-W41-43 (325.8 mblb). e) Contact between a fragment of impact melt (on the left) and the impact breccia (on the right). The contact is marked by a layer of clay, probably from the drilling mud, injected in the open fractures. Picture 3 cm wide. Thin section scan. Sample 101Q6-W11-13 (326.6 mblb). f) Impact melt. Note the extensive vesiculation. The darker portions may represent unmelted material. Picture 3 cm wide. Thin section scan. Sample 101Q8-W41-43 (327.6 mblb). g) The impact breccia matrix. Portion of the impact breccia with a glassy appearance and with rounded vesicles filled by secondary minerals. Sample 99Q3W17-19 (319.1 mblb). Plane-polarized light microphotograph. h) The same area but under cross-polarized light. The glassy matrix is pervasively devitrified. Sample 99Q3-W17-19 (319.1 mblb). Cross polarized light microphotograph.

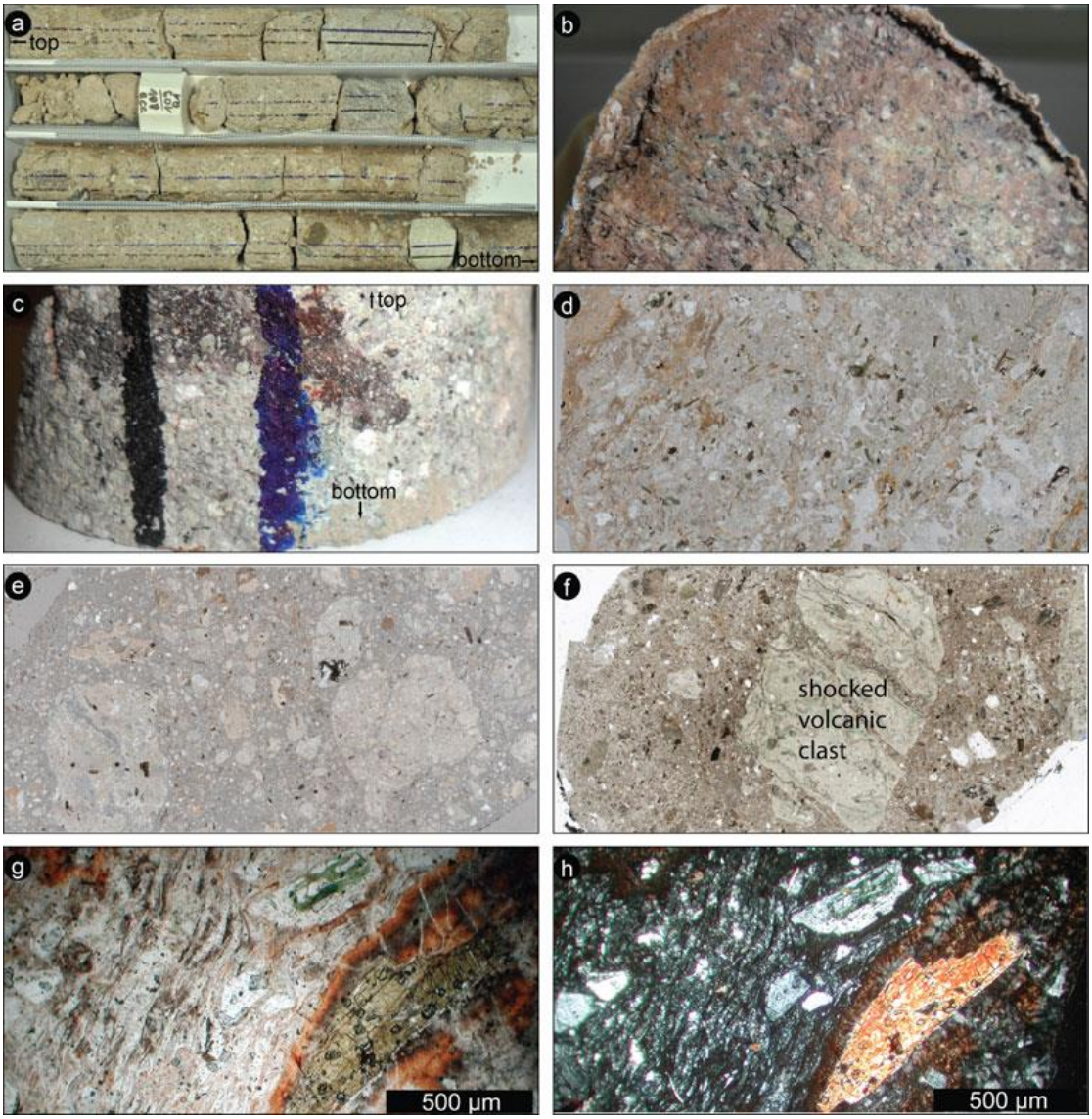

Figure 2.13 (a-h): Interval 328-390 mblb. a) Box containing part of the core runs 108 and 109 (approximately 344-350 mblb). The core width is 6 cm. The lacustrine sediment contribution is negligible in this unit, which has a more homogenous appearance. Impact melt bodies are less abundant, whereas in the lower row of the box, a small block of ignimbrite (greenish in color) is visible. b) Sample of impact breccia, with abundant clasts of mm size in a reddish matrix. Sample 6 cm wide. Sample 123Q2- W36-39 (384.4 mblb). c) Sample of ignimbrite (volcanic), with cm-sized pumice fragment. The ignimbrite clearly contains whitish mineral clasts in a grayish matrix. Note the blue and black ink stripes, marking the core orientation (blue on right means "up"). Sample 6 cm wide. Sample 114Q-CC (361.7 mblb). d) Ignimbrite/tuff clast, with strong layering marked by flattened pumice fragments and preferred orientation of the mineral grains. Picture 3 cm wide. Thin section scan. Sample 109Q1-W17-19 (348.6 mblb). e) Impact breccia, with poorly sorted clasts of volcanic rocks in a clastic matrix. Picture 3 cm wide. Thin section scan. Sample 112Q1-W18-20 (355.8 mblb). f) Large rhyolite clast in the impact breccia. Detailed petrographic analysis revealed that the clast is shocked, with plagioclase and quartz phenocrysts containing multiple sets of PDF. Picture 3 cm wide. Thin section scan. Sample 124Q2-W18-20 (387.2 mblb). g) Strong flow fabric in a likely volcanic particle. Sample 109Q1W17-19 (348.6 mblb). Plane-polarized light microphotograph. h) The same area but under cross-polarized light, to note the progress of devitrification in glassy areas and of alteration in phenocrysts. Sample 109Q1-W17-19 (348.6 mblb). Cross-polarized light microphotograph.

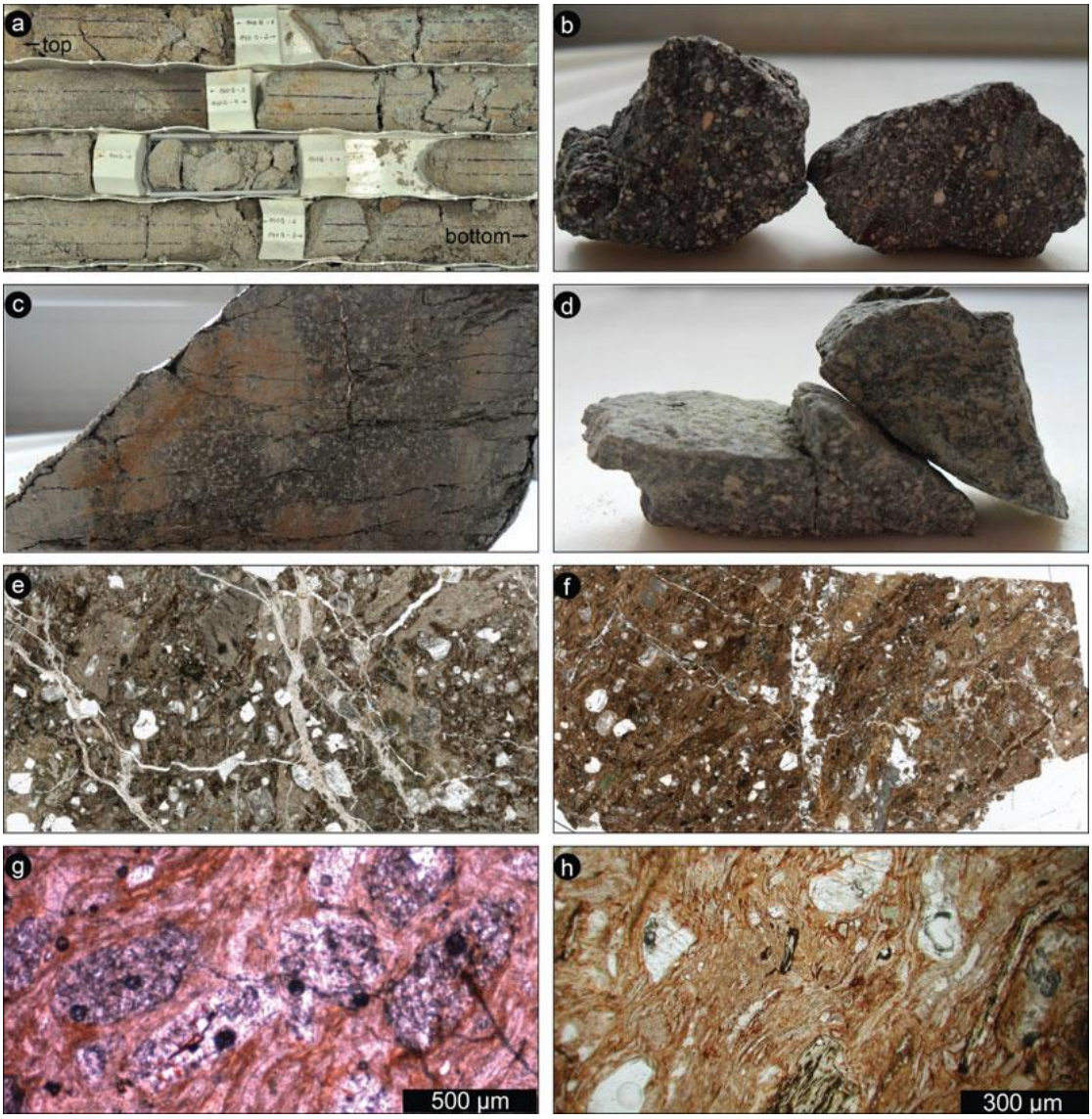

Figure 2.14 (a-h): Interval 390-423 mblb: Intermediate layer. a) Box containing part of the core runs 140 and 141 (approximately 416-420 mblb). The core width is 6 cm. The layer includes different lithologies, but the rock is highly altered, making classification difficult. b) Fragments of a layered blackish volcanic rock. Fragments 3 cm wide each. Sample 134Q1-W7-9 (399.6 mblb). c) Sample of a fractured volcanic rock, showing abundant whitish grains in a blackish matrix. Sample 6 cm wide. Sample 142Q2-W1-3 (420.6 mblb). d) Fragments of a greenish volcanic rock, which was classified as basalt by geochemistry. Fragments about 3 cm wide each. Sample 142Q3-W13-15 (420.9 mblb). e) Internal structure of one of the volcanic lithologies in this core section. Subrounded quartz grains are embedded in a brownish matrix, which includes probably pumice lapilli. The sample is crosscut by a network of open fractures. Thin section scan. Sample 137Q1-W5-7 (407.3 mblb). f) Rhyolitic sample with few subrounded quartz phenocrysts in a layered brownish matrix, which shows a strong layering/flow fabric. The sample is crosscut by open fractures, which are discordant with respect to the magmatic foliation. Picture 3 cm wide. Thin section scan. Sample 139Q6-W4-6 (414.8 mblb). g) Strong flow fabric in an andesitic volcanic rock, with abundant altered feldspar grains enveloped by the flowing matrix. Sample 130Q1W15-17 (395.4 mblb). Plane-polarized light microphotograph. h) Felsic volcanic rock with quartz, feldspar, and altered amphibole grains in a glassy welded matrix. Sample 139Q6-W4-6 (414.8 mblb). Plane-polarized light microphotograph.

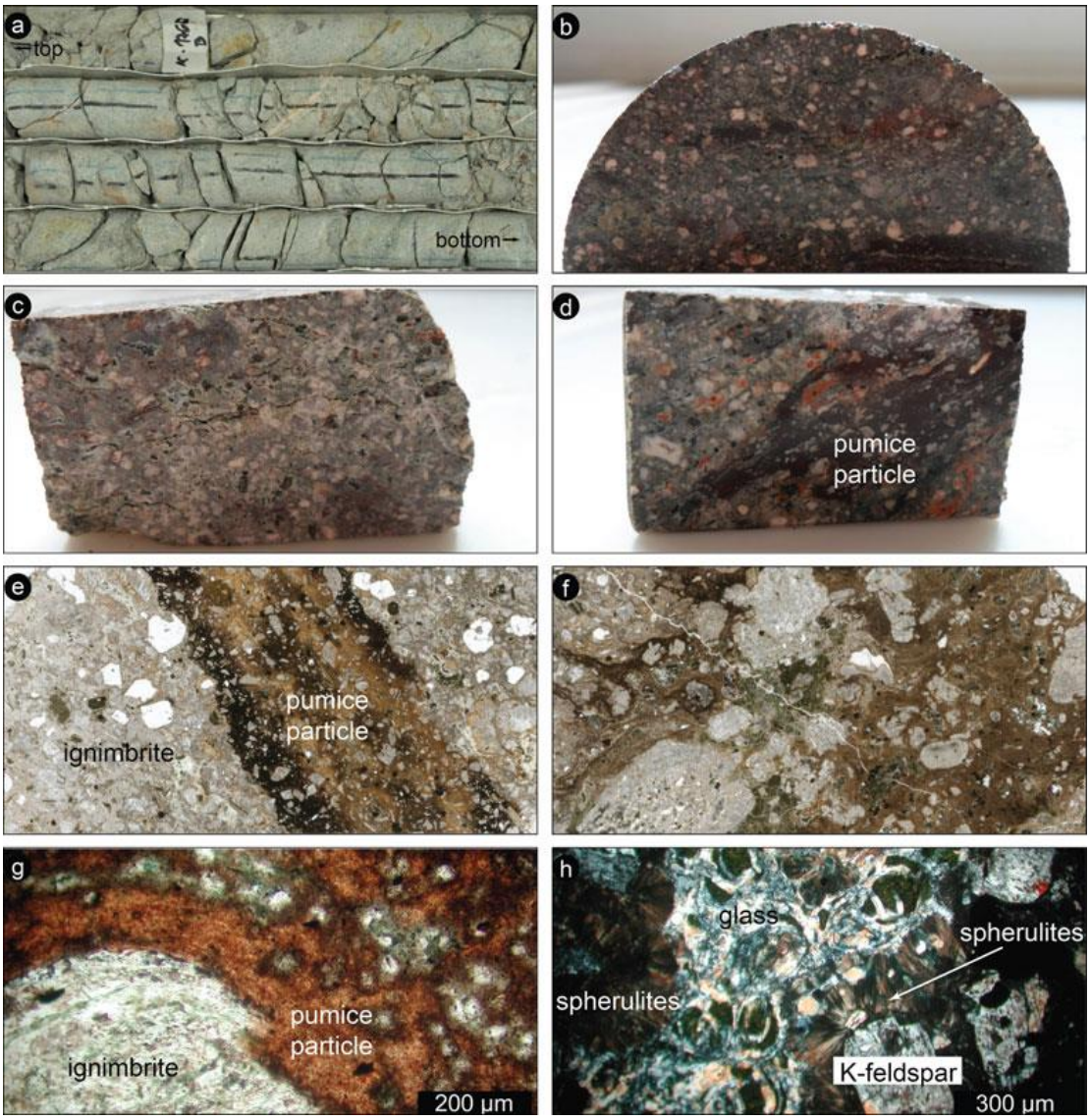

Figure 2.15 (a-h): Interval 423-517 mblb: Rhyodacitic ignimbrite. a) Box containing part of the core run 176 (approximately 507-510 mblb). The core width is 6 cm. The core consists of an apparently homogenous greenish ignimbrite, crosscut by fractures and whitish veins filled by both carbonates and zeolites. Fractures and veins are developed with an angle between 15 and 45° with respect to the core axis. b) Cross section of a large pumice clast in the ignimbrite, cut parallel to the flow plane. Note the blackish glassy matrix and the abundant equigranular mineral grains. Sample 6 cm wide. Sample 147Q2-W40-41 (431.8 mblb). c) Pumice-free portion of the ignimbrite. Note the greenish glass preserved in the upper part of the sample. Sample 3 cm wide. Sample 162Q5-W24-26 (470 mblb). d) Ignimbrite containing a large flattened pumice inclusion. Sample is 3 cm wide. Sample 173Q5-W25-27 (501.3 mblb). e) Internal structure of a pumice particle in the ignimbrite. Note the darker color of the matrix and the more abundant feldspar grains at the contact with the host rock, forming the typical "chilled" margins. Thin section scan. Sample 149Q1-W26-28 (435.7 mblb). f) Internal structure of a large pumice particle, with a random distribution of feldspar grains and glass fragments (greenish) in a brownish matrix, characterized by a strong layering. Image width 3 cm. Thin section scan. Sample 164Q3-W35-37 (475.2 mblb). g) Detail of the contact between a pumice particle and host rock matrix. Sample 164Q3-W26-28 (475.1 mblb). Plane-polarized light microphotograph. h) Detail of strongly altered glass (chloritization or devitrification) preserved in the ignimbrite, with the characteristic perlitic fracturing. Note also the extensive development of spherulites at the margins of feldspar grains. Sample 148Q1-W20-30 (433.5 mblb). Cross-polarized light microphotograph.

with a general angle of approximately 45° to the core axis. Locally, conjugate systems of fractures were observed. The veins are generally filled by whitish to reddish or greenish materials, classified as carbonate (likely calcite) or zeolites depending on the reaction to dilute HCl. The overall unit is quite fresh, except for the obvious devitrification of the glassy portions.

The unit is crosscut by an impact breccia dyke between 471.4 and 471.9 mblb. This breccia consists of melt particles and mineral fragments in a glass-bearing clastic, unconsolidated matrix. The contact with the ignimbrite is sharp and no evidence of cataclasis was observed. The breccia was lately better characterized by detailed petrographic studies, revealing the occurrence of shocked minerals (see Pittarello et al. 2013; Raschke et al. 2013; Wittmann et al. 2013).

2.9 RESULTS OF IMPACTITE STUDIES

Detailed petrographic and geochemical studies of the core samples were performed by three independent groups, in Vienna (Pittarello et al. 2013), Berlin (Raschke et al. 2013b), and Houston/St. Louis (Wittmann et al. 2013). As the three studies involved a different number of samples, and because there is a natural variation in sample characteristics even within a few centimeters of the core, there are differences in the assignment of the exact breccia nomenclature, but the general classification is about the same. In particular, there is still some disagreement regarding the extent to which the uppermost unit is termed a suevite or a reworked suevite.

In a detailed petrographic and geochemical study of the complete drill core, involving over 100 samples for petrography and 35 for geochemistry, Pittarello et al. (2013) found evidence to classify the almost 75 m-thick core section, from about 316 to 390 mblb, beginning with a mixed zone of fallback breccia and lacustrine sediments, as suevite, whereas they assign the remaining part of the core to slightly shocked to unshocked volcanic rocks. These authors noted that the suevite contains abundant melt fragments, as well as shocked minerals. The volcanic rocks that make up polymict and monomict impact breccia comprise a pervasively altered volcanic sequence. Pittarello and co-workers also provide a comparison between the rocks found in the drill core and a representative suite of target rock samples collected at and around the crater. Geochemical studies confirm that the rock types found as parts of the various breccia types are also represented among the target rocks, although the variation in the drill core samples is somewhat limited. As an exception, mafic rocks from the intermediate layer in the drill core cannot be directly correlated with the mafic samples from the target, but Hf-Nd isotopic compositions indicate that the two different types of these rocks represent different stages of the same magmatic evolution.

Raschke et al. (2013a) give an account of the curation and preparation of the impactite cores and discuss the classification of that core according to their observations. These authors concluded that below the zone of reworked impact breccia at the top (316.75-328 mblb), there is a section of what they conservatively refer to as polymict impact breccia (328-390 mblb), followed by two units of variously brecciated volcanic bedrock. The upper bedrock (a unit of various volcanics) and the lower bedrock (rhyodacitic ignimbrite) (391.79-422.71 mblb and 422.71-517.09 mblb). Raschke et al. (2013b) provide detailed petrographic and geochemical observations on their large set of samples that represent the complete impactite core.

Wittmann et al. (2013) performed petrographic and geochemical analyses of a number of drill core samples in comparison with impact melt rocks from the surface and several glass spherules from outside the crater (cf. also Adolph and Deutsch 2009, 2010). Although there are some limited differences between the details of their lithological classifications and those of Pittarello et al. (2013) and Raschke et al. (2013a), due to more limited number of samples and a natural variation in the investigated materials, these researchers still arrive at the same succession of fallback material, suevite, polymict breccia, and monomict breccia as the other authors. Wittmann et al. (2013) quantify the abundance of glassy impact melt shards <1 cm in size in the upper 10 m of suevite to about 1 vol%. Like the other two groups, they also note the finding of glass spherules in the reworked fallout deposit that caps the suevite and is at the transition to lacustrine sedimentation, similar to what was recovered at the top of the Bosumtwi fallback sequence (Koeberl et al. 2007b). Some of the spherules contain Ni-rich spinel and admixtures of an ultramafic component, and this zone also contains a relatively higher abundance of shock metamorphosed lithic clasts. Wittmann et al. (2013) interpret this unit as allochthonous breccia from the vicinity of the central ring uplift of the El'gygytgyn structure.

A main problem in the study of the drill core samples from El'gygytgyn concerns the question how it might be possible to distinguish volcanic melt fragments that are part of the target from those melts and glasses that formed during the impact event. One possibility is the presence of shocked mineral clasts within the glasses, but this opportunity does not always present itself. Recent studies of the cathodoluminescence (CL) properties of volcanic melts and impact melt rocks and glasses from the El'gygytgyn drill core by Pittarello and Koeberl (2013a) indicate that CL parameters might be helpful in distinguishing the two formation processes. Another possibility is the application of quantitative petrography, such as the study of clast size distribution (CSD), as in the study by Pittarello and Koeberl (2013b). Such a technique has been applied to melt rocks in earlier studies, including lunar rocks. These authors show that geometrical characterization provides a reproducible technique for

quantitative description of impact lithologies, even though the studied suevite blurs the distinctions due to local variability that averages out on a larger scale. Nevertheless, this method allows the identification of unshocked to slightly shocked volcanic clasts within the suevite.

Pittarello and Koeberl (2013c) studied impact glass samples from the El'gygytgyn structure, to constrain the formation of these glasses and their cooling history. They found that the glasses can be grouped into two types, one that has formed early in the impact process and consists of pure glass (deposited as glass bombs) and a second type that includes composite samples with impact melt breccia lenses embedded in silica glass. These mixed glasses probably resulted from inclusion of unmelted portions into melted portions during ejection and deposition and were probably formed during the crater excavation and modification phase.

Hellevang et al. (2013) report on laboratory hydrothermal alteration experiments, geochemical modeling, and mineralogical analyses of El'gygytgyn impact melt rock in comparison with two volcanic glass samples (not from the El'gygytgyn region), to better understand the alteration of the El'gygytgyn impact melt and possible relations to the surface of Mars. In their alteration experiments, they found that phases such as cristobalite form; however, as the El'gygytgyn melt rock already contained secondary alteration phases, including zeolites, it was not clear if any additional such phases formed during the experiment.

Goderis et al. (2013) present one of two studies that try to constrain the meteoritic component at El'gygytgyn. In their work, they compare the geochemical composition of impactites from the drill core with that of impact melt rock fragments at the crater surface. They determined siderophile element abundance data and Os isotope ratios and concluded, with the help of mixing calculations taking into account an indigeneous component, that there is evidence for a small (approximately 0.05 wt% carbonaceous chondrite equivalent) meteoritic component at the bottom of a reworked fallout deposit, in a polymict impact breccia, and in some impact melt rock fragments. The exact impactor type could not be derived, but Goderis et al. (2013) suggest, based on siderophile element abundances and ratios of spherule samples that might be part of the uppermost fallback sequence, that an impactor with ordinary chondritic composition is more likely than a primitive achondritic source, even though they do not exclude this possibility completely.

In another study on the meteoritic component within El'gygytgyn impactites, Foriel et al. (2013) note a variation in Cr, Co, and Ni contents in the various breccia and impact glass samples, which does not give a clear signal, but they found that the Cr isotopic composition of

an impact glass sample yielded a nonterrestrial $\varepsilon^{54}Cr$ value of -0.72 ± 0.31 (2 SE). This negative $\varepsilon^{54}Cr$ differs from values for carbonaceous chondrites ($\varepsilon^{54}Cr$ of +0.95 to +1.65), but is nearly identical to reported values for ureilites (approximately -0.77), and, within error, similar to values for eucrites (approximately -0.38) and ordinary chondrites (approximately -0.42). Foriel et al. (2013) conclude that the similarity of the El'gygytgyn Cr isotopic data with those of ureilites, and other chemical evidence such as very low Ir contents, suggests that a ureilitic source was involved, or maybe the asteroid could have been an F-type asteroid of mixed composition, similar to the recent Almahata Sitta fall in Sudan.

Finally, an analysis of the physical properties of the drill core from the El'gygytgyn impact structure was performed by Maharaj et al. (2013). These authors studied petrophysical parameters, such as the densities and porosities, and detected structural and textural changes down the drill core, but not changes in lithology. Nevertheless, these parameters can indicate fracturing and brecciation as a result of the impact event, in that they allow the identification of the transition from a consolidated fine-grained matrix structure to a more crystalline structure. These authors suggest that there is a boundary between the differently brecciated rock sections at around 415 mblb. Maharaj et al. (2013) also used paleomagnetic methods to re-orientate the drill core and found that the re-oriented core has natural remanent magnetic components with mainly normal polarity, but also some components with reverse polarity. The magnetic properties suggest that the main magnetic minerals are ferrimagnetic iron-titanium oxides with high titanium contents, as is common for young igneous rocks. These authors note that the variations in magnetic properties are probably caused by differences in the oxidation/reduction state of these ferrimagnetic minerals.

2.10 CONCLUSIONS

The El'gygytgyn impact structure, 3.6 Ma old and 18 km in diameter, was excavated in Late Cretaceous siliceous volcanic rocks of the central Chukotka, northeastern Russia. It is the only known terrestrial impact structure formed in siliceous volcanic target and thus enables us to investigate shock metamorphism in such lithologies. The impact structure, filled by a lake 12 km in diameter, was drilled in 2009 during an ICDP drilling project. The drill core penetrated through postimpact sediments, impactites, and the fractured igneous basement. The impactite portion of the core was recovered from 316.08 to 517.30 m in depth below the lake bottom.

The main rock types of the crater basement are ignimbrite, tuff, and lava of rhyolitic to dacitic composition; rarely basaltic and andesitic compositions were analyzed. The simplified stratigraphy of the core is: (a) 316-390 m - impact breccia including volcanic and impact melt clasts that locally contain shocked minerals, in a fine-grained clastic matrix; (b)

385-423 m - a volcanic sequence including both felsic (likely felsic tuffs) and mafic (basalt) members; (c) 423-517 m - greenish rhyo-dacitic ignimbrite, with abundant (volcanic) melt particles, quartz-free and elongated parallel to flattening direction. This latter formation is crosscut by abundant fractures locally filled by carbonate, silicate, and clay veins. Over the whole length of the impactite core, the abundance of shock features decreases rapidly from the top to the bottom of the studied core section, being almost absent in the lower brecciated volcanics.

A comparison between the similar sized Bosumtwi and El'gygytgyn impact craters is quite interesting, despite the difference in target rocks. Initial expectations of large amounts of impact melt within either of those craters were not confirmed. A large variety of stratigraphic, petrographic, geochemical, isotopic, and petrophysical analyses were made on the impactite core segment by several research teams and are reported in a series of companion papers to this introduction and overview.

Acknowledgments

Funding for this research was provided by the International Continental Scientific Drilling Program (ICDP), the US National Science Foundation (NSF), the German Federal Ministry of Education and Research (BMBF), Alfred Wegener Institute (AWI) and GeoForschungsZentrum (GFZ), the Russian Academy of Sciences Far East Branch (RAS FEB), the Russian Foundation for Basic Research (RFBR), and the Austrian Federal Ministry of Science and Research (BMWF). The current work was supported by the Austrian Science Foundation FWF, project P21821-N19 (to C.K.). The Russian GLAD 800 drilling system was developed and operated by DOSECC Inc., and the down-hole logging was performed by the ICDP-Operational Support Group. We are grateful to M. Voevodskaya (Russian Academy of Sciences/CRDF) who tirelessly worked to enable logistics in Russia. In Pevek, D. Koselov from Chukotrosgidromet was very helpful for all local arrangements. At the drill site, N. Vasilenko and his colleagues from the Chaun Mining Corporation were responsible for the efficient and safe daily operations in the base camp and during drilling crew shifts. Contracts for the camp were organized by CH2MHill. We are particularly grateful to the personnel in the Pevek office of the Kinross Gold Corporation for their assistance. Ice pad preparation and safety monitoring were carried out by EBA Engineering Consultants Ltd., Canada. We are grateful to J. Plescia and H. Newsom for helpful reviews and J. Spray for editorial comments.

Editorial Handling - Dr. John Spray

Note: In comparison to the published original manuscript a few spelling and grammatical mistakes had to be corrected. In addition, some references were updated with "a" or "b".

CHAPTER 3

LITHOSTRATIGRAPHY OF THE IMPACTITE AND BEDROCK SECTION OF ICDP DRILL CORE D1C FROM THE EL'GYGYTGYN IMPACT CRATER, RUSSIA.

This Chapter was published as the following peer-reviewed article:

Raschke U., Reimold W. U., Zaag P. T., Pittarello L., and Koeberl C. 2013a. Lithostratigraphy of the impactite and bedrock section in ICDP drill core D1c from the El'gygytgyn impact crater, Russia. *Meteoritics and Planetary Science* 48:1143-1159, http://dx.doi.org/10.1111/maps.12072.

3.1 ABSTRACT

In 2008/2009, the International Continental Scientific Drilling Program (ICDP) obtained drill cores from the El'gygytgyn impact structure located on the Chukotka Peninsula (Russia). These cores provide the most complete geological section ever obtained from an impact structure in siliceous volcanic rock. The lithostratigraphy comprises a thick sequence of lacustrine sediments overlying impact breccias and deformed target rock. The interval from 316 m (below lake floor-blf) to the end of the core at 517 m depth can be subdivided into four lithological sequences. At 316 m depth, the first mesoscopic clasts of shocked target rock occur in lacustrine sediments. The growing abundance of target rock clasts with increasing depth and corresponding decrease of lacustrine sediment components indicate the extent of this transition zone to 328 m depth. It constitutes a zone of mixed reworked impact breccia and lacustrine sediments. Volcanic clasts in this reworked suevite section show all stages of shock metamorphism, up to melting. The underlying unit (328-390 m depth) represents a suevite package, a polymict impact breccia, with considerable evidence of shock deformation in a wide variety of volcanic clasts. This includes fragments with quartz that exhibit planar fractures and planar deformation features (PDF). In addition, at three depths, several centimeter-sized clasts with shatter cones were detected. Due to microanalytical identification of relatively rare, microscopic impact melt particles in the matrix of this breccia, this material can be confidently labeled a suevite. Also in this sequence, three unshocked, <1 m thick intersections of volcanic blocks occur at 333.83, 351.52, and 383.00 m depths. The upper bedrock unit begins at 390.74 m depth, has a thickness of 30.15 m, and represents a sequence of different volcanic rocks - an upper part with basaltic composition from 390.74 to 391.79 m depth overlying a lower, rhyodacitic part from 391.79 to 420.27 m depth. This (parautochthonous) basement unit is only very weakly affected by the impact: only one shocked quartz grain with two sets of PDF was recorded at 391.72 m depth. The lower

bedrock unit (420.89-517.09 m depth [end of core]) is a brittly deformed, rather homogeneous welded ignimbrite that in part can be considered a cataclasite. The top three meters of this section are sheared, which could represent pre-impact tectonic deformation. A 54 cm thick injection of polymict impact breccia occurs at 471.42–471.96 m depth.

3.2 INTRODUCTION

The Pliocene age (3.58 ± 0.04 Ma; Layer 2000) El'gygytgyn impact structure is the best preserved impact structure on Earth in felsic volcanics (Koeberl et al. 2013). The complex impact structure (Fig. 3.1) with a diameter of 18 km is largely filled with Lake El'gygytgyn of 12 km width.

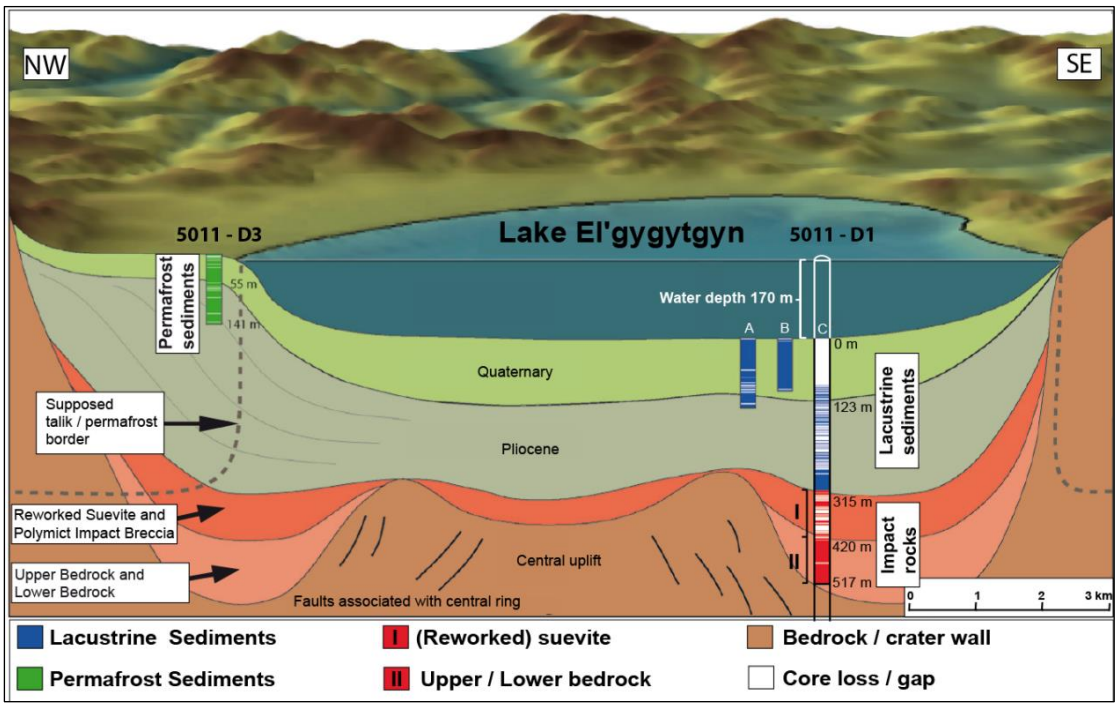

Figure 3.1: Schematic outline of the El'gygytgyn impact structure (vertically exaggerated) and the geological framework of target rocks with the position of drill sites and drilling depths (numerical data in meters below lake level). Based on geophysical interpretation; modified after Melles et al. (2011).

The structure has a prominent rim with elevations up to 180 m above lake level. However, degradation must have been significant, as much of the ejecta blanket around the crater structure has been removed by erosion. The impact event took place into the Late Mesozoic Ochotsk-Chukotsky Volcanic Belt of Chukotka (Northeast Siberia). The crater is centered on 67°30′N and 17°05′ E. El'gygytgyn crater is one of only few terrestrial impact structures known to have formed in volcanic target rocks. The El'gygytgyn target comprises silicious volcanic rocks (Gurov and Gurova 1979, 1991) that are thought to belong to the Late Cretaceous Pykarvaam and Milguveem series (Belyi 1969; Feldman et al. 1981). ^{40}Ar-^{39}Ar dating of some volcanic rocks from the area around the crater yielded ages of 83-94 Ma (Layer 2000; Ispolatov et al. 2004; see Fig. 3.2).

From December 2008 until April 2009, a drilling campaign was conducted at Lake El'gygytgyn by the International Continental Scientific Drilling Program (ICDP). The project had two main purposes: to investigate the lacustrine sedimentary crater fill for information about the paleoclimatic record for the high Arctic latitudes and to study the effects of the impact event on the felsic volcanic target (Melles et al. 2003, 2011). A first drill hole was located on the western lake terrace and was terminated at about 140 m depth. The purpose for this drilling was to investigate the development of permafrost. The second borehole, the focus of our work, was sunk against the outer slope of the central uplift of the impact structure, as determined by geophysical studies (e.g., Melles et al. 2011) from a drilling-rig on the frozen lake (Koeberl et al. 2013). This "D1" drill core consists of three sections from separate boreholes. D1a and D1b reached depths of 112 and 147 m below lake floor (mblf) and only recorded the postimpact sediment section. Only the 517 m long core D1c intersected the impact rocks below the lake sediments (Melles et al. 2011).

Group	Formation	Lithologies *(Belyi, 1977)*	Age in Ma *(Ispolatov 2004)*	Age in Ma *(Stone et al. 2009)*	Age in Ma *(Kelly 1999)*	Occurrence in crater area *(Stone et al. 2009)*
Chauna - Group	Koekvun' Fm.	550 m basalts, andesites, minor dacites and volcano-clastic rocks		~83.2	87 ± 6	SE crater rim and Enmyvaam valley
	Voron´in Fm.	50-550 m felsic to intermediate tuffs and ignimbrites		91.1 ± 0.9	94 ± 7	NE crater rim
	Pykarvaam Fm.	50-100 m rhyolitic ignimbrites and tuffs		~88	94 ± 7	Whole crater rim SE and NE
	Kalenmuvaam Fm.	800-900 m andesite-dacite ignimbrites, lava and tuffs				Not exposed in the region
	Alkakvun Fm.	1000-1200 m rhyolitic ignimbrites and tuffs, tuffaceous sedimentary rocks	~87.3		95 ± 6	Not exposed in the region

Figure 3.2: Combined lithostratigraphic table of the Lake El'gygytgyn region. Title of the geological group, their formation and stratigraphic column after Belyi (1977, 1988, 1994), Belyi and Belaya, 1998. Ages after Ispolatov et al. (2004), Kelley et al. (1999) and Stone et al. (2009).

The section of lake sediments can be divided into two different units. The upper sediment layer to 123 mblf is well stratified. The lower sediment layer appears more massive and ends against a mixed sediment-impact breccia transition zone at approximately 316.75 m depth. (Note: all depths in core D1c given here are uncorrected field depths; see below.)

Below this unit, ICDP drill core D1c contains a sequence of different impactites and volcanic bedrock (to 517.09 m). This sequence can be divided into a zone of reworked impact breccia at the top (316.75-328 m), a polymict impact breccia (328-390.74 m), and two units of volcanic bedrock (391.79-422.71 m and 422.71-517.09 m, respectively). Core recovery for the two impact sections was, on average, 54% and for the bedrock units 87%. The lake sediment part of the drill core is curated at the University of Cologne; the lower part with the impactite sequence has been curated and is currently stored at the Museum für Naturkunde Berlin. In autumn 2009, our team began with core curation (according to ICDP protocol, which includes a first lithological description supported by scanned images covering the entire drill core). This was followed by a first sampling party for the consortium science team members in May 2010. After this, detailed petrographic and geochemical analysis of the impactites was undertaken (e.g., Raschke et al. 2013b; Pittarello et al. 2013).

In this contribution, we provide a general lithostratigraphic description of the sub-316 m portion of core D1c. The companion paper by Raschke et al. (2013b) presents detailed petrographic and geochemical records for the impactites and bedrock sections.

3.3 GEOLOGICAL BACKGROUND

The El'gygytgyn impact structure is located in the central part of the Late Mesozoic Ochotsk-Chukotsky Volcanic Belt (OCVB) and at the southeastern slope of the Academician Obruchev Ridge in central Chukotka. The relatively young crater has a well-preserved morphological expression with a circular basin, surrounded by a crystalline rim with the highest elevation on the eastern side of the structure (Dietz and McHone 1976; Gurov et al. 1978) (Fig. 3.3). The approximately 14 km wide crater floor is largely covered by the nearly circular Lake El'gygytgyn, which is up to 170 m deep in its central part. The lake is somewhat offset from the center relative to the crater rim. The displacement toward the SE was confirmed by the observation that more rapid sedimentary accumulation occurred in the west (Gurov and Koeberl 2004). A complex system of lacustrine terraces surrounds the lake to an elevation of approximately 80 m above lake level (Gurov et al. 2007). According to seismic investigation (Niessen et al. 2006), a central peak is not exposed on the recent surface of the crater floor, nor is it evident in the bathymetric record of the lake bottom. However, from gravity measurements, Dabizha and Feldman (1982) suggested the presence of an approximately 2 km wide central peak underneath postimpact sediments - centered relative to

the crater outline. In contrast, Nolan et al. (2003) suggested that a central uplift was centered on the lake. Recent seismic work (Melles et al. 2011) has been interpreted to confirm that the central uplift is centered relative to the crater rim, and not to the lake.

The geology and structure of the crater are mostly known from the work of Gurov et al. (1978, 1979a), Gurov and Gurova (1983), and Gurov and Yamnichenko (1995). The crater is surrounded by an uplifted rim that has an asymmetrical cross section, with steep inner walls and gentle outer slopes. The crater was formed in a sequence of volcanic rocks that forms a monoclinic structure that dips to the east at 6–10°. The target rocks are disturbed in the vicinity of the crater by a complex system of faults that extend to a distance of 2.7 crater radii (approximately 24 km) from the center of the structure (Gurov and Gurova 1983).

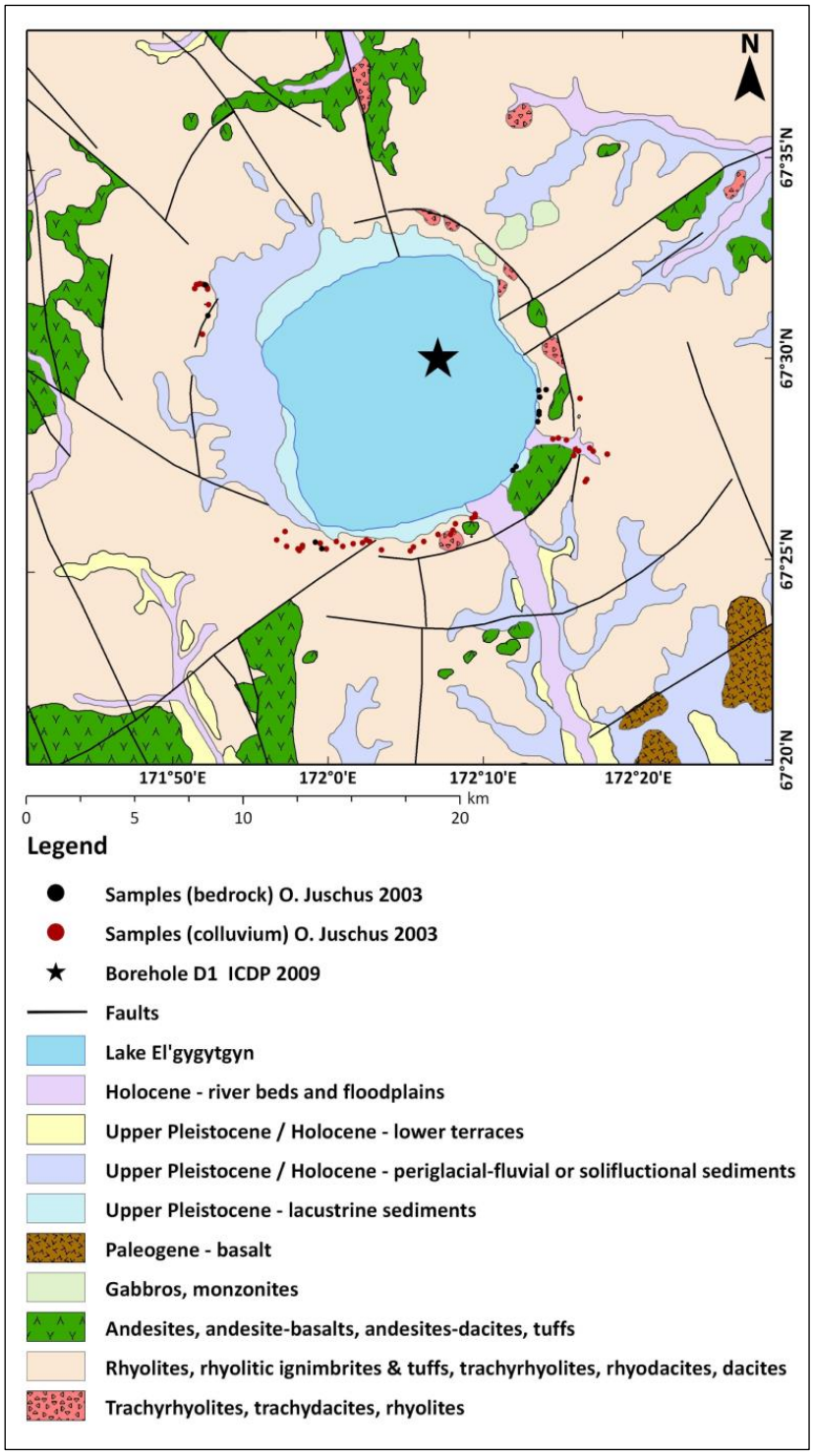

Figure 3.3: Simplified geological map after Nowaczyk et al. (2002), with location of the ICDP drill hole D1c and the location of samples obtained courtesy of O. Juschus (TU Berlin, collected in 2003).

The volcanic rocks of this region were described as the Late Cretaceous Okhotsk-Chukotka Volcanic Belt (OC-VB). They comprise five different forma-

tions (Alkakvun, Kalenmuvaam, Pykarvaam, Voron'in, and Koekvun', see Fig. 3.2). These rocks constitute the Chauna Group (Belyi 1977; Kelley et al. 1999; Stone et al. 2009), which represents, after a traditional geochronologic model, the early Albian-Cenomanian (approximately 106-97 Ma) phase of the evolution of the OCVB (Belyi and Belaya 1998). New investigations from Ispolatov et al. (2004) and Stone et al. (2009), based on the work of Belyi (1994) and Belyi and Belaya (1998), implied that the major part of the crater, except the SE part, was located in volcanics of the Pykarvaam Formation thought to have an age of more than 91 Ma. However, both Ispolatov et al. (2004) and Stone et al. (2009) measured younger paleomagnetic ages for the Pykarvaam Formation (approximately 88 Ma). Ispolatov et al. (2004) created a new timeline for the evolution of the OCVB (very short and strong volcanism), Stone et al. (2009) suggested that the impact event and the formation of the El'gygytgyn crater could have reset the magnetic minerals in the rocks. The SE crater rim is part of the Koekvun' Formation with an age of 83.1 ± 0.4 Ma (Stone et al. 2009).

3.4 REGIONAL LITHOSTRATIGRAPHY

The lithologies of the different formations in the target area include (from top of section): ignimbrites (250 m); tuffs and rhyolitic lava (200 m); tuffs and andesitic lava (70 m); and ash tuffs and welded tuffs of rhyolitic and dacitic compositions (100 m) (Gurov et al. 2005, 2007). Thus, rhyolitic rocks amount to 89% and andesitic rocks to 11% of the target composition. Rocks from the crater rim do not display any characteristic shock metamorphic effects. Megabreccia deposits are widespread in some areas of the inner crater wall, especially in the northern and northwestern sectors (Gurov and Gurova 1983; Gurov and Yamnichenko 1995). A more detailed map, updated with recent geological observations and incorporating a host of information from Russian sources, is in preparation by our group.

Shocked target rocks and impact melt rocks occur on the surface, within and adjacent to the El'gygytgyn impact structure, as redeposited material. They are found in lacustrine terraces inside the crater and, locally, in terraces along little streams on the outer slopes of the crater rim (e.g., Gurov and Gurova 1983; Smirnov et al. 2011). Brecciated target rocks (impact breccias) occur under the lake sediments in the central part of the crater as encountered by the 2009 ICDP drill core (see below). The source of the terrace deposits (a mixture of unshocked and shocked rocks, and fragments of impact melt rock) was the ejecta blanket in and around the impact crater, which has been completely eroded. In the absence of ice transport, the material was probably transported to the areas of final deposition in the terraces due to slumping off the rim (in line with the irregular shapes of blocks indicating short-distance transport). Rounded cobbles/pebbles (2-15 cm in size) of reworked impact rocks and blocks of dark impact melt breccia occur only on recent terraces (Smirnov et al. 2011). Aerodynamically shaped glass bombs occur together with shock metamorphosed rocks

in the lacustrine terraces inside the crater and also in terraces along some streams around it. All types of impactites are generally fresh and most of them do not display significant postimpact hydrothermal alteration and weathering (Gurov and Koeberl 2004; Pittarello et al. 2013).

3.5 METHODS

The general information about the depth reached in the D1c drilling was based on drillers' depth. This specification was also used at the sampling party in May 2010. Until now, all scientists working with the impactite section of D1c have been using these depths as discussed in the introductory paper to this issue by Koeberl et al. (2013). Other groups from the El'gygytgyn scientific party have recently adopted slightly different depths, after correlation with a previously drilled shallow core (Lz 1024) from 2003. The result is an offset of exactly three meters (e.g., end of hole at 520.09 m instead of 517.09 mblf). To avoid confusion among the impact science team, we use the field depths.

The core interval from 316 to 517 m depth arrived at the Museum für Naturkunde Berlin in October 2009. Soon thereafter, a complete survey was started of the content of boxes and depths marked on the drilled rocks, which included (1) handling of the core boxes with numbers 1 to 41, which contained consolidated hard rock (129 Q-1 or 393.55 (mblf) to the end at 179 Q-6 or 517.09 mblf); Q is the caliber of the drilling rod (2.5 inches/6.35 cm in diameter). (2) The cores were cut out of their plastic tubes, in which the unconsolidated rocks had been stored after retrieval from the core catcher (98 Q-2 or 316.77 mblf to 128 Q-CC or 393.14 mblf); they had not yet lithified. (3) The cores were carefully washed with fresh water and repacked into new clean and dry core boxes. Also, the fines and remnants of the washing procedure were collected and stored. (4) The drilling depths were checked and all data were logged into the ICDP database. No exact information about drilling depths and intervals of core loss had been provided, so it was decided to set the core loss at the bottom of each core run. In some cases, a core loss of more than 1 m per single core run (a core run with 100% recovery measures normally 3 m) was encountered. (5) This was followed by detailed visual, macroscopic description of the cores, particularly recording lithological properties. The data recorded included texture of groundmass, clast content, the occurrence of melt particles, and deformation features such as fractures and shatter cones, or veining. Color was determined for all parts of the drill core interval according to Munsell's rock color chart. All this information was uploaded with the core scans onto the ICDP webpage (http://www.icdp-online.org/projects/world/asia/lake-elgygytgyn/details/#loaded).

In preparation of the sampling party in May 2010 at the Museum für Naturkunde Berlin, several meters of core were halved, and, subsequently, most of the core was halved.

Following the sampling party, over 600 samples requested by the individual members of the scientific consortium were cut and shipped. The Berlin and Vienna groups obtained approximately 200 samples each. By now, the Berlin group has studied some 140 polished thin sections of core samples and further 35 of country rocks from the collections of the MfN and a first batch of samples collected during the 2011 crater expedition (Raschke et al. 2013b). Optical microscopy was used for lithological classification and first shock deformation analysis. We have also carried out XRF analyses of 150 samples for major and trace elements, 115 of which are from the drill core (Raschke et al. 2013b). MicroRAMAN spectroscopy was used for the analysis of secondary minerals (in particular, zeolites), which were found as infill of glassy spherules in the uppermost part of the impactites and as fracture fill in the lower part of the core interval. First scanning electron microscopic studies of impact breccia groundmass and melt particles were carried out. Instrumental details are given in Raschke et al. (2013b).

In Vienna, 93 samples (38 from the impact breccia and 55 from the bedrock) were selected for petrographic studies, which were conducted by optical and electron microscopy. Further 35 representative samples (20 from the impact breccia and 15 from the bedrock) were selected for chemical analysis. Major and selected minor elements were investigated by X-ray fluorescence spectrometry (XRF), whereas the majority of trace elements were investigated by instrumental neutron activation analysis (INAA). In addition, 19 samples from the unshocked target were prepared for petrographic and geochemical analysis. Details of instruments and methods, as well as data, are provided in Pittarello et al. (2013).

For the description of the lithologies, we used standard terminology (Neuendorf et al. 2005); in the case of the impactites, this follows the International Union of Geological Sciences (IUGS) recommended classification (Stöffler and Grieve 2007). This procedure was also successfully applied for the lithological description of rocks from the Chesapeake Bay ICDP-USGS drilling campaign (Horton et al. 2009). "Suevite" is a polymict impact breccia that contains cogenetic particles of impact melt rock and clasts, which show different degrees of shock metamorphism. The term "polymict impact breccia" is used for impact breccias of polymict clast content, but where it is not clear yet whether they represent lithic impact breccia, suevite, or impact melt rock (Stöffler and Grieve 2007). So far, it has been rather difficult to distinguish volcanic and impact melt particles by optical methodology alone. At this time, 13 samples have been investigated at MfN by microanalytics (electron microprobe analysis). Five of them from the reworked suevite sequence (317.99, 318.13, 318.24, 318.39, 326.51 mblf), six from the suevite (344.17, 352.19, 359.92, 374.93, 382.09, and 389.91 mblf) and one each from the bedrock unit (438.09 mblf) and surface collection (UR-2011_9.11c). We analyzed and compared the impact melt particles from the surface with those from the

drill core. Furthermore, we studied the volcanic melt particles from the lower bedrock unit, from the volcanic clasts in impact breccia, and from surface samples. We established some groups of melt with typical characters in texture and geochemical properties. Now, with these new data, we are able to distinguish, at least in some cases, the impact-related melt from volcanic melt (see Raschke et al. 2013b). As a result, we recognized the polymict impact breccia sequence as a suevite sequence (328 to 390 mblf).

3.6 LITHOLOGICAL UNITS

The 202 m long sequence of impactites and bedrock of drill core D1c shows a wide range of macroscopically discernible properties. Generally, the drilled rocks are strongly altered. This is a major contributing factor to the rather wide color variance observed for the different units. In the upper approximately 100 m, colors range from light gray (sediments and clasts) to red (polymict impact breccia) to black (basaltic block). Obviously, some drilling mud could not be washed out of the cores (especially out of some fractures) or they would have been reduced to silt and sand, so that some color variation must be blamed on this remnant contamination. The lowermost part of this core interval (approximately 100 m ignimbrite) is generally light greenish in color.

During our field trip to the crater in summer 2011 (Zaag et al. 2011), we collected samples from the crater rim that have a similar mineralogy and color to the lower bedrock unit (Raschke et al. 2013b). Only on the surfaces of fractures in the core do secondary minerals, especially calcite and zeolite, occur. In general, the rocks of the upper bedrock sequence appear strongly weathered, with more intense coloration and replacement of minerals and a network of thin calcite veins. The entire core from the impactite interval is fractured, but the upper polymict impact breccia section (328-390 mblf) is dominated by relatively unconsolidated breccia, in which fewer open fractures have been preserved than in the more indurated rocks below. Thus, it does appear that fracture abundance increases with depth. The lowermost hundred meters are locally - and frequently - crushed (cataclastically deformed to monomict-brecciated bedrock).

Apparent core loss produced during the drilling process is very high in the poorly or unconsolidated upper units (316.77-390.74 mblf), with an average loss of 46%. In the relatively homogeneous bedrock units (390.74-517.09 mblf, end of coring), the core loss amounts to an average of 13%. The 202 m impactite sequence was divided into four main lithologies (see stratigraphic column, Fig. 3.4). The uppermost lithology consists of reworked impact breccia (316.77-328.00 mblf) that contains abundant shocked clasts of different target lithologies and melt particles in a sedimentary (sandy) matrix. Because of the definite presence of impact glass beads, this breccia package was classified as reworked suevite. The

underlying polymict impact breccia (328.00-390.74 mblf) has a fine-grained, clast-supported matrix (without apparent sedimentary component) and also does not carry sediment-derived clasts. Abundant melt fragments are mixed in with the clastic component and occur in the fine-grained matrix (Fig. 3.4). Only with electron microscopic studies was it possible to determine the nature of these melt particles and to identify tiny impact melt particles (Raschke et al. 2013b) and, thus, classify this polymict impact breccia as suevite.

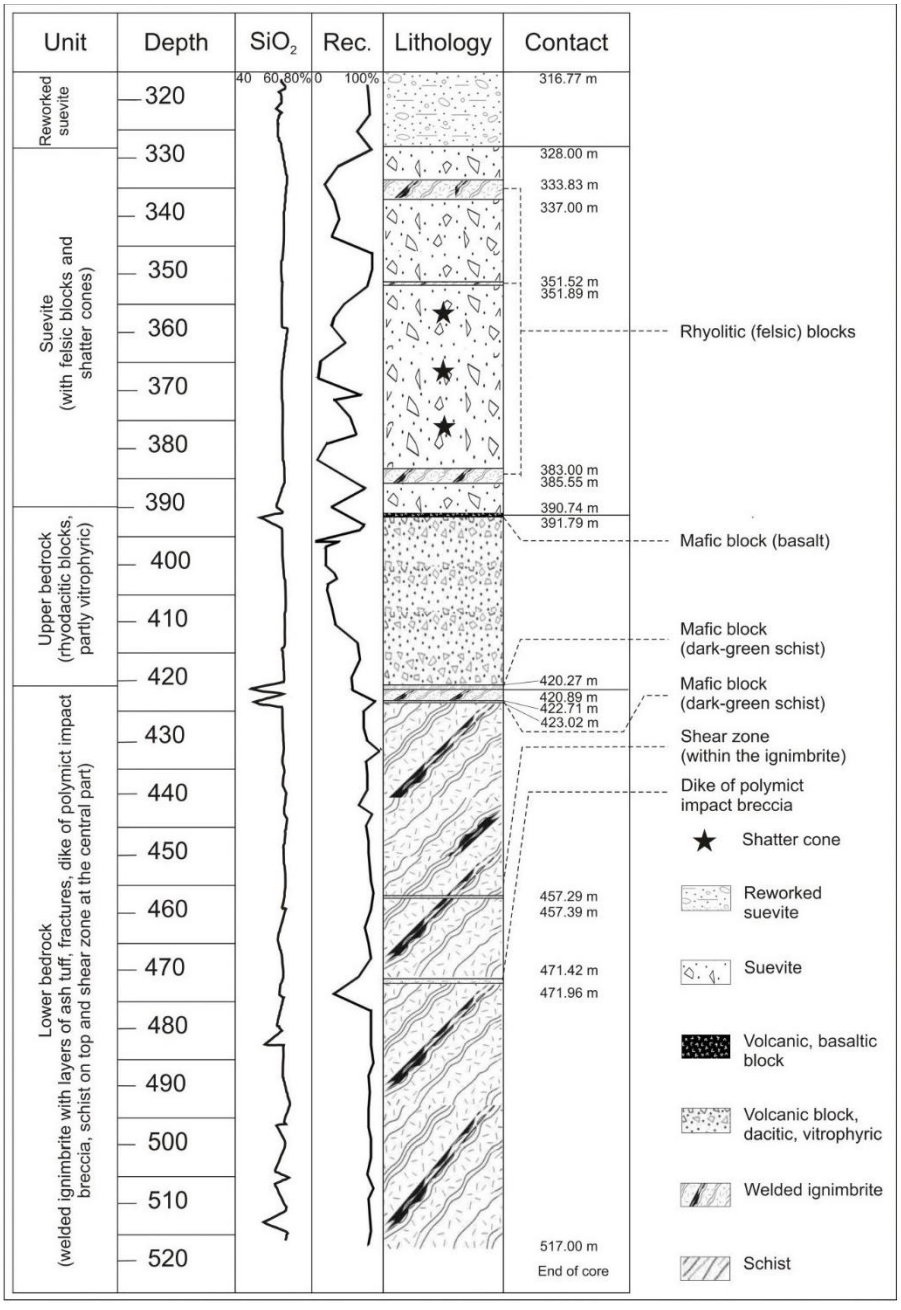

Figure 3.4: Stratigraphic column of the impactite sequence of the El'gygytgyn ICDP drill core. The abbreviation "Rec." means "core recovery."

The sequence below the polymict impact breccia is named the "upper bedrock unit," comprising two different volcanic rock types. The upper one (390.74-391.79 mblf) is from a basaltic lava flow (approximately 1 m), and the second rock type is a dacitic volcanic formation. The lower bedrock unit (421.80-517.09 mblf) is strongly brecciated and consists of a rhyodacitic ignimbrite.

In some cases, it is difficult to determine an exact contact between the units. On the one hand, this could be a result of the drilling, whereby contacts may have been lost due to poor core recovery. On the other hand, there are only slight variations in the compositions of some rocks. For example, the boundary between unit one (reworked suevite) and unit 2 (suevite) is seemingly gradational and only marked by apparent reduction in sedimentary clasts or fine-grained sediment bands (silt, sand) in the impact breccia component.

In the following parts, we provide general descriptions of the individual units. We begin with the description of the contact zone between lake sediments and uppermost impact breccia.

3.6.1 The Transition Zone (313.73-316.77 mblf)

With the support of our colleagues at the universities in Cologne and Amherst, we were able to examine the three meters of core directly above the reworked suevite, which form the Transition Zone between the lowermost true lake sediment and uppermost reworked suevite. As the core curation at Cologne was not completed yet by the time this paper was compiled, exact top depths of the core runs are still unknown. We, thus, give preliminary depths in brackets at this time.

An important first-order observation is that in this transition zone, isolated clasts of up to 3 cm diameter of possible impact rocks occur - like drop stones - in bedded lacustrine sediment (see Fig. 3.5A, top of run 97 Q-1). Then follows a greywacke-like sediment with fine- to coarse-grained sand clasts (middle of 97 Q-1). Below that is an approximately 10 cm wide zone of fine-grained, laminated silt to sand. At the end of 97 Q-1 (depth 314.73 m) occurs fine- to coarse-grained sediment, partly with cross-bedding and some small (approximately 1 cm) lithic clasts. At the top of 97 Q-2 (Fig. 3.5B, 314.80 mblf), a large clast of possible impact breccia, of approximately 5 cm size, was recovered. This clast is embedded in fine-grained sand layers with thicknesses up to 10 cm. Below that occur fine- to coarse-grained, well-bedded layers with clasts up to 2 cm in size (middle of 97 Q-2). At the end of this section, the number and size of clasts increase, with abundant clasts up to 5 cm in size.

3.6.2 The Reworked Suevite (316.77-328.00 mblf)

This approximately 11 m thick unit contains clasts of centimeter to decimeter size of all known target lithologies in a fine-grained, sandy matrix. With increasing depth, clasts are

becoming larger (up to 20 cm), and the sediment layers thinner and more silty. With the disappearance of these layers, the bottom end of this unit is reached, at just about 328 m depth. This unit begins at the top of core run 98 Q-2 (316.77 m) and displays relatively well-sorted matrix of coarse sand (grain size up to 2 mm). There are only several small (approximately 1 cm sized) clasts present. The next core run (98 Q-5, top depth 317.97 mblf)

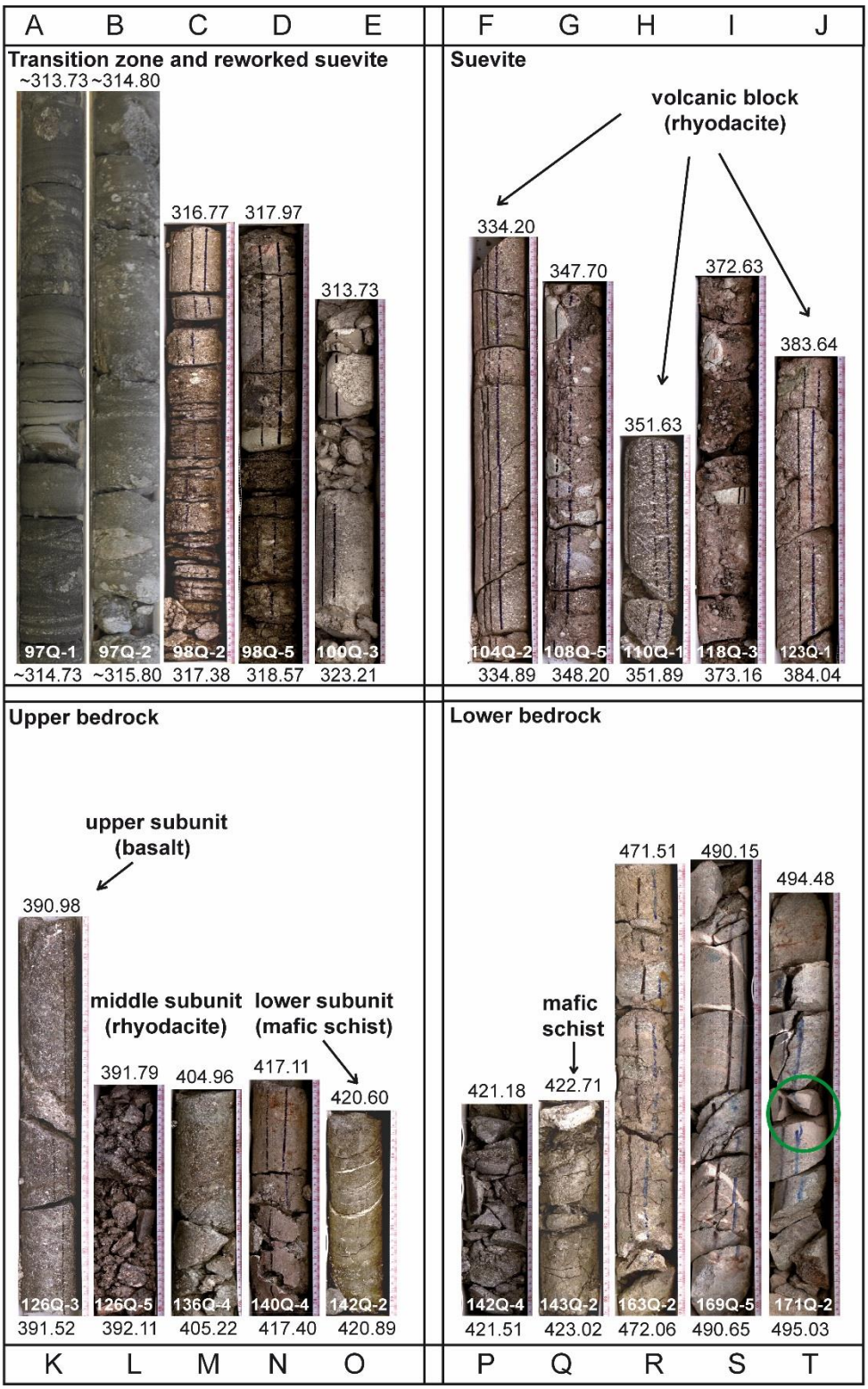

Figure 3.5: Photographs of drill core (diameter: 6.5 cm; depths in mblf, core run indicated by Q-number). A–E) Reworked suevite: A, B) 97 Q-1 and 97-2 are dominated by laminated sedimentary matrix of varied grain sizes (fine to coarse, i.e., mud to sand). Rock fragments and clasts of cm size occur isolated in the matrix. C) Here, with increasing depth, rock fragments and clasts of impactites are more abundant and the matrix shows grain size up to coarse sand. D) This core shows in the consolidated upper part some clasts of 1 to 6 cm sizes, which have different colors. On top is a reddish, 3 cm sized clast of rhyolite; 10 cm lower, an approximately 6 cm wide, gray volcanic clast is embedded in the unsorted matrix. At the middle of the core run occurs a light green clast, which corresponds obviously to the ignimbritic lower bedrock. The matrix contains many blackish clasts of up to 2 cm size. E) In the upper third of core run 100 Q-3 is a pumice-like clast of approximately 6 cm width, which is surrounded by a rim of clay. F–J) Polymict impact breccia: F) 104 Q-2 is a boulder of coherent volcanic rock. G) 108 Q-5 shows clasts of different lithologies in reddish, fine-grained, poorly sorted matrix. H) 110 Q-1 is part of a dark gray, coherent, volcanic boulder. I) 118 Q-3 consists of typical polymict impact breccia with different clasts in a poorly sorted matrix. J) 123 Q-1 is the lowermost volcanic block in the breccia. K–O) Upper bedrock: K) 126 Q-3 represents the basaltic lava flow. L–N) 126 Q-5, 136 Q-4, and 140 Q-4 are representative for the second subunit of rhyodacitic composition, and O) 142 Q-2 is also from the same lithology, but overprinted by tectonic deformation (foliation and fractures, partly filled with white calcite veins). P–T) Lower bedrock: All core runs shown represent the fractured, greenish welded ignimbrite. P) 142 Q-4 is of the uppermost part of the lower bedrock sequence, a strongly brecciated section. Q) shows the small block with dark greenish, fine-grained matrix that does not show phenocrysts. 143 Q-2 is also strongly affected by tectonic deformation. R) 163 Q-2 is part of a 54 cm long section, in which a polymict breccia vein occurs within the bedrock sequence. Different colored clasts are included in reddish to brownish, fine grained, poorly sorted matrix. S) 169 Q-5 contains some of the veins that represent calcite fracture fill. T) 171 Q-2 shows a 3 cm thick reddish vein ash tuff injection (green circle).

with gray matrix has the character of poorly sorted and unlithified sediment with a grain size between fine sand and gravel (0.63-2.0 mm, see Fig. 3.5D, 98 Q-5). In this matrix, no lamination was observed. At 319.70 m depth, there are abundant, although isolated, glassy spherules with sizes between 150 and 400 µm (Fig. 3.6A). They are often filled with zeolites (see also Raschke et al. 2013b). Clasts in the matrix have sizes up to 6 cm and are characterized by varied color ranging from red to gray to black (Fig. 3.5D, 98 Q-5, 317.97-318.57 m depth). Pumice fragments with characteristic beige color and high porosity occur very often in this section of the drill core (Fig. 3.5E, upper third). From 319 to 328 m depth, the matrix-supported character of this breccia changes to a clast-supported one. The unsorted, fine- to coarse-grained matrix consists of the same lithoclasts as the larger fragments. Additionally, there are blackish melt fragments with sizes <10 mm (see also Raschke et al. 2013b). We noted thin veins of clay or fine sand surrounding some larger clasts (Fig. 3.5E, 100 Q-3, 322.68-323.21 m depth). Many clasts show evidence of shock metamorphism. At 319.70 m, we found many shocked quartz grains with up to 4 different orientations of sets of planar deformation features (PDF; Fig. 3.6B). At 321.39 m depth, we discovered a melt clast (Fig. 3.6C) that contains some melted mineral clasts. Figures 3.6C and 3.6D demonstrate that melt clast and inclusions are completely isotropic (impact glass). This thin section image also shows at the margin of this clast the contact between locally recrystallized melt and fine-grained matrix.

Between 317 and 322 mblf, the groundmass contains many small, impact-produced glass spherules with sizes between 150 and 400 µm. Some of these spherules have narrow

glass rims but otherwise are hollow, and others are partly or completely filled with melts after quartz, feldspar, or pyroxene (Raschke et al. 2013b; Wittmann et al. 2013). We propose that this is evidence of impact-melted material and consequently classify this section of core as reworked suevite (see Raschke et al. 2013b).

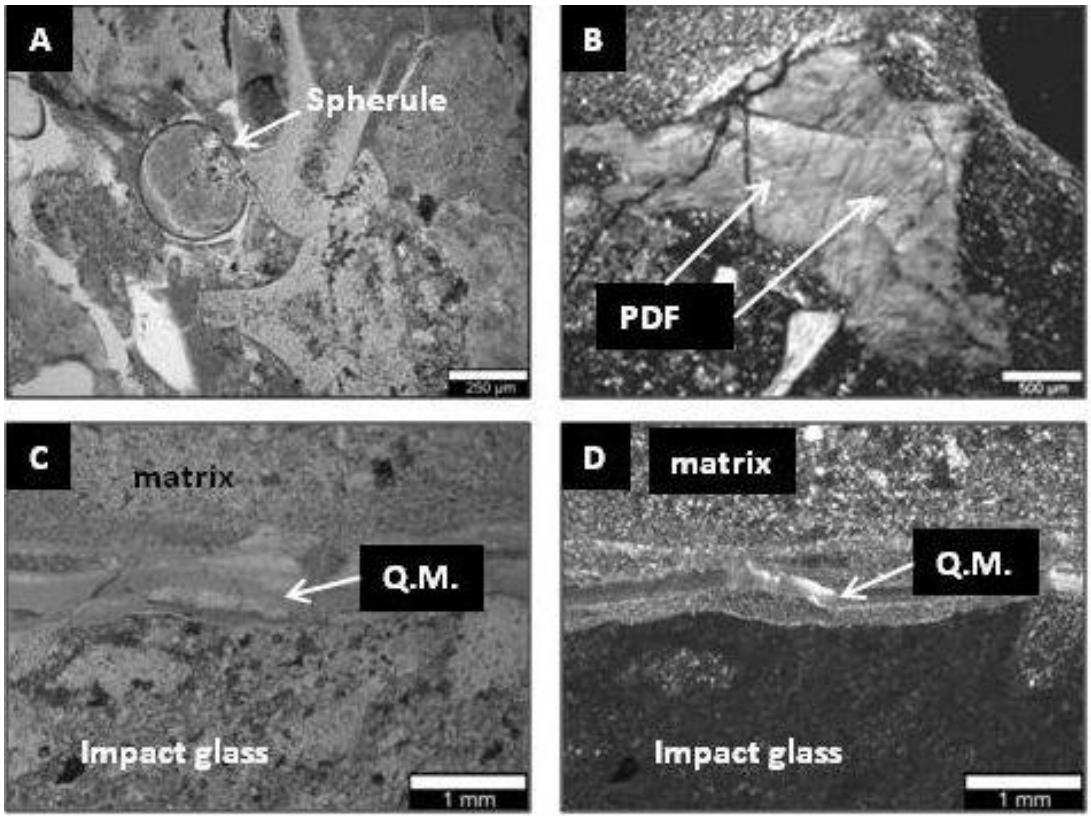

Figure 3.6: Microphotographs. A–D) Reworked suevite: A) Spherule (approximately 450 lm size) filled with zeolite in a fine-grained, polymict matrix (317.90 m). It is thought that this glassy spherule was produced in the vapor plume during the impact and was accumulated into the uppermost part of impact breccia. B) Highly shocked quartz grain with four sets of PDF in a microcrystalline matrix (also 317.90 mblf). C, D) Two images of the same thin section (321.39 m depth) show suevitic breccia with impact glass in the lower half of the images. C: plane polarized light. D: cross polarized light. Above this glassy melt fragment occurs a narrow quench margin (Q.M.), followed by microcrystalline matrix. This type of glass is thought to represent impact melt and was not observed in volcanic deposits such as ignimbrites or lava flows.

3.6.3 The Suevite (328.00-390.74 mblf)

The matrix of this unit is characterized by a reddish to gray color that is dominant over the entire length of this section (Fig. 3.5G, 108 Q-5, 347.70-348.20 m depth). The groundmass is unsorted and only slightly lithified (i.e., the breccia is quite unconsolidated and crumbles easily). Generally, the grain size of the groundmass ranges from fine to coarse sand (0.63-2.0 mm). The lithic microclasts represent the same lithologies as the larger clasts. They seem to be derived from all known target lithologies (basalt, andesite, dacite, and rhyolite). Felsic clasts (i.e., those different from basalt) dominate the population, in keeping with the regional distribution of different country rock types. Presence of melt is not obvious at the

macroscopic scale. But thin section studies show that the matrix contains tiny (<1 mm) melt particles. Only detailed submicroscopic studies provide further information on the genesis of these particles (derived from volcanic target rock or impact-melted). We analyzed six samples of this suevite (344.17, 352.19, 359.92, 374.93, 382.09, and 389.91 mblf) with an electron microprobe and managed to distinguish some different melts with characteristic chemical compositions. Together with the analysis of impact melt breccia from surface and volcanic melt from the lower bedrock unit, it is possible to distinguish melts of impact and volcanic origin (Raschke et al. 2013b).

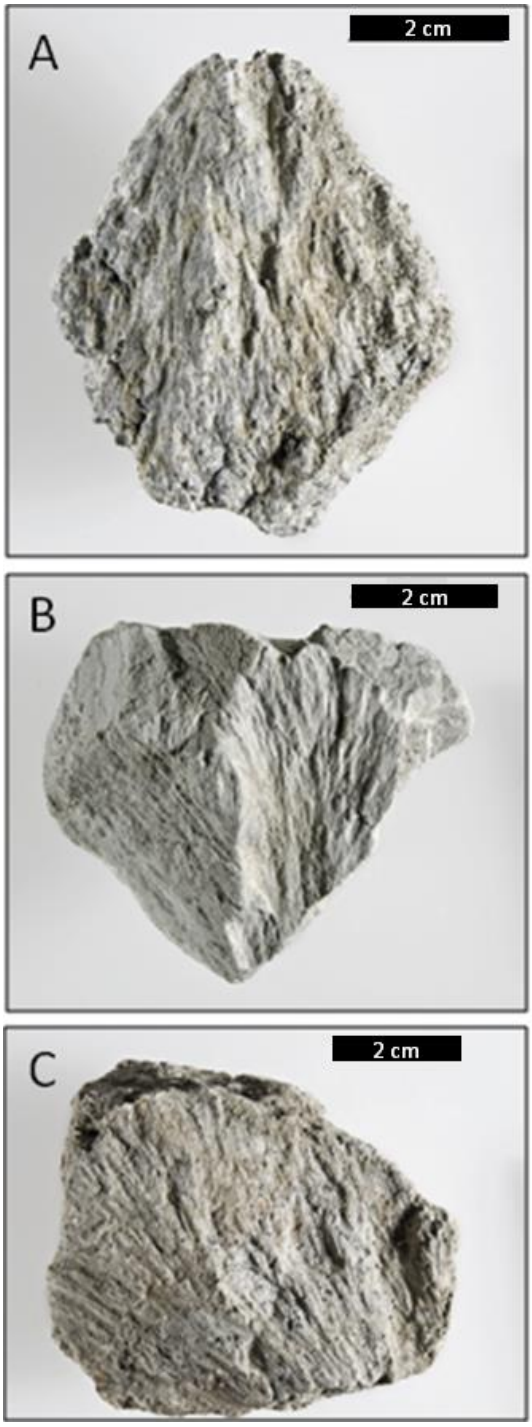

Figure 3.7: Photos of shatter cones in the suevite sequence. A) Shatter cone at 351.79 m depth. B) Shatter cone at 368.35 mblf. C) Shatter cone at 376.24 mblf.

The population of lithic clasts in the suevite interval comprises angular, often brecciated (strongly fractured to cataclastic) clasts ranging in size from 5 mm to 20 cm; they also display a wide range of colors (Fig. 3.5I, 118 Q-3, 372.63-373.16 m depth). Pumice fragments are not as abundant as in the uppermost part of reworked suevite. There are light green clasts of rhyodacitic ignimbrite and typically dark andesitic and basaltic clasts (Fig. 3.5G and 3.5I). Melt particles were not obvious macroscopically. The detailed petrographic analysis (Raschke et al. 2013) showed that many lithic clasts and mineral microclasts are shock deformed. We found evidence for shock metamorphism in quartz in the form of planar fractures (PF), up to four sets of PDF (Fig. 3.6B) per host grain, and very rare diaplectic glass. Within this unit, we detected three clasts of rhyodacite with well-developed shatter cones (Figs. 3.7A-C). This fracturing phenomenon has been considered the only true, mesoscopic indicator of impact ever since its earliest description by Dietz (1947); see also French and Koeberl (2010). The first shatter cone is located on top of a coherent volcanic block of 0.37 m thickness at 351.79 mblf (Fig. 3.7A). The other two were discovered in

larger, and approximately 8 cm wide, clasts from 368.35 and 376.24 mblf (Figs. 3.7B and 3.7C).

At 333-336 and 383-386 m depth, we found two approximately 3 m thick subunits that are interpreted to represent larger blocks of volcanic rock incorporated into the polymict impact breccia. The upper block (333.83-337.32 mblf) is a homogeneous rock with a fluidal texture and a light brown to reddish groundmass. This block includes up to 4 mm large, white to light reddish phenocrysts of alkali feldspar, and darker ones of mafic minerals (<2 mm), as well as melt fragments of up to 3 cm size. This rock is fractured, with fractures spaced at 10 cm or larger intervals. They are oriented at approximately 45° to the core axis (Fig. 3.5F, 104 Q-2, 334.20-334.89 m depth). The geochemical composition showed a high SiO_2 and alkali-element content and corresponds to that of a rhyodacite (Raschke et al. 2013). According to our microscopic studies, shock features in this block are very rare, with only a few planar deformation features (PDF) having been noted in some quartz grains.

At 351.51-351.89 m depth, a small, coherent volcanic block (0.4 m, Fig. 3.5H, 110 Q-1) occurs. It is similar to the block described just before, but its color is slightly darker (dark gray to dark green) and the melt particles are smaller (<1 cm). Shock deformation features could be observed only in the shatter coned specimen. The other parts of this block show no more shock features. Geochemistry and petrography suggest that this is a block of pyroclastic dacite. The texture of this block is different from that of the main lithology in this unit that also comprises fluidal-textured melt particles.

A large clast of similar volcanic rock exists at 383.00-385.55 mblf. This block of an ignimbritic lithology is entirely unshocked (Fig. 3.5J, 123 Q-1). The fine-grained matrix shows many recrystallized minerals, especially tiny quartz crystals. Furthermore, there exist finest needles in the form of radial, spherulitic growths around larger minerals or microclasts. SEM-EDX analysis indicates that they have a feldspathic composition. The small mineral clasts are up to 4 mm in size and consist of feldspar, quartz, and mafic minerals (biotite and rare amphibole). A moderate level of alteration is shown by secondary calcite. The small impact melt particles are mainly weathered to phyllosilicates, mostly chlorite. Iron oxides are dispersed throughout the matrix.

3.6.4 The Upper Bedrock Unit (390.74-420.89 mblf)

This unit can be classified as a monomict breccia. It comprises three subunits. Generally, these rocks display dark colors ranging from brown to black. Numerous fractures occur over the entire length of this section, and below 419.47 m depth, they are frequently filled with calcite. Altogether, this unit is strongly altered, as evidenced by macro- and microscale observations. In the upper part, from 390.74 m to 391.79 m depth, there is a

section of black, homogeneous, and rather massive, although fractured rock. In contrast, the rocks of the underlying bedrock section are not only fractured but actually cataclastically deformed (brecciated).

The upper subunit (390.74-391.79 mblf) is a relatively coherent volcanic section (Fig. 3.5K, 126 Q-3, 391.52 m depth). The brownish groundmass is fine-grained (<2 mm). There are no visible clasts, but white phenocrysts with up to 4 mm sizes. Furthermore, dark, brownish melt particles and thin reddish and white veins can be observed. The vein fillings are commonly secondary calcite. Thin section petrography and geochemical results verify that this section represents a basaltic volcanic flow. In the groundmass, we could identify feldspar, pyroxene (generally of <1 mm grain size), and minor quartz. The quartz grains have slightly larger size (1-2 mm) than the other mineral grains. Rarely - and only in thin sections from the uppermost part of this section - there is evidence of shock metamorphism with up to four sets of PDF in quartz. However, while this section is still characterized by rare, heterogeneously distributed occurrences of shocked grains (cf. also Raschke et al. 2013b), there is no more evidence for shock deformation in samples from the entire core section obtained below 391.79 mblf.

The thin section at 391.72 mblf was taken from an approximately 12 cm reddish-brownish clast occurring within the basaltic flow. Microanalysis shows that this clast represents a rhyodacitic ignimbrite with a microcrystalline matrix with fluidal texture. We also identified pumice fragments and phenocrysts of feldspar, quartz, biotite, hornblende, and a few grains of ore minerals.

The contact to the next subunit of the upper bedrock (between 391.79 and 420.27 mblf) is not present and was lost in the core catcher. This second subunit is composed of moderately to strongly brecciated, reddish-brownish to black volcanic rocks (see Figs. 3.5L-N, 126 Q-5, 136 Q-4, and 140 Q-4). The colors of the fine-grained matrix change from light to dark brown. The groundmass is composed of feldspar, quartz, and mafic minerals, and contains up to 5 mm sized phenocrysts - mostly feldspar, with subordinate quartz. Thin section analysis shows that the occurrence and abundance of vitrophyric glass particles are responsible for the changes in color within this subunit. These dark brownish, glassy melt particles are elongated and orientated preferentially at 90° to the long axis of the drill core. According to major element analysis (Raschke et al. 2013b), this subunit has a uniform, rhyodacitic composition.

From 391.79 to 404.48 mblf, a blackish and moderately brecciated volcanic rock occurs. With a gradual transition follow the underlying rocks (from 404.48 to 407.28 mblf) that are reddish to brownish and strongly brecciated. Vitrophyric glass particles are not abundant; in contrast, reddish pumice fragments are important. This succession characterized

by changing color and varied predominance of different volcanic melt phases is repeated over the next meters of underlying rocks. From 407.28 to 413.60 mblf, the dark, vitrophyric glass particles are predominant. The transition to the rocks above this vitrophyric volcanic flow is obviously gradual with a several centimeter-wide zone of reworked reddish rock fragments. At 413.60 mblf, a relatively sharp contact with an abrupt change to the reddish-brownish ignimbrite with characteristic pumice fragments occurs. These rocks and the whole subunit are ending at 420.27 mblf.

The transition to the third, lowermost, schistose subunit between 420.27 and 420.89 mblf is sharp, but not well preserved. This third subunit comprises a dark green volcanic rock with a closely spaced foliation and, in places, significant grain size reduction to clay particle size. The foliation forms an angle of approximately 45° to the long axis of the core (believed to have had vertical orientation). Thin calcite veins fill some open joints (Fig. 3.5O, 142 Q-2, 422.71 mblf depth). Microscopic analysis revealed that this part has the same fluidal texture as the rest of this subunit. Besides this, it is enriched in some metal elements (e.g., Ni, Cr, Fe) compared with the other volcanic units in this drill core (for more detail, refer to Raschke et al. 2013b). The contact to the underlying lower bedrock unit is again clearly defined and sharp.

3.6.5 The Lower Bedrock Unit (420.89–517.09 mblf)

This sequence is - on first impression - a homogeneous volcanic rock without significant changes over its entire length of almost hundred meters. Closer inspection, however, reveals some special features. Generally, the rather consolidated drill core has light green color and numerous dark gray to black melt particles of generally elongated, often undulating forms. Most are about 1 cm wide and up to 6 cm in length. An additional feature of this package is the strong brecciation of the core, with abundant fractures at all depths, especially in the uppermost part of this unit. Fractures are variably oriented with angles of 30-45° to the core axis in the upper part. With increasing depth, the angle changes to approximately 75° to the long axis of the drill core (see Raschke et al. 2013b). They are often filled with white to yellowish minerals (calcite and zeolite, Fig. 3.5S, 169 Q-5, 490.15-490.65 mblf). A unique, 54 cm wide vein with a filling of variegated polymict breccia occurs as 471.42-471.96 m depth (see Figs. 3.5R and 3.8E). Microscopy revealed that some quartz grains are shock deformed (up to three sets of PDF per host quartz grain), which allows us to conclude that this vein represents an injection of polymict impact breccia into the bedrock. Melt particles were recorded, but it is not clear yet whether they are volcanic or impact melt.

The groundmass of this volcanic rock consists of microclasts of up to 4 mm size. They include small grains of plagioclase, alkali feldspar, quartz, biotite, and amphibole.

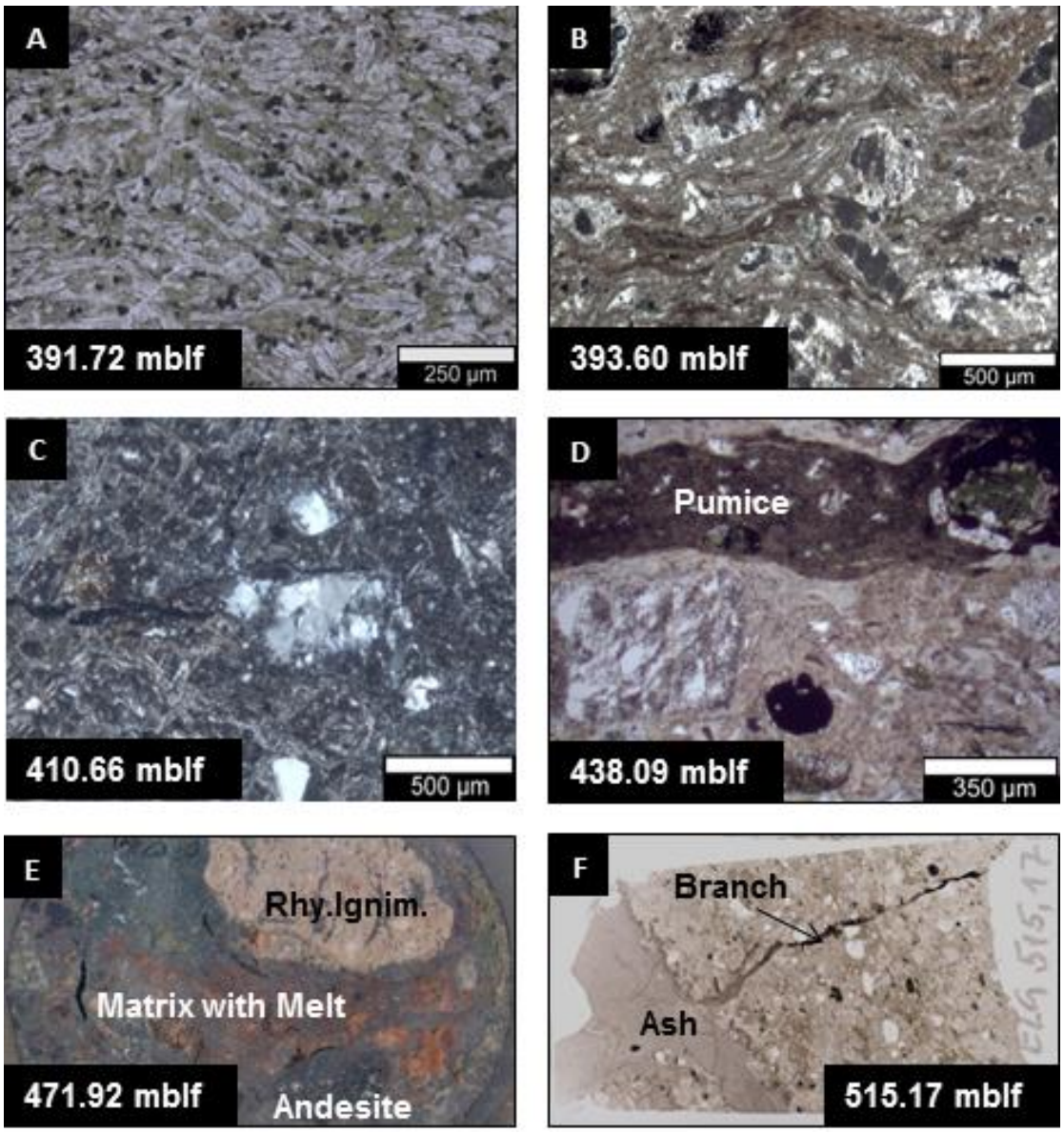

Figure 3.8: Microphotographs of thin section scans. A-C) Upper bedrock: A) Thin section of a sample from 391.72 m depth shows an intersertal fabric dominated by feldspar crystals, typical for a basalt; cross polarized light. B) Characteristic fluidal texture of the volcanic boulder at 393.60 m depth; plane polarized light. C) Microphotograph (cross polarized light) of a thin section of a sample from 410.66 m depth displays a vitrophyric matrix with few quartz and feldspar crystals. D-F) Lower bedrock; D) Detail of pumice melt fragment from 438.09 m depth; plane polarized light. D) Thin section scan of a typical welded ignimbrite with melt (pumice) fragments and phenocrysts of feldspar and quartz, 438.09 mblf, plane polarized light. E) Image of drill core (size 6 x 4 cm) from 471.92 mblf depth, with a large clast of ignimbrite and a smaller clast of andesite in fine-grained, melt poor matrix. F) Thin section scan (area shown is 48x24 mm wide) of a reddish, finest grained vein with a vein branching off across some phenocrysts in the ignimbrite, at 515.17 mblf depth, plane polarized light.

Large phenocrysts are not present, but melt particles up to 6 cm size are common. The macroscopically visible melt inclusions are pumice fragments that include the same minerals as the groundmass, except quartz. Such pumice fragments are called "fiamme" in the current volcanological nomenclature (McBirney 1968; Sparks et al. 1999), and are a characteristic

feature of ignimbrites (hot pyroclastic volcanic flow). In this lower bedrock section, these small fiamme bodies are mostly oriented at 45° to the long axis of the drill core (see Fig. 5T, 171 Q-2, 494.48-495.03 mblf). The fractures are developed subparallel to the magmatic foliation, which is determined by pumice fiamme alignment due to compaction, following the original emplacement.

The uppermost part of the lower bedrock unit at 420.89-421.51 m depth, the ignimbritic bedrock, is strongly fractured (as shown in Fig. 3.5P, 142 Q-1). From 422.71 to 423.02 m depth occurs an isolated block of dark green volcanic rock of 31 cm length. It has a fine grained matrix (grains <1 mm) and a close-spaced foliation (Fig. 3.5Q, 143 Q-2). We interpret this block as a xenolith picked up by the ignimbrite mass.

In the lowermost part of the unit (423.03-517.09 mblf), we found some red to brownish veins of 2 mm to 3 cm width and aligned along the preferred orientation of the melt particles in this unit (Figs. 3.5S, 169 Q-5, 490.15-490.65 m depth and 3.5T, 171 Q-2, 494.48-495.03 mblf). The thin section scan shows in Fig. 3.8F a vein of 2 cm width. From this vein, a smaller one branches off and penetrates the host rock cutting through its idiomorphic phenocrysts. The vein filling consists of finest material of what could be fine-ash particles (<10 µm in average). At 515.94 m depth, a similar vein was observed that contains some zeolite grains as well. It is surrounded by a very fine grained cataclastic zone, which is in transition to larger crystals and fragments of the ignimbrite bedrock. Further investigations are necessary to determine the true character(s) of these veins in the lowermost part of the drill core. One thought that is currently entertained is that they could represent ash tuff injections into fractures off the surface of a volcanic flow.

Geochemical compositions (Raschke et al. 2013b) demonstrate that the whole unit has a rhyodacitic composition, except for the small greenish section located at the top of this unit. Here, the SiO_2 content is relatively depleted and the basaltic composition is similar to that of the greenish block at the end of the upper bedrock unit. The polymict vein around 471.92 m depth and the reddish veins at the end of the core have essentially similar compositions to the rhyodacitic volcanics. The presence of fiamme and the microscopic character of this section (Raschke et al. 2013b) indicate that this lower brecciated bedrock unit is a welded ignimbrite of rhyodacitic composition.

3.7 DISCUSSION AND CONCLUSION

The 517 m long ICDP drill core D1c from the Lake El'gygytgyn can be subdivided into an upper sedimentary part and a lower impactite (i.e., impact-generated breccia or impact-affected volcanic rock) part. The 202 m studied section exhibits a range of impact lithologies and bedrock varieties. On top, from 316.77 (contact not sharp) to approximately

328.00 m, occurs the zone of reworked suevite. This mixture contains lacustrine sediments and intercalated, often strongly shocked, rock fragments of various target lithologies. It also includes impact melt particles, impact melt spherules, shocked minerals with PF and PDF, and some rare diaplectic glass (see Raschke et al. 2013b). Thin section studies revealed shock features in mineral inclusions within glassy melt particles. These are similar to our observations on samples of impact melt breccia from the surface of the outer crater provided by C. Koeberl in 2009.

The underlying unit (328.00-390.74 m) is a sequence of altered, polymict impact breccia with crystalline clasts and melt particles in a clast-rich, fine-grained groundmass. We observed several types of melt at the thin section scale. Further investigations by electron microscopy and with the electron microprobe allowed us to distinguish the phases and determine the nature of these melt particles. We have been able to verify the existence of impact melt particles and, thus, to confirm that this unit represents suevite. The clasts in this unit show evidence for various stages of shock metamorphism (unshocked particles to rare diaplectic glass, i.e., they cover the shock range from <5 to 30 GPa). Additionally, we found three shatter cones at different depths in this unit. Three sizable volcanic blocks of coherent target material are incorporated in this sequence as well. The upper two of these show evidence of weak shock metamorphism (rare PDF and a shatter cone). The lower block is completely unshocked. It is obvious that these blocks have their origin in the outer zone of the transient crater and were included into the polymict impact breccia during collapse/crater modification.

The upper bedrock unit consists of two different volcanic rocks. These rocks are strongly altered. The upper subunit has a basaltic composition and shows some evidence of shock metamorphism. The second volcanic block has a rhyodacitic chemical composition and is completely unshocked. The contact to the underlying lower bedrock unit is characterized by quite strongly sheared dark green volcanic rock. This subunit shows a very low SiO_2 content and is much enriched in some metals compared with the other lithologies. Additionally, there are many thin calcite veins that are oriented parallel to the foliation of this unit. The strongly altered nature of this section suggests that this could be the actual crater floor that has been strongly affected by hydrothermal alteration.

The lower 90 m are a homogeneous welded ignimbrite that is also present in the crater area as recently observed during a field expedition in July 2011 (Raschke et al. 2013b). This unit does not show any traces of shock metamorphism, and hydrothermal alteration is much reduced. Fracturing is still strong and part of this section is actually cataclastically overprinted. Fractures are partly filled with calcite or zeolite and show the same orientation as the fiamme structures in this ignimbrite. From 471.42 to 472.06 m depth, a vein of polymict

impact breccia is injected. During the collapse of the central uplift, this polymict impact breccia might have been injected into an opening fracture in the basement.

Over the last meter of drill core, several centimeter-wide veins of a fine-grained material occur. They could represent ash tuff fillings of joints in the ignimbrite emplaced during or after the accumulation of this pyroclastic rock. This would be consistent with the microcrystalline content of these veins. On the other hand, we see that the veins cut phenocrysts of the ignimbrite and that veins are rimmed by cataclastic layers (see Figs. 3.5P and 3.5Q). This could suggest that the veins have their origin in the impact process and that they were emplaced in the course of impact-induced tectonic movement in the subcrater basement. Additional work on these injections is required.

In contrast to Wittmann et al. (2013), who consider these lowermost sequence blocks derived from an outer part of the impact structure, we favor that these volcanics represent crater basement. Our argument is based on the observation that the moderate-to-steep attitudes of these rocks as illustrated by the considerable angles of foliation, fractures, and fiamme alignment are consistent with the drilled location being located on the central uplift of the El'gygytgyn impact structure, where a somewhat deformed bedrock sequence must be expected.

Acknowledgments

This work has been funded by the German Science Foundation through DFG projects Re 528/10-1, RE 528/10-2, and RE 528/12-1 to WUR and by Austrian Science Foundation (FWF) project P21821-N19 to CK. Drilling and logistics were supported by ICDP, the U.S. National Science Foundation, the German Ministry of Research and Education, the Russian Academy of Sciences, and the Austrian Ministry for Science and Research. DOSECC is acknowledged for collecting the core, partner negotiations, equipment innovation, and drilling expertise. We owe special thanks to the technicians at the Museum für Naturkunde Berlin: Hans-Rudolf Knoefler and Kathrin Krahn for the preparation of thin sections and sample preparation for geochemical analysis, and Kirsten Born for support with scanning electron microscopy. Patrice Zaag was highly supportive in the lab and in the field. Discussions with our colleagues at the University of Cologne were very helpful with regard to the nature and stratigraphy of the Transition Zone and Reworked Suevite units.

Editorial Handling - Dr. John Spray

Note: This chapter was also updated for more correctness in spelling and grammar. Some references were specified with "a" or "b". On page 47: ages cited in the text were corrected. On page 64: the figure caption was slightly modified for more clarity.

CHAPTER 4

PETROGRAPHY AND GEOCHEMISTRY OF IMPACTITES AND VOLCANIC BEDROCK IN THE ICDP DRILL CORE D1C FROM LAKE EL'GYGYTGYN, NE RUSSIA.

This Chapter has been published as the following peer-reviewed article:

Raschke U., Schmitt R. T., and Reimold W. U. 2013b. Petrography and geochemistry of impactites and volcanic bedrock in the ICDP drill core D1c from lake El'gygytgyn, NE Russia. *Meteoritics and Planetary Science* 48:1251-1286, http://dx.doi.org/10.1111/maps.12087.

4.1 ABSTRACT

The 3.6 Ma old and 18 km diameter El'gygytgyn impact structure in NE Siberia was drilled in 2008/09 by ICDP (International Continental Scientific Drilling Program). A 517 m long core hole (D1c) was drilled into the outer flank of the central uplift structure, with an overall core recovery of approximately 63%. Thereby, approximately 315 m lake sediments and approximately 202 m impactites were recovered. Here, we present a detailed petrographic and geochemical assessment of the impact breccia and bedrock sections in this core. The 97 m long lower bedrock unit (517-420 m below lake floor [blf]) consists of an ignimbrite. In the overlying upper bedrock unit (420-390 mblf), the core recovered a sequence of similar ignimbrite and several decimeters of mafic rocks. We interpret these units as rocks that are located close to their former, preimpact position, but have been somewhat rotated due to collapse of the central uplift (i.e., it represents parautochthonous basement). From about 390 to 328 mblf occurs a suevite package with an impact melt-poor, clast-dominated matrix, and lithic and mineral clasts that cover the entire range of volcanic target rocks known from the El'gygytgyn region. All stages of shock metamorphism (unshocked to melted) were observed in clasts, and in microclasts of the matrix, of suevite from different depths. Immediately below this package, at the contact to the underlying bedrock, occurs a 1 m wide sheared zone within vitrophyric ignimbrite, which we consider the actual crater floor. The uppermost approximately 12 m, from 328-316 mblf depth, seem to comprise reworked suevite, consisting of a mixture of sediments and suevite with more and, on average, stronger shocked minerals than found in the main suevite unit. This includes a small component of glassy spherules and impact melt fragments. Toward the top of this unit, lake sediments progressively become the dominant material in this section. We assume that this unit contains a fallback component from the ejecta plume that was mixed with the first sediments of the

postimpact crater lake, and possibly some rocks that slumped off the inner crater wall - similar to a thin layer at the base of the sediment section of borehole LB-5A recovered in Lake Bosumtwi (Ghana).

4.2 INTRODUCTION

The 3.58 ± 0.04 Ma old (Layer 2000) El'gygytgyn impact structure is located on the Chukotka Peninsula of northeast Russia (Gurov et al. 1978; Gurov and Koeberl 2004; Koeberl et al. 2013). The 18 km diameter, complex impact structure was formed in a siliceous volcanic target of the Anadyr mountain belt, which is part of the Ochotsk-Chukotka Volcanic Belt (Belyi 1977; Gurov et al. 1979; Gurov and Gurova 1991). The crater structure (Fig. 4.1) is largely covered by Lake El'gygytgyn. Seismic investigations suggested that the 12 km wide and 170 m deep crater lake (Nolan et al. 2003) is underlain by lacustrine sediments with a thickness of 360-420 m. The lake is somewhat offset from the crater center. The crater basin consists of an approximately 7.2 km wide central ring depression around an approximately 4 km wide central uplift (Gebhardt et al. 2006).

The target lithologies were described by Gurov et al. (1978) and Gurov and Gurova (1983) based on geological exploration along the crater rim and in its environs. The target lithologies comprise a suite of volcanic rocks that belong to the approximately 88 Ma old Pykarvaam Formation and the 83.1 ± 0.4 Ma old Koekvun' Formation (Stone et al. 2009). This suite is supposed to encompass (from top to bottom) ignimbrites (250 m), tuffs and rhyolitic lava (200 m), tuffs and andesitic lava (70 m, especially to the southwest of the crater), and ash tuffs and welded tuffs of rhyolitic and dacitic compositions (100 m) (Gurov et al. 2005, 2007). In addition, remnants of an approximately 110 m thick basalt sill occur at the northeastern crater rim, and Paleogene basalt was found approximately 15 km downstream along the Enmyvaam river (Gurov et al. 2005; U. Raschke and P. T. Zaag, Museum für Naturkunde Berlin, unpublished results). The general attitude of the pyroclastic flows and lava beds at the crater and in its surrounding area shows a gentle dip with 6-10° to the east-southeast (Gurov et al. 2007).

The crater rim is almost completely preserved, except for the southeastern part that has been breached by the Enmyvaam river that constitutes a periodic outflow from the lake. Rocks of the crater rim do not display any characteristic shock metamorphic effects (Gurov et al. 2007). The ejecta blanket around the impact crater has been nearly completely eroded by arctic weathering. Remnants can only be found in the form of redeposited material in lacustrine and fluvial terraces inside and outside of the crater rim (Smirnov et al. 2011).

Petrographic studies of these rocks have shown various impact-induced shock features. Planar deformation features (PDF), diaplectic glass, and high pressure polymorphs of quartz (coesite and stishovite) were found by Gurov et al. (1978, 1979b, 2005). In addition, Glushkova and Smirnov (2007) found glassy spherules in lake terrace deposits in the southern part of the crater structure and in fluvial terraces of the Enmyvaam river. Such spherules were analyzed by Adolf and Deutsch (2010), Smirnov et al. (2011), and Wittmann et al. (2013). They are considered impact-produced droplets deposited from the collapsing ejecta plume. In addition, impact rocks ranging in size from lapilli to bombs were also found at lake terraces (Gurov and Koeberl 2004; Pittarello and Koeberl 2013).

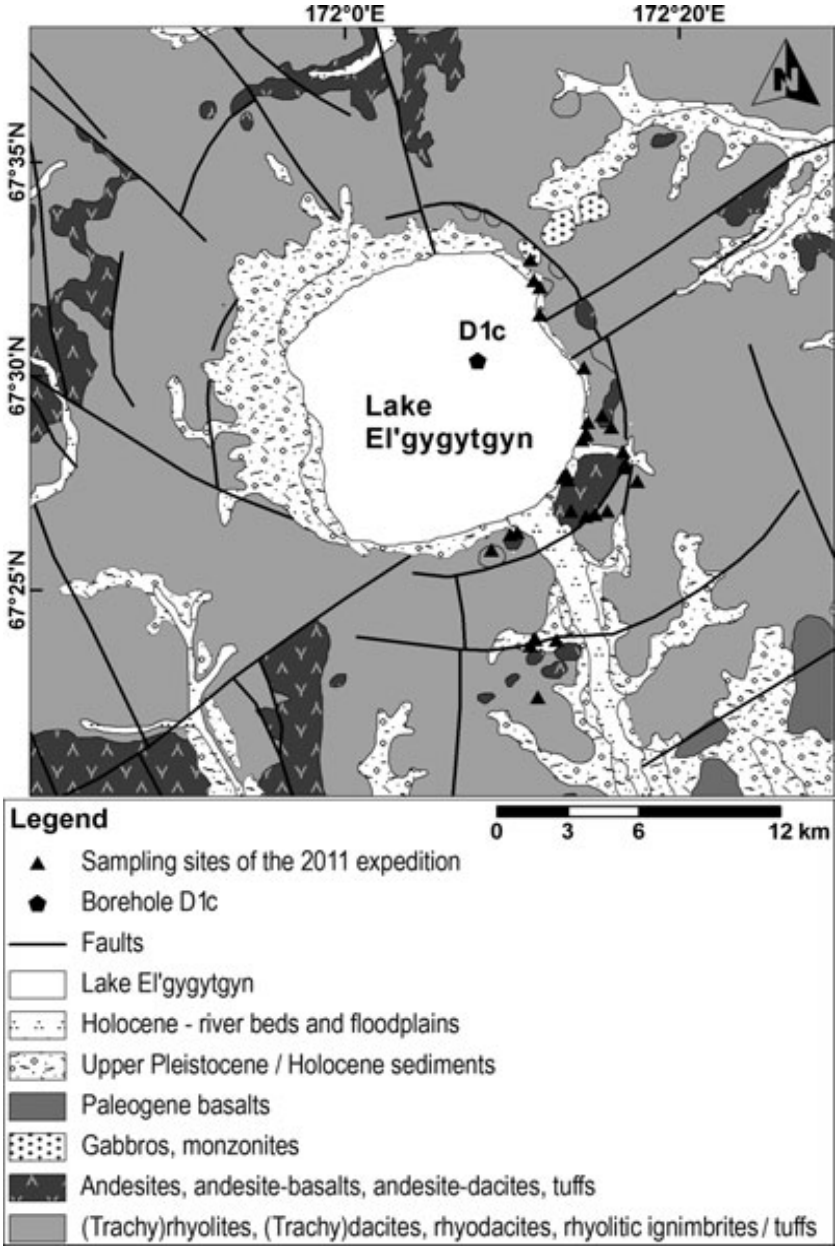

Figure 4.1: Simplified geological sketch map of the El'gygytgyn impact structure based on the Russian geological map (Raevsky and Potapova 1984; Zheltovsky and Sosunov 1985).

During winter 2008/2009 a drilling campaign was conducted at Lake El'gygytgyn by the International Continental Scientific Drilling Program (ICDP). Three boreholes were drilled from the frozen crater-lake surface (Koeberl et al. 2013; their figs. 5 and 6). The deepest drill hole D1c (Fig. 4.1) was presumably sunk against the outer slope of the central uplift. It penetrated 225.3 m lacustrine sediments and, below that, 207.5 m of impact rocks. Core recovery for this latter sequence is 157.4 m, or 76%. Drilling was terminated at a depth of 517 m below lake floor (mblf) (Melles et al. 2011). A detailed stratigraphic description of the impactite section of the core is contained in Raschke et al. (2013a; see also Fig. 4.2).

The general information about the depth reached in the D1c drilling was based on drillers' depths. This specification was also used at the sampling party in May 2010. Until now, all scientists working with the impactite section of drill core D1c have been using these depths as discussed in the introductory paper to this issue (Koeberl et al. 2013). Other groups from the El'gygytgyn scientific party have recently adopted slightly different depths, after correlation with a previously drilled shallow core from 2003 (drill core Lz exactly three meters (e.g., end of drill hole at 520.09 mblf instead of 517.09 mblf, as applied here).

In this contribution, we present petrographic observations and geochemical data for the different units of core D1c, which describe the typical character of the various formations present. Particular emphasis is placed on the nature of the impact breccias and shock metamorphic observations. In addition, we compare the chemical character of the core units with the geochemistry of the volcanics sampled in the environs of the crater.

4.3 SAMPLES AND METHODOLOGY

From October 2009 to May 2010 the impactite section of the drill core (from 316 to 517 mblf depth) was curated at the Museum für Naturkunde Berlin. The initial core description is available on the ICDP homepage (http://elgygytgyn.icdp-online.org). In May 2010, an international sampling party was held in Berlin, and after that the preparation of the samples for petrographic and geochemical analysis was started (see Raschke et al. 2013; Koeberl et al. 2013). Currently, we have 143 thin sections for the 202 m impactite sequence at our disposal. For the description of the different lithologies of target rocks and impactites we applied standard terminologies, which were also successfully used in 2009 for the Chesapeake Bay ICDP drill core description (Horton et al. 2009; Raschke et al. 2013a).

Petrographic analysis was carried out with standard polarizing microscopic equipment. For higher magnification analysis a scanning electron microscope (SEM) of the type JEOL JSM-6610LV, equipped with a LaB_6-cathode and a BRUKER Quantax 800 energy-dispersive X-ray spectrometry (EDX) system, was applied.

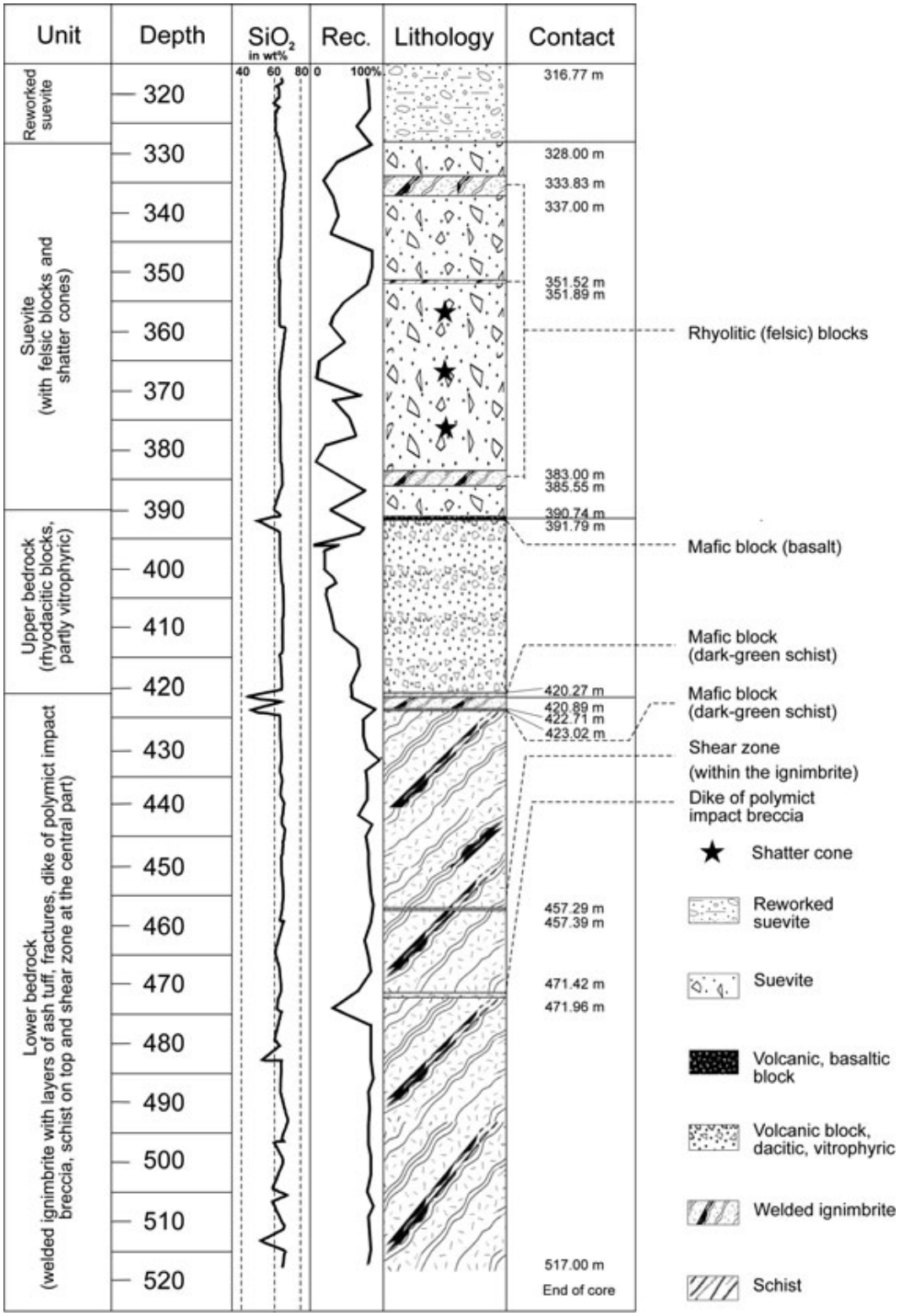

Figure 4.2: Stratigraphic column of the impactite sequence of the El'gygytgyn-ICDP drill core D1c. The abbreviation "Rec." means "core recovery."

Compositional and back-scattered electron (BSE) images and chemical analyses of melt particles were obtained using a JEOL Superprobe JXA-8500F electron microprobe (EMP) with online data reduction. A cup current of 15-20 nA with an acceleration potential of 15 keV and an electron beam diameter of 1 to 2 µm were used for single spot and profile analyses (EMPA) to minimize loss of sodium during the measurements. Peak counting time was 30 s for most elements with the exception of Na and Mn with counting times of 20 and 40 s, respectively. The background was evaluated for 15 s on either side of each peak. For mineral identification we used a DILOR LabRam Raman spectrometer with an integrated HeNe-Laser of 632.8 nm wave length. All three instruments reside at the Museum für Naturkunde Berlin.

For whole-rock chemical analysis we used 20 to 50 g per sample, depending on available sample size, grain size, and density. The samples were taken from the center of drill core specimens, and special attention was employed to avoid contamination due to the drilling process. Samples from the reworked suevite and suevite, and from a polymict impact breccia dike in the lower bedrock were prepared for analysis by avoiding lithic clasts with diameters larger than about 0.3 cm. If necessary, relatively large visible lithic clasts were removed manually. Samples were ground using sintercorundum grinding devices.

Whole-rock chemical analysis was carried out by X-ray fluorescence spectroscopy (XRF) with a BRUKER AXS S8 TIGER instrument on fused samples (major elements) and powder pellets (trace elements). For production of the fused samples we used 0.6 g of powdered sample material, which was dried at 105 °C, 3.6 g of di-lithiumtetraborate, and, depending on the oxidation grade of the sample, between 0.5 and 2.0 g NH_4NO_3. Fused samples were produced in Pt/Au crucibles (950/50) on an OXIFLUX burner chain. Major elements were measured using an analytical program based on 40 certified international rock standards (CERAM 2CAS11, CCRMP MRG-1, CCRMP SY-3, HUN BaH, IGEM MK-1 [VS 2125-81], IGEM MO-2 [VS 2116-81], IGEM MO-3 [VS 2117-81], IGEM MO-5 [VS 2119-81], IGEM MO-6 [VS 2120-81], IGEM MO-7 [VS 1046-94], IGEM MO-13 [VS 1044- 94], IGEM MO-15 [VS 1017-94], IGEM MW-1 [VS 2121-81], IGEM MW-2 [VS 2122-81], IGEM MW-3 [VS 2123-81], IGI BIL-1 [VS 7126-95], IGI BIL-2 [VS 7176-95], MINTEK NIM-D [SARM 6], MINTEK NIM-G [SARM 1], MINTEK NIM-L [SARM 3], MINTEK NIM-N [SARM 4], MINTEK NIM-P [SARM 5], MINTEK NIM-S [SARM 2], MINTEK SARM 39 [X-39], MINTEK SARM 40 [X-40], MINTEK SARM 41 [X-41], MINTEK SARM 44 [X-44], MINTEK SARM 45 [X-45], MINTEK SARM 46 [X-46], MINTEK SARM 50 [X-50], RIAP OOPE401 [VS 5370-90], RIAP OOPE501 [VS 5372-90], UNS SpS, ZGI BM, ZGI FK, ZGI GM, ZGI GNA, ZGI SW, ZGI TB, ZGI TB2, ZGI TS; see Govindaraju [1994] for description of these standards and analytical data), and 10 reference

standards (SIEM-01–SIEM-10) by SIEMENS AG, Karlsruhe. For the powder pellets 9.00 g of powdered sample material, dried at 105 °C, were mixed with nine grinding aid tablets (POLAB of POLYSIUS AG). The powder pellets were pressed with a HERZOG tablet press (HTP) at a force of 15 t and under constant force for a duration of 20 s. The determination of trace element concentrations uses the BRUKER AXS GEOQUANT V1.3 measurement program, which was also calibrated using international rock standards. Detection limits are as follows: 1.0 wt% for SiO_2; 0.5 wt% for Al_2O_3; 0.05 wt% for Fe_2O_3; 0.01 wt% for TiO_2, MnO, MgO, CaO, Na_2O, K_2O, and P_2O_5; 15 ppm for Cu, Zn, and Pb; 10 ppm for Y, Zr, Nb, Ba, La, and Ce; and 5 ppm for Sc, V, Cr, Co, Ni, Rb, and Sr. Accuracy values on data presented here are 0.5 wt% for SiO_2; 0.1 wt% for Al_2O_3; 0.05 wt% for Fe_2O_3, MgO, CaO, Na_2O, and K_2O; 0.01 wt% for TiO_2, MnO, and P_2O_5; 30 ppm for Ba; 25 ppm for Cu; 20 ppm for Zn, La, Ce, and Pb; and 5 ppm for Sc, V, Cr, Co, Ni, Rb, Sr, Y, Zr, and Nb. The precision values on these data are about the same order or lower.

To determine loss on ignition (LOI), about 1 g of powderized sample material, dried for four hours at 105 °C, was used. The sample was heated in porcelain crucibles for four hours at 1000 °C. LOI was calculated using the weight difference between measurements before and after heating. Detection limit, precision, and accuracy values for LOI are about 0.1 wt%.

4.4 THE STRATIGRAPHY OF THE IMPACTITES BETWEEN 517.09 AND 316.77 MBLF DEPTH

The 202 m long section of impact/impact-affected rocks of the ICDP drill core D1c can be divided into four major units (Fig. 4.2), as discussed in detail by Raschke et al. (2013). From the end of the core at 517 mblf to 421 mblf, a relatively homogeneous ignimbrite of porphyritic texture constitutes the lower bedrock unit. No evidence for shock metamorphism was observed here. From 421 to 390.74 mblf a sequence of different volcanic blocks was intersected, which range in composition from basaltic to rhyolitic; this section is termed the upper bedrock unit. At the top of this strongly altered sequence the lowermost occurrence of shock metamorphosed minerals was recorded (at 391.72 mblf depth). Above this, up to 328 mblf, a unit of polymict impact breccia dominates. In this unit, shocked minerals and melt clasts abound. In the following we will present evidence that this unit contains impact melt particles and, consequently, represents a suevite unit, consistent with the definition by Stöffler and Grieve (2007). In addition, three larger blocks of almost unshocked volcanics are included in this breccia. Three shatter cones were observed during sample cutting (Raschke et al. 2013). A gradual transition from the suevite to the uppermost unit, classified as reworked suevite, begins at 328 mblf. This uppermost unit ends at 316.77 mblf, where the lake sediment

section is reached (Melles et al. 2012). Major components in this unit are fragments of lacustrine sediments and shock metamorphosed volcanic clasts. In the upper 2-3 m of this unit we recognized a general trend of fining upward (normal gradation). Here, an abundance of clasts with shock evidence (e.g., PDF in quartz grains) and occurrence of impact glass are observed. In the upper part of the reworked suevite, the matrix has a sedimentary character, and above 316.77 mblf depth the lacustrine accumulations dominate the core. There are some isolated volcanic rock clasts of up to 20 cm length in this unit as well (Raschke et al. 2013).

4.5 RESULTS

4.5.1 Petrographic Analysis

4.5.1.1 The Lower Bedrock (517.09 to 420.89 mblf)

This unit comprises dominantly the lower bedrock, but there are also a dike of polymict impact breccia, thin ash veins, and a mafic block at the top (see also Raschke et al. 2013a). The lower bedrock is mainly composed of a relatively homogeneous, trachyrhyodacitic (see below), welded ignimbrite. Petrographic observation shows some variation in texture. This lithological section can be subdivided into two intervals of ignimbrite. The first one occurs between 517.09 and 457.45 mblf, and the second one between 457.39 and 420.89 mblf. The distinction between these two subunits is based on petrographic observations and geochemical results. In both sections we observe a typical ignimbritic texture with elongated pumice fragments, so-called "fiamme" (Figs. 4.3A and 4.3B), in a greenish, fine-grained matrix. From 471.42 m to 471.96 m depth a dike of polymict impact breccia is present (see Raschke et al. 2013a) that contains some shocked quartz grains. At the top of this section (422.71-423.02 mblf) occurs an approximately 30 cm wide, dark green block of basaltic composition. The extremely fractured block has a sharp contact to the ignimbrite bedrock around this isolated block.

4.5.1.2 The Welded Ignimbrite

This lithology occurs from 517.09 to 423.02 mblf, and from 422.71 to 420.89 mblf. The light greenish rock has a micro-crystalline matrix that consists of crystals or crystal fragments of feldspar (mostly plagioclase that is partly seriticized), clear quartz, and some alkali feldspar. The mafic minerals are biotite and minor amphibole. At the edge of the crystals spherulitic recrystallization of SiO_2-rich melt is observed. These radial growth structures are typical for magmatic (or volcanic) rocks (see also Pittarello et al. 2013) and indicate relatively rapid quenching of the pyroclastic flow. Supported by the matrix occur larger, elongated, and flattened pumice fragments (fiamme) with a width of up to 3 cm and a length of up to 8 cm (Fig. 4.3A). "Fiamme" are lens-shaped particles, usually millimeters to a

few centimeters in size. They can occur in welded pyroclastic fall deposits and, especially, in ignimbrites, which are the deposits of felsic pumiceous, pyroclastic density currents. The name fiamme has a relation to the Italian word for flames, which describes their shape. The term is descriptive and is not used for genetic interpretation (see Kobberger and Schmincke 1999). These brownish to blackish glassy melt particles contain the same minerals that also occur in the groundmass, and which constitute a typically eutaxitic texture. Furthermore, the pumice fragments have an irregular, interfingering contact to the surrounding microcrystalline matrix and show remnants of gas bubbles (see also Pittarello et al. 2013). These vesicles have a rim of glass which is often altered with a reddish color and devitrified (see Fig. 4.3B). This is characteristic for a welded ignimbrite (e.g., McBirney 1968; Kobberger and Schmincke 1999; Pittarello et al. 2013). The pumice fragments are characteristically oriented at approximately 45° to the core axis, but higher angles are possible as well (e.g., Fig. 4.3A) and most fractures are also oriented parallel to this dominant orientation. The pumice fragments are generally moderately altered and some have a thin greenish alteration, which is caused by the presence of chlorite, along the contacts to the groundmass. Smaller (<5 mm) melt particles are mostly completely altered to chlorite and other phyllosilicates.

4.5.1.3 The Contact or Shear Zone Between the Two Subunits of Ignimbrite

Macroscopically we found between 457.29 and 457.39 mblf a narrow zone of light greenish, finest-grained material with a sharp contact to the bedrock above and below. The contact zone, which is only a few millimeters wide, is indicated by a darker color, in comparison to the surrounding ignimbrite. The cause of this coloration is thought to be a grain-size reduction (cataclasis, Fig. 4.3C). Studies of thin sections have shown that the light gray to greenish matrix includes fragments of minerals (especially feldspar and quartz) with relatively smaller grain size in comparison to the minerals in the host rock above and below. These phenocrysts occur in this zone, together with clasts, in a locally parallel arrangement. Local displacements of mineral fragments (Fig. 4.3D) are also observed. We interpret these observations as evidence for the presence of a narrow shear zone. We observed microfractures in this narrow shear zone that are mainly filled by secondary, reddish carbonate. Only with microscopic observation we could identify another small shear effect. The microphotograph of the sample from 498.97 mblf (Fig. 4.3E) shows a rotated rigid clast enveloped by fiamme.

A similar observation was reported by Kobberger and Schmincke (1999) from Gran Canaria. The approximately 20 m thick rhyodacitic ignimbrite can be divided into four structural subzones. The vitrophyric basal zone with uniaxial flattening of pumice fragments is overlain by a shear zone with synthetically rotated boudins, shear bands, and strongly

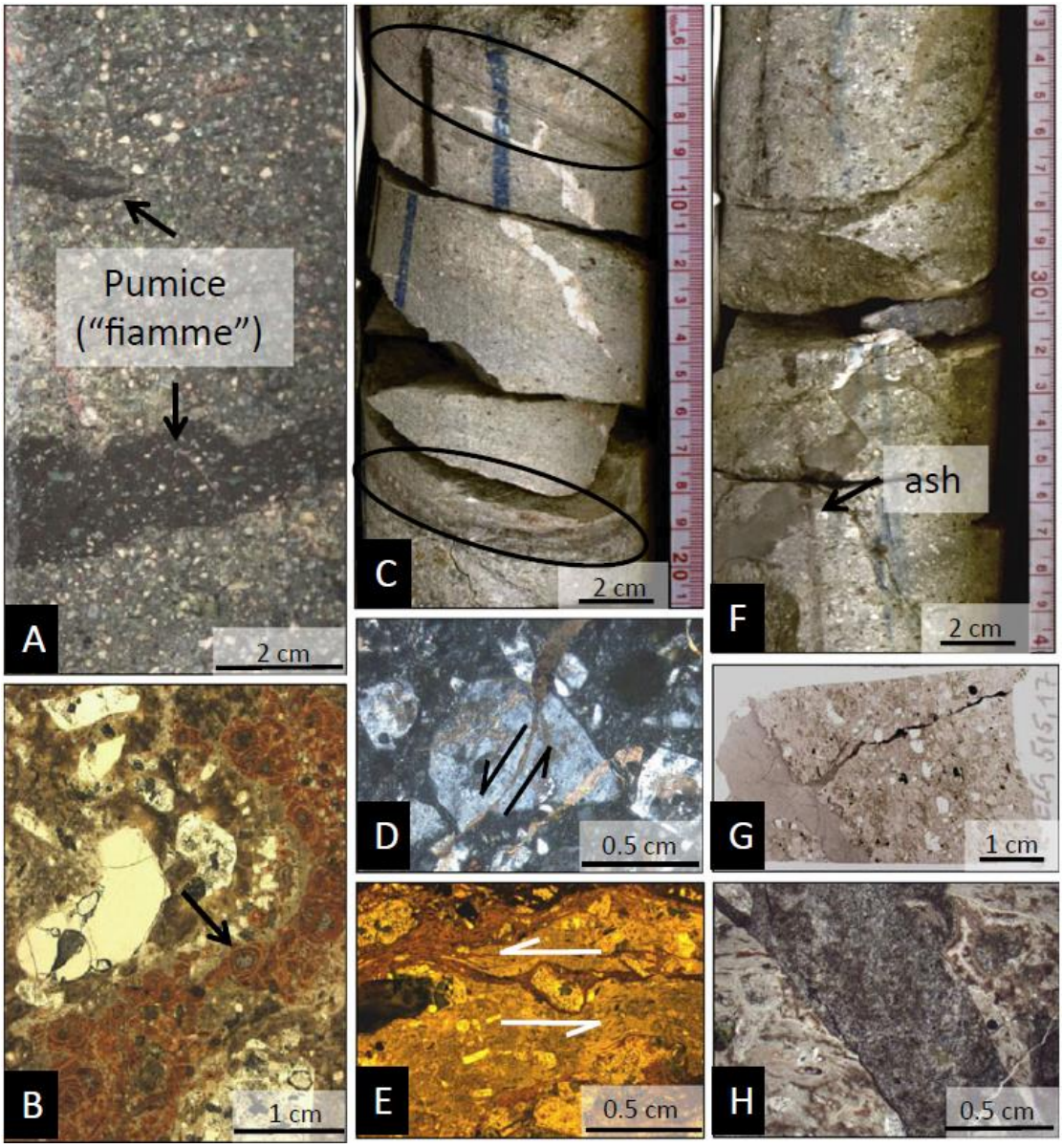

Figure 4.3: Images of the lower bedrock unit. A) Elongated pumice particles, oriented at high angles to the long axis of the drill core (506.12-505.95 mblf, length approximately 16 cm). B) Pumice fragment ("fiamme") and phenocrysts in the ignimbrite at 498.94 mblf depth. Note that the fiamme contains small, round vesicles. These red-brown bubbles (arrow) are filled with crystalline material. C) Cataclastic and shear zone in the ignimbrite at 457.39 mblf. This zone is about 10 cm wide and shows a grain-size reduction close to the contact to the ignimbritic host rock (black circles). D) Cataclastic fabric with broken and displaced quartz grain in the center (457.32 mblf depth, cross polarized light). E) Microphotograph (plane polarized light) from a sample at 498.97 mblf showing a rotated rigid clast enveloped by fiamme. F) Sample from a half drill core at 515.17 mblf showing the red-brownish ash vein with a sharp contact to the ignimbritic host rock. Note the offset of this vein, obviously a result of postvolcanic stress. G) Thin section scan from the same depth; the dark ash vein has a narrow branch that filled a very narrow fracture in the ignimbritic host rock. H) Microphotograph of the same structure (plane polarized light). The central ash vein has a well-defined contact to the surrounding ignimbrite.

foliated inclined fiamme. The central zone consists of flattening and stretching with symmetrical pressure features and is strongly foliated, but without shear bands. The top zone shows slight uniaxial flattening with brecciation (e.g., conjugate, extension cracks). Pumice fragments are abundant in all zones, and with increasing pressure from the weight of the ignimbrite flow they are successively more flattened. The development of a shear zone is dependent on the highest shear strain, occurring near the basal zone.

4.5.1.4 The Ash Tuff Veins

From approximately 490 mblf to the end of the drill core there are a number of red to brownish veins of 2 mm to 3 cm width that are oriented more or less parallel to the preferred orientation of the pumice particles in this unit. First petrographic observations suggest that they are veins of volcanic ash, which were injected into fractures off paleo-surfaces within this ignimbrite sequence (see also Raschke et al. 2013). Figure 4.3F shows such a "vein" from 515.17 mblf depth. A thin section scan (Fig. 4.3G) displays that this ash vein is approximately 1 cm in width and has a small branch, which has filled a narrow fracture in the volcanic rock. A microphotograph (Fig. 4.3H) illustrates a close-up of the sharp contact between host rock and ash vein. Further SEM and EMPA investigation of this material is still necessary to fully evaluate the character of these veins.

4.5.1.5 Shock Metamorphism

Within this entire unit we did not find any clear evidence for shock metamorphism, except within the polymict breccia dike at 471 mblf depth. This dike is discussed below in comparison with the main polymict impact breccia (suevite) package. In contrast to our observations on this lower bedrock unit, Pittarello et al. (2013) observed a single quartz phenocryst with basal planar fractures (PF) and PDF in a thin section of a sample from 431.80 mblf depth. This, too, does not emphasize significant shock metamorphic overprint of this unit. The lower bedrock unit is strongly brecciated and the fractures have a general orientation of about 45° relative to the long axis of the core. The fractures are partly filled by secondary minerals (zeolite and calcite).

4.5.1.6 The Upper Bedrock Unit (420.89 to 390.74 mblf)

This unit contains two mafic blocks between 420.89 and 390.74 mblf. Between them, from 420.27 to 391.79 mblf, occurs a pyroclastic, volcanic block that with regard to mineral composition and texture is generally similar to the trachyrhyodacitic ignimbrite of the lower bedrock. Vitrophyric glass particles are abundant and dominate two zones from 413.60-407.28 and 404.28-391.79 mblf (Raschke et al. 2013). They likely represent two separate volcanic flows. They are composed mainly of crystal fragments that are set into a

microcrystalline matrix. Typical phenocrysts are mainly feldspar, quartz, and biotite. The groundmass contains dark brownish, vitrophyric melt particles in a fluidal texture (Fig. 4.4A).

The interval between the vitrophyric flows is filled by a reddish, pumice-rich ignimbritic rock. Here, parallel-oriented melt fragments occur in a feldspar-dominated, fine-grained, fluidal-textured matrix. The pumice fragments are smaller (up to 10 mm long and a few mm thick) than those in the lower bedrock ignimbrite. They are aligned at an angle of approximately 90° to the core axis. Alkali feldspar forms the largest mineral grains, with sizes up to 3 mm. Quartz, plagioclase, biotite, and some opaque minerals (e.g., titanomagnetite) constitute the micro-crystalline groundmass. This, and the elongated melt fragments, gives this lithology a character similar to that of the ignimbrite from the lower bedrock.

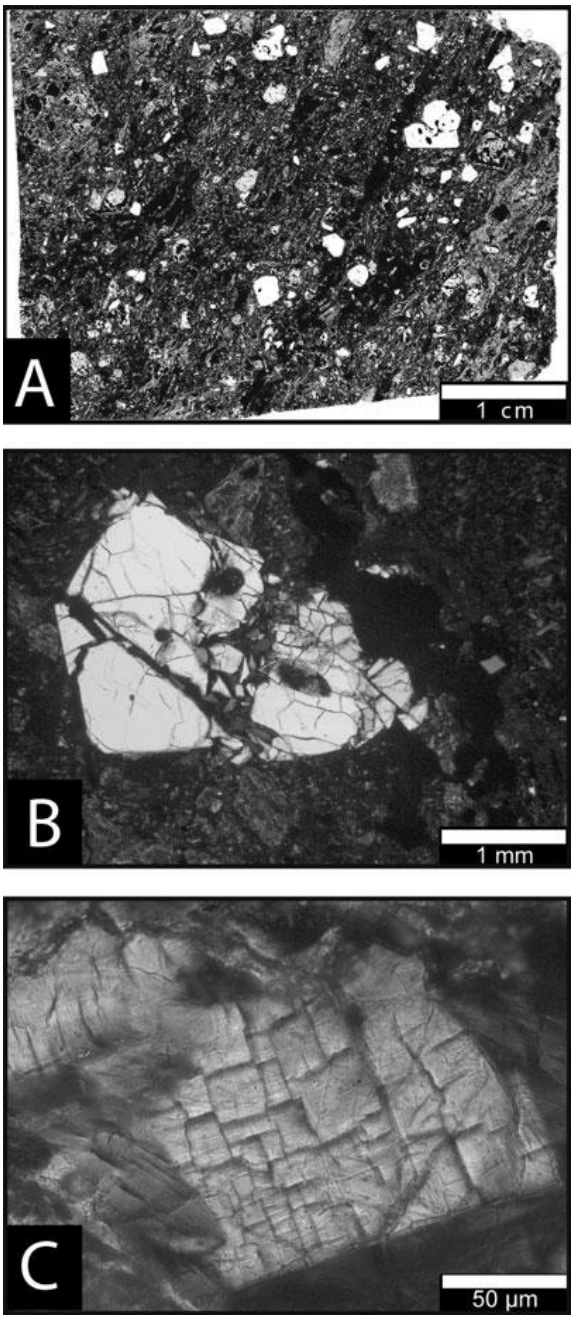

Figure 4.4: Upper bedrock. A) Thin section scan from the sample at 393.60 mblf showing elongated, vitrophyric particles together with larger, mainly feldspar phenocrysts. B) Thin section image (cross polarized light) of a strongly fractured quartz grain in the sample from 404.79 mblf. C) Another image from the same thin section (cross polarized light) shows a subhedral, intricately fractured quartz grain.

The rock has a rather fractured character, which has certainly contributed to its local disintegration during drilling. This is also illustrated, at the microscopic scale, in Figs. 4.4B and 4.4C (sample from 404.79 mblf). The broken quartz grain in the center of the microphotograph of Fig. 4.4B is typical for the mineral fraction in this unit. Figure 4.4C shows an unusual style of mineral brecciation. It is possible that this feature represents crude rectilinear PF related to weak shock metamorphism. But this feature is not typical and, in fact, we have not found other diagnostic evidence for shock metamorphism in this interval. The strong alteration of this interval is represented by thin reddish

calcite veins that occur throughout the whole unit and which are visible also in the central part of Fig. 4.4A, and by microscopically visible alteration of the different minerals. Ferromagnetic or mafic minerals (biotite, hornblende) show chloritization and partial replacement by carbonate. Alkali feldspar is often sericitized. Plagioclase contains abundant secondary carbonate at grain margins.

4.5.1.7 The Mafic Blocks in the Lower and Upper Bedrock Units

The first block with a size of about 30 cm occurs at the top of the lower bedrock unit between 423.02 and 422.71 mblf. The dark green rock is extremely weathered and brecciated, with local comminution to clay particle size; thus, it appears similar to a greenschist. The rock contains relatively few plagioclase phenocrysts in a microcrystalline matrix that is dominated by greenish phyllosilicate minerals (chlorite). The second mafic block of the upper bedrock occurs between 420.89 and 420.27 mblf and appears similar to the first one. It is penetrated by thin, white calcite veins that are oriented parallel to each other at an angle of approximately 45° to the core axis (Fig. 4.5A). Microscopy and geochemistry (see below) indicate that this block represents basalt, dominated by up to 4 mm large crystals of feldspar and pyroxene (Fig. 4.5B). The minerals are strongly altered; plagioclase and biotite are frequently replaced by calcite, and are embedded in a microcrystalline matrix of the same minerals. This groundmass has a green to brown color, is largely altered to phyllosilicates, and contains small, roundish vugs that are filled by chlorite and calcite. It is assumed that the roundish vugs (Fig. 4.5C) were gas bubbles inside a lava flow.

At the top of the upper bedrock unit, from 391.79 to 390.74 mblf, occurs the last mafic block of this unit. A thin section from the sample from 391.72 mblf (see Raschke et al. 2013, their fig. 3.8A) shows typical, fine-grained basalt with a matrix dominated by small plagioclase crystals. Together with relatively few pyroxene crystals, they constitute a porphyric texture. Small black dots in the microphotograph are opaque minerals (mainly Fe- and Fe-Ti oxides). Furthermore, thin white to reddish veins can be identified as fractures filled by secondary calcite. Rare shocked quartz grains are recognized in a thin section of the sample from 391.72 mblf (Fig. 4.5D), which constitutes the lowermost occurrence of significant shock deformation. The illustrated quartz crystal contains at least two differently oriented sets of PDF. In addition, we found feather features (FF), another effect of shock metamorphism (Poelchau and Kenkmann 2011). Alteration of this rock is quite strong, but not as extensive as that of the lower mafic blocks.

A sample from 391.72 mblf shows a completely different texture. Glassy melt particles are dominant in the matrix, where they display a fluidal-texture arrangement. Phenocrysts are formed by feldspar, quartz, rare biotite, and amphibole. This clast is a

rhyolitic ignimbrite, which is strongly fractured and altered. The feldspar minerals have been partly replaced by carbonate. Fracturing is illustrated by a crushed plagioclase grain in Fig. 4.5E. Here, both shearing and displacement of fragments are apparent.

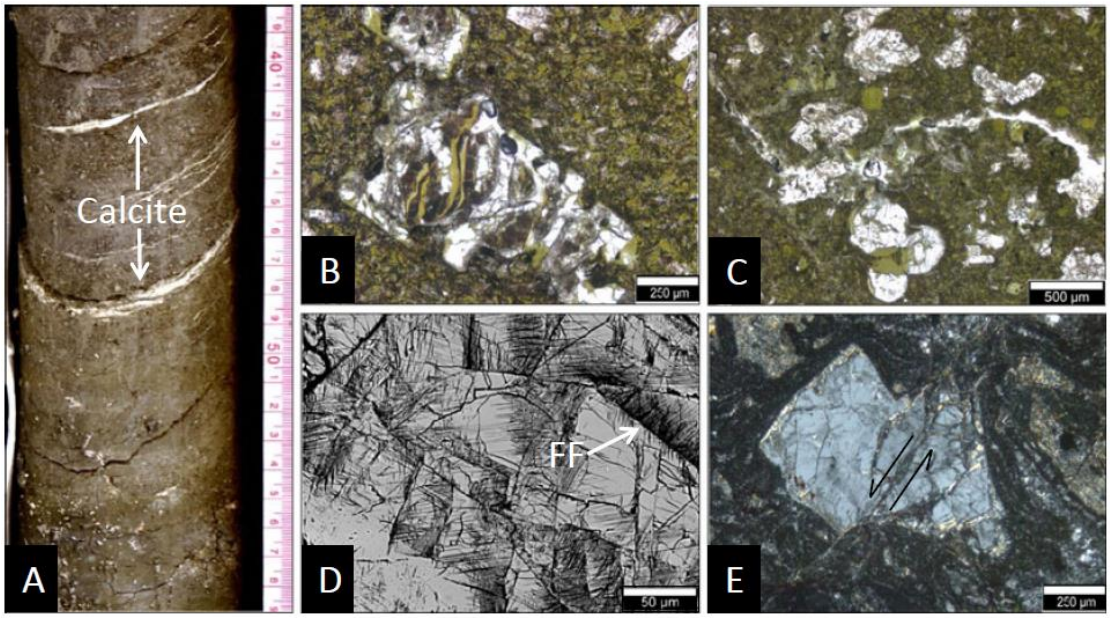

Figure 4.5 (a-e): Mafic blocks. A) Scan of drill core from 420.89 to 420.69 mblf. The thin white veins are calcite fillings of narrow fractures, which are oriented at about 45° to the core axis. Scale in centimeters. B) Thin section scan for a specimen from 420.60 mblf. The light to dark green color of the sample stems from the fact that matrix and pyroxene porphyroblasts are strongly chloritized. C) Thin section image (plane polarized light, sample from 420.60 mblf) showing the strongly altered groundmass with chlorite (green) and rare vesicles, which are filled with calcite. D) Backscattered electron image of a quartz grain from a sample at 371.73 mblf depth. At least two sets of planar deformation features (PDF) occur and in the upper right corner of the image feather features (FF) are visible coming off both sides of a subplanar fracture. E) Thin section image (cross polarized light) for a sample from the uppermost part of this unit at 391.72 mblf. The groundmass consists of glassy fragments with fluidal texture and phenocrysts, which are often crushed. The fragments of the brittle feldspar grain show obvious displacement.

In summary, this uppermost mafic block shows an internal transition from an intact basaltic flow to a monomict breccia of this material. The lower part is a typical basalt flow with plagioclase, pyroxene, opaque minerals, and some rare shocked quartz grains. Brecciation and alteration are relatively severe. Secondary minerals are abundant and occur as white to pinkish single crystals or as thin, penetrative veins. The upper part is an assemblage of vitrophyric particles (fragments of glass shards) and fragments of basalt. This assemblage has been brecciated as well and is weathered to the same secondary minerals. This upper section represents the contact zone to the overlying polymict impact breccia. All three mafic blocks are extremely brecciated, with evidence of local shearing and crushing. Hydrothermal alteration was very effective, as indicated by the high LOI of the chemical analyses (Table S1).

4.5.1.8 The Polymict Impact Breccia Revealed as Suevite (390.74 to 328 mblf)

The polymict impact breccia unit occurs from 328.00 to 390.74 mblf. In addition, a small dike of very similar polymict impact breccia occurs between 471.42 and 471.96 mblf in the lower bedrock unit. A general overview of this lithology and the included felsic blocks has been given in Raschke et al. (2013a). Here, we present additional information on different kinds of melt particles and clasts, many of which display shock metamorphism.

The breccia is matrix-supported. Groundmass contains both lithic and mineral clasts. Larger clasts range in size from 5 mm to 20 cm and cover the full range of volcanic rocks found within the wider crater area. This includes blackish basalt and andesite, reddish trachyrhyolite and dacite, and greenish ignimbrite (Fig. 4.6A). The breccia is poorly sorted, especially in the upper part where many clasts reach sizes up to 20 cm. With increasing depth, the clast size variation is somewhat less and the breccia appears more sorted. This trend is also supported by the analysis of the clast population discussed below.

Many clasts show a porphyric texture with euhedral to subhedral feldspar and quartz crystals in a microcrystalline matrix, similar to the rocks that make up the bulk of the upper and lower bedrock units. Most of the rock fragments are unshocked. In addition, there are light colored clasts with pumice-like, fluidal textures that contain some subhedral phenocrysts of feldspar and quartz in a glassy matrix. We could not observe clear evidence of shock features in such clasts and we consider that these melt clasts originate from a possible pumiceous lithology, such as that described by Gurov et al. (1979a, 2005) from the crater environs. In addition, three larger blocks of felsic volcanics occur at depths of 385.55-383.00, 351.89-351.52, and 337.00-333.83 mblf (see also Raschke et al. 2013a).

Generally, the groundmass of the polymict impact breccia has a reddish color. Partly responsible could be remnants of the drilling mud that penetrated into the otherwise almost unconsolidated material during the drilling process. It was not advisable to completely remove this clayey deposit during core preparation, as this would have risked complete disintegration of the breccia. Mineral and lithic clasts from this unit are strongly altered, and secondary minerals (calcite, zeolite) occur throughout this package in the form of single crystals or fillings of thin veins of white to light reddish or pink color. Some of this secondary material was revealed to represent carbonate.

The groundmass of this unit consists of microfragments derived from the same volcanic rocks also forming the larger clasts, besides single crystals of their minerals, and small melt particles (Fig. 4.6B). The crystals, with grain sizes up to 4 mm, mostly have subangular to subrounded forms. An approximately 2 mm long microfragment of ignimbritic target rock is embedded in the fine-grained matrix (Fig. 4.6C). Quartz is generally fresh;

plagioclase and biotite are moderately to strongly altered and partly coated by, or converted to, carbonate, chlorite, and sericite. Further minerals found are pyroxene, alkali feldspar, amphibole, and zircon. Few quartz and feldspar grains show evidence of shock

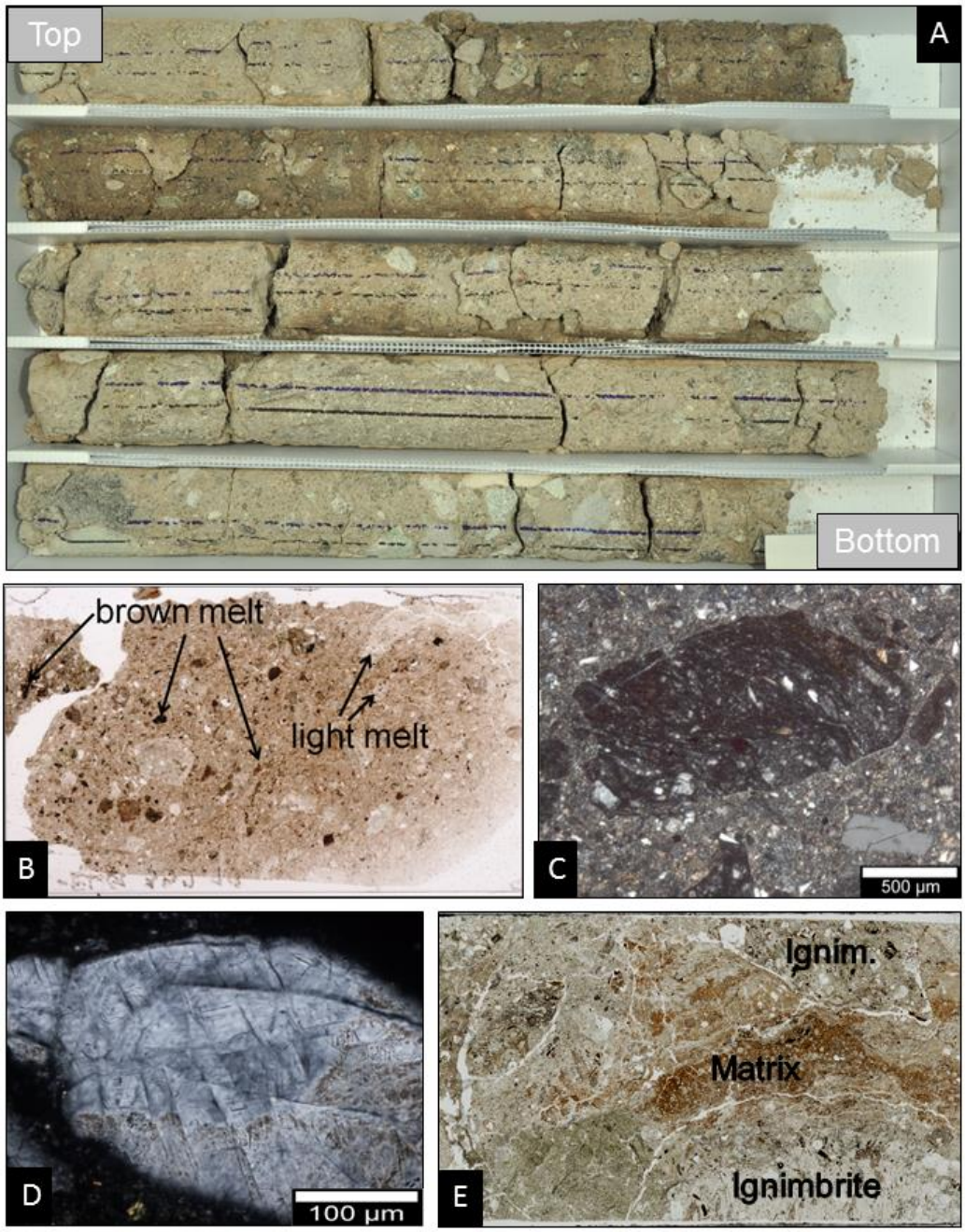

Figure 4.6 (a-e): A) Photograph of a representative core box (depth interval from 348.20 to 345.67 mblf). Clasts of different size and color are embedded in a clastic, light reddish matrix. B) Scan of a thin section from 352.19 mblf with clasts of different sizes and colors. Melt particles are small, dark, or light colored, and larger ones show - at higher magnification - "schlieren" (as in the particles indicated by arrows). C) Thin section (cross polarized light) from 386.35 mblf showing a fragment of ignimbritic target rock, which is embedded in a fine-grained matrix. D) Microphotograph (cross polarized light) of a shock metamorphosed quartz grain with at least three sets of planar fractures (379.72 mblf). E) Scan of a thin section from a sample of the polymict impact breccia dike at 471.92 mblf depth. This dike is incorporated into the lower, ignimbritic bedrock; it contains evidence of shock metamorphism (PDF) in quartz.

metamorphism in the form of PF and PDF (Fig. 4.6D). We did find weakly or moderately to strongly (single or multiple PDF sets) shocked mineral grains over the entire length of this unit; however, the total amount of shocked material is generally very limited, estimated at much less than 0.1 vol%. With decreasing depth, the abundance of strongly shocked mineral grains with three or more PDF sets does increase, with the highest abundance of shocked mineral grains occurring in the uppermost part of this sequence. In particular, seven thin sections from samples between 328.77 and 349.77 mblf contain shocked mineral grains, with PF and PDF in quartz and feldspar - at up to three sets per grain. Thin sections from the lower part of this unit, in contrast, show rare evidence for shock metamorphism. Only in four of twenty samples did we identify shocked minerals (samples from 359.69, 359.92, 373.22, and 382.38 mblf depth). Here, only one or two grains with shock microdeformation features (up to 2-3 sets of PDF) occur in each thin section. We also found some mineral grains that are isotropic to be included in melt fragments. This diaplectic glass is a good indicator for elevated shock metamorphism (25-30 and 30-40 GPa for quartz and feldspar, respectively; e.g., Grieve et al. 1996; Ostertag 1983). In addition, we found three shatter cones (376.20, 368.32, and 351.79 mblf) in volcanic rock clasts (see Raschke et al. 2013), which are meso- to macroscopic features for low to moderate shock metamorphism (e.g., Dietz 1968).

4.5.1.9 The Polymict Impact Breccia Dike (471.96–471.42 mblf)

Between 471.96 and 471.42 mblf in the lower bedrock unit a dike of brecciated material is located that contains fragments of different colored lithologies in a fine-grained matrix (see Raschke et al. 2013). Gray clasts derived from a pyroclastic flow with parallel oriented melt particles (possibly fragments of ignimbrite) and dark greenish clasts derived from andesite or basalt occur together in a red-brownish matrix (Fig. 4.6E). The groundmass contains small melt particles up to several millimeters in size. At this time, it is not clear whether these melt particles are impact-generated or not. Many microscopic mineral fragments show evidence of shock metamorphism. We found shocked grains of quartz and feldspar with PF and single or multiple sets of PDF.

4.5.1.10 Micro-Analysis of Melt Particles Within Suevite and Reworked Suevite

Small melt particles, which are not visible macroscopically or by inspection with a hand lens, do occur in many samples of the polymict impact breccia. At the thin section scale (for example, Fig. 4.6B), these small fragments exhibit different colors and grain sizes (0.1 to 5 mm). Brownish, small, round to angular melt particles occur together with light colored, relatively larger, sometimes elongated melt fragments. Submicroscopic analysis (by EMPA) provided detailed information on the nature and origin of these different melt particles - whether they are derived from the volcanic target rocks or could represent impact-melted

material. So far, we have analyzed six samples (from 344.17, 352.19, 359.92, 374.93, 382.09, and 389.91 mblf depth) to distinguish different melt particles. Furthermore, we analyzed samples of the reworked suevite sequence (317.99, 318.13, 318.24, 318.39, and 326.51 mblf), as well as volcanic melt from the lower bedrock unit (438.09 mblf), and a single sample of impact melt breccia collected at the surface in the eastern sector of the crater (UR-2011-9.1c). This enables us to establish some criteria to distinguish melts of impact or volcanic origin.

Impact melt appears as holohyaline particles or glassy "schlieren" in a fluidal-textured groundmass (Fig. 4.7A, 326.51 mblf). The melt has generally a feldspathic or rhyolitic composition. The glassy melt is vesicle-rich and does not have many strongly shocked mineral clasts (mainly quartz). We found this impact glass within the suevite and reworked suevite. Impact glass spherules were observed only in the reworked suevite unit (especially at 318 mblf depth). Their chemical composition is also dominantly rhyodacitic, except for very rare spherules with mafic melt and crystals. Tiny melt particles and shards were found in the matrix of the suevite and reworked suevite unit (Fig. 4.7B). Figure 4.7C shows an element mapping from a sample of the reworked suevite unit (326.51 mblf). This is an impact glass particle with an intricate micro-banding with "schlieren" of lechatelierite and various feldspathic compositions, interspersed with elongated vesicles. Such melt particles with schlieren rarely have mafic bands. Clearly the precursors of such impact melt particles must have been felsic, likely rhyolitic to dacitic, in composition.

We analyzed with EMPA several glass spherules from thin sections of the samples from 318.13, 318.24, 318.39, and 359.92 mblf. One group of spherules is hollow with a glassy rim. The other group contains spherules which are filled with glass and where a distinct rim or outer seam was not observed. Figure 4.7D shows such a filled void with an apparent size of 200 x 50 µm. Its fill has a nearly homogeneous composition dominated by Si, Al, and Na (see selected element maps in Fig. 4.7D). Another round vesicle of approximately 110 µm diameter is filled with aluminosilicate (approximately 67 wt% SiO_2, 18 wt% $Al_2 O_3$, and 3 wt% FeO; all element concentrations are based on element-oxide calculations with EDS-generated data; analyses were normalized to 100 wt%). Mafic microcrystals, seemingly of Mg-pyroxene composition, occur in this melt (Fig. 4.7E). Two spherules from 318.13 mblf and one from 318.39 mblf are hollow with a narrow rim and have crystal inclusions that line part of the rim. These three spherules are nearly round and have apparent diameters between 300 and 500 µm. Energy-dispersive X-ray spectrometry analyses show a very high content of SiO_2 for the rim crystals along the inner rim, with additional contents of Al_2O_3 and CaO (<5 wt%). Spherule 1 from sample 318.13 mblf (Fig. 4.7F) contains microcrystals with a ferroalumino-silicate composition (approximately 80 wt% SiO_2, 10 wt% FeO, and 8.4 wt% Al_2O_3). The rim was also analyzed and shows a different chemical composition of

approximately 62 wt% SiO_2, 15 wt% CaO, 11 wt% FeO, 6 wt% Al_2O_3, 3 wt% Na_2O, and 2.7 wt% K_2O. Spherule 2 from the same sample (Fig. 4.7G) and the spherule from the sample from 318.39 mblf cover the same range of chemical compositions but have a significant SiO_2 enrichment (besides additions of Ca, Fe, Al, and K) of the crystal inclusions. Wittmann et al. (2013) made similar observations for impact spherules collected to the southeast of the crater rim.

A thin section from a specimen derived from an approximately 1 m large block of impact melt breccia observed at the crater surface (0551829/7483040, UTM, WGS84, Fig. 4.7H). It reveals a largely crystalline nature, with dense aggregates of plagioclase microlites and felty assemblages of often skeletal pyroxene crystallites. Defocused beam EMPA (electron beam about 15 µm wide) determined a feldspathic bulk composition that is dominated by Si, Al, Ca, and Na. The distribution of these elements is heterogeneous, clearly depending on varying proportions of different microcrystal varieties. Similar elemental abundances were observed in impact glass particles from 326.51 mblf. Further comprehensive and quantitative analysis of impact melt particles is in progress.

The presence of impact melt particles resolved in this study allows us to conclude that the polymict impact breccia package constitutes suevite. Seemingly, however, the proportion of bona fide impact melt in this unit is rather limited, considering both the proportion of impact melt in the clast fraction and the melt content of groundmass.

A general characteristic of the volcanic melt particles is a finely crystalline to aphanitic (vitrophyric) groundmass with heterogeneous compositions ranging from basaltic to rhyolitic. Euhedral phenocrysts of quartz and feldspar, mafic minerals such as biotite and amphibole, and accessory ore minerals are included in the mesostasis. Brownish, flattened pumice fragments ("fiamme") and black glass shards are typical for the ignimbrite of the lower and, partly, for the upper bedrock. We also found rare accretionary lapilli within the ignimbrite. In a thin section of a rhyodacitic ignimbrite sample from 438.09 mblf in the lower bedrock unit some volcanic melt particles were analyzed (e.g., the particle shown in Fig. 4.7I). In contrast to the impact melt particles of variable compositions, these volcanic particles have the same chemical composition as the bulk composition of the ignimbritic host rock. A characteristic feature that is not observed in the presumed impact melt fragments of the polymict impact breccia is the widespread occurrence of Fe-Ti-oxides in the groundmass of these volcanic melt particles. Fragments of such volcanic melt rock occur abundantly in the polymict impact breccia as mostly sharply defined, angular clasts with an internal, fluidal texture.

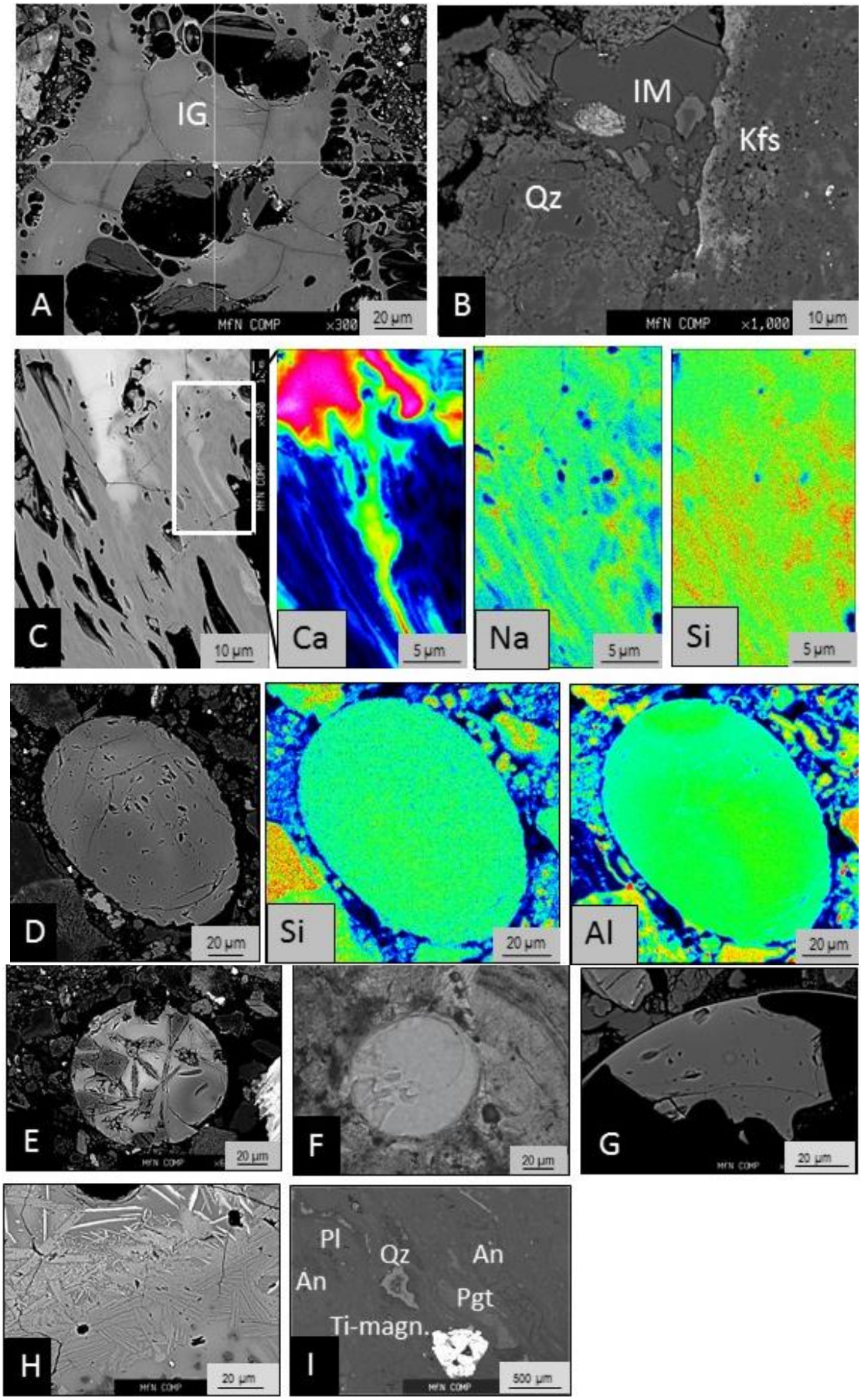
IG
A
MfN COMP
×300
20 µm
IM
Kfs
Qz
B
MfN COMP
×1,000
10 µm
C
10 µm
Ca
5 µm
Na
5 µm
Si
5 µm
D
20 µm
Si
20 µm
Al
20 µm
E
20 µm
F
20 µm
G
20 µm
H
20 µm
Pl
Qz
An
An
Pgt
Ti-magn.
I
500 µm

Figure 4.7: A) Vesicle-rich impact glass particle (IG). EMP-BSE image of the sample from 326.51 mblf (reworked suevite). Wavelength-dispersive element mapping showed that Si and Al dominate the chemical composition, with other elements only accounting for <5 wt%. B) SEM-SE (secondary electron) image of a sample from 359.92 mblf (suevite) with a small impact melt particle (IM) in the upper mid part of this image. EDX point measurements show a composition of aluminosilicate with a high proportion (about 14 wt%) of Al_2O_3. The surrounding minerals are potassium feldspar (Kfs) and quartz (Qz). C) Various EMP element maps of part of an impact glass particle from the sample from 326.51 mblf (reworked suevite). This glass is constituted of chemically very different schlieren. Dark gray phases are SiO_2-rich, and light gray or even white schlieren are rich in Ca and Na. The color range for element maps signifies high concentrations of a given element in reddish color, green indicates moderate concentrations, and blue means poor or very low concentration. D-G) Spherules from the sample taken at 318.13 mblf depth (reworked suevite); SEM-BSE images (D, E, G) and microphotograph (F), respectively. D) This round spherule contains glass of aluminosilicate composition. Si and Al concentrations are about equal. Other elements do not show significant abundances. E) This spherule is filled by glass with a high Si and Al concentration. The dark gray crystals have a Mg-pyroxene composition. F) This partially hollow spherule has a glass rim of aluminosilicate composition. A microcrystalline area occurs inside the rim. Its composition is Si-dominated and similar to all measured within-spherule crystals. Note: In the right part of this image occurs a fragment of an accretionary lapilli of presumed volcanic origin. G) Close-up of the crystalline part of a second, almost hollow spherule fragment. The mark of the electron beam is visible in the center. This particle is representative for all analyzed intraspherule crystals and consists of approximately 87 wt% SiO_2, 4.7 wt% FeO, 4.5 wt% CaO, and 1.2 wt% K_2O. H) SEM-BSE image of an impact melt sample from an approximately 1 m sized boulder at the eastern shore of Lake El'gygytgyn. Defocused beam analyses of this material indicate a feldspathic composition with respect to Si, Al, Ca, and Na. Light crystals have high concentrations in Fe and are possibly Fe-oxide. I) This EMP composite image of a sample from 438.09 mblf (ignimbrite) exhibits the typical fluidal texture of a volcanic melt particle. Partially molten minerals are anorthite, plagioclase (Pl), quartz (Qz), pigeonite (Pgt), and Ti-magnetite. The occurrence of ore minerals is typical for volcanic melt fragments and was not observed in any of our presumed impact melt particles.

4.5.1.11 The Reworked Suevite Unit (approximately 328-316.77 mblf)

The reworked suevite deposit begins at about 328 mblf and extends to about 316.77 mblf depth (Raschke et al. 2013a). The contact to the underlying impact breccia unit is not clearly defined. The contact is taken here where the first, significant occurrence of clay and fine sand has been noted. The variably fine- to coarse-grained matrix is supported by lacustrine sediment (clay to sand) with an increasing abundance toward the top of this section. Figure 4.8A shows a core box (No.100, 318.83-316.77 mblf) with the uppermost two meters of this unit. It is easy to recognize that the larger fragments and clasts are located in the bottom segments of this box. In slot 3 of this core box (part 3 in Fig. 4.8A) occur large volcanic clasts with a size up to approximately 8 cm. Their colors are variable from white (pumice) to black (andesite or basalt). In slot 2 of the box (part 2 in Fig. 4.8A) occurs the same variation of clasts, but with a smaller size (at max. 3 cm clast sizes). The uppermost slot of the box (part 1 in Fig. 4.8A) contains the smallest clasts with sizes of approximately 1 cm.

Toward the top of this box the sediments show upward fining (normal gradation). We did not observe several (allegedly, up to seven) fining upward cycles in this unit, as reported

by Wittmann et al. (2013). The unit is matrix-supported and has a micro-clastic matrix that is generally similar to that of the polymict impact breccia below, also including small melt particles that are mixed with fine sand and clay size minerals (Fig. 4.8B). Rock fragments, up to 20 cm in length, occur as well and are derived from the members of the volcanic target rocks (Gurov et al. 2005). Similar to the underlying suevite, we found clasts from basaltic to rhyolitic composition. Here, also pumice-like clasts occur that are gray in color and often have an internal fluidal texture. Brownish melt particles of millimeter to centimeter size are dispersed in the groundmass. Wittmann et al. (2013) also reported possible impact melt particles with a size up to 1 mm in the matrix. These particles have mainly a slight light brownish color and many have elongated or shard shapes. In addition, we found a number of diaplectic quartz glass particles with sizes up to 1.5 mm.

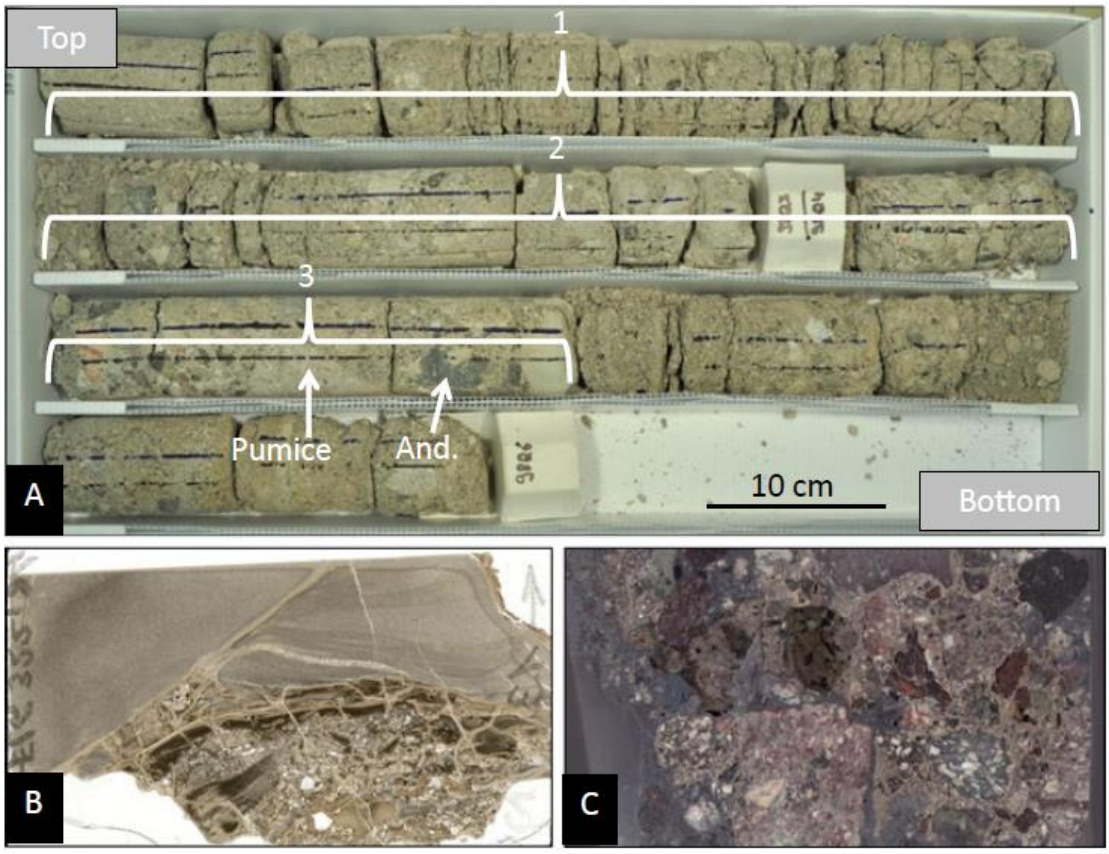

Figure 4.8: Reworked suevite. A) Complete core box No. 100, Q98-2- Q98-6, from 318.83 to 316.77 mblf, showing the different sizes and colors of the clasts from the transition zone. Suevitic matrix and lacustrine sediments are present. The image shows a normal gradation of the clast size. Larger clasts in part 3 have sizes of up to about 8 cm. "And." points to an andesitic rock clast. In part two the clasts become smaller (approximately 2 cm in diameter), and in the uppermost part 1 the clasts are <1 cm in size. B) Thin section scan (true size: 24 x 48 mm) for a sample from 322.84 mblf with fine- to coarse-grained suevitic groundmass in contact to lacustrine, laminated sediment of silt to clay grain size. The orientation of the sample is marked in the upper right corner (arrow shows toward the top). C) This thin section (true size: 24 x 48 mm) scan illustrates the polymict character of this unit (318.06 mblf).

The thin section for a sample from 318.06 mblf (Fig. 4.8C) shows the polymict character of this breccia that combines fragments of many different rock types in the clast population as well as in the polymict, heterogranular groundmass. The rock fragments belong to a dark brown andesite, a greenish ignimbrite, and a reddish trachyrhyolite. The groundmass also contains brown to blackish melt particles. These melt particles have a glassy mesostasis that is full of vesicles. Our microscopic studies from surface samples of impact glass bombs (samples collected by O. Juschus in 2003 and C. Koeberl in 2009) show the same character as these melt clasts. Similar melt fragments are described by Pittarello and Koeberl (2013) from surface-derived impact melt rocks collected by C. Koeberl in 2009 from a western lake terrace. Our group observed them in the suevite core, and Wittmann et al. (2013) reported them from impact melt rocks collected near the western crater rim. All three groups consider such melt particles as impact melt.

Figure 4.9A represents a close-up of an area in the same thin section from 318.06 mblf that shows a mélange of vesicle-rich melt that is partially altered to finest-grained, brownish phyllosilicate accumulations. In addition, one sees in this image a few mineral inclusions and a crystal-lined vesicle. These crystals are thought to be zeolite. Microspherules with up to approximately 0.8 mm size are embedded in the groundmass in the upper part of this unit. The highest concentration of these spherules was found between 317 and 322 mblf. The spherules have a glassy margin and may contain some crystal inclusions or microfragments of different minerals (e.g., quartz and feldspar, or zeolite). The crystals have grown inwards from the outer rims. Another type of spherules is filled by aluminosilicate glassy melt that contains some crystals with feldspathic or mafic composition (see the Micro-Analysis of Melt Particles Within Suevite and Reworked Suevite section).

In a thin section from a sample from 323.01 mblf we found a partially melted pyroxene in fluidal-textured (variably light brownish to translucent schlieren) impact glass (Fig. 4.9B). A plagioclase crystal with microfaulting is shown in Fig. 4.9C (317.64 mblf). This and abundant similar microfracturing of mineral and rock clasts is likely the result of shock overprint. Sets of PDF with multiple orientations are common throughout this unit. They occur both in quartz (Fig. 4.9D) and feldspar fragments.

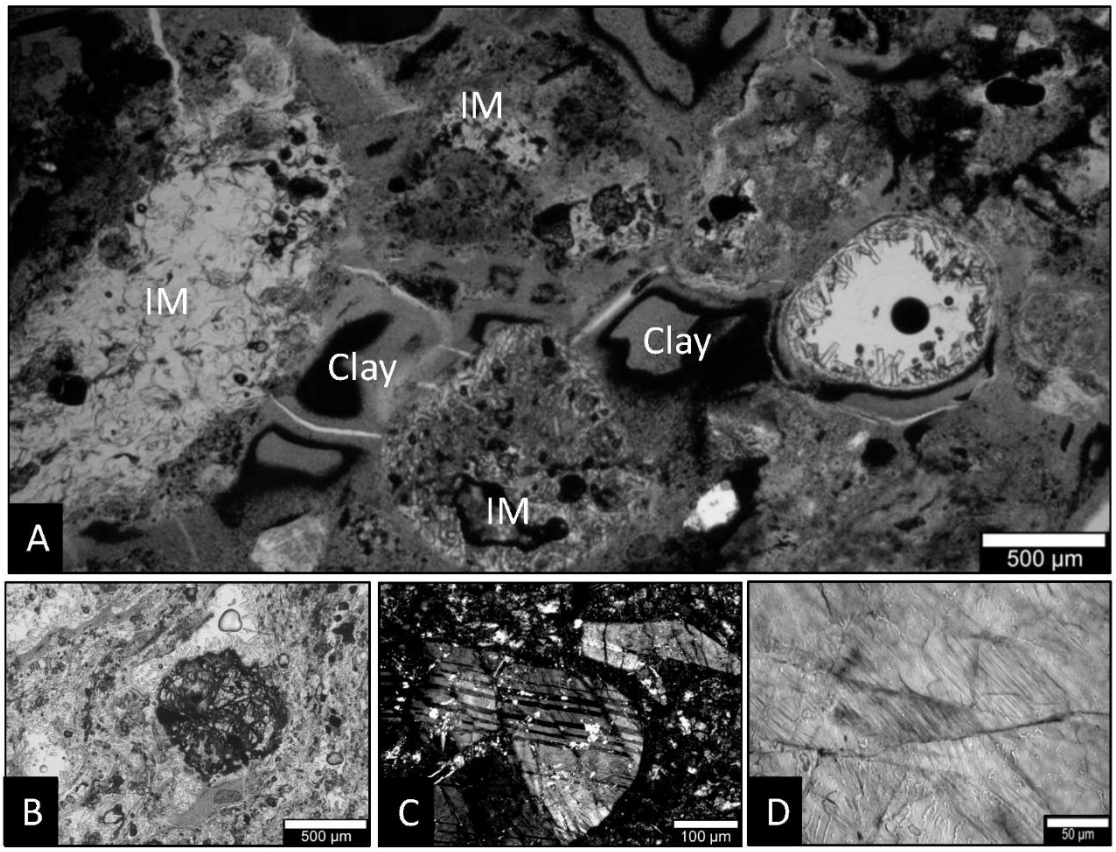

Figure 4.9: Reworked suevite. A) Two combined thin section images (320.95 mblf depth, plane polarized light) showing a mixture of vesicle-rich impact melt, secondary phyllosilicate minerals, and clay. The large, white clast on the left is nearly translucent impact melt (IM) and shows some crystals of feldspathic composition. The two round areas in the middle, marked IM, are also impact glass, but here occur tiny inclusions (black dots) and phyllosilicates, so that these glass particles are not translucent. The hollow vesicle in the right part of this image is filled by small columnar crystals that are lining the rim and grow radial-symmetrically. Their composition is Si-dominated and similar to the other within-spherule crystals (see Fig. 4.7G). B) Thin section image (plane polarized light, 323.01 mblf depth) of impact melt with a former pyroxene mineral that is strongly shocked and partially converted to diaplectic glass. C) Thin section shows a cracked feldspar grain with displaced fragments (cross polarized light, sample from 317.64 mblf depth). D) Microphotograph (cross polarized light) of the sample from 319.82 mblf with shock features (PDF, at minimum 4 sets) in quartz.

4.5.2 The Fractures

Over the whole length of the impactite sequence strong brecciation and/or fracturing are observed. Fractures are often parallel to other aspects of the fabric. Conjugate fracture systems have also been noted repeatedly, especially in the bedrock units and the felsic blocks. The fractures are partly filled by secondary minerals, which excludes that the fracturing is a result of the core extraction process.

In the lower bedrock unit, the melt particles ("fiamme") in the trachyrhyodacitic ignimbrite and the fractures are generally oriented at 45° to the long axis of the drill core, i.e., often parallel to the orientation of the flow structure of the ignimbrite as indicated by the preferred orientation of pumice fragments. Some of the fractures form conjugate systems in

what the fractures are oriented at 30 or 120° to each other. We have observed some slight variation in the abundance and orientation of fractures with depth. A first trend is noted in the lower part of the ignimbrite bedrock unit (approximately 503 to 512 mblf), where the fractures are oriented at 45 to about 80° to the long axis of the drill core (Fig. S1A). Above this, up to approximately 490 mblf, the abundance of fractures decreases (Fig. S1B) and their orientation is predominantly about 45° to the core axis. This changes again between 483 and 473 mblf with a trend to subparallel fractures oriented at frequently more shallow angles to the core axis (45° to 5°, Fig. S1C). Similar orientations are dominant from approximately 444 to 441 mblf. At the top of the lower bedrock unit fractures are very common and generally oriented at about 45° to the core axis, often occurring as conjugate fracture sets with an angle of about 90º between them. The isolated mafic block at 423.03 to 422.71 mblf is characterized by significant grain-size reduction, locally to grain sizes lower than 20 µm (Fig. S1D).

At the bottom of the upper bedrock unit a mafic block occurs between 420.89 and 420.27 mblf depth, which is also fractured (with fractures at angles of about 45° to the core axis). Thin white calcite veins have filled many of these originally open fractures (Fig. 4.4A). Above this block, the core material is more competent and moderately brecciated. The fractures in the suevite and reworked suevite are frequently located along the edges of larger clasts and do not cut the clasts. While the fractures in the bedrock are mostly filled by secondary minerals, the fractures in the upper units are filled by fine-grained polymict material or with clay injections, especially in the uppermost part of the reworked suevite.

4.5.3 Analysis of the Clast Population and Its Grain-Size Variation Throughout the Impactite Section

In the reworked suevite, suevite, and strongly brecciated upper bedrock (316.77-420.89 mblf) the distribution of different clast types and the maximum clast sizes were recorded. We carried out a macroscopic clast investigation over the whole length of these units. The technique applied is identical to that used by Ormö et al. (2009) on the Chesapeake Bay ICDP core from the Eyreville drilling site in the Chesapeake Bay impact structure. All clasts or fragments larger than 5 mm were counted and classified according to their lithology. In addition, fabric and color were noted. Altogether, 589 clasts were evaluated. Forty-two percent of these have clast sizes smaller than 10 mm (Fig. 4.10A). The variation of clast distribution and the variation of their sizes with depth are summarized in Figs. 4.10B-D. The macroscopic and microscopic analysis of the clast population in breccias has shown that most clasts have sizes up to 20 mm. A similar trend was also observed for impact breccias by Ormö

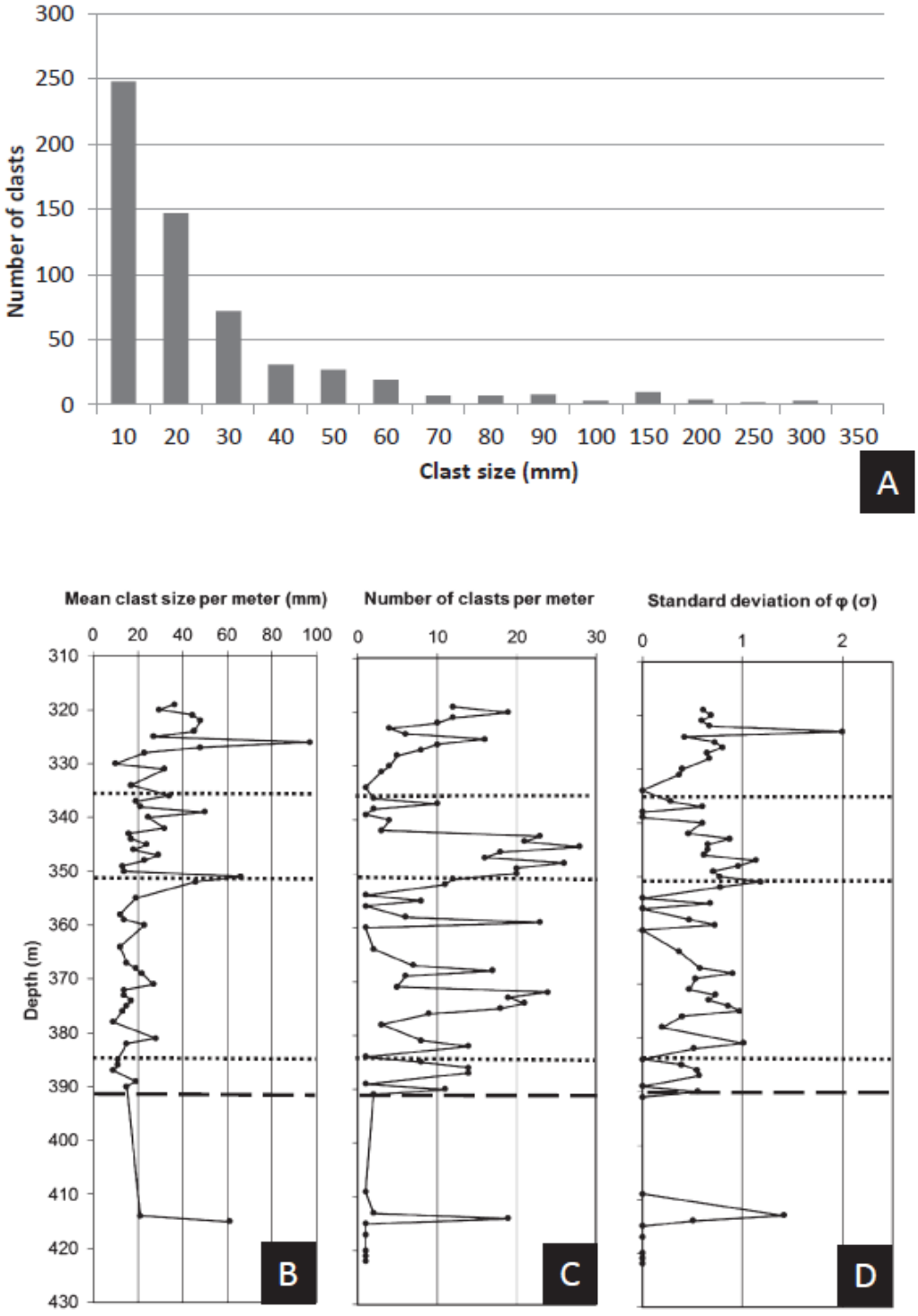

Figure 4.10: Clast population. A) The clast size (up to 1 m) is divided into classes with a range of 10 mm (x-axis). Most of the 589 clasts evaluated belong to the first size class up to 10 mm in diameter. Over 90% of the clasts have sizes up to 50 mm. B-D) In these three diagrams the clast properties are plotted against depth. The dashed line marks the contact between suevite and upper bedrock. The three dotted lines illustrate the locations of the three felsic blocks. B) The mean clast size per meter is plotted, with a maximum size of 100 mm (x-axis) in relation to the drill core depth (y-axis). The three volcanic blocks are broken into several pieces that have been counted separately. C) A plot of numbers of clasts per meter clearly shows that the most clasts belong to the suevite. D) The standard deviation of the clast size φ shows a normal deviation. Small clasts have relatively high values for the standard deviation (up to factor 2); with increasing size of the clasts the deviation decreases with values of φ less than 1.

et al. (2009). The number of clasts per meter is very high for the suevite unit. The uppermost reworked suevite has slightly reduced clast abundance, with notable occurrence of many large clasts of lake sediment, and where the addition of sedimentary material to the breccia matrix is responsible for a lowering of the clast per meter values. It is possible to identify in Fig. 4.10B the larger felsic blocks (dotted lines) and the transition to the more coherent pyroclastic rocks of the upper bedrock, respectively (421-391 mblf).

A number of issues must be considered when trying to assess the significance of this clast investigation. We analyzed a small (1 cm wide) strip parallel to the long axis of the drill core - and the statistical significance of this can only be evaluated by further studies parallel to this narrow band. There is also a problem with core loss and with the, admittedly small, sample sections that had been removed already before this analysis began, during the sampling party.

Comparing the values for the mean clast size per meter readily allows recognizing the three felsic blocks in the polymict breccia sequence, at 385.5-383.00, 351.89-351.52, and 337.00-333.83 mblf depths. The upper bedrock is characterized by a single block (420.89 to approximately 391 mblf) that comprises two vitrophyric pyroclastic layers and two ignimbritic layers in alternating order. The graph for the number of clasts per meter (Fig. 4.10C) corresponds well to these findings and displays, naturally, an inverse trend: the larger blocks have low values and the polymict impact breccia and the reworked suevite contain a comparatively larger number of clasts per meter. The standard deviation of the clast size φ (Fig. 4.10D) shows a normal deviation, which means that the small clasts have relatively high values for the standard deviation (up to a factor of 2). With increasing size of the clasts the deviation decreases with values of φ less than 1. A possible explanation for this could be increased measuring error by measuring of smaller clasts.

4.5.4 Chemical Analysis of the D1c Lithologies

For whole-rock chemical analysis 96 samples covering the entire impactite section of drill core D1c were chosen. Sample statistics according to drill core sequences and lithostratigraphy are given in Table 4.1.

Table 4.1: Sample statistics for whole-rock chemical analysis.

Drill core section	Depth range (m (blf))	Rock type	Number of samples
Reworked suevite unit	316.77 – ~328	Reworked suevite	17
Suevite unit	~328 – 390.74	Suevite	16
		Felsic blocks	4
Upper bedrock unit	390.74 – 420.89	Upper bedrock	10
		Mafic blocks	2
Lower bedrock unit	420.89 – 517.09	Lower bedrock (ignimbrite)	40
		Mafic blocks	3
		Ash tuffs	2
		Polymict impact breccia dike	2

The chemical analyses are compiled, according to increasing sample depth, in the supporting information (Table S1). The content of the major element oxides SiO_2, TiO_2, Al_2O_3, Fe_2O_3, MgO, CaO, Na_2O, K_2O, and P_2O_5 are plotted against depth in the drill core to display general chemical trends (Figs. 4.11A-I).

Generally, with the exception of the mafic blocks, the chemical composition of the rocks in drill core D1c shows a high degree of uniformity throughout the whole core. Average chemical compositions and the ranges of rock compositions are given for the reworked suevite, suevite, and the upper and lower bedrock in Table 4.2.

4.5.4.1 Chemistry of Felsic Target Lithologies

The felsic target lithologies comprise the lower and upper bedrock, ash tuffs within the upper bedrock unit, and larger felsic blocks within the suevite unit (Fig. 4.2).

Lower and Upper Bedrock

The lower bedrock (517.09-420.89 mblf) is subdivided by a shear zone at 457.39 mblf into two subunits. This boundary is also clearly visible in the chemical compositions of samples by systematic variations of the SiO_2, TiO_2, Fe_2O_3, MgO, P_2O_5, Sc, V, Zn, and Zr contents with depth (Figs. 4.11A-B, D-E, I, and 4.12). Both subunits are characterized by an increase in TiO_2, Fe_2O_3, MgO, P_2O_5, Sc, V, Zn, and Zr contents, and a concomitant decrease

in the SiO_2 content, with decreasing depth. This effect is most prominent toward the top of the lower subunit near the shear zone between approximately 470 and 457.39 mblf depth. At the shear zone, a distinct change in the SiO_2, TiO_2, Fe_2O_3, MgO, P_2O_5, Sc, V, Zn, and Zr abundances is recognized (Figs. 4.11A-B, D-E, I, and 4.12).

The upper bedrock (420.89-390.74 mblf depth) generally has a similar chemical composition as the upper subunit of the lower bedrock, with the exception of the alkali (especially Na_2O) and alkaline oxides (Figs. 4.11A-I and 4.12). Especially the immobile chemical oxides and elements (TiO_2, P_2O_5, V, and Zr, see Figs. 4.11B, 11I, and 4.12; compare Arikas [1986] and Middelburg et al. [1988]) do not allow a chemical distinction between the upper subunit of the lower bedrock and the upper bedrock. The samples of the lower part (419.40-404.79 mblf) of the upper bedrock have distinctly lower Na_2O contents in comparison to those of the lower bedrock (Fig. 4.11G). This part of the upper bedrock is characterized by intense brecciation, which most likely led to removal of Na_2O. This possible removal of Na_2O in this part of the upper bedrock is not associated with distinct changes of the MgO, CaO, K_2O, Rb, Sr, and Ba abundances. In contrast, two samples from the top of the upper bedrock (393.60 and 398.34 mblf) again have Na_2O contents that are similar to those of most of the lower bedrock samples (Fig. 4.11G).

In the total alkali-silica (TAS) plot after Cox et al. (1979) the samples of the lower bedrock plot into the rhyolite, dacite, and trachydacite fields and cluster around the triple point of these three fields (Fig. 4.13A). The average composition of the lower bedrock (Table 4.2) plots also near this triple point. Therefore, the lower bedrock has chemically a trachyrhyodacitic composition. In contrast, most of the upper bedrock samples plot in the TAS diagram within the dacite field near the boundary to the rhyolite field; only one sample from 413.76 mblf depth is clearly located in the middle of the dacite field (Fig. 4.13B). The average upper bedrock plots in the TAS diagram in the dacite field near the boundary to the rhyolite field. The upper bedrock has therefore a rhyodacitic composition. The lower and upper bedrock both have a subalkaline character (Irvine and Baragar 1971) and belong to the calc-alkaline suite based on the Zr versus TiO_2 discrimination diagram (Figs. 4.14A and 4.14B). Average target rock compositions of El'gygytgyn reported by Gurov et al. (2005) plot in the TAS diagram (Fig. 4.13B) in the rhyolite field (rhyolite and rhyolitic tuff), on the boundary between rhyolite and dacite (rhyolitic ignimbrite), and between the dacite and andesite fields (andesite/andesitic tuff).

Average compositions of lower and upper bedrock (Table 4.2), as well as Harker diagrams for samples from these units (Figs. 4.15A-G), also indicate a similar chemical composition for both bedrock units.

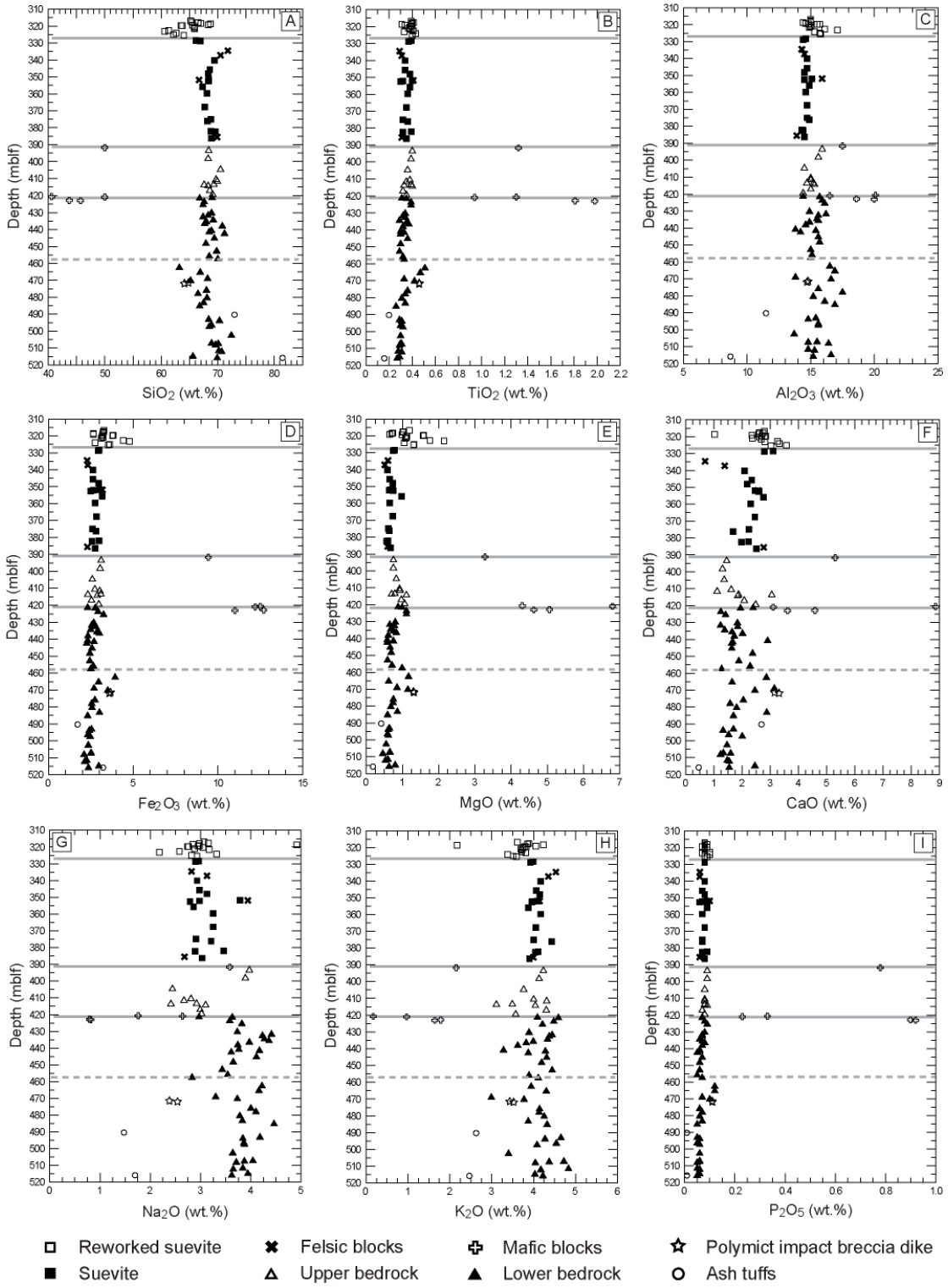

Figure 4.11: Variations of the SiO_2 (A), TiO_2 (B), Al_2O_3 (C), Fe_2O_3 (D), MgO (E), CaO (F), Na_2O (G), K_2O (H), and P_2O_5 (I) abundances plotted versus depth for the impactite section of El'gygytgyn drill core D1c. Note that the boundaries between the core units lower/upper bedrock, upper bedrock/suevite, and suevite/reworked suevite at depths of 420.89, 390.74, and approximately 328 mblf, respectively, are indicated by gray lines. A gray broken line within the lower bedrock unit at a depth of 457.39 mblf indicates the occurrence of a shear zone separating the lower bedrock into two subunits.

In the Harker diagrams the field of the upper bedrock is - for most of the major oxides (TiO_2, Al_2O_3, Fe_2O_3, MgO, CaO, and K_2O) - included in the field of the lower bedrock (Figs. 4.15A-E, G). The only exception is the Na_2O versus SiO_2 plot, which shows a significantly lower Na_2O content in the upper bedrock in comparison to the lower bedrock (Fig. 4.15F). This was most likely caused by removal of Na_2O by post-impact solutions. In the lower part of the upper bedrock intense brecciation is observed that produced an increase in the surface area amenable to attack by solutions in contrast to the underlying lower bedrock. A similar preferential removal of Na_2O in brecciated and/or altered rhyolitic rocks of Southern Germany was, for example, described by Arikas (1986).

Slight differences occur between the average compositions of both rocks (Table 4.2). The TiO_2, Fe_2O_3, M_gO, and K_2O abundances are slightly higher in the upper bedrock in comparison to the lower bedrock. Most prominent is the difference in the Na_2O content, which is distinctly lower in the lower part of the upper bedrock (Figs. 4.11G and 4.15F). This is most likely the result of the already suggested Na_2O removal. The lower and upper bedrock are chemically distinct from the average rhyolite and rhyolitic tuff (Figs. 4.15A-G) from surface outcrops reported by Gurov et al. (2005). The average rhyolitic ignimbrite of Gurov et al. (2005) shows - for most major elements (SiO_2, TiO_2, Al_2O_3, Fe_2O_3 MgO, and K_2O) - only slight differences to the average lower and upper bedrock (Figs. 4.15A-G). Nevertheless, there are differences in the CaO and Na_2O abundances (Figs. 4.15E and 4.15F), which are lower in the averages for lower and upper bedrock and higher in those for the lower bedrock, respectively, in comparison to the average rhyolitic ignimbrite of Gurov et al. (2005). The surface samples of rhyolitic ignimbrite analyzed by Gurov et al. (2005) might have undergone preferential Na_2O removal during weathering at surface, a process reported for many rhyolite localities worldwide (e.g., Arikas 1986; Middelburg et al. 1988).

Ash Tuffs

Two ash tuff samples within the lower bedrock unit, at 490.43 and 515.94 mblf depths (for petrographic descriptions see Raschke et al. 2013a), have exotic chemical compositions, and are also different in chemical composition in comparison to the average rhyolitic ash tuff (lower horizon) reported by Gurov et al. (2005). Both ash tuff samples have high SiO_2 contents (73.0 and 81.5 wt%, respectively) and indicate therefore a connection to the rhyolitic volcanic rocks. The ash tuff at 490.43 mblf depth is chemically characterized by high Sr (3895 ppm) and low Zr (<10 ppm) contents that are distinctly different from all other felsic bedrock samples. Nevertheless, the high Sr content is not correlated to other alkaline earth metals abundances (CaO and Ba). The other analyzed ash tuff at 515.94 mblf depth

displays an unusually high SiO_2 content (81.5 wt%), which is not typical for rhyolitic volcanic rocks and most likely the result of secondary silicification.

Felsic Blocks

In the suevite unit three larger felsic blocks (385.55-383.00, 351.89-351.52, and 337.00-333.83 mblf depth, compare Fig. 4.2) occur. Samples from 334.54, 337.00, 351.87, and 385.54 mblf were analyzed (compare Figs. 4.11A-I). Based on the TAS diagram after Cox et al. (1979) the samples from 385.54 and 351.87 mblf depth plot into the dacite and trachydacite fields, respectively (Fig. 4.13B). The two samples from 337.00 and 334.54 mblf have a rhyolitic composition in the TAS diagram (Fig. 4.13B). Both samples have calc-alkaline character similar to the lower and upper bedrock (Fig. 4.14C).

Thus, individual chemical analyses of these blocks display distinctly different chemical compositions. The variations of the chemical compositions of the lower and upper bedrock samples are prominent, and in the Harker diagrams these felsic block samples plot for most oxides into the field of the lower bedrock (Figs. 4.15A-G).

4.5.4.2 Compositions of Mafic Target Lithologies

Mafic target lithologies occur as blocks in the drill core section und are comparatively scarce with respect to the dominance of felsic target lithologies (Fig. 4.2). Five mafic rock samples were analyzed, comprising two samples from the upper bedrock unit (391.72 and 420.60 mblf) and three from the lower bedrock unit (420.90, 422.80, and 422.98 mblf). The mafic blocks stand out clearly in the depth profiles (Figs. 4.11A-I) due to their low SiO_2 and K_2O, and high TiO_2, Al_2O_3, Fe_2O_3, and MgO abundances in comparison to the dominant felsic target lithologies. The trace element abundances of Sc, V, Cr, Co, Ni, Cu, Zn, Ga, Y, and Zr are also significantly higher in the mafic blocks than in the felsic target lithologies. The SiO_2 abundances of the mafic blocks vary between 40.6 and 50.0 wt% and indicate an ultramafic to mafic composition. The MgO abundances that range from 3.28 to 6.80 wt% are not typical for ultramafic rocks. Based on the TAS diagram after Cox et al. (1979) the sample from 391.72 mblf depth has a trachybasaltic, the samples from 420.90 and 422.98 mblf a basaltic, and those from 420.60 and 422.80 mblf a picrobasaltic composition (Fig. 4.13B). In contrast, the Zr versus TiO_2 discrimination diagram (Fig. 4.14C) after Pearce (1980) based on immobile elements indicates for the samples from 379.72, 420.90, 420.80, and 422.98 mblf have an intermediate composition, whereas the sample from 420.60 mblf depth shows a basaltic composition. High LOI values between 5.6 and 9.2 wt% for all five mafic block samples indicate strong alteration that obviously obstructs the geochemical classification of these rocks.

Table 4.2: Average chemical composition, standard deviation and range of rock compositions for the reworked suevite, suevite, upper and lower bedrock. Felsic and basic blocks were excluded for these calculations.

Rock type	Reworked suevite					Suevite					Upper bedrock					Lower bedrock (ignimbrite)				
Depth range (mblf)	316.77 – ~328					~328–390.74					390.74 – 420.89					420.89–517.09				
	Mean	SD[a]	Min	Max	n[c]	Mean	Sd[a]	Min	Max	n[c]	Mean	SD[a]	Min	Max	n[c]	Mean	SD[a]	Min	Max	n[c]
wt%																				
SiO_2	64.8	2.3	60.6	68.7	17	68.2	0.9	66.1	69.6	16	69.0	0.9	67.6	70.5	10	68.5	1.7	63.2	72.4	40
TiO_2	0.38	0.03	0.31	0.43	17	0.35	0.03	0.30	0.40	16	0.37	0.03	0.32	0.40	10	0.33	0.05	0.26	0.51	40
Al_2O_3	15.3	0.6	14.4	17.1	17	14.6	0.2	14.3	15.1	16	15.1	0.5	14.4	15.9	10	15.5	0.9	13.7	17.5	40
Fe_2O_3[b]	3.39	0.57	2.65	4.78	17	2.80	0.19	2.50	3.17	16	2.83	0.27	2.32	3.11	10	2.62	0.37	2.10	3.93	40
MnO	0.07	0.01	0.06	0.12	17	0.06	0.01	0.04	0.08	16	0.04	0.01	0.03	0.06	10	0.05	0.01	0.03	0.07	40
MgO	1.20	0.39	0.65	2.15	17	0.69	0.10	0.56	0.98	16	0.88	0.14	0.70	1.11	10	0.74	0.18	0.46	1.17	40
CaO	2.71	0.54	1.02	3.57	17	2.39	0.34	1.68	3.10	16	1.81	0.59	1.11	3.05	10	1.84	0.50	1.23	3.14	40
Na_2O	3.02	0.55	2.18	4.91	17	3.08	0.26	2.79	3.78	16	3.02	0.53	2.41	3.97	10	3.84	0.35	2.83	4.46	40
K_2O	3.67	0.43	2.17	4.23	17	4.05	0.14	3.87	4.43	16	3.89	0.40	3.11	4.31	10	4.13	0.38	2.99	4.83	40
P_2O_5	0.08	0.01	0.07	0.10	17	0.08	0.01	0.06	0.09	16	0.08	0.01	0.07	0.09	10	0.07	0.01	0.05	0.12	40
LOI	4.8	0.9	3.3	6.9	17	3.1	0.7	1.5	4.5	16	2.4	0.8	1.1	4.2	10	1.9	0.7	0.9	3.9	40
ppm																				
Sc	7	2	6	11	16	6	1	<5	9	15	7	1	5	8	10	6	1	<5	10	24
V	37	6	18	43	16	29	4	24	41	16	29	3	26	35	10	25	7	17	58	40
Cr	12	5	<5	21	14	<5		<5	20		<5		<5	<5		<5		<5	<5	
Co	<5		<5	5		<5		<5	<5		<5		<5	<5		<5		<5	6	
Ni	13	3	<5	20	15	6	2	<5	10	11	<5		<5	6		<5		<5	12	
Zn	49	4	36	54	16	45	1	41	48	16	43	5	36	51	10	41	4	<15	55	40
Rb	125	22	53	142	16	132	6	118	144	16	123	17	92	144	10	125	12	83	148	40
Sr	257	124	185	704	16	251	70	164	392	16	219	25	175	270	10	379	283	87	1506	40
Y	23	2	19	27	16	20	1	11	22	16	19	1	17	21	10	18	2	16	23	40
Zr	151	16	118	179	16	155	10	137	174	16	159	13	140	177	10	141	15	68	186	40
Ba	652	200	372	1302	16	702	47	599	815	16	777	65	656	871	10	726	65	343	871	40
La	34	9	23	57	16	31	3	26	37	16	29	3	23	33	10	30	4	19	37	40
Ce	80	10	61	108	16	77	5	67	86	16	67	4	59	73	10	68	5	45	80	40
Pb	20	2	16	27	16	17	2	11	22	16	17	1	16	20	10	20	8	<15	63	32

[a]SD = standard deviation.
[b]Total Fe as Fe_2O_3.
[c]n = number of analyses used for calculation of mean and standard deviation.

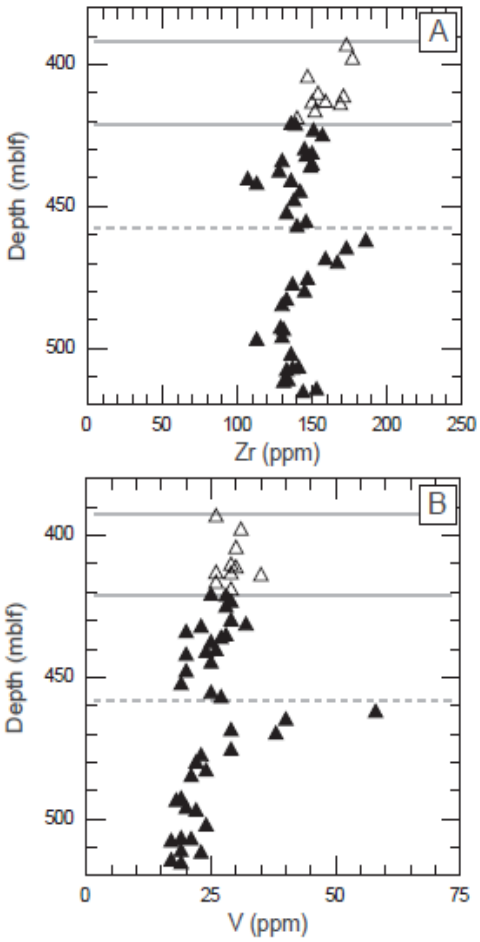

Figure 4.12: Variations of Zr (A) and V (B) abundances versus depth for the lower and upper bedrock in the drill core D1c. For symbols see Fig. 4.11. The boundaries between the core units lower/upper bedrock and upper bedrock/suevite at depths of 420.89 and 390.74 mblf, respectively, are indicated by gray lines. A gray broken line within the lower bedrock unit at a depth of 457.39 mblf indicates a shear zone separating the lower bedrock into two subunits. Note the significant variations of the Zr and V contents in the lower subunit of the lower bedrock unit below this shear zone.

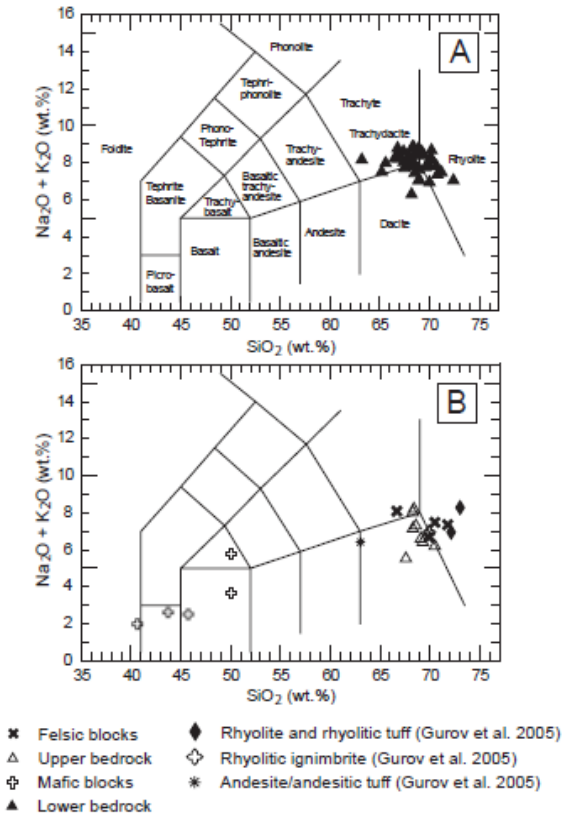

Figure 4.13: Total alkali-silica (TAS) plots after Cox et al. (1979) for target lithologies of the El'gygytgyn crater. A) Lower bedrock from the drill core D1c. B) Upper bedrock, and felsic and mafic blocks from the suevite and the lower and upper bedrock units of drill core D1c, respectively. For comparison, this diagram shows additionally the average rhyolitic ignimbrite, rhyolite, rhyolitic tuff, and andesite/andesitic tuff calculated for surface samples after Gurov et al. (2005).

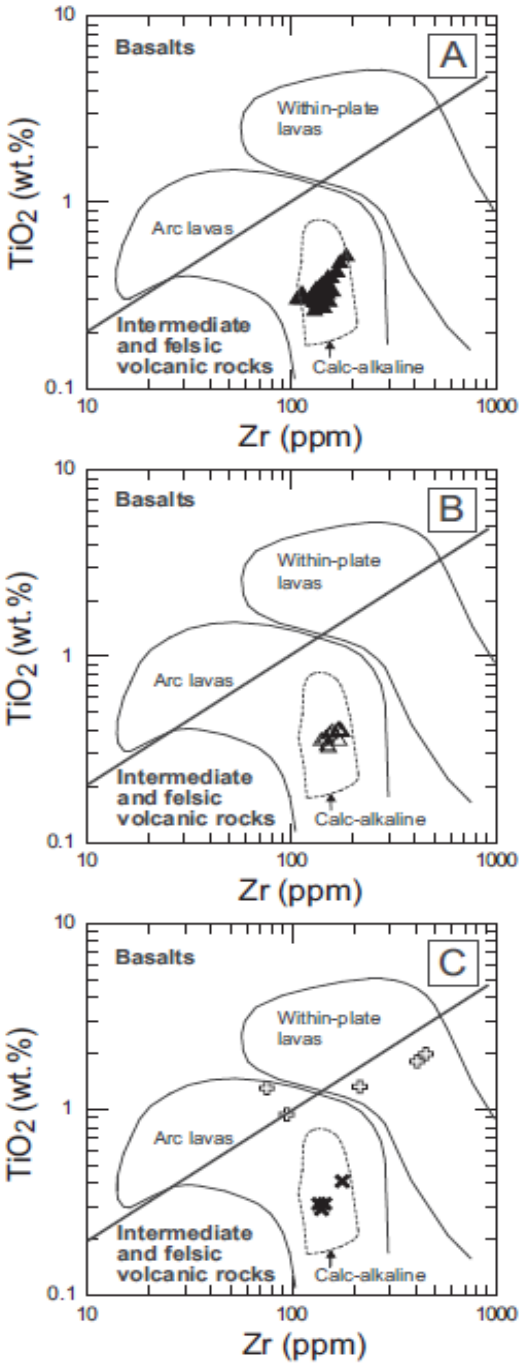

Figure 4.14: Zr versus TiO_2 discrimination diagram (Leat and Thorpe 1986), showing the line separating basalts and intermediate and felsic volcanic rocks and the fields for arc and within-plate lavas after Pearce (1980). Within the arc lavas, a field for calc-alkaline volcanic rocks is marked using the data of Ewart (1979). These diagrams show A) the lower bedrock, B) upper bedrock, and C) felsic and mafic blocks from the suevite and the lower and upper bedrock units, respectively. For symbols see Fig. 4.11.

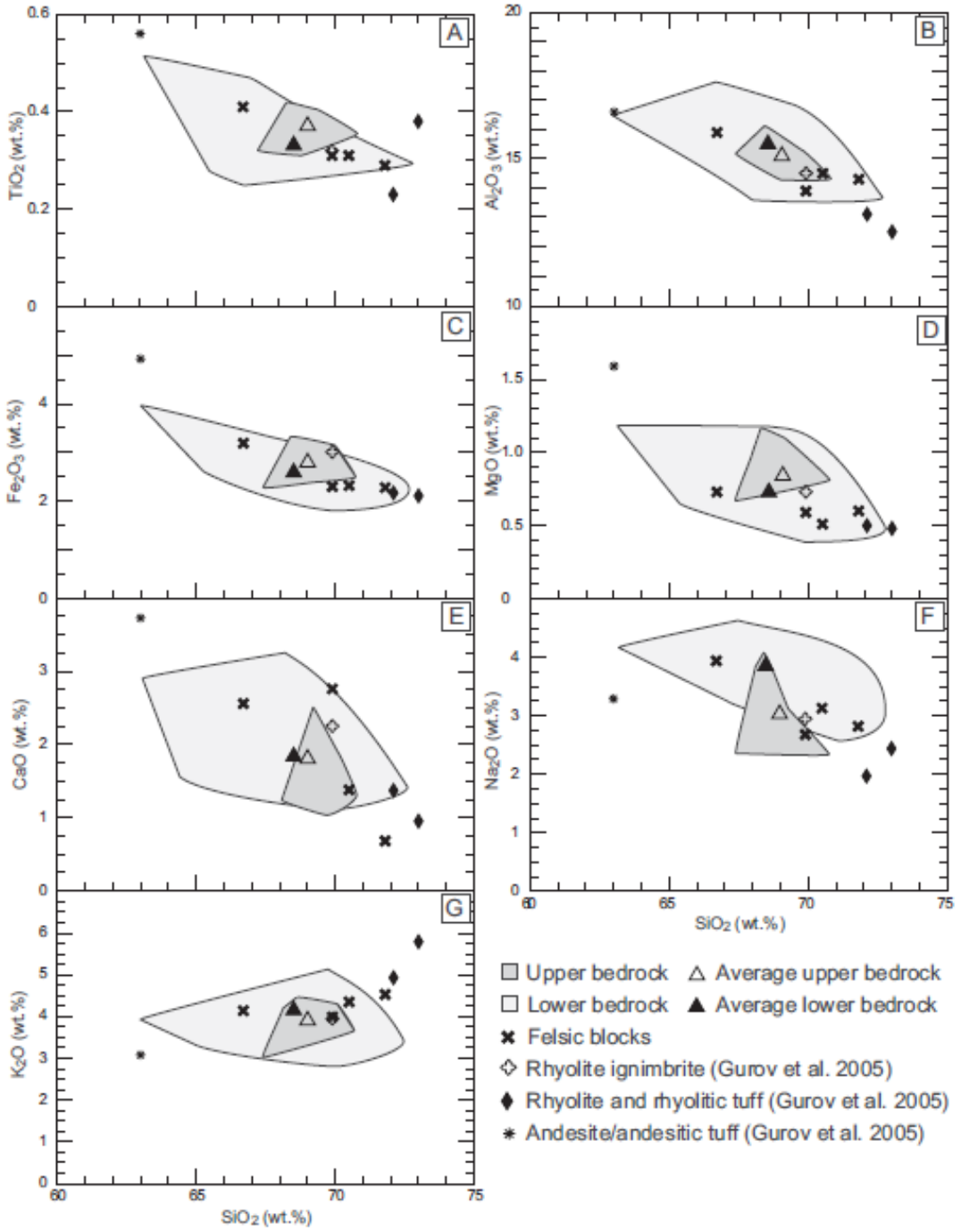

Figure 4.15: Harker diagrams (SiO_2 versus TiO_2, Al_2O_3, Fe_2O_3, MgO, CaO, Na_2O, and K_2O; A-G) for felsic target lithologies of the El'gygytgyn crater. The diagrams display the compositional fields of upper and lower bedrock and their average abundances in comparison to the felsic blocks from the suevite unit of drill core D1c and average rhyolitic ignimbrite, rhyolite, rhyolitic tuff, and andesite/andesitic tuff calculated from analyses of surface samples (Gurov et al. 2005).

4.5.4.3 Chemical Composition of Suevite and Polymict Impact Breccia Dike

Suevite samples from the 390.74 to 328 mblf depth interval and the polymict impact breccia dike at 471.96-471.42 mblf depth in the lower bedrock unit (Fig. 4.2) were analyzed

chemically as well. The suevite unit represents a chemically rather homogeneous sequence. This is also demonstrated by the small standard deviations of the average suevite composition (Table 4.2). In the TAS diagram after Cox et al. (1979) the suevite displays a dacitic composition very similar to that of the upper bedrock (Fig. 4.16).

The average composition of the suevite (Table 4.2) is similar to those of the lower and especially the upper bedrock. Nevertheless, the alkali and alkaline oxides display some differences. The CaO content of the suevite is higher in comparison to the lower and upper bedrock, the Na_2O content of the suevite is similar to that of the upper bedrock but distinctly lower than that of the lower bedrock, and the MgO content is slightly lower than that of the upper bedrock. Harker diagrams of the suevite in comparison to those for the bedrocks of the D1c drill core and to compositions of surface impactites and target rocks reported by Gurov et al. (2005) are displayed in Figs. 4.17A-G. The Harker diagrams for suevite samples suggest that the suevite could be a mixture of a dominant felsic and a minor mafic component. The felsic component can be represented by both the upper and lower bedrock of the D1c drill core, but also by the rhyolitic ignimbrite, rhyolite, and rhyolitic tuff after Gurov et al. (2005).

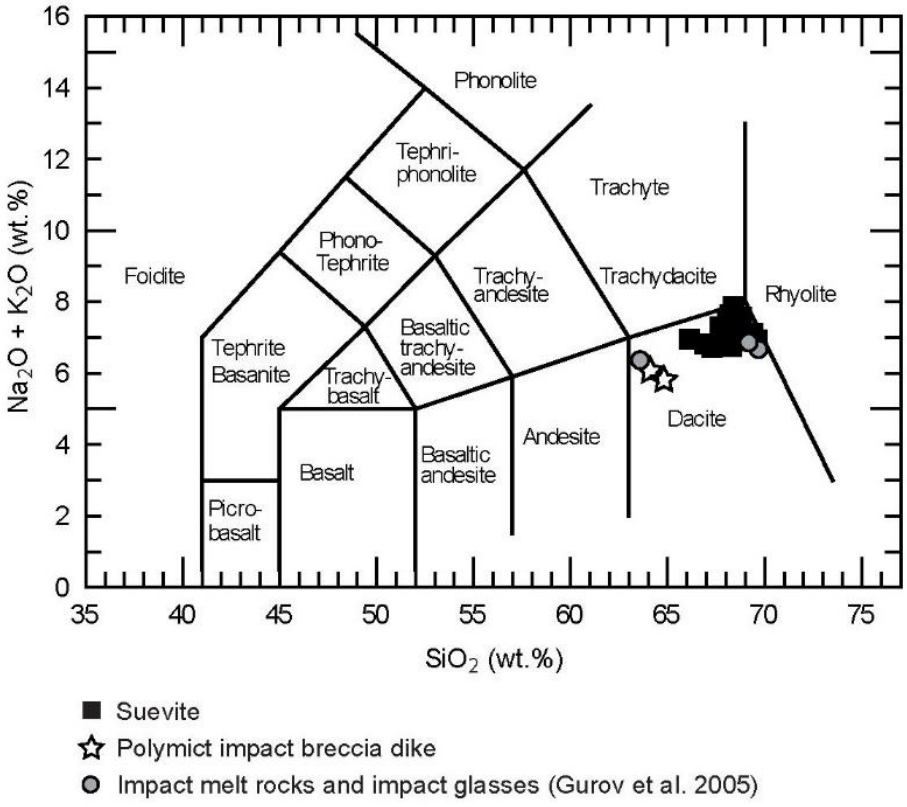

Figure 4.16: Total alkali-silica (TAS) plot after Cox et al. (1979) for the suevite and polymict impact breccia dike of drill core D1c, and average impact melt rocks and impact glasses from surface outcrops (Gurov et al. 2005). All these rock types plot in the dacite field.

The mafic component could well be the andesite/andesitic tuff of Gurov et al. (2005) or a more mafic component such as that indicated by the mafic blocks of the D1c drill core. It is conspicuous that the CaO and especially the Na_2O contents do not show this clear mixing trend in the Harker diagrams (Figs. 4.17E and 4.17F). This is most likely caused by alteration process(es) that lead to the removal of Na_2O in combination with a slight carbonatization, as indicated by comparatively higher CaO and LOI contents in many of the analyzed samples (and as discussed in the previous section of this paper). Also the surface samples reported by Gurov et al. (2005) have undergone alteration leading to changes in the Na_2O and CaO abundances.

The average impact melt rocks and impact glasses according to Gurov et al. (2005) display a similar mixing trend as the suevite of the D1c drill core. The average for impact glasses from the whole crater (SiO_2 content 69.7 wt%) and impact melt rocks from the SW, W, NW, N, and NE parts of the crater (SiO_2 content 69.2 wt%) given by Gurov et al. (2005) plot in the Harker diagrams close to the field of the suevite (Figs. 4.17A-G). In contrast, the average impact melt rocks from the S part of the crater (SiO_2 content 63.6 wt%) after Gurov et al. (2005) show a more mafic composition and plot close to the average andesite/andesitic tuff reported by Gurov et al. (2005).

The samples from the polymict impact breccia dike (from 471.92 and 471.45 mblf) in the lower bedrock unit do not plot in the Harker diagrams into the field of the main suevite unit (Figs. 4.17A-G). These dike samples display a slightly more mafic composition as indicated especially by lower SiO_2 and higher MgO, V, and Cr contents in comparison to the average suevite. In the TAS diagram after Cox et al. (1979) the polymict impact breccia dike samples plot in the dacite field (Fig. 4.16). The chemical composition of the polymict impact breccia dike is more or less in the range of the compositions for the ignimbrite of the environs of the dike in the drill core, and indicates therefore a partially locally derived impact breccia. Nevertheless, slightly higher MgO, V, and Cr abundances indicate the admixture of a mafic component. The Na_2O abundances of the polymict impact breccia dike are clearly lower in comparison to the local host rock (Fig. 4.11G) and indicate alteration leading to the removal of Na_2O. This is also supported by the high LOI (5.6 wt%) of the polymict impact breccia dike samples.

4.5.4.4 Chemical Composition of the Reworked Suevite

The reworked suevite occurs in the depth interval from about 328 to 316.77 mblf (Fig.4.2). The oxide and element abundances are more variable within this sequence than those of the underlying suevite unit (Figs. 4.11A-I). This is also demonstrated by the relatively higher standard deviations of the average reworked suevite (Table 4.2). Slightly

positive correlation of SiO_2, K_2O, and Zr, and negative correlation of MgO, CaO, LOI, and Sc contents with decreasing depth can be recognized for this unit, whereas the other elements (e.g., TiO_2, P_2O_5) do not show clear trends against depth. The average reworked suevite (Table 4.2) has - in comparison to the average suevite - lower SiO_2 and K_2O, and higher Al_2O_3, Fe_2O_3, MgO, and CaO abundances. Generally, the reworked suevite has a more mafic composition (SiO_2 abundance: average 64.8 wt%, range 60.6-68.7 wt%) than the suevite (SiO_2 abundance: average 68.2 wt%, range 66.1-69.6 wt%), which is also visible in the Harker diagrams of the reworked suevite (Figs. 4.18A-G). The Harker diagrams indicate that the reworked suevite could be - similar to the suevite - a mixture of a dominant felsic and a minor mafic component (Figs. 4.18A-G) - which is also borne out of the clast population. In contrast to the suevite the portion of the mafic component in the reworked suevite must be distinctly higher. This mafic component is also more mafic than the average andesite/andesitic tuff composition reported by Gurov et al. (2005) and seems to have an affinity toward the more mafic composition of the mafic blocks of drill core D1c. In the SiO_2/Al_2O_3 versus Fe_2O_3/K_2O discrimination diagram of Herron (1988) for the chemical classification of sedimentary rocks the reworked suevite plots into the field of graywacke (Fig. 4.19).

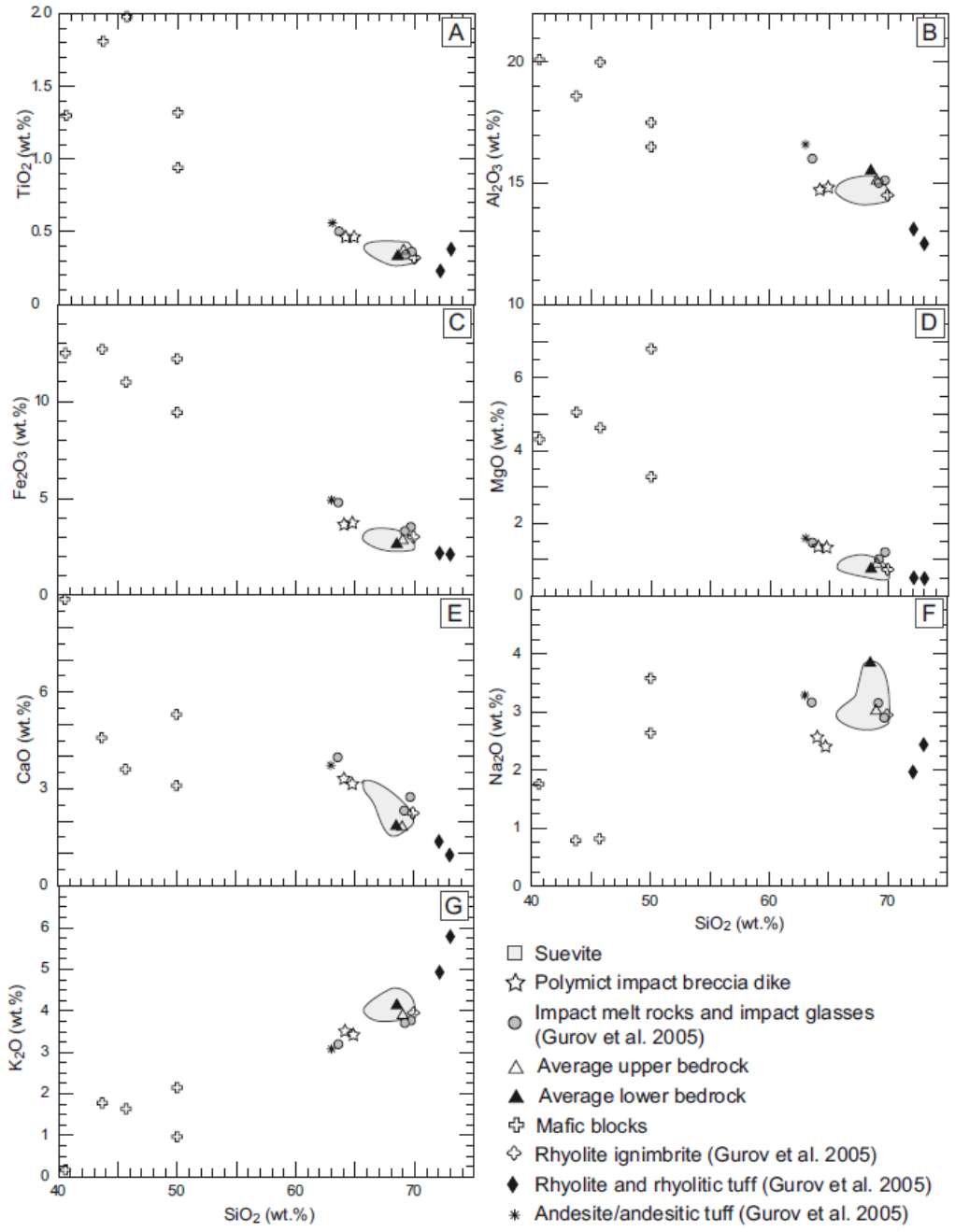

Figure 4.17: Harker diagrams (SiO_2 versus TiO_2, Al_2O_3, Fe_2O_3, MgO, CaO, Na_2O, and K_2O; A-G) for impactites, suevite, and polymict impact breccia dike of drill core D1c; average impact melt rocks and impact glasses from surface outcrops (after Gurov et al. 2005) and target lithologies (average lower and upper bedrock and mafic blocks of drill core D1c; average rhyolitic ignimbrite, rhyolite, rhyolitic tuff, and andesite/andesitic tuff from surface outcrops by Gurov et al. 2005). The compositional area for the suevite is shown as a gray area without individual compositions, while the compositions for the other lithologies are shown as individual data points (polymict impact breccia dike, mafic blocks) or averages. These diagrams indicate that the suevite is a mixture between a dominant felsic and a minor mafic component.

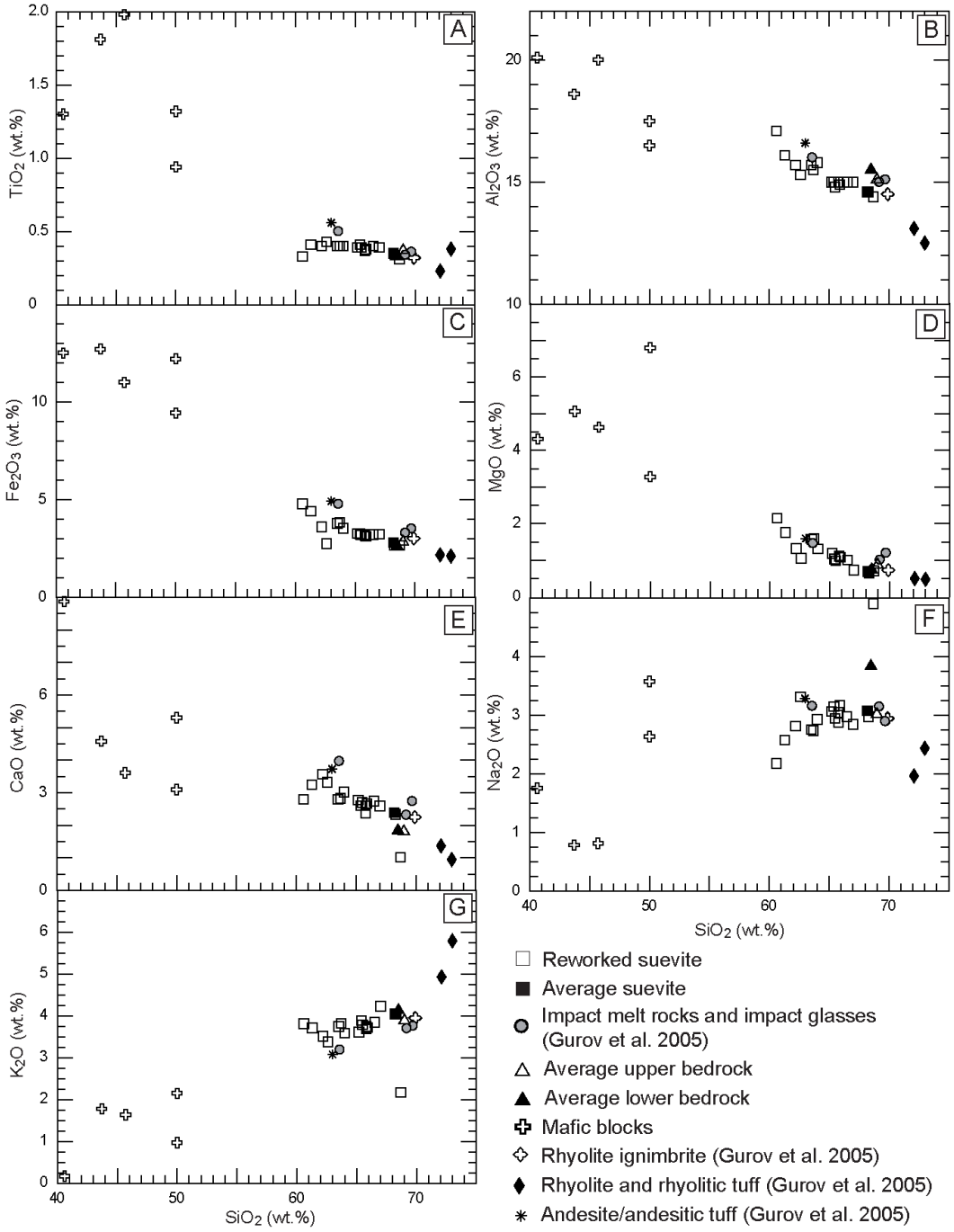

Figure 4.18: Harker diagrams (SiO_2 versus TiO_2, Al_2O_3, Fe_2O_3, MgO, CaO, Na_2O, and K_2O; A-G) for reworked suevite. For comparison, the average suevite, lower, and upper bedrock, and mafic blocks of drill core D1c and the average rhyolitic ignimbrite, rhyolite, rhyolitic tuff, and andesite/andesitic tuff for samples from surface outcrops (Gurov et al. 2005) are shown.

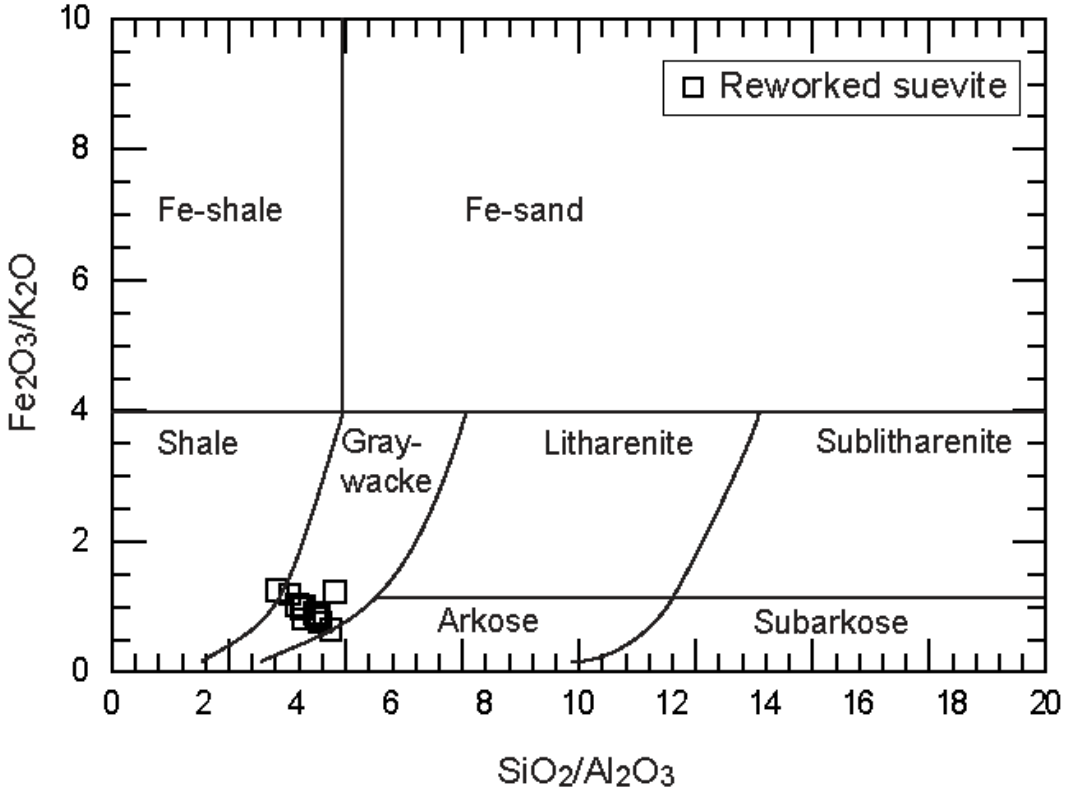

Figure 4.19: SiO_2/Al_2O_3 versus Fe_2O_3/K_2O discrimination diagram for sedimentary rocks, modified after Herron (1988). The samples of the reworked suevite are all plotting into the graywacke field.

4.6 DISCUSSION

We have carried out a detailed petrographic and chemical analysis of the impactite unit intersected in ICDP drill core D1c from the El'gygytgyn impact structure. In the following the results are discussed in terms of the formation of these units and their emplacement.

4.6.1 Petrography of the Impact Rocks and Their Origin

4.6.1.1. The Lower Bedrock Unit (517.09 to 420.89 mblf)

This unit is strongly fractured and contains pumice fragments. These elongated particles ("fiamme") are aligned at approximately 45° to the long axis of the drill core. The fractures in this core interval dip at angles from 15 to approximately 70° to the long axis of the core. In the context of this local geology it is possible to estimate the expansion and accumulation of the pyroclastic flow. The normal dip of the pumice fragments within the volcanics in the wider crater region is 6–10° (Gurov et al. 2007; and our own observations of summer 2011). Generally, the evolution of the flattened fiamme structures in ignimbrites is based on interaction with gravity and is nearly parallel orientated to the depositional surfaces

(Fisher and Schmincke 1984). A geological setting, in which all fiamme is synsedimentarily arranged with an angle of nearly 45° to the base of a flow (as in drill core D1c), seems unrealistic. This clear inclination of all fiamme particles with a general dip of about 45° indicates a post volcanic and likely impact-related adjustment of these rocks. This can be explained by assuming rotation of blocks of the ignimbritic bedrock incurred during the modification of the original impact crater, namely the creation and collapse of the central uplift, from whose flank the drill core was extracted. This also implies that the lower bedrock could represent parautochthonous target rock. Contrary to Wittmann et al.'s (2013) opinion, it is not necessary that this megablock was derived from a laterally removed site. In addition, the weakly cataclastic nature of this unit and the occurrence of a shear zone at 457 mblf depth is consistent with a minor, crater modification-related tectonic overprint of the ignimbrite bedrock.

At 471 mblf occurs an injected dike of polymict impact breccia with sharp contacts to the host rock, most likely also formed during the collapse phase of cratering. Such injections of impact breccia dikes into the crater floor or central uplift bedrock have been observed at many other impact structures, including the Rochechouart structure in France (e.g., Lambert 1981). The sharp contact of this dike to the surrounding ignimbritic bedrock likely occurred along a fracture that is oriented parallel to the general trend in this block. The mineralogical composition of the dike material includes fragments of the ignimbrite host rock, but also clasts from basalt, andesite, and trachyrhyolite in a brownish, clastic matrix composed of microscopic lithic and mineral fragments, as well as small glassy melt fragments of either volcanic or impact origin. In addition, we found many shocked quartz and feldspar grains (see also Pittarello et al. 2013), with PF and multiple PDF sets, indicating variable shock levels. This injected material shows the same petrographic and geochemical properties as the suevite from the upper part of this drill core; however, in the absence of definite proof for presence of impact melt in this dike injection, characterizing this breccia as a suevite is not possible at this stage.

In contrast to our own observations and those of Pittarello et al. (2013), Wittmann et al. (2013) apparently did not find any evidence of shock metamorphism in this dike (they only report subplanar fractures in quartz). Therefore, they hypothesize that this polymict material could represent a sliver between two ignimbrite blocks, along which radial transport over a distance of 2-4 km from the transient crater rim could have been facilitated - in analogy to the model for the emplacement of large blocks drilled at Eyreville in the inner part of the Chesapeake Bay impact structure. For that case, Kenkmann et al. (2009) modeled that these blocks could have been derived from the inner flank of the crater rim, several kilometers from the drill site. Wittmann et al. (2013) proposed that blocks of ignimbrite were derived far from

their original position in the outer reaches of El'gygytgyn crater as well - mainly because they find (as we did) only a low-shock overprint on these bedrock strata that would be consistent with shock deformation of less than 10 GPa.

However, we feel that this idea is difficult to reconcile with the observation that the two postulated units of ignimbrite, separated by the polymict impact breccia dike, show very similar orientation of pumice fragments (on average, about 45°). Furthermore, the chemical fingerprint does not separate these units at the depth of occurrence of the polymict impact breccia vein (471 m), but rather at 457 mblf. At this depth we have found petrographic evidence for a shear zone within the ignimbrite. Our preferred hypothesis is that the entire lower bedrock, i.e., the ignimbrite section, is a rotated and uplifted parautochthonous megablock with fractures and shear zones that is still located close to - or at - its original position.

4.6.1.2 The Upper Bedrock Unit (420.89 to 390.74 mblf)

This unit (420.89–390.74 mblf) consisting of a volcanic rock is generally similar to that of the lower bedrock unit. This upper pyroclastic bedrock generally lacks shock features, but it is strongly brecciated and altered. At the bottom (420.89–420.27 mblf) and at the top (391.79–390.74 mblf) occur two basaltic blocks. Between them is a pyroclastic flow with a heterogeneous composition. Here, a reddish and pumice-rich zone is overlain by a blackish, vitrophyr-rich zone. This sequence ranges from 420.27 to 407.28 mblf and is then repeated from this depth toward the top at 391.79 mblf, where it is covered by a basaltic rock (391.79-390.74 mblf). The contact zones between these subunits are gradual and not sharp. The different character of layers within this volcanic block is well known for the internal stratigraphy of a pyroclastic (ignimbritic) flow (Freundt and Schmincke 1995; Kobberger and Schmincke 1999). These authors described such a section as typical for an ignimbritic pyroclastic flow.

Mafic blocks occur between the top of the lower bedrock and the bottom of the upper bedrock. They are dark green in color, are strongly altered with severe chloritization and extremely fractured with cataclastic grain-size reduction, and local (cm wide) shear zones. Obviously, these blocks were overprinted by significant tectonic deformation that could have been incurred at preimpact time. In both mafic blocks we measured enhanced concentrations of metal oxides, in comparison to the other lithologies in this drill core. This may be an effect of intense hydrothermal alteration - possibly after the impact.

At the top of the upper bedrock unit occurs a dark gray to blackish block with an apparent width of about 1 m and a basaltic composition. Here, we found in the bedrock unit the first evidence of shock metamorphism (two sets of PDF in a quartz grain). In the top few

meters of this unit a shear zone with clasts of basalt, glass shards, and fragments of the overlying suevite occurs. The formation of this thin brecciated layer is considered to be the result of the likely turbulent emplacement of the suevite onto the crater floor, or alternatively, as a consequence of brecciation related to the modification stage of cratering. The observed sequence of mafic blocks and ignimbrite corresponds to the stratigraphy observed in the southern part of the crater area (Belyi 1977), where a swarm of mafic dikes in a rhyodacitic basement was observed. Another explanation for this stratigraphic sequence can be derived from an observation at the north-eastern crater rim. According to Gurov et al. (2005), the hills in this sector are composed of rhyolitic volcanics at the base and overlying andesites and basalts. This was confirmed by our results of the 2011 expedition. The suggestion by Wittmann et al. (2013) that the mafic blocks are possible intersections of Paleogene basalt sills (they refer to a reference by Glushkova and Smirnov 2005) is strange, as a basis for this cannot be found in that work. In summer 2011, we sampled Paleogene basalt approximately 17 km southeast of the crater rim and are currently analyzing thin sections for comparison with this mafic core intersection.

4.6.1.3 The Massive Suevite Unit (390.74 to 328 mblf)

The massive suevite occurs in the core between 390.74 and 328 mblf. The petrographic character of this package is characterized by a very fine-grained (clastic) matrix with a polymict population of lithic and mineral clasts and melt particles. The lithic clasts represent all known target lithologies and many of them display evidence for shock metamorphism covering the shock level range from <10 to >45 GPa. We found different kinds of melt particles that often contain a fine-grained crystallized matrix. We assume that these melts are of volcanic origin.

In addition, we observed light colored, transparent glassy melt particles, often with fluidal texture and frequently with many tiny vesicles. Also, some clasts with diaplectic quartz glass were noted in such melt particles of likely impact origin. A similar range of melt textures was observed in our thin sections of samples of impact glass collected on surface over the crater area by O. Juschus (then at the University of Leipzig, currently at the Technische Universität Berlin, Germany) in 2003 and by C. Koeberl (University of Vienna) in 2009. Quite a few of such melt particles from drill core samples also contain shocked mineral fragments. EMPA results have shown that many of these variegated, fluidal-textured and porous melt particles have variable chemical compositions, with the compositions of individual schlieren ranging from pure silica to apparent silica-feldspar mixtures. In contrast, volcanic melts analyzed in ignimbrite samples have basaltic to rhyodacitic compositions, similar to those of their host rocks. We presume that the variegated melts represent impact melt fragments, formed from silica or quartz-feldspar-mafic mineral combinations.

Consequently, we must assign the polymict impact breccia the status of a suevite that comprises clastic debris from target rocks mixed with impact-generated melt fragments (Stöffler and Grieve 2007).

During our sampling along the core we found three shatter cones at the depths of 376.20, 368.32, and 351.79 mblf in relatively larger clasts of volcanic rock in the breccia (see Raschke et al. 2013a). Shatter cones have been described in the regime from <5 to >30 GPa shock pressure (e.g., review in French and Koeberl 2010). Also in this sequence, three weakly shocked blocks of volcanic rocks (large fragments from a pyroclastic flow) occur around 333.83 mblf, 351.52 mblf, and 383.00 mblf depth. They show comparatively rare shock features (PF and FF in quartz grains) with the exception of the upper part of the uppermost block, where we found the first shatter cone and, in thin section, PF with FF. The latter are thought to be formed in crystalline rock at shock pressures <10 GPa (Poelchau and Kenkmann 2011). Of the three felsic blocks, only the uppermost one is weakly shocked, whereas the other two do not display any evidence of shock deformation.

Evidence for more severe shock deformation was observed in mineral grains within the fine-grained breccia matrix. We analyzed 39 thin sections from this unit (389.91-328.78 mblf), and in seven of them we found shocked quartz grains with three or more PDF sets, between 344.71 and 382.38 mblf depth. Further eight thin sections showed evidence for slight shock overprint in the form of one or two PDF sets in quartz and feldspar. These thin sections cover a large part of this breccia interval. Finally, another eight thin sections showed no evidence of shock deformation. In summary, the distribution of shock deformation in the breccia interval is heterogeneous and does not show any trend with depth. Remarkably, Wittmann et al. (2013) have not found any clear evidence for shock metamorphism over the interval from 419.30 to 330.80 mblf. It must be concluded that the suevitic impact breccia is characterized by a relatively small proportion of significantly shocked debris.

4.6.1.4 The Reworked Suevite Unit (Approximately 328-316.77 mblf)

Generally, the reworked suevite unit shows a similar litho-composition comprising a fine-grained matrix and polymict clast population as the suevite below this unit. In addition, the groundmass of the reworked suevite unit contains a large proportion of sand to clay size mineral grains, as well as larger clasts, of which some have sedimentary bedding structures. The presence of such sedimentary material is clearly the reason for the poor consolidation of this lithology. In contrast to the suevite below, the clast content is dominated by many white to dark gray tuff clasts (pumice).

Throughout this reworked suevite interval there is a considerable proportion of clasts derived from different lacustrine sediment facies. The heterogeneous groundmass is

composed of lacustrine sediments and a polymict micro-clastic matrix that includes melt fragments. In addition, tiny glassy spherules occur in both types of groundmass. Many glassy micro-spherules occur in the top five meters of this unit (e.g., Figs. 4.7D-G). We assume, based on our chemical results, that these spherules were produced during the impact process and were deposited from the ejecta plume (see also Wittmann et al. 2013). Impact spherules are droplets that were created from vaporized material, which includes components of target rocks and, possibly, projectile component (Symes et al. 1998). Impact spherules were also found in the ICDP drill core LB-5 from the Bosumtwi crater in Ghana. This complex crater has a size of 10 km diameter, which is roughly in the same size range as El'gygytgyn. The spherules were preserved in what has been interpreted as the youngest fallback deposit (Koeberl et al. 2007), together with tiny accretionary lapilli and ample shocked quartz. Quantitative chemical analysis by EMPA-EDX indicated that the glasses in such spherules from the Bosumtwi crater are compositionally heterogeneous.

Wittmann et al. (2013) compare such spherules with others that were collected on the terraces along the Enmyvaam river, approximately 20 km outside the crater. They measured a variable abundance of siderophile elements and a high Ni-content from 300 to 2000 ppm, and suggest that this could be derived from the meteoritic projectile. So far, we have not noted any significant enrichment of siderophile elements in spherules analyzed by us. Small (up to 5 mm in size), variegated melt particles occur in the micro-clastic matrix. Brownish melt fragments display a micro-crystalline texture in contrast to the light to transparent glass particles. We found inclusions of diaplectic glass and of shocked mineral grains in this kind of melt glass (see also Pittarello and Koeberl 2013), and thus we conclude that these particles are impact-produced melt.

Toward the top of the section, the abundance of lacustrine sediment increases. We observe a general trend of gradation with a fining upward sequence over the uppermost 2-3 meters, just below the transition to proper lacustrine sediment at 316 mblf depth. Larger clasts of sediment or volcanics (up to 20 cm in size) are often surrounded by a fine clay layer and a mixture of sediments of different grain size.

Wittmann et al. (2013) claim to have identified seven separate fining upward cycles in this interval. Our colleagues from the University of Cologne are also working on this section (V. Wennrich, University of Cologne, personal communication). They interpret the thin clay covering on clasts and the fine sand filling of open spaces (including a slight gradation) as the possible result of initial lake formation. After the impact, the crater was a geomorphologic depression that was periodically filled by rain and/or groundwater. The higher temperature of the rocks could have been responsible for rapid evaporation and the lake could have dried up on occasion. It is possible that a net of open, shrinking fractures penetrated the uppermost

layers of sediment and fallback impact materials. Thus, the clayey and fine sand material could have become injected into the uppermost meter of this reworked suevite interval.

We conclude that this unit is the result of mixing of impact fallout from the ejecta plume with slumped material from the inner slope of the crater rim, and sediment from the evolving crater lake. Clearly, a lot of suevitic material is mixed into this section, so that we consider the term "reworked suevite" justified.

4.6.1.5 Distribution of Shock Features Throughout the Impactites in D1c

The distribution of shock features over the whole 200 m of impactites is as expected. We found evidence for the highest shock level at the top of the drilled impact rocks, in the reworked suevite and uppermost suevite units. Below that follows a rapid decrease in shock metamorphic observations. In the upper and lower bedrocks rare mineral grains with shock features signify a very weak shock level. From the bottom up, we identified the first clear shock feature (at least 2 PDF sets in a single quartz grain) at 391.72 mblf. The distribution of the particles with shock features in the suevite is highly heterogeneous. Strongly shocked mineral grains commonly occur together with rare weakly or unshocked particles due to intense mixing of target rock fragments and melt particles. There is strong debate at this time about the nature and timing of the suevite formation process, and whether the particles are derived partially from the ejecta plume or whether all this material was kept in the form of a ground surge in the crater. It is debated whether secondary explosions caused by a fuel-coolant interaction-like process involving hot impact melt and sudden water influx could have resulted and re-mixed and re-distributed the crater fill (Grieve et al. 2010; Artemieva et al. 2013; Stöffler et al. 2013).

Wittmann et al. (2013) observed, like us and Pittarello et al. (2013), that the shock level in the bedrock sampled by core D1c is very low or, at best, <10 GPa. They use this as an argument for their hypothesis that these bedrock sections were derived from the outer part of the crater structure. However, not only is there a problem to easily move these blocks into their current positions (as discussed above), but it is also not impossible that parautochthonous crater basement could have low-shock overprint, as is observed here. For example, numerical modeling for impact structures of crater size comparable to that of El'gygytgyn (18 km) - namely for Sierra Madera (USA, 12-13 km diameter) and a hypothetical impact structure approximately 16 km in diameter by Goldin et al. (2006), and for Serra da Cangalha (Brazil, 13 km) by Vasconcelos et al. (2012) - hasshown that material below the crater floor in central parts of these structures can be reasonably expected to incur shock overprint of the order of <10 GPa. Thus, application of this argument of low-shock pressure in favor of long-distance transfer and derivation of blocks drilled at the flank of the central uplift of the El'gygytgyn impact structure does not hold.

4.6.1.6 Alteration

The entire recovered core is altered. In the lower bedrock unit, the greenish ignimbrite displays numerous fractures filled by secondary minerals (calcite and zeolite). During our expedition in 2011, we collected samples of a similar lithology, a rhyodacitic ignimbrite, inside the crater rim on surface in the eastern parts of the impact structure. These samples have the same light greenish color as the samples from the drill core. We assume that this alteration represents the usual alteration process of the approximately 85 Ma old volcanic rocks in the Arctic environment and must be considered independent of the impact overprint.

The upper bedrock and the mafic blocks are also strongly brecciated and altered; the intensity of alteration is much more pronounced than in the underlying lower bedrock. They could represent the immediate crater floor section below the crater itself, and would have been therefore strongly affected by the hydrothermal post-impact alteration. The chemical analysis of both rock types supported this observation of a strong alteration. The lower bedrock shows a distinct removal of Na_2O, whereas the mafic blocks are characterized by significant enhancement of the LOI.

The suevite is also strongly altered and the matrix shows a reddish color that we tentatively (bar further analysis) relate to the oxidation of iron. Secondary minerals occurring in fractures and pods of the poorly consolidated breccia include secondary carbonate and zeolites. The reworked suevite unit contains rock fragments that are also strongly weathered, but the impact melt particles and impact spherules are commonly quite fresh.

4.6.1.7 Chemical Composition of Impact Breccias and Target Rocks

The El'gygytgyn drill core D1c acquired about 62.7 m of suevite, which for the first time provides a representative mixture of all rocks that occurred in the target area to this impact crater. The average chemical composition of the suevite from drill core D1c (Table 4.2) approximates therefore an average target composition of the El'gygytgyn area. Previous estimates of the average target composition by Gurov and Koeberl (2004) and Gurov et al. (2005) were calculated using the relative thickness of the main volcanic rock types in the stratigraphy of the basement exposed in the wider crater area.

The comparison of the drill core suevite and the target rock average compositions (Table 4.3) displays slightly higher TiO_2, Al_2O_3, CaO, and Na_2O, lower SiO_2 and K_2O, and similar Fe_2O_3, MnO, MgO, and P_2O_5 abundances in the suevite than in the previously estimated (Gurov et al. 2005) target composition. Due to weathering (e.g., Arikas 1986; Middelburg et al. 1988) and alteration effects in both the surface rocks and the impactites of the drill core the interpretation of the CaO and Na_2O data is somewhat problematic. Nevertheless, the observed differences in SiO_2, TiO_2, Al_2O_3, and K_2O abundances indicate a

slightly more mafic composition of the target area than previously assumed. Therefore, mafic rocks, such as basalts reported from the northeast sector of the crater (geological map in Gurov et al. 2005), should have been present at a slightly higher proportion in the target area than previously considered for the calculation of the average target composition. This issue will be studied further through the upcoming geochemical analysis of a new surface sample suite from the eastern part of the crater structure and environs, which was obtained during the summer 2011 expedition.

Generally, the suevite can be considered a mixture between dominant felsic and minor mafic target components, as discussed above. Apart from the dominant felsic target components the involvement of mafic target components, e.g., andesite, andesitic tuffs, and basalts, in the suevite is confirmed (e.g., Fig. 4.17). Also the petrographic observations provided here and by Pittarello et al. (2013) support this observation. Nevertheless, the number of major target lithologies observed in the D1c drill core and available data of unshocked target rock compositions, especially for trace elements, from the literature is insufficient. Further detailed investigations and mixing calculations require additional chemical investigations of, especially, the mafic target rocks. This data shortfall also pertains to the mixing calculation results presented by Wittmann et al. (2013).

The El'gygytgyn area is part of the Okhotsk-Chukotka volcanic belt (e.g., Belyi 1977; Gurov et al. 1979; Gurov and Gurova 1991; Tikhomirov et al. 2008), which is one of the largest subduction-related volcanic provinces on Earth and most likely related to the subduction of Paleo-Pacific plates under the northeastern Asian terranes (Tikhomirov et al. 2008). Typical for the Okhotsk-Chukotka volcanic belt is the dominance of felsic magmatites that attained over 70% of the total magma volume (Tikhomirov et al. 2008). The felsic target lithologies of the El'gygytgyn drill core D1c (Figs. 4.13 and 4.15) display similar chemical composition and geochemical trends in the Harker diagrams in comparison to those from other parts of the Okhotsk-Chukotka volcanic belt (Tikhomirov et al. 2008). Both the rhyolitic volcanic rocks of the Okhotsk-Chukotka volcanic belt (Tikhomirov et al. 2008) and the felsic target lithologies of the El'gygytgyn drill core D1c (Fig. 4.14) plot in the Zr versus TiO_2 diagram in the arc lava field, supporting the formation of the volcanic rocks in a subduction-related regime.

Table 4.3: Average chemical composition and standard deviation for the suevite of the El´gygytgyn drill core D1c in comparison to the average target composition based on the regional stratigraphy for the El'gygytgyn area by Gurov and Koeberl (2004) and Gurov et al. (2005). *sd = standard deviation; †total Fe as Fe_2O_3.

	Average suevite		Average target composition
	mean	sd*	
wt.%			
SiO_2	68.2	0.9	70.72
TiO_2	0.35	0.03	0.29
Al_2O_3	14.6	0.2	13.90
$Fe_2O_3^{\dagger}$	2.80	0.19	2.72
MnO	0.06	0.01	0.06
MgO	0.69	0.10	0.72
CaO	2.39	0.34	2.01
Na_2O	3.08	0.26	2.57
K_2O	4.05	0.14	4.48
P_2O_5	0.08	0.01	0.10

4.7 CONCLUSIONS

We report the results of a detailed petrographic and geochemical investigation of the impact breccias and underlying bedrock lithologies intersected by the ICDP D1c drill core from the outer flank of the central uplift of the El'gygytgyn impact structure. Major outcomes of this work include:

(1) The lower bedrock is made up of a trachyrhyodacitic ignimbrite that can be subdivided into lower and upper parts divided by a narrow shear zone at 457.3 mblf depth. Petrographic and geochemical studies show a significant chemical variation across the shear zone. The upper bedrock is a felsic pyroclastic flow that displayed the lowermost occurrence of shock metamorphism detected in this study at 391.72 mblf depth. In general, the bedrock section is only very weakly shocked below this depth, with only one confirmed observation of shock deformation at 431.80 mblf by Pittarello et al. (2013).

(2) Both bedrock units are fractured and altered. In comparison to the other units of the drill core and to the observations of surface samples from the crater, this alteration does not seem to be influenced by the hydrothermal alteration that was established within the crater cavity after the impact.

(3) The three mafic blocks that are part of the lower and upper bedrock units represent basalt. These blocks are strongly brecciated and display a foliation, as well as cataclastic grain-size reduction and local occurrence of shear zones. They are strongly altered and locally show extraordinarily high concentration of metals (e.g., Cr, Co, Ni), in comparison to the rest of the core. It is thought that this core interval constitutes the hydrothermally altered crater floor.

(4) The suevite contains different kinds of melt particles (some of which are likely impact generated) and clasts that display the entire range of shock metamorphism. The distribution of shock features against depth does not show a significant trend but their number seems to be somewhat enhanced in the upper part of the breccia.

(5) The reworked suevite is an assemblage of lacustrine sediments and minor fallout material from the ejecta plume. We could identify all stages of shock metamorphism in the form of shocked mineral grains with PF and PDF, and presence of diaplectic glass. In addition, there are impact melt particles and impact glass spherules. Spherules have siliceous compositions with highly varied contents of other major elements. The abundance of lacustrine sediments increases toward the top and exhibits a gradually fining-upward sequence.

(6) Shocked particles are particularly enriched in the uppermost core section, the reworked suevite. In the suevite, shocked clasts occur at limited abundance at all depths but are relatively more abundant in the upper part of the suevite package. Samples from the upper bedrock unit show only very rarely slight evidence for shock metamorphism, and the lower bedrock is entirely unshocked.

(7) The trend of rapidly decreasing evidence of shock metamorphism with depth suggests that the bedrock sequence represents crater floor. The variably tilted attitude of the bedrock blocks is not inconsistent with this interpretation, as the core was obtained at the outer flank of the collapsed central uplift structure.

(8) At a depth of 471.92 mblf occurs a dike of polymict impact breccia. The clast content is dominated by particles from an ignimbritic precursor. In addition, there are many clasts of andesite, basalt, and trachyrhyolite. The fine-grained matrix contains many shocked quartz and feldspar grains and some glassy melt fragments. The origin of these melt particles is not absolutely certain at this stage, so that we avoid using the term "suevite" for this dike for now.

(9) The drill core is strongly brecciated over its entire length. Most fractures occur in the lower and upper bedrock unit and are commonly oriented at about 45° to the core axis. Open fractures are often filled by secondary minerals (calcite and zeolite), the deposition of which must have been late in the history of these rocks. It is, thus, possible that these late precipitations were caused by impact generated hydrothermal fluids.

Acknowledgments

This study has been funded by the Deutsche Forschungsgemeinschaft within the ICDP priority program through projects Re 528/10-1 and 10-2 to WUR and RTS. Drilling was carried out by DOSECC, Inc., together with the logistics supported by the International Continental Drilling Program (ICDP), the US National Science Foundation (NSF), the German Ministry of Research and Education, the Russian Academy of Sciences, and the

Austrian Ministry for Science and Research. We especially thank Hans-Rudolf Knöfler for thin section preparation, Kathrin Krahn for sample preparation for geochemical analysis, Kirsten Born for support with scanning electron microscopy, and Patrice Zaag for various technical and scientific support. We acknowledge helpful discussions with Lidia Pittarello and Christian Koeberl (University of Vienna and Natural History Museum, Austria). Reviewers Cristiano Lana and especially Bevan French, as well as the Associate Editor Christian Koeberl, are thanked for extensive comments that strongly improved the manuscript.

Editorial Handling - Dr. Christian Koeberl

Note: This chapter was also updated for more correctness in spelling and grammar. Some references were extended with "a" or "b". On page 79, in line 5 "occur" was inserted. On page 85, lines 10 and 11 were changed from "rare in" to "does not have many". On page 86, line 11 and on page 88 in the figure caption, the word "X-ray" was corrected with "electron beam". On page 91, last line the word "that" was replaced by the words "in what". On page 98, second last line, the words "alkaline earth metal" were inserted and "K_2O" was deleted.

SUPPLEMENTARY MATERIAL

Table S1: Whole rock chemical compositions of individual samples from the impactite section of the El'gygytgyn drill core D1c.

Table S1: Whole rock chemical compositions of individual samples from the impactite section of the El´gygytgyn drill core D1c.

Sample	UR-ELG	UR-ELG	UR-ELG	UR-ELG	UR-ELG	UR-ELG	UR-ELG	UR-ELG	UR-ELG	UR-ELG	UR-ELG	UR-ELG	UR-ELG	UR-ELG	UR-ELG	UR-ELG	UR-ELG	UR-ELG	UR-ELG	UR-ELG
Depth (mblf)	316.79	317.64	317.89	318.39	318.65	319.19	319.40	319.70	319.82	320.27	320.95	321.56	322.67	323.16	324.10	325.04	325.38	328.43	328.78	334.54
Type*	rsv	rsv	rsv	rsv	rsv	rsv	rsv	rsv	rsv	rsv	rsv	rsv	rsv	rsv	rsv	rsv	rsv	sv	sv	felsic block
wt.%																				
SiO_2	65.2	65.4	66.5	67.0	68.7	68.3	65.5	63.7	63.5	65.8	65.8	65.9	61.3	60.6	62.6	62.2	64.0	66.1	66.9	71.8
TiO_2	0.39	0.41	0.40	0.39	0.31	0.34	0.39	0.40	0.40	0.38	0.37	0.38	0.41	0.33	0.43	0.40	0.40	0.39	0.37	0.29
Al_2O_3	15.0	15.0	15.0	15.0	14.4	14.6	14.8	15.5	15.7	15.0	15.0	14.9	16.1	17.1	15.3	15.7	15.8	14.6	14.4	14.3
Fe_2O_3[†]	3.27	3.24	3.21	3.22	2.65	2.66	3.20	3.83	3.78	3.18	3.21	3.12	4.41	4.78	2.75	3.60	3.54	2.98	2.93	2.28
MnO	0.07	0.06	0.07	0.06	0.06	0.06	0.07	0.08	0.08	0.07	0.07	0.07	0.09	0.12	0.06	0.08	0.08	0.07	0.06	0.02
MgO	1.19	1.03	1.01	0.73	0.71	0.65	0.99	1.59	1.57	1.12	1.11	1.08	1.76	2.15	1.05	1.32	1.31	0.78	0.75	0.60
CaO	2.78	2.61	2.74	2.59	1.02	2.34	2.70	2.83	2.80	2.61	2.37	2.67	3.25	2.80	3.32	3.57	3.02	3.10	2.78	0.68
Na_2O	3.07	3.15	2.98	2.85	4.91	2.98	2.95	2.74	2.76	3.05	2.88	3.17	2.58	2.18	3.32	2.82	2.93	2.96	2.90	2.82
K_2O	3.61	3.89	3.85	4.23	2.17	4.05	3.79	3.82	3.75	3.75	3.69	3.72	3.71	3.81	3.38	3.51	3.59	3.99	3.92	4.53
P_2O_5	0.08	0.08	0.09	0.08	0.08	0.07	0.09	0.09	0.08	0.08	0.08	0.08	0.10	0.07	0.10	0.08	0.09	0.08	0.08	0.06
LOI	4.6	4.6	3.9	3.4	4.5	3.3	5.3	4.6	4.9	4.2	5.2	4.6	5.7	5.7	6.9	6.0	5.0	4.4	4.5	1.8
Total	99.26	99.47	99.75	99.55	99.51	99.35	99.78	99.18	99.32	99.24	99.78	99.69	99.41	99.64	99.21	99.28	99.76	99.45	99.59	99.18
ppm																				
Sc	7	7	7	10	6	n.a.[§]	10	9	10	6	11	8	8	10	9	9	11	7	7	<5
V	38	41	36	38	18	n.a.	43	39	42	34	33	35	38	38	39	38	39	33	31	19
Cr	19	14	10	21	<5	n.a.	18	14	11	7	<5	9	10	5	13	7	11	5	5	<5
Co	<5	<5	<5	<5	<5	n.a.	<5	<5	5	<5	<5	<5	5	<5	<5	<5	<5	<5	<5	<5
Ni	13	11	10	7	<5	n.a.	20	14	14	10	11	10	17	16	12	12	13	8	10	<5
Cu	15	15	<15	<15	<15	n.a.	16	16	15	<15	<15	<15	17	<15	<15	16	<15	<15	<15	<15
Zn	51	49	48	49	36	n.a.	49	53	54	48	48	48	54	53	46	51	50	47	46	37
Rb	124	132	129	137	53	n.a.	119	141	142	129	139	133	131	139	93	125	128	126	123	136
Sr	205	202	197	285	216	n.a.	247	199	202	218	185	215	313	273	704	223	220	329	392	151
Y	23	24	22	20	19	n.a.	21	25	25	21	22	23	26	27	21	24	23	20	19	17
Zr	164	179	169	150	158	n.a.	141	157	159	150	154	159	132	118	123	144	157	154	146	139
Nb	<10	<10	<10	<10	<10	n.a.	<10	<10	<10	<10	<10	10	10	<10	<10	<10	<10	<10	<10	<10
Ba	622	646	600	775	372	n.a.	532	597	532	635	623	627	750	750	1302	537	531	762	815	809
La	29	26	40	33	34	n.a.	30	31	34	24	28	32	44	57	23	45	31	33	26	36
Ce	79	77	78	72	78	n.a.	73	82	89	74	61	75	80	108	81	90	80	75	70	81
Pb	18	20	20	27	20	n.a.	19	23	22	18	21	18	20	21	16	21	20	20	19	17

*Abbreviations: rsv = reworked suevite, sv = suevite, ub = upper bedrock, lb = lower bedrock, pib dike = polymict impact breccia dike. [†]total Fe as Fe_2O_3. [§]n.a. = not analyzed.

Table S1 (continued): Whole rock chemical compositions of individual samples from the impactite section of the El´gygytgyn drill core D1c.

Sample	UR-ELG	UR-ELG	UR-ELG	UR-ELG	UR-ELG	UR-ELG	UR-ELG	UR-ELG	UR-ELG	UR-ELG	UR-ELG	UR-ELG	UR-ELG	UR-ELG	UR-ELG	UR-ELG	UR-ELG	UR-ELG	UR-ELG	UR-ELG
Depth (m (blf))	337.00	340.12	345.70	347.99	351.87	351.89	352.19	352.58	355.81	359.69	367.69	374.99	376.20	382.09	382.38	385.54	386.35	391.72	393.60	398.34
Type*	felsic block	sv	sv	sv	felsic block	sv	sv	sv	sv	sv	sv	sv	sv	sv	sv	felsic block	sv	mafic block	ub	ub
wt.%																				
SiO_2	70.5	69.4	68.6	68.3	66.7	68.4	68.4	68.3	67.3	68.1	67.7	68.8	68.2	68.8	69.6	69.9	68.9	50.0	68.4	68.3
TiO_2	0.31	0.34	0.34	0.38	0.41	0.40	0.32	0.30	0.38	0.36	0.35	0.32	0.36	0.39	0.32	0.31	0.35	1.32	0.40	0.39
Al_2O_3	14.5	14.7	14.7	14.5	15.9	15.1	14.5	14.5	14.9	14.6	14.7	14.7	14.9	14.3	14.4	13.9	14.5	17.5	15.9	15.6
Fe_2O_3†	2.32	2.63	2.63	2.95	3.19	3.05	2.66	2.50	3.17	2.75	2.83	2.59	2.81	2.98	2.58	2.30	2.75	9.43	3.11	3.05
MnO	0.03	0.05	0.06	0.06	0.09	0.08	0.05	0.07	0.07	0.06	0.06	0.06	0.04	0.07	0.05	0.06	0.06	0.44	0.06	0.06
MgO	0.51	0.59	0.65	0.73	0.73	0.67	0.64	0.75	0.98	0.65	0.73	0.61	0.64	0.60	0.56	0.59	0.67	3.28	0.75	0.75
CaO	1.38	2.08	2.34	2.17	2.56	2.46	2.60	2.58	2.75	2.30	2.45	2.24	1.68	2.23	1.97	2.76	2.50	5.30	1.45	1.30
Na_2O	3.13	2.93	2.98	3.13	3.94	3.78	2.98	2.79	2.86	3.25	3.25	2.91	3.21	3.46	2.89	2.68	3.03	3.58	3.97	3.89
K_2O	4.35	4.17	4.06	4.15	4.14	4.08	3.97	3.96	3.87	4.17	4.05	4.00	4.43	4.11	4.04	3.99	3.90	2.15	4.23	4.13
P_2O_5	0.06	0.08	0.07	0.08	0.10	0.09	0.07	0.06	0.09	0.07	0.08	0.07	0.07	0.09	0.07	0.06	0.08	0.78	0.09	0.09
LOI	2.3	2.6	3.4	2.9	1.7	1.5	3.5	3.5	3.4	2.8	3.3	3.0	2.7	2.4	2.9	2.9	3.1	5.6	1.1	2.0
Total	99.39	99.57	99.83	99.35	99.46	99.61	99.69	99.31	99.77	99.11	99.50	99.30	99.04	99.43	99.38	99.45	99.84	99.38	99.46	99.56
ppm																				
Sc	<5	6	5	5	7	7	<5	5	9	6	7	5	7	5	7	6	5	23	7	6
V	24	28	30	30	29	28	29	28	41	28	29	26	28	27	24	29	31	171	26	31
Cr	<5	<5	<5	<5	<5	<5	<5	<5	20	<5	<5	<5	<5	<5	<5	<5	<5	63	<5	<5
Co	<5	<5	<5	<5	<5	<5	<5	<5	<5	<5	<5	<5	<5	<5	<5	<5	<5	20	<5	<5
Ni	<5	6	5	5	5	5	<5	6	9	5	5	<5	6	<5	<5	<5	<5	60	5	6
Cu	<15	<15	<15	<15	<15	<15	<15	<15	<15	<15	<15	<15	<15	<15	<15	<15	<15	47	<15	<15
Zn	43	45	47	47	45	41	44	44	48	45	45	43	45	46	44	42	43	105	51	48
Rb	139	134	134	130	134	127	131	118	128	135	137	136	144	136	133	115	134	37	139	144
Sr	165	174	232	235	376	372	309	204	281	209	279	195	164	250	199	143	197	554	224	270
Y	18	21	18	22	21	19	20	18	20	21	20	19	18	22	20	17	19	29	17	19
Zr	144	151	153	174	176	164	146	137	146	161	155	151	163	173	150	135	155	214	173	177
Nb	<10	<10	<10	<10	<10	<10	10	<10	<10	<10	<10	<10	<10	<10	<10	<10	<10	13	10	<10
Ba	744	684	710	599	706	712	694	707	711	666	682	693	689	736	722	761	650	903	834	814
La	31	33	27	34	29	30	28	33	33	28	35	33	37	33	29	32	29	61	28	33
Ce	73	67	80	76	73	83	76	86	81	79	76	78	81	83	73	67	72	147	65	73
Pb	18	17	18	22	15	18	16	16	18	16	16	18	16	15	17	18	16	16	16	16

*Abbreviations: rsv = reworked suevite, sv = suevite, ub = upper bedrock, lb = lower bedrock, pib dike = polymict impact breccia dike. †total Fe as Fe_2O_3. §n.a. = not detected.

Table S1 (continued): Whole rock chemical compositions of individual samples from the impactite section of the El´gygytgyn drill core D1c.

Sample	UR-ELG	UR-ELG	UR-ELG	UR-ELG	UR-ELG	UR-ELG	UR-ELG	UR-ELG	UR-ELG	UR-ELG	UR-ELG	UR-ELG	UR-ELG	UR-ELG	UR-ELG	UR-ELG	UR-ELG	UR-ELG	UR-ELG	UR-ELG
Depth (m (blf))	404.79	410.66	411.69	413.55	413.76	414.37	416.99	419.40	420.60	420.90	421.36	421.61	422.80	422.98	423.69	425.47	430.31	431.77	432.56	434.45
Type*	ub	ub	ub	ub	ub	ub	ub	ub	mafic block	mafic block	lb	lb	mafic block	mafic block	lb	lb	lb	lb	lb	lb
wt.%																				
SiO_2	70.5	69.7	69.9	69.3	67.6	68.3	68.6	69.1	40.6	50.0	69.0	66.8	43.7	45.7	67.6	67.4	68.9	68.3	67.4	69.2
TiO_2	0.36	0.38	0.35	0.39	0.33	0.40	0.32	0.35	1.30	0.94	0.31	0.35	1.81	1.98	0.39	0.39	0.34	0.32	0.34	0.29
Al_2O_3	14.5	15.0	15.0	14.7	15.2	15.3	15.0	14.4	20.1	16.5	14.4	15.7	18.6	20.0	15.9	16.1	14.9	16.2	15.6	15.5
Fe_2O_3†	2.59	2.74	3.03	3.09	2.32	2.88	2.54	2.97	12.5	12.2	2.31	2.76	12.7	11.0	2.93	3.25	2.67	2.55	2.79	2.49
MnO	0.03	0.04	0.04	0.04	0.03	0.04	0.04	0.06	0.35	0.16	0.05	0.05	0.21	0.16	0.04	0.05	0.05	0.04	0.05	0.05
MgO	0.83	0.92	0.93	0.79	0.70	1.11	0.97	1.06	4.31	6.80	0.88	0.99	5.06	4.63	1.11	1.11	0.80	0.65	0.78	0.68
CaO	1.36	1.61	1.11	1.87	3.05	1.84	2.07	2.48	8.87	3.10	2.39	1.94	4.58	3.61	1.24	1.41	1.83	1.23	1.84	1.38
Na_2O	2.44	2.81	2.67	2.92	2.41	3.10	2.99	3.02	1.76	2.64	2.97	3.63	0.79	0.82	3.58	3.82	3.73	4.41	4.23	4.27
K_2O	3.76	4.00	4.31	3.49	3.11	4.04	4.30	3.57	0.17	0.97	4.09	4.59	1.78	1.64	4.48	4.21	3.89	4.44	4.37	4.33
P_2O_5	0.08	0.08	0.08	0.08	0.08	0.09	0.07	0.08	0.33	0.23	0.07	0.07	0.90	0.92	0.08	0.09	0.08	0.07	0.07	0.06
LOI	2.7	2.6	2.1	2.4	4.2	2.6	2.4	2.2	9.2	5.9	2.6	2.4	9.2	8.7	1.9	1.9	2.0	1.1	1.6	1.3
Total	99.15	99.88	99.52	99.07	99.03	99.70	99.30	99.29	99.49	99.44	99.05	99.28	99.33	99.16	99.25	99.73	99.19	99.31	99.07	99.55
ppm																				
Sc	5	8	6	7	7	7	6	8	50	34	<5	<5	49	51	8	5	<5	<5	5	<5
V	30	29	30	26	29	35	26	29	288	191	25	28	310	327	29	28	29	32	23	20
Cr	<5	<5	<5	<5	<5	<5	<5	<5	603	340	<5	<5	945	940	<5	<5	<5	<5	<5	<5
Co	<5	<5	<5	<5	<5	<5	<5	<5	31	29	<5	<5	52	43	<5	<5	<5	<5	<5	<5
Ni	<5	<5	<5	<5	<5	5	<5	<5	112	78	5	<5	278	251	8	5	6	5	<5	<5
Cu	<15	<15	<15	<15	<15	<15	<15	<15	56	38	<15	<15	90	97	<15	<15	<15	<15	<15	<15
Zn	36	41	49	43	36	44	40	42	298	81	38	41	111	96	41	46	39	46	39	36
Rb	126	123	132	105	92	126	136	103	<5	25	117	132	70	73	137	139	117	127	129	126
Sr	175	211	188	219	225	218	223	233	507	249	207	187	268	265	205	203	248	316	269	209
Y	17	18	21	19	19	21	19	17	27	25	16	17	53	64	19	19	19	21	18	18
Zr	147	154	171	159	150	169	152	140	75	94	136	139	409	450	151	157	145	150	146	130
Nb	<10	<10	<10	<10	<10	<10	<10	<10	<10	<10	<10	<10	19	20	<10	<10	<10	<10	<10	<10
Ba	711	772	763	774	761	824	871	646	107	192	871	770	596	463	750	718	756	761	733	762
La	30	30	33	23	25	29	30	33	32	29	30	32	73	72	29	30	29	24	26	30
Ce	67	65	71	59	69	64	71	63	50	39	74	69	151	158	60	68	64	67	63	67
Pb	17	17	17	18	16	18	20	16	<15	<15	17	<15	16	<15	15	<15	19	25	16	<15

*Abbreviations: rsv = reworked suevite, sv = suevite, ub = upper bedrock, lb = lower bedrock, pib dike = polymict impact breccia dike. †total Fe as Fe_2O_3. §n.a. = not detected.

Table S1 (continued): Whole rock chemical compositions of individual samples from the impactite section of the El´gygytgyn drill core D1c.

Sample	UR-ELG	UR-ELG	UR-ELG	UR-ELG	UR-ELG	UR-ELG	UR-ELG	UR-ELG	UR-ELG	UR-ELG	UR-ELG	UR-ELG	UR-ELG	UR-ELG	UR-ELG	UR-ELG	UR-ELG	UR-ELG	UR-ELG	UR-ELG
Depth (m (blf))	435.63	436.48	438.09	440.86	441.47	442.45	445.25	448.31	452.81	455.88	457.45	462.59	465.34	469.08	470.28	471.45	471.92	475.98	478.02	480.46
Type*	lb	lb	lb	lb	lb	lb	lb	lb	lb	lb	lb	lb	lb	lb	lb	pib dike	pib dike	lb	lb	lb
wt.%																				
SiO_2	68.0	67.7	70.8	68.9	68.5	71.2	69.4	67.9	69.8	68.5	70.0	63.2	66.9	68.2	65.2	64.8	64.1	68.0	66.5	68.1
TiO_2	0.35	0.37	0.32	0.30	0.33	0.30	0.36	0.30	0.29	0.32	0.33	0.51	0.47	0.33	0.42	0.46	0.46	0.36	0.34	0.31
Al_2O_3	15.6	14.9	14.6	13.8	15.4	14.2	15.6	15.7	15.0	15.1	15.0	16.5	16.9	13.8	16.6	14.8	14.7	15.6	17.5	15.2
Fe_2O_3†	2.87	3.00	2.33	2.31	2.69	2.26	2.57	2.44	2.44	2.65	2.50	3.93	2.96	2.69	3.50	3.67	3.59	2.74	2.55	2.57
MnO	0.05	0.06	0.05	0.05	0.05	0.04	0.05	0.06	0.05	0.04	0.03	0.07	0.04	0.05	0.07	0.07	0.08	0.05	0.05	0.05
MgO	0.76	0.83	0.61	0.58	0.75	0.58	0.66	0.69	0.59	0.71	0.99	1.17	0.62	0.85	1.15	1.30	1.32	0.75	0.74	0.68
CaO	1.64	2.01	1.72	2.90	1.66	1.62	1.63	2.37	1.88	2.28	1.27	2.86	1.64	3.14	2.45	3.15	3.31	2.04	1.57	1.80
Na_2O	4.36	3.97	3.74	3.76	4.17	3.61	4.11	3.65	3.43	3.54	2.83	4.22	4.16	3.30	3.73	2.38	2.54	4.00	4.10	3.78
K_2O	3.99	3.82	3.62	3.28	4.28	3.87	4.31	4.19	4.44	3.89	4.11	3.94	4.30	2.99	3.77	3.43	3.52	4.14	4.13	4.25
P_2O_5	0.07	0.08	0.07	0.06	0.06	0.05	0.07	0.06	0.06	0.05	0.07	0.12	0.12	0.07	0.10	0.11	0.11	0.06	0.07	0.06
LOI	1.5	2.7	1.5	3.6	1.6	1.7	0.9	2.4	1.5	2.2	2.7	3.0	1.5	3.9	2.9	5.6	5.6	1.4	1.7	2.9
Total	99.19	99.44	99.36	99.54	99.49	99.43	99.66	99.76	99.48	99.28	99.83	99.52	99.61	99.32	99.89	99.77	99.33	99.14	99.25	99.70
ppm																				
Sc	6	<5	5	5	6	<5	5	6	<5	5	<5	10	7	5	6	8	11	6	5	6
V	28	27	25	26	24	20	25	20	19	25	27	58	40	29	38	53	58	29	23	22
Cr	<5	<5	<5	<5	<5	<5	<5	<5	<5	<5	<5	<5	<5	<5	<5	48	44	<5	<5	<5
Co	<5	<5	<5	<5	<5	<5	<5	<5	<5	<5	<5	6	<5	<5	<5	5	5	<5	<5	<5
Ni	<5	5	<5	<5	5	<5	<5	6	5	<5	<5	12	<5	<5	5	15	15	5	5	<5
Cu	<15	<15	<15	<15	<15	<15	<15	<15	<15	<15	<15	15	<15	<15	<15	17	16	<15	<15	<15
Zn	41	44	38	42	39	34	43	36	38	39	39	55	46	38	49	50	49	44	42	38
Rb	124	117	107	117	120	112	134	125	133	114	135	124	145	83	133	115	113	111	119	116
Sr	268	507	594	1274	453	893	226	315	283	219	109	210	237	192	302	334	300	298	472	219
Y	20	20	18	16	17	16	19	17	18	18	17	19	21	16	23	19	20	20	18	19
Zr	150	149	128	107	136	113	142	138	133	146	140	186	173	159	167	146	142	147	137	145
Nb	<10	10	<10	<10	<10	<10	<10	<10	<10	<10	<10	<10	<10	<10	<10	<10	<10	<10	<10	<10
Ba	679	783	762	708	811	678	642	699	731	624	819	716	861	686	684	662	660	767	751	600
La	35	34	36	34	33	26	36	29	34	33	36	26	31	29	33	25	29	36	27	29
Ce	72	68	72	80	63	67	68	64	70	72	68	58	78	64	76	70	66	61	68	61
Pb	18	17	17	15	20	17	19	<15	18	20	63	<15	19	<15	<15	18	17	26	21	<15

*Abbreviations: rsv = reworked suevite, sv = suevite, ub = upper bedrock, lb = lower bedrock, pib dike = polymict impact breccia dike. †total Fe as Fe_2O_3. §n.a. = not detected.

Table S1 (continued): Whole rock chemical compositions of individual samples from the impactite section of the El´gygytgyn drill core D1c.

Sample	UR-ELG	UR-ELG	UR-ELG	UR-ELG	UR-ELG	UR-ELG	UR-ELG	UR-ELG	UR-ELG	UR-ELG	UR-ELG	UR-ELG	UR-ELG	UR-ELG	UR-ELG	UR-ELG
Depth (m (blf))	483.34	485.26	490.43	493.20	493.92	496.49	497.42	502.65	507.27	507.54	508.19	511.65	512.29	514.97	515.94	515.94
Type*	lb	lb	ash tuff	lb	lb	lb	lb	lb	lb	lb	lb	lb	lb	lb	ash tuff	lb
wt.%																
SiO_2	67.5	66.8	73.0	68.4	70.3	68.9	68.5	72.4	68.9	70.1	69.6	70.2	70.7	65.6	81.5	69.9
TiO_2	0.34	0.26	0.20	0.29	0.31	0.30	0.32	0.30	0.30	0.31	0.29	0.28	0.31	0.29	0.16	0.27
Al_2O_3	16.1	16.9	11.5	15.4	14.8	15.6	15.6	13.7	15.5	14.8	16.4	14.8	15.3	16.6	8.7	15.2
Fe_2O_3†	3.01	2.31	1.73	2.54	2.41	2.32	2.46	2.35	2.52	2.49	2.10	2.26	2.14	2.97	3.23	2.36
MnO	0.07	0.04	0.03	0.05	0.05	0.04	0.05	0.05	0.05	0.05	0.04	0.05	0.04	0.07	0.02	0.06
MgO	0.86	0.59	0.42	0.64	0.61	0.59	0.61	0.55	0.65	0.66	0.46	0.60	0.53	0.80	0.19	0.63
CaO	2.87	1.69	2.69	1.69	1.32	1.52	2.00	1.46	1.33	1.59	1.23	1.47	1.54	2.45	0.46	1.54
Na_2O	3.83	4.46	1.48	4.18	3.84	3.86	3.87	3.64	4.04	3.87	3.71	3.84	3.65	3.94	1.70	3.62
K_2O	3.87	4.32	2.63	4.65	4.27	4.54	4.08	3.40	4.72	4.37	4.04	4.83	4.17	4.03	2.47	4.22
P_2O_5	0.07	0.05	0.01	0.05	0.06	0.05	0.06	0.06	0.06	0.06	0.05	0.05	0.06	0.06	0.01	0.05
LOI	1.0	1.8	5.4	1.6	1.6	1.7	2.0	1.3	1.4	1.5	1.4	1.4	1.4	2.6	0.8	1.5
Total	99.52	99.22	99.09	99.49	99.57	99.42	99.55	99.21	99.47	99.80	99.32	99.78	99.84	99.41	99.24	99.35
ppm																
Sc	6	<5	<5	5	<5	6	6	<5	5	<5	<5	6	<5	6	<5	<5
V	24	21	15	19	18	20	22	24	19	21	17	19	23	17	12	19
Cr	<5	<5	<5	<5	<5	<5	<5	<5	<5	<5	<5	<5	<5	<5	<5	<5
Co	<5	<5	<5	<5	<5	<5	<5	<5	<5	<5	<5	<5	<5	<5	<5	<5
Ni	<5	5	<5	<5	<5	<5	6	<5	<5	<5	5	<5	<5	<5	5	<5
Cu	<15	<15	17	<15	<15	<15	<15	<15	<15	<15	<15	<15	<15	<15	16	<15
Zn	40	39	52	39	41	42	43	37	38	37	34	37	41	48	<15	41
Rb	129	125	106	140	129	134	135	110	148	132	123	133	119	127	104	131
Sr	403	636	3895	425	413	537	1506	411	190	221	197	422	463	206	87	202
Y	18	20	13	18	18	17	17	19	18	19	18	18	19	22	23	18
Zr	133	130	<10	129	131	130	113	136	141	137	133	134	131	153	68	144
Nb	<10	<10	<10	<10	<10	<10	10	<10	10	<10	<10	<10	<10	<10	<10	<10
Ba	769	620	311	702	721	742	693	579	764	716	663	795	787	648	343	717
La	29	28	18	34	35	26	37	27	31	23	20	29	30	36	19	26
Ce	62	59	53	71	62	69	78	66	70	68	70	69	68	79	45	69
Pb	18	17	17	18	19	17	20	17	17	18	19	20	20	20	16	20

*Abbreviations: rsv = reworked suevite, sv = suevite, ub = upper bedrock, lb = lower bedrock, pib dike = polymict impact breccia dike. †total Fe as Fe_2O_3. §n.a. = not detected.

CHAPTER 5

THE 2011 EXPEDITION TO THE EL'GYGYTGYN IMPACT STRUCTURE, NORTHEASTERN RUSSIA: TOWARD A NEW GEOLOGICAL MAP FOR THE CRATER AREA.

This Chapter has been published as the following peer-reviewed article:

Raschke U., Zaag P. T., Schmitt R. T., and Reimold W. U. 2014. The 2011 expedition to the El'gygytgyn impact structure, Northeast Russia: Towards a new geological map for the crater area. *Meteoritics and Planetary Science* 49:978-1006, http://dx.doi.org/10.1111/maps.12306.

5.1 ABSTRACT

El'gygytgyn is a 3.6 Ma, 18 km diameter, impact crater formed in an approximately 88 Ma old volcanic target in Northeast Siberia. The structure has been the subject of a recent ICDP drilling project. In parallel to those efforts, a Russian-German expedition was undertaken in summer 2011 to investigate the permafrost soil, lake terraces, and the volcanic rocks of the southern and eastern crater rim. This provided the unique opportunity for mapping and sampling of the volcanic target rocks around a large part of this complex impact structure. Samples from 43 outcrops were collected and analyzed petrographically and geochemically. The results were combined with earlier mapping outcomes to create a new geological map of this impact structure and its immediate environs, at the scale of 1:50,000. Compositions of our rock suites are compared with the lithologies of the 2009 ICDP drill core. The ignimbrite described as lower bedrock in the ICDP drill core shows petrographically and chemically strong similarities to the rhyolitic and rhyodacitic ignimbrites observed on surface. The suevite sequence exposed in the ICDP drill core is a mixture of all observed target rocks at their respective proportions in the area. In contrast to previous studies, the calculated average target composition of El'gygytgyn takes the contribution of the basic target rocks into consideration: mafic and intermediate rocks approximately 7.5%, and felsic rocks approximately 92.5%.

5.2 INTRODUCTION

The El'gygytgyn impact structure is located about 100 km north of the Arctic Circle on the Chukotka Peninsula of far northeast Russia, centered at 67°300 N and 172°340 E (Fig. 5.1a). The 18 km diameter, circular depression was discovered in 1933 through early remote

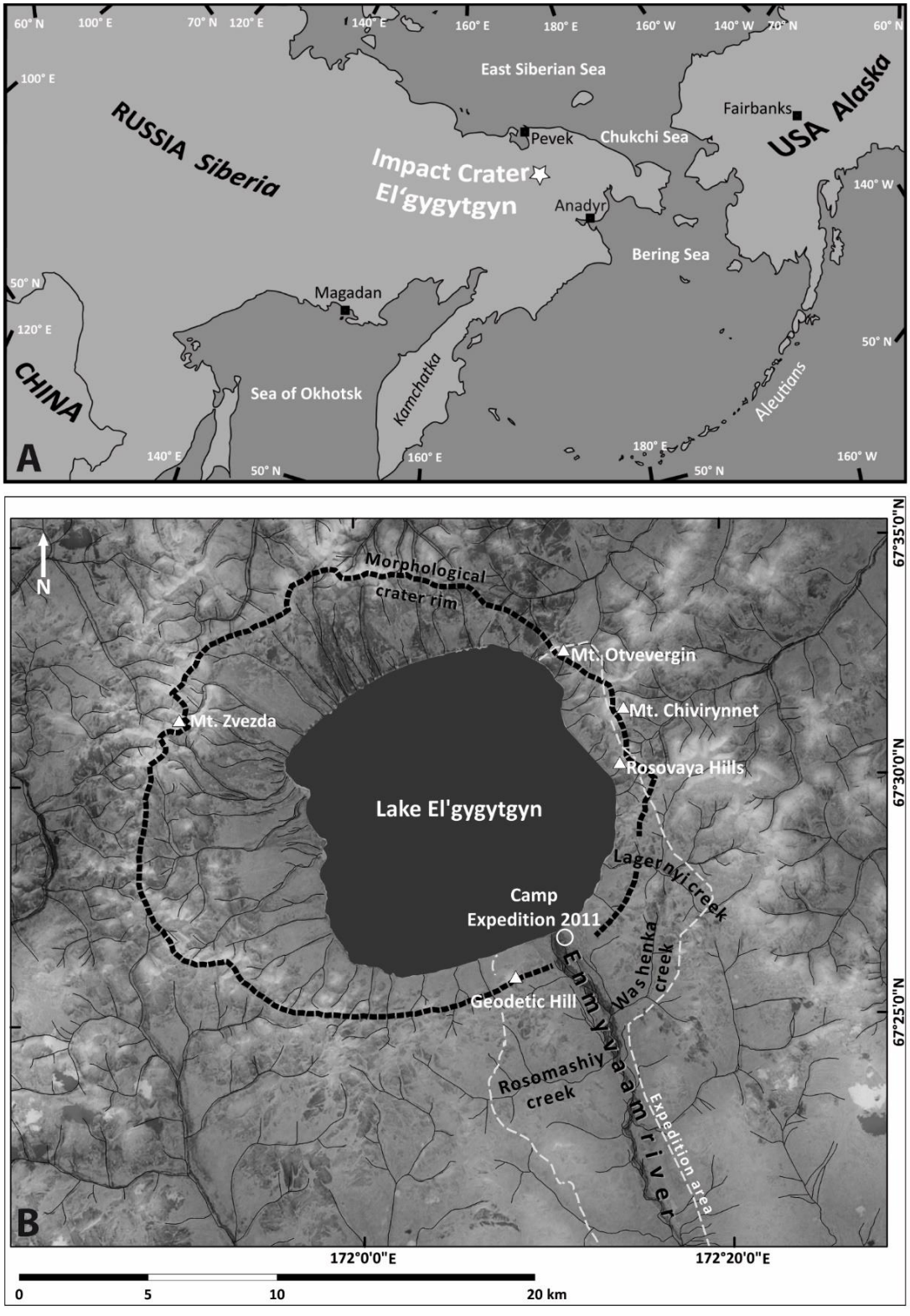

Figure 5.1: A) Geographic location of the El'gygytgyn impact structure in NE Russia, Chukotka Peninsula. Map based on Google Earth image. This image is part of the new geological map. B) Simplified geographic overview of the entire crater region with respect to the most important locations referred to in this work. Hill shaded digital elevation model based on ASTER GDEM V2.

sensing studies (Obruchev 1957) and then thought to represent a depression of volcanic origin. In the mid-20th century, field investigation of the Anadyr Mountains that are part of the Ochotsk-Chukotsky Volcanic Belt (OCVB) began. In 1958, V.F. Belyi and K.V. Parakezov compiled the first geological map of this region at the 1:500,000 scale (Belyi 1958). Nekrasov and Raudonis (1963) were the first to propose a possible impact origin for the El'gygytgyn crater structure. Between 1972 and 1974, a major geological mapping campaign was undertaken of the crater and its surroundings, especially over the Enmyvaam area to the south of the crater (Fig. 5.1b). The official geological maps for this region (sheets Q-59 III-IV, scale 1:200,000) were published by the Russian Ministry of Geology and edited by Raevsky and Potapova (1984) and Zheltovsky and Sosunov (1985), respectively. Dietz and McHone (1976) studied LANDSAT images of this area and concluded that El'gygytgyn probably was the largest Quaternary impact crater on Earth. Gurov et al. (1979a) confirmed the impact origin of this crater structure by analyzing shocked rocks (impactites) sampled during a field campaign in 1977/78 (for further results on this sample suite, see also Gurov et al. [2005] and Pittarello et al. [2013]).

The age of the El'gygytgyn impact was investigated by several authors. First, Storzer and Wagner (1979) obtained an age of 4.52 ± 0.11 Ma from fission-track dating of impact glass and melt rocks. Komarov et al. (1983) suggested an age of 3.45 ± 0.15 Ma, also from fission-track dating of impactites. K-Ar dating by Gurov et al. (1979b) yielded a similar age of 3.5 ± 0.5 Ma and, later, Layer (2000) obtained an age of 3.58 ± 0.04 Ma for impact glass particles by $^{40}Ar/^{39}Ar$ dating. This is currently the preferred age for this impact event.

Here, we present a petrographic and chemical characterization of surface lithologies of the eastern El'gygytgyn crater area, as sampled during the crater expedition of 2011 and including samples collected in 2003 by O. Juschus (HNE Eberswalde). The results of this study were combined with literature data to create a new geological map of the El'gygytgyn crater area and for a comprehensive discussion of the chemical characteristics of El'gygytgyn country rocks in the crater environs and drilled by ICDP in 2009/2010 (cf. Koeberl et al. 2013). We have found (Raschke et al. 2013a, 2013b) that the suevite sequence exposed in the ICDP drill core is a mixture of all observed target rocks, at their respective proportions in the area. In contrast to previous studies, the calculated average target composition of El'gygytgyn takes the contribution of the basic target rocks into consideration.

5.2.1 Geological and Stratigraphic Background

The El'gygytgyn impact structure was formed in the central part of the Late Mesozoic OCVB and at the southeastern slope of the Academician Obruchev Ridge in central Chukotka (Gurov and Koeberl 2004; Koeberl et al. 2013). The regional geological setting is mostly

known from the work of Belyi (1977, 1988, 1994, 2004, 2010) and Belyi and Belaya (1998). The volcanic rocks of this region were described as Late Cretaceous units (Albian to Campanian/Maastrichtian age) of the OCVB (Belyi and Belaya 1998). There are eight different formations: the Alkakvun, Kalenmuvaam, Pykarvaam, Voron'in, and Koekvun' formations that constitute the Chauna Group with ages between approximately 82 and 106 Ma, and the Ergyvaam, Emuneretveem, and Enmyvaam formations that are younger than the Chauna Group with a Turonian to Campanian/Maastrichtian age (74-82 Ma, Table 5.1; Belyi and Belaya 1998; Stone et al. 2009). The same authors analyzed samples from the El'gygytgyn region and the area to the south along the Enmyvaam, Ergyvaam, and Mechekrynnetveem Rivers (and others) up to a distance of approximately 40 km from the crater. They reported petrological, palynological, and geochemical analyses, including K-Ar and ^{40}Ar-^{39}Ar dating. Stratigraphic and chronological information is compiled in Table 5.1. The age of the Chauna Group volcanics (100-87 Ma) is still under debate. Kelley et al. (1999) analyzed samples taken at a tributary of the Palyavaam River, approximately 120 km NE of El'gygytgyn Lake. They determined an ^{40}Ar/^{39}Ar age of approximately 88 Ma for these rocks. In 2004, Ispolatov et al. reported an ^{40}Ar/^{39}Ar age of 87.6 ± 0.5 Ma for samples also from the northern part of the OCVB. Both groups suggested a relatively short eruption phase for the Chauna Group (1-6 Ma) during Coniacian time. Overall, the stratigraphy for the entire area of the OCVB is still not firm. Here, we are focusing on the relatively small region of the actual crater and its immediate environs, to which the stratigraphic map of Stone et al. (2009) applies (a modified version of which is shown as Fig. 5.2).

The description of the El'gygytgyn crater structure as a complex impact structure is strongly based on the work of Eugene P. Gurov (e.g., Gurov et al. 1978, 1979a; Gurov and Gurova 1982; Gurov and Koeberl 2004). The approximately 14 km wide crater basin is almost completely covered by the nearly circular Lake El'gygytgyn (Fig. 5.3). The 170 m deep center of the lake is somewhat offset with respect to the center of the crater (Gebhardt et al. 2006). This southeasterly displacement is the result of the establishment of a complex system of lacustrine terraces in the immediate surroundings of the lake. In the western and northern parts of the lake environs, the terraces are up to a few kilometers wide and the oldest terraces have reached elevations of approximately 80 m above lake level (Gurov and Koeberl 2004; Gurov et al. 2007). An approximately 2 km wide central peak underneath postimpact sediments was suggested by Feldman et al. (1981). Seismic investigations during a 2003

Table 5.1: Compilation of different stratigraphic units of the northern Ochotsk-Chukotsky Volcanic Belt (OCVB). Age determination and lithological composition by Belyi and Belaya (1998) are results of $^{39}Ar/^{40}Ar$ and K/Ar-dating and petrochemical studies of samples from the entire volcanic province. Stone et al. (2009) analyzed samples from the crater region and the area towards the southeast along the Enmyvaam River. GSSP means Global Stratotype Section and Point (Gradstein et al. 2012).

Stage/ Age *[Ma (after GSSP 2012)]*	**Group**	**Formation**	**Lithologies** *(Belyi 1977; Belyi & Belaya 1998)*	**Age (Ma)** *(Belyi & Belaya, 1998)*	**Age (Ma)** *(Stone et al. 2009)*	**Occurrence in crater area** *(Stone et al. 2009)*
66.0±0.05 **Maastrichtian**		Enmyvaam Fm.	Max. 100 m ignimbrites and basalts	73.9±0.4	69.0±0.9 73.9±0.4	Far SE area
72.1±0.2 **Campanian**		Emuneretveem Fm.	400 m felsic ignimbrites, tuffs	78.7±3.8	75.2±0.3	Not exposed in the crater region
		Ergyvaam Fm.	Max. 900 m rhyolitic, partly vitrophyric ignimbrites	82.0±3.0	78.1±0.7	NE crater rim (Mt. Otvevergin); along Enmyvaam River
83.6±0.5 **Santonian**	**C h a u n a G r o u p**	Koekvun' Fm.	550 m basalts, andesites, minor dacites and volcaniclastic rocks	83.2±0.3	82.3±1.3	SE crater rim and in Enmyvaam River and floodplain
86.3±0.5 **Coniacian**		Voron´in Fm.	50 – 550 m felsic to intermediate tuffs and ignimbrites	87.1±0.3	91.1±0.9	NE crater rim
89.8±0.3 **Turonian**		Pykarvaam Fm.	400 – 500 m rhyolitic ignimbrites, tuffs	88.9±0.7	88.5±2.7	Whole crater rim SE, NE environs
		Kalenmuvaam Fm.	800 – 900 m andesite-dacite ignimbrites, lava and tuffs			Not exposed in the crater region
93.9±0.2 **Cenomanian** 100.5±0.4		Alkakvun Fm.	1000 – 1200 m rhyolitic ignimbrites and tuffs and tuffaceous sediments			Not exposed in the crater region

field campaign in preparation of the ICDP drilling project confirmed that a central peak is not exposed on the recent surface of the crater floor, but occurs buried under 320-350 m of lacustrine sediments, with a probable diameter of approximately 4 km (Nolan et al. 2003; Gebhardt et al. 2006).

The El'gygytgyn crater is surrounded by a complex system of faults (Raevsky and Potapova 1984; Zheltovsky and Sosunov 1985; Gurov et al. 2007). Short faults, oriented more or less radial to the center of the crater, are dominant. Concentric faults and some other orientations are subordinate. The apparently impact-related faults disappear at a distance of 2.7 crater radii (Gurov and Gurova 1982).

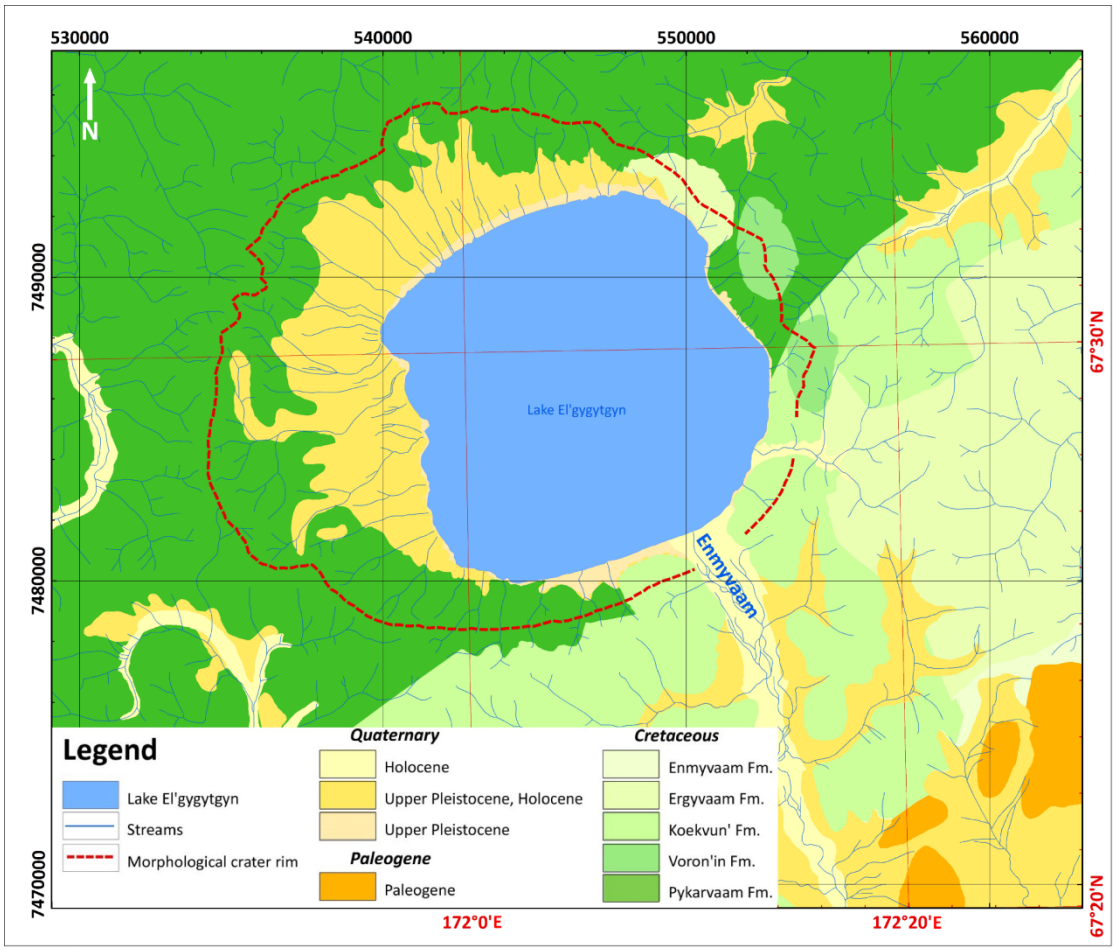

Figure 5.2: Stratigraphic map of the El'gygytgyn crater area, modified after Stone et al. (2009).

The target lithologies are generally known from the work of Belyi (1977, 1988, 1994) and Belyi and Belaya (1998), and from Gurov and coworkers (Gurov et al. 1978, 2005, 2007; Gurov and Gurova 1982). They described the rocks as a suite encompassing (from top to bottom) ignimbrites (mainly felsic, 250 m), tuffs and rhyolitic lava (200 m), tuffs and andesitic lava (70 m, occurring especially to the southwest of the crater), ash tuffs, and welded tuffs of rhyolitic and dacitic compositions (100 m). Additionally, an approximately 110 m thick basalt sill occurs as a plateau at the northeastern crater rim (Gurov et al. 2005).

The general bedding of the pyroclastic rocks and lava flows at the crater rim and in its environs dips gently at 6-10° to the east-southeast (Gurov and Koeberl 2004). Dips up to 33° have been measured locally in this investigation (see below).

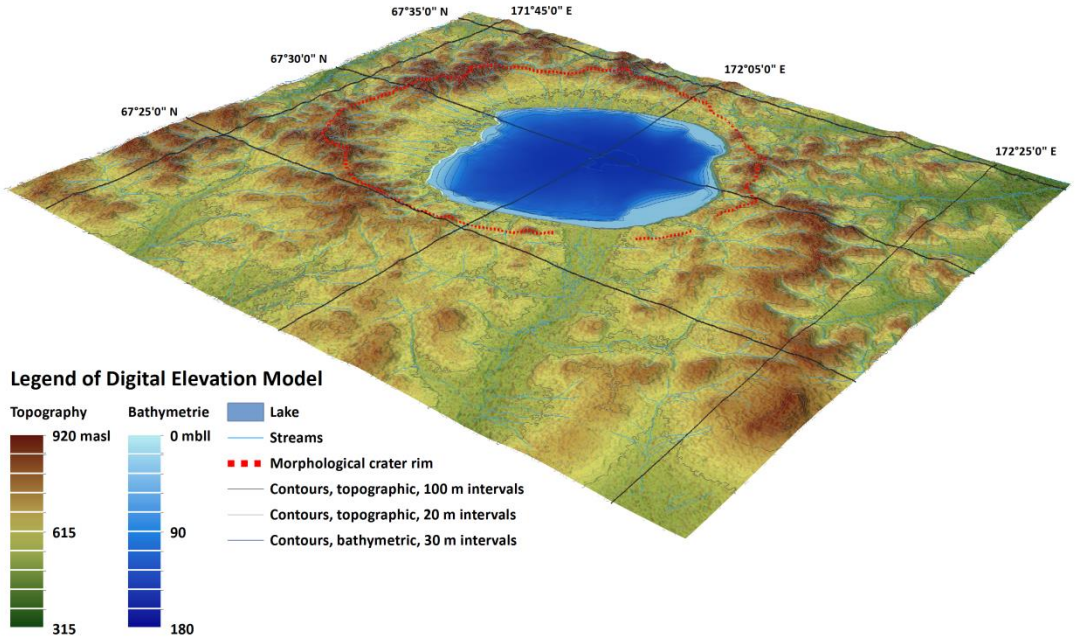

Figure 5.3: Digital elevation model for the El'gygytgyn impact structure with a 2 times elevation factor, produced with ArcScene 10, based on ASTER DEM data; bathymetric data kindly provided by A. Lack, AWI Potsdam.

The crater rim is almost completely preserved, except for the southeastern part that has been degraded by the Enmyvaam River, a periodic (i.e., during summertime) outflow from the lake. Rocks of the crater rim did not reveal any characteristic shock metamorphic effects (Gurov et al. 2007; this work). The original ejecta blanket (a mixture of unshocked and shocked rocks, and fragments of impact melt breccia) around the impact crater has been nearly completely eroded by arctic weathering. Only a few remnants can be found, embedded in the lacustrine and fluvial terraces, inside and outside of the crater rim (Gurov et al. 1979a; Smirnov et al. 2011; Wittmann et al. 2013; this work). In the absence of ice or glacial transport (Glushkova and Smirnov 2007), the material was probably transported to the lower terraces by slumping off the rim (the irregular shapes of blocks indicate limited local transport). Rounded cobbles (2-15 cm in size) of impact rocks and larger, meter-sized blocks of dark impact melt breccia occur only on recent terraces (Gurov and Koeberl 2004; Smirnov et al. 2011; Pittarello and Koeberl 2013; this work). Aerodynamically shaped glass bombs occur together with shock metamorphosed rocks in the lacustrine terraces inside the crater and also in terraces along some streams in the environs of the crater (e.g., along the Enmyvaam River) (Gurov et al. 1978, 1979a). All recorded types of impactites are generally fresh and

most of the samples described do not display significant postimpact hydrothermal alteration and weathering (Gurov et al. 1979a, 1979b; Gurov and Koeberl 2004; this work).

Petrographic analysis of these impactites has demonstrated various impact-induced shock features. Planar fractures (PF), planar deformation features (PDF), and diaplectic glass of quartz and feldspar were identified by Gurov et al. (1978, 1979a, 1979b, 2005) in quartz phenocrysts of shock metamorphosed glassy rhyolite (liparite) and andesite. High-pressure polymorphs of quartz (coesite and stishovite) were determined in two specimens of rhyolitic tuff (Gurov et al. 1979a). Tiny impact glass spherules were found in lake terrace deposits in the southern part of the crater structure and in fluvial terraces along the Enmyvaam River (Gurov et al. 1979a; Glushkova and Smirnov 2007). Such spherules were also analyzed by Adolph and Deutsch (2010), Smirnov et al. (2011), and Wittmann et al. (2013), who concluded that they represent impact-produced melt droplets that had been deposited from the collapsing ejecta plume into a thin layer on the juvenile surface of the impact structure. Brecciated target rocks (impact breccias) occur under the lake sediments in the central part of the crater, as shown by the results of the 2009 ICDP drill core (e.g., Koeberl et al. 2013; Pittarello et al. 2013; Raschke et al. 2013a, 2013b; Wittmann et al. 2013).

The development of the lake terraces was investigated via geomorphic, lithological, and stratigraphic field studies (including pollen analysis) by Glushkova and Smirnov (2007). They concluded that the accumulation of three main terraces can be identified, beginning in the middle Pleistocene and ending in the young Holocene, approximately 5000 a ago.

The oldest lake terrace was deposited 35-40 m above the actual lake level. Generally, this terrace follows the 530 m topographic contour and has a middle to upper Pleistocene age (beginning in the middle Pleistocene and ending with the transition to the upper Pleistocene). This terrace represents the highest stand of Lake El'gygytgyn, when its diameter was increased in the western and northern parts of the El'gygytgyn depression by more than 2 km over the modern shoreline. In the eastern and southern parts, the extension was of the order of tens of meters to some hundreds of meters (Glushkova and Smirnov 2007). Remnants of this accumulation were also identified in the wide valley of the Enmyvaam River (10 km upstream of the lake outlet) and also in the basin of the Lagernyi creek (compare Fig. 5.2).

In the upper Pleistocene, the terrace at 9-11 m above present lake level was accumulated and the lake extent was much reduced, according to the 500 m contour. Thus, the valley of the Enmyvaam River attained its modern relief during the upper Pleistocene (Glushkova and Smirnov 2007).

The youngest terrace was accumulated approximately 3 m above the current lake level. Detailed studies of lacustrine and flood plain sediments by pollen and radio-carbon

analysis revealed an age of 9125 ± 30 ^{14}C years BP (MAG-994) to 7450 ± 55 ^{14}C years BP (MAG-1433) for this deposit (see Glushkova and Smirnov 2007). This age is close to the transition from the late Pleistocene to the Holocene at about 12.3 ka (Shilo et al. 2001). From this time, the lake level has decreased and reached the present niveau. The modern contours of the lake shoreline formed in the last 5000 a.

5.2.2 Drilling Campaign 2008/09

During winter 2008/2009, an international deep drilling campaign was carried out at Lake El'gygytgyn by the International Continental Scientific Drilling Program (ICDP). Three localities were selected for drilling, two (D1 and D2) on the frozen lake surface and D3 at the western slope of the largest terrace (Melles et al. 2011; Koeberl et al. 2013). The purpose for the D3 drilling was the investigation of the development of permafrost; this drilling was successfully terminated at about 140 m depth. Both the D1 and D2 boreholes had been planned to reach the slope of the central uplift structure and to sample the entire stack of postimpact sediments for paleo-climate investigations, as well as the impact breccias and target rocks of the inner crater. During the drilling of D1, a lot of technical problems were incurred and it took three attempts to reach the final depth of 517.3 m (Melles et al. 2011; Koeberl et al. 2013). Thus, the plan to drill D2 had to be abandoned. The first two drillings at the D1 site (D1a and D1b) reached depths of 112 and 147 m below lake floor (mblf) and only penetrated the postimpact lake sediments. The deepest drill hole D1c (see Fig. 5.4) is thought to have been sunk against the outer slope of the central uplift. It penetrated 320 m of lacustrine sediments and, below that, 207.5 m of impactite and impact-affected volcanics. Core recovery for this latter sequence is 157.4 m, or 76%.

Since the end of the ICDP drilling campaign (May 2009), our team has been involved in the scientific investigation of the impactite section of drill core D1c. We have curated these rocks at the Museum für Naturkunde Berlin according to ICDP standard and presented a first lithological description and drill core stratigraphy. In May 2010, we held an international sampling party and organized the distribution of some 600 drill core samples to the El'gygytgyn impactite consortium. A special issue of *Meteoritics and Planetary Science* has been published with a first round of scientific outcomes of this consortium effort regarding the impactite section of drill core D1c (Koeberl et al. 2013). Detailed stratigraphic, petrographic, and geochemical investigations are published in papers by Raschke et al. (2013a, 2013b), Pittarello et al. (2013), and Wittmann et al. (2013).

The section of lacustrine sediments, drilled at D1c with a thickness of 320 m, can be subdivided into an upper, well-stratified subunit and a lower, more chaotic sedimentary subunit (Gebhardt et al. 2013). Below this unit, drill core D1c exposes a suite of different impactites (to 390 mblf) and volcanic bedrocks (to 517 mblf). This assemblage can be -

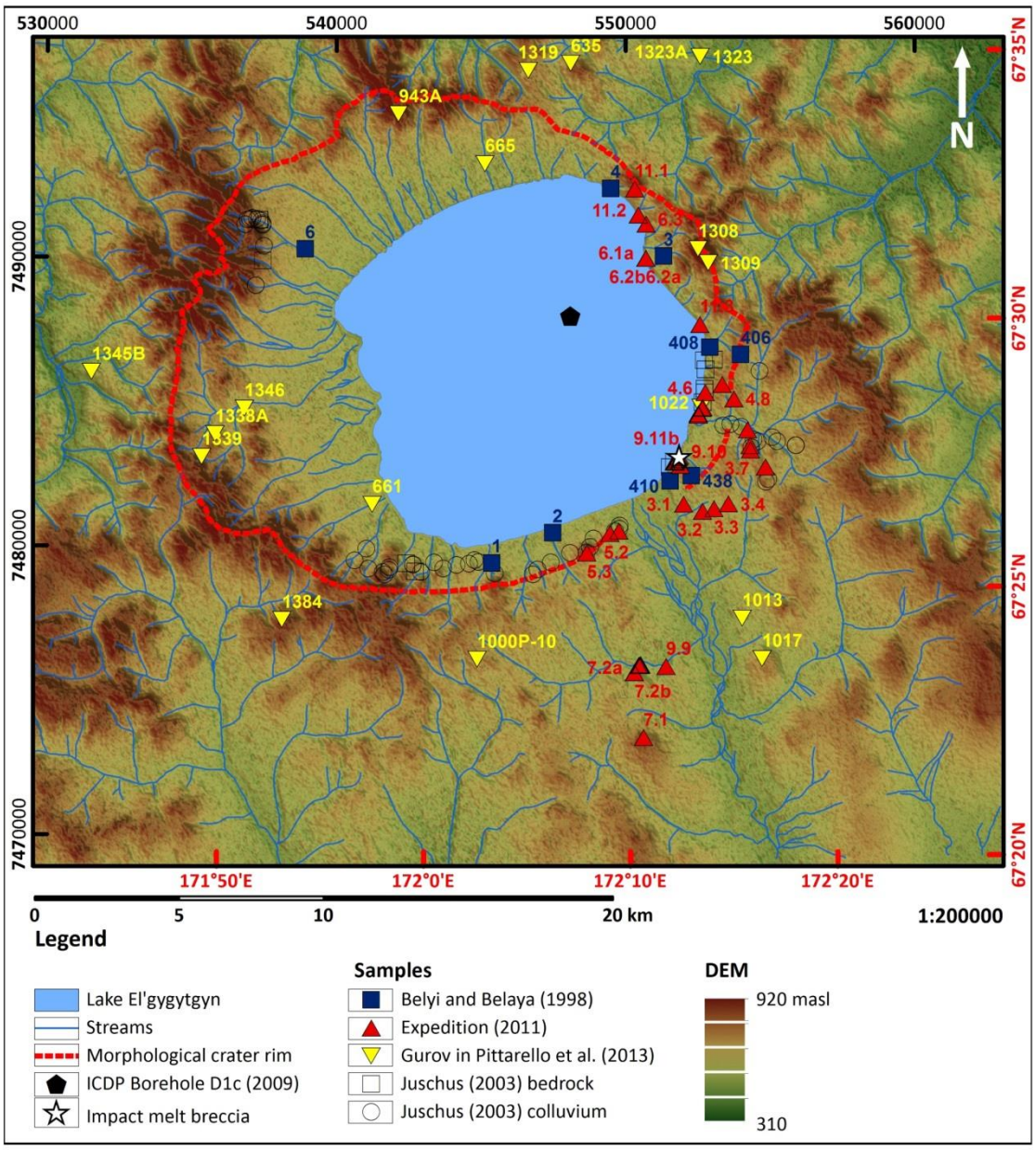

Figure 5.4: Overview map showing all locations that were sampled by the different authors or groups named in the legend. To avoid clutter, the samples by O. Juschus are not numbered. Exact sampling coordinates are given in the short sample description in the supporting information Table S1. Impact melt breccia was found only at the SE lake terrace. Possible other occurrences could not be confirmed and, thus, are not indicated on the map. DEM scale is given in meters above sea level (masl).

following Raschke et al. (2013a, 2013b) - divided into: (1) A transition zone at the top, which contains a mixture of lacustrine sediments and impact rock clasts and has been called *reworked suevite* (316-328 mblf). Between 318 and 322 mblf depth, this unit contains a significant amount of impact glass spherules (Raschke et al. 2013a, 2013b; Wittmann et al.

2013). (2) *Suevite*, an impact breccia with a relatively poor content of impact melt clasts and shocked, clastic, target-derived particles, was intersected between 328 and 391 mblf depth. (3) The *upper bedrock* unit (391-423 mblf) has revealed rare shock deformation only to 391.72 mblf depth, but is otherwise unshocked. It is composed of a basaltic to rhyolitic ignimbrite succession. (4) The *lower bedrock* unit from 423 mblf to the end of core at 517.3 mblf consists of an, in long parts, monomictly brecciated rhyolitic ignimbrite. Note that our group (Raschke et al. 2013a, 2013b) favors these volcanic rocks to represent the narrow shocked zone directly below the crater floor and unshocked country rock underneath, whereas others (Wittmann et al. 2013) prefer that this is an intersection of a large block derived from an outer part of the crater structure and transported to its current place during crater modification.

5.2.3 The 2011 Expedition to El'gygytgyn Crater

In 2011, a joint expedition by staff from the Alfred-Wegener-Institute (AWI)-Potsdam, the Arctic and Antarctic Research Institute (AARI)-St. Petersburg, Cologne University, and Museum für Naturkunde Berlin to the impact structure provided us with the unique opportunity to investigate the geology of a significant part of the crater. One objective for our project was sampling of the rocks on the southern and eastern crater rim for a petrographic and geochemical study in comparison with the target rocks exhumed in the D1c drill core, as we noted that this area was underrepresented in the previous work by the Belyi and Gurov teams. After petrographic-geochemical classification of the country rock samples from this expedition (complemented by an earlier sample series obtained from O. Juschus, HNE, Eberswalde), we could compare these rocks with the drilled rocks of the ICDP borehole D1c. Together with access (courtesy of our Russian colleagues who participated in the expedition) to the older Russian geological map (Raevsky and Potapova 1984; Zheltovsky and Sosunov 1985) and compiling all data available in the mostly Russian literature, this enabled us to create a new, updated geological map of the El'gygytgyn impact structure at the scale of 1:50,000.

5.3 METHODOLOGY

5.3.1 Preparation for the Expedition

For the field trip, we compiled previous mapping information, which included the simplified geological map of Gurov's (Gurov and Koeberl 2004), the modified geological map by Nowaczyk et al. (2002) based on the geological map by Belyi and Raikevich (1994), and the Russian topographic map of the crater area (topographic maps Q-59-19, -20 of 1984 by the Chukotka Autonomous Area of the Magadan Region). O. Juschus (HNE Eberswalde) provided some surface samples with location information from his field campaign in 2003,

which were investigated by optical microscopy, scanning electron microscope (SEM), and, where sample size permitted, X-ray fluorescence (XRF) analysis.

5.3.2 Field Work and Sampling

The expedition lasted from 13 July to 19 August 2011. During this time, we had 26 days in the field; however, weather conditions were highly unstable, with frequent north wind with heavy snowfall, especially in early August. In essence, only 11 days could be used for sampling and mapping. The focus was directed on the southern and eastern crater rim areas. Additionally, an attempt was made to extend the mapping to the Mechekrynnetveem River about 20 km south of the lake, for sampling of impact-produced glass fragments in allochthonous materials of river terraces (Glushkova and Smirnov 2007). But this aim was too ambitious for the prevailing harsh weather conditions, so this traverse had to be abandoned at a distance of 17 km from the lake.

The whole region is affected by highly effective arctic weathering. Generally, the hills of the crater rim and its vicinity have slopes with low angles that are covered with locally eroded material. Due to the strong influence of permafrost that becomes partly molten in its upper few decimeters during the short Arctic summer, the effects of landslides and solifluction are widespread. In summary, denudation of the landscape is dominant in this Arctic tundra region (see Fig. S1 for overview images of the crater rim). This also explains why it was not possible to observe a single fault or contact between country rock types. The transitions from individual strata could only be approximated to a few meters by shifting eroded material on the slope surfaces. However, a large number of orientations of fractures could be recorded on a handful of outcrops on the cliffs of the Rosovaya Hills at the eastern lakeshore at 552700/7486300 (UTM coordinates). Altogether, we sampled 60 country rock specimens at 43 outcrop locations, among them a, for this region, previously unknown type of basaltic-andesitic tuff to the south of the lake. Most of the hand specimens are not oriented, but at 10 locations, it was possible to take oriented samples that had been requested by two groups from Finland (University of Helsinki) and Germany (Karlsruher Institut für Technologie) for the determination of magnetic parameters.

At the end of 2011, the samples arrived in Berlin. The collection of El'gygytgyn country rock samples comprises a large suite of different samples from at and around the crater. First of all, this comprises our own samples collected during the field campaign in 2011 (named with prefix UR-2011). The second group of samples is the suite from O. Juschus from his 2003 expedition, which was increased after the expedition by additional donations and supplemented by 30 samples obtained from N. Nowaczyk (GFZ Potsdam). In summary, we could analyze 72 samples from the 2003 expedition, labeled with prefix PM. Juschus had collected bedrock and colluvium samples with geographic coordinates. Thin sections were

produced for all these samples, and it was possible to generate a set of 38 XRF analyses from samples that were large enough. In addition, some chemical data that are discussed against our own results were published by Pittarello et al. (2013), who analyzed 19 samples collected by E. P. Gurov (and for which coordinates are available as well). The final sample information that could be used here had been published by Belyi and Belaya (1998), who described 11 samples with geographic coordinates from the crater region. The location of almost all samples used here is shown in the overview outcrop map (Fig. 5.4). Most of the Juschus samples have not been plotted, however, as they represent colluvium and, consequently, are not relevant to this new bedrock map. Gurov's samples (referenced in Pittarello et al. 2013) include one derived from outside our map area to the East (#612) and another one (#665) obviously had been collected at the northern lake terrace. We have excluded both of these samples from our work.

5.3.3 Petrographic and Geochemical Analysis

Petrographic analysis was carried out by standard polarized light microscopy. For higher magnification analysis, a scanning electron microscope (SEM) of the type JEOL JSM-6610LV, equipped with a LaB_6-cathode and a BRUKER Quantax 800 energy-dispersive X-ray spectrometer, was applied. Backscattered electron (BSE) images and chemical mineral analyses were obtained with a JEOL Superprobe JXA-8500F field-emission cathode electron microprobe. A cup current of 15-20 nA with an acceleration potential of 15 keV and an electron beam diameter of 1-2 µm were used for single spot and profile analyses by EMPA to minimize loss of sodium during the measurements. Peak counting time was 30 s for most elements, with the exception of Na and Mn with counting times of 20 and 40 s, respectively. The background was evaluated for 15 s on either side of the peak. Both these instruments reside at the Museum für Naturkunde Berlin.

For whole rock chemical analysis, we used 20-50 g per sample, depending on available sample, and grain, size. The samples were taken from the center of fresh hand specimens to avoid altered parts. For chemical analysis, we used samples from the 2011 crater expedition and additional samples collected by Juschus. Samples were ground using sinter-corundum grinding devices. Some samples from the 2003 crater expedition were too small to yield enough material for trace element analysis. In this case, we used petrographically similar samples from the neighborhood of those sampling sites.

Whole rock chemical analysis was carried out by X-ray fluorescence spectrometry (XRF) with a BRUKER AXS S8 TIGER instrument on fused samples (major elements) and powder pellets (trace elements) at the Museum für Naturkunde Berlin. Details of sample preparation, analytical programs, and reference materials employed are reported in Raschke et al. (2013b). Accuracy values on data presented here are 0.5 wt% for SiO_2; 0.1 wt% for Al_2O_3;

0.05 wt% for Fe_2O_3, MgO, CaO, Na_2O, and K_2O; 0.01 wt% for TiO_2, MnO, and P_2O_5; 30 ppm for Ba; 25 ppm for Cu; 20 ppm for Zn, La, Ce, and Pb; and 5 ppm for Sc, V, Cr, Co, Ni, Rb, Sr, Y, Zr, and Nb. The precision values on these data are of about the same order or lower. Detection limits are as follows: 1.0 wt% for SiO_2; 0.5 wt% for Al_2O_3; 0.05 wt% for Fe_2O_3; 0.01 wt% for TiO_2, MnO, MgO, CaO, Na_2O, K_2O, and P_2O_5; 15 ppm for Cu, Zn, and Pb; 10 ppm for Y, Zr, Nb, Ba, La, and Ce; and 5 ppm for Sc, V, Cr, Co, Ni, Rb, and Sr.

For the determination of loss on ignition (LOI), about 1 g of powderized sample material, dried for 4 h at 105 °C, was used. The sample was heated in porcelain crucibles for 4 h at 1000 °C. LOI was calculated using the weight difference between measurements before and after heating. Detection limit, precision, and accuracy values for LOI are about 0.1 wt%.

5.3.4 Creating the Map

For computing and drawing of the new geological map, the ArcGis 10.0 software by ESRI was used. In addition, we utilized open-file ASTER data for the georeferencing and for creation of a digital elevation model (DEM). For the bathymetry of the lake, we used another DEM created by M. Lack (AWI, Potsdam). For the discrimination of the rocks in the suitable stratigraphic units, we used the data by Stone et al. (2009), who combined the ages of Belyi and Belaya (1998) and Kelley et al. (1999), and developed a modern stratigraphy for this region. The different stratigraphic units are illustrated with a range of green colors that are typical for Cretaceous rocks. For representation of the different lithologies in the map, we used pattern symbols according to the common standard textures (USGS standard classification, including ArcGis10-U.S. Geological Survey 2005).

5.4 RESULTS

5.4.1 The Lithological Groups

The samples can be classified into nine lithological groups (basalt, basaltic andesite, andesite, rhyodacitic ignimbrites, rhyolitic ignimbrites, andesitic-dacitic tuff, basaltic-andesitic tuff, rhyodacitic tuff, impact melt breccia) with respect to the previous classification by Gurov and Belyi, and their coworkers (Belyi and Belaya 1998; Gurov and Koeberl 2004; Pittarello et al. 2013). Here, we give short descriptions for these groups using samples from the 2003 and 2011 crater expeditions and additional data given by Belyi and Belaya (1998) and Pittarello et al. (2013). For the individual samples of the 2003 and 2011 crater expeditions, a short petrographic description, including a thin section scan as well as their location (geographical coordinates on the UTM grid) is given in the supporting information Table S1. The electronic supplement referred to here as Figs. S1-S9 contains also additional outcrop and sample images. The chemical analyses of these samples are compiled together with additional analyses of Belyi and Belaya (1998) and Pittarello et al. (2013) in Table S2.

Average chemical compositions and the range of rock compositions (excluding highly altered samples) are given for the lithological groups of basalt, basaltic andesite, rhyodacitic ignimbrites, rhyolitic ignimbrites, andesitic-dacitic tuff, basaltic-andesitic tuff, and rhyodacitic tuff in Table 5.2.

The division of the samples into these nine lithological groups is based on petrographic observations as well as the total alkali-silica (TAS) plot (Fig. 5.5) after Le Maitre et al. (1989). It should be noted that quite a few of our samples did not measure more than 5-8 cm in size, and that it is likely that some of the compositional overlap between these lithological groups is due to not fully representative sample sizes. At the beginning of each litho-description, the respective sample suites are introduced.

5.4.1.1 Basalt

Expedition 2011: UR-2011_3.1/3.2/3.7/3.8/5.2/8.1/8.2; Belyi and Belaya (1998): 438-1/438-3; Juschus (2003): PM-34; Gurov in Pittarello et al. (2013): 1308/1309

Location/outcrop: A 0.7 km^2 basalt sheet occurs both on the NE crater rim in the form of a plateau that is well exposed at Mt. Chivirynnet (Figs. 5.1b and S1a, 552660/7490845 UTM coordinates, Gurov samples #1308/1309 in Pittarello et al. 2013) and in the SE study region (438-1 and 438-3, Belyi and Belaya 1998). We have confirmed both of these occurrences and, in addition, could identify patchy basalt outcrops in the southeast, at the same elevation as the exposures in the other areas at the top of shallow hills. This creates weathering-resistant miniplateaus, which are underlain by andesitic basalts and rhyolites (Figs. S2a and S2b). Samples UR-2011_5.2 and PM-34 (by Juschus) were taken from the same outcrop at the top of an approximately 40 m high (above lake level) hill, near the prominent geodetic hill at the southern lakeshore (548649/7479864 UTM coordinates, 235 m above lake level).

Microscopic and geochemical description: The typically blackish rocks are cracked by the Arctic weathering (Figs. S2c and S2d), have a fine-grained (generally used here for submillimeter-sized; <1 mm) crystalline matrix that is rich in plagioclase, and contain rare larger porphyroblasts of olivine and pyroxene (the intersertal matrix texture is shown in Fig. S2e). Fractures at mm spacing occur in form of a fine grid and are filled with secondary quartz. The chemical analyses (Tables 5.1 and S2) show high-alumina basalts with an alkaline trend (Wimmenauer 1985). In the TAS plot after Le Maitre et al. (1989), these samples plot into the basalt, trachy-basalt, basaltic andesite, and basaltic trachy-andesite fields (Fig. 5.5).

5.4.1.2 Basaltic Andesite

Expedition 2011: UR-2011_4.1b/4.2/4.4; Juschus (2003): PM-66

Location/outcrop: There are two places where this lithology was found. Sample PM-66 (by Juschus) comes from the NW crater rim and belongs to a handful of specimens collected from colluvium. We took our three samples from the eastern part of the crater, just north of the Lagernyi creek (Fig. 1b); GPS 552513/7484506 (UR-2011_4.1), 552639/7484745 (UR-2011_4.2), and 552669/7484762 (UR-2011_4.4; see Fig. S3a). The position is approximately 20-30 m above lake level, on the slopes of the cliffs, near the shoreline.

Microscopic and geochemical description: All samples are dark gray to light green in color, which is related to the many greenish particles that are possibly devitrified glassy melt (especially in sample UR-2011_4.2). Typical for all samples of this lithology is the fine-grained crystalline matrix composed mainly of plagioclase, with larger phenocrysts of feldspar (plagioclase) and olivine (Figs. S3b and S3c). Alteration is generally strong and includes a high content of secondary carbonate, which is also recognizable in the high CaO and LOI contents of these samples (Table S2). Therefore, no average composition is given for this lithological group.

5.4.1.3 Andesite

Expedition 2011: UR-2011_4.1e/7.2/9.6/11.2; Juschus (2003): PM-24/PM-72; Gurov in Pittarello et al. (2013): #1323/1346

Location/outcrop: Apparently, outcrops UR-2011_4.1e and PM-24 belong to the same andesitic lava flow occurring to the north and south of the mouth of the Lagernyi creek. Location 4.1e is located approximately 10 m above lake level (approximately 500 m NN) at the top of a slope. PM-24 was sampled 2.1 km east of the lake at the Lagernyi creek. Sample UR-2011_7.2 was taken from the slope of a hill to the south of the lake. At the other side of this hill, we found a sizable outcrop at the Rosomashiy creek (GPS 550516/74785856). All samples UR-2011_9.1 to 9.9 were obtained here (see the Basaltic-Andesitic Tuff section). This outcrop is approximately 25 m wide and 60 m long. It was opened up due to erosion caused by the small creek. Sample UR- 2011_9.6 was taken from the base of the outcrop directly at the creek. On the slope of a shallow hill at the NE edge of the lake, hand specimen UR-2011_11.2 was collected. Here, it was evident that a huge sequence of ignimbrites (Mt. Otvevergin, the Rhyolitic Ignimbrite section) is in close contact with the andesite. The ignimbrites occur at significantly higher elevation than the andesite. Samples PM-72 and #1346 (by Gurov in Pittarello et al. 2013) were obtained at the western crater rim. We could not visit these locations and, thus, cannot confirm the maximum extension of these outcrops. The same applies for sample #1323 (by Gurov in Pittarello et al. 2013) that was taken at the northern crater rim.

Microscopic and geochemical description: Fine-grained crystalline, feldspar-rich matrix with porphyritic texture. There are larger phenocrysts of pyroxene (hypersthene), biotite, amphibole, and rare olivine. Alteration is moderate with some secondary calcite. The andesites (Tables 5.2 and S2) are of varied chemical composition ranging in SiO_2 content from 57.9 to 64.5 wt%. In the TAS diagram after Le Maitre et al. (1989), the petrographically grouped andesites plot into the andesite (samples UR-2011_7.2/9.6, PM-72), trachyandesite (sample UR-2011_11.2), and dacite (samples #1323, #1346 by Gurov in Pittarello et al. 2013) fields.

5.4.1.4 Rhyodacitic Ignimbrite

Expedition: UR-2011_9.12a/10.1; Juschus (2003): PM- 3/PM-5/PM-6/PM-15/PM-40/PM-43/PM46/PM-47/ PM-74/PM-75; Gurov in Pittarello et al. (2013): 1319

Location/outcrop: This lithology constitutes the entire western half of the crater rim. It was assumed by Raevsky and Potapova (1984) and by Zheltovsky and Sosunov (1985) that this formation belongs to the Pykarvaam Formation. In our expedition area, we only found samples of this lithology at the SE crater rim. An approximately 50 m wide slope along the southern shoreline allows investigating this rhyodacitic tuff (UR- 2011_10.2). At the northern extension (approximately 25 m), this slope (or shallow cliff) is 8–10 m high and consists of a similar lithology, the greenish rhyodacitic ignimbrite (Fig. S4a). Sample 1319 by Gurov in Pittarello et al. (2013) was obtained in the low hills of the northern crater rim. PM-samples 3, 5, and 6 originate from the eastern area, north of Lagernyi creek. PM-15, 40, 43, 46, and 47 were collected in the SW area of the crater rim, and PM-74 and 75 from the hills of the western rim. All these locations (see Fig. 5.4) were outside of our expedition area, so we cannot confirm these, but they correlate quite well with the information on the older Russian map.

Table 5.2: Average chemical composition, standard deviation and range of rock compositions for various surface lithologies. Highly altered samples (UR 2011_1.1, PM 59, PM 72) were excluded from these calculations. The individual analyses are compiled in Table S2.

	Basalt					Andesite					Rhyodacitic ignimbrite					Rhyolitic ignimbrite				
Lithology	Mean	SD	Min	Max	*n*	Mean	SD	Min	Max	*n*	Mean	SD	Min	Max	*n*	Mean	SD	Min	Max	*n*
wt%																				
SiO_2	53.30	2.50	49.90	56.90	11	61.40	3.20	57.90	64.50	5	68.50	2.70	63.10	72.40	8	70.80	2.50	68.20	79.10	22
TiO_2	0.97	0.23	0.70	1.42	11	0.69	0.15	0.53	0.84	5	0.34	0.09	0.19	0.48	8	0.29	0.08	0.12	0.39	22
Al_2O_3	17.60	0.80	16.30	18.90	11	17.30	1.00	16.20	18.30	5	15.50	1.80	13.70	19.10	8	14.60	1.40	9.90	16.30	22
Fe_2O_3[a]	8.58	0.79	7.45	9.61	11	5.83	1.43	4.28	7.36	5	2.78	0.66	1.76	3.88	8	2.29	0.54	0.92	2.94	22
MnO	0.15	0.02	0.12	0.17	11	0.12	0.04	0.06	0.16	5	0.07	0.03	0.05	0.14	8	0.05	0.02	0.02	0.10	22
MgO	4.50	1.13	2.78	5.97	11	1.73	0.54	1.30	2.33	5	0.73	0.29	0.36	1.29	8	0.49	0.16	0.14	0.75	22
CaO	8.02	1.19	6.32	9.90	11	4.43	1.11	3.55	5.65	5	1.81	0.72	0.92	3.33	8	1.54	0.70	0.21	2.51	22
Na_2O	2.87	0.50	2.32	3.67	11	3.57	0.16	3.42	3.83	5	3.58	0.37	3.02	4.01	8	3.38	1.18	0.40	6.21	22
K_2O	1.69	0.36	1.29	2.36	11	2.96	0.59	2.33	3.57	5	4.16	0.44	3.52	5.09	8	4.37	1.35	1.78	8.49	22
P_2O_5	0.35	0.24	0.12	0.88	11	0.28	0.14	0.15	0.42	5	0.08	0.03	0.03	0.12	8	0.07	0.02	0.03	0.09	22
LOI	1.80	0.80	0.80	3.10	11	1.10	0.30	0.90	1.50	5	2.10	0.80	1.30	3.60	8	1.80	0.09	0.70	3.90	22
Total	99.83					99.41					99.65					99.68				
ppm																				
Sc	23	6	15	32	8	12	1	11	14	5	6	2	6	9	5	5	2	<5	7	11
V	167	42	103	231	8	62	16	50	81	5	28	15	8	51	5	17	8	<5	27	11
Cr	62	50	<5	148	9	16	1	<5	16	2	10	3	<5	12	2	6	5	<5	13	15
Co	27	21	11	73	10	7	1	<5	8	4	<5		<5	<5		<5		<5	8	15
Ni	27	21	10	74	10	9	2	<5	11	3	8	3	<5	10	3	<5		<5	13	17
Zn	85	23	49	115	10	81	10	70	92	5	47	4	42	53	5	37	20	14	79	22
Rb	40	12	27	65	10	94	33	59	131	5	123	17	110	152	5	142	35	76	257	22
Sr	514	193	343	951	10	389	114	282	518	5	230	76	131	318	5	218	176	27	876	22
Y	22	5	15	33	10	26	4	22	31	5	22	4	19	28	5	21	4	16	32	22
Zr	138	68	71	248	10	207	99	124	332	5	179	25	152	214	5	174	53	69	290	22
Ba	514	194	308	826	8	572	40	503	600	5	761	228	470	1108	5	658	250	259	1197	22
La	24	15	14	58	8	28	6	22	35	5	32	3	28	36	5	32	5	22	41	13
Ce	56	32	31	118	8	59	6	51	67	5	68	9	60	82	5	64	9	53	82	13

Table 5.2. Continued

	Andesitic-dacitic tuff					Basaltic-andesitic tuff					Rhyodacitic tuff				
Lithology	Mean	SD	Min	Max	*n*	Mean	SD	Min	Max	*n*	Mean	SD	Min	Max	*n*
wt%															
SiO_2	60.80	2.10	57.10	63.00	7	53.30	1.60	50.80	55.30	9	70.60	3.10	65.70	75.80	15
TiO_2	0.60	0.05	0.62	0.78	7	0.87	0.05	0.79	0.93	9	0.38	0.21	0.18	0.85	15
Al_2O_3	16.80	0.40	16.20	17.40	7	15.70	0.60	14.60	16.30	9	14.00	1.40	11.10	15.70	15
Fe_2O_3[a]	5.70	1.00	4.53	7.80	7	7.30	0.81	6.38	8.83	9	2.68	1.17	0.91	5.33	15
MnO	0.11	0.03	0.08	0.17	7	0.13	0.02	0.10	0.16	9	0.07	0.04	0.02	0.15	15
MgO	1.81	0.35	1.33	2.26	7	3.10	0.86	2.05	4.17	9	0.58	0.33	0.18	1.49	15
CaO	4.81	1.03	3.29	5.83	7	6.43	1.03	4.37	8.22	9	1.24	1.16	0.14	4.70	15
Na_2O	3.52	0.55	2.40	4.10	7	2.91	1.41	1.08	5.97	9	2.68	1.47	0.42	6.06	15
K_2O	2.81	1.03	1.13	3.73	7	1.73	0.94	0.55	2.82	9	4.91	2.26	1.62	10.90	15
P_2O_5	0.19	0.02	0.16	0.22	7	0.28	0.04	0.21	0.35	9	0.09	0.01	0.02	0.23	15
LOI	2.50	1.40	1.00	4.90	7	7.90	1.70	5.10	10.40	9	2.10	0.80	1.00	3.40	15
ppm															
Sc	16	10	9	27	3	22	5	15	27	9	9	4	<5	15	7
V	83	35	62	124	3	151	28	106	183	9	38	41	9	122	11
Cr	20	25	<5	65	5	47	40	<5	117	7	<5		<5	26	
Co	19	9	<5	31	6	15	5	11	24	9	<5		<5	9	
Ni	6	3	3	9	7	22	5	18	32	9	<5		<5	15	
Zn	110	83	41	283	7	78	13	61	106	9	60	22	39	102	11
Rb	83	37	29	145	7	48	32	10	106	9	121	43	50	190	11
Sr	523	203	220	860	7	490	246	171	900	9	173	88	51	381	11
Y	25	6	20	39	7	23	3	19	28	9	21	5	12	28	11
Zr	182	12	170	206	7	128	42	99	232	9	192	58	89	279	11
Ba	631	359	217	841	3	451	224	131	773	9	643	234	316	1084	11
La	26	2	24	27	3	19	5	14	27	9	27	9	<10	36	9
Ce	59	6	53	65	3	44	9	30	59	9	51	21	23	82	11

[a]Total Fe as Fe_2O_3.
n = number of analyses used for calculation of mean and standard deviation.

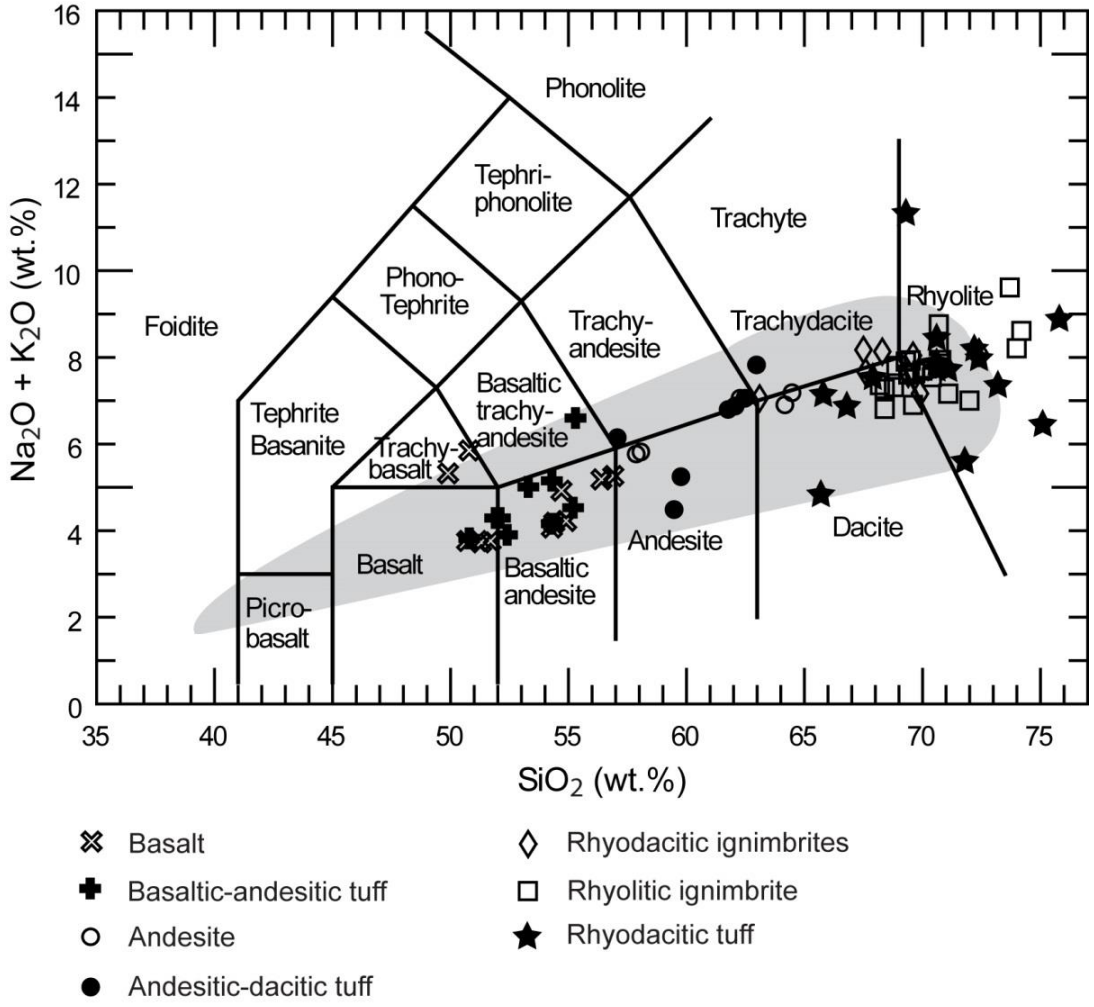

Figure 5.5: Total alkali-silica (TAS) plot after Le Maitre et al. (1989) for samples from surface lithologies at El'gygytgyn crater. The shaded field indicates the spread of data for bedrock samples from the D1c drill core (Raschke et al. 2013b).

Microscopic and geochemical description: The samples have a greenish, fine-grained crystalline matrix with fluidal texture. Medium-sized (approximately 4 mm in size) subangular feldspar phenocrysts occur together with rare biotite, hornblende, and quartz phenocrysts. Elongated and deformed pumice fragments (often as devitrified glass) contain larger crystal fragments (up to 3 mm) that can be recognized macroscopically (Figs. S4a and S4b). Often they show an interfingering contact with the surrounding matrix that seems to be typical for this rock. In both samples, we found fragments of accretionary lapilli (Fig. S4c), small particles produced by agglutination of dust grains in a presumable moist eruption cloud (Fisher and Schmincke 1984). Alteration is moderate to strong with sericitization of feldspar, especially along Carlsbad twin lamellae, and chloritization of biotite. In the TAS plot after Le Maitre et al. (1989), the samples of the rhyodacitic ignimbrite (Tables 2 and S2) plot into the rhyolite, dacite, and trachydacite fields, close to the triple point formed by these three fields (Fig. 5). The rhyodacitic ignimbrite is chemically similar to the rhyolitic ignimbrite (Table 2),

but differences could be observed in the TiO_2, Fe_2O_3, and MgO contents, which are slightly higher in the rhyodacitic ignimbrite in comparison to the rhyolitic ignimbrite.

5.4.1.5 Rhyolitic Ignimbrite

Expedition 2011: UR-2011_5.3/6.1/6.2/6.3/10.1b/10.2a/10.2b/11.1/11.3; Juschus (2003): PM-18/PM-37; Belyi and Belaya (1998): 1/3/6/6-1/405/408-7/410-1/4-1/403; Gurov in Pittarello et al. (2013): #635/661/943A/1017/1339/1384

Location/outcrop: This lithology dominates the eastern half of the crater rim and seems to have been emplaced over a wide stratigraphic age range, from the oldest Pykarvaam to the youngest Ergyvaam Formation. Most of the investigated samples represent this rock type. In summary, there are four exposures, from which most of the samples originate: In the NE, Mt. Otvevergin (see Fig. 1b) and down its slope to the lakeshore (UR- 2011_11.1/11.3 and 3/4-1 of Belyi and Belaya 1998; and from somewhat further north, Gurov's samples 635/943A referred in Pittarello et al. 2013). Here, the ignimbrite shows varied color. The brownish pumice fragments are embedded into a greenish to reddish matrix, which is enriched in iron oxides (Figs. S5a–c). The second outcrop is located at the eastern shoreline, at the "Rosovaya" Hills, where several high cliffs occur (UR-2011_6.1/6.2/6.3 and 408-7 of Belyi and Belaya 1998). We found another lithology as well, the rhyodacitic tuff. At this place, both rock types commonly occur together, which is also observed at the SE shoreline. The transition between tuff and ignimbrite is gradational and we have distinguished these rock types by the occurrence of pumice fragments, which is a characteristic criterion for felsic ignimbrites (Fisher and Schmincke 1984). The Mt. Otvevergin and Rosovaya Hills locations, both displaying rhyolitic welded tuffs (ignimbrites), are separated by a section of andesite that occurs over several hundred meters at the lake shoreline (UR-2011_11.2, see the Andesite section). The third occurrence of this lithology is directly north of the Enmyvaam fluviatile terrace in the SE, from which samples UR-2011_10.1b/10.2a/10.2b/11.1/11.3 and 410 of Belyi and Belaya (1998) are derived. And the last prominent location is the "Geodetic Hill" in the SE, at GPS 548655/7479736 near the outflow of the Enmyvaam River (UR-2011_5.3 and PM-37, see Figs. S5d–S5f). There are more occurrences represented by single samples of this lithology, e.g., Gurov's #1017-a piece from the shallow hills north of the Enmyvaam terraces. Locations of several other sampled locations (PM-18 and #661 of Gurov in Pittarello et al. 2013) could not be confirmed in the field. It appears, however, that these samples were collected as surface samples at lake terraces. Gurov's samples #1339 and #1384 were located outside of our study area; #1384 corresponds with the old geological map in contrast to sample #1339. This is situated in the (lithologically similar) rhyodacitic ignimbrite area.

Microscopic and geochemical description: The rocks are composed of a fine-grained crystalline matrix with elongated pumice fragments that, in part, are vesicle-rich. Moderately

sized phenocrysts (max. 3 mm in size) of quartz and rare primary calcite occur together with feldspar, biotite, and weathered amphibole (hornblende) in the matrix. Moderate to strong alteration with sericitization of feldspar is common. Weathered biotite is often enclosed by fine-grained opaques (hematite). The rhyolitic ignimbrite (Tables 2 and S2) is chemically (for both major and trace elements) comparable with the rhyodacitic ignimbrite. The range of compositions of the rhyolitic ignimbrite extends to higher SiO_2 contents than that of the rhyodacitic ignimbrite. In the TAS diagram after Le Maitre et al. (1989), the samples of the rhyolitic ignimbrite fall into the dacite and rhyolite fields (Fig. 5).

5.4.1.6 Andesitic-Dacitic Tuff

Expedition 2011: UR-2011_1.1/4.1a/4.1d/7.1/; Juschus (2003): PM-19/PM-25/PM-56-1/PM-64-1; Belyi and Belaya (1998): 406-(1-5); Gurov in Pittarello et al. (2013): #1345B

Location/outcrop: This tuffaceous rock is present at a small outcrop at the uppermost reaches of the slope of the SE crater rim, directly north of the Enmyvaam River (GPS 552513/7484506; UR-2011_4.1a/4.1d). Another location is at the northern flank of the Lagernyi creek valley, approximately 4 km NNW of the first outcrop (sample 406 by Belyi and Belaya 1998). Here, this tuff occurs together with other pyroclastics, e.g., rhyodacitic tuffs and rhyolitic ignimbrites. The third location is on the top of a prominent hill (689 masl; see Fig. S6a) in the southern part of the study area, approximately 2 km west of the Enmyvaan River (GPS 550616/7473341; UR-2011_7.1). The outcrops are strongly weathered and fractured. Generally, they are covered with subarctic, green to black lichen (Fig. S6b).

Microscopic and geochemical description: The matrix is fine-grained crystalline and/or ash-supported. Typically crystal fragments are abundant and have similar sizes to the clastic groundmass particles (Fig. S6c, thin section scan of sample UR-2011_7.1). Prominent minerals are feldspar, pyroxene, olivine, and kaersutite. Also abundant are ore minerals, mostly pyrite, and a few zircon grains occur. Sample PM-25 (Lagernyi creek valley) by Juschus shows a similar mineralogy (see Fig. S6d). Microscopic, round vesicles and larger phenocrysts of feldspar occur in a finest-grained ash groundmass (see Fig. S6e). Alteration is moderate to strong and exhibited by secondary calcite and chlorite. The samples of the andesitic-dacitic tuff (Tables 2 and S2) are chemically similar, with regard to major and trace elements, to those of andesite. In the TAS diagram after Le Maitre et al. (1989), they also plot into the fields for andesite, trachy-andesite, and dacite (Fig. 5).

5.4.1.7 Basaltic-Andesitic Tuff

Expedition 2011: UR-2011_9.1/9.2/9.3/9.4/9.5/9.7/9.8/9.9; Gurov in Pittarello et al. (2013): #1000P10

Location/outcrop: This lithology was completely unknown in the older literature about the El'gygytgyn crater and its vicinity. We discovered a very instructive location 5.7 km SSE of the southern lakeshore (GPS 550516/74785856), at lake level. The outcrop is approximately 60 m long and 25 m wide (Fig. S7a). It is located at the northern slope of a shallow hill and is truncated by the Rosomashiy creek, a tributary of the Enmyvaam River. We sampled upstream, beginning with the lowermost part of the tuffaceous sequence. In general, the different layers of tuff show dips of 14-33° to the east-southeast, which corresponds to the general dip direction of bedrock in the entire crater region (Gurov et al. 2007). The tuffs differ in color and grain size. Samples UR-2011_9.1, 9.2, and 9.3 are gray and their lithics have varied sizes. Sample 9.1 comes from a very fine-grained (<1 mm) ash layer that is well sorted. It was not possible to measure the true thickness, but we estimated that this layer is more than 20 cm thick. The overlying layer (sample 9.2) is comparatively coarse-grained with larger, subrounded clasts up to 1 cm in size. This stratum is approximately 15-20 cm thick. The upper layer represented by sample 9.3 is of medium grain size (2-5 mm) and more than 40 cm thick (Fig. S7b).

A few meters upstream, the next stratigraphically higher layer could be sampled (UR-2011_9.4 and 9.5). This is a reddish, fine-grained tuff with well-sorted layers of ash and intercalations of fine-grained lithic clasts (lapilli) (Fig. S7c). The orientations of the bedding planes are 191/24 and 146/33 SE. At the next outcrop, approximately 5 m upstream, sample 9.6 was obtained and an orientation of 141/21 (strike/dip) was measured. Approximately 20 m upstream, the reddish, fine-grained ash tuff has up to 10 cm thick intercalations of polymict volcanoclastic breccias (UR- 2011_9.7). These breccias show larger (up to 1 cm sized) clasts of different lithologies, including ignimbrites, rhyolites, basalts, and andesites (Fig. S7d). The thickness of this sequence could not be estimated, because the rocks were buried by talus off the slope. A further 300 m downstream, an outcrop of 15x9x3 m extent occurs (541403/7475730). The rock there (sample UR-2011_9.9) is similar to those described before (Fig. S7e), but chemical analysis shows significantly higher MgO and Na_2O, and lower K_2O, contents than obtained for the other samples (Table S2). Gurov also found these tuffs in the environs of the crater to the south (sample #1000P10 in Pittarello et al. 2013).

Microscopic and geochemical description: The gray-colored tuffs (UR-2011_9.1/9.2/9.3) consist of a microclastic matrix with larger mineral grains and clasts up to 10 mm in size (see Figs. S6f, S6h, and S6i). The lithic micro-clasts belong to different lithologies including andesitic to rhyolitic ignimbrites and andesitic or basaltic lavas. The clasts are poorly sorted and angular to round. A phreatomagmatic eruption as origin for this rock type seems plausible. The alteration is moderate to strong with abundant secondary calcite that often fills vesicles (Fig. S7j).

The reddish tuffs (UR-2011_9.4/9.5) are fine-grained, with a grain size mainly <1 mm. These fine ash layers follow a bedding structure and are intercalated by somewhat coarser grained layers (1–2 mm in size, see Fig. S7g). Tiny mineral grains are magmatic feldspars and quartz, and calcite (secondary). This sequence is slightly to moderately weathered. Occasionally, translucent to opaque glass shards, vesicles, and pumice fragments occur (Fig. S7k). The chemical analysis of these samples (Table 2, supporting information Table S2) does not reveal a clear chemical trend for this sequence. Typical for all these samples are high values of LOI, which can be correlated with the CaO contents (Tables 2 and S2) and originate from the formation of secondary calcite. In the TAS diagram after Le Maitre et al. (1989), the basaltic-andesitic tuff samples fall into the fields of basalt, basaltic andesite, and basaltic trachy-andesite (only sample 9.9) (Fig. 5). A recalculation of these analyses excluding the LOI will shift these samples to the fields of basaltic andesite, andesite, and trachy-andesite.

5.4.1.8 Rhyodacitic Tuff

Expedition 2011: UR-2011_3.5/4.1c/4.5/4.6;10.2 Juschus (2003): PM-16/PM-37/PM-59/PM-61-1/PM-63/PM-65/PM-67/PM-68-1/PM-70/PM-71; Gurov in Pittarello et al. (2013): #1013/1022/1323A/1338A

Location/outcrop: This lithology was observed and sampled at five locations. First, two small outcrops occur north and south of the Lagernyi creek at the top of low hills (UR-2011_3.5/4.1c, see Fig. S8a; UTM: 554161/7481888 and 552513/7484506), and #1022 by Gurov in Pittarello et al. 2013). Sample UR-2011_4.5 (UTM: 552669/7484762) was taken on a slope covered by talus more than a half meter thick. After the examination of solid rocks, we took the two oriented samples. The exposure is about 5-7 m above lake level. Here, and in the wider southeastern part of the study area, the rhyolitic or rhyodacitic rocks constitute the basis of the volcanic sequence. The second location is approximately 200 m north at the shoreline, and it forms the "Rosovaya Hills," one of the best outcrops in the entire region (Fig. S7b, sample UR-2011_4.6). They form several approximately 30 m high cliffs that are covered by reddish Arctic lichen. The same rocks occur over the next few hundred meters north, but not so prominent, and they are buried under a large apron of eroded material. At the southern crater rim PM-16 and 37 had been sampled by O. Juschus. The fifth occurrence should be in the SE near the Washenka creek (sample #1022 by Gurov in Pittarello et al. 2013). We did find at the SE shoreline rhyodacitic tuff (sample UR-2011_10.2). This outcrop is approximately 50 m long. At the southern end, we sampled a greenish tuff, but at the northern end occurs grayish rhyodacitic ignimbrite with dark pumice fragments (see the Rhyodacitic Ignimbrite section). The transition between these lithologies is not clear; explicit contacts were not observed. Other samples (by O. Juschus) were collected in the NW hills at a

single location and possibly represent colluvium (PM-59, 61, 63, 65, 67, 68, 70, and 71). For this reason, this lithology was not included there on the new geological map.

Microscopic and geochemical description: The rhyodacitic tuff (Table 2 and S2) is chemically comparable to the rhyodacitic and rhyolitic ignimbrites. Nevertheless, the abundances of the alkali elements display a greater scatter in comparison to the ignimbrites. In the TAS plot after Le Maitre et al. (1989), the samples of rhyodacitic tuff are located in the rhyolite, dacite, and trachydacite fields (Fig. 5). The petrographic appearance of the rhyodacitic tuff is very heterogeneous. The fine-grained matrix (particle sizes <2 mm) is constituted of ash or melt fragments (e.g., UR-2011_4.1c, see Fig. S8c), or contains glassy shards. According to the nomenclature of tuffaceous rocks, this unit displays the full range from crystal tuff to lithic and vitric tuffs (Schmid 1981). The brownish ash matrix contains larger phenocrysts of feldspar (plagioclase), quartz (often recrystallized), biotite, amphibole (hornblende), and chlorite (Figs. S7d and S7e). Additional (accessory) minerals are opaques (e.g., UR-2011_3.5, Fig. S8f) and zircon. Small melt particles could be also observed. The alteration (e.g., sericitization of feldspar) is moderate to strong. Most samples are poorly sorted due to the mixing of finest groundmass with larger lithic or crystal components.

5.4.1.9 Impact Melt Breccia

Expedition 2011: UR-2011_9.10/9.11b, c/10a

Location/outcrop: The impact melt breccia occurs in the form of bombs (sizes from 5 to 20 cm) or blocks (1–3 m), which are incorporated into the lower lake terraces. Gurov and Koeberl (2004) described several places of accumulation of impact melt breccia and glassy bombs along the entire lake shoreline. We only found some larger blocks of meter size at the recent 3 m terrace between the Enmyvaam River and the Lagernyi creek in the SE sector (Fig. S9a). They show a mélange of blackish glass particles (up to 30 cm long "schlieren") and brownish scoria-like parts with large, whitish phenocrysts of centimeter size. These rocks are extremely porous and sharp-edged at freshly broken surfaces. A detailed discussion of such materials is given by Pittarello and Koeberl (2013). In addition, we collected well-rounded pieces of impact melt rock, whose origin by either aerodynamically formed bombs or rounded pieces of large blocks of impact melt breccia can be speculated upon (see Pittarello and Koeberl [2013] for a discussion). This material was found at various lake terraces and on the low pebble ridges along the entire shoreline (Fig. S9b).

Microscopic and geochemical description: The three thin sections show different melt phases with translucent glass, brownish glassy schlieren, and blackish glass particles, which all are vesicle-rich (Figs. S9c and S9d). Occasionally, we could identify (in all melt phases) separate minerals or single clasts that are not completely molten. Within these minerals

(especially quartz and feldspar), we found evidence for shock metamorphism in the form of planar features (PF), planar deformation features (PDF), and diaplectic glass (Fig. S9e). Pittarello and Koeberl (2013) also analyzed different hand specimens of impact melt breccia from the western lake terrace and divided these into two groups, of which the first was characterized as blackish, glassy, and homogeneous and the second as similar to a heterogeneous lava scoria. The two chemically analyzed samples (Table S2) are similar in composition to the average impact melt rocks and impact glasses reported by Gurov et al. (2005).

5.4.1.10 Quaternary Deposits

In the new geological map, we have used the classification for the quaternary deposits according to the older Russian map (Raevsky and Potapova 1984; Zheltovsky and Sosunov 1985). The upper Pleistocene deposits contain the 35-40 m terrace (middle to upper Pliocene age) as well as the 9-11 m terrace (upper Pleistocene age). The second unit, the upper Pleistocene/Holocene, represents the 3 m terrace. The third unit, the Holocene, is classified for the development of the present shoreline and its deposits of up to 1 m above present lake level (Fig. 5.6).

5.4.1.11 The New Map

The characteristics of the different stratigraphic units occurring in the whole region were described by Belyi and Belaya (1998). The units do not involve separate volcanic rock types; in contrast, they are often constituted of similar volcanic lavas, pyroclastic rocks, and tuffs. In the crater region, not all units occur with their full stratigraphic range of lithologies. Thus, it is difficult to identify the respective stratigraphic unit based only on petrographic observations. In the framework of this project, we could make chemical analyses, but could not carry out age determination for our rocks.

The new geological map is available in the supporting information (Fig. S10). The new map contains two main parts, the stratigraphy and the lithology. The stratigraphic discrimination for the crater region is based on the older Russian geological map (Raevsky and Potapova 1984; Zheltovsky and Sosunov 1985), which was used as the base map for our work. But this stratigraphy is in several points not clear and a lot of localities had to be labeled with question marks. Therefore, we used additional information from Stone et al. (2009), who compiled the analytical work by Belyi (1994), Belyi and Belaya (1998), and Raikevich (1995). They updated the old stratigraphy in several aspects, but they never combined this information with the older Russian geological map (Raevsky and Potapova 1984; Zheltovsky and Sosunov 1985). This has been done, however, for our new geological map and is discussed in the Distribution of Stratigraphic Formations section.

The second part of the new map - the lithological distribution - is also generally based on the old Russian geological map (Raevsky and Potapova 1984; Zheltovsky and Sosunov 1985). But besides this, a huge portfolio of new samples from our expedition and the expedition of O. Juschus, and additional literature information on samples (Belyi and Belaya 1998; Gurov in Pittarello et al. 2013) were available for our work. In summary, the location and petrography of most of the samples from Belyi and Belaya (1998), of the bedrock samples by O. Juschus, and of the samples of Gurov (in Pittarello et al. 2013) could be confirmed in the field or by reciprocal plausibility checks, and could therefore be used for the new map. Some of the colluvium samples by O. Juschus and one sample by Gurov (#665 in Pittarello et al. 2013) show other compositions than expected, but could also be applied to our map. The doubtful Juschus samples, which cover a complete range of all volcanic rocks, were collected at the northwestern crater rim, at a single location (see lithological description). We could not investigate these doubtful places during our field campaign and we have had no information about these outcrops, their conditions, and extensions. We decided to show these samples in the overview outcrop map (Fig. 5.4) and use them for petrographic and geochemical description, but not to include these samples in the geological map.

Based on the significantly enlarged data set, we were able to update the old map in several aspects, especially in the eastern half of the crater area. Here, we found outcrops which were partly completely unknown up to now or their lithological interpretation was unclear or wrong. Sometimes, we used more unusual patterns for the depiction of some rocks for a better understanding and readability of the map. We labeled all geomorphological points of interest and created a digital elevation model based on Landsat images depicting landscape and lake. Almost all faults and boundaries in our new geological map are based on previous work by Gurov (e.g., Gurov and Gurova 1982) and Belyi (2004), and the older Russian geological map (Raevsky and Potapova 1984; Zheltovsky and Sosunov 1985). We could confirm or determine some new boundaries in the SE crater area where we found the best outcrop conditions in the region.

Based on the new geological map, the surface proportions for the different lithologies were calculated. For this, we have isolated and exported all polygons of the several layers from the ArcGis project, which include the lithologies, the rivers and terraces, the quaternary deposits, and the lake (Table 3). These surface area proportions were used to calculate a new average target composition by using the average chemical composition of the individual lithologies given in Table 2 and multiplying them with their respective surface area proportions. Due to the strong alteration of the available basaltic andesite samples, the surface area proportions for andesite and basaltic andesite were combined and the average composition of andesite was used for both lithologies.

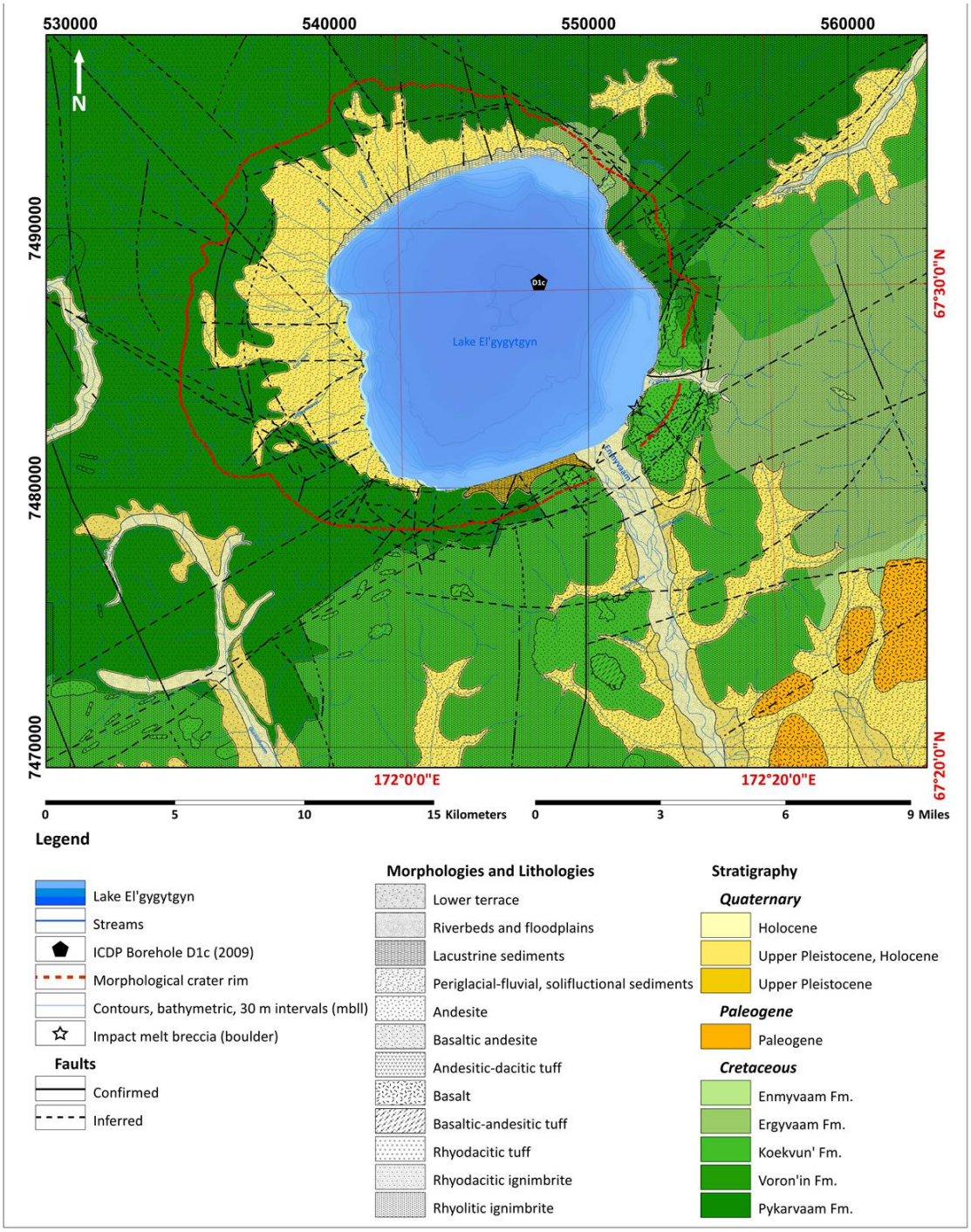

Figure 5.6: Geological map of the El'gygytgyn impact crater. This map, shown here at reduced resolution, is the main part of the higher resolution version of the new map (Fig. S10).

5.5 DISCUSSION

5.5.1 Geological Setting of the El'gygytgyn Area

The lithologies occurring at surface in the El'gygytgyn area represent a more or less continuous suite of volcanic rocks ranging in chemical character from felsic to mafic (Fig. 5).

The felsic volcanic rocks dominate clearly and occupy the major part of the El'gygytgyn area (about 90%), which is typical for the OCVB that contains generally over 70% felsic magmatites (e.g., Tikhomirov et al. 2008). The major and trace elements of the volcanic rocks of the El'gygytgyn area follow in Harker diagrams (e.g., Fig. S11) the same geochemical trends as those previously described for the OCVB (Tikhomirov et al. 2008). Nearly all of the rocks have a subalkaline character (Irvine and Baragar 1971; Fig. 5.7a), and belong, based on the Zr versus TiO_2 discrimination diagram (Leat and Thorpe 1986), to the field for arc lavas (Fig. 5.7b). This diagram additionally displays that the mafic rocks of the El'gygytgyn area have more or less an intermediate rather than a typically mafic character. The Ta + Yb versus Rb discrimination diagram (Pearce et al. 1984) for felsic lithologies indicates that the volcanics were formed in a volcanic arc geological setting (Fig. 5.7c). A similar trend is also visible for the mafic lithologies in the FeO-MgO-Al_2O_3 discrimination diagram (Pearce et al. 1977) (Fig. 5.7d), which shows these rocks fall into the field for orogenic formation. Overall, the chemical data for the surface rocks of the El'gygytgyn area indicate a cogenetic volcanic suite that could have formed in a subduction-related geodynamic regime as also suggested by previous workers (e.g., Tikhomirov et al. 2008; Pittarello et al. 2013).

The average target composition based on the new geological map (Table 5.3) corresponds somewhat better to the average composition of the suevite of the D1c drill core than the previously given average target composition by Gurov and Koeberl (2004) and Gurov et al. (2005). This shows the relevance of a small mafic component within the target for the formation of the suevite as proposed already by Raschke et al. (2013b). Slight differences in the CaO and Na2O contents between the average target composition and the average suevite composition of D1c drill core are the result of the notable alteration of the suevite as described by Raschke et al. (2013b) and Pittarello et al. (2013). Based on the new data, the average target composition could be expanded for some trace elements (Table 5.4), which also display good agreement with average suevite of the D1c drill core. As the concentrations of Cr, Co, and Ni in

Table 5.2: Percentage of the different target lithologies occurring around the El'gygytgyn impact crater. The calculation is based on the new geological map.

Lithology	Area (km²)	Area (%)
Basalt	23.7	3.6
Basaltic andesite	19.9	3.0
Andesite	2.4	0.4
Rhyodacitic ignimbrite	251.1	37.8
Rhyolitic ignimbrite	361.9	54.5
Andesitic-dacitic tuff	0.7	0.1
Basaltic-andesitic tuff	1.7	0.3
Rhyodacitic tuff	2.1	0.3
Sum	**663.7**	**100.0**
River, terrace deposits	185.8	
Lake area	118.9	
Total surface area	**968.4**	

most samples are below the detection limits of our analyses, we are not able to constrain an average target composition for these elements.

5.5.2 Distribution of Stratigraphic Formations

The occurrence of the different stratigraphic formations in the El'gygytgyn area is discussed based on their chronology and extents, given by Stone et al. (2009). Nevertheless, the assignment of the new samples to these stratigraphic formations is only tentative without availability of further age dating, because all these formations display a great variability in rock composition. Here, we have considered the geology of the respective locations as given in the literature and state where we can confirm earlier lithological observations through findings from our expedition. The newly discovered outcrops are also included in this scheme. The overall results of this work are presented in the stratigraphy as displayed in the updated map.

5.5.2.1 Pykarvaam Formation

This stratigraphic unit represents the country rocks in more than half of the entire crater region, mainly in the western sector (see also the old geological maps by Raevsky and Potapova [1984] and Zheltovsky and Sosunov [1985]). In our own expedition area, this formation occurs only with a minor occurrence on the NE crater rim, where we found andesites, in agreement with the old map. But we could not find relicts of contact metamorphism from the intrusion of these subvolcanic bodies, as had been reported in the explanation to the previous map (Raevsky and Potapova 1984; Zheltovsky and Sosunov 1985). In contrast, the andesites surrounding the basalt plateau (Mt. Chivirynnet) are of younger, Voron'in age, because of the age determination by Stone et al. (2009).

5.5.2.2 Voron'in Formation

Only two locations with material assigned to this formation occur in the crater area. First, there is Mt. Chivirynnet (approximately 800 masl), a basalt (Gurov et al. 1979a) or andesitic basalt plateau (Raevsky and Potapova 1984; Zheltovsky and Sosunov 1985; this work). The second location is approximately 2 km farther south (north of Lagernyi creek), also represented by a prominent hill (small plateau). According to the old map, andesite or andesitic dacite occurs here, together with rhyolitic tuff at the shoreline. We found at this location a greater variation of rock compositions with basalt, andesitic basalt, and andesite, mostly on top of the hills. These rocks are more resistant against weathering than their environs, so that they create positive morphology. Rhyolitic ignimbrite and rhyodacitic tuff constitute the base of these hills. Our study revealed a subhorizontal succession of these lithologies.

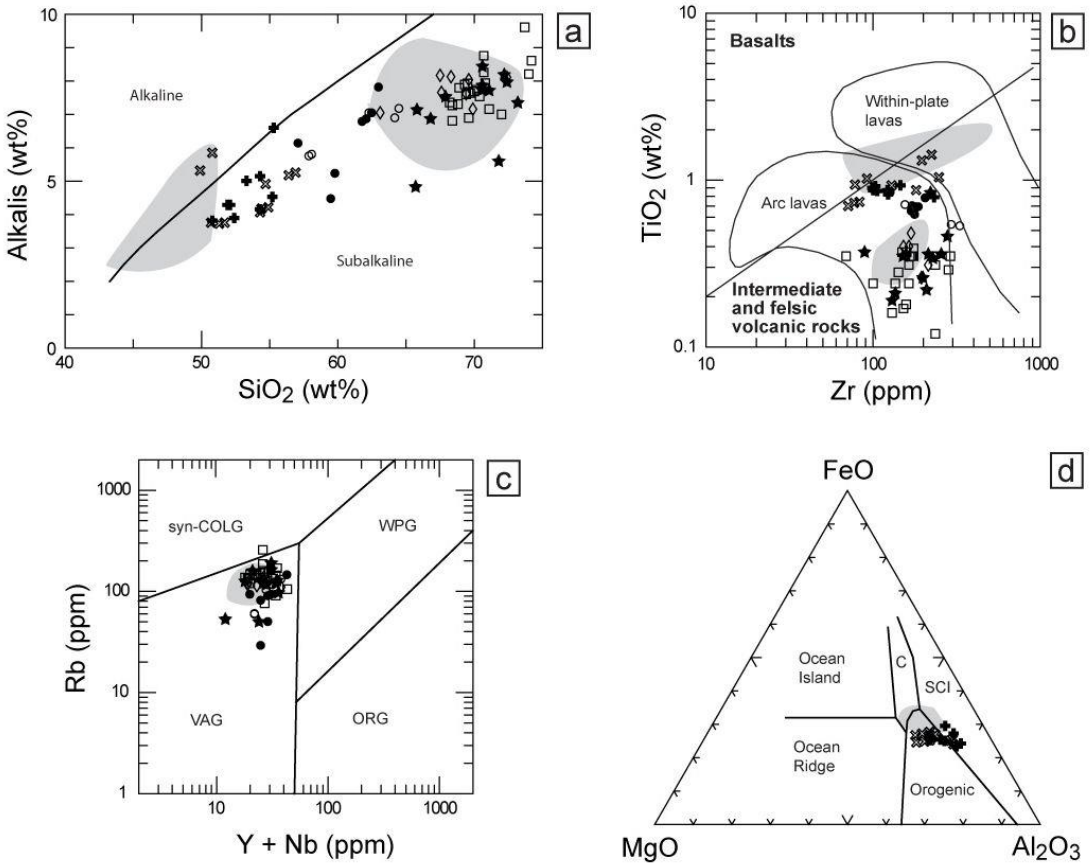

Figure 5.7: a) SiO_2 versus alkali element abundance discrimination diagram (Irvine and Baragar 1971) for the differentiation between alkaline and subalkaline rocks. Nearly all samples plot into the field for subalkaline rocks. b) Zr versus TiO_2 abundance diagram. The discrimination line (in bold) separating basalts and intermediate and felsic volcanic rocks (Leat and Thorpe 1986) is also shown, as are the fields (thin lines) for arc and within-plate lavas after Pearce (1980). Nearly all samples lie in the arc lava field. c) Discrimination diagram of Yb+Ta versus Rb abundances for felsic rocks after Pearce et al. (1984) showing the fields of volcanic-arc felsites (VAG), syn-collisional felsites (syn-COLG), within-plate felsites (WPG), and ocean-ridge felsites (ORG). Nearly all samples plot into the VAG field, which is consistent with the provenance of the OCVB province (e.g., Tikhomirov et al. 2008). d) Ternary plot of FeO (total iron as FeO)-MgO-Al_2O_3 for the discrimination of the tectonic setting of mafic rocks after Pearce et al. (1977). C = continental, SCI = spreading center island. All basalt samples plot into the field for an orogenic setting, whereas some of the basaltic-andesitic tuff samples extend into the SCI field. For symbols compare Fig. 5.5. The shaded fields indicate data for bedrock samples (plotted separately for the felsic and mafic lithologies) from the D1c drill core (Raschke et al. 2013b).

.

5.5.2.3 Koekvun' Formation

Our study area in the eastern sector of the crater area is dominated by the Koekvun' Formation, which is typically constituted of mafic lavas and tuffs, as well as rhyolitic ignimbrite at the northern flank of the Enmyvaam River Valley (Belyi and Belaya 1998). These rocks should be younger in age (according to Stone et al. 2009) than indicated on the older Russian map (Raevsky and Potapova 1984; Zheltovsky and Sosunov 1985). The map was updated by us, accordingly. The new outcrop of basaltic-andesitic tuff to the south of the lake should also belong to this formation, because its location is surrounded by rocks of the same age (according the stratigraphic order by Stone et al. 2009).

Table 5.3: Average chemical composition and standard deviation for the suevite of the El'gygytgyn drill core D1c in comparison to average target compositions based on the regional stratigraphy for the El'gygytgyn area.

	Average suevite D1c drill core Raschke et al. (2013)		Average target composition based on new map		Average target composition Gurov and Koeberl (2004), Gurov et al. (2005)
	mean	sd*	mean	sd*	
wt.%					
SiO_2	68.2	0.9	68.9	2.6	70.72
TiO_2	0.35	0.03	0.35	0.09	0.29
Al_2O_3	14.6	0.2	15.1	1.5	13.90
Fe_2O_3[†]	2.80	0.19	2.84	0.63	2.72
MnO	0.06	0.01	0.06	0.02	0.06
MgO	0.69	0.10	0.77	0.26	0.72
CaO	2.39	0.34	1.98	0.74	2.01
Na_2O	3.08	0.26	3.44	0.82	2.57
K_2O	4.05	0.14	4.14	0.95	4.48
P_2O_5	0.08	0.01	0.09	0.04	0.10
LOI	3.1	0.7	1.9	0.4	2.53[#]
Total	99.40		99.57		100.10
ppm					
Sc	6	1	6	2	
V	29	4	28	12	
Zn	45	1	44	14	
Rb	132	6	129	27	
Sr	251	70	240	137	
Y	20	1	22	4	
Zr	155	10	176	44	
Ba	702	47	688	232	
La	31	3	32	5	
Ce	77	5	65	10	

(Total Fe as Fe_2O_3; LOI includes H_2O and CO_2, *sd = standard deviation)

5.5.2.4 Ergyvaam Formation

This unit is seemingly present only in the eastern crater region. The prominent Mt. Otvevergin is composed of reddish to greenish ignimbrite. On the old map (Raevsky and Potapova 1984; Zheltovsky and Sosunov 1985), this was expressed as "Gabbro or Monzonite" intrusive rock and not as ignimbrite. In the same region, at the upper part of the Otvevergin creek basin, Gurov and Koeberl (2004) identified rocks with a granodiorite-diorite composition. For both cases, we could not identify such intrusive rocks in the entire eastern crater area. All rocks observed are effusive or explosive volcanics. The major occurrence of this unit is just outside of the eastern crater rim, in the hinterland of the Lagernyi creek. We did not investigate this area, so we could not confirm the lithological data given on the older Russian map (Raevsky and Potapova 1984; Zheltovsky and Sosunov 1985), but we have changed the age for this area according to the age determination by Stone et al. (2009), from Koekvun' to Ergyvaam Formation age.

5.5.2.5 Enmyvaam Formation

This unit is not present in our mapping area, but we could assign on our map a small occurrence to this unit, approximately 10 km SE of the lake, according to Stone et al. (2009). This unit was not included in the older Russian map (Raevsky and Potapova 1984; Zheltovsky and Sosunov 1985).

5.5.2.6 Paleogene

Further afield from the crater (>10 km to the south), the meander of the River Enmyvaam exposes formidable basalt cliffs of 10–20 m height. These rocks were described as basalts of Paleogene age (Gurov and Koeberl 2004). We also sampled these lithologies (UR-2011_8.1/8.2), but the outcrops are located outside of our map area.

5.5.3 Comparison of Surface Volcanics with the Bedrock drilled by the ICDP Project

Rhyolitic and rhyodacitic ignimbrite is the most prominent lithology of the entire crater region, which is overlain in the southeastern area by volcanic rocks of basaltic to andesitic composition forming local plateaus of up to 2 km^2 extent. The rhyolitic and rhyodacitic ignimbrites are very similar in petrographic appearance and chemical composition (Table 2), but differ in age according to previous work: rhyodacitic ignimbrite belongs to the Pykarvaam Formation and the rhyolitic ignimbrite to the Koekvun' Formation, respectively (Stone et al. 2009). The rhyodacitic ignimbrite displays slight differences from the rhyolitic ignimbrite in TiO_2, Fe_2O_3, MgO, CaO, and V contents, which are slightly higher, and in the SiO_2 content, which is slightly lower (Table 2). A clear distinction between these two ignimbrites based on immobile major elements (e.g., Ti) or trace elements has not been possible.

The rhyolitic and rhyodacitic ignimbrites are also similar to the ignimbrite found as lower bedrock in ICDP drill core D1c (e.g., Pittarello et al. 2013; Raschke et al. 2013a, 2013b). The different ignimbrites are very similar in texture and mineralogical composition. The lower bedrock of the drill core (Raschke et al. 2013b) (Table 2) is chemically more similar to the rhyodacitic ignimbrite based on higher Fe_2O_3, MgO, CaO, and V contents than to the rhyolitic ignimbrite (Fig. 8). Nevertheless, a clear assignment of the lower bedrock of the ICDP drill core to a distinct ignimbrite surface lithology requires measurement of additional trace elements, and proper correlation can only be made once age data have become available.

The felsic part of the upper bedrock of the ICDP drill core (e.g., Pittarello et al. 2013; Raschke et al. 2013a, 2013b; Wittmann et al. 2013) is chemically (Raschke et al. 2013b) (Table 2) also more similar to the rhyodacitic than to the rhyolitic ignimbrite, but displays differences in petrography, such as smaller or even missing pumice fragments, and a distinctly different color. The surface outcrops of both ignimbrite varieties also have certain variability in their textural appearance (with respect to color and pumice content) and chemical compositions that partially overlap with those of the ignimbrites within the lower and upper bedrock of the ICDP drill core.

For the mafic blocks of the ICPD drill core (e.g., Raschke et al. 2013a, 2013b; Table S1; Pittarello et al. 2013), a correlation with surface basalts or basaltic-andesitic tuffs can be based on the abundances of the immobile elements Ti and Zr, for the two blocks at 391.8 to 390.7, and 423.0 to 422.7 mblf. The extremely high concentrations of especially V, Cr, and Ni observed in these mafic blocks do, however, not match any mafic surface lithology. The ratios of TiO_2/P_2O_5, Cr/Co, and Cr/Ni for the mafic blocks display more or less the same trend as observed within the surface basalts. This may support the suggestion by Raschke et al. (2013b) that these metal enrichments could be related to impact-induced hydrothermal overprint at the crater floor. The precursor of these mafic blocks observed in the D1c drill core is, therefore, most likely the surface basalt of the crater area.

5.5.4 Tectonic Setting

Most of the ignimbrites contain a lot of elongated pumice fragments or particles (see Raschke et al. 2013a, 2013b). In general, ignimbrites cover the landscape and level the topographic relief (McBirney 1968). Normally, pumice fragments are (sub)horizontally oriented with their long axes indicating the direction of flow (Fisher and Schmincke 1984). If the pumice fragments display different orientations, it can be assumed that the rock has been moved, or turned, after deposition by tectonic processes.

We could measure an orientation of 252/35 at the SE crater rim (GPS 551698/7482888), but for a single outcrop (UR-2011_9.12a/10.1) of surface ignimbrite only. The NW half of the crater rim where the majority of the rhyodacitic ignimbrites occur could not be visited during our field trip. For the lower bedrock unit of the drill core, we found the pumice fragments in orientations of 30 to 70° to the long axis of the not oriented core (Raschke et al. 2013a, 2013b). These steeper dips are accordingly suggestive of a possible deformation at the flank of the central uplift or slight rotation of these rocks during the cratering process.

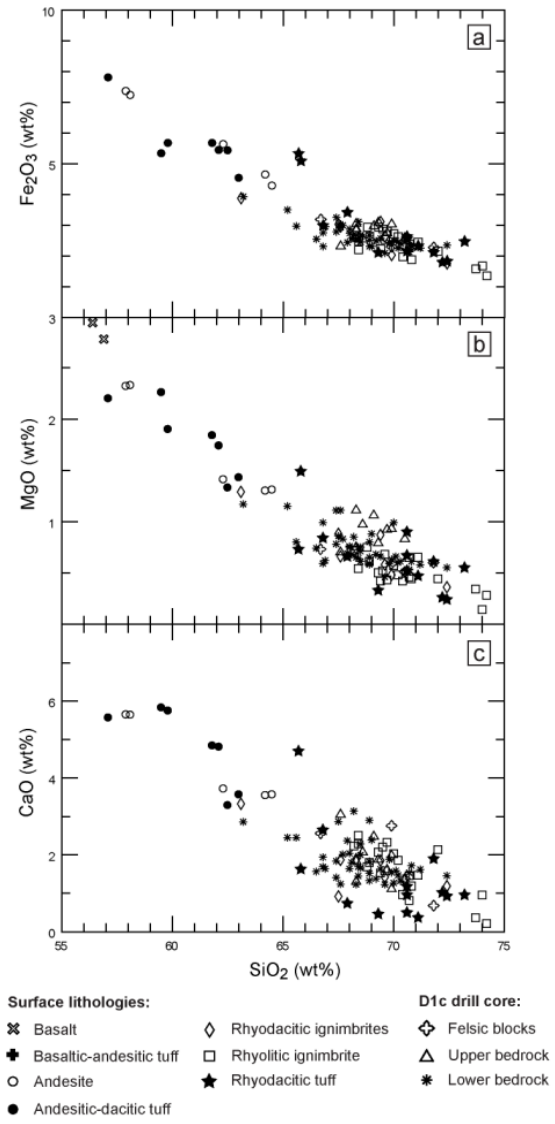

Figure 5.8: Harker diagrams for a) Fe_2O_3, b) MgO, and c) CaO versus SiO_2 contents for the comparison between the felsic surface lithologies of the El'gygytgyn area with samples from the ICDP drill core D1c (Raschke et al. 2013b). Note the similarity between the felsic lithologies from the surface (especially the rhyolitic and rhyodacitic ignimbrites) and the major bedrock lithologies of the ICDP drill core D1c.

A complete reconstruction of the tectonic setting (including a structural map) seems very difficult, because the orientation data we collected in the field cannot be considered as representative, due to the weather condition that prevented a more extensive structural analysis and due to the weathering and fracturing processes that have obliterated the original structures. We could not find a single outcrop of shock metamorphosed rocks in their original position. Most of the other outcrops were covered with up to several meter-thick talus composed of eroded blocks or stones. Only a few cliffs at the shoreline of Lake El'gygytgyn provided suitable locations for measuring and sampling oriented specimens.

5.6 CONCLUSIONS

We provide an update of the Russian Geological Map of the El'gygytgyn area (Raevsky and Potapova 1984; Zheltovsky and Sosunov 1985) based on our results of a 2011 field campaign, which revealed new aspects of the volcanic rocks that represent the target rocks for the El'gygytgyn impact. The most important outcomes are:

1. Impact melt breccia occurs as blocks of up to meter size in the 3 m terrace at the southern shoreline, and as smaller pieces (<5–8 cm) in the pebble ridges.

2. The ignimbrites in the SE sector of the crater, which belong mainly to the Koekvun' Formation, form the base for the overlying mafic rocks. Basalt and andesite occur as lava flow or, partly, as tephra (tuff).

3. The NE sector of the crater with prominent Mt. Otvevergin does not exhibit intrusive gabbro or monzonite. Our analysis shows that, at this place, a rhyolitic ignimbrite occurs. The presence of granodiorite or diorite in the same sector could not be confirmed.

4. A new outcrop of basaltic-andesitic tuff was found to the south of the crater and is indicative of a phreatomagmatic event. The wide range of tuffs, all with ash matrices, but different clast sizes, is generally of andesitic composition. The orientation of these tuff layers dips shallowly (<33°) to the SE in correspondence to the regional trend.

5. Faults across and boundaries between the lithological units could not be mapped due to severe Arctic weather conditions and extensive talus cover. Only at the eastern crater rim could we estimate a lithological transition, from rhyolitic ignimbrite to andesite and basalt, over a zone of several meters width.

6. The rhyolitic and rhyodacitic ignimbrites observed at the surface in the El'gygytgyn area are similar in petrographic appearance and chemical composition to the ignimbrites of the lower and upper bedrock of the ICDP drill core. Based on the available chemical date, a correlation of the lower bedrock ignimbrite with the rhyodacitic ignimbrite observed on surface is preferred, but for a reliable correlation additional trace element analyses and isotope studies/age dating are mandatory.

Acknowledgments

Funding for the participation of UR and PZ in the 2011 expedition was provided by the Deutsche Forschungsgemeinschaft (DFG) through grant RE 528/12-1 (to WUR). The expedition was organized and conducted by G. Federov (AARI, St. Petersburg) and G. Schwamborn (AWI Potsdam). These two were also responsible for sample transfer from Russia to Germany. We thank N. Ostanin (State University, St. Petersburg) for making information, previously published in Russian, available to us, which includes the Russian

Geological Map. The investigation of the 2011 expedition samples was also supported by the DFG through grant RE 528/10-2 to WUR and RTS. O. Juschus (HNE Eberswalde) provided numerous rock samples and data from his 2003 crater expedition, and N. Nowaczyk (GFZ Potsdam) provided information, and rock samples that greatly expanded our collection. L. Pittarello supplied the geographical coordinates for the samples by E. Gurov. M. Sauerbrey (University of Cologne) is thanked for nice photographs of the lithologies around the crater that we could use for this work. M. Lack (AWI Forschergruppe Potsdam) developed a first digital elevation model that we could use for the bathymetry of the Lake El'gygytgyn. Aster satellite data were employed for creation of all other digital elevation models. Aster (GDEM) is a product of METI and NASA. Additional support for the publication of the map and this paper was obtained from the Museum für Naturkunde Berlin. H.-R. Knöfler (Museum für Naturkunde Berlin) did a great job preparing a large number of polished thin sections of El'gygytgyn samples (including the drill core samples, totaling >300 samples). K. Krahn (Museum für Naturkunde Berlin) is thanked for sample preparation for the XRF geochemical analyses. And special thanks go to E. A. Raschke for translation of the Russian literature.

Reviewers E. Gurov and L. Pittarello, as well as Associate Editor C. Koeberl, provided constructive input that significantly improved the manuscript.

Editorial Handling - Dr. Christian Koeberl

*Note: This chapter was also updated for more correctness in spelling and grammar. On page 143 the figure caption updated (delete: "distinguished", insert: "various"). On page 157 the figure was modified. Deleted: the word "Alkalies" and replaced by "Alkalis". On page 157, line 10 was insert "*according the stratigraphic order". *On page 182 was deleted "moderately altered with secondary calcite being common" and insert "slightly altered".*

5.7 SUPPLEMENTARY MATERIAL

This subchapter contains additional figures and tables, which were published online only.

Figure S1: a) Aerial photograph of the north-eastern crater rim (view towards East). Mt. Otvevergin (761.2 masl) is centered on the photograph. Note the colorful slopes covered by ignimbrites. b) At the slope near the top of Mt. Otvevergin (sample location UR-2011_11.1). View over the entire eastern crater rim with the basalt plateau (Mt. Chivirynnet, 806.4 masl) prominent in the background.

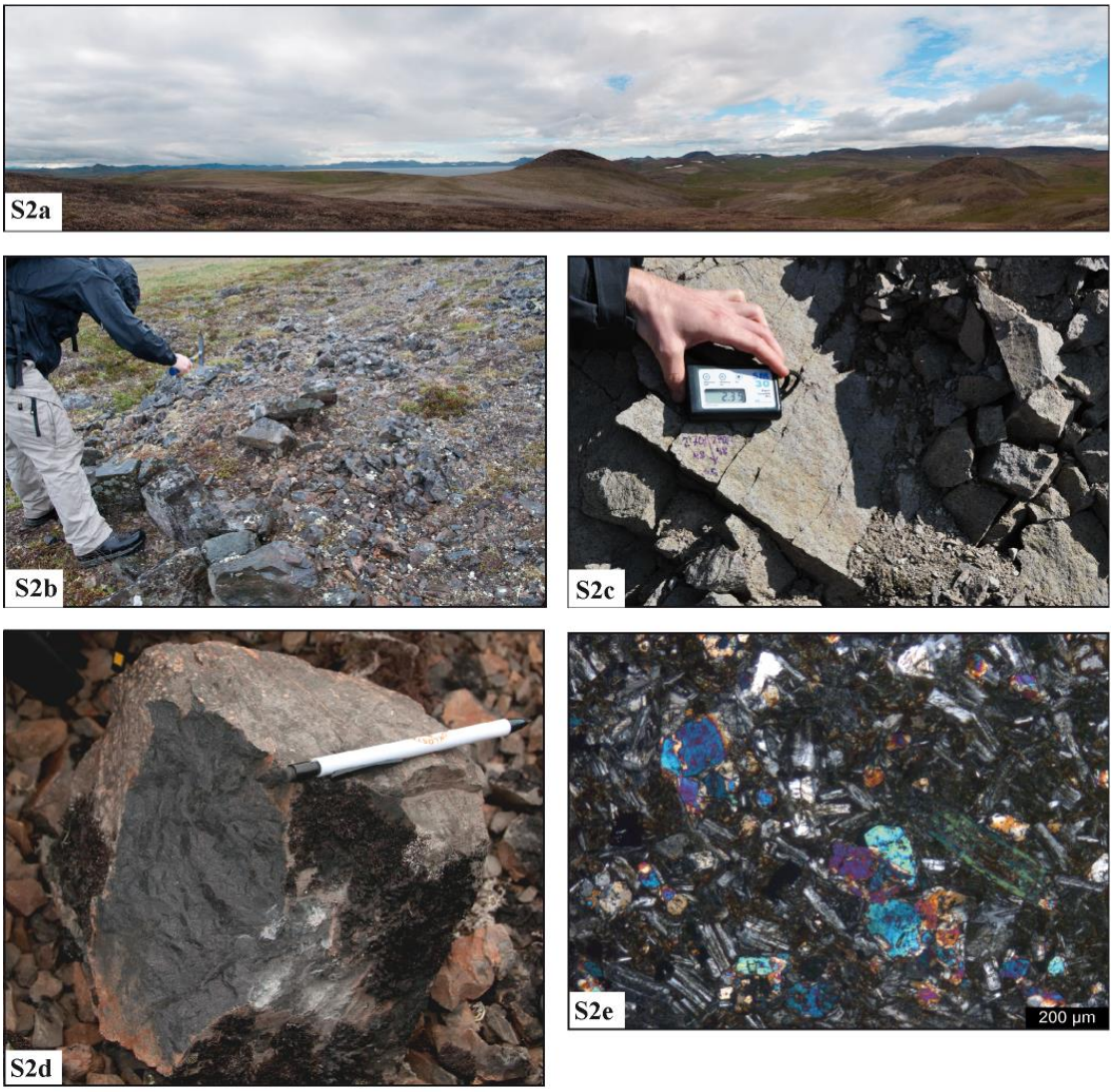

Figure S2 (a-e): Basalt. a) Panoramic view over the south-eastern crater rim towards the NW. Note the low hills (the upper parts of which are composed of basalt) in the central and right parts of the picture. In the background the NE basalt plateau is visible. b) Typical basalt outcrop (UR-2011_3.2, UTM: 552659/7481179). c) After having exposed bedrock we noted the geographical orientation (blue arrows) and measured the electrical conductivity. d) Freshly hammered piece of basalt. e) Microphotograph in cross polarized light of a typical basalt sample with a few olivine phenocrysts, sampleUR-2011_3.1.

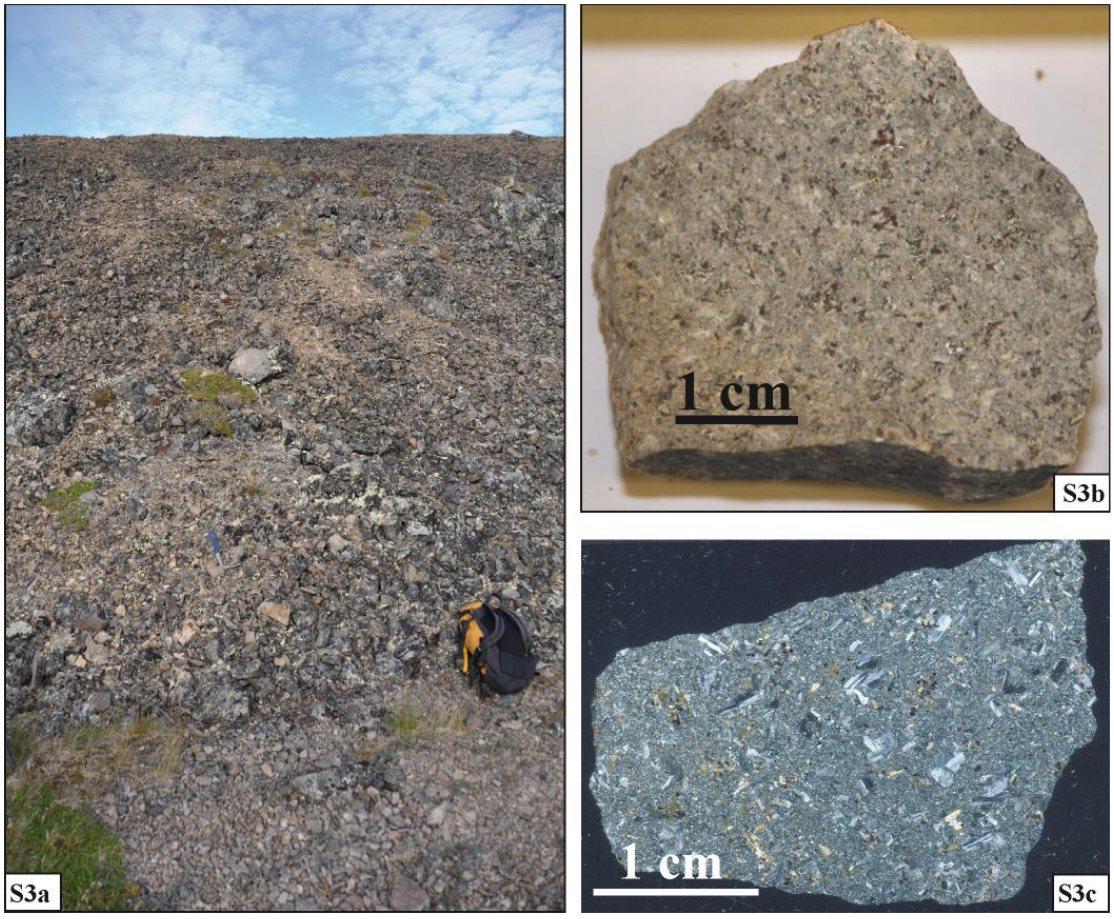

Figure S3 (a-c): Andesitic basalt. a) Outcrop at the slope of a low hill at UTM: 552669/7484762 largely covered by weathered material; backpack for scale. b) Hand specimen of andesitic basalt from this outcrop. c) Thin section scan with characteristic fine-grained matrix and medium-grained feldspar phenocrysts.

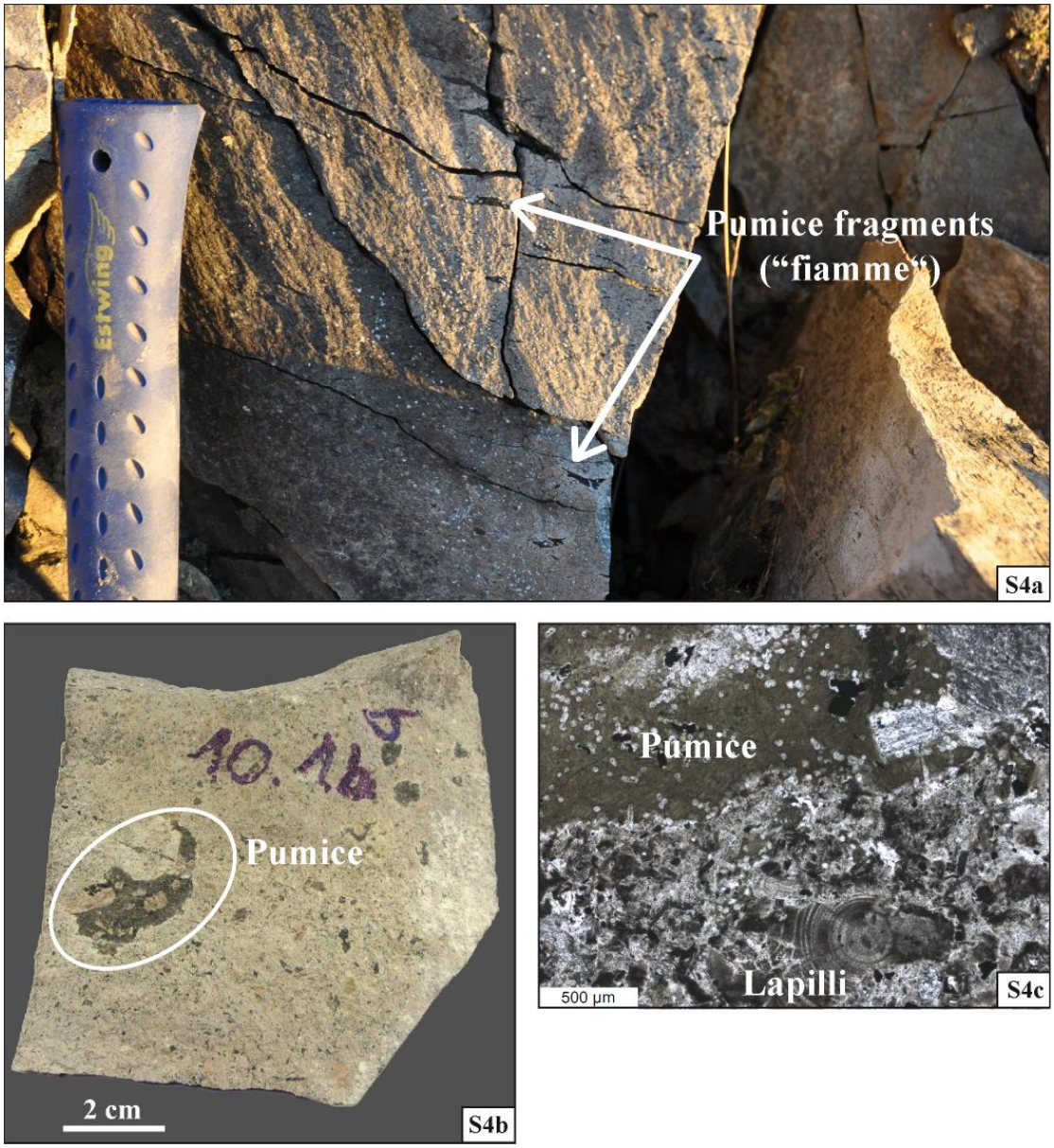

Figure S4: (a-c): Rhyodacitic ignimbrite. a) Well preserved outcrop (UR-2011_9.12a/10.1, UTM: 551698/7482888) of a leucocratic ignimbrite at the SE crater rim. The deformed pumice fragments ("fiamme") occur as dark lenses with a parallel orientation (labelled with white arrows). b) Hand specimen from this location. Note the feldspar porphyroblasts included in the pumice fragments. c) Microphotograph of a thin section with a fine-grained (ash) matrix and vesicle-rich pumice and lapilli fragment (UR-2011_9.12a, plane polarized light).

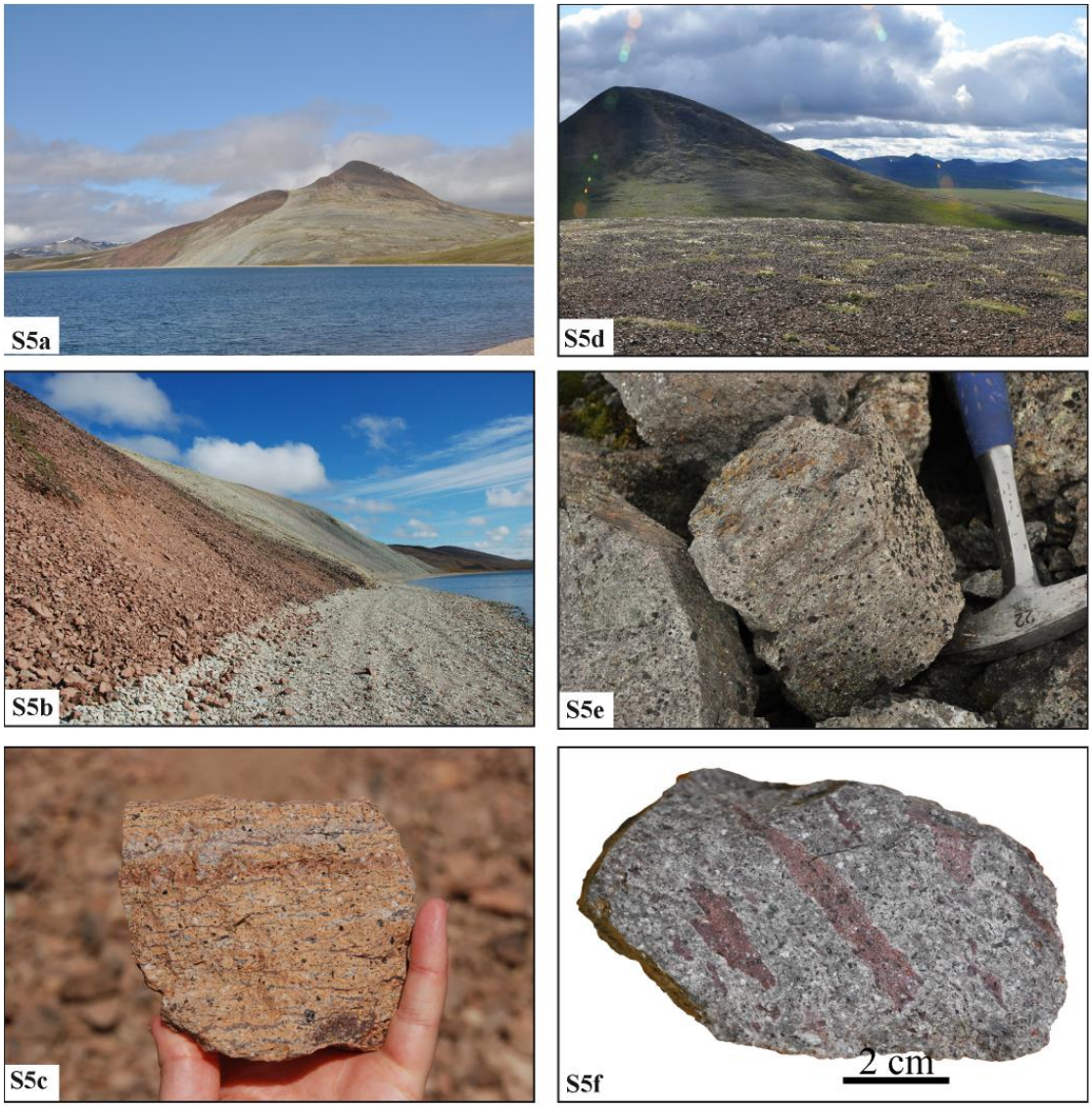

Figure S5: (a-f): Rhyolitic ignimbrite. a) Mt. Otvevergin (700 masl) at the NE end of Lake El'gygytgyn. b) Shore line at Mt. Otvevergin. Two different colored ignimbrites occur together. Note: The beach is covered with greenish rocks instead of reddish ones that occur at the foothill, because the water circulation transported the pebbles and cobbles from east to west (counterclockwise). Photograph by M. Sauerbrey. c) Hand specimen of the reddish ignimbrite with parallel oriented pumice ("fiamme") fragments. Photograph by M. Sauerbrey. d) Geodetic Hill at the southern crater rim, view from east to west. e) Outcrop of grayish ignimbrite at the top of Geodetic Hill (727.2 masl). f) Hand specimen of this ignimbrite with red-brown pumice ("fiamme") fragments.

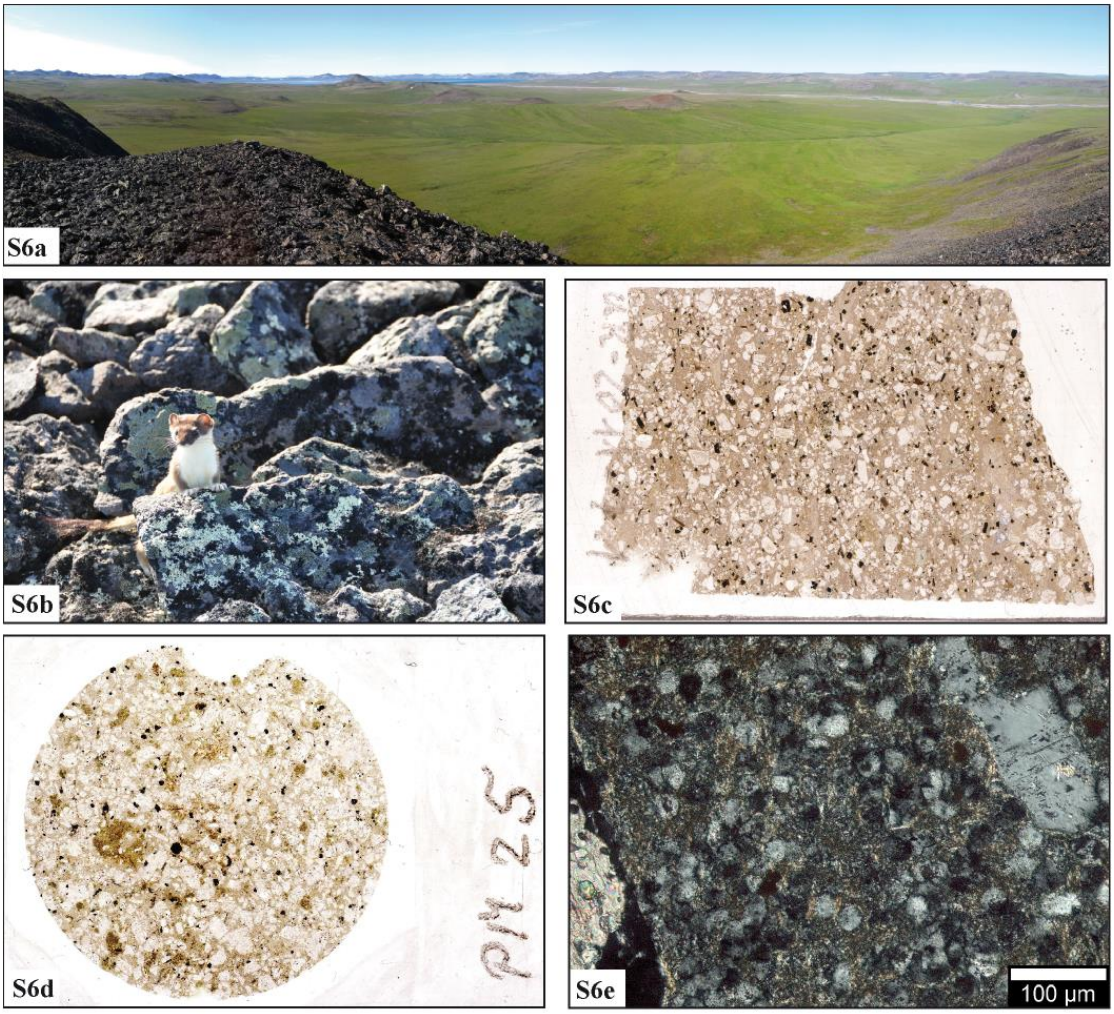

Figure S6: (a-e): Andesitic-dacitic tuff. a) Panorama view towards the north from the top of a prominent hill south of the crater (location UR-2011_7.1). Lake El'gygytgyn and the Geodetic Hill lie in the background, somewhat offset from the center of the picture. b) Hermelin at the top of this hill. The rocks show colorful weathering crusts and are partially covered by lichen. c) Thin section scan (48x22 mm) of sample UR-2011_7.1 with crystal fragments (mostly feldspar) in an ash matrix. Mafic minerals, especially biotite and amphibole, occur widespread. d) Thin section scan (48x22 mm) of sample PM-25 by O. Juschus, collected at the Lagernyi valley. Also visible is the crystal tuff texture. e) Finest ash matrix with round vesicles filled with feldspar, and a larger plagioclase phenocryst (microphotograph of a thin section under cross polarized light).

S7a

S7b

S7c

S7d

S7e

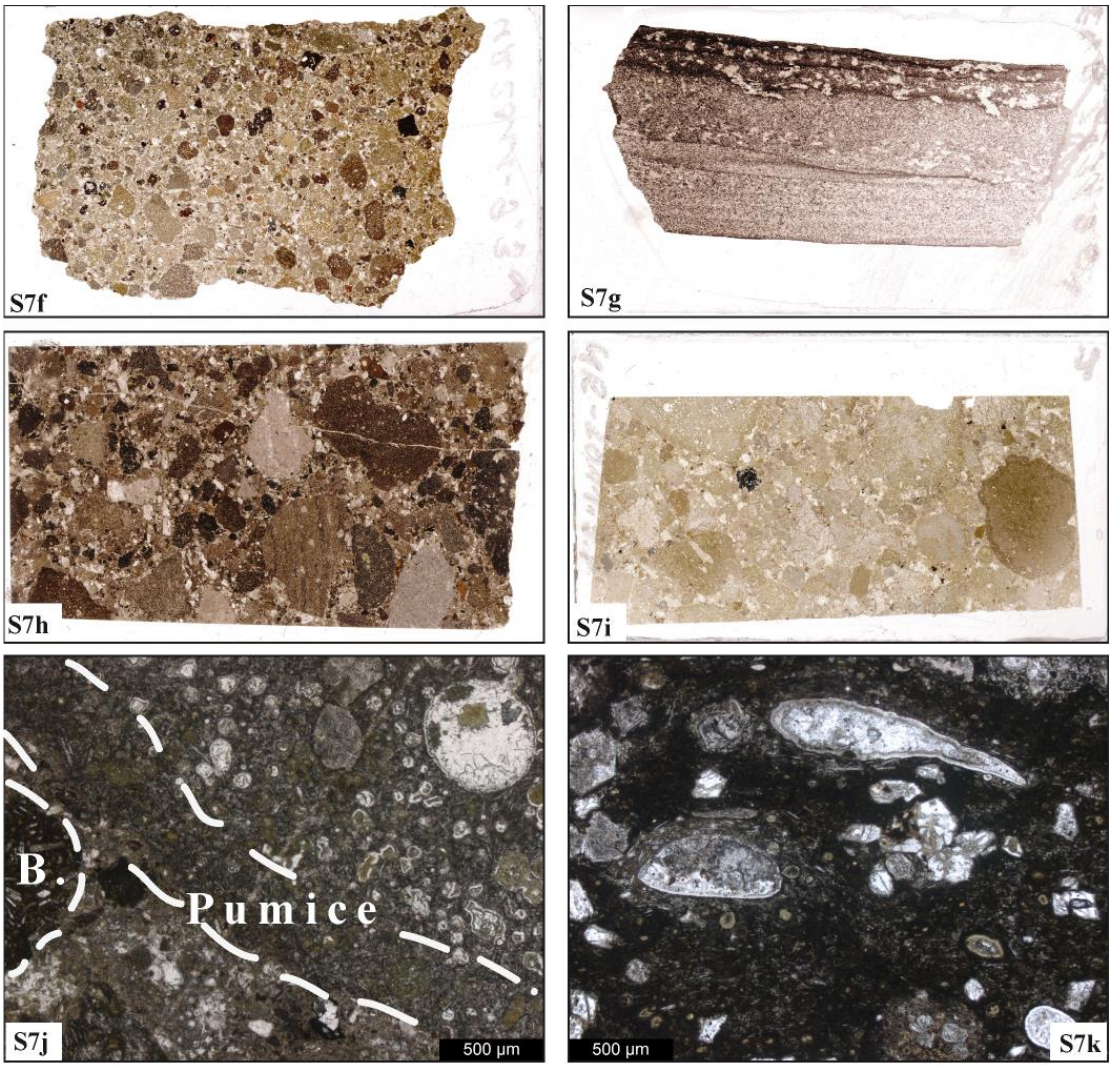

Figure S7: (a-k): Basaltic-andesitic tuff. a) New outcrop to the south of the crater lake (550517/7475857), ca 60 m long and 15-20 m high. View from east to west with different types of tuffaceous rocks. Photograph by M. Sauerbrey. b) Location UR-2011_9.3 with an oriented hand specimen of a medium-grained tuff. c) Reddish, laminated ash tuff, sample UR-2011_9.5. d) Sample UR-2011_9.7 composed of lithic fragments in size up to 15 mm. Fragments and matrix are light greenish in color. e) Crystal tuff with grayish matrix with clasts up to cm-size (sample UR-2011_9.9, ca. 300 m east at the Washenka river). f) Thin section scan (48x22 mm) of sample UR-2011_9.3 showing a composition of different lithic clasts and crystal fragments in a fine ash groundmass. The fragments are subangular, typically of phreatomagmatic tuffs. g) Thin section scan (48x22 mm) from sample UR-2011_9.5, fine-laminated ash tuff. h) Chaotic texture of lithic tuff (also possible phreatomagmatic tuff) with clasts of several lithologies and different sizes (thin section scan, 48x22 mm, UR-2011_9.8, parallel polarized light). i) Thin section scan (48x22 mm), sample UR-2011_9.9, ca. 300 m downstream showing larger (up to 10 mm in size) clasts of ash particles which have a high porosity. j) Microphotograph of sample UR-2011_9.7, with a diagonally oriented pumice fragment, which contains a number of vesicles (a larger one at right upper corner). These are filled by calcite or other secondary minerals (e.g., chlorite). At the left edge, a basalt fragment (B.) is visible. Plane polarized light. k) Pumice fragment in a vesicle-rich ash matix, similar to S6j. Microphotograph, cross polarized light.

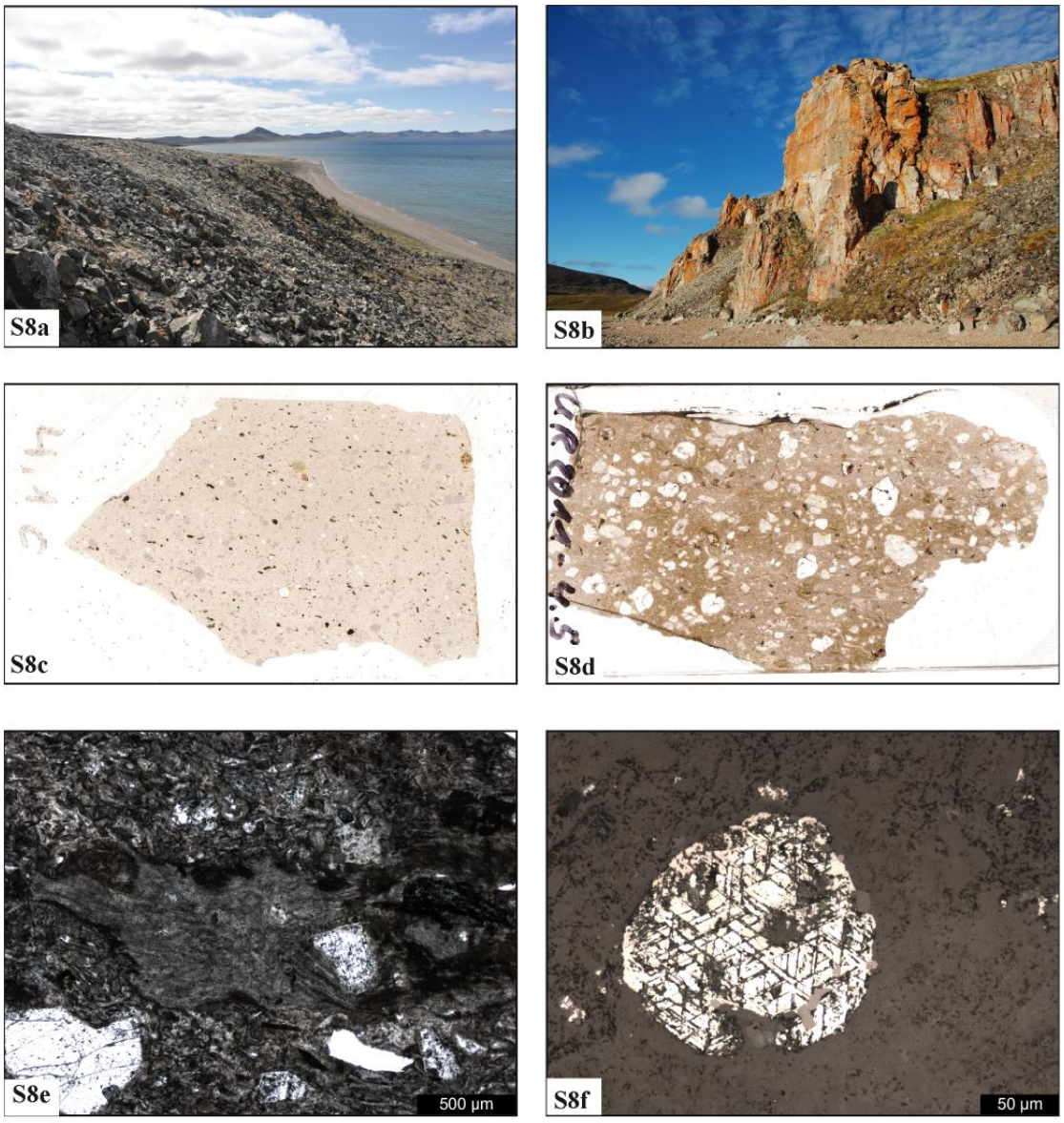

Figure S8: (a-f): Rhyodacitic tuff. a) Outcrop at the eastern shoreline, north of the Lagernyi creek (UR-2011_4.1c, UTM: 552513/74844556). View to south. b) "Rosavaya-Hills", prominent cliff at the north eastern shoreline (UR-2011_4.5). The reddish color is an algae cover that is growing especially on the surface of the felsic tuffs. c) Thin section scan (48x22 mm) of UR-2011_4.1c, an ash matrix supported tuff with small (< 1 mm in size) crystal fragments. d) Thin section scan (48x22 mm) of UR-2011_4.5 with larger crystal fragments (mostly feldspar) in a finest grained ash matrix. e) Microphotograph of an elongated ash-particle in the center and few crystal fragments of feldspar (included in the ash particle and outside at the left, lower corner (microphotograph, parallel polarized light). f) Microphotograph showing a haematite with "Martinite"-structure, UR-2011_3.5, reflected light.

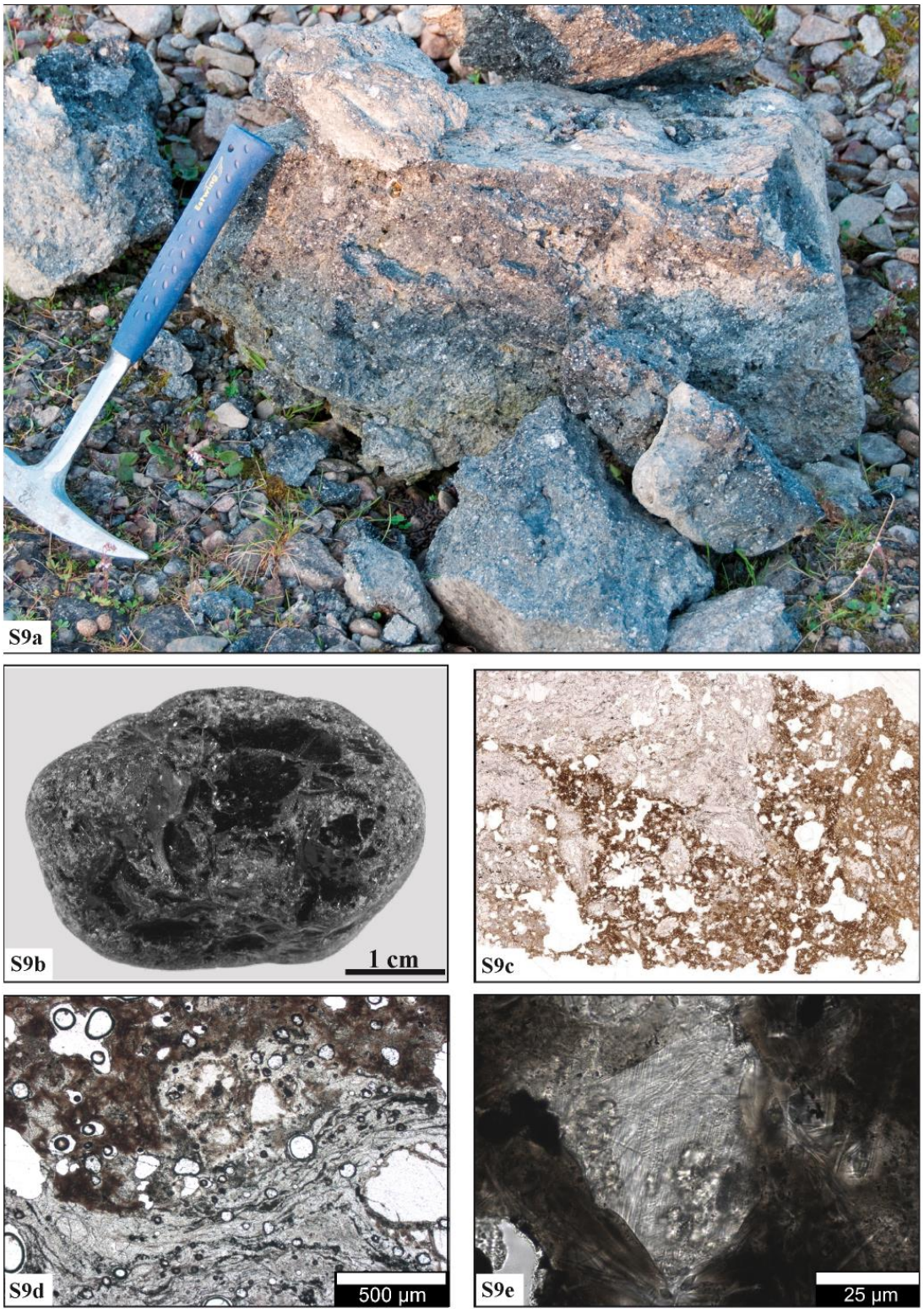

Figure S9: (a-e): Impact melt breccia. a) Block of impact melt breccia at the SE shoreline (GPS: 551863/7483086, UR-2011_9.10). Note the scoria-like texture with black glassy "schlieren" and porous parts with inclusions of light colored crystal fragments. b) Round pebble of impact melt breccia, sampled at the southern lake terrace. c) Thin section scan (length 3 cm) of sample UR-2011_9.11, another, similar block of impact melt breccia. Two different kinds of melt are visible (brownish and translucent), both with a high content of vesicles. d) Close-up of the same thin section (under plane polarized light) emphasizes the contact between the glassy, translucent and brownish melts. e) Two sets of planar deformation features (PDF) in a small quartz grain embedded into the brownish part of impact glass (UR-2011_9.11, microphotograph taken with plane polarized light).

Geological Map of El´gygytgyn Impact Crater - Chukotka, NE Siberia, Russia 1:50 000

Compiled by U. Raschke [1], P. T. Zaag [1], R. T. Schmitt [1] and W. U. Reimold [1,2], [1] Museum für Naturkunde Berlin, Invalidenstraße 43, 10115 Berlin, Germany (E-mail: ulli.raschke@outlook.com),
[2] Humboldt-Universität zu Berlin, Unter den Linden 6, 10099 Berlin, Germany

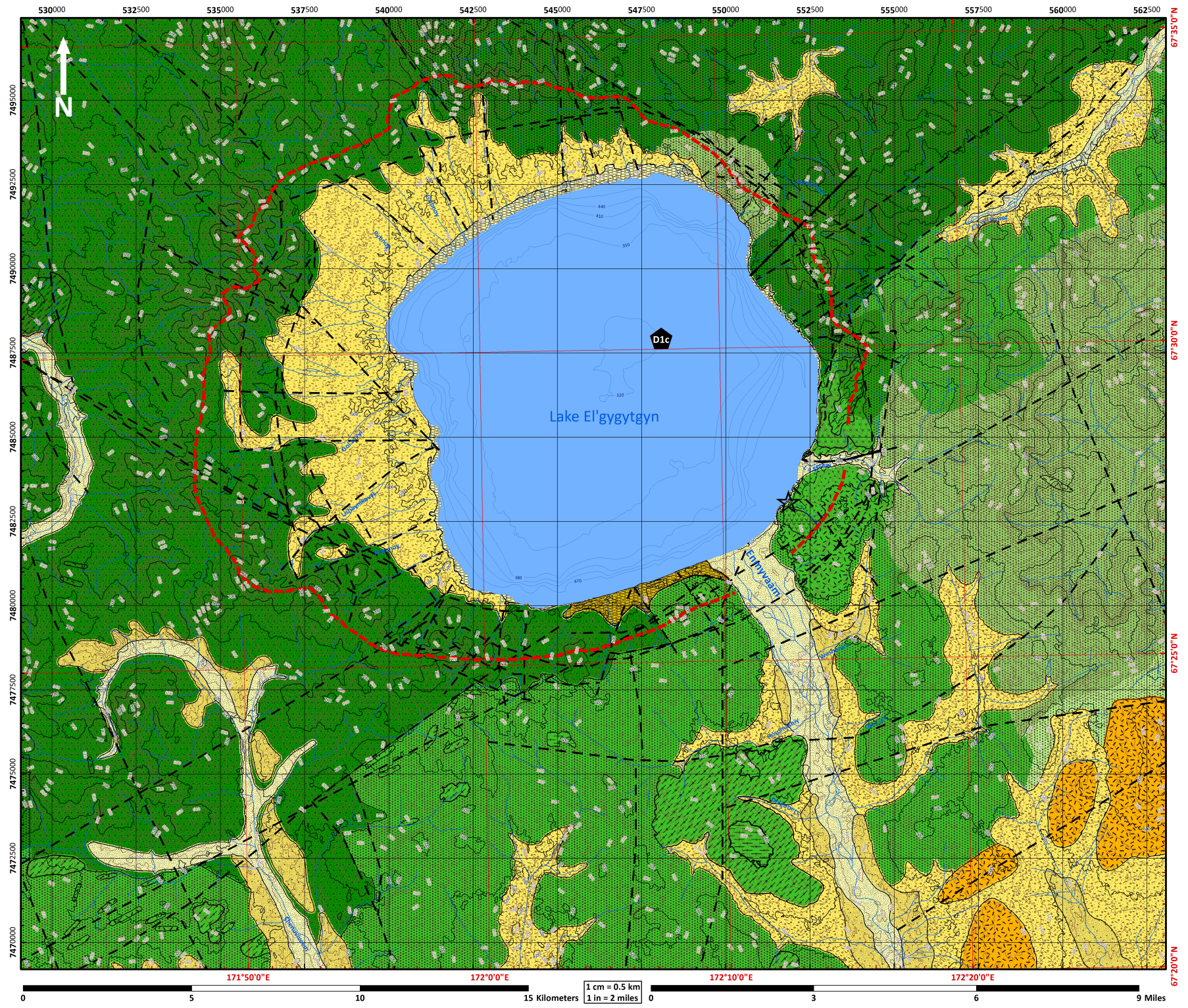

Legend

- Lake El'gygytgyn
- Streams
- ICDP Borehole D1c (2009)
- Morphological crater rim
- Contours, bathymetric, 30 m intervals (mbll)
- Contours, topographic, 100 m intervals (masl)
- Contours, topographic, 20 m intervals (masl)

Samples

- Belyi and Belaya (1998)
- Expedition (2011)
- Gurov in Pittarello et al. (2013)
- Juschus (2003) bedrock
- Juschus (2003) colluvium
- Impact melt breccia (boulder)

Faults

- Confirmed
- Inferred

Morphologies and Lithologies

- Lower terrace
- Riverbeds and floodplains
- Lacustrine sediments
- Periglacial-fluvial, solifluctional sediments
- Andesite
- Basaltic andesite
- Andesitic-dacitic tuff
- Basalt
- Basaltic-andesitic tuff
- Rhyodacitic tuff
- Rhyodacitic ignimbrite
- Rhyolitic ignimbrite

Stratigraphy

Quaternary

- Holocene
- Upper Pleistocene, Holocene
- Upper Pleistocene

Paleogene

- Paleogene

Cretaceous

- Enmyvaam Fm.
- Ergyvaam Fm.
- Koekvun' Fm.
- Voron'in Fm.
- Pykarvaam Fm.

Elevation (masl): 920, 715, 510, 310
Bathymetry (mbll): 0, 60, 120, 180

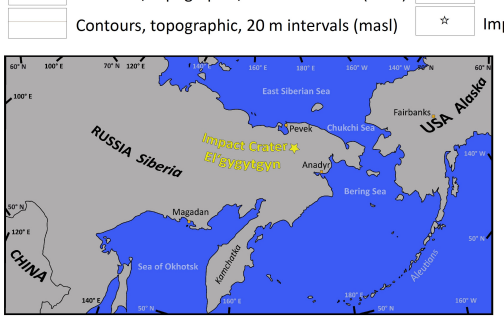

Schematic map indicating the location of El'gygytgyn Impact Crater.

Coordinate System: WGS 1984 UTM Zone 59N
Projection: Transverse Mercator
Datum: WGS 1984
False Easting: 500,000.000
False Northing: 0.000
Central Meridian: 171.000
Scale Factor: 0.9996

Abbreviations: masl = meters above sea level; mbll = meters below lake level

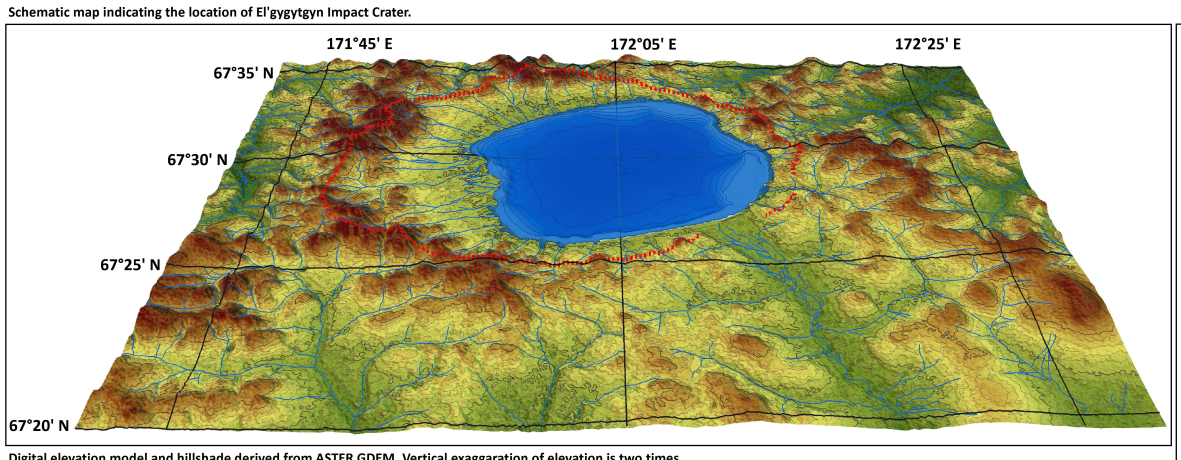

Digital elevation model and hillshade derived from ASTER GDEM. Vertical exaggaration of elevation is two times.

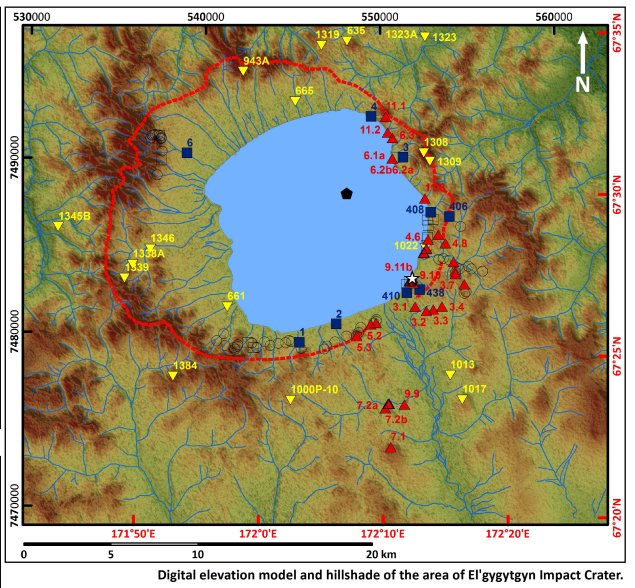

Digital elevation model and hillshade of the area of El'gygytgyn Impact Crater.

Acknowledgements:
This work was funded by the Deutsche Forschungsgemeinschaft (project RE 528/12-1 to WUR). We especially thank G. Schwamborn from the Alfred-Wegener-Institute (Potsdam) and G. Federov from the Arctic and Antarctic Research Institute (St. Petersburg) for the organization of the 2011 expedition to Lake El'gygytgyn. N. Ostanin (State University, St. Petersburg, Russia) is thanked for making information, previously published in Russian, available to us. O. Juschus (HNE Eberswalde), who obtained rock samples during a 2003 expedition, and N. Nowaczyk (Geoforschungszentrum Potsdam) provided information, as well as rock samples that greatly expanded our own collection. For the generation of the digital elevation model ASTER satellite data were employed. ASTER GDEM is a product of METI and NASA.

References:

1) Belyi V. F. and Raikevich M. I. 1994. The Elgygytgyn Lake Hollow. Russian Academy of Sciences, Far East Branch, Northeast Interdisciplinary Research Institute. Magadan. 27 pp. In Russian. 2) Belyi V. F. and Belaya B. V. 1998. The Late Stage of the Okhotsk - Chukchi Volcanic Belt Development (the Enmyvaam River Upper run Area). North East Interdisciplinary Research Institute, Magadan, Russian Academy of Sciences Far East Branch. 108 pp. In Russian. 3) Lack M. 2011. GIS El'gygytgyn v. 1.0. Alfred-Wegener-Institut für Polar- und Meeresforschung, Forschungsstelle. 4) Melles M., Minyuk P., Brigham-Grette J., Juschus O. 2003, Bericht Polar & Meeresforsch., 509, ISSN 1618-3193. 84 pp. 5) Pittarello L., Schulz T. and Koeberl C. 2013. Petrography, geochemistry and Hf-Nd isotope evolution of drill core and target rocks from the El'gygytgyn impact crater, NE Chukotka, Arctic Russia. Meteoritics and Planetary Science, 48:1160-1198. 6) Stone D. B., Layer P. W. and Raikevich M. I. 2009. Age and paleomagmatism of the Okhotsk-Chukotka Volcanic Belt (OCVB) near Lake El´gygytgyn, Chukotka, Russia. Stephan Mueller Special Publication Series (EGU-Copernicus Publ. 4:243–260. 7) Raevsky F. B. and Potapova E. P. 1984. Geological map of the Anadyr region, sheet Q-59-III, IV. In: Official geological map of the USSR. Eds: Ministry of Geology, USSR. In Russian. 8) Topographical map Q-59-19, 20. 1984. Chukot Autonomous Area of the Magadan region, Magadan, Russia. 9) Zheltovsky V. G. and Sosunov G. M. 1985. Geological map of the Anadyr region, sheet Q-59-V, VI. In: Official geological map of the USSR. Ministry of Geology, Moscow, USSR. In Russian.

© 2014 Museum für Naturkunde Berlin, Germany.

Figure S10: This figure shows the complete new geological map of the El'gygytgyn impact structure at still reduced resolution. This map is also available as fully high-resolution file on the Pangea server by MAPS. The map contains three additional maps which are also presented in this paper (Figs. 5.1a, 5.3, and 5.4)

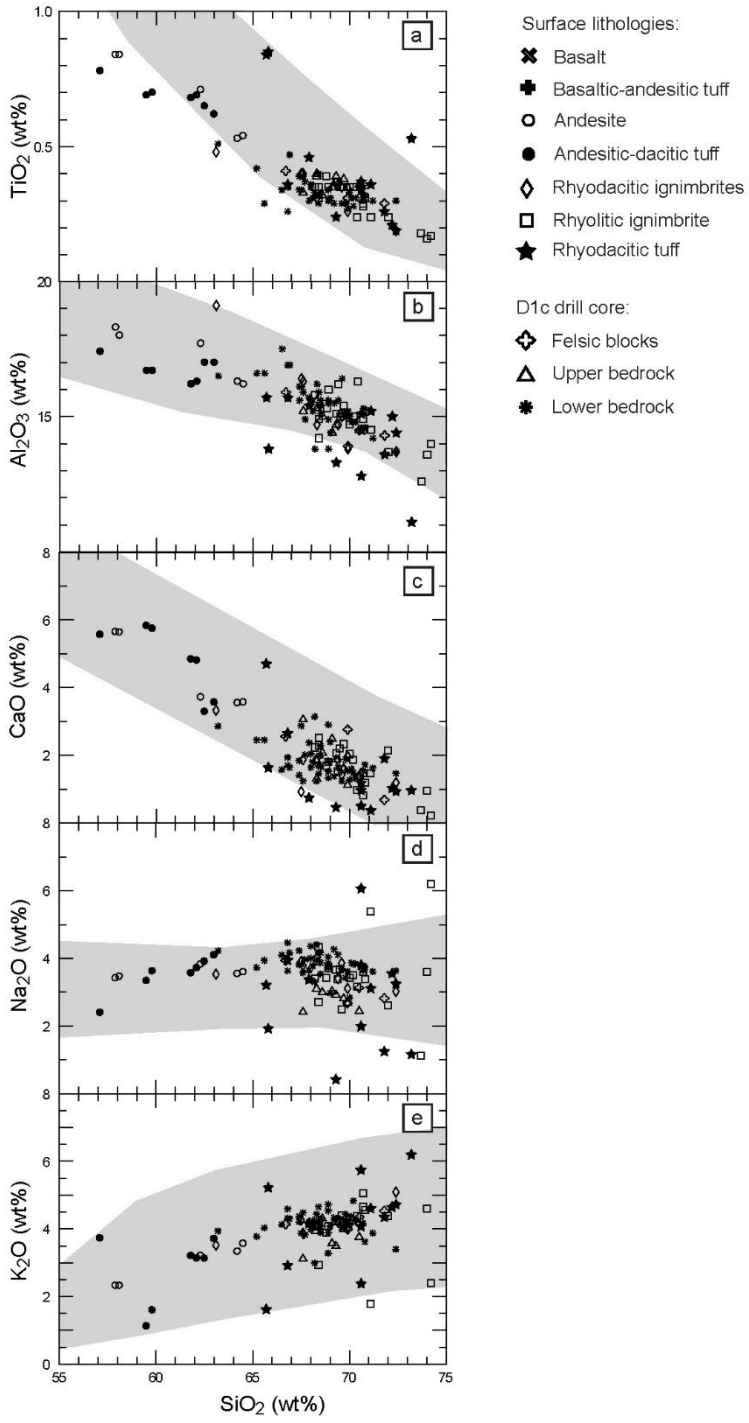

Figure S11: Harker diagrams for a) TiO_2, b) Al_2O_3, c) CaO, d) Na_2O and e) K_2O for El'gygytgyn surface lithologies and felsic bedrocks from the D1c drill core (Raschke et al. 2013b). For comparison the trend for the OCVB (including the Berlozhya magmatic assemblage) is shown as shaded field (based on data of Tikhomirov et al. 2008). Note that most the El´gygytgyn samples plot within the field of the OCVB.

Table S1. Locations and short lithological descriptions of surface samples from the El'gygytgyn impact structure that were collected during the 2003 and 2011 expeditions (images are thin section scans, 48x24 mm)

1. Group: Basalt

UR-2011_3.1 (552011/7481422): Fine grained crystalline matrix (intersertal texture) of feldspar, mainly plagioclase, and a few larger crystals of olivine and pyroxene. No shock features visible and a relatively fresh sample, with weathering crust only.

UR-2011_3.2 (552659/7481179): Similar to sample UR-2011_3.1, but with larger (~4 mm) feldspar (plagioclase and alkali-feldspar) porphyroblasts, widespread occurrence of tiny ore mineral grains (Fe-oxides).

UR-2011_3.7 (554315/7483300): This sample is similar to UR-2011_3.2.

UR-2011_3.8 (554304/7483455): This sample is also similar to UR-2001_3.2/3.7, but displays a stronger alteration at the surface (weathering crust) and along some narrow cracks.

UR-2011_5.2 (549459/7480410): Fine grained crystalline matrix of plagioclase and a few larger vesicles (up to ~3 mm in diameter), which are filled by recrystallized quartz. No shock features were observed. Brownish iron oxides are widespread. This sample is strongly altered and much secondary carbonate occurs.

UR-2011_8.1 (556305/:7464188): Fine grained crystalline matrix (intersertal texture) of feldspar, mainly plagioclase, and a few larger biotite plates. Hornblende and biotite are uralitized. No shock features were observed. In contrast to other basalts, the K_2O content is enriched (Table S2).

UR-2011_8.2 (556232/:7466410): This sample is very similar to UR-2011_8.1, and also enriched in K_2O (Table S2).

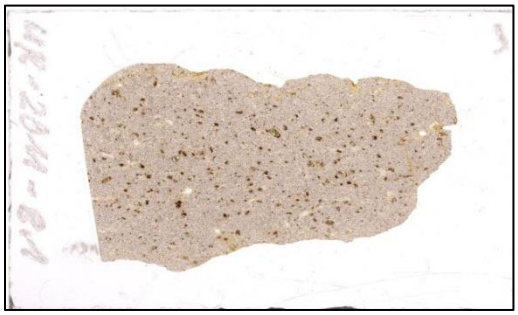

PM-34 (549640/7480487): Fine grained crystalline matrix with plagioclase and only a few larger pyroxene and other feldspar grains. Intersertal texture. No quartz and shock features visible, but moderately weathered with many reddish iron oxide particles.

PM-51 (554356/7483385): Fine grained crystalline matrix of plagioclase and a few larger pyroxene crystals. No olivine and no shock features found. Somewhat altered.

2. Group: Basaltic Andesite

UR-2011_4.1b (552513/7484506): Fine grained crystalline matrix (intersertal texture) with feldspar (albite with Carlsbad twinning), some quartz crystals and tiny ore mineral crystals. No shock features were found, but a strong alteration with much calcite and chlorite (pseudomorphs after pyroxene).

UR-2011_4.2 (552639/7484745): Fine grained crystalline matrix with much feldspar, mainly plagioclase, and larger feldspar phenocrysts. Some olivine crystals are included in the intersertal texture. The whole sample is greenish, possibly due to presence of devitrified melt. No shock features were observed, but strong alteration with secondary chlorite and carbonate. The chemical analysis shows a high LOI and CaO content reflecting the strong alteration (Table S2).

UR-2011_4.4 (552669/7484762): Fine grained crystalline matrix with plagioclase and larger phenocrysts of feldspar and quartz. Intersertal texture with tiny brownish iron oxides and greenish chlorite (after glass). Secondary calcite is further evidence for comparatively stronger alteration. One possibly shocked quartz grain was found. Strong alteration is also expressed in high LOI and CaO contents (Table S2).

PM-66 (537333/7491268): Homogeneous, fine grained crystalline matrix with much plagioclase and a few larger feldspar crystals (with Carlsbad twinning), and rare, small quartz grains. Intersertal texture with few vesicles in a flow structure. Somewhat weathered.

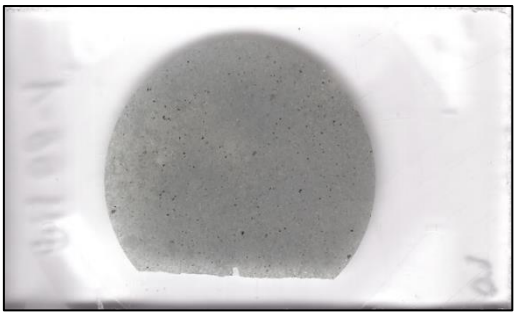

3. Group: Andesite

UR-2011_4.1e (552513/7484556): Fine grained crystalline, light to dark brownish matrix with a porphyritic texture and larger phenocrysts (~4 mm) of plagioclase, amphibole, olivine and biotite. Moderate alteration (some chlorite).

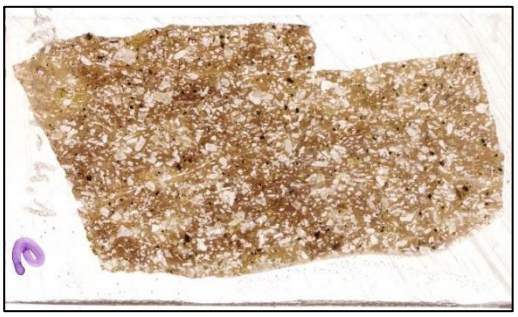

UR-2011_7.2 (550306/7475590): Very fine grained crystalline matrix with micro-feldspar-needles, flow texture, and a few, tiny quartz crystals.

UR-2011_9.6 (550446/7475839): Similar to UR-2011_7.2. Very fine grained crystalline matrix with a few larger phenocrysts of feldspar and pyroxene in a fluidal texture. Fractures are filled by secondary quartz. Widespread occurrence of tiny ore mineral grains. Moderately weathered (secondary carbonate).

UR-2011_11.2 (550443/7491434): The fine grained crystalline matrix (intersertal texture) consists of plagioclase and pyroxene (augite). These minerals occur also as larger phenocrysts. Tiny (oxidized) ore mineral gains (<1 mm). Relatively fresh.

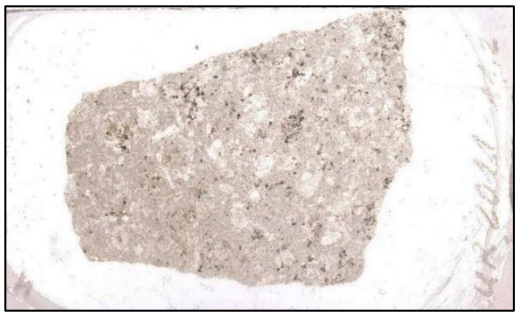

PM-24 (554429/7483666): Fine grained crystalline matrix with plagioclase and some larger pyroxene and tiny, widespread ore mineral grains. Intersertal texture. Moderately weathered (secondary carbonate).

PM-72 (537333/7491268): Fine grained crystalline matrix with plagioclase and some larger crystals (<3 mm) of feldspar, pyroxene (hypersthene), biotite, and hornblende, and a few tiny ore mineral grains. Quartz is very rare. Porphyritic texture. Strongly weathered.

4. Group: Rhyodacitic ignimbrite

UR-2011_9.12a (551698/7482888): Microcrystalline matrix with spherulitic growth structures in brownish to greenish mesostasis. Larger phenocrysts are quartz, feldspar, hornblende, and a few primary calcite grains. Some ore mineral grains. Strong alteration as indicated by greenish alteration of glass.

PM-3 (552740/7485416): Fine grained crystalline matrix with fluidal texture. Up to ~4 mm subangular phenocrysts of alkali feldspar, hornblende, biotite, plagioclase and quartz. Elongated pumice fragments with interfingering contacts. Spherulitic growth structures in glass. No shock features; moderate to strong alteration with sericitisation of feldspar, and overgrowths of calcite on feldspar.

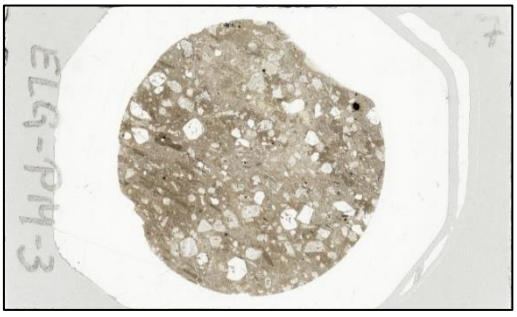

PM-5 (552720/7486400): Fine grained crystalline matrix with fluidal texture. Up to ~3 mm rounded phenocrysts of plagioclase, alkali feldspar, hornblende, large biotite crystals, and quartz. Elongated pumice fragments are very small. No shock features, and moderate to strong alteration.

PM-6 (553069/7486426): Similar to PM-5. Fine grained crystalline matrix with fluidal texture. Medium sized (~4 mm), subangular phenocrysts of plagioclase, alkali feldspar, hornblende, biotite and quartz. Elongated pumice fragments. No shock features; strong alteration, also indicated by the alteration of glass to chlorite.

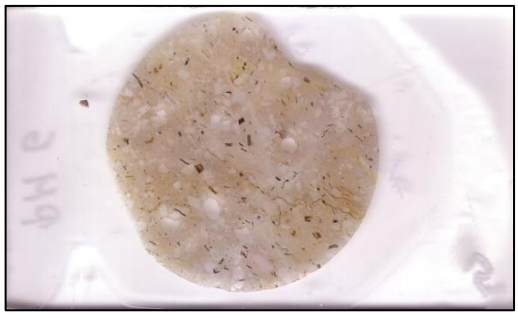

PM-15 (546951/7479155): Fine grained, crystalline, dark reddish matrix with fluidal texture. Medium sized (~3 mm) subangular phenocrysts of plagioclase, alkali feldspar, biotite, and quartz. Elongated pumice fragments with small vesicles. No shock features; moderate to strong alteration with sericitisation of feldspar and chloritisation of biotite.

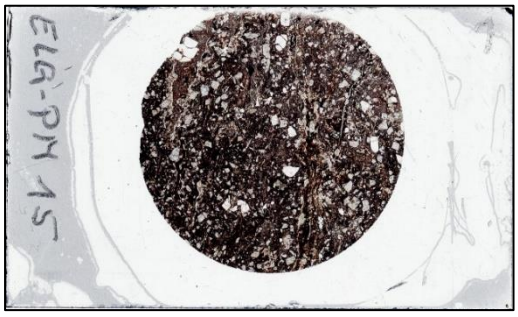

PM-40 (542717/7479084): Fine grained crystalline matrix with fluidal texture. Medium sized (~4 mm), subangular phenocrysts of alkali feldspar, hornblende, biotite, and quartz. Elongated, vesicle-rich pumice fragments and glass shards. Moderate alteration.

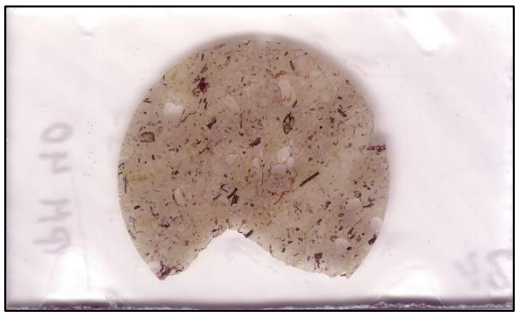

PM-43 (542413/7479377): Similar to PM-40 with comparatively larger glass particles.

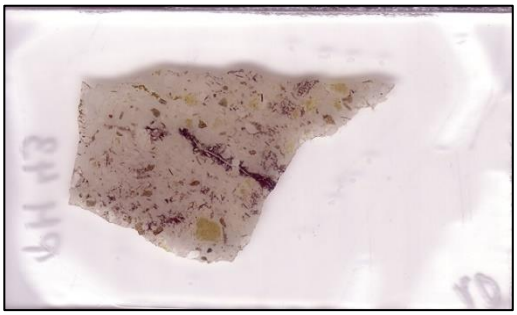

PM-46 (541662/7478993): Fine grained crystalline matrix with fluidal texture. Medium sized (~4 mm), subangular phenocrysts of alkali feldspar, hornblende, plagioclase, biotite, and quartz. Some pyrite grains. Elongated, vesicle-rich pumice fragments with interfingering contacts. Strong alteration with sericitisation of feldspar and chloritisation of biotite and hornblende.

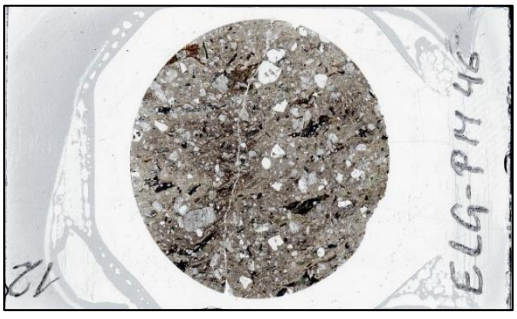

PM-47 (541604/7479066): Similar to PM-46, but with larger pumice fragments (~2 cm in size); secondary calcite (alteration).

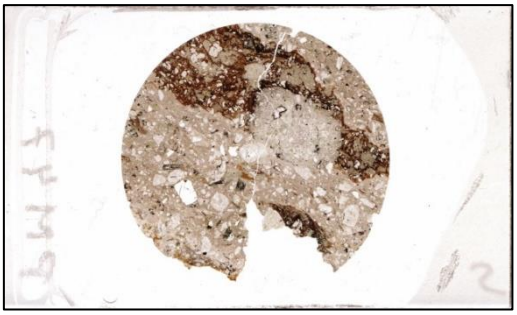

PM-74 (537452/7489857): Fine grained crystalline matrix with fluidal texture. Medium sized (~3 mm), subangular phenocrysts of feldspar, hornblende, biotite, and quartz. Elongated, reddish pumice fragments (~ 2 cm). Moderate to strong alteration (sericite).

PM-75 (537201/7488999): Similar to PM-74, but completely reddish matrix with phenocrysts of quartz (up to 2 mm in size) and euhedral crystals of amphibole. Pumice fragments are vesicle-rich. Moderate alteration.

5. Group: Rhyolitic ignimbrite

UR-2011_5.3 (548655/7479736): Fine grained, crystalline matrix with elongated melt fragments and larger, vesicle-rich, pumice fragments. Phenocrysts (max. 3 mm size) of quartz, primary calcite, feldspar, biotite, and weathered amphibole (hornblende). Strong alteration (feldspar partly replaced by secondary carbonate).

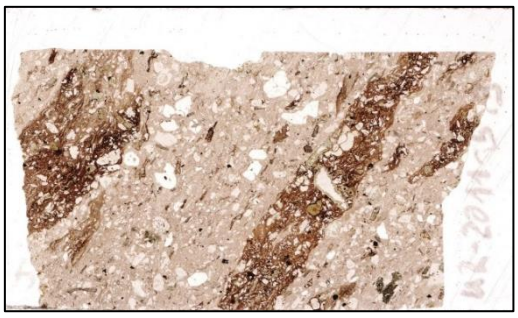

UR-2011_6.1 (550702/7489941): The two parts of the thin section are, first, a clast-rich melt on the left side (below) and a crystal tuff on the right side. Larger minerals in both parts are feldspar and quartz. Additionally occur plates of biotite, hornblende, and a few ore mineral grains. Small veins penetrate tuff and melt. They are filled by ash particles, glass shards and tiny crystals. Alteration is very strong. A few parts of ash are replaced by calcite.

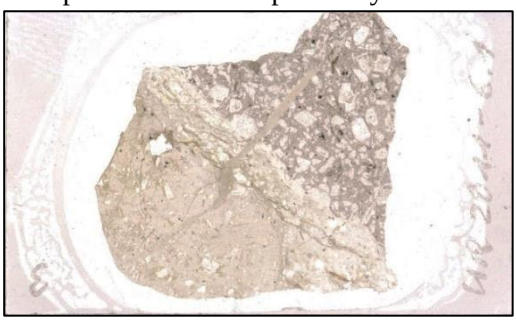

UR-2011_6.2 (550702/7489941): Fine grained matrix with fluidal texture includes crystal fragments of plagioclase and biotite. Tiny pumice particles occur. Moderate to strong alteration with sericitisation of feldspar.

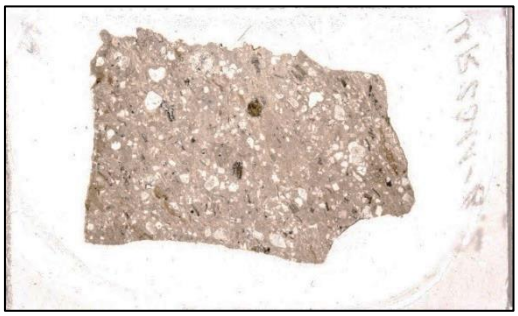

UR-2011_6.3 (550708/7491126): Similar to UR-2011_6.2; matrix with fragments of plagioclase, quartz (< 4 mm in size), biotite, and hornblende. Elongated (20 x 5 mm) pumice particles with frayed edges occur. Moderate to strong alteration with sericitisation of feldspar.

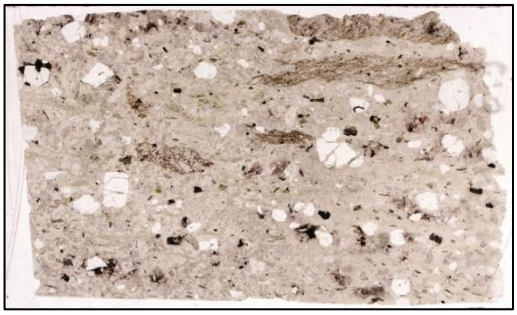

UR-2011_10.1b (551782/7482975): Fine grained matrix with fluidal texture includes parallel oriented glass shards and melt fragments, which are often altered to calcite. Crystals are (altered) plagioclase and quartz. A few ore mineral grains, and some tiny lapilli are embedded.

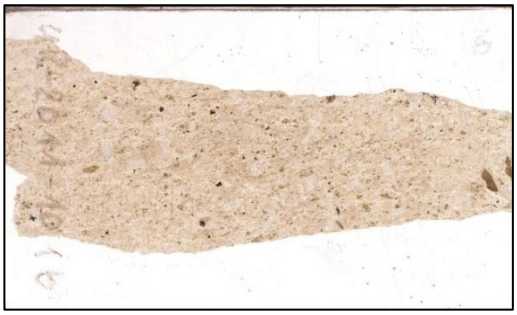

UR-2011_10.2a (551720/7482914): Very fine grained ash matrix with mineral fragments of feldspar, biotite, hornblende and minor quartz. Widespread calcite (due to secondary alteration) occurs. The sample presumably represents an ash layer within the ignimbrite sequence.

UR-2011_10.2b (551720/7482914): Very similar to UR-2011_10.2a. Biotite is coated by tiny ore mineral grains, and feldspar is partly replaced by calcite. Ash layer in ignimbrite.

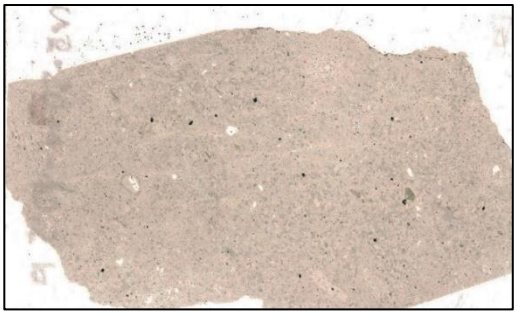

UR-2011_11.1 (550308/7492339): Fine grained matrix with fluidal texture and pumice fragments. Mineral clasts of different sizes are feldspar, quartz, biotite, and hornblende. Strongly weathered, e.g. feldspar partially transformed to calcite.

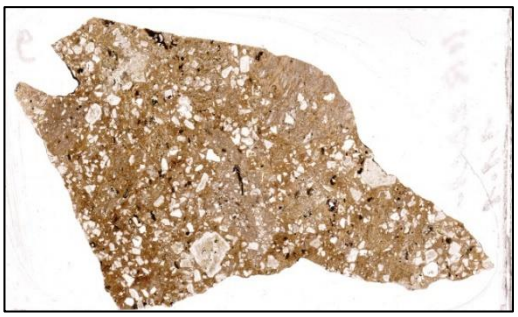

UR-2011_11.3 (552567/7487648): Fine grained matrix with fluidal texture containing phenocrysts (different sizes) of

feldspar, quartz, biotite, and hornblende. Strongly altered: feldspar is partially replaced by calcite.

PM-18 (551531/7482697): Similar to 11.3. Matrix with brownish ash particles and phenocrysts of feldspar, quartz, and biotite. Strongly altered, e.g., feldspar partially transformed to calcite, and chloritisation of biotite. A large fragment of ash (ca. 2 cm in size) is incorporated.

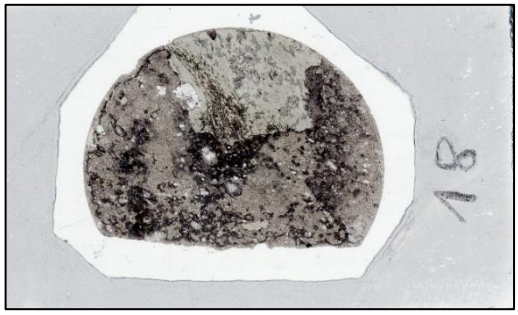

PM-37 (548888/7480231): Fine grained matrix with fluidal texture; phenocrysts of feldspar, biotite, and rare (recrystallized) quartz. A few tiny ore mineral grains occur. Moderately weathered.

6. Andesitic-dacitic tuff

UR-2011_1.1 (551894/7482774): The fine grained matrix is cemented by carbonate. Crystal and mineral fragments of feldspar, quartz, and kaersutite occur at different sizes and are arranged in well sorted layers. Alteration of feldspar is moderate.

UR-2011_4.1a (552769/7486085): Very fine grained matrix, dominated by tiny plagioclase crystals. Few larger feldspar grains, and only one crystal of quartz shows planar fractures (PF), as possible shock indication. Moderate alteration.

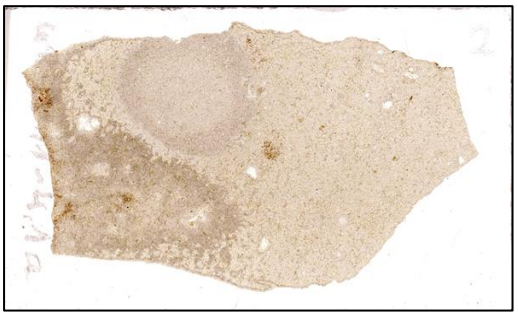

UR-2011_4.1d (552513/7484506): Micro-crystalline matrix with larger fragments of feldspar and olivine. Many brownish glass shards. Chaotic texture with a few veins filled by ash. Vesicles are common and partly filled by quartz. Many ore mineral grains and a few zircon crystals are included. The rock is only slightly altered.

UR-2011_7.1 (550616/7473341): Fine grained matrix, dominated by feldspar with larger amounts (up to 3 mm in size) of subangular crystals of feldspar, biotite, hornblende and olivine. No quartz. Relatively fresh.

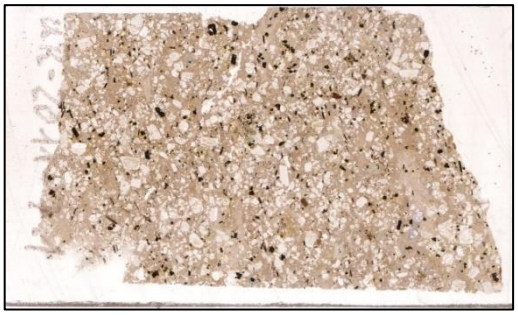

UR-2011_10.1 (551782/7482975): Fine grained matrix with fluidal texture that includes parallel oriented glass shards and melt particles, which are often altered to calcite. Phenocrysts are (weathered) plagioclase; some lapilli occur.

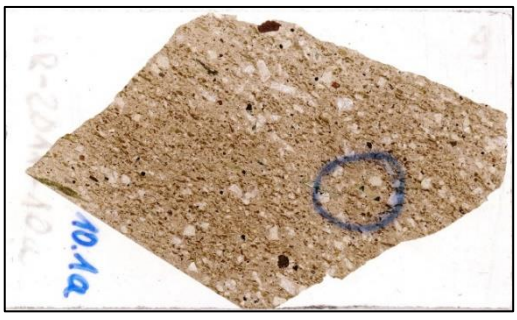

PM-19 (551687/7482886): Microcrystalline matrix with crystal fragments of plagioclase (up to 4 mm in size). Poorly sorted crystal tuff with moderate alteration (chloritisation of feldspar).

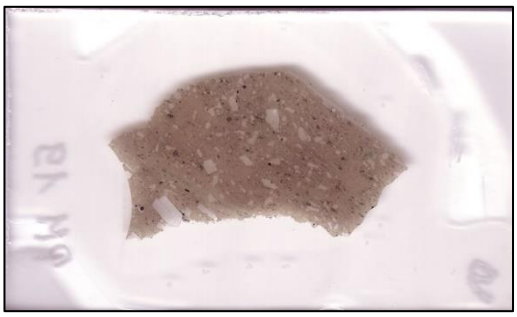

PM-25 (554566/7483594): Microcrystalline matrix with small, rounded vesicles, which are filled by feldspar. Larger crystals are feldspar, rare quartz, a few ore mineral grains, and fine grained secondary calcite. The rock is strongly weathered.

PM-56 (5537333/7491268): Fine grained, brownish, microcrystalline matrix with many small to medium sized (max. 3 mm in size) crystals of feldspar, biotite, hornblende, and kaersutite. The rock is strongly altered.

PM-64 (5537333/7491268): Similar to PM-56. Poorly sorted crystal tuff.

7. Basaltic-andesitic Tuff (phreatomagmatic)

UR-2011_9.1 (550517/7475857): Fine grained crystalline matrix with medium sized (< 2 mm) sub-angular crystals of feldspar, quartz, and many ore mineral grains. Strongly altered with chloritisation of feldspar.

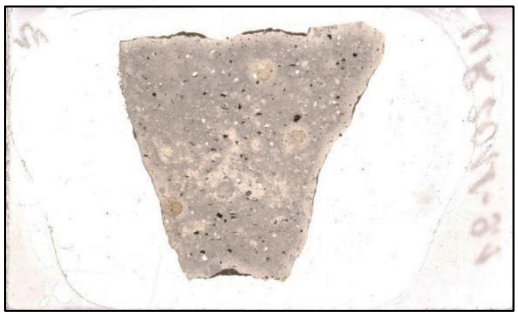

UR-2011_9.2 (550517/7475857): Fine grained, crystalline matrix (porphyritic texture); relatively large (max. 6 mm) subangular fragments and/or crystals of sideromelane, plagioclase, augite, olivine, and clinopyroxene. Pumice fragments are also included. Slightly altered.

UR-2011_9.3 (550517/7475857): Fine grained, clastic matrix includes larger mineral fragments or lithic clasts up to 5 mm in size. The clasts belong to different lithologies, such as (andesitic to rhyolitic) ignimbrites and andesitic or basaltic lavas. Slightly altered.

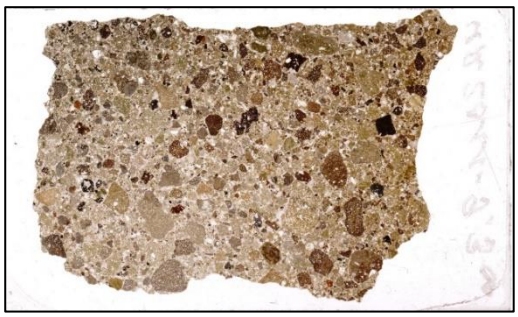

UR-2011_9.4 (550503/7475843): Fine grained (ash) matrix with medium sized crystals (< 2 mm) of feldspar and secondary calcite. Translucent to opaque glass shards and vesicles are included. Slightly altered.

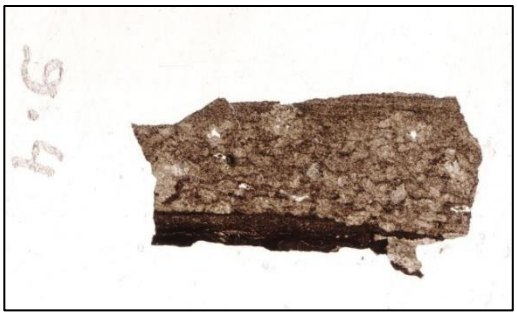

UR-2011_9.5 (550487/7475845): Similar to UR-2011_9.4. Ash matrix with crystals (max. 2 mm in size) of quartz and feldspar, and secondary calcite. Translucent to opaque glass shards and vesicles are included. Slightly altered.

UR-2011_9.7 (550446/7475839): Fine grained, clastic matrix with mineral grains or lithic clasts up to 10 mm in size. The clasts belong to different rocks, such as ignimbrites and andesitic or basaltic lavas.

Pumice fragments, small lapilli and ash agglutinates are also included. Slightly to moderately altered with secondary calcite and chlorite.

UR-2011_9.8 (550446/7475839): Similar to UR-2011_9.7 with a polymict lithic clast population at sizes up to 20 mm. Stronger alteration in comparison with 9.7 with much secondary calcite.

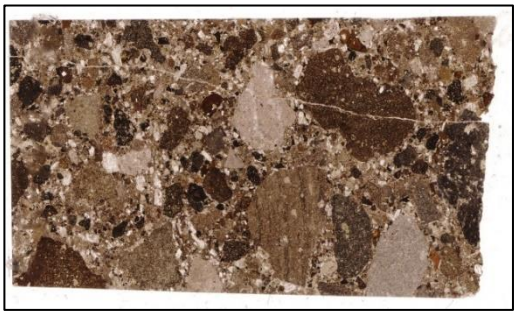

UR-2011_9.9 (551401/7475806): Similar to UR-2001_9.7/9.8, but the average clast size is much smaller (~2 mm in size). Moderate alteration (secondary calcite).

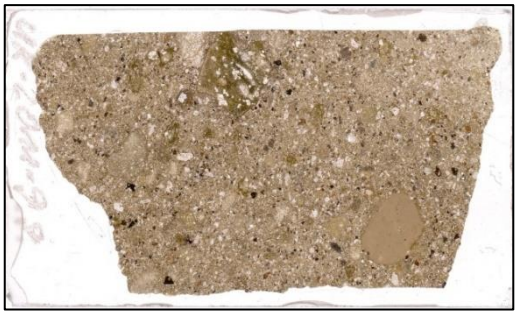

8. Rhyodacitic tuff

UR-2011_3.5 (554161/4818830): Crystal tuff with a fine ash matrix, wherein included are lithic clasts or fragments of different minerals (including feldspar, hornblende, amphibole, and chlorite, pumice and basaltic fragments). The pumice fragments are round and not deformed. In addition, we found iron oxide mineral grains, i.e. hematite with exsolution lamellae. Strongly altered feldspar.

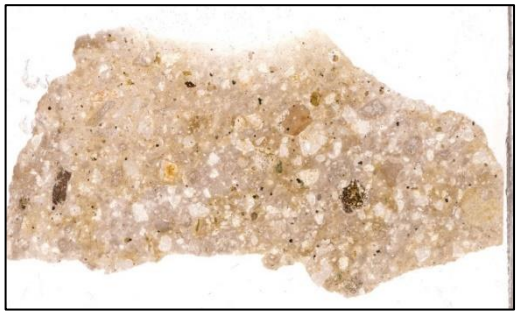

UR-2011_4.1c (552513/7484506): Ash tuff (matrix dominated) with clasts of feldspar, quartz, hornblende, and biotite. Moderately sorted. Strongly altered feldspars.

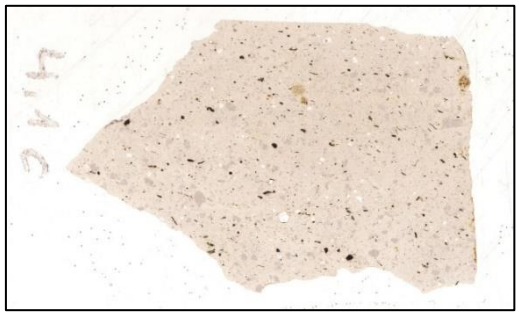

UR-2011_4.5 (55268/7484520): Fine grained, crystalline matrix with spherulitic growth structures. Relatively large (max. 5 mm) phenocrysts of alkali feldspar, together with rare biotite and hornblende. Moderate alteration, feldspar is partially transformed to calcite.

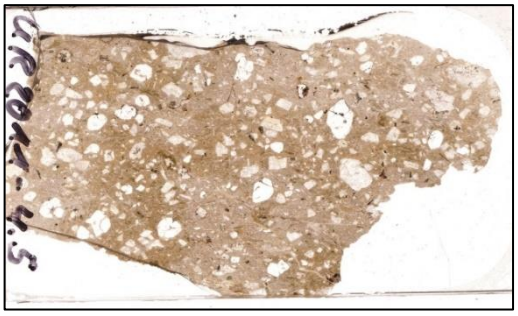

UR-2011_4.6 (552746/7485282): Similar to UR-2011_4.5. Fine grained crystalline, brownish matrix with spherulitic growth structures. Medium sized (< 3 mm) phenocrysts of alkali feldspar and quartz, with remnants of biotite and hornblende. In places, feldspar is altered to calcite.

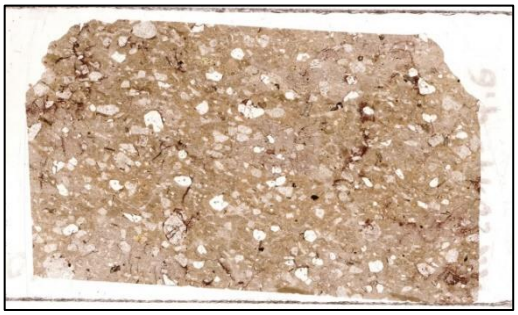

PM-16 (547418/7479405): Fine grained (max. 2 mm) ash matrix with phenocrysts of feldspar, quartz, and biotite. Well sorted. Strongly altered feldspar.

PM-59 (536920/7491280): Fine grained crystalline matrix with fluidal texture that contains parallel oriented melt particles (pumice). Small plagioclase phenocrysts and some somewhat larger phenocrysts (<3 mm) of pyroxene, biotite, quartz, and hornblende. Tiny, widespread ore mineral grains. Moderately altered with secondary calcite.

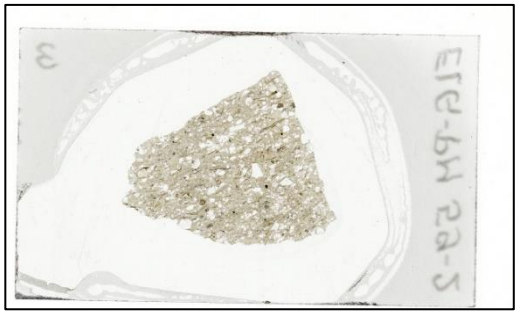

PM-61 (537090/7491339): Fine grained ash matrix (max. 2 mm) with mineral grains of feldspar, biotite, quartz (often recrystallized) and minor kaersutite. Accretionary lapilli with sizes up to 5 mm are incorporated. Well sorted, and strongly altered; feldspar displays sericitisation.

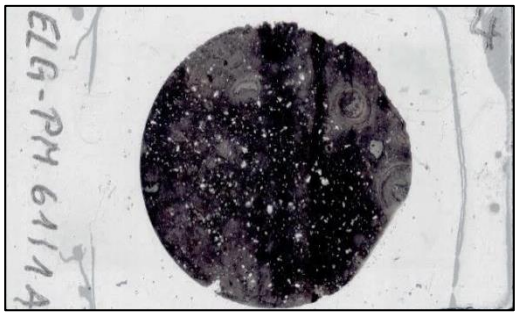

PM-63 (537333/7491268): Fine grained ash matrix (max. 1.5 mm in size) with phenocrysts of feldspar, rare quartz, and a few grains of ore minerals. Well sorted and moderately altered, with some secondary chlorite.

PM-65 (537333/7491268): Very fine grained matrix (ash) with larger fragments of pumice and phenocrysts of feldspar, biotite, hornblende, and quartz. Poorly sorted and moderately altered.

PM-67 (537333/7491268):
Microcrystalline matrix (no fluidal texture) with brownish glass particles and small (max. 1.5 mm) phenocrysts of quartz. Slightly weathered.

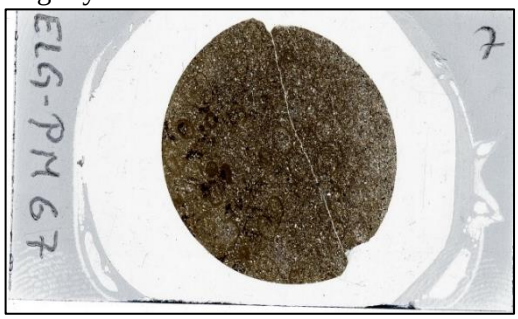

PM-68 (537333/7491268): Very-fine grained, brownish and well sorted ash matrix with melt particles and fragments of feldspar and quartz. Also included are a few ore mineral grains, zircon, and small vesicles. Relatively well sorted rock with an average grain size of ~1.5 mm.

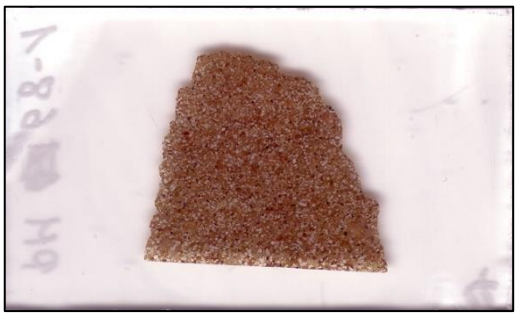

PM-70 (537090/7491339): Dark green, finest grained matrix with medium sized (< 4 mm) fragments of lithic clasts (basalt, ignimbrite) and mineral clasts (quartz, feldspar). Poorly sorted and slightly altered.

PM-71 (537090/7491339): Fine ash matrix with small clasts of feldspar, quartz, biotite, and hornblende. Well sorted with clast sizes up to 2 mm. Moderately altered (biotite plates are coated by iron oxides).

9. Impact melt breccia

UR-2011_9.10 (551863/74833086): Different vesicle-rich melt phases including translucent glass, brownish schlieren, and small black glass particles. Quartz and feldspar grains only occur in brownish parts. Quartz and feldspar display PDF.

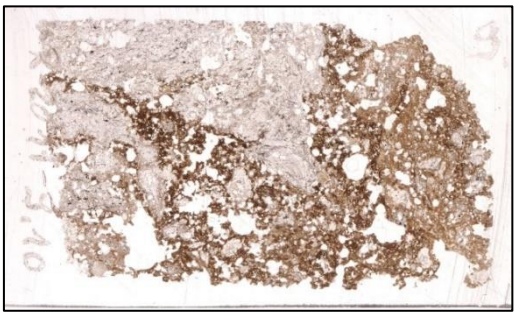

UR-2011_9.11(b/c) (551863/74833086): Similar to UR-2011_9.10. Shocked quartz and feldspar grains contain PDF (in bright glass). Amphiboles occur within a larger (~10 mm in size) basalt clast (9.11b).

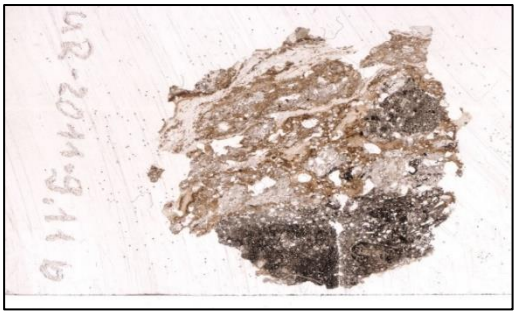

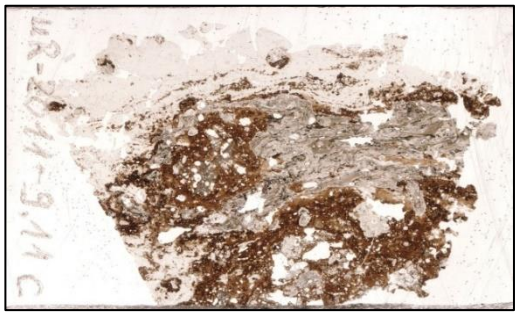

UR-2011_10a (551829/7483040): Different melt phases including translucent glass, brownish schlieren, and small black glass particles. Vesicle rich. Quartz (with PDF) and feldspar occur in lithic clasts.

Table S2: Compilation of whole rock compositions of surface samples from the El'gygytgyn area.

Sample	UR-2011_3.1	UR-2011_3.2	UR-2011_3.7	UR-2011_5.2	UR-2011_8.1	UR-2011_8.2	PM 34	438-1	438-3	1308	1309	UR-2011_4.2	UR-2011_4.4	UR-2011_7.2	UR-2011_9.6	UR-2011_11.2	PM 72	1323	1346	UR-2011_9.12a
Type*	basalt	basalt	basalt	basalt	basalt	basalt	basalt	basalt	basalt	basalt	basalt	basalt. andes.	basalt. andes.	ande-site	ande-site	ande-site	ande-site	ande-site	ande-site	rhyo-dac ign.
Source*	Exped	Exped	Exped	Exped	Exped	Exped	OJ	Belyi	Belyi	Pittar.	Pittar.	Exped	Exped	Exped	Exped	Exped	OJ	Pittar.	Pittar.	Exped
wt.%																				
SiO_2	54.9	51.7	56.4	50.7	49.9	50.8	51.3	54.3	54.4	56.9	54.7	45.0	49.2	57.9	58.1	62.3	57.2	64.2	64.5	68.3
TiO_2	0.74	1.02	0.93	0.94	1.31	1.42	0.94	0.70	0.73	0.87	1.04	1.03	0.99	0.84	0.84	0.71	0.70	0.53	0.54	0.31
Al_2O_3	17.2	17.0	18.3	18.3	17.9	17.7	17.7	16.4	16.3	17.9	18.9	17.0	16.8	18.3	18.0	17.7	16.6	16.3	16.2	14.7
Fe_2O_3†	8.20	9.31	7.45	9.29	9.60	8.97	9.61	8.06	7.81	7.84	8.22	11.1	10.1	7.36	7.23	5.63	6.17	4.64	4.28	2.82
MnO	0.14	0.16	0.13	0.16	0.17	0.12	0.17	0.13	0.15	0.14	0.16	0.26	0.20	0.15	0.16	0.13	0.11	0.06	0.08	0.14
MgO	4.69	5.97	2.94	4.97	4.62	4.11	5.41	5.86	4.98	2.78	3.14	4.45	4.35	2.32	2.33	1.41	1.36	1.30	1.31	0.74
CaO	8.43	9.18	6.52	9.90	8.62	6.91	9.31	7.52	8.26	6.32	7.30	8.79	8.33	5.65	5.64	3.72	5.44	3.55	3.57	1.89
Na_2O	2.54	2.32	3.67	2.44	2.96	3.67	2.44	2.69	2.50	3.25	3.16	2.04	1.77	3.42	3.47	3.83	2.16	3.55	3.60	4.01
K_2O	1.68	1.44	1.51	1.32	2.36	2.18	1.29	1.38	1.68	2.01	1.76	1.12	0.94	2.33	2.33	3.21	2.86	3.34	3.57	4.12
P_2O_5	0.17	0.25	0.34	0.23	0.68	0.88	0.23	0.12	0.13	0.43	0.42	0.24	0.24	0.42	0.42	0.24	0.17	0.15	0.15	0.07
LOI	1.3	1.8	1.5	0.8	2.0	2.9	1.0	2.9	3.1	1.2	1.1	8.6	7.1	0.9	0.9	0.9	6.7	1.5	1.4	2.7
Total	99.99	100.15	99.69	99.05	100.12	99.66	99.40	100.06	100.04	99.64	99.90	99.62	100.02	99.59	99.42	99.78	99.47	99.12	99.20	99.80
ppm																				
Sc	27	32	15	28	25	22	n.d.	n.d.§	n.d.	14.9	19	34	35	11	11	14	14	11.1	10.5	6
V	183	231	118	193	194	161	n.d.	n.d.	n.d.	103	156	181	163	81	77	51	73	50	49.5	25
Cr	31	117	<5	93	148	87	n.d.	33.7	28.5	11.1	9.2	26	21	<5	<5	<5	<5	15.1	15.9	<5
Co	18	21	11	21	22	20	n.d.	72.9	58.5	12.1	14.7	21	21	7	8	<5	<5	7.1	6.5	<5
Ni	16	24	12	20	74	53	n.d.	13.3	10.1	24.3	26.4	17	19	10	11	7	8	<33	<31	8
Cu	24	29	18	27	42	47	n.d.	20.2	19.2	5.6	9.2	35	30	12	16	<15	<15	5.3	4.3	<15
Zn	72	87	83	82	93	115	n.d.	52.1	49.0	113	101	97	84	92	83	70	64	72.4	87.9	49
Ga	19	20	20	18	20	23	n.d.	19.0	15.5	21.2	50.9	18	16	20	20	19	20	20.7	15.7	16
Rb	36	27	65	28	49	36	n.d.	32	35	54	41	27	16	59	60	103	96	131	116	110
Sr	343	486	548	461	743	951	n.d.	379	347	423	462	391	367	498	518	363	82	282	284	173
Y	19	26	20	19	24	25	n.d.	15	16	25.2	32.6	20	20	22	22	28	18	30.6	25.2	28
Zr	83	92	129	78	196	224	n.d.	71	77	181	248	79	79	124	127	156	137	332	295	214
Nb	<10	<10	<10	<10	11	19	n.d.	4	4	5.9	5.1	<10	<10	<10	<10	<10	<10	7	7.3	10
Ba	498	389	586	308	763	826	n.d.	n.d.	n.d.	394	348	292	371	593	600	592	436	572	503	762
La	16	14	24	15	32	58	n.d.	n.d.	n.d.	17.1	18.4	12	14	23	22	26	22	31.6	34.7	36
Ce	32	42	60	31	93	118	n.d.	n.d.	n.d.	36.9	37.1	28	32	51	55	67	31	58.6	61.2	82
Pb	<15	<15	15	<15	<15	37	n.d.	n.d.	n.d.	12.4	11.5	<15	<15	<15	<15	18	17	18.4	17.9	18

*Abbreviations: Exped = El'gygytgyn crater expedition 2011, analysed at MfN Berlin; Pittar. = samples by Gurov and analysed by Pittarello et al. (2013); OJ = samples from the 2003 crater expedition by Olaf Juschus, analysed at MfN Berlin; Belyi = recalculated analyses from Belyi and Belaya (1998); basalt. andes. = basaltic andesite; rhyo-dac ign. = rhyodacitic ignimbrite; rhyo. ign. = rhyolitic ignimbrite; and-dac. tuff = andesitic-dacitic tuff; bas-and. tuff = basaltic-andesitic tuff; rhyo-dac. tuff = rhyodacitic tuff; †total Fe as Fe_2O_3. §n.d. = not determined.

Table S2 (continued).

Sample	UR-2011_10.1	PM 03	PM 15	PM 46	PM 47	PM 75	1319	UR-2011_5.3	UR-2011_6.1	UR-2011_6.2	UR-2011_6.3	UR-2011_11.1	UR-2011_11.3	PM 18	1	3	4-1	6	6-1	405
Type*	rhyo-dac ign.	rhyo-dac ign.	rhyo-dac ign.	rhyo-dac ign.	rhyo-dac ign.	rhyo-dac ign.	rhyo-dac ign.	rhyo. ign.	rhyo. ign.	rhyo. ign.	rhyo. ign.	rhyo. ign.	rhyo. ign.	rhyo. ign.	rhyo. ign.	rhyo. ign.	rhyo. ign.	rhyo. ign.	rhyo. ign.	rhyo. ign.
Source*	Exped.	OJ	OJ	OJ	OJ	OJ	Pittar.	Exped	Exped	Exped	Exped	Exped	Exped	OJ	Belyi	Belyi	Belyi	Belyi	Belyi	Belyi
wt.%																				
SiO_2	63.1	72.4	67.5	69.6	67.6	69.4	69.9	68.8	69.4	68.9	70.7	68.2	70.4	70.8	69.6	70.2	69.7	69.5	68.4	69.3
TiO_2	0.48	0.19	0.40	0.35	0.40	0.36	0.26	0.39	0.37	0.35	0.28	0.35	0.24	0.31	0.35	0.35	0.35	0.35	0.31	0.37
Al_2O_3	19.1	13.7	16.4	15.0	16.3	14.7	13.8	15.3	16.2	16.0	14.9	15.8	16.3	15.2	15.1	15.0	15.4	15.0	14.9	15.1
$Fe_2O_3^T$	3.88	1.76	3.03	2.64	2.96	3.11	2.03	2.94	2.23	2.64	2.39	2.62	1.98	1.88	2.54	2.63	2.81	2.88	2.47	2.94
MnO	0.08	0.06	0.05	0.06	0.07	0.06	0.05	0.06	0.04	0.06	0.05	0.05	0.10	0.07	0.05	0.05	0.06	0.05	0.05	0.05
MgO	1.29	0.36	0.88	0.58	0.66	0.87	0.48	0.75	0.42	0.61	0.46	0.72	0.42	0.44	0.68	0.48	0.43	0.52	0.54	0.50
CaO	3.33	1.19	0.92	1.42	1.87	1.85	1.97	1.69	1.53	1.80	0.81	2.23	0.97	1.19	1.58	1.86	2.33	2.20	2.51	2.07
Na_2O	3.53	3.02	3.91	3.86	3.79	3.41	3.11	3.42	3.38	3.71	3.70	3.40	3.16	3.38	2.49	3.50	3.53	3.69	4.34	3.67
K_2O	3.52	5.09	4.26	4.18	3.87	4.21	4.05	3.89	4.22	4.09	5.06	3.96	4.38	4.56	4.41	4.24	4.11	4.24	2.93	4.23
P_2O_5	0.12	0.03	0.09	0.07	0.09	0.08	0.06	0.09	0.08	0.08	0.06	0.08	0.06	0.05	0.09	0.08	0.08	0.07	0.06	0.09
LOI	1.7	1.7	2.0	1.4	2.2	1.3	3.6	2.7	1.3	1.2	1.4	2.1	1.6	2.0	3.1	1.6	1.2	1.5	3.5	1.7
Total	100.13	99.50	99.44	99.18	99.81	99.35	99.31	100.03	99.17	99.44	99.81	99.51	99.61	99.88	99.99	99.99	100.00	100.00	100.01	100.02
ppm																				
Sc	9	n.d.	7	n.d.	6	n.d.	4	6	6	5	<5	5	<5	7	n.d.	n.d.	n.d.	n.d.	n.d.	n.d.
V	51	n.d.	27	n.d.	28	n.d.	7.6	27	22	24	18	22	13	9	n.d.	n.d.	n.d.	n.d.	n.d.	n.d.
Cr	8	n.d.	<5	n.d.	<5	n.d.	11.5	<5	<5	<5	<5	<5	<5	<5	2.2	2.2	2.2	2.2	2.2	2.2
Co	<5	n.d.	<5	n.d.	<5	n.d.	2.3	<5	<5	<5	<5	<5	<5	<5	4.0	4.6	7.1	4.4	7.8	6.2
Ni	10	n.d.	5	n.d.	<5	n.d.	<25	<5	6	<5	6	<5	5	5	1.3	11.1	2.2	0.9	1.7	0.6
Cu	0	n.d.	<15	n.d.	<15	n.d.	4	<15	<15	<15	8	9	<15	<15	4.4	3.6	6.0	3.0	7.0	5.1
Zn	53	n.d.	46	n.d.	42	n.d.	47	46	41	43	34	40	49	76	15.7	13.9	19.8	14.1	30.8	18.1
Ga	18	n.d.	16	n.d.	15	n.d.	15.6	15	15	15	15	16	15	16	11.1	12.8	16.0	7.1	20.7	14.1
Rb	114	n.d.	117	n.d.	120	n.d.	152	134	120	133	137	132	147	105	152	147	136	138	148	143
Sr	318	n.d.	263	n.d.	266	n.d.	131	236	245	245	167	227	136	76	182	294	372	270	319	276
Y	23	n.d.	19	n.d.	19	n.d.	20	22	20	19	18	20	23	32	21	17	17	18	16	17
Zr	169	n.d.	164	n.d.	152	n.d.	195	175	149	166	142	172	136	236	69	175	174	170	164	159
Nb	<10	n.d.	<10	n.d.	<10	n.d.	7.5	10	<10	<10	<10	<10	<10	11	4	3	8	9	7	6
Ba	701	n.d.	1108	n.d.	762	n.d.	470	833	1197	810	729	838	696	800	n.d.	n.d.	n.d.	n.d.	n.d.	n.d.
La	28	n.d.	31	n.d.	30	n.d.	33	35	26	31	22	31	41	35	n.d.	n.d.	n.d.	n.d.	n.d.	n.d.
Ce	65	n.d.	72	n.d.	63	n.d.	59.8	66	65	68	67	66	78	82	n.d.	n.d.	n.d.	n.d.	n.d.	n.d.
Pb	18	n.d.	20	n.d.	17	n.d.	22.8	19	20	21	17	21	20	20	n.d.	n.d.	n.d.	n.d.	n.d.	n.d.

Table S2 (continued).

Sample	408-7	410-1	403-2	635	661	943A	1017	1339	1384	UR-2011_1.1	UR-2011_4.1	UR-2011_7.1	406-1	406-2	406-4	406-5	1345B	UR-2011_9.1	UR-2011_9.2	UR-2011_9.3
Type*	rhyo. ign.	rhyo. ign.	rhyo. ign.	rhyo. ign.	rhyo. ign.	rhyo. ign.	rhyo. ign.	rhyo. ign.	rhyo. ign.	and-dac. tuff	and-dac. tuff	and-dac. tuff	and-dac. tuff	and-dac. tuff	and-dac. tuff	and-dac. tuff	and-dac. tuff	bas-and. tuff	bas-and. tuff	bas-and. tuff
Source*	Belyi	Belyi	Belyi	Pittar.	Pittar.	Pittar.	Pittar.	Pittar.	Pittar.	Exped	Exped	Exped	Belyi	Belyi	Belyi	Belyi	Pittar.	Exped	Exped	Exped
wt.%																				
SiO_2	74.0	71.1	72.0	74.2	73.7	79.1	68.4	70.7	70.0	50.8	62.5	63.0	59.5	59.8	61.8	62.1	57.1	54.3	50.8	52.1
TiO_2	0.16	0.24	0.24	0.17	0.18	0.12	0.35	0.29	0.35	0.58	0.65	0.62	0.69	0.70	0.68	0.69	0.78	0.84	0.87	0.92
Al_2O_3	13.6	14.5	13.7	14.0	12.6	9.9	14.2	14.5	14.7	16.6	17.0	17.0	16.7	16.7	16.2	16.3	17.4	16.3	16.3	15.6
$Fe_2O_3^{\dagger}$	1.68	2.45	2.16	1.36	1.58	0.92	2.20	2.28	2.72	4.72	5.43	4.53	5.33	5.67	5.67	5.44	7.80	6.38	8.83	7.95
MnO	0.06	0.08	0.05	0.03	0.04	0.02	0.04	0.06	0.06	0.25	0.13	0.08	0.10	0.10	0.08	0.10	0.17	0.11	0.15	0.14
MgO	0.14	0.65	0.44	0.28	0.34	0.20	0.54	0.65	0.57	2.14	1.33	1.43	2.26	1.90	1.84	1.74	2.20	2.45	2.66	4.17
CaO	0.96	1.47	2.14	0.21	0.37	0.28	2.29	1.46	2.03	12.2	3.29	3.57	5.83	5.75	4.84	4.81	5.57	6.19	7.17	6.29
Na_2O	3.61	5.38	2.61	6.21	1.12	0.40	2.71	3.61	3.42	3.25	3.91	4.10	3.34	3.63	3.57	3.72	2.40	2.40	3.26	2.56
K_2O	4.60	1.78	4.39	2.40	8.49	7.10	4.10	4.65	4.27	1.14	3.13	3.71	1.13	1.60	3.21	3.14	3.73	2.75	0.56	1.73
P_2O_5	0.03	0.06	0.05	0.04	0.04	0.03	0.06	0.07	0.09	0.20	0.22	0.21	0.20	0.18	0.18	0.18	0.16	0.30	0.27	0.29
LOI	1.2	2.3	2.3	0.7	1.0	1.0	3.9	0.9	0.9	7.6	1.8	1.0	4.9	4.0	1.9	1.9	2.2	7.5	9.1	8.1
Total	100.04	100.01	100.08	99.60	99.46	99.07	98.79	99.17	99.09	99.48	99.39	99.25	99.98	100.03	99.97	100.12	99.51	99.52	99.97	99.85
ppm																				
Sc	n.d.	n.d.	n.d.	2	2.6	2	6.2	4.6	5.8	13	11	9	n.d.	n.d.	n.d.	n.d.	27.2	16	23	27
V	n.d.	n.d.	n.d.	<1	0.7	0	8.3	19.3	19.6	90	62	64	n.d.	n.d.	n.d.	n.d.	124	135	183	173
Cr	2.2	2.2	2.2	9.2	11.3	11	13	12.7	10.5	27	<5	<5	9.6	11.6	8.5	7.2	64.6	7	<5	44
Co	4.5	3.7	4.4	1.4	1.7	1	2.1	2.7	3.2	5	6	<5	13.7	30.5	23.8	19.3	17.5	11	12	17
Ni	1.1	2.2	0.9	6.7	<20	5	12.8	<25	9.7	13	8	9	2.6	5.0	3.9	3.3	8.4	18	20	20
Cu	4.4	3.9	3.0	3	1.6	2	2.8	1.4	2.8	19	15	17	10.7	13.4	16.7	10.6	11.5	30	26	27
Zn	18.5	16.6	14.1	39	45	32	79	66.5	58.6	55	75	60	40.8	128.6	283.0	63.6	119	61	89	74
Ga	13.6	10.9	7.1	<36	<9	14	7.3	16.7	7.9	18	19	19	21.5	18.1	15.2	13.2	27.9	15	20	17
Rb	159	128	143	76	257	186	91	170	144	19	81	93	29	50	93	90	145	55	18	41
Sr	195	42	876	41	27	38	154	158	223	847	429	525	860	686	463	479	220	684	224	564
Y	19	19	20	19.4	18.2	20	26	26.5	26.2	14	25	20	23	23	23	22	38.7	22	19	23
Zr	130	100	164	152	158	236	227	283	290	70	170	178	179	172	181	187	206	123	100	103
Nb	7	9	2	7.5	7.6	6	8.4	7.7	7.5	<10	<10	<10	2	6	8	7	4	<10	<10	<10
Ba	n.d.	n.d.	n.d.	357	445	0	535	570	490	642	841	835	n.d.	n.d.	n.d.	n.d.	217	640	131	480
La	n.d.	n.d.	n.d.	35.6	30.1	259	28.1	30.5	31.5	14	26	24	n.d.	n.d.	n.d.	n.d.	26.9	16	27	18
Ce	n.d.	n.d.	n.d.	56.9	53	35	54.8	57.5	58.9	39	65	58	n.d.	n.d.	n.d.	n.d.	52.5	42	38	39
Pb	n.d.	n.d.	n.d.	28.9	24	62	15.6	22.3	20.2	<15	16	15	n.d.	n.d.	n.d.	n.d.	9.8	<15	<15	<15

Table S2 (continued).

Sample	UR-2011_9.4	UR-2011_9.5	UR-2011_9.7	UR-2011_9.8	UR-2011_9.9	1000P-10	UR-2011_3.5	UR-2011_4.1c	UR-2011_4.5	UR-2011_4.6	UR-2011_10.2	PM 16	PM 37	PM 59	PM 61	PM 67	PM 70	PM 71	1013	1022
Type*	bas-and. tuff	bas-and. tuff	bas-and. tuff	bas-and. tuff	bas-and. tuff	bas-and. tuff	rhyo-dac. tuff	rhyo-dac. tuff	rhyo-dac. tuff	rhyo-dac. tuff	rhyo-dac. tuff	rhyo-dac. tuff	rhyo-dac. tuff	rhyo-dac. tuff	rhyo-dac. tuff	rhyo-dac. tuff	rhyo-dac. tuff	rhyo-dac. tuff	rhyo-dac. tuff	rhyo-dac. tuff
Source*	Exped	Exped	Exped	Exped	Exped	Pittar.	Exped	Exped	Exped	Exped	Exped	OJ	OJ	OJ	OJ	OJ	OJ	OJ	Pittar.	Pittar.
wt.%																				
SiO_2	52.4	55.2	51.9	54.3	55.3	53.3	71.1	70.6	72.2	72.4	70.6	75.1	75.8	67.4	69.3	73.2	65.8	70.6	67.9	65.7
TiO_2	0.93	0.86	0.90	0.87	0.82	0.79	0.36	0.35	0.21	0.19	0.34	0.22	0.18	0.29	0.24	0.53	0.85	0.37	0.46	0.84
Al_2O_3	15.5	15.3	16.3	14.6	15.2	16.0	15.2	15.1	15.0	14.4	14.5	12.6	12.0	14.4	13.3	11.1	13.8	12.8	15.4	15.7
$Fe_2O_3^T$	7.35	7.05	6.53	6.48	7.24	7.86	2.33	2.63	1.80	1.83	2.16	2.40	0.91	2.32	2.11	2.47	5.09	2.56	3.42	5.33
MnO	0.10	0.14	0.16	0.10	0.15	0.14	0.06	0.05	0.05	0.05	0.07	0.04	0.02	0.07	0.03	0.15	0.08	0.03	0.11	0.12
MgO	2.15	3.29	2.05	2.87	4.07	4.16	0.47	0.67	0.26	0.24	0.52	0.31	0.18	0.87	0.33	0.55	1.49	0.90	0.66	0.73
CaO	6.83	6.65	8.22	6.17	4.37	6.02	0.37	0.50	1.02	0.93	1.18	0.40	0.14	3.76	0.46	0.96	1.63	0.96	0.74	4.70
Na_2O	1.08	2.57	3.74	1.54	5.97	3.07	3.11	6.06	3.55	3.25	3.80	2.33	0.90	1.56	0.42	1.16	1.92	1.99	3.37	3.21
K_2O	2.82	1.96	0.55	2.62	0.63	1.94	4.61	2.38	4.64	4.72	4.07	4.12	7.98	3.00	10.9	6.19	5.22	5.74	4.16	1.62
P_2O_5	0.35	0.27	0.26	0.31	0.26	0.21	0.06	0.10	0.04	0.03	0.06	0.02	0.02	0.06	0.04	0.19	0.23	0.09	0.13	0.22
LOI	10.4	6.9	9.0	9.3	5.1	6.1	1.6	1.0	1.3	1.1	2.3	1.9	1.3	5.5	1.8	2.9	3.4	3.1	2.3	1.4
Total	99.91	100.19	99.61	99.16	99.11	99.63	99.27	99.44	100.07	99.14	99.60	99.44	99.43	99.23	98.93	99.40	99.51	99.14	98.65	99.59
ppm																				
Sc	15	21	26	16	27	26.9	6	<5	<5	<5	<5	6	n.d.	n.d.	n.d.	n.d.	n.d.	15	8	14.9
V	116	147	178	106	152	173	14	31	10	9	14	13	n.d.	n.d.	n.d.	n.d.	n.d.	122	38.1	115
Cr	<5	<5	29	12	117	82.9	<5	<5	<5	<5	<5	<5	n.d.	n.d.	n.d.	n.d.	n.d.	<5	15.2	26.1
Co	11	14	24	12	14	20.7	<5	<5	<5	<5	<5	<5	n.d.	n.d.	n.d.	n.d.	n.d.	7	2.1	8.5
Ni	20	20	19	19	27	32.3	<5	6	<5	<5	<5	<5	n.d.	n.d.	n.d.	n.d.	n.d.	11	14.8	<36
Cu	24	25	26	24	31	14.6	<15	<15	<15	<15	<15	<15	n.d.	n.d.	n.d.	n.d.	n.d.	25	13.3	2.4
Zn	77	75	70	81	73	106	69	44	39	43	51	47	n.d.	n.d.	n.d.	n.d.	n.d.	57	102	100
Ga	19	16	17	17	15	23	17	<15	15	<15	16	<15	n.d.	n.d.	n.d.	n.d.	n.d.	18	<10	7.2
Rb	106	50	14	83	10	57	117	53	159	164	120	128	n.d.	n.d.	n.d.	n.d.	n.d.	126	122	50
Sr	725	459	324	900	171	356	128	201	164	127	101	118	n.d.	n.d.	n.d.	n.d.	n.d.	224	178	381
Y	26	20	20	23	24	27.9	17	12	21	21	26	24	n.d.	n.d.	n.d.	n.d.	n.d.	18	26.1	19.1
Zr	146	106	99	122	123	232	256	151	136	130	228	209	n.d.	n.d.	n.d.	n.d.	n.d.	89	279	221
Nb	<10	<10	<10	<10	<10	4	11	<10	<10	10	<10	11	n.d.	n.d.	n.d.	n.d.	n.d.	<10	7.5	4.6
Ba	773	610	213	617	259	338	1084	589	671	602	851	877	n.d.	n.d.	n.d.	n.d.	n.d.	316	749	377
La	27	16	15	16	23	14.4	<10	<10	27	33	32	34	n.d.	n.d.	n.d.	n.d.	n.d.	18	13.6	15.7
Ce	59	50	35	52	50	30	42	28	67	67	74	77	n.d.	n.d.	n.d.	n.d.	n.d.	23	28.2	32.3
Pb	<15	<15	19	<15	<15	10.2	32	16	27	20	17	15	n.d.	n.d.	n.d.	n.d.	n.d.	<15	21.6	12.7

Table S2 (continued).

Sample	1323A	1338A	UR-2011_9.10	UR-2011_9.11
Type*	rhyo-dac. tuff	rhyo-dac. tuff	impact melt breccia	impact melt breccia
Source*	Pittar.	Pittar.	Exped	Exped
wt.%				
SiO_2	66.8	71.8	68.7	68.3
TiO_2	0.36	0.26	0.39	0.42
Al_2O_3	15.7	13.6	15.2	15.3
$Fe_2O_3^T$	2.99	2.12	2.91	3.26
MnO	0.09	0.06	0.06	0.07
MgO	0.84	0.61	0.72	1.05
CaO	2.65	1.90	2.51	2.86
Na_2O	3.95	1.25	3.44	3.29
K_2O	2.92	4.35	3.95	3.90
P_2O_5	0.09	0.07	0.09	0.11
LOI	2.9	3.4	1.3	1.0
Total	99.29	99.42	99.27	99.56
ppm				
Sc	6.6	4.4	7	6
V	24.1	31	27	37
Cr	12.7	11.8	<5	<5
Co	4.1	2.6	<5	<5
Ni	<26	<27	9	8
Cu	2.8	2.1	<15	<15
Zn	54.9	49	48	51
Ga	12.3	9.6	16	16
Rb	97	190	135	132
Sr	235	51	268	289
Y	27.6	23	22	22
Zr	214	199	170	165
Nb	7.7	7.5	<10	<10
Ba	523	431	751	705
La	33.2	35.6	37	33
Ce	63.1	61.1	73	72
Pb	18.2	21.1	21	21

CHAPTER 6

GEOCHEMICAL STUDIES OF IMPACT BRECCIAS AND COUNTRY ROCKS FROM THE EL'GYGYTGYN IMPACT STRUCTURE, RUSSIA.

This Chapter has been published as the following peer-reviewed article:

Raschke U., Zaag P. T., Schmitt R. T., McDonald I., Reimold W. U., Mader D., and Koeberl C. 2015. Geochemical Studies of impact breccias and country rocks from the El'gygytgyn impact structure, Russia. *Meteoritics and Planetary Science* 50:1071-1088, http://dx.doi.org/10.1111/maps.12455.

6.1 ABSTRACT

The complex impact structure El'gygytgyn in northeastern Russia (age 3.6 Ma, diameter 18 km) was formed in ~88 Ma old volcanic target rocks of the Ochotsk-Chukotsky Volcanic Belt (OCVB). In 2009, El'gygytgyn was the target of a drilling project of the International Continental Scientific Drilling Program (ICDP), and in summer 2011 it was investigated further by a Russian-German expedition. Drill core material and surface samples, including volcanic target rocks and impactites, have been investigated by various geochemical techniques in order to improve the record of trace element characteristics for these lithologies and to attempt to detect and constrain a possible meteoritic component. The bedrock units of the ICDP drill core reflect the felsic volcanics that are predominant in the crater vicinity. The overlying suevites comprise a mixture of all currently known target lithologies, dominated by felsic rocks but lacking a discernable meteoritic component based on platinum group element (PGE) abundances. The reworked suevite, directly overlain by lake sediments, is not only comparatively enriched in shocked minerals and impact glass spherules, but also contains the highest concentrations of Os, Ir, Ru, and Rh compared to other El'gygytgyn impactites. This is - to a lesser extent - the result of admixture of a mafic component, but more likely the signature of a chondritic meteoritic component. However, the highly siderophile element contribution from target material akin to the mafic blocks of the ICDP drill core to the impactites remains poorly constrained.

6.2 INTRODUCTION AND GEOLOGICAL BACKGROUND

The El'gygytgyn impact structure is located on the Chukotka Peninsula of far northeast Russia; it is centered at 67°30´N and 172°34´E (Fig. 1). The 18 km diameter, near-circular depression is largely filled by the 12 km wide Lake El'gygytgyn. The impact age was determined at 3.58 ± 0.04 Ma (Layer 2000). The volcanic target rocks belong to the Late

Cretaceous Ochotsk-Chukotsky Volcanic Belt (OCVB) that is of Albian to Campanian/Maastrichtian (86-106 Ma) age (Belyi and Belaya 1998; Raschke et al. 2014 and references therein). The target lithologies are generally known from the work of Belyi (1994), Belyi and Belaya (1998), and from Gurov and co-workers (Gurov et al. 1978, 2005, 2007; Gurov and Gurova 1983). These authors described the OCVB rocks as a suite comprising (from top to bottom): ignimbrites (mainly felsic, 250 m); tuffs and rhyolitic lavas (200 m);

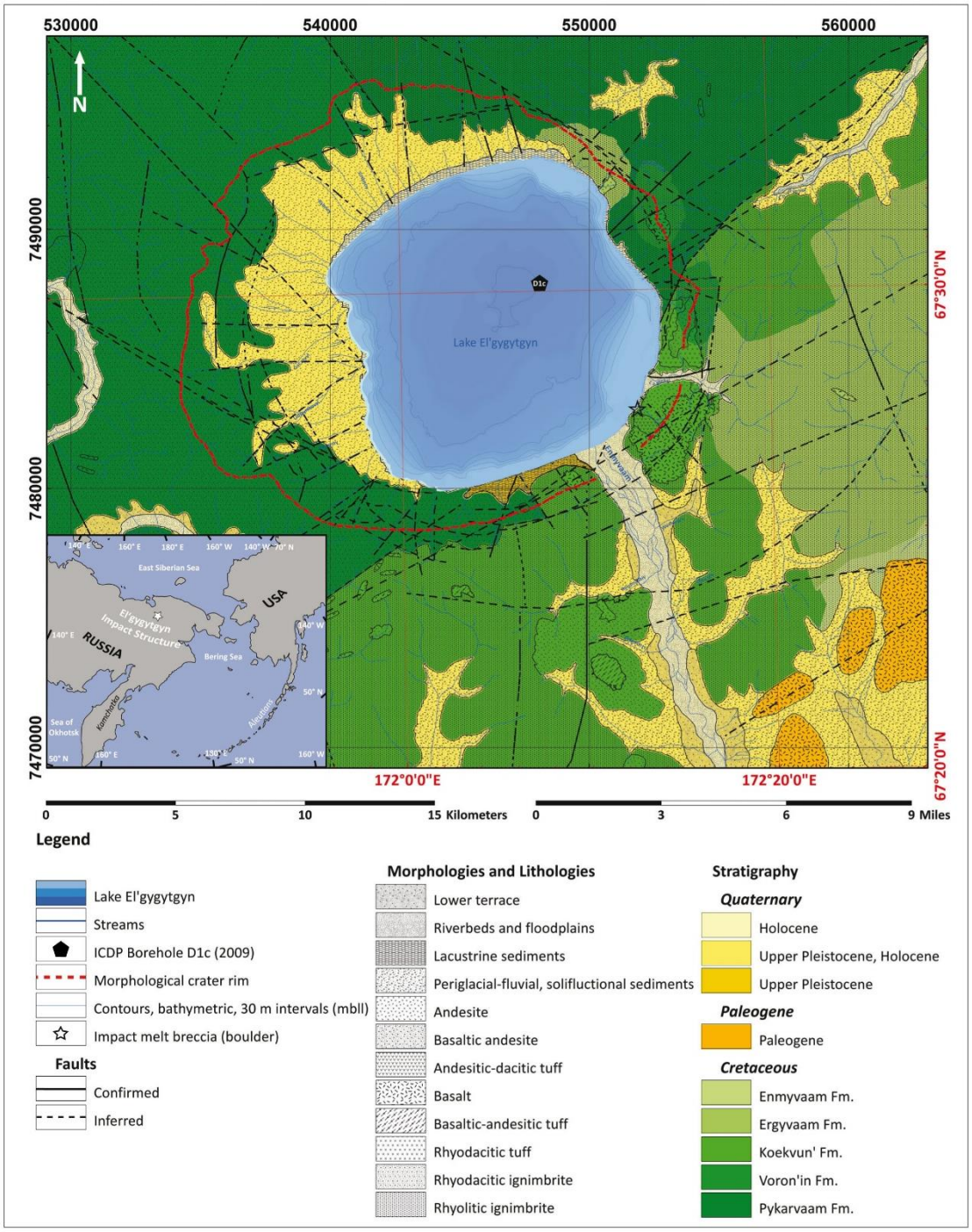

Figure 6.1: Geological map of the El'gygytgyn impact crater with drill core location and small inset for a geographic overview (Raschke et al. 2014)

tuffs and andesitic lava (70 m, occurring especially to the southwest of the crater); and finally, ash and welded tuffs of rhyolitic and dacitic compositions (100 m). Above this sequence a ca. 110 m thick basalt sill occurs as a plateau at the northeastern crater rim (Gurov et al. 2004). Additionally, there are previously unknown lithologies at the southeastern crater rim that were defined for the first time by Raschke et al. (2014). Mount Otvevergin, on the northeastern lakeshore, is composed of reddish and greenish ignimbrites. In the southeastern sector of the lake several mini-plateaus occur that are made up of (sub)horizontal basalt or andesite layers; they are, on aggregate, ~2 km^2 in area extent. To the south of the lake, a suite of gray to reddish, basaltic-andesitic tuffs is present (see Fig.6.1).

The crater rim is well preserved, except for the southeastern part that has been eroded by the Enmyvaam River, a periodic outflow from the lake. Previous studies have shown that rocks of the crater rim did not reveal any characteristic shock metamorphic effects (Gurov et al. 2007; Raschke et al. 2014). The originally in situ ejecta deposits (comprising a mélange of unshocked and shocked rocks, and fragments of impact melt breccia) around the impact crater have been nearly completely eroded by arctic weathering. Only a few allochthonous remnants have been found, embedded in the lacustrine and fluvial terraces inside and outside of the crater rim. These include rounded cobbles (2-15 cm in size), and larger, meter-sized blocks of dark impact melt breccia (Raschke et al. 2014; Pittarello et al., 2013; and references therein). Aerodynamically shaped glass bombs occur together with shock metamorphosed rocks in the lacustrine terraces inside the crater and also in terraces along some streams (e.g., along the Enmyvaam river) in the environs of the crater. All recorded types of impactites from the wider crater area are generally fresh and most of the samples described do not display significant post-impact hydrothermal alteration and weathering (Gurov and Koeberl 2004; Raschke et al. 2014). The impact origin was confirmed by Gurov and co-workers, who found evidence for shock metamorphism in some samples from the crater region (Gurov et al. 1978, 1979, 2005). That includes planar deformation features in quartz, diaplectic quartz glass, coesite and stishovite, and planar fractures in quartz (which by themselves are not shock diagnostic).

In spring 2009 an International Continental Scientific Drilling Program (ICDP) drilling campaign (summarized in Koeberl et al. 2013) recovered a ~520 m long drill core, comprising ~318 m of lacustrine sediments and ~200 m of impactites (drilling location shown in the cross-section of Fig. 6.2). The drilled impactites can be stratigraphically divided (from top to bottom, see Fig. 6.3) into ~12 m of reworked suevite (316.77–328.00 m below lake floor [mblf]), ~63 m of suevite (328.00-390.74 mblf), and ~30 m of upper (390.74-420.89 mblf) and ~96 m of lower bedrock (420.89-517.00 mblf) (Raschke et al. 2013a). The lower bedrock is interpreted as (parautochthonous) crater basement. It is crosscut by a single, thin

polymict impact breccia dike at 471.42 - 471.96 mblf depth. The upper bedrock unit contains different ignimbrites, and three meter-sized mafic blocks (at ~391, 420, and 422 mblf depth). The bedrock units are mainly unshocked but intensely fractured.

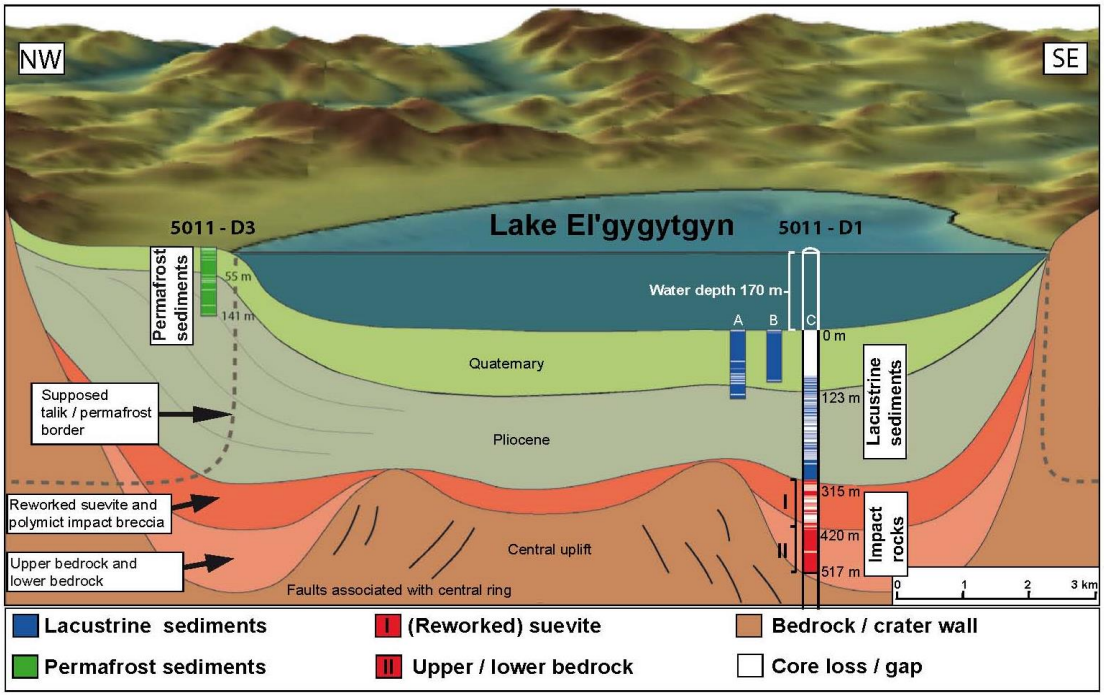

Figure 6.2: Simplified NW-SE cross-section through the El'gygytgyn impact structure, showing the drill core location and drilled lithologies. For more detail see Raschke et al. (2013a) and Koeberl et al. (2013). Based on a diagram by Melles et al. (2011).

The suevitic units contain shocked minerals and relatively rare impact melt particles. Only in the reworked suevite, at the top of the drilled sequence, stronger shocked lithic clasts, melt particles and impact-produced glass spherules are abundant (cf. also Wittmann et al. 2013). All drilled rocks are moderately to strongly weathered (for detailed petrographic information, see Raschke et al. 2013b, Pittarello et al. 2013).

In addition, one of us (UR) participated in a 2011 Russian-German expedition to El'gygytgyn to supplement the existing surface geological data base with new mapping results and to obtain surface samples of country rocks and impactites for comparison with drill core lithologies. Based on the 2011 surface exploration, an upgraded geological map of the El'gygytgyn area was compiled (Raschke et al. 2014). The Zr/TiO_2 vs. Nb/Y diagram of Fig. 6.4 (data from Raschke et al. 2013b, 2014) illustrates the variability of the compositions of the drill core and surface samples. Both sample sets cover the same range of compositions. Obviously, the predominance of target rocks in the basaltic or andesitic-basaltic field of Fig. 6.4 is based on the proportionally higher number of samples analyzed from these lithologies.

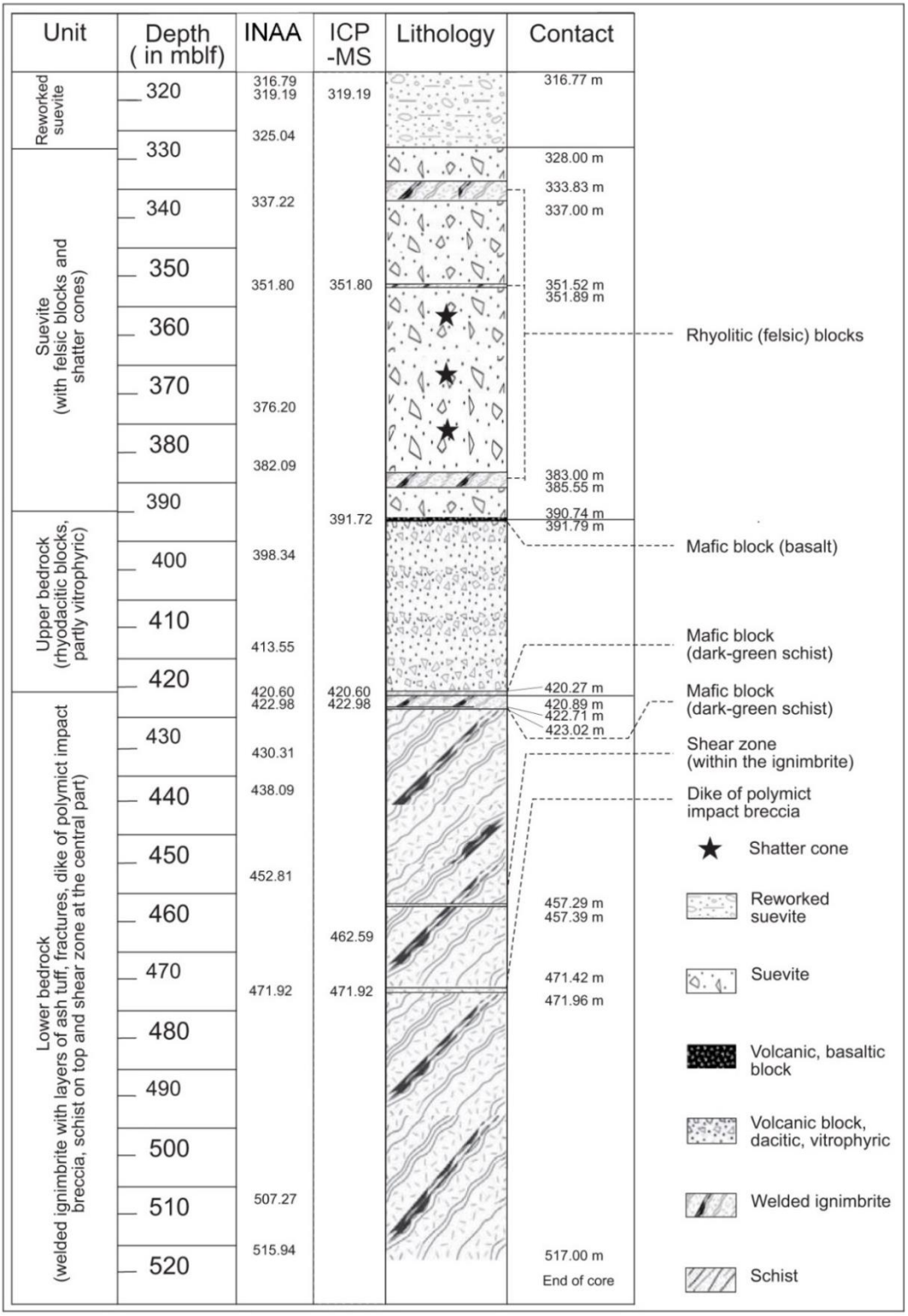

Figure 6.3: Stratigraphic column of the ICDP drill core (modified after Raschke et al. 2013a). The stratigraphic positions of samples used for INAA and PGE analyses are indicated, as well as those of samples analyzed by INAA from Pittarello et al. (2013) used in this work.

6.2.1 Impact and Volcanic Melt Rocks in the Crater Area and in the Drill Core

The distinction between the volcanic and impact melt rocks has proven to be a complex task in the study of the El'gygytgyn crater (cf. Pittarello and Koeberl 2013a).

In contrast to the majority of other impact craters on Earth, the classification of melt particles is a basic requirement for the distinction between impact-generated and volcanic melt particles. Furthermore, the determination of a meteoritic component in impact produced melt particles can help to confirm the type of projectile and its role as well as its dissipation in the impact process.

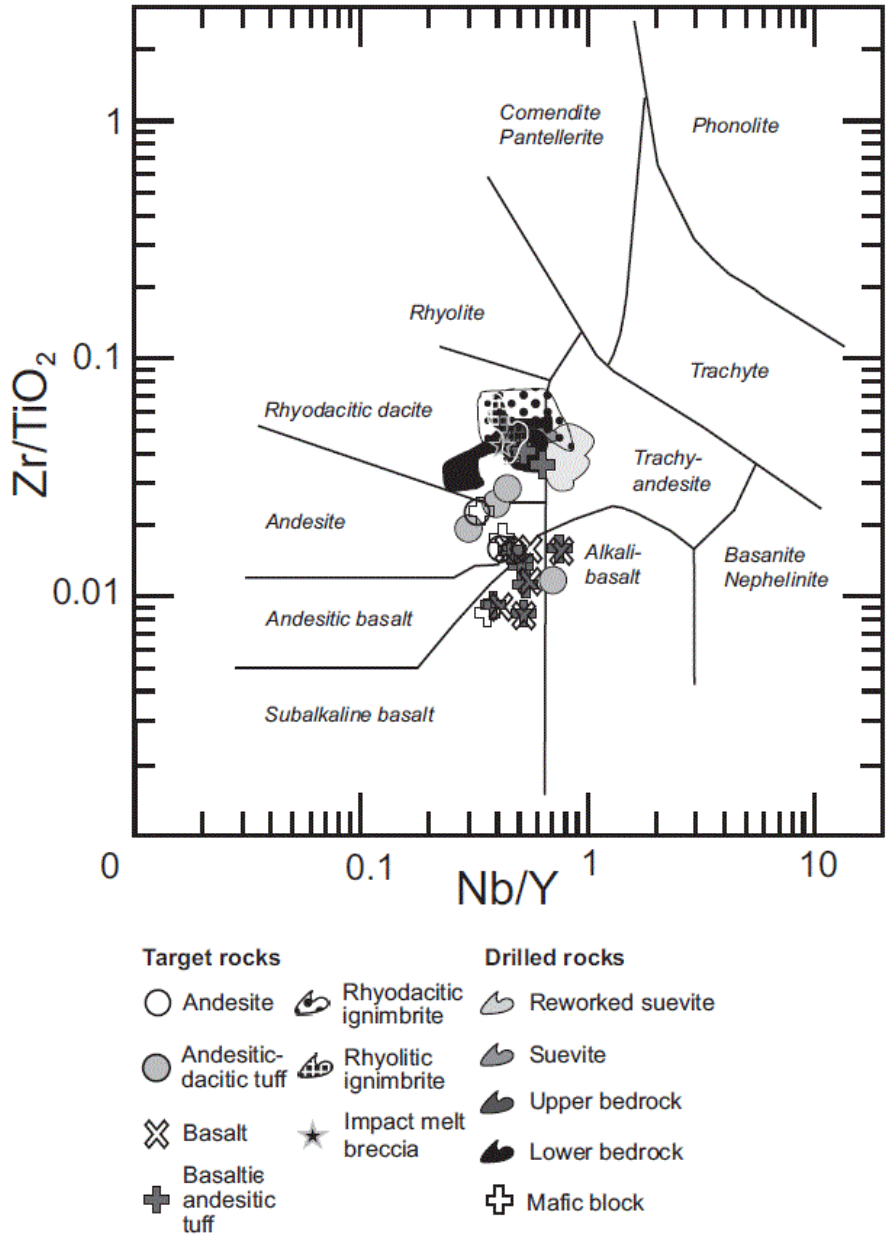

Figure 6.4: Zr/TiO_2 versus Nb/Y diagram for classification of volcanic rocks after Winchester and Floyd (1977). Note: The suevitic units (incl. reworked suevite) plot in the same field as the upper and lower bedrock of the drill core as well as the rhyolitic and rhyodacitic ignimbrites from the crater rim. These lithologies are illustrated by differently shaded fields that each include a larger number of data. Each symbol for a sample from a mafic unit represents an individual analysis. Data from Raschke et al. (2013b, 2014).

Volcanic melt particles occur in the ignimbritic rocks of the upper and lower bedrock. They are generally recrystallized and similar in their composition to the rhyolitic or rhyodacitic host rocks. Alkali feldspar and mafic minerals (biotite and amphibole) occur as phenocrysts in the fine-grained melt. Altered glassy fragments are found inside the pumice fragments of the rhyolitic or rhyodacitic ignimbrite. A detailed description of these volcanic melt particles was given by Raschke et al. (2013b, 2014).

Impact melt occurs in four different settings: i) blocks of impact melt breccia and glass bombs in the lake terraces; ii) tiny (0.5 - 1.5 mm) glass spherules on the lake terrace and along the Enmyvaam River (Glushkova and Smirnoff 2007); iii) similar spherules in the reworked suevite section of the ICDP drill core (Wittmann et al. 2013; Goderis et al. 2013); and iv) small (altered) melt particles in the drilled suevite section (Pittarello et al. 2013; Raschke et al. 2013b).

1. Impact melt breccia sampled on the surface (Gurov and Koeberl 2004) outside the crater structure occurs as a fresh, heterogeneous mélange of glassy, mostly blackish but also translucent "schlieren", which may be rich in vesicles, but relatively poor in mineral or lithic inclusions. Other melt breccia resembles a volcanic scoria with larger clasts of unmelted or only partially molten rock fragments. The composition of such breccia depends on the host rock material and can include pieces of, e.g., pumice, ignimbrite, andesite, or basalt. The minerals in these clasts often show shock features, for example planar fractures, planar deformation features, and diaplectic glass (see Raschke et al. 2013b; Pittarello and Koeberl 2013b).

2. Up to 1.5 mm sized glass spherules found in lacustrine sediments to the south of the crater (during the Quaternary, Lake El'gygytgyn covered a larger surface area and had a higher lake level) and in fluvial terraces along the Enmyvaam River (Gurov 1979; Glushkova and Smirnov 2007) were analyzed by Adolph and Deutsch (2010), Smirnov et al. (2011), and Wittmann et al. (2013). All these authors concluded, on the basis of geochemical data, that the spherules were impact-produced melt droplets that had been deposited from the collapsing ejecta plume (with lithic debris) in a thin layer on the juvenile post-impact surface. Overall, the spherules are strongly heterogeneous, ranging in composition from basaltic to rhyolitic, and are probably derived from the different volcanic lithologies in the target area, which requires, in turn, that the spherules did not undergo homogenization in the ejecta plume (see Wittmann et al. 2013).

3. An accumulation of spherules occurs on top of the reworked suevite section between 317 and 322 mblf. The spherules are very heterogeneous and occur in different types. First, there are hollow spherules with a glassy margin and that may contain a few crystal

inclusions or microfragments of different minerals (e.g., feldspar, quartz and zeolite). Another type of spherule is filled by aluminosilicate glassy melt, which contains microlites of feldspar or of mafic composition (Raschke et al. 2013b and references therein).

4. Impact melt was identified in the matrix of the suevite section of the drill core between 328 and 391 mblf (Raschke et al. 2013b). This comprises very small melt particles, ~1 mm in size, which are generally altered to secondary phyllosilicates (e.g., smectites and chlorites). These particles amount to much less than 1 vol% of the whole suevite package.

6.2.2 Previous Studies of Siderophile Elements, Platinum Group Elements, and Rare Earth Elements

Pittarello et al. (2013) analyzed rare earth element (REE) concentrations of drill core rocks and compared these with volcanic rocks from the regional geological setting. With the exception of data for the mafic blocks from the drill core, all other impactite samples, including the suevites, plot in the same space as the volcanic target rocks. Raschke et al.'s (2014) chemical comparison between impactites of the drill core and regionally occurring lithologies revealed very similar chemical compositions of upper and lower bedrock and the suevitic units, as well as the surface rocks from the crater rim that are dominated by the rhyolitic or rhyodacitic ignimbrites.

The enrichment of siderophile elements in microtektites (or microkrystites) is generally a very useful tool for the determination of a projectile signature (Koeberl 2014; Koeberl et al. 2012). According to Wittmann et al. (2013), the siderophile element contents in the spherules of the reworked suevite are highly variable. The El'gygytgyn glass spherules show a wide range of compositions, reflecting the geochemical signature of the target lithology assemblage composed of both mafic and felsic rocks (Raschke et al. 2013b; Wittmann et al., 2013). The siderophile element contents of the spherules in the reworked suevite are highly variable (Ni ~30 to 1400 ppm), similar to the spherules from outside of the crater (Ni ~300 to 1100 ppm), and are probably related to projectile contamination (see also Wittmann et al. 2013).

Foriel et al. (2013) found that some impact glass samples from the surface of the El'gygytgyn area have a chromium isotopic anomaly that agrees best with a ureilite source. They suggested that the impactor could have had a composition similar to that of the Almahata Sitta meteorite from Sudan, which is a ureilite with clasts of ordinary chondrite (Jenniskens et al. 2009).

Platinum group element (PGE) analyses were undertaken by Goderis et al. (2013) on the spherule-bearing deposits, as well as on a few hand specimens of impact melt recovered

from the crater rim. Together with their Os isotope and Ir concentration analysis, these authors concluded that rather than an achrondritic (ureilitic) impactor composition, an ordinary chondrite type was probable.

Based on these previous studies, especially the instrumental neutron activation analysis (INAA) data of Pittarello et al. (2013), as well as work done on drill core and country rock samples by Raschke et al. (2013b, 2014), we decided to try to derive more information about the geochemical character of the impactites and their target rocks, including the comparison with impact melt breccia that was collected on the lake terraces within the crater. Another goal has been the identification of a meteoritic component using siderophile element abundances in impactites from the El'gygytgyn crater.

6.3 SAMPLES AND ANALYTICAL METHODS

A suite of 17 samples from the ICDP drill core (impactites, including suevite and bedrock lithologies) was selected for INAA. A second suite of samples (7 ICDP drill core and 10 surface specimens) was used for PGE analysis. Some petrographic and chemical details about the surface samples have previously been presented in Raschke et al. (2014). Sampled drill core depths (this work and from Pittarello et al. 2013) are given in Table 6.1.

The measurements by INAA were carried out at the Department of Lithospheric Research, University of Vienna. The contents of some major (Na, K, and Fe) and many trace elements (including the REE) were determined using this method. In general, about 130 mg of powdered sample was sealed in a polyethylene capsule and irradiated in the 250 kW Triga Mark-II reactor of the Atomic Institute in Vienna. For calibration three international rock standards were used: (i) Allende carbonaceous chondrite (Smithsonian Institution, Washington DC, see Jarosewich et al. 1987); (ii) Ailsa Craig Granite AC-E (Centre de Recherche Petrographique et Geochimique, Nancy, France, see Govindaraju 1989); and (iii) Devonian Ohio Shale SDO-1 (USGS, see Govindaraju 1994). Further details about the method, technique, and accuracy of results is given by Koeberl (1993) and Mader and Koeberl (2009). The INAA data for the various lithologies of the ICDP drill core are reported in Table 6.2.

The contents of the PGE and Au were determined in Cardiff by inductively coupled plasma-mass spectrometry (ICP-MS) after pre-concentration by Ni-sulfide fire assay with co-precipitation, using external calibration. For each sample, 15 grams of material was used. Two reference materials with low-level concentrationswere used for the validation of PGE analysis: i) WITS-1 (a silicified komatiite and ultramafic rock from the Barberton

Table 6.1: List of ICDP drill core samples for analytical studies.

Sample	ID	Lithology*
(this work)	*(by Pittarello et al. 2013)*	
UR-ELG_316.79	98Q2-W03-07 (316.80)	rsv
UR-ELG_319.19	98Q5-W28-31 (318.20)	rsv
UR-ELG_325.04	99Q2-W12-15 (319.50)	rsv
UR-ELG_337.22		rsv
UR-ELG_351.80	104Q2-W39-41 (334.70)	sv
UR-ELG_376.20	107Q1-W14-16 (342.70)	sv
UR-ELG_382.09	109Q7-W14-16 (351.40)	sv
	112Q7-W04-07 (355.40)	sv
	114QCC-W02-05 (361.70)	sv
	118Q1-W00-03 (371.30)	sv
	119Q2-W23-25 (374.90)	sv
	123Q1-W22-24 (383.90)	sv
UR-ELG_398.34	125Q1-W33-35 (390.20)	ub
UR-ELG_413.55	134Q1-W07-09 (399.60)	ub
	135Q3-W05-08 (401.80)	ub
	138Q8-W00-03 (412.20)	ub
	139Q5-W07-09 (414.50)	ub
UR-ELG_391.72	126Q4-W17-18 (391.70)	mb
UR-ELG_420.60	142Q3-W13-15 (420.90)	mb
UR-ELG_422.98	143Q2-W06-08 (422.90)	mb
UR-ELG_422.98	146Q2-W11-14 (429.70)	lb
UR-ELG_430.31	151Q2-W05-07 (440.40)	lb
UR-ELG_438.01	155QCC-W07-10(451.40)	lb
UR-ELG_452.81	158Q2-W20-23 (456.90)	lb
UR-ELG_462.59	161Q1-W12-14 (465.10)	lb
	162Q2-W27-30 (468.30)	lb
	162Q5-W24-26 (470.20)	lb
	167Q1-W22-25 (483.10)	lb
	168Q5- W24-26 (487.40)	lb
UR-ELG_507.27	173Q3-W15-18 (500.00)	lb
UR-ELG_515.94	174Q4-W26-28 (503.90)	lb
	178Q4W51-53 (514.30)	lb
UR-ELG_471.92		pibd

rsv = reworked suevite, sv = suevite, ub = upper bedrock, lb = lower bedrock, mb = mafic block, pibd = polymict impact breccia dike.

area, South Africa), and ii) TDB-1, a basaltic (diabase) rock sample from Canada (Tredoux and McDonald 1996). More details regarding the analytical technique and the related precision and accuracy values have been published in Huber et al. (2001) and McDonald and Viljoen (2006). For drill core and surface samples the PGE and Au abundance data are reported in Table 6.3.

In addition, we used the datasets of siderophile elements from petrographic and geochemical studies, which we have already published for the drill core material (Raschke et al. 2013b) and for the surface samples of the wider crater region (Raschke et al. 2014). Additional trace element data for the ICDP drill core from Pittarello et al. (2013) measured by INAA in the same laboratory as our samples were used to extend the data set, especially for scarce lithologies such as the mafic blocks. All samples are listed in Table 6.1 and Fig. 6.3. Using this large data set we tried to discriminate special characteristics of the reworked suevite (including layers of impact produced glass spherules) and the other impactites from the drill core in contrast to the target rocks from the crater vicinity, inclusive of impact melt breccia from the lake terrace. Furthermore, we compared our results with respect to the data of Goderis et al. (2013), Wittmann et al. (2013), Foriel et al. (2013), and Pittarello et al. (2013).

6.4 RESULTS

6.4.1 Composition of the drill core material and target rocks

The El'gygytgyn drill core material and the surface samples mainly comprise felsic volcanic rocks. Rhyolitic or rhyodacitic ignimbrites are the predominant rock types in the drill core (lower bedrock unit, ~50 % of the impactite section) as well as regarding the country rocks. In the vicinity of the crater more than 90 % of the country rocks are SiO_2-rich volcanics (Raschke et al. 2014). The mafic rocks, i.e., basalts, andesitic basalts, and their eruptive equivalents (phreatomagmatic tuffs), form a minor contribution in the area and are only found in the southeastern sector of the crater environs. In this work, we focus on four types of lithologies for chemical discrimination and interpretation: (1) the reworked suevite with accumulated impact glass spherules in the groundmass (see Raschke et al. 2013b and Wittmann et al. 2013, as well as references therein); (2) the impact melt breccia from the lake terrace that might carry a possible meteoritic component; (3) the suevite, a mélange of all possible target lithologies and impact melt particles; and (4) the mafic blocks from the drill core between upper and lower bedrock unit. These blocks are possibly derived from basaltic intrusions (sills) and are highly altered and fractured. These altered samples are characterized by a high loss on ignition (LOI) as well as an extraordinary chemical signature in comparison to all other target rocks; they are enriched in a wide range of metal oxides and easily recognizable in the compositional discrimination diagrams.

6.4.2 Rare Earth Elements

The average REE contents of the different lithologies of the ICDP drill core from this and previous studies are summarized in Table 4. The CI chondrite normalized REE patterns for sampled lithologies are shown in Figs. 5a-c. The patterns of the average upper and lower bedrock of the ICDP drill core (Fig. 5a) are very similar. They indicate enrichments for the average upper and lower bedrock by factors of 75 to 89 for La, and 10 to 8 for Yb, respectively, compared to CI chondrite composition. The light REE (LREE) are enriched compared to the heavy REE (HREE) (average La_N/Yb_N 8-10), and a negative Eu anomaly (average Eu/Eu* ~ 0.6 to 0.7; $Eu/Eu^* = Eu_N/(Sm_N \times Gd_N)^{0.5}$) is characteristic for these rocks. Another prominent feature of the upper and lower bedrock is a flat pattern of HREE. In comparison to the rocks of the Ochotsk-Chukotsky Volcanic Belt (OCVB), the upper and lower bedrock show less fractionation and slightly lower REE ratios, namely La_N/Yb_N ratios of 7.9 and 10.8 for the upper and lower bedrock, respectively, compared to ~ 8 to 18 for the OCVB, and La/Sm ratios of 3.7 and 4.9, respectively, compared to 5 to 8 for the OCVB (Tikhomirov et al. 2008). In contrast to the felsic target rocks, the mafic blocks of the ICDP drill core display different REE patterns (Fig. 5b). The CI chondrite-normalized REE patterns

Table 6.2: Selected major and trace element abundances of samples from the ICDP drill core D1c of the El'gygytgyn impact structure, as detected by instrumental neutron activation analysis.

Sample	UR-ELG	UR-ELG	UR-ELG	UR-ELG	UR-ELG	UR-ELG	UR-ELG	UR-ELG	UR-ELG	UR-ELG	UR-ELG	UR-ELG	UR-ELG	UR-ELG	UR-ELG	UR-ELG	UR-ELG
Depth (mblf)	316.79	319.19	325.04	337.22	351.8	376.2	382.09	398.34	413.55	420.6	422.98	430.31	438.09	452.81	471.92	507.27	515.94
Lithology*	rsv	rsv	rsv	sv	sv	sv	sv	ub	ub	mb	mb	lb	lb	lb	pibd	lb	lb
ppm																	
Na (wt%)	2.48	2.02	2.00	2.21	2.57	2.22	2.41	2.81	2.09	1.25	0.53	2.76	3.03	2.52	1.89	3.19	1.28
K (wt%)	3.09	3.09	2.88	3.00	3.26	3.17	3.03	2.99	2.50	<0.7	0.91	2.94	3.36	3.30	2.66	4.07	2.04
Fe (wt%)	2.41	2.87	2.26	1.51	1.90	1.78	1.91	1.99	2.01	7.97	7.16	1.75	1.70	1.62	2.42	1.72	2.27
Sc	9.17	11.1	7.95	4.48	6.09	5.38	6.07	6.45	6.14	36.9	42.0	5.46	5.59	4.22	9.04	4.65	2.1
Cr	43.2	92.7	26.1	10.7	11.8	19.8	12.4	18.7	13.6	544	872	13.7	10.2	10	58.6	10.5	11.6
Co	6.03	8.38	5.45	2.92	3.52	3.23	3.54	3.69	3.30	30.8	42.7	3.44	3.23	2.71	6.99	3.24	1.01
Ni	28	41	<26	<20	12	4	11	17	3	98	276	6	<24	<21	24	<22	<20
Zn	67	66	56	49	53	47	56	56	57	348	121	50	50	46	58	51	13
Ga	4.9	3.6	6.9	3.4	5.2	4.1	2.8	4.8	6.1	232	19	3.2	<3.7	5.5	5.3	4.5	3.1
As	15.4	16.2	11.4	4.42	9.57	5.96	7.87	8.96	5.72	42.2	91.5	34.9	19.1	8.91	18.3	14.3	47.8
Se	0.03	<1.7	<1.5	<1.3	<1.4	<1.3	<1.4	<1.4	<1.4	<2.8	7.72	<1.4	<1.5	<1.3	<1.6	<1.4	<1.3
Rb	146	118	115	131	132	138	128	136	107	9.51	75.6	115	129	137	121	174	119
Sr	171	318	153	122	283	122	161	196	165	401	172	178	518	217	235	169	76
Zr	241	241	172	193	218	208	222	234	217	166	678	220	229	187	237	221	127
Sb	1.57	1.55	0.98	0.92	1.39	1.17	1.46	1.69	1.54	1.01	4.09	1.55	1.61	0.97	1.84	1.15	2.37
Cs	9.84	7.64	9.22	8.67	4.55	10.3	8.26	6.64	6.85	3.54	30.1	3.83	4.17	4.94	9.18	5.21	5.76
Ba	464	596	299	431	469	417	439	495	481	65	260	481	569	493	419	592	235
La	34.3	28.3	35.7	30.8	30.1	31.5	31.4	30.4	27.8	19.2	51.1	31.7	34.3	41.6	28.9	37.3	24.6
Ce	64.8	56.1	64.7	57.6	56.7	58.9	60.8	58	53.3	34	111	58.8	64.5	72.9	53.5	68.5	39.8
Nd	25	22.6	22.9	19	20.5	20.4	21.9	20.8	19.2	15.6	59	18.7	21.5	22.2	18.7	22.1	13.1
Sm	5.79	5.08	5.03	3.79	4.3	4.06	4.25	4.2	4.13	4.39	13.7	4.05	4.68	4.43	4.3	4.8	3.05
Eu	0.98	0.89	0.84	0.75	0.88	0.77	0.9	0.93	0.77	1.70	3.84	0.81	0.86	0.76	0.93	0.80	0.44
Gd	5.03	4.54	3.86	3.8	4.26	3.25	3.54	3.67	2.99	4.66	10.2	3.11	4.55	4	3.99	4.67	2.61
Tb	0.78	0.71	0.63	0.46	0.55	0.49	0.56	0.52	0.54	0.7	1.59	0.50	0.59	0.5	0.54	0.57	0.48
Tm	0.4	0.34	0.3	0.27	0.3	0.27	0.27	0.29	0.3	0.34	0.61	0.31	0.33	0.26	0.32	0.34	0.38
Yb	2.54	2.35	2.27	1.78	2.04	1.94	2.10	1.98	1.98	2.17	3.65	1.98	2.13	2.01	2.08	2.13	3.19
Lu	0.43	0.41	0.38	0.3	0.34	0.34	0.35	0.33	0.34	0.32	0.56	0.33	0.34	0.33	0.34	0.38	0.57
Hf	5.28	4.71	4.14	4.17	4.59	4.48	4.57	4.74	4.89	2.04	12.3	4.55	4.46	4.11	4.5	4.88	2.17
Ta	0.89	0.67	0.64	0.69	0.65	0.70	0.64	0.66	0.66	0.33	1.1	0.68	0.79	0.73	0.65	0.93	0.63
Au (ppb)	13	<1.3	0.6	0.6	<1.3	<1.1	<1.5	<1.4	<1.2	<1.5	1.7	<1.5	<1.7	<1.3	<0.9	<1.6	<1.3
Th	15.8	11.9	11.8	15.1	13.3	15.1	13.9	13.3	13.1	1.51	5.32	14.9	16.5	17.8	12.7	19.4	12.6
U	4.69	3.33	3.38	3.55	3.69	3.40	3.16	3.49	3.25	0.36	5.98	3.77	5.15	4.00	3.66	5.04	4.81

Abbrevations: rsv = reworked suevite, sv = suevite, ub = upper bedrock; lb = lower bedrock; mb = mafic block; pibd = polymict impact breccia dike.

Table 6.3: Concentrations of platinum group elements and Au in impactites and target lithologies from the ICDP drill core D1c and surface outcrops.

Sample	Lithology	Os (ppb)	Ir (ppb)	Ru (ppb)	Rh (ppb)	Pt (ppb)	Pd (ppb)	Au (ppb)
ICDP drill core								
UR-ELG 319.19 mblf	reworked suevite	0.40	0.42	0.64	0.19	0.76	0.89	4.15
UR-ELG 351.8 mblf	suevite	0.07	0.09	0.14	0.12	3.46	1.23	3.87
UR-ELG 391.72 mblf	mafic block	<0.03	0.04	0.11	0.07	3.38	1.13	0.60
UR-ELG 420.6 mblf	mafic block	0.41	0.52	0.78	0.20	2.04	1.94	18.65
UR-ELG 422.8 mblf	mafic block	0.16	0.20	0.30	0.19	2.86	2.62	2.11
UR-ELG 462.59 mblf	lower bedrock	0.15	0.10	0.15	0.12	1.00	4.84	4.26
UR-ELG 471.92 mblf	polym. impact breccia dike	<0.03	0.04	0.10	0.07	0.22	0.26	0.35
Surface outcrops								
UR-2011_1.1	andesitic-dacitic tuff	<0.03	<0.03	0.06	0.06	0.26	0.25	1.20
UR-2011_3.7	basalt	0.06	0.07	0.12	0.14	0.98	1.31	0.70
UR-2011_4.4	basaltic andesite	0.09	0.11	0.27	0.06	0.95	0.31	1.39
UR-2011_4.5	rhyodacitic tuff	0.11	0.09	0.10	0.12	4.41	2.25	5.10
UR-2011_5.3	rhyolitic ignimbrite	0.04	0.05	0.06	0.02	1.41	0.70	0.17
UR-2011_7.2	andesite	0.04	0.04	0.11	0.09	0.56	0.25	1.29
UR-2011_9.2	basaltic-andesitic tuff	0.06	0.03	0.09	0.12	1.04	2.93	8.82
UR-2011_9.11b	impact melt	0.05	0.05	0.11	0.07	2.13	0.46	0.50
UR-2011_9.12a	rhyodacitic ignimbrite	<0.03	0.04	0.22	0.08	0.20	0.25	0.31
UR-2011_10.1a	rhyodacitic ignimbrite	<0.03	0.04	0.05	0.08	1.16	2.07	2.93

of the mafic block samples show comparable signatures characterized by an enrichment of the LREE compared to the HREE and a slightly fractionated profile for the HREE. The REE patterns show different enrichments for the mafic blocks at 391, 420 and 422 mblf by factors of 134, 50, and 143 for La, and 9, 9, and 15 for Yb, respectively, compared to CI chondrite composition. The enrichment of the LREE is more prominent in the blocks at 391 and 422 mblf with La_N/Yb_N ratios of 14 and 9.5, respectively, compared to the block at 420 mblf with a La_N/Yb_N ratio of 5.9. The REE patterns for the mafic blocks at 422 and 420 mblf do not show distinct Eu anomalies, whereas the block at 391 mblf displays - in contrast to all other lithologies - a slightly positive Eu anomaly with a Eu/Eu* ratio of 1.16. However, these blocks are very heterogeneous, and it is difficult to compare these with each other or with other lithologies from the drill core, crater, and the OCVB.

The average signatures for suevite, the polymict impact breccia dike, and the reworked suevite of the ICDP drill core display similar REE patterns (Fig. 5c). All lithologies show an enrichment of the REE compared to the CI chondrite composition by factors of 90,

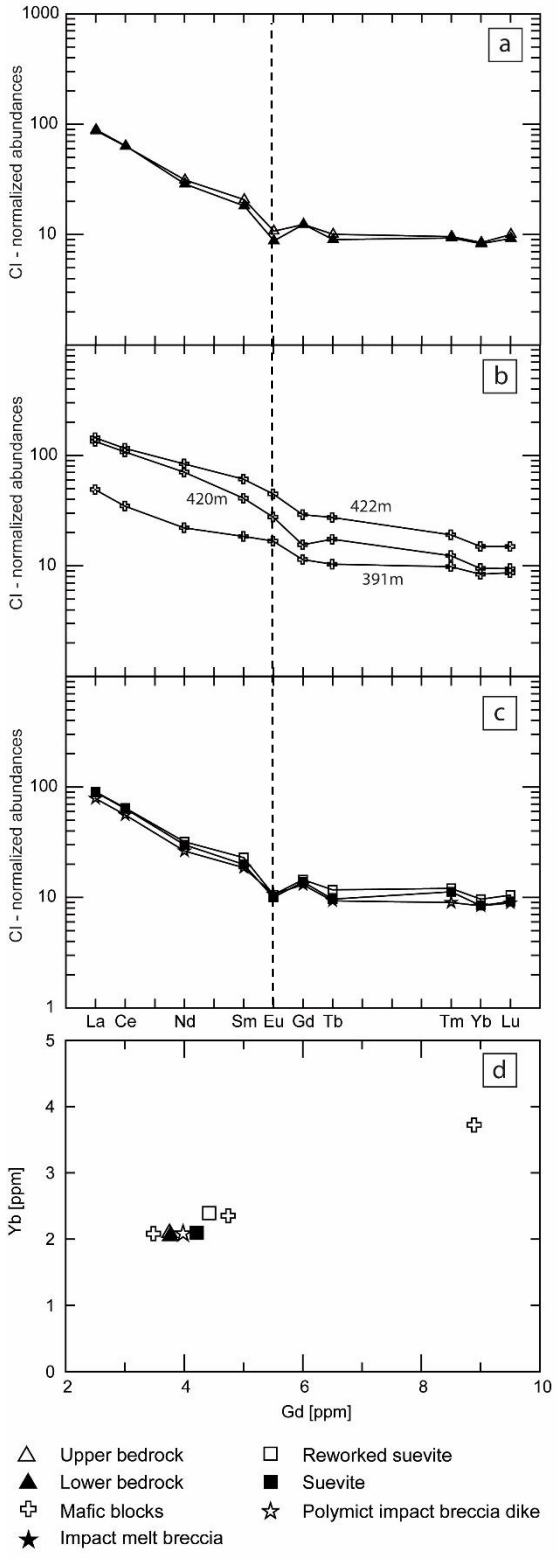

79, and 90 for La, and 8, 8, and 10 for Yb for the suevite, polymict impact breccia dike, and reworked suevite, respectively. The LREE are enriched compared to the HREE in these lithologies with La_N/Yb_N ratios of 10.6, 9.4, and 9.4, respectively, and negative Eu anomalies are present, with Eu/Eu* ratios of 0.60, 0.69, and 0.58 for the suevite, polymict impact breccia dike, and reworked suevite, respectively. The REE patterns of the suevite and polymict impact breccia dike show strong similarities to those of the upper and lower bedrock, and indicate that the suevite mainly formed from these target lithologies. This is also visible in the Yb vs. Gd diagram (Fig. 5d). The reworked suevite indicates some slight differences in the REE patterns from those for the suevite. The absolute concentrations of the REE and the enrichments of the REE compared to CI chondrite composition are slightly higher, and the negative Eu anomaly is lower in the reworked suevite in comparison to the suevite and the lower and upper bedrock. This behavior could be explained by an additional admixture of mafic material in the reworked suevite compared to the suevite, as suggested in the Yb vs. Gd diagram (Fig. 6.5d).

Figure 6.5: CI chondrite - normalized REE patterns (normalization values from Taylor and McLennan 1985) of analyses for samples of the ICDP drill core (see table 6.2): (a) upper and lower bedrock; (b) three mafic blocks at depths of 391, 420, and 422 mblf; (c) reworked suevite, suevite, and polymict impact breccia dike. Dotted line for better comparison of Eu-values. (d) Yb vs. Gd-diagram displaying the distinctly increased concentrations of Gd and Yb in the mafic blocks at 391 and 422 mblf, and the admixture of such a mafic component to the reworked suevite. Note that surface volcanic target lithologies and impact melt breccia are not plotted in this figure.

Table 6.4: Compilation of the average REE contents, their standard deviations, and the Eu/Eu* and LaN/YbN ratios of the ICDP El'gygytgyn drill core lithologies.

ppm	Reworked suevite avg. (n = 6)	Suevite avg. (n = 12)	Polymict impact breccia dike ~471 mblf (n = 1)	Upper bedrock avg. (n = 7)	Lower bedrock avg. (n = 17)	Mafic block ~391 mblf (n = 1)	Mafic block ~420 mblf avg. (n = 2)	Mafic block ~422 mblf avg. (n = 2)
La	33.2 ± 3.5	32.9 ± 2.3	28.9	31.8 ± 3.0	32.5 ± 4.1	49.2	18.0 ± 1.4	53.0 ± 1.9
Ce	61.8 ± 5.8	61.0 ± 3.9	53.5	60.0 ± 5.6	60.5 ± 7.7	103.0	33.3 ± 1.0	111 ± 1
Nd	22.7 ± 1.6	21.3 ± 1.9	18.7	22.1 ± 2.9	20.3 ± 2.2	50.2	15.7 ± 0.1	59.6 ± 0.8
Sm	5.30 ± 0.66	4.50 ± 0.56	4.30	4.76 ± 0.72	4.18 ± 0.47	9.47	4.27 ± 0.18	14.1 ± 0.6
Eu	0.92 ± 0.08	0.87 ± 0.13	0.93	0.93 ± 0.18	0.76 ± 0.11	2.41	1.46 ± 0.35	3.90 ± 0.09
Gd	4.43 ± 0.59	4.22 ± 0.66	3.99	3.76 ± 0.67	3.77 ± 0.66	4.75	3.49 ± 1.67	8.90 ± 1.90
Tb	0.68 ± 0.11	0.56 ± 0.08	0.54	0.58 ± 0.09	0.52 ± 0.05	1.01	0.60 ± 0.14	1.59 ± 0.00
Tm	0.43 ± 0.11	0.40 ± 0.10	0.32	0.34 ± 0.05	0.33 ± 0.03	0.44	0.35 ± 0.01	0.68 ± 0.01
Yb	2.39 ± 0.26	2.09 ± 0.22	2.08	2.09 ± 0.20	2.04 ± 0.33	2.35	2.08 ± 0.13	3.72 ± 0.10
Lu	0.40 ± 0.04	0.35 ± 0.03	0.34	0.38 ± 0.04	0.35 ± 0.06	0.36	0.33 ± 0.01	0.57 ± 0.01
Eu_{avg}/Eu_{avg}*	0.58	0.61	0.69	0.67	0.59	1.10	1.16	1.06
La_{avgN}/Yb_{avgN}	9.39	10.64	9.39	10.28	10.77	14.15	5.85	9.63

Based on data of this work and from Pittarello et al. (2013); average Eu/Eu = 0.77; $Eu/Eu^* = Eu_N/[Sm_N \times Gd_N]^{0.5}$

n = number of samples, normalization values from Taylor and McLennan, 1985.

6.4.3 Siderophile Elements

The concentrations of the siderophile elements Co, Ni, and Cr, and the Ni/Cr, Ni/Co, and Cr/Co ratios are summarized for the different lithologies of the ICDP drill core in Table 6.5. Our results show that, in general, the siderophile element concentrations are low in the felsic (lower and upper bedrock) and distinctly higher in the mafic target lithologies (mafic blocks), with the highest concentrations of siderophile elements having been measured for the mafic block at ~420 mblf. The concentrations of the siderophile elements and their ratios within the suevite are quite similar to the respective concentrations and ratios in the lower and upper bedrock. The concentrations of siderophile elements reported for impact melt rocks and glass bombs collected at the surface around the crater are also in this range, with concentrations of <50 ppm Cr, <7 ppm Co, and <21 ppm Ni (Gurov and Koeberl 2004; Gurov et al. 2005). Therefore, a contamination of the suevite and the impact melt rocks by a meteoritic component is not obvious in these siderophile element abundances. Slightly higher concentrations of siderophile elements together with lower Ni/Cr and higher Ni/Co and Cr/Co ratios in comparison to the suevite unit are observed in the reworked suevite and within a polymict impact breccia dike occurring in the lower bedrock at ~471 mblf. For the impact spherules (Wittmann et al. 2013) the contents of siderophile elements (measured by LA-ICP-MS) are much higher in comparison to all other target lithologies (Table 6.5), e.g., the Ni data for some samples (sph6 at 317.60 mblf) show high values up to 1400 ppm (Wittmann et al. 2013). Regarding to the moderately siderophile element budget of the reworked suevite (Table 6.5), these spherules are negligible. These observations agree with the results of Pittarello et al. (2013) and Goderis et al. (2013). Therefore, the higher concentrations of siderophile elements in the reworked suevite and polymict impact breccia dike, and their

different ratios in comparison to the suevite, are most likely the result of a higher amount of mafic material within these impactites. Overall, the observed siderophile element ratios for the suevite, reworked suevite, and polymict impact breccia dike do not match meteoritic ratios (e.g., Tagle and Berlin 2008; Koeberl 2014).

Table 6.5: Compilation of the average Cr, Co, and Ni contents, their standard deviations, and their ratios for the ICDP El'gygytgyn drill core lithologies[a]; for comparison data for impact spherules from the El'gygytgyn crater are also reported. [b]

ppm	Reworked suevite avg. (n = 6)	Suevite avg. (n = 12)	Polymict impact breccia dike ~471 mblf (n = 1)	Upper bedrock avg. (n = 7)	Lower bedrock avg. (n = 17)	Mafic block ~391 mblf (n = 1)	Mafic block ~420 mblf avg. (n = 2)	Mafic block ~422 mblf avg. (n = 2)	Impact spherules[b] (n = 13)
Cr	34.8 ± 31.4	12.3 ± 13.8	58.6	13.2 ± 7.4	8.1 ± 4.0	95.1	499 ± 64	1061 ± 267	329 ± 267
Co	5.89 ± 1.48	3.97 ± 1.52	6.99	4.49 ± 1.62	3.10 ± 0.60	29.2	32.4 ± 2.2	54.6 ± 16.7	44.4 ± 26.2
Ni	24.9 ± 13.7	10.7 ± 5.2	24	11.8 ± 6.4	10.7 ± 3.4	76.9	100 ± 3	331 ± 77	564 ± 467
Ni_{avg}/Cr_{avg}	0.72	0.87	0.40	0.89	1.32	0.81	0.20	0.31	1.71
Ni_{avg}/Co_{avg}	4.22	2.70	3.43	2.63	3.45	2.63	3.09	6.06	12.70
Cr_{avg}/Co_{avg}	5.91	3.10	8.38	4.00	2.61	3.26	15.40	19.43	7.41

[a]Based on data of this work and from Pittarello et al. (2013).
[b]Based on data from Wittmann et al. (2013); these impact spherules originate from the reworked suevite of the ICDP El'gygytgyn drill core and from outside of the crater.
n = number of samples.

6.4.4 Platinum Group Element analysis – the Presence of a Meteoritic Component

Results of the PGE and Au analysis are given in Table 6.3 and plotted in Figs. 6.6 and 6.7. The Ir contents of the target rocks vary between < 0.03 and 0.52 ppb (Table 6.3). The Ir concentrations of the felsic lithologies are generally low (< 0.10 ppb), whereas higher Ir contents (0.52 ppb) were measured for the basaltic target lithologies, especially for the highly altered and metal oxide enriched mafic blocks at ~420 and 422 mblf in the drill core. The high Ir concentrations in the mafic blocks are associated with high Os concentrations, but also with elevated concentrations of Pt, Pd, and Au that are typical of many mafic lavas (e.g., Barnes et al. 1985; Tredoux et al. 1995; McDonald 1998; Crocket 2002).

The Ir contents of the suevite, impact melt breccia and polymict impact breccia dike samples are in the range of 0.04 to 0.09 ppb, and in good agreement with data previously presented by Goderis et al. (2013), who determined a range from 0.05 to 0.20 ppb for similar samples. Gurov and Koeberl (2004) reported Ir concentrations of 0.02 to 0.11 ppb for impact melt rocks and glass bombs from El'gygytgyn, which also corresponds well with our new measurements.

Notably part of the reworked suevite has a significantly higher PGE concentration in comparison to the suevite, impact melt breccia, and polymict impact breccia dike, as well as most of the felsic and mafic target lithologies (Table 6.3), in terms of Os (0.40 ppb), Ir (0.42 ppb), Ru (0.64 ppb), and Rh (0.19 ppb) (Fig. 6.6c). Additionally, these values are very similar to those for the mafic block at ~420 mblf, but also considerably increased in comparison with

the mafic blocks at ~391 and 422 mblf. The Os/Ir ratio of the reworked suevite is higher (~1) compared to the values for the mafic blocks at ~420 and 422 mblf (~0.8; an Os/Ir-ratio < 1 is typical for mafic magmas (Barnes et al. 1985).

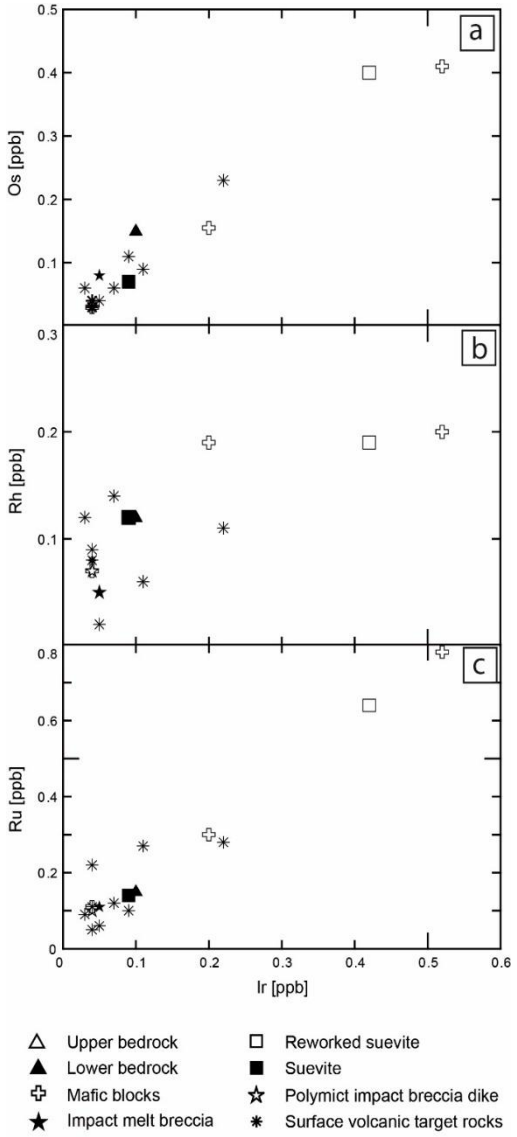

Figure 6.6: (a) Os vs. Ir, (b) Rh vs. Ir, and (c) Ru vs. Ir abundance plots. Note the high concentrations of these elements in the mafic block at 420 mblf and the reworked suevite.

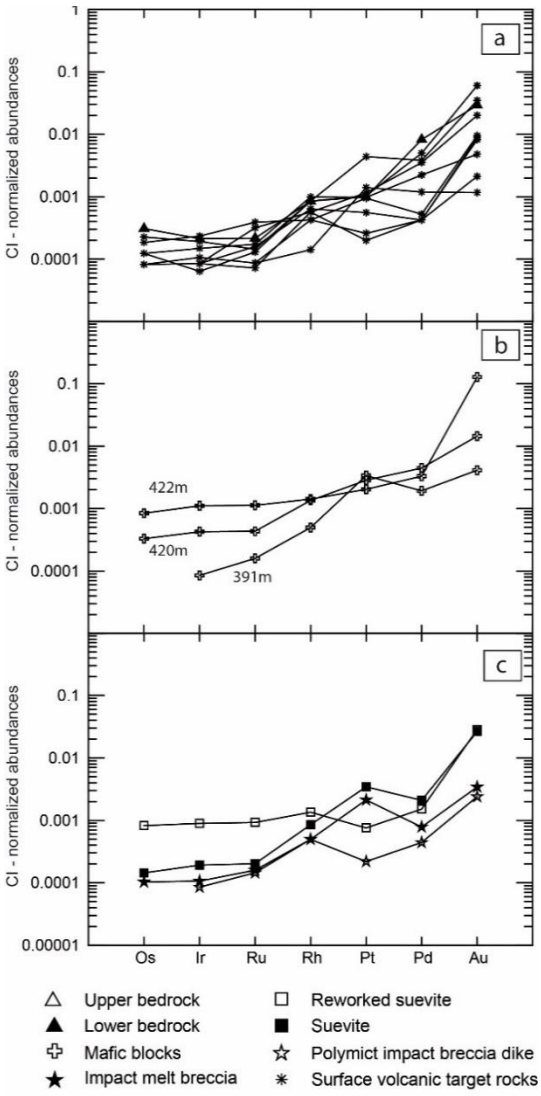

Figure 6.7: CI-normalized PGE plots (normalization values from Lodders 2003) of (a) surface volcanic rocks including rhyolitic ignimbrite, rhydodacitic ignimbrite, andesite, andesitic-dacitic tuff, basalt, and basaltic-andesitic tuff, (b) the three mafic blocks in the ICDP drill core at 391, 420, and 422 mblf depths, and (c) reworked suevite, suevite, impact melt breccia, and polymict impact breccia dike. Note the significantly higher concentrations of Os, Ir, Ru, and Rh in the reworked suevite.

6.5 DISCUSSION

Goderis et al. (2013) analysed a wide range of siderophile element contents in the mafic block at ~391 mblf, in the dike of polymict impact breccia (471 mblf), and in the reworked suevite at 318.9 mblf (named by these authors as "bottom of reworked fallout deposit") of the ICDP drill core. Raschke et al. (2013b) also reported high concentrations of Ni, Cr, and Co for the mafic blocks from the drill core (423 to 391 mblf). Goderis et al. (2013) reported that the $^{187}Os/^{188}Os$ isotopic signal of the mafic block at 391.6 mblf is much more radiogenic (2.8 +/- 0.1) than the reworked suevite (0.148 +/- 0.001 - 0.239 +/- 0.006). This suggests the Os in the reworked suevite cannot be derived from the mafic component. Consequently, the mafic blocks and similar lithologies cannot be the only contributors to the moderate siderophile element budget of the drilled impactites. The Ni/Cr and Cr/Co abundance for some samples are between the values of chondritic and primitive achondritic (ureilitic) meteoritic components, especially for impact glass spherules from outside of the crater. The Ni/Co ratios fall between values for ureilites, brachinites, and chondrites (Warren et al. 2006).

The distribution of spherules in the reworked suevite section is reminiscent of similar impact spherules found in the ICDP drill core LB-5 from the Bosumtwi crater in Ghana (Koeberl et al. 2007). Bosumtwi is a 10.5-km diameter complex impact structure in the same size range as El'gygytgyn. These spherules were preserved in what has been interpreted as the youngest fallback deposit (Koeberl et al. 2007). At Bosumtwi, despite the presence of a high indigenous component linked to ultramafic target rocks, the spherule-bearing deposit shows a slightly elevated and distinct (i.e., unfractionated) PGE signature (Goderis et al. 2007).

Quantitative chemical analysis by EMPA-EDX has indicated that the glasses in these spherules are compositionally heterogeneous (Koeberl et al. 2007a). The detection of the projectile component is a difficult and complicated task, because some of the target lithologies with high PGE contents mask the presence of an extraterrestrial component. For the El'gygytgyn impact crater, Goderis et al. (2013) determined generally very low PGE contents in the impactites (> 50 % under quantification limit) with the result that Ir, Ru, Pt, and Rh are slightly enriched in the reworked suevite and the impact melt breccia, while Pd and Au are not equally elevated. In general, the PGE and Au plots show that the El'gygytgyn samples are generally comparable to chondritic patterns. Based on the slight Ir enrichment with flat, nonfractionated CI-normalized PGE patterns for the reworked suevite, Os isotope ratios for the spherule-bearing deposit that are inconsistent with the target rock composition, and mixing models for the major and Cr, Co, and Ni composition of the spherules characterized by LA-ICP-MS, Goderis et al. (2013) favored an ordinary chondrite (possible LL-type) as the most likely type of projectile for El'gygytgyn.

Foriel et al. (2013) compiled analytical data from Pittarello et al. (2013) of the ICDP drill core and a glass bomb, which was collected at the crater surface. Additionally, these authors used data by Val´ter et al. (1982) and Gurov and Koeberl (2004). Similar to Goderis et al. (2013), Foriel et al. (2013) found an enrichment of siderophile elements (Cr, Co, and Ni) for the suevite of the drill core, but could not substantiate a meteoritic component, because it was not possible to constrain the influence of mafic target rocks (indigenous component). Nonetheless, they found in one of their impact glass samples non-terrestrial Cr isotopic values. Such values are close to those of ureilitic meteorites, but also within analytical error of the range determined for eucrites and ordinary chondrites. These authors concluded that the ratios for siderophile elements did match neither chondritic nor achondritic meteorite compositions. Based on the Cr isotope data, Foriel et al. (2013) favored a ureilite type impactor, although an ordinary chondrite could not be excluded. Other types of meteorites were considered unlikely though.

Here, we present new results on trace element compositions, including siderophile elements, especially the PGE, of the impactites and target rocks from the El'gygytgyn impact crater (Tables 6.2-6.5). The concentrations of the siderophile elements (Cr, Co, and Ni) are typically very low in the felsic volcanics/ignimbrites, but slightly enriched in the mafic target lithologies and extraordinarily high in the three mafic blocks of the drill core (Raschke et al. 2013b, 2014; Pittarello et al. 2013). The siderophile element, as well as the REE abundances and patterns, for the upper and lower bedrock of the drill core correspond to those for suevite samples (Figs. 5a-c, Tables 4, 5). These observations are in agreement with those of Goderis et al. (2013). Therefore, the suevite represents mixtures of all target lithologies in accordance with their regional proportions. The contribution of the mafic target lithologies (~ 7 % based on surface geology, Raschke et al. 2014) to the trace element budget of the suevite is negligible.

Generally, the PGE concentrations (Table 6.3), their ratios (Fig. 6.6), and the CI-normalized PGE patterns (Fig. 6.7) for the suevite are also in the same range as the data for the felsic to intermediate target lithologies. The PGE data confirm the observations based on siderophile element abundances, and, therefore, a meteoritic component could not be detected in the suevite based on trace element data alone. The parautochthonous origin of the lower bedrock drilled in the crater basement, as discussed in Raschke et al. (2013b), could be confirmed by these trace element data. The chemical characteristics of the felsic surface rocks and the lower bedrock are similar and represent the same lithology, namely rhyodacitic ignimbrite.

The reworked suevite at the top of the impactite section of the drill core contains a larger amount of strongly shocked lithoclasts, impact melt particles, and impact glass

spherules, and is chemically characterized by an enrichment of Fe-, Al-, and Mg-oxides compared with all other impactites (Raschke et al. 2013b). Also, the REE concentrations and patterns (Fig. 6.5, Table 6.4) display a slight difference to the suevites and the felsic target lithologies. A comparatively higher proportion of a mafic component in the reworked suevite could provide an explanation for these differences. For this process two different scenarios, or a combination of these, can be imagined: (i) First, suevite is formed as a ground surge inside the inner crater. This is followed by addition of highly shocked clasts from all target rock types, and intercalation of mafic and intermediate rocks especially at the top of the suevite sequence due to debris coming off the collapsing crater rim - besides mixing in of some material from the ejecta plume. (ii) Second, the pre-impact geology of the target volume could have contained a higher proportion of mafic and intermediate rocks than indicated by the crater environs today. This could be supported by the actual stratigraphy of the crater rim (Raschke et al. 2014). The older rocks (felsic ignimbrites of the Pykarvaam Formation) are partly covered in the SE and E of the crater by sub-horizontal layers of younger (Voron'in and Koekvun' formations) basalts and andesites. In addition, phreatomagmatic tuffs of basaltic-andesitic composition occur to the south of the crater (Raschke et al. 2014).

However, the siderophile elements and PGE are significantly enriched in the reworked suevite in comparison to all other impactites and most of the target lithologies (Figs. 6.6, 6.7, Tables 6.3, 6.5). The idea of admixture of a mafic component to form the package of reworked suevite, as mentioned before, cannot explain the high values of Os, Ir, Ru, and Rh found for this unit, in comparison to the composition of the mafic target lithologies (Table 6.3). Only the mafic blocks drilled in the ICDP core, especially the mafic block at ~420 mblf, have significantly enriched PGE values, which are in the range of the PGE values of the reworked suevite. Nevertheless, it is not plausible that a very strong mafic contamination similar to the composition of the mafic blocks would alone be responsible for the high PGE concentrations in the reworked suevite based on mass balance for the major and other trace elements, including the REE and iron (see Figs. 5-7). However, a hitherto undiscovered, additional ultramafic lithology is possible but so far remains hypothetical. Therefore, a contamination by a meteoritic component in this uppermost reworked suevite seems plausible. A combination of the two scenarios described above, a mixing of ground surge suevite with debris (coming off the collapsing crater rim) as well as accumulated material from the ejecta plume with an additional input from meteoritic components and a proportion of basaltic target rocks, would probably be the best-fit hypothesis. This is similar to the findings of Goderis et al. (2013), who also suggested the likely admixture of a meteoritic component to the reworked suevite.

Table 6.6: Average PGE composition of the El'gygytgyn target in comparison to the reworked suevite and calculated mix of impactites and projectiles.

PGE	Average El'gygytgyn target	Reworked suevite (319 mblf)	Average target + 0.12% ureilite	Average target + 0.10% LL chondrite	Average target + 0.07% CI chondrite
ppb					
Os	0.04	0.40	0.40	0.40	0.39
Ir	0.05	0.42	0.34	0.39	0.38
Ru	0.07	0.64	0.51	0.59	0.57
Rh	0.03	0.19	n.a.	0.14	0.12
Pt	1.38	0.76	1.87	2.09	2.05
Pd	0.72	0.89	0.79	1.22	1.11
Au	0.27	4.15	0.30	0.39	0.37

[a]Data based on the average El'gygytgyn target with an admixture of 0.12% average ureilite, 0.10% average LL chondrite, and 0.07% average CI chondrite, respectively.
Data for ureilite (based on 24 samples) by Warren et al. (2006) and for LL and CI chondrites by Tagle and Berlin (2008).
n.a. = not available.

The average PGE concentrations of the El'gygytgyn target (Table 6.6) were calculated using the surface area proportions of the target lithologies from Raschke et al. (2014), and the PGE concentrations of these lithologies from Table 6.3. Based on these data, we attempt to reproduce the PGE content of the reworked suevite, especially the Os, Ir, and Ru concentrations, by mixing the average El'gygytgyn target with different proportions of average ureilite (Warren et al. 2006), LL and CI chondrite (Tagle and Berlin 2008). The best fits for these mixtures, based on a fixed Os concentration according to the content of the reworked suevite, were achieved with an admixture of 0.12 % ureilite, 0.10 % LL chondrite, and 0.07 % CI chondrite component, respectively (see Table 6.6). A comparison between these three meteoritic components shows that the best match could be achieved with admixture of both chondritic components. A better calculation including major and siderophile elements is currently not possible, because the majority of data were measured by XRF and not by INAA or LA-ICP-MS.

A similar finding is revealed by comparison of the Os/Ir and Os/Ru ratios, which are 0.95 and 0.63, 1.23 and 0.82, 1.08 and 0.70, and 1.06 and 0.70, for the reworked suevite, average ureilite, LL, and CI chondrite, respectively (data for ureilites from Warren et al. 2006, and for chondrites from Tagle and Berlin 2008). These results suggest the possible admixture of a chondritic component to the reworked suevite similar to the findings of Goderis et al. (2013). Taking into account the moderately siderophile element ratios reported by these authors for the spherules in the reworked suevite section, an ordinary chondrite component seems to provide the best option as a possible impactor for the El'gygytgyn impact, based on the PGE data.

The method used by Foriel et al. (2013) to determine the nature of projectile component by Cr isotopic measurements would be difficult to use on the reworked suevite samples, because the Cr isotope method is generally capable of detecting only ≥ 1 % extraterrestrial component, whereas PGE abundances allow to determine somewhat lower meteoritic admixtures (in rare cases to about 0.2 %) (cf. Koeberl 2014; Koeberl et al. 2002).

Nevertheless, the uncertainties about the role of the mafic blocks with their relatively high PGE concentrations and their possible contribution to the reworked suevite prevent the unambiguous detection of a meteoritic component. The nature of these impactites requires further investigation.

6.6 CONCLUSIONS

Impact melt breccia found at the surface is obviously a mélange of mainly rhyo(dacitic) ignimbrite and rare basaltic andesite, based on major and trace element compositions. Compared with the drilled rocks, the composition of the suevite and the upper bedrock unit closely matches the impact melt breccia. The PGE content of the impact melt breccia is also similar to that of the suevite sequence between 328 and 391 mblf of the ICDP drill core. Based on PGE analyses, the suevite in the drill core does not show evidence of any unambiguous meteoritic contamination.

The mafic blocks of the drill core (between suevite and lower bedrock) at ~420 and 422 mblf are very unusual in their composition, compared to all other drill core and surface lithologies. Their siderophile and PGE concentrations are much higher than the respective concentrations of investigated basaltic rocks at the surface. The probable enrichment with metal oxides (TiO_2, Al_2O_3, Fe_2O_3, MgO) and trace elements (Sc, V, Cr, Co, Ni, Cu, Zn), as well as the PGE, during a hydrothermal alteration process seems plausible as indicated by a high loss on ignition (LOI) and the strongly altered state of these blocks.

The concentrations of PGE in the reworked suevite are much higher compared to all other impactites. These elevated PGE contents are most likely the result of an admixture of a meteoritic component, probably of chondritic composition – in good agreement with the previous work of Goderis et al. (2013) and Gurov and Koeberl (2004).

Nevertheless, the reworked suevite contains also a higher proportion of a mafic component, as indicated by the REE content, in comparison to the suevite. The composition of this mafic component and its PGE content cannot clearly be determined because of the possible contribution of the chemically unusual mafic blocks to the element budget. Therefore, it is not possible at this stage to unambiguously determine the nature of the meteoritic projectile from the new results of this study either.

Acknowledgments

Funding for the El'gygytgyn drilling project was provided by the International Continental Scientific Drilling Program (ICDP), the U.S. National Science Foundation (NSF), the German Federal Ministry of Education and Research (BMBF), Alfred Wegener Institute (AWI), Deutsches GeoForschungsZentrum Potsdam (GFZ), the Russian Academy of

Sciences Far East Branch (RAS FEB), the Russian Foundation for Basic Research (RFBR), the Arctic and Antarctic Research Institute (AARI) in St. Petersburg, and the Austrian Federal Ministry of Science and Research (BMWF). The Russian GLAD 800 drilling system was developed and operated by DOSECC Inc., and the downhole logging was performed by the ICDP-OSG. The work in Vienna was supported by the Austrian Science Foundation (FWF), project P21821-N19. This work is supported by Deutsche Forschungsgemeinschaft (DFG) grant RE 528/10-2 to WUR and RTS. Special thanks go to the reviewers B. Simonson and S. Goderis for their helpful comments and suggestions to improve the quality of the original manuscript.

Editorial Handling - Dr. Michael Poelchau

Note: This chapter was also updated for more correctness in spelling and grammar. On page 201 the depth values were changed: old: "391, 422, and 420", new: 422, 420, and 391", and "1.16" was applied instead of "1.15" for the value of the Eu-anomaly. On page 208, lines 30-32, additional text was inserted: "mixing of ground surge suevite with debris (coming off the collapsing crater rim) as well as accumulated material from the ejecta plume".

CHAPTER 7

7. GENERAL DISCUSSION

The objectives of this thesis as listed in Chapter 1.1 can be summarized in the following statement: “Petrographic and geochemical characterization and classification of drilled impactites and country rocks from the El’gygytgyn crater toward a better understanding of the cratering process for the formation of this impact structure”. The outcome of this work was published in five peer-reviewed articles (Chapters 2-6) and can be described in short, as the following major topics.

7.1 The obtained drill core material (impactites) and its different stratigraphic interpretations

7.2. The new geological map of the El’gygytgyn impact structure

7.3 Emplacement of basal impact rocks

7.4 Formation of the suevite

7.5 The distribution of shock metamorphism over the entire length of the drill core

7.6 Distinction of impact produced melt and volcanic melt

7.7 Identification of a meteoritic component

7.8 What did this work on the El’gygytgyn impact crater yield with respect to other craters?

7.1 OBTAINED DRILL CORE MATERIAL (IMPACTITES) AND ITS DIFFERENT STRATIGRAPHIC INTERPRETATIONS

The drilling campaign entailed to drill three boreholes at different localities within the crater structure (see chapter 1.1.2). Borehole D1c achieved 52% recovery for lake sediments and 76% for the sequence of impact rocks at 315-517 mblf. For detailed information see Chapter 2 and Melles et al. (2011). In May 2010, an international consortium of impact geologists was invited to form the sampling party, and three of them developed stratigraphic profiles for the drill core. A. Wittmann took 23 samples from the 202 m long drill core material. L. Pittarello obtained ~200 samples, and the PhD candidate for this work ~200 samples. The petrographic observations and geochemical studies resulted in three stratigraphic columns, which are mostly in accordance with each other, in particular between Pittarello and this work. But some significant discrepancies occur as well, especially against that of Wittmann. Figure 7.1 shows the three stratigraphic columns in one chart for a better overview.

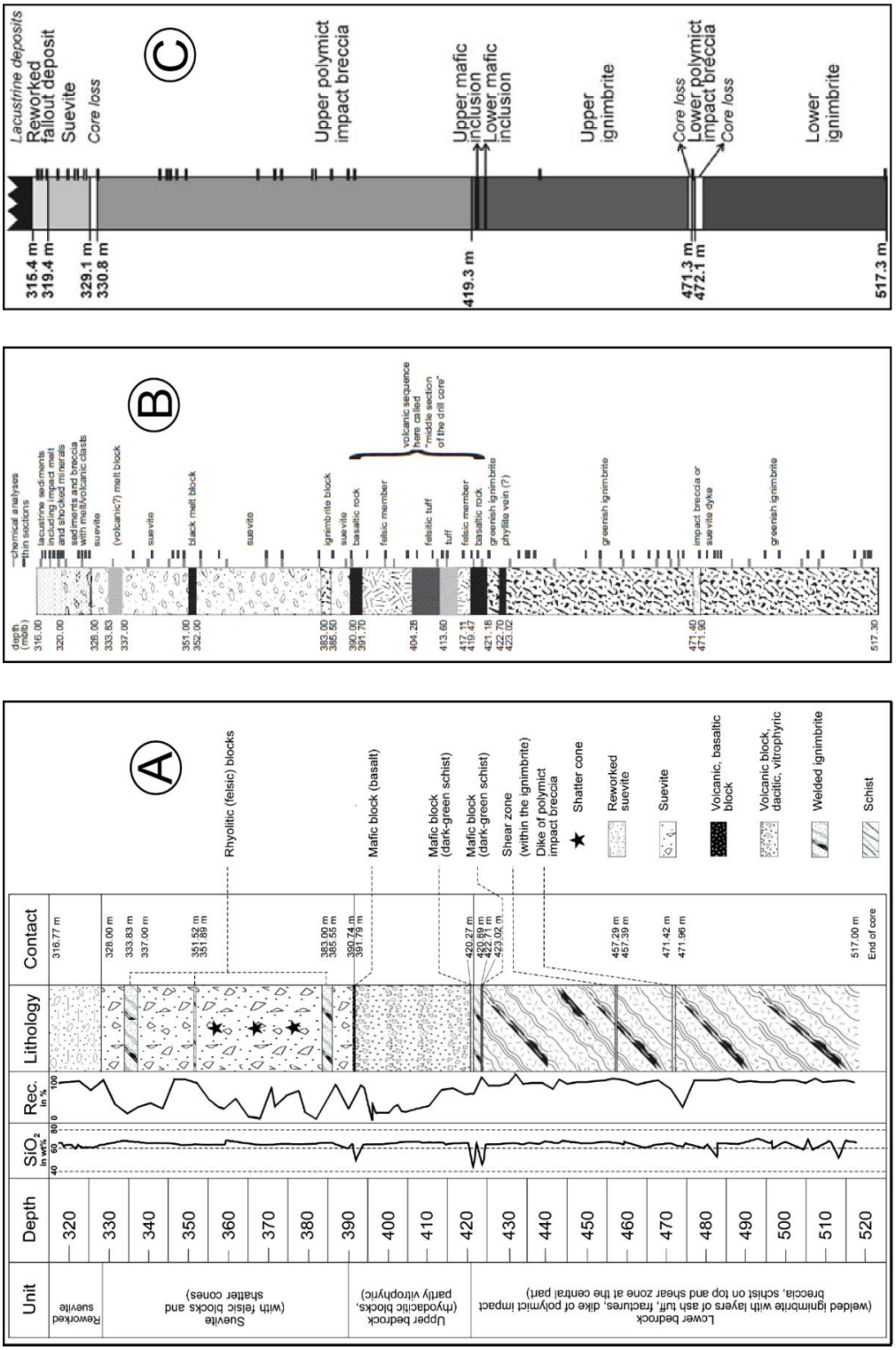

Figure 7.1: Stratigraphic columns for the impactite sequence of the El'gygytgyn ICDP drill core D1c. A) by PhD candidate, published in manuscripts (Chapters 2, 3); B) by Pittarello et al. (2013); C) by Wittmann et al. (2013).

The lithostratigraphy of the drill core developed by the PhD candidate (labeled "A" in Fig. 7.1) and by L. Pittarello (labeled "B" in Fig. 7.1) is based on the study of numerous samples, followed by an extensive discussion, especially about the lithologies and their

subdivision. As a result, the classification of the geological units and their positions within the drill core are similar for most parts.

Pittarello et al. (2013) and Koeberl et al. (2013 – Chapter 2) divided the drill core into three sections: (1) the suevite on top (316-390 mblf) with intercalated lacustrine sediments in the upper 10 m, and locally containing large blocks (up to 40 cm) of melt rocks distributed throughout the profile; (2) a "Middle section" (390-420 mblf) that consists of different volcanic rocks, varying from rhyolitic to basaltic lavas, tuffs, and ignimbrites; and (3) the "Ignimbrite" (420-517 mblf) as short term for the welded rhyodacitic ignimbrite, which dominates the lowermost section. Only for their "middle section" slight differences between their interpretation and that of this work occur (more details in the section below).

Besides these similar interpretations of the stratigraphic order of the drilled rocks, the interpretation of the lithostratigraphy by Wittmann et al. (2013) is partially different and will be discussed here and in Chapter 7.3. This is necessary, because the lithostratigraphy is the basis for the interpretation of the cratering process. The amount of core loss was difficult to estimate in a few cases. As a result, slight differences in the borehole depth need to be considered, when comparing the lithological units or subunits.

The lower bedrock unit can be subdivided into an upper and lower subunit, intersected by a narrow shear zone at 457 mblf. A small (~1 m) dike of polymict impact breccia crosscuts at 471 mblf. This is consistent in all three works. Wittmann et al. (2013) described these units as "upper ignimbrite" and "lower ignimbrite" (419.3 to 517.3 mblf), intersected by a "lower polymict impact breccia" at 471.3 to 472.1 mblf. The classification of the ignimbrite is widely accepted and comparable with this work and the work of Pittarello et al. (2013). However, the separation of this rock type by Wittmann et al. at a depth of ~471 mblf is in contrast to the petrographic and geochemical findings in this work, which reveal a separation of two similar ignimbritic flows at ~457 mblf.

The "Middle section" after Pittarello et al. (2013) is, in general, comparable with the findings of this work for the upper bedrock unit, but differs in detail. In this thesis, an internal stratigraphy has been developed for this unit in the form of a sequence of several pyroclastic flows of more or less vitrophyric character (more detailed information in Chapter 4.5). Pittarello et al. (2013) did not classify various pyroclastic flows, but instead different volcanic rocks, such as "tuff", "felsic tuff", and "felsic members". In strong contrast, Wittmann et al. (2013) included this whole unit into the next, upper unit of "polymict impact breccia" (419.3-330.8 mblf). Basaltic layers (e.g., mafic intrusion in an ignimbrite boulder at 391.66 mblf) also belong to this unit. Additionally, at this depth Wittmann et al. (2013) did not find shock effects in minerals, in contrast to the results of this work (cf. Chapter 3.6).

The stratigraphic columns “A” and “B” for the suevitic units (Fig. 7.1) are almost comparable to each other, except that Pittarello et al. (2013) included the uppermost unit, the reworked suevite into the suevite. However, they also identified this unit as suevite, due to occurrence of impact melt particles and shock effects in minerals, especially quartz. Again, in strong contrast, Wittmann et al. (2013) named this unit the “upper polymict impact breccia” (419.3-330.8 mblf), because they did not find impact melt fragments, but they obtained (only) three clasts with minerals that show possible shock effects. These samples were taken from 390.1, 382.3, and 374.4 mblf, and contain PF and associated feather features, which indicate a peak shock pressure of <10 GPa (Poelchau and Kenkmann 2011).

The uppermost layer, the reworked suevite, was named by Wittmann et al. (2013) as a “suevite” with similar description as in this work and the work of Pittarello et al. (2013). The interpretations for the origin of this unit as a mélange of fallout material from the ejecta plume and lacustrine sediments are similar in all three works.

7.2 THE NEW GEOLOGICAL MAP OF THE EL’GYGYTGYN IMPACT STRUCTURE

During the 2011 expedition to the El’gygytgyn impact crater, hand specimens of country rocks were sampled along the eastern crater rim and later analyzed in the laboratory. The outcome, in comparison with the drilled impact rocks, revealed some differences to previously published work. However, it was mostly possible to confirm the old geological maps of the crater region by Raevsky and Potapova (1984) and Zheltovsky and Sosunov (1985).

The new and relevant results or differences are:

- The impact melt breccia also occurs as meter-size blocks within the 3-m terrace at the southern shoreline, and as smaller pieces (<8 cm) in the pebble ridges around the lake.
- Trachy/rhyolitic ignimbrites in the SE sector of the crater occur in a larger area than known previously and belong mainly to the Koekvun’ Formation. They are the base for the overlying mafic (basalts and andesites) lava flows or tephra (tuff).
- Mt. Otvevergin (NE of the crater rim) does not exhibit intrusive gabbro or monzonite as claimed by Raevsky and Potapova (1984) and Zheltovsky and Sosunov (1985). The analysis shows that, at this place, a rhyolitic ignimbrite occurs. The presence of granodiorite or diorite in close vicinity, as postulated by the same authors, could not be confirmed, either.

- A newly discovered basaltic-andesitic tuff (south of the crater) indicates a phreato-magmatic event. This tuff layer dips shallowly (<33°) to the SE in correspondence with the regional trend.
- Faults across, and boundaries between, the lithological units could not be mapped due to severe Arctic weather conditions and extensive talus cover. Only at the eastern crater rim was it possible to estimate a lithological transition. The fold system according to the previous map(s) could, thus, not be confirmed.
- The rhyolitic and rhyodacitic ignimbrites observed at surface in the El'gygytgyn area are similar in petrographic character and chemical composition to the ignimbrites of the lower and upper bedrock units of the ICDP drill core (D1c). They represent the main target rock type.

7.3 EMPLACEMENT OF BASAL IMPACT ROCKS

The outcomes of the investigation of impactites (Chapters 2, 3, 4, and 6) and target rocks (Chapter 5) allows speculation about scenarios for the cratering process (emplacement and modification) of the El'gygytgyn impact, and the nature of the projectile that formed the impact structure (Chapter 6).

There is a predominance of trachy-/rhyolitic to rhyodacitic ignimbrites in the drilled impactites (lower and upper bedrock, as well as the main clast component of the suevite) and the country rocks. The orientation of volcanic, elongated melt particles (fiamme) in the ignimbrites is sub-horizontal at the SE crater rim (Raschke et al. 2014 – Chapter 5). This is in accordance with the work of Gurov et al. (2007) and corresponds to the gravity controlled, nearly parallel deposition typical for many ignimbrites (Fisher and Schmincke 1984). The drilled lower bedrock unit consists of a similar lithology, but the orientation of the fiamme structures is roughly 45° to the core axis. This implies a tilting of the lower bedrock (as a mega-block) during the crater modification stage. The position of the drill hole at the eastern flank of the central uplift supports the idea that this crater lithology is parautochthonous. In addition, the weakly cataclastic nature of this unit and the occurrence of a shear zone at 457 mblf depth are consistent with a minor, crater modification-related tectonic overprint on the ignimbrite bedrock.

Wittmann et al. (2013) speculated that the drilled section represented a mega-block that could have been derived from a laterally removed site during the collapse of the transient crater cavity. This is based on a scenario by Kenkmann et al. (2004, 2009) for the original position of a drilled mega-block at the Chesapeake Bay impact structure and appears reasonable, at first glance. However, the following arguments show that this idea seems to be implausible on close examination.

At 471 mblf an injected dike of polymict impact breccia occurs. It contains shocked quartz and feldspar grains (Chapter 3 and Pittarello et al. 2013) with PF and multiple sets of PDF. Such injections of impact breccia dikes into the crater floor or central uplift bedrock have been observed at many other impact structures, e.g., the Rochechouart impact structure in France (e.g., Lambert 1981). In contrast, Wittmann et al. (2013) did not find any evidence of shock metamorphism in this dike (they only report subplanar fractures in quartz). They hypothesized that this polymict material could represent a sliver of breccia between two ignimbrite blocks (lower and upper ignimbrite), which possibly was emplaced during lateral transport over a distance of 2-4 km from the transient crater rim. Further, they concluded that an additional argument for the original position of ignimbritic blocks at the crater rim was that these bedrock units are overprinted only (in agreement with this work) by low shock pressure of less than 10 GPa. However, not only at the crater rim occurs such a low shock pressure regime. It can also be expected in lower parts of central uplifts. This hypothesis is supported by numerical models for impact structures of a crater size comparable to that of El'gygytgyn (18 km) - for Sierra Madera (USA, 12-13 km diameter) and a hypothetical impact structure approximately 16 km in diameter by Goldin et al. (2006), as well as for Serra da Cangalha (Brazil, 13 km) by Vasconcelos et al. (2012). These models have shown that material below the crater floor in central parts of these structures can be reasonably expected to incur a shock overprint of the order of <10 GPa. Thus, low shock pressure does not necessarily imply long-distance transport.

A further result is that the lower bedrock unit consists of two ignimbritic flows which are slightly different in their chemical composition and separated by a shear zone at ~457 mblf (and not by the polymict impact breccia dike at 471 mblf, as suggested by Wittmann et al. 2013). The same orientation of the fiamme structures in both flows supports a common pre-impact accumulation of these rocks. In the case of distal transport of these blocks over several kilometers, it would be highly likely that the rocks would be more rotated, with regard to one another. In conclusion, the present work favours that the entire lower bedrock, i.e., the ignimbrite section, is a somewhat rotated and uplifted parautochthonous mega-block with fractures and shear zones, which is still located close to - or at - its original position near the crater center.

The upper bedrock contains a pyroclastic flow with a heterogeneous composition comprising a reddish pumice-rich zone, a blackish vitrophyre-rich zone, and an uppermost zone of a basaltic rock. The contact zones between these subunits are gradual. The different characters of layers within this unit were compared to the typical internal stratigraphy of a pyroclastic (ignimbritic) flow (Freundt and Schmincke 1995; Kobberger and Schmincke 1999). In contrast, Wittmann et al. (2013) defined this unit, including the overlying suevite, as the `upper polymict impact breccia´, which is `blocky debris mostly derived from felsic

volcanics to matrix-supported materials that are mixtures of felsic and mafic volcanics´ (cf. Wittmann et al. 2013, page 1225). This is a correct description for the upper bedrock unit, but it is incomplete. Differences to Wittmann et al. (2013) that are noted for this unit are that it is composed of different pyroclastic flows and not of a polymict impact breccia. Here, it is assumed that the upper bedrock unit represents the crater floor. At the top of this sequence is the lowermost occurrence of shock metamorphism, and the polymict suevite is partially mixed with the uppermost part of the basaltic flow, possibly as a result of turbulent emplacement of the suevite on top of the crater floor.

The two mafic blocks of upper and lower bedrock (at 420 and 422 mblf) are exotic, and perhaps were intercalated by (post)impact crater modification tectonics and influenced by post-impact hydrothermal alteration. The existence of such ultramafic blocks or layers in the pre-impact target cannot be excluded, although there are no hints from the regional geological setting (cf. Chapter 5).

7.4 FORMATION OF THE SUEVITE

The polymict impact breccia between 390.74 and 328 mblf contains two different kinds of melt particles (impact-derived melt and volcanic melt – Chapter 7.6), as well as the full range of shock metamorphic effects occurring in mineral and lithic clasts. Accordingly, this rock type is classified as suevite (after Stöffler and Grieve 2007).

Thirty-nine thin sections from this unit (389.91-328.78 mblf) were analyzed. In seven samples, shocked quartz grains with three or more sets of PDF were found. Eight other thin sections showed evidence of a slight shock overprint in the form of one or two sets of PDF, mostly in quartz, and rarely in feldspar. Pittarello et al. (2013) also found many grains of quartz and feldspar within this unit that show multiple sets of PDF. In summary, the distribution of shock deformation in the suevite interval is relatively heterogeneous; it does not show a specific trend of decreasing abundance with increasing depth (note: the decrease of shock metamorphism for the entire length of the drill core is - in contrast - obvious). It should be noted that Wittmann et al. (2013), in contrast, did not find clear evidence of shock metamorphism, only ’scarce shock metamorphic features’, in 14 samples from this entire interval from 419.30 to 330.80 mblf. They termed this unit ’upper polymict impact breccia’ (cf. Wittmann et al. 2013, page 1225).

Also in this sequence, three blocks of volcanic rocks (large fragments from an ignimbritic flow) occur at around 333.83 mblf, 351.52 mblf, and 383.00 mblf depth. Only the uppermost one is weakly shocked (containing a shatter cone), whereas the other two do not display any evidence of shock deformation.

The heterogeneous distribution of shock effects within the 63 m thick suevite sequence could be the result of an extensive mixing process known as a ground surge within the crater depression (Stöffler et al. 2004). Possibly, the incorporated blocks represent lateral transport of unshocked material from the crater rim, or vertical transport from the crater floor, into the suevite body. Furthermore, the low impact melt content of 1 to 2 vol% is comparable to craters with similar size but other target materials (cf. Bosumtwi with 1.6 to 6.8 vol%; average of ~3.6 vol% impact melt content of, what they termed, the upper impactite unit, see Coney et al. 2007).

The overlying reworked suevite unit reflects the air fall sedimentation from the ejecta plume that was mixed with lacustrine sediments (sand to clay minerals). These sediments are partially sorted (graded) showing at least one fining upward sequence at 318.70 mblf. Wittmann et al. (2013) claimed to have found up to seven cycles in the groundmass of polymict, micro-clastic material. The embedded clasts mostly consist of white to dark-gray tuff (pumice) – in contrast to the suevite below. These clasts and mineral grains show all stages of shock metamorphism, ranging from unshocked to impact melt rock and glass spherule occurrence. Furthermore, detailed petrographic studies revealed an admixture of vapor plume-derived ash to the uppermost meter of this suevitic crater-fill accumulation. The finest ash particles impregnated shrinking cracks, which were likely created by cooling of the surface of the hot suevitic material. A micro-photograph (Fig. 7.2, 318.24 mblf) shows such an ash filled fracture, and additionally, this fracture crosscuts a shocked quartz grain containing PDF of several orientations. Glass spherules were also found in the uppermost

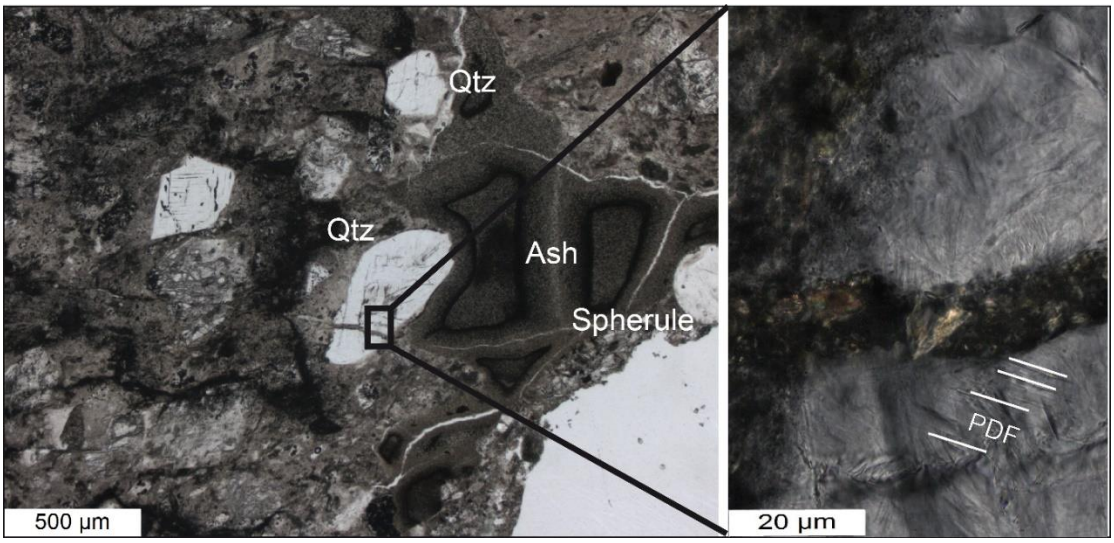

Figure 7.2: Left: Thin section from the reworked suevite at 318.24 mblf, in plane polarized light. In the uppermost meter of suevite shocked quartz grains, ash pockets and glass spherules occur. Right: High-magnification microphotograph of a shocked quartz grain with PDF of several orientations (position indicated in the left image by a black rectangle). Best developed planar deformation feature (PDF) is marked, in cross polarized light. The fracture is filled by fine ash particles, probably generated in the ejecta plume.

meter of this unit. According to the results of Wittmann et al. (2013), the spherules are likely impact produced and formed within the vapor plume. The arguments for this is, that melt droplets were found near nuclear bomb test sites, in the vicinity of terrestrial impact craters and in lunar samples (Wittmann et al. 2013, and references therein). For the latter, laboratory experiments were undertaken to constrain the crystallization conditions of such lunar spherules. Symes et al. (1998) proposed that these particles were probably formed by large (basin-forming) impact events during their residence in large ejecta plumes.

The lithostratigraphic occurrence of glass spherules and ash at the top of the suevite, as well as the increasing intercalation of the amount of post-impact lake sediment upward, indicate relatively continuous accumulation (see Chapter 3). This infers that the crater formation, and the formation of suevite, were continuous. At this point, the model of secondary suevite formation by Stöffler et al. (2013) and Artemieva et al. (2013) seems inapplicable for the El'gygytgyn crater. A secondary ejecta plume would be accompanied by a large scale, chaotic mixing process within the internal stratigraphy of the suevitic units.

7.5 THE DISTRIBUTION OF SHOCK METAMORPHISM OVER THE ENTIRE LENGTH OF THE DRILL CORE

In general, the quality and quantity of shock metamorphic effects decreases rapidly from the top as depth increases over the whole ~200 m sequence of impactites, only the suevite sequence (~93 m) is heterogeneous in their shock occurrence. The resulting implications for crater modification and emplacement of impactites are discussed above (Chapter 7.3). The unshocked lower bedrock corresponds to the parautochthonous crater basement; the upper bedrock with rare evidence of shock deformation to the transient crater floor, and the suevitic units with stronger shocked material represent the crater fill.

The uppermost occurrence of shock features in the impactite section occurs at the top of the drilled impact rocks, in the reworked suevite. The underlying suevite is highly heterogeneous. Strongly shocked mineral grains and impact melt particles occur together with low- to unshocked mineral fragments and lithic clasts. In the upper and lower bedrock, mineral grains with shock features (PDF) occur very infrequently; this signifies a very low shock level. The lowermost shock feature was identified at 391.72 mblf. (top of the upper bedrock unit). Wittmann et al. (2013) noted, like the author and Pittarello et al. (2013), that the shock level in the bedrock samples of core D1c is very low at generally <10 GPa. Wittmann et al. (2013) used this as an argument for their hypothesis that these bedrock sections derived from the outer part of the crater structure – refuted in section 7.3 above.

7.6 DISTINCTION OF IMPACT PRODUCED MELT AND VOLCANIC MELT

Melt is a general feature of impact structures, in particular of large ones. The generation of impact melt is caused by two different processes. Firstly, shock melting of rock-forming minerals occurs during the contact and compression phase with pressure exceeding 45-60 GPa (Kenkmann et al. 2014). After unloading of the shock pressure, the associated post-shock temperatures may exceed the melting temperature of the target rock minerals. The products of this process range from tiny glass spherules, through melt fragments/bodies within suevite, up to thick sheets of coherent impact melt. The volume of produced impact melt rocks is directly correlated to the volume of the transient crater cavity (Grieve et al. 1977). In the case of small craters, the impact melt is a small proportion of the transient crater volume. It is thought that at first a heterogeneously distributed and thin melt sheet forms on the crater wall, which is then redistributed by the mass movements during the modification stage (ground surge, slumping of blocks from the crater rim, etc.). In the case of larger impact structures, the preservation of a thick (up to several kilometers thick) melt sheet is possible. For example, the Popigai crater in Russia with a diameter of ~ 100 km contains a 600 m thick melt sheet (Masaitis 1998). The ~1850 Ma old Sudbury impact structure in Canada has a 2.5-3.0 km thick melt sheet that is well known as “Sudbury Igneous Complex” (Therriault et al. 2002).

Another process for the generation of melt is frictional melting during coseismic faulting, gravitational sliding, and perhaps decompression related processes upon rise and collapse of a central uplift (e.g., Kenkmann et al. 2014; Mohr-Westheide and Reimold 2011; Reimold et al. 2016). The result is the formation of what is historically and non-discriminatingly known as “pseudotachylite”. In 1916, Shand used the (old spelling) term “pseudotachylyte” for the enigmatic melt breccias of the Vredefort Dome. Today, ‘‘pseudotachylite’’ is reserved in structural geology for friction melts only. For such breccias in impact structures, the genetic process(es) is(are) still under debate, and a number of different scenarios are possible for formation of such breccias in impact structures. These processes are: i) Genesis under compression and immediate decompression during the early stage of cratering (formation of shock veins). ii) Friction melting. iii) The combination of compression and friction melting. And iv) The frictional movement of large blocks during the modification phase of the cratering process, at the time when central uplifts form and collapse. For detail, see Mohr-Westheide and Reimold (2010, 2011) or Reimold et al. (2015, 2016). Reimold (1995) coined the term ’pseudotachylitic breccia (PTB)’ for such rocks whose genesis cannot be resolved easily, and that should be used until such time that formation as a specific breccia type (friction melt = pseudotachylite, impact melt injection, cataclasite/ultracataclasite of impact or non-impact origin, etc.) has been determined.

7.6.1 The Impact Produced Melt Volume in Drill Core D1c

The production of melt depends on the impact velocity, the impact angle, the size and composition of the projectile, and the lithological properties of the target rocks. An output of this thesis work is that the El'gygytgyn impact structure has a relatively small volume of impact-produced melt. In detail, a low impact velocity, and a very low angle of impact (~15°) would yield a relatively small volume of impact melt in the crater (e.g., Pierazzo and Melosh 2000). However, the nearly circular shape of the El'gygytgyn crater is in contradiction with a very low angle of impact. The shape of the crater cavity becomes ellipsoidal for impact angles below 10-15° to the target surface (Gault and Wedekind 1978; Bottke et al. 2000). In the case of El'gygytgyn, an impact angle of nearly 15° could satisfy the case of melt poor suevite and a roughly circular crater shape.

The composition, density and water content of the target rocks are also very important for the formation of impact melt. Wittmann et al. (2013) pointed out that, if the target rock suite consisted of porous ignimbrites, lavas, and tuffs, comparable with water-saturated sediments, then a coherent impact produced melt sheet could have been dispersed and much of the melt ejected (see also Kieffer and Simonds 1980). Furthermore, they concluded that 'this may explain the eroded fragments of impact melt that occur with sizes up to approximately 1 m in terrace outcrops of the crater (e.g., Gurov et al. 2005), whereas the largest confirmed impact melt fragment in the drill core is smaller than 1 cm' (ibid. page 1218). The present work is in agreement with the statement by Wittmann et al. (2013) and has also shown that the blocks of impact melt breccia on the lake terrace are likely derived from the dispersed impact melt. But, in contrast to Wittmann et al. (2013), impact melt clasts of up to 40 cm size have been found within the uppermost suevitic breccia of the drill core (Chapter 2). Further, it is agreed with Wittmann et al. (2013) that the position of the drill site at the flank of the central uplift (Gebhardt et al. 2006) allowed sampling of only a relatively thin layer of suevite, because most material could be accumulated in lower parts of the ring syncline. However, a similar poor melt content in the crater suevite is well known from the Bosumtwi crater (Coney et al. 2007). A further comparison with focus on the outer suevite is not possible, because in the case of El'gygytgyn, deposits outside the crater were completely removed by the intense arctic erosion and denudation processes.

Calculation of the volume of impact-produced melt is always a difficult task and needs (for accuracy) a site-specific numerical model for each impact event. Nevertheless, Wittmann et al. (2013) attempted to calculate the possible thickness of impact melt, based on a 1 vol% impact melt contribution to the suevite, combined with the thickness of the suevite and reworked fallout deposits, and obtained a 1.4 m thick layer of impact melt across the structure. Notably they made the calculation with a combined thickness of 13.7 m (suevite

and reworked suevite). On the contrary, this work yields a combined thickness of 75.02 m of suevitic breccias, which is roughly 5 times greater than the value proposed by Wittmann et al. (2013). This means that the thickness of a possible melt layer should be much larger than the 1.4 m proposed by them. Seismic refraction and reflection data were acquired during two expeditions in 2000 and 2003. A breccia that was interpreted as allochthonous fallback (suevite) occurs beneath the lake sediments, which has a thickness of 100 m on top of the central rise, increasing to 400 m thickness in the surrounding basin (Gebhardt et al. 2006). The drill core recovery of ~75 m of suevitic breccia is slightly less than the proposed thickness. Possible reasons are core loss and the position of the drill hole on the flank of the central uplift structure.

7.6.2 Occurrences of Melt at El'gygytgyn Crater

The distinction of volcanic melt and impact melt was a complex task in the context of this study of the El'gygytgyn crater (cf. also Pittarello and Koeberl 2013a). In contrast to the majority of other impact craters on Earth that formed in non-volcanic targets, at El'gygytgyn a proper classification of melt particles is a fundamental requirement for the distinction of impact-generated and volcanic melt material. Impact melt occurs in the lacustrine terraces in the form of blackish impact glass bombs or cobbles (Gurov et al. 1995, Chapter 4 and 5), blackish to brownish blocks of impact melt breccia (Fig. 7.3; Pittarello et al. 2013, and Chapters 4 and 5), and micro-spherules or glass beads (Wittmann et al. 2013, Chapter 4).

7.6.2.1 Glass Bombs and Blocks of Impact Melt Breccia

Aerodynamically shaped glass bombs occur together with rounded pebbles (2-15 cm in size) of impact breccia on the recent terraces inside the crater, and also in terraces along some streams in the environs of the crater, e.g., along the Enmyvaam River (Gurov et al. 1978, 1979a; Smirnov et al. 2011; Pittarello and Koeberl 2013a; this work, Chapter 5). All recorded types of impactites are generally fresh, and do not display significant post-impact hydrothermal alteration and weathering (Gurov et al. 1979a, 1979b; Gurov and Koeberl 2004). Petrographic analysis of these impactites has revealed various impact-induced shock features. Planar fractures (PF), planar deformation features (PDF), and diaplectic glass of quartz and feldspar were identified by Gurov et al. (1978, 1979a, 1979b, 2005) and in this work (Chapter 5) in quartz phenocrysts of shock metamorphosed glassy rhyolite (liparite) and andesite. High-pressure polymorphs of quartz (coesite and stishovite) were identified in two specimens of rhyolitic tuff (Gurov et al. 1979a).

Impact melt breccia occurs as blocks of up to meter size. Gurov and Koeberl (2004) described several places of accumulation of impact melt breccia and glassy bombs along the entire lake shoreline. However, during the 2011 expedition such blocks were only found at the recent 3 m terrace in the SE sector. These blocks show a scoria-like mélange of dark glassy

schlieren with lithic clasts (up to 30 cm long) and brownish scoria-like parts with large, whitish phenocrysts of centimeter size. These rocks are extremely porous and sharp-edged at freshly broken surfaces. All melt phases contain mineral clasts that were not completely molten. Within these clasts (especially in quartz), evidence was found for shock metamorphism in the form of planar fractures (PF), planar deformation features (PDF), and diaplectic glass. Geochemical studies reveal that impact melt breccia is obviously a mélange of mainly rhyo(dacitic) ignimbrite and rare basaltic andesite, based on major and trace element compositions. Compared with the drilled rocks, the composition of the suevite and the upper bedrock unit closely match these impact melt breccias. The PGE content of the impact melt breccia is also similar to that of the suevite sequence between 328 and 391 mblf of the ICDP drill core (cf. Chapter 6). These blocks of impact melt breccia may have been part of a larger body of clast-rich impact melt rock (after Stöffler and Grieve 2007) within the inner crater and at the top of the melt-poor suevite. Due to erosion and remobilization (e.g., solifluction, lake ice drift and break water at the shore line), blocks of impact melt breccia could have been separated and incorporated into the post-impact crater-fill. Please note that the highest (post-impact) lake level was roughly 40 m higher than today, as evidenced by the proposed 40 m terrace (Glushkova and Smirnov 2007).

Pittarello et al. (2013) investigated impact glass bombs and impact melt breccia that were collected during the drilling campaign in April 2009. They divided the samples into two main groups: type 1, a mainly pure, blackish impact melt glass (partially porous and pumice-like with whitish melt blebs), and scoria-like type 2 samples that contain unmelted portions of lithic breccia incorporated into black-brownish, homogeneous bands of glass. They analyzed, via electron microprobe, a schlieren-structure within type 1 (blackish glass) and interpreted this as immiscibility of Fe and Si within the melt fragment. The present work has also detected, by electron microprobe, bands of high Fe-content within a melt particle from a sample of a meter-sized block of impact melt breccia (Chapter 5). The type 2 melt breccia is very similar to the description of the large blocks of impact melt breccia, but with lenticular shapes and unsorted angular clasts, with random orientation, embedded in a brownish matrix. The microanalysis shows additional features, such as a chilled margin within the transition from glass parts to the melt breccia bands. In both types of melt shock features (PF, PDF) occur commonly, as detected during this work. For type 1, Pittarello et al. (2013) interpreted the homogeneous melting as formation of impact melts during the early stages of the impact process (excavation). The melts of type 2 differ in their thermal history and were interpreted as early formed - excavated and aerodynamically transported - melt mixed with impact melt breccia intercalations, derived from the crater floor.

In summary, this present work, as well as the work by Pittarello et al. (2013), has found two different kinds of impact melt: A pure, blackish glass and a scoria-like breccia with

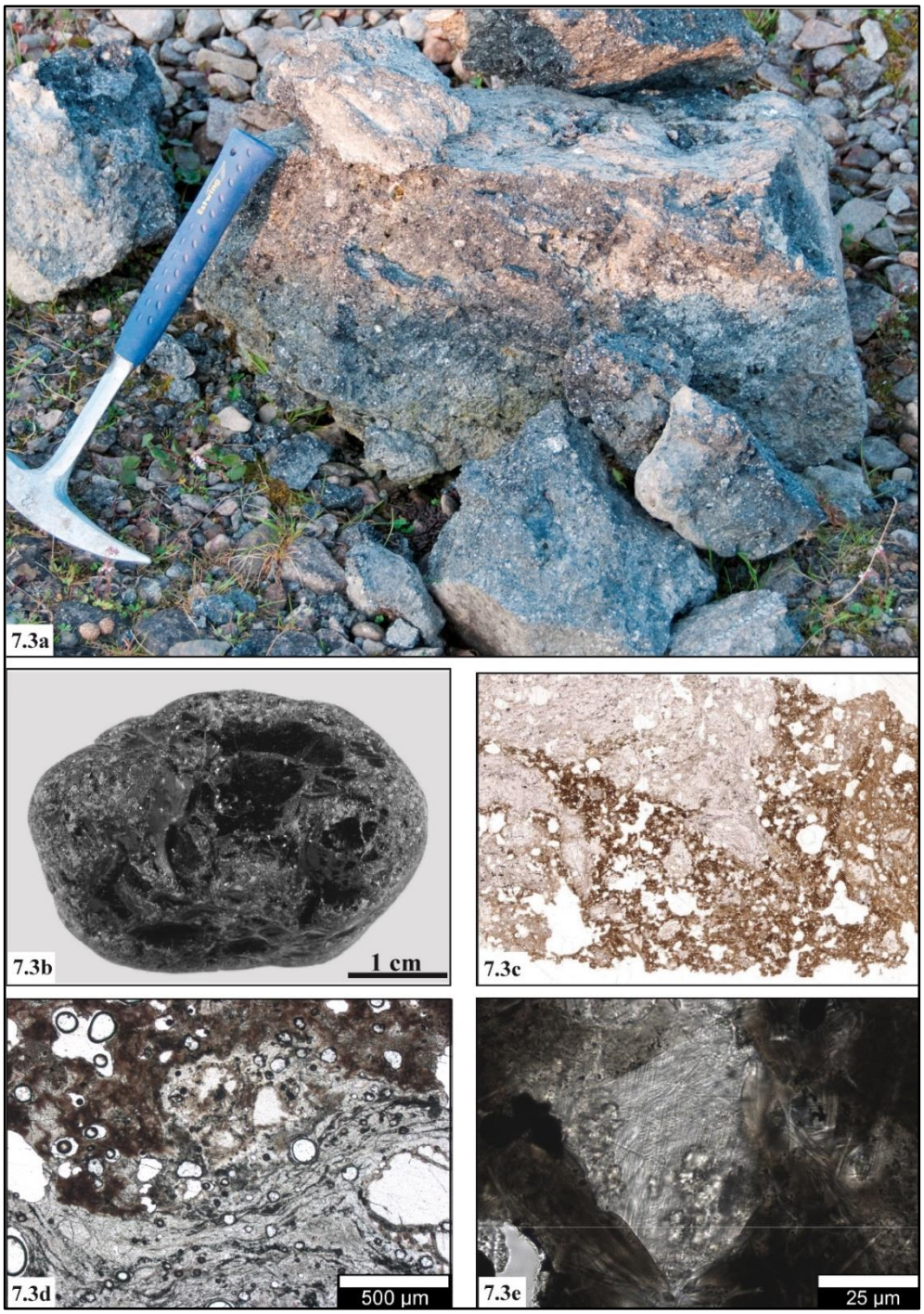

Figure 7.3 (a-e): Impact melt breccia: a) Block of impact melt breccia at the SE shoreline (GPS: 551863/7483086, UR-2011_9.10). Note the scoria-like texture with black glassy "schlieren" and porous parts with inclusions of light colored crystal fragments. b) Round pebble of impact melt breccia, sampled at the southern lake terrace. c) Thin section scan (length 3 cm) of sample UR-2011_9.11, another, similar block of impact melt breccia. Two different kinds of melt are visible (brownish and translucent), both with a high content of vesicles. d) Close-up of the same thin section (under plane polarized light) emphasizes the contact between the glassy, translucent and brownish melts. e) Two sets of planar deformation features (PDF) in a small quartz grain embedded into the brownish part of impact glass (UR-2011_9.11, microphotograph taken with plane polarized light). This figure was published as Fig. S8 of the supplementary material of Chapter 5.

glass particles. The first one was probably generated during the excavation process and later accumulated as fallback ejecta, within and around the crater. Hence, the occurrence of impact glass as the highest shocked stage and the clearly aerodynamically modified shape of these rocks. Type two is a mixture of lenses of impact melt breccia that are embedded in silicate glass, probably as a result of inclusions of unmelted, rigid impact debris within the melt flow.

On the other hand, it is also possible that the pebbles of melt type 1 were not aerodynamically formed, and rather are eroded parts from large blocks of impact melt breccia, similar to what we have found at the recent shoreline. Furthermore, these pebbles are more resistant against erosion than the lithic and brecciated parts of the scoria-like breccia. So, it is still possible that only one type of impact melt breccia formed during the cratering process and later, post-impact, two separate types developed in the course of erosion.

7.6.2.2 Impact Melt of the Drill Core

The groundmass of the uppermost suevite in D1c also contains micro-fragments of the volcanic rocks forming the larger clasts, besides single crystals of their minerals and small melt particles. These particles exhibit different colors and sizes (0.1 to 5 mm). Brownish, small, round to angular melt particles occur together with light colored, relatively larger, sometimes elongated melt fragments. Electron microprobe analysis (see Chapter 3) provided detailed information on the nature and origin of these different melt particles, whether they are derived from the volcanic target rocks or they could represent impact-melted material.

Impact melt appears as holohyaline particles or glassy “schlieren” in a fluidal-textured groundmass and has generally a rhyolitic composition. The melt is vesicle-rich and has inclusions of diaplectic glass and of shocked mineral grains with PDF (see also Pittarello and Koeberl 2013b, c). Thus, it can be concluded that these particles are impact-produced melt. These shock effects were not found in confirmed volcanic melt fragments (e.g., pumice of the ignimbrites) from the drilled bedrocks or from the crater rim. Gurov et al. (1978, 1979a, 1979b, 2005) found hand specimens of rhyolite (liparite) on the lake terraces, which showed shock metamorphism. In summary, the amount of impact melt fragments within the suevitic units is very low, at <<1 vol. %. However, it is and remains very difficult to separate impact induced melt from volcanic melt, where specific shock-textural indicators are missing (Chapter 3).

Recently published results by Pittarello et al. (2015) show that it may be possible to discriminate impact produced melt from volcanic melt via Cathodoluminescence (CL), combined with an optical microscope and SEM (SEM-CL). They analyzed six samples of impact breccia, including non- to strongly shocked clasts of the target rocks from the lake terrace and the ICDP drill core D1c. The impact generated melts display a very low luminescence (SEM-CL) in comparison to the unshocked volcanic rocks from the crater. Peak

shock pressure was inversely correlated to the intensity of luminescence that is decreasing with increasing shock pressure, as supported by CL spectral analysis. This might have been caused by the progressive destruction of the crystal lattice of the rock-forming minerals due to the passage of the shock front. It may also be due to devitrification and recrystallization of impact melt in comparison to the groundmass of the significantly older volcanic target materials (see Pittarello et al. 2015). However, this new method of melt analysis should be tested with more impact melt samples from this site, and also from other impact structures, and volcanic rocks to assess its wider applicability.

7.6.2.3 Spherules

Besides the discussed melt particles, glass occurs in the form of spherules that were found both in the groundmass of the uppermost part of the drill core, as well as in the lake and river terraces. There are two types of spherules. Firstly, the most abundant type of spherules has a glassy margin and may contain some crystal inclusions or micro-fragments of different minerals (e.g., quartz and feldspar, or zeolite). The other type of spherules is filled by aluminosilicate glass that contains some crystals with feldspathic or mafic composition (Chapter 3). Based on the chemical results presented in Chapter 3, it seems certain that these spherules were produced during the impact process and deposited directly from the ejecta plume (see also Wittmann et al. 2013). Impact spherules are droplets, which incorporate components of target rocks and, possibly, projectile material (Symes et al. 1998). Impact spherules were also found in the ICDP drill core LB-5 from the Bosumtwi crater in Ghana. This complex crater has a size of 10 km diameter, which is roughly the same size as El'gygytgyn. The spherules were preserved in what has been interpreted as the youngest fallback deposit (Koeberl et al. 2007), together with tiny accretionary lapilli and plenty of shocked quartz. Quantitative chemical analysis by EMPA-EDX indicates that the glasses in such spherules of the Bosumtwi crater (Ghana) are compositionally heterogeneous. So, glass spherules are a common feature for the latest deposits of impact-produced ejected material, likely originating from the ejecta plume.

7.6.2.4 Volcanic Melt of the Crater Rim and from the drilled Rocks

The lower bedrock unit of the drill core, as well as the majority of the crater rim is formed of rhyolitic to rhyodacitic ignimbrite. Elongated and flattened pumice fragments (fiamme) of up to 3 cm width and up to 8 cm length are typical for this rock. Fiamme are lens-shaped particles, usually millimeters to a few centimeters in size. These brownish to blackish glassy melt particles contain the same minerals that occur in the groundmass of these small bodies, where they typically constitute a eutaxitic texture. Furthermore, the pumice fragments have an irregular, interfingering contact to the surrounding micro-crystalline matrix and show remnants of gas bubbles (see also Pittarello et al. 2013). These vesicles have a rim

of glass, which is often devitrified and altered to a reddish color. This is characteristic for a welded ignimbrite (e.g., McBirney 1968; Kobberger and Schmincke 1999; Pittarello et al. 2013). Generally, the pumice fragments are moderately altered and some show a greenish alteration color, which is caused by the presence of chlorite along the contact to groundmass. Smaller (<5 mm) melt particles are mostly altered to chlorite and other phyllosilicates. The typical composition and shape of such fiamme structures is a criterion for the distinction of volcanic melt from impact melt.

7.7 IDENTIFICATION OF A METEORITIC COMPONENT

For the determination of an extraterrestrial projectile component, samples from all drill core lithologies and country rocks from the crater rim were selected. They were analyzed by X-ray fluorescence spectroscopy (XRF) for siderophile elements, instrumental neutron activation analysis (INAA) for many trace elements, including the REE, and by inductively coupled plasma-mass spectrometry (ICP-MS) for PGE and Au.

7.7.1 Siderophile Elements

The concentrations of the siderophile elements (Cr, Co, and Ni) are typically very low in the felsic volcanics/ignimbrites, but slightly enriched in the mafic target lithologies, and very high in the three mafic blocks of the drill core, especially the one occurring at 422 mblf (this work, Chapters 3 and 4, and Pittarello et al. 2013). The concentrations of the siderophile elements and their ratios within the suevite are quite similar to the respective concentrations and ratios in the lower and upper bedrock. The concentrations of siderophile elements reported for impact melt rocks and glass bombs collected at the surface around the crater are also in this range, with concentrations of <50 ppm Cr, <7 ppm Co, and <21 ppm Ni (Gurov and Koeberl 2004; Gurov et al. 2005). Therefore, a contamination of the suevite and the impact melt rocks by a meteoritic component is not obvious in these siderophile element abundances (see this work, Chapter 6).

Goderis et al. (2013) reported that the $^{187}Os/^{188}Os$ isotopic signal of the mafic block at 391.6 mblf is much more radiogenic than the reworked suevite. They concluded that the mafic blocks and similar lithologies cannot be the only contributors to the budget of the moderately siderophile elements of the drilled impactites. The Ni/Cr and Cr/Co abundances for some samples are intermediate between the values of chondritic and primitive achondritic (ureilitic) meteoritic components, especially for impact glass spherules from outside of the crater. The Ni/Co ratios fall between values for ureilites, brachinites, and chondrites (Warren et al. 2006).

Foriel et al. (2013) also found an enrichment of siderophile elements (Cr, Co, and Ni) for the suevite of the drill core, as compared with felsic volcanic rocks in the lower part of the core and from surface samples. But they could not substantiate a meteoritic component with

this method, because it was not possible to constrain the influence of mafic target rocks on the target component. Nonetheless, they found a non-terrestrial Cr isotopic value in one of their impact glass samples. This value is close to those of ureilitic meteorites, but also within analytical error of the range determined for eucrites and ordinary chondrites. These authors concluded that the ratios for siderophile elements did not match chondritic or achondritic meteorite compositions. Based on the Cr isotope data, Foriel et al. (2013) favored a ureilite type impactor, although an ordinary chondrite could not be excluded. Other types of meteorites were considered unlikely though.

Wittmann et al. (2013) focused on impact spherules from the drill core (uppermost suevite) and others that were collected on the terraces along the Enmyvaam River (~ 20 km south of the crater). Additionally, they analyzed samples of impact melt breccia from the lake terrace. They measured variable abundances of siderophile elements and high Ni contents of 300 to 2000 ppm for the impact spherules (from both locations) in comparison to the other target lithologies, and suggested that this could be derived from the meteoritic projectile.

7.7.2 Platinum Group Elements (PGE) and Rare Earth Elements (REE)

The Ir contents of the target rocks vary between <0.03 and 0.52 ppb (Table 6.3 and Figures 6.6 and 6.7). The Ir concentrations of the felsic lithologies are generally low (<0.10 ppb). Higher Ir contents (0.52 ppb) were measured for the basaltic target lithologies, especially for the highly altered and metal oxide enriched mafic blocks at ~420 and 422 mblf in the drill core. High Os concentrations follow this Ir trend, but there are also elevated concentrations of Pt, Pd, and Au that are typical of many mafic lavas (e.g., Barnes et al. 1985; Tredoux et al. 1995; McDonald 1998; Crocket 2002).

The Ir contents of the suevite, impact melt breccia, and polymict impact breccia dike samples are in the range of 0.04-0.09 ppb, and in good agreement with data previously obtained by Goderis et al. (2013), who determined a range from 0.05 to 0.20 ppb for similar samples. Gurov and Koeberl (2004) reported Ir concentrations of 0.02-0.11 ppb for impact melt rocks and glass bombs from El'gygytgyn, which also correspond well with these new measurements.

The reworked suevite has a significantly higher Platinum Group Element (PGE) concentration in comparison to the suevite, impact melt breccia samples, and polymict impact breccia dike, as well as most of the felsic and mafic target lithologies (Table 6.3), in terms of Os (0.40 ppb), Ir (0.42 ppb), Ru (0.64 ppb), and Rh (0.19 ppb) (Table 6.3). These values are very similar to those for the mafic block at ~420 mblf, but also considerably increased in comparison with the mafic blocks at ~391 and 422 mblf. The Os/Ir ratio of the reworked suevite is higher (~1) compared to the values for the mafic blocks at ~420 and 422 mblf (~0.8; an Os/Ir-ratio <1 is typical for mafic magmas; Barnes et al. 1985). The Rare Earth Element

(REE) concentrations (Chapter 6) cannot provide a hint for the presence of a projectile component; nevertheless, they display a slight difference between the reworked suevite, on the one hand, and the suevite and felsic target lithologies, on the other (Chapter 6). This is interpreted to indicate a comparatively higher proportion of mafic component in the reworked suevite. A comparatively higher proportion of a mafic component in the reworked suevite would provide an explanation, in part, for these differences between reworked suevite and the underlying suevite. To achieve this, two different scenarios, or a combination of these, can be imagined: (i) First, the suevite is formed as a ground surge inside the inner crater. This is followed by addition of highly shocked clasts from all target rock types, and intercalation of mafic and intermediate rocks, especially at the top of the suevite sequence, due to debris coming off the collapsing crater rim. Besides this, some material from the ejecta plume would also be incorporated. (ii) Second, the pre-impact geology of the target volume could have contained a higher proportion of mafic and intermediate rocks than indicated by the crater environs today. This could be supported by the actual stratigraphy of the crater rim (Chapter 5) that includes a comparatively higher abundance of basalts and andesites in the SE and E area of the crater. A hitherto undiscovered, additional ultramafic lithology is possible, but so far remains hypothetical. So, it seems unlikely that a very strong mafic contamination, similar to the composition of the mafic blocks, would be solely responsible for the high PGE concentrations in the reworked suevite (see Chapter 6). Therefore, contamination by a meteoritic component in this uppermost reworked suevite remains possible. A combination of target rock mixing during crater collapse with additional input from a meteoritic component and a proportion of basaltic target rock would probably be the best hypothesis. This is in good agreement with the previous work of Gurov and Koeberl (2004), who also suggested the likely admixture of a meteoritic component, probably of chondritic composition.

Goderis et al. (2013) determined generally very low PGE contents in the impactites - with the result that Ir, Ru, Pt, and Rh are slightly enriched in the reworked suevite and the impact melt breccia, whereas Pd and Au are not equally elevated. The slight Ir enrichment shows flat, not fractionated CI-normalized PGE patterns for the reworked suevite. In general, the PGE and Au plots show that the El'gygytgyn PGE systematics are generally comparable to chondritic patterns. The Os isotope ratios for the spherule-bearing deposit are inconsistent with the target rock composition., On that basis and supported by mixing models for the major elements and Cr, Co, and Ni contents of spherules characterized by LA-ICP-MS, Goderis et al. (2013) favored an ordinary chondrite (possible LL-type) as the most likely type of impactor for El'gygytgyn.

7.7.3 Mixing Calculations

The calculation of the PGE content for the mixing calculation is based on the proportions of the target lithologies in the crater area and their respective PGE concentrations. An attempt was made to reproduce the PGE content of the reworked suevite, by admixture of different proportions of typical meteorites: Ureilite (Warren et al. 020063), LL-, and CI–chondrite (Tagle and Berlin 2008). The result is that the best match could be achieved with an admixture of either chondritic component (Table 6.6). This is similar to the findings of Goderis et al. (2013) for the PGE content, as well as for the moderate siderophile element ratios from spherules in the reworked suevite section.

Foriel et al. (2013) used Cr isotope measurements to determine the nature of the projectile component. However, this method is only suitable for a relatively high amount of extraterrestrial component above about 1%, whereas PGE abundances allow determining somewhat lower meteoritic admixtures (in rare cases to about 0.2 %) (cf. Koeberl 2014; Koeberl et al. 2002). However, the mafic blocks with their high PGE concentrations and their possible contribution to the reworked suevite prevent the unambiguous detection of a meteoritic component. The chemical nature of these impactites requires further investigation.

7.8 WHAT DID THIS WORK ON THE EL'GYGYTGYN IMPACT CRATER YIELD WITH RESPECT TO OTHER CRATERS?

Impact structures in siliceous volcanic targets are very rare and mostly deeply eroded, or buried under sediments or colluvium. Thus, El'gygytgyn impact crater is outstanding and the best studied crater of this type on Earth. Volcanism and impact cratering are the most important geological processes on the planetary scale (Melosh 1989). The surface-near geology of all other terrestrial planets of our solar system (e.g., Earth, Mars, Venus) is also dominated by impact cratering processes (French 1998). Earth´s hydrosphere and atmosphere were formed by degassing of the Earth, a process largely accomplished by volcanic eruption (Fisher and Schmincke 1984). Through the existence of an atmosphere and liquid water on Earth, a complex system of erosion, transport and sedimentation processes could be established. This is not unique in our solar system. Mars had a significant hydrosphere with aqueous erosion and transport (Carr 1996). Titan has a methane based 'hydrosphere' with seas, rivers, rain and erosion (Lorenz and Lunine 1996). The other important process for planetary geology is the impact of asteroids and comets. The comparability of terrestrial and planetary impact structures, as well as the analogies of impact processes in different target rocks, play a major role in current impact research. The extensive study of such impact craters as El'gygytgyn can provide a wider and better insight into the geology of impact structures in volcanic targets.

The results of this thesis and from other researchers of the El'gygytgyn scientific party suggest that the fundamental processes involved in El'gygytgyn impact cratering are very similar to those of other impact structures with other target material.

The first cratering stage (contact and compression) seems broadly similar for each crater type. The passage of the shock wave metamorphoses the target rocks and the projectile and results in a range of effects from crystallographic shock effects, over the generation of melt, to vaporization of the rocks. These features are characteristic for all larger impact structures, including the El'gygytgyn crater. The target porosity has a strong influence on the shock deformation of target rocks (Kowitz et al. 2013a, b, 2016). The El'gygytgyn region is indeed characterized by different types of volcanic rocks (and porosities), but a comparison of shock metamorphism in the different target lithologies, that are part of the (drilled) suevitic units, is almost impossible, due to the strong heterogeneity of their mineralogical compositions. A shock determination of surface-rocks is not possible, because the impactites at the surface around the crater are largely absent.

The second cratering stage (excavation) depends on criteria such as impact velocity, impact angle, and size of impactor (Melosh 1989 and references therein). The distribution of proximal and distal ejecta from El'gygytgyn is comparable to other complex craters. The lack of fallback suevite outside the crater can be explained by the very effective erosion that removed all traces of suevitic or "Bunte Breccia"-type impact breccia. Only a few blocks of impact melt breccia, cobbles at the lake shore and tiny droplets of melt, which were formed within the ejecta plume, were found as redeposited material within the lake and river terraces.

The type of target rocks and the impact angle influence the third stage of impact cratering (modification). Almost all craters on Earth have a circular shape, also El'gygytgyn. Only Matt Wilson (N.T. Australia), which is ellipsoidal and well exposed with a central uplift, formed through a highly oblique impact (Kenkmann and Poelchau 2009).

Finally, there are many comparable elements of the impact cratering processes on sedimentary and crystalline target rocks (majority of all craters) as well as in felsic volcanic rocks as at El'gygytgyn. However, each impact structure has its own individuality and special characteristics.

CHAPTER 8

CONCLUSIONS

Major outcomes of this PhD thesis are the development of a complete lithostratigraphy of the drilled impactites and country rocks of the El'gygytgyn impact structure, including the creation of an updated geological map. Additionally, the distribution of shock effects over the entire length of the drill core as well as determination of the downhole clast size distribution was achieved. Comprehensive petrographic and geochemical studies were necessary. On that basis, it was possible to interpret the origin of different impactites for this impact structure. Finally, it was attempted to reconstruct the cratering process, including identification of the projectile that formed the impact structure:

(1) The lower bedrock (~97 m) consists of a (trachy)rhyodacitic ignimbrite that can be subdivided into lower and upper parts divided by a narrow shear zone at 457.3 mblf depth. The upper bedrock (~20 m) is a felsic pyroclastic flow that displayed the lowermost occurrence of shock metamorphism detected in this study at 391.72 mblf depth. Both bedrock units are fractured and altered. In comparison to the other units of the drill core and to the observations of surface samples from the crater, this alteration does not seem to be influenced by the hydrothermal alteration that was established within the crater cavity after the impact. These units are interpreted to represent the parautochthonous crater floor at the flank of the central uplift.

(2) The three mafic blocks that are part of the lower and upper bedrock units likely represent the hydrothermally altered crater floor. These blocks are strongly brecciated and display a foliation, as well as cataclastic grain-size reduction and local occurrence of shear zones.

(3) The ~63 m melt-poor suevite contains different kinds of melt particles (some of which are likely impact generated) and clasts that display a wide range of shock metamorphism. The distribution of shock features against depth does not show a significant trend but their number seems to be somewhat enhanced in the upper part of the breccia. The chemical composition reflects the regional geological setting, i.e., the suevite is a mixture of all known target lithologies at their different proportions. It is interpreted to have formed as a ground surge within the crater cavity.

(4) The reworked suevite (~12 m) is an assemblage of lacustrine sediments and fallout material from the ejecta plume and contains clasts that show all stages of shock metamorphism. There are impact melt particles and impact glass spherules that have a siliceous composition. The abundance of lacustrine sediments increases toward the top. The sediments are deposited in a gradually fining-upward sequence.

(5) The drill core is strongly brecciated over its entire length. Most fractures occur in the lower and upper bedrock unit and are commonly oriented at about 45° to the core axis. Open fractures are often filled by secondary minerals (calcite and zeolite). It is likely that these late precipitations were caused by impact generated hydrothermal fluids.

(6) The study of the country rocks shows that the entire crater rim is completely unshocked and that the drilled impactites can be well related (with their composition) to the target lithologies.

(7) The investigation of siderophile elements, PGE, and REE revealed that it is problematic to identify the nature of the extraterrestrial projectile that formed the El'gygytgyn structure, because the presence of mafic rocks partially masks the extraterrestrial PGE component. However, mixing calculations show that the best chemical model for the El'gygytgyn suevitic rocks involves a chondrite component.

(8) A further, important result is the creation of a new geological map for the crater region. This map is based on the Russian maps from the 1980s, combining all data obtained by later workers that could be obtained from the literature. Finally, the results of the 2011 expedition completed this new, updated map for the El'gygytgyn impact structure.

REFERENCES

Adolph L. and Deutsch A. 2009. Glass spherules related to the El'gygytgyn impact crater (Siberia) (abstract #1116). *40th Lunar and Planetary Science Conference*. Houston, USA. CD-ROM.

Adolph L. and Deutsch A. 2010. Trace element analysis of impact glass spherules of the El'gygytgyn crater, Siberia (abstract #2421). *41st Lunar and Planetary Science Conference*. Houston, USA. CD-ROM.

Alwmark C., Ferrière L., Holm-Alwmark S., Ormö J., Leroux H., and Sturkell E. 2015. Impact origin for the Hummeln structure (Sweden) and its link to the Ordovician disruption of the L chondrite parent body. *Geology* 43/4:279-282, doi: 0.1130/G36429.1

Arikas K. 1986. Geochemie und Petrologie der permischen Rhyolithe in Südwestdeutschland (Saar-Nahe-Pfalz-Gebiet, Odenwald, Schwarzwald) und in den Vogesen. *Pollichia Buch* 8:1-321.

Arp G., Kolepka C., Simon K., Karius V., Nolte N., and Hansen T. 2013. New evidence for persistent impact-generated hydrothermal activity in the Miocene Ries impact structure, Germany. *Meteoritics and Planetary Science* 48:2491-2516, doi: 10.1111/maps.12235.

Artemieva N. A., Wünnemann K., Krien F., Reimold W. U., and Stöffler D. 2013. Ries crater and suevite revisited - Observations and modeling Part II: Modeling. *Meteoritics and Planetary Science* 48:590-627, doi: 10.1111/maps.12085.

Baratoux D. and Melosh H. J. 2003. The formation of shatter cones by shock wave interference during impacting. *Earth and Planetary Science Letters* 216:43-54, doi: 10.1016/S0012-821X (03)00474-6.

Baratoux D. and Reimold W. U. 2016. The current state of knowledge about shatter cone genesis: An introduction to the special issue. *Meteoritics and Planetary Science* 51:1389-1434, doi: 10.1111/maps.12678.

Barnes S. J., Naldrett A. J., and Gorton M. P. 1985. The origin of platinum-group elements in terrestrial magmas. *Chemical Geology* 53:303-323, doi: 10.1016/0009-2541(85)90076-2.

Belyi V. F. 1958. Схема тектоники и вулканизм южной части Чаун-Чукотки. *Геологический сборник Львовского геологического общества*. [The tectonic

setting and volcanism of south Chaun-Chukotka. *A summary of the geological work at the University of Lemberg*]. Львов: изд-во Львовского университета 5-6:264-281. In Russian.

Belyi V. F. 1969. *Volcanic formations and stratigraphy of the northern part of the Ochotsk-Chukotsky belt.* Nauka Press. Moscow. 176 p. In Russian.

Belyi V. F. 1977. *Stratigraphy and structures of the Okhotsk-Chukotsky volcanic belt.* Nauka Press. Moscow. 171 p. In Russian.

Belyi V. F. 1982. Basin of the El'gygytgyn Lake-Meteorite crater or geological structure of a recent stage of evolution of Central Chukotka? *Tichookeanskaya Geologia* 5:85-92. In Russian.

Belyi V. F. 1988. *Topical questions of phytostratigraphy of middle Cretaceous of North-East USSR*. NEISRI FEB RAS. Magadan, Russia. 34 p. In Russian.

Belyi V. F., 1994. *The Geology of Okhotsk-Chukotsky Volcanogenic Belt*. NEISRI FEB RAS. Magadan, Russia. 76 p. In Russian.

Belyi V. F. 1998. Impactogenesis and volcanism of the El'gygytgyn depression. *Journal of Petrology* 6:86-99. In Russian.

Belyi V. F. 2004. Геохимические признаки связи импактитов и позднекайнозойских вулканитов впадины Эльгыгытгын (Чукотка) [Geochemical criteria for the relation between impactites and late Cenozoic volcanics at the El'gygytgyn depression]. *Doklady Akademii Nauk* 397/26: 247-252. In Russian.

Belyi V. F. 2010. Impactite generation in the El'gygytgyn depression, Northeast Russia, as a volcanic phenomenon. 2. On the Petrography and geochemistry of the impactites. *Journal of Volcanology and Seismology* 4/3:149-163. Original Russian Text © V.F. Belyi. 2010, published in *Vulkanologiya i Seismologiya*, 3:3-18.

Belyi V. F. and Raikevich M. I. 1994. *The El'gygytgyn Lake hollow*. NEISRI FEB RAS. Magadan, Russia. 27 p. In Russian.

Belyi V. F. and Belaya B. V. 1998. *The Late Stage of the Okhotsk-Chukotsky Volcanogenic Belt Development (the Enmyvaam River Upperrun Area)*. NEISRI FEB RAS. Magadan, Russia.108 p. In Russian.

Bottke W. F., Love S. G., Tytell D., and Glotch T. 2000. Interpreting the elliptical crater populations on Mars, Venus, and the Moon. *Icarus* 145:108-121, doi: 10.1006/icar.1999.6323.

Branca W. and Fraas E. 1905. *Das kryptovulkanische Becken von Steinheim*. Königlich-Preußische Akademie der Wissenschaften. Verlag G. Reimer, Berlin. 64 p.

Brigham-Grette J., Melles M., Minyuk P., and Scientific Party. 2007. Overview and significance of a 250 ka paleoclimate record from El'gygytgyn Crater Lake, NE Russia. *Journal of Paleolimnology* 37:1-16, doi: 10.1007/s10933-006-9017-6.

Brigham-Grette J., Melles M., Minyuk P., Andreev A., Tarasov P., DeConto R., Koenig S., Nowaczyk N., Wennrich V., Rosen P., Haltia E., Cook T., Gebhardt C., Meyer-Jacob C., Snyder J., and Herzschuh U. 2013. Pliocene warmth, polar amplification, and stepped Pleistocene cooling recorded in NE Arctic Russia. *Science* 340:1421-1427, doi: 10.1126/science.1233137.

Canup R. M. and Asphaug E. 2001. Origin of the Moon in a giant impact near the end of the Earth's formation. *Nature* 412:708-712, doi:10.1038/35089010.

Carr M. H. 1996. Water erosion on Mars and its biologic implications. *Endeavour* 20:56-60, doi:10.1016/0160-9327(96)10013-2.

Coney L., Reimold W. U., Hancox P. J., Mader D., Koeberl C., McDonald I., Struck U., Vajda V., and Kamo S. L. 2007. Geochemical and mineralogical investigation of the Permian-Triassic boundary in the continental realm of the southern Karoo Basin, South Africa. *Palaeoworld* 16:67-104, doi:10.1016/j.palwor.2007.05.003.

Cox K. G., Bell J. D., and Pankhurst R. J. 1979. *The interpretation of igneous rocks*. London: Allen and Unwin. 450 p, doi: 10.1007/978-94-017-3373-1_3.

Crocket J. H. 2002. Platinum-group element geochemistry of mafic and ultramafic rocks. In: *The Geology, Geochemistry, Mineralogy and mineral benefication of Platinum-group elements*. Special Volume 54, edited by L. J. Cabri. Canadian Institute of Mining, Metallurgy and Petroleum, pp. 177-210.

Dabizha A. I. and Feldman V. I. 1982. Geophysical characteristics of some astroblemes of USSR. *Meteoritika* 40:91-101. In Russian.

Dachille, F., Gigl, P., Simons, P. Y., 1968. Experimental and analytical studies of crystalline damage useful for the recognition of impact structures. In *Shock Metamorphism of Natural Materials*. Edited by French, B. M., Short, N. M. Mono Book Corp, Baltimore, MD, pp. 555-569.

Dietz R. S. 1947. Meteorite impact suggested by the orientation of shatter-cones at the Kentland, Indiana, disturbance. *Science* 105:42-43, doi: 10.1126/science.105.2715.42.

Dietz R. S. 1968. Shatter cones in cryptoexplosion structures. In *Shock Metamorphism of Natural Materials*. Edited by French, B. M., Short, N. M. Mono Book Corp, Baltimore, MD, pp. 267-285.

Dietz R. S. 1977. El'gygytgyn crater, Siberia: Probable source of Australasian tektite field (and bediasites from Popigai*). Meteoritics* 12:145-157, doi: 10.1111/j.1945-5100.1977.tb00339.

Dietz R. S. and McHone J. F. 1976. El'gygytgyn: Probably the world's largest meteorite crater. *Geology* 4:391-392, doi: 10.1130/0091-7613(1976)4<391:EPWLMC>2.0.CO; 2.

Engelhardt W. von 1997. Suevite breccia of the Ries impact crater, Germany: Petrography, chemistry, and shock metamorphism of crystalline clasts. *Meteoritics and Planetary Science* 32:545-554.

Ewart A. 1979. A review of the mineralogy and chemistry of Tertiary-Recent dacitic, latitic, rhyolithic and related salic volcanic rocks. In *Trondhjemites, dacites and related rocks*. Edited by Barker F. Elsevier. Amsterdam. pp. 13-132.

Feldman V. I., Granovsky L. B., Kapustkina I. G., Karoteeva N. N., Sazonova L. V., and Dabizha A. I. 1981. Meteorite crater El'gygytgyn. In *Impactites*, edited by Marakhushev A. A. Moscow: Moscow State University Press. pp. 70-92. In Russian.

Ferrière L., Koeberl C., Libowitzky E., Reimold W. U., Greshake A., and Brandstätter F. 2010. Ballen quartz and cristobalite in impactites: New investigations, In *Large Meteorite Impacts and Planetary Evolution IV*: edited by Gibson R. L., and Reimold, W. U. *Geological Society of America Special Paper* 465, p. 609-618, doi: 10.1130/2010.2465(29).

Fisher R. V. and Schmincke H. U. 1984. Pyroclastic flow deposits. In *Pyroclastic rocks*, edited by Wilson L. Lancaster, UK: Elsevier. pp. 187-230. ISBN 3-540-51341-8.

Foriel J., Moynier F., Schulz T., and Koeberl C. 2013. Chromium isotope anomaly in an El'gygytgyn crater impactite: Evidence for an ureilite projectile. *Meteoritics and Planetary Science* 48:1339-1350, doi: 10.1111/maps.12116.

French B. M. 1998. *Traces of Catastrophe: A Handbook of Shock-Metamorphic Effects in Terrestrial Meteorite Impact Structures*. LPI Contribution 954, Lunar and Planetary Institute, Houston. 120 p.

French B. M. and Koeberl C. 2010. The convincing identification of terrestrial meteorite impact structures: What works, what doesn't, and why. *Earth-Science Reviews* 98:123-170, doi:10.1016/j.earscirev.2009.10.009.

French B. M. Cordua W. S and Plescia J. B. (2004) The Rock Elm meteorite impact structure, Wisconsin: Geology and shock-metamorphic effects in quartz. *Geological Society of America Bulletin* 116:200-218, doi: 10.1130/B25207.1.

Freundt A. and Schmincke H. U. 1995. Petrogenesis of rhyolite-trachyte-basalt composite ignimbrite P1, Gran Canaria, Canary Islands. *Journal of Geophysical Research* 100:455-474, doi: 10.1029/94JB02478.

Gault D. E. and Wedekind J. A. 1978.Experimental studies of oblique impact. In: *Proceedings 9th Lunar and Planetary Science Conference*. Houston, USA. pp. 3843-3875.

Gebhardt A. C., Niessen F., and Kopsch C. 2006. Central ring structure identified in one of the world's best-preserved impact craters. *Geology* 34:145-148, doi: 10.1130/G22278.1.

Gebhardt A. C., Franke A., Kück J., Sauerbrey M. A., Niessen F., Wennrich V., and Melles M. 2013. Petrophysical characterization of the lacustrine sediment succession drilled in Lake El'gygytgyn, Far East Russian Arctic. *Climate of the Past* 9:1933-1947, doi: 10.5194/cp-9-1933-2013.

Gieré R., Wimmenauer W. Müller-Sigmund H., Wirth R., Lumpkin G. R., and Smith K. L. 2015. Lightning-induced shock lamellae in quartz. *American Mineralogist* 100:1645-1648, doi: 10.2138/am-2015-5218.

Glushkova O. and Smirnov V. 2005. General geology and geography. In *Berichte zur Polar- und Meeresforschung* 509, edited by Minyuk P. and Brigham-Grette J. Bremerhaven, Germany: Alfred Wegener Institute for Polar and Marine Research. pp. 14-18.

Glushkkova O. Y., and Smirnov V. N. 2007. Pliocene to Holocene geomorphic evolution and paleogeography of the El'gygytgyn Lake region, NE Russia. *Journal of Paleolimnology* 37:37-47, doi: 0.1007/s10933-006-9021-x.

Goderis S., Wittmann A., Zaiss J., Elburg M., Ravizza G., Vanhaecke F., Deutsch A., and Claeys P. 2013. Testing the ureilite projectile hypothesis for the El'gygytgyn impact: Determination of siderophile element abundances and Os isotope ratios in ICDP drill core samples and melt rocks. *Meteoritics and Planetary Science* 48:1296-1324, doi: 10.1111/maps.12047.

Gohn G. S., Koeberl C., Miller K. G., Reimold W. U., Browning J. V., Cockell C. S., Horton J. W., Kenkmann T., Kulpecz A. A., Powars D. S., Sanford W. E., and Voytek M. A. 2008. Deep drilling into the Chesapeake Bay impact structure. *Science* 320:1740-1745, doi: 10.1126/science.1158708.

Gohn G. S., Koeberl C., Miller K. G., and Reimold W. U. 2009. Deep drilling in the Chesapeake Bay impact structure - An overview. *The ICDP-USGS Deep Drilling Project in the Chesapeake Bay Impact Structure: Results from the Eyreville Core Holes*, edited by Gohn G. S., Koeberl C., Miller K. G., and Reimold W. U. *Geological Society of America Special Paper* 458:1-20, doi: 10.1130/2009.2458(01).

Goldin T. J., Wünnemann K., Melosh H. J., and Collins G. S. 2006. Hydrocode modeling of the Sierra Madera impact structure. *Meteoritics and Planetary Science* 41:1947-1958, doi: 10.1111/j.1945-5100.2006.tb00462.x.

Govindaraju K. 1989. Compilation of working values and sample description for 272 geostandards. *Geostandards Newsletter* 13:1-113, doi: 10.1111/j.1751-908X.1989. tb00476.x.

Govindaraju K. 1994. 1994 compilation of working values and samples description for 383 geostandards. *Geostandards Newsletter* 18:1-158, doi: 10.1046/j.1365-2494.1998. 53202081.x-i1.

Gradstein F. M., Ogg J. G., Schmitz M. D., and Ogg G. M. 2012. *The Geologic Time Scale 2012*. 1/2. Oxford: Elsevier. 1145 p.

Grieve R. A. F. 2006. *Impact structures in Canada*. St. John's, Canada: Geological Association of Canada, 210 p.

Grieve R. A. F., Langenhorst F., and Stöffler D. 1996. Shock metamorphism of quartz in nature and experiment: II. Significance in geoscience. *Meteoritics and Planetary Science* 31:6-35, doi: 10.1111/j.1945-5100.1996.tb02049.x.

Grieve R. A. F., Osinski G. R. and Chanou A. 2015. The suevite conundrum: A general perspective (abstract #1036). *Bridging the Gap III: Impact cratering in Nature, Experiments, and Modeling*, Freiburg, Germany.

Gurov E. P. and Gurova E. P. 1979. Stages of shock metamorphism of volcanic rocks of siliceous composition on example of the El'gygytgyn crater (Chukotka). *Doklady Academii Nauk* USSR 249:1197-1201. In Russian.

Gurov E. P. and Gurova E. P. 1983. Regularities of fault spreading around meteorite craters (an example of the El'gygytgyn crater). *Doklady Academii Nauk* 269:1150-1153. In Russian.

Gurov E. P. and Gurova E. P. 1991. *Geological structure and rock composition of impact structures.* Naukova Dumka Press. Kiev. 160 p. In Russian.

Gurov E. P. and Yamnichenko A. Y. 1995. Morphology of rim of complex terrestrial craters (abstract). *26th Lunar and Planetary Science Conference*. Houston, USA. p. 533.

Gurov E. P., and Koeberl C. 2004. Shocked rocks and impact glasses from the El'gygytgyn impact structure (Russia). *Meteoritics and Planetary Science* 39:1495-1508, doi: 10.1111/j.1945-5100.2004.tb00124.x.

Gurov E. P., Valter A. A., Gurova E. P., and Serebrennikov A. I. 1978. Meteorite impact crater El'gygytgyn in Chukotka. *Doklady Akademii Nauk* USSR 240:1407-1410. In Russian.

Gurov E. P., Valter A., A. Gurova E. P., and Kotlovskaya F. I. 1979a. El'gygytgyn impact crater, Chukotka: Shock metamorphism of volcanic rocks (abstract). *10th Lunar and Planetary Science Conference* pp. 479-481.

Gurov E. P., Gurova E. P., and Rakitskaia R. B. 1979b. Stishovite and coesite in shock-metamorphosed rocks of the El'gygytgyn crater in Chukotka. *Doklady Akademii Nauk* USSR 248:213-216. In Russian.

Gurov E. P., Koeberl C., Reimold W. U., Brandstätter F., and Amare K. 2005. Shock metamorphism of siliceous volcanic rocks of the El'gygytgyn impact crater (Chukotka, Russia). In: *Large Meteorite Impacts III*, edited by Kenkmann T., Hörz F. and Deutsch A. *Geological Society of America Special Paper* 384:391-412, doi: 10.1130/0-8137-2384-1.391.

Gurov E. P., Koeberl C., and Yamnichenkov A. 2007. El'gygytgyn impact crater, Russia: Structure, tectonics, and morphology. *Meteoritics and Planetary Science* 42:307-319, doi: 10.1111/j.1945-5100.2007.tb00235.x.

Harms U., Koeberl C., and Zoback M. D., eds. 2007. *Continental Scientific Drilling*. Heidelberg: Springer. 366 p.

Hasch M., Reimold W. U., Raschke U., and Zaag P. 2016. Shatter cones at the Keurusselkä impact structure and their relation to local jointing. *Meteoritics and Planetary Science* 51:1534-1551, doi: 10.1111/maps.12676.

Hellevang H., Dypvik H., Kalleson E., Pittarello L., and Koeberl C. 2013. Can alteration experiments on impact melts from El'gygytgyn and volcanic glasses shed new light on the formation of the Martian surface? *Meteoritics and Planetary Science* 48:1287-1295, doi:10.1111/maps. 12046.

Herron M. M. 1988. Geochemical classification of terrigenous sands and shales from core or log data. *Journal of Sedimentary Petrology* 58:820-829.

Horton Jr. J. W., Gibson R. L., Reimold W. U., Wittmann A., Gohn G. S., and Edwards L. E. 2009. Geologic columns for the ICDP-USGS Eyreville B core, Chesapeake Bay impact structure: Impactites and crystalline rocks, 1766 to 1096 m depth. In *The*

ICDP-USGS Deep Drilling Project in the Chesapeake Bay Impact Structure: Results from the Eyreville Core Holes, edited by Gohn G. S., Koeberl C., Miller K. G., and Reimold W. U. *Geological Society of America Special Paper* 458:21-49, doi: 10.1130/2009.2458(02).

Huber H., Koeberl C., McDonald I., and Reimold W. U. 2001. Geochemistry and petrology of Witwatersrand and Dwyka diamictites from South Africa: search for an extraterrestrial component. *Geochimica et Cosmochimica Acta* 65:2007-2016, doi: 10.1016/S0016-7037(01)00569-5.

Huffman A. R. and Reimold W. U. 1996. Experimental constraints on shock-induced microstructures in naturally deformed silicates. *Tectonophysics* 256:165-217, doi:10.1016/0040-1951(95) 00162-X.

Irvine T. N. and Baragar W. R. A. 1971. A guide to the chemical classification of the common volcanic rocks. *Canadian Journal of Earth Science* 8:523-548, doi: 10.1139/e71-055.

Ispolatov V. O., Tikhomirov P. L., Heizler M., and Cherepanova I. Yu. 2004. New $^{40}Ar/^{39}Ar$ ages of Cretaceous continental volcanics from central Chukotka: Implications for initiation and duration of volcanism within the northern part of the Okhotsk Chukotka Volcanic Belt (northeastern Eurasia). *Journal of Geology* 112:369-377, doi: 10.1086/382765.

Jarosewich E., Clarke R. S., and Barrows J. N. 1987. The Allende Meteorite Reference Sample. *Smithsonian Contributions to the Earth Sciences* 27. 49 p.

Jenniskens P., Shaddad M. H., Numan D., Elsir S., Kudoda A. M., Zolensky M. E., Le L., Robinson G. A., Friedrich J. M., Rumble D., Steele A., Chesley S. R., Fitzsimmons A., Duddy S., Hsieh H. H., Ramsay G., Brown P. G., Edwards W. N., Tagliaferri E., Boslough M. B., Spalding R. E., Dantowitz R., Kozubal M., Pravec P., Borovicka J., Charvat Z., Vaubaillon J., Kuiper J., Albers J., Bishop J. L., Mancinelli R. L., Sandford S. A., Milam S. N., Nuevo M., Worden S. P. 2009. The impact and recovery of asteroid 2008 TC(3). *Nature* 458:485-488, doi :10.1038/nature07920.

Johnson G. P. and Talbot R. J. 1964. *A theoretical study of the shock wave origin of shatter cones*. M.Sc. Thesis. Air Force Institute of Technology, Wright-Patterson Airforce Base, Dayton, Ohio, USA. 103 p.

Kelley S. P., Spicer R. A., and Herman A. B. 1999. New $^{40}Ar/^{39}Ar$ dates for Cretaceous Chauna Group tephra, north-eastern Russia, and their implications for the geologic history and floral evolution of the North Pacific region. *Cretaceous Research* 20:97-106, doi:10.1006 /cres.1998.0140.

Kenkmann T. and Poelchau M. H. 2009. Low-angle collision with Earth: the elliptical impact crater Matt Wilson, Northern Territory, Australia. *Geology* 37: 459-462, doi: 10.1130/G25378A.1.

Kenkmann T., Wittmann A., and Scherler D. 2004. Structure and impact indicators of the Cretaceous sequence of the ICDP drill core Yaxcopoil-1, Chicxulub impact crater, Mexico. *Meteoritics and Planetary Science* 39:1069-1088, doi: 10.1111/j.1945-5100.2004.tb01129.x.

Kenkmann T., Collins G. S., Wittmann A., Wünnemann K., Reimold W. U., and Melosh H. J. 2009. A model for the formation of the Chesapeake Bay impact crater as revealed by drilling and numerical simulation. In *The ICDP-USGS Deep Drilling Project in the Chesapeake Bay Impact Structure: Results from the Eyreville Core Holes*, edited by Gohn G. S., Koeberl C., Miller K. G., and Reimold W. U. *Geological Society of America Special Paper* 458:571-585, doi: 10.1130/2009.2458(25).

Kenkmann T., Poelchau M. H., Trullenque G., Hoerth T., Schäfer F., Thoma K., and Deutsch A. 2012. Shatter cones formed in a MEMIN impact cratering experiment (abstract #5092). *75th Annual Meeting of the Meteoritical Society*, Cairns, Australia.

Kenkmann T., Poelchau M. H., and Wulf G. 2014. Structural geology of impact craters. *Journal of Structural Geology* 62:156-182, doi: 10.1016/j.jsg.2014.01.015.

Kieffer S. W. and Simonds C. H. 1980. The role of volatiles and lithology in the impact cratering process. *Review of Geophysics and Space Physics* 18:143-181.

Kobberger G. and Schmincke H. U. 1999. Deposition of rheomorphic ignimbrite D (Mogán Formation), Gran Canaria, Canary Islands, Spain. *Bulletin of Volcanology* 60:465-485, doi: 10.1007/s004450050246.

Koeberl C. 1993. Instrumental neutron activation analysis of geochemical and cosmochemical samples: A fast and proven method for small sample analysis. *Journal of Radioanalytical and Nuclear Chemistry* I68:47-50, doi: 10.1007/BF02040877.

Koeberl C. 2014. The Geochemistry and Cosmochemistry of Impacts. In: Holland H. D. and Turekian K. K. (eds.) *Treatise on Geochemistry, Second Edition, vol. 2 (Planets, Asteroids, Comets and The Solar System)*, pp. 73-118. Oxford. Elsevier.

Koeberl C. and Reimold W. U. 2005. Bosumtwi impact crater, Ghana (West Africa): An updated and revised geological map, with explanations. *Jahrbuch der Geologischen Bundesanstalt*, Wien (Yearbook of the Austrian Geological Survey) 145:31-70, (+1 map, 1:50,000).

Koeberl C. and Milkereit B. 2007. Continental drilling and the study of impact craters and processes-An ICDP perspective. In *Continental Scientific Drilling*, edited by Harms U., Koeberl C., and Zoback M. D. Heidelberg: Springer. pp. 95-161.

Koeberl C., Peucker-Ehrenbrink B., Reimold W. U., Shukolyukov A., and Lugmair G. W. 2002. A comparison of the osmium and chromium isotopic methods for the detection of meteoritic components in impactites: Examples from the Morokweng and Vredefort impact structures, South Africa. In *Catastrophic Events and Mass Extinctions: Impacts and Beyond.* Edited by C. Koeberl and K.G. MacLeod. *Geological Society of America Special Paper* 356:607-618.

Koeberl C., Brandstätter F., Glass B. P., Hecht L., Mader D., and Reimold W. U. 2007a. Uppermost impact fallback layer in the Bosumtwi crater (Ghana): Mineralogy, geochemistry, and comparison with Ivory Coast tektites. *Meteoritics and Planetary Science* 42:709-729, doi: 10.1111/j.1945-5100.2007.tb01069.

Koeberl C., Milkereit B., Overpeck J. T., Scholz C. A., Amoako P. Y. O., Boamah D., Danuor S., Karp T., Kueck J., Hecky R. E., King J. W., and Peck J. A. 2007b. An international and multidisciplinary drilling project into a young complex impact structure: The 2004 ICDP Bosumtwi Crater Drilling Project - An overview. *Meteoritics and Planetary Science* 42:483-511, doi: 10.1111/j.1945-5100.2007.tb01057.x.

Koeberl, C., Claeys, P., Hecht, L., and McDonald, I. 2012. Geochemistry of impactites. *Elements* 8:37-42, doi: 10.2113/gselements.8.1.37.

Koeberl C., Pittarello L., Reimold W. U., Raschke U., Brigham-Grette J., Melles M., and Minyuk P. 2013. El'gygytgyn impact crater, Chukotka, Arctic Russia: Impact cratering aspects of the 2009 ICDP drilling project. *Meteoritics and Planetary Science* 48:1108-1129, doi:10.1111/maps.12146.

Komarov A. N., Koltsova T. V., Gurova E. P., and Gurov E. P. 1983. Determination of the El'gygytgyn crater impactites' age by the fission track method. *Doklady Academii Nauk UkrSSR* 10:11-13. In Russian.

Kowitz A., Schmitt R. T., Reimold W. U. and Hornemann U. 2013a. The first MEMIN shock recovery experiments at low shock pressure (5-12.5 GPa) with dry, porous sandstone. *Meteoritics and Planetary Science* 48:99-114, doi:10.1111/maps.12030.

Kowitz A., Güldemeister N., Reimold W. U., Schmitt R. T. and Wünnemann K. 2013b. Diaplectic quartz glass and SiO_2 melt experimentally generated at only 5 GPa shock pressure in porous sandstone: laboratory observations and meso-scale numerical

modeling. *Earth and Planetary Science Letters* 384:17-26, doi:10.1016/j.epsl.2013.09.021.

Kowitz A., Güldemeister N., Schmitt R. T., Reimold W. U., Wünnemann K., and Holzwarth A. 2016. Revision and recalibration of existing shock classifications for quartzose rocks using low-shock pressure (2.5-20 GPa) recovery experiments and meso-scale numerical modeling. *Meteoritics and Planetary Science* 51:1741-1761, doi:10.1111/maps.12712.

Lambert P. 1981. Breccia dikes: Geological constrains on the formation of complex craters. In *Multi-ring basins: Formation and evolution*; *Proceedings, 12th Lunar and Planetary Science Conference*, part A:59-78 (A82-39033 19-91). *Geochimica et Cosmochimica Acta*, Supplement 15. New York: Pergamon Press.

Langenhorst F. and Deutsch A. 1994. Shock experiments on pre-heated α- and β-quartz: 1. Optical and density data. *Earth and Planetary Science Letters* 125:407-420, doi: 10.1016/0012-821X(94)90229-1.

Langenhorst F. and Deutsch A. 2012. Shock metamorphism of minerals. *Elements* 8:31-36.

Layer P. W. 2000. ^{40}Argon/^{39}Argon age of the El'gygytgyn event, Chukotka, Russia. *Meteoritics and Planetary Science* 35:591-599, doi: 10.1111/j.1945-5100.2000.tb01439.

Leat P. T. and Thorpe R. S. 1986. Geochemistry of an Ordovician basalt-trachybasalt-subalkaline/peralkaline rhyolithe association from the Lleyn Peninsula, North Wales, U.K. *Geological Journal* 21:29-43, doi: 10.1002/gj.3350210103.

Le Maitre R. W., Bateman P., Dudek A., Keller J., Lameyre J., Le Bas M. J., Sabine P. A., Schmid R., Sorensen H., Streckeisen A., Woolley A. R., and Zanettin B. 1989. *A classification of igneous rocks and glossary of terms: Recommendations of the International Union of Geological Sciences Subcommission on the Systematics of Igneous Rocks.* Oxford, UK: Blackwell Scientific Publications. 193 p., ISBN 063202593X.

Lodders K. 2003. Solar system abundances and condensation temperatures of elements. *The Astrophysical Journal* 591:1220-1247, doi: 10.1086/375492.

Lorenz R. D. and Lunine J. I. 1996. Erosion on Titan: Past and present. *Icarus* 122:79-91, doi:10.1006/icar.1996.0110.

Mader D. and Koeberl C. 2009. Using Instrumental Neutron Activation Analysis for geochemical analyses of terrestrial impact structures: Current analytical procedures at

the University of Vienna Geochemistry Activation Analysis Laboratory. *Applied Radiation and Isotopes* 67:2100-2103, doi: 10.1016/j.apradiso.2009.04.014.

Mader M. M. and Osinski G. R. 2015. Impactites of the Mistastin Lake impact structure, Canada: Insights into impact ejecta emplacement (abstract #1033). *Bridging the Gap III: Impact Cratering in Nature, Experiments, and Modeling*, Freiburg, Germany.

Maharaj D., Elbra T., and Pesonen L. J. 2013. Physical properties of the drill core from the El'gygytgyn impact structure, NE Russia. *Meteoritics and Planetary Science* 48:1130-1142, doi:10.1111/maps.12064.

Masaitis, V. L., 1998. Popigai crater: origin and distribution of diamond-bearing impactites. *Meteoritics and Planetary Science* 33:349-359, doi: 10.1111/j.1945-5100.1998.tb01639.

McBirney A. R. 1968. Second additional theory of origin of fiamme in ignimbrites. *Nature* 217:938, doi: 10.1038/217938a0.

McDonald I. 1998. The need for a common framework for collection and interpretation of data in platinum-group element geochemistry. *Geostandards Newsletter* 22:85-91, doi: 10.1111/j.1751-908X.1998.tb00547.x.

McDonald I. and Viljoen K. S. 2006. Platinum-group element geochemistry of mantle eclogites: A reconnaissance study of xenoliths from the Orapa kimberlite, Botswana. *Transactions of the Institution of Mining and Metallurgy, Section B* 115:81-93, doi: 10.1179/174327506X138904.

Melles M., Minyuk P., Brigham-Grette J., and Niessen F. 2003. Successful completion of pre-site survey for deepdrilling at El'gygytgyn crater lake. *American Geophysical Union Fall Meeting Abstracts* p. 0287.

Melles M., Minyuk P., and Brigham-Grette J. 2005. The expedition El'gygytgyn Lake 2003 (Siberian Arctic). In *Berichte zur Polar- und Meeresforschung* 509, edited by Minyuk P. and Brigham-Grette J. Bremerhaven: Alfred Wegener Institute for Polar and Marine Research. 139 p.

Melles M., Brigham-Grette J., Minyuk P., Koeberl C., Andreev A., Cook T., Fedorov G., Gebhardt C., Haltia-Hovi E., Kukkonen M., Nowaczyk N. R., Schwamborn G., Wennrich V. and the El'gygytgyn Scientific Party. 2011. The Lake El'gygytgyn Scientific Drilling Project – Conquering Arctic Challenges through Continental Drilling. *Scientific Drilling* 11:29-40, doi: 10.2204/iodp.sd.11.03.2011.

Melles M., Brigham-Grette J., Minyuk P. S., Nowaczyk N. R., Wennrich V., DeConto R. M., Anderson P. M., Andreev A. A., Coletti A., Cook T. L., Haltia-Hovi E., Kukkonen

M., Lozhkin A. V., Rosen P., Tarasov P., Vogel H., and Wagner B. 2012. 2.8 million years of Arctic climate change from Lake El'gygytgyn, NE Russia. *Science* 337:315-320, doi: 10.1126/science.1222135.

Melosh H. J. 1989. *Impact Cratering: A Geologic Process.* Oxford monographs on geology and geophysics. Oxford University Press. New York, NY. 245 p.

Middelburg J. J., Van der Weijden C. H., and Woittiez J. R. W. 1988. Chemical processes affecting the mobility of major, minor and trace elements during weathering of granitic rocks. *Chemical Geology* 68:253-273, doi: 10.1016/0009-2541(88)90025-3.

Mohr-Westheide T. and Reimold W. U., 2010. Microchemical investigation of smallscale pseudotachylitic breccias from the Archean gneiss of the Vredefort dome, South Africa. In *Large Meteorite Impacts and Planetary Evolution IV*. Edited by Gibson, R.L., Reimold, W.U. *Geological Society of America Special Paper* 465, pp. 619-643, doi: 10.1130/2010.2465(30).

Mohr-Westheide T. and Reimold W. U. 2011. Formation of pseudotachylitic breccias in the central uplifts of very large impact structures: scaling the melt formation. *Meteoritics and Planetary Science* 46:543-555, doi: 10.1111/j.1945-5100.2011.01173.x.

Nekrasov I. A. and Raudonis P. A. 1963. Meteorite craters. *Priroda* 1:102–104. In Russian.

Neuendorf K. K. E., Mehl Jr. J. P., and Jackson J. A., eds. 2005. *Glossary of Geology*, 5th ed. Alexandria, Virginia: American Geological Institute. 779 p.

Niessen F., Gebhardt A. C., and Kopsch C. 2007. Seismic investigation of the El'gygytgyn impact crater lake (Central Chukotka, NE Siberia): Preliminary results. *Journal of Paleolimnology* 37:49-63, doi: 10.1007/s10933-006-9022-9.

Nolan M., Liston G., Prokein P., Brigham-Grette J., Sharpton V. L., and Huntzinger R. 2003. Analyses of lake ice dynamics and morphology on Lake El'gygytgyn, NE Siberia, using synthetic aperture radar (SAR) and Landsat. *Journal of Geophysical Research* 108:8162, doi: 10.1029/2001JD000934.

Nowaczyk N. R., Minyuk P., Melles M., Brigham-Grette J., Glushkova O., Nolan M., Lozhkin A. V., Stetsenko T. V., Andersen P. M., and Forman S. L. 2002. Magnetostratigraphic results from impact crater Lake El'gygytgyn, northeastern Siberia: A 300 kyr long high-resolution terrestrial palaeoclimatic record from the Arctic. *Geophysical Journal International* 150:109-126, doi: 10.1046/j.1365-246X.2002.01625.x.

Obruchev S. V. 1957. *Across the tundra and mountains of Chukotka.* State Press of Geography. Moskow. 198 p. In Russian.

Öpik E. J. 1973. Comets and the formation of Planets. *Astrophysics Space Science* 21:307-398, doi: 10.1007/BF00643104.

Ormö J., Sturkell E., Horton J. W. Jr., Powars D. S., and Edwards L. E. 2009. Comparison of clast frequency and size in the resurge deposits at the Chesapeake Bay impact structure (Eyreville and Langley cores): Clues to the resurge process. In *The ICDP-USGS Deep Drilling Project in the Chesapeake Bay Impact Structure: Results from the Eyreville Core Holes*, edited by Gohn G. S., Koeberl C., Miller K. G., and Reimold W. U. *Geological Society of America Special Paper* 458:617-632, doi: 10.1130/2009.2458(27).

Osinski G. R., Grieve R. A. F., and Spray J. G. 2004. The nature of the groundmass of surficial suevite from the Ries impact structure, Germany, and constraints on its origin. *Meteoritics and Planetary Science* 39:1655-1683, doi: 10.1111/j.1945-5100.2004.tb00065.x.

Osinski G. R., Grieve R. A. F., Collins G. S., Marion C., and Sylvester P. 2008. The effect of target lithology on the products of impact melting. *Meteoritics and Planetary Science* 43:1939-1954, doi: 10.1111/j.1945-5100.2008.tb00654.x.

Osinski G. R., Tornabene L. L., Banerjee N. R., Cockell C. S., Flemming R., Izawa M. R. M., McCutcheon J., Parnell J., Preston L., Pickersgill A. E., Pontefract A., Sapers H. M., and Southam G. 2013. Impact-generated hydrothermal systems on Earth and Mars. *Icarus* 224:347-363, doi 10.1016/j.icarus.2012.08.030.

Ostertag R. 1983. Shock experiments on feldspar crystals. Proccedings 14th Lunar and Planetary Science Conference, *Journal of Gepohysical Research: Solid Earth* 88(S01) pp. B364-B376, doi: 10.1029/JB088iS01p0B364.

Pearce J. 1980. Geochemical evidence for the genesis and eruptive setting of lavas from Tethyan opholithes. In *Proceedings of the International Ophiolite Symposium, Cyprus 1979*. pp. 261-272. Ministry of Agriculture and Natural Resources, Cyprus.

Pearce T. H., Gorman B. E., and Birkett T. C. 1977. The relationship between major element chemistry and tectonic environment of basic and intermediate volcanic rock. *Earth and Planetary Science Letters* 36:121-132, doi: 10.1016/0012-821X(77)90193-5.

Pearce J. A., Harris N. B. W., and Tindle A. G. 1984. Trace element discrimination diagrams for the tectonic interpretation of granitic rocks. *Journal of Petrology* 25:956-983, doi: 10.1093/petrology/25.4.956.

Pierazzo E. and Melosh H. J. 2000. Melt production in oblique impacts. *Icarus* 145:252-261, doi: 10.1006/icar.1999.6332.

Pittarello L. and Koeberl C. 2013a. A cathodoluminescence study of impact melts and rocks from El'gygytgyn: A method to distinguish impact and volcanic melts? (abstract #1459). *44th Lunar and Planetary Science Conference*. Houston, USA.

Pittarello L. and Koeberl C. 2013b. Clast size distribution (CSD) and other geometrical features in shocked and unshocked rocks from the El'gygytgyn impact structure. *Meteoritics and Planetary Science* 48:1325-1338, doi: 10.1111/maps.12070.

Pittarello L. and Koeberl C. 2013c. Petrography of impact glasses and melt breccias from the El'gygytgyn impact structure, Russia. *Meteoritics and Planetary Science* 48:1236-1250 doi: 10.1111/maps.12048.

Pittarello L., Schulz T., Koeberl C., Hoffmann J. E., and Münker C. 2013. Petrography, geochemistry and Hf-Nd isotope evolution of drill core samples and target rocks from the El'gygytgyn impact crater, NE Chukotka, Arctic Russia. *Meteoritics and Planetary Science* 48:1160-1198, doi: 10.1111/maps.12088.

Pittarello L, Roszjar J., Mader D., Debaille V., Claeys P., and Koeberl C. 2015. Cathodo-luminescence as a tool to discriminate impact melt, shocked and unshocked volcanics: A case study of samples from the El'gygytgyn impact structure. *Meteoritics and Planetary Science* 50:1954-1969, doi: 10.1111/maps.12559.

Poelchau M. H. and Kenkmann T. 2008. Asymmetric signatures in simple craters as an indicator for an oblique impact direction. *Meteoritics and Planetary Science* 43:2059-2072, doi: 10.1111/j.1945-5100.2008.tb00661.x.

Poelchau M. H. and Kenkmann T. 2011. Feather features: A low-shock-pressure indicator in quartz. *Journal of Geophysical Research: Solid Earth* 116(B02201). 13 p. doi:10. 1029/2010 JB007803.

Pohl J., Poschlod K., Reimold W. U., Meyer C., and Jacob J. 2010. Ries crater, Germany: The Enkingen magnetic anomaly and associated drill core SUBO 18. *Geological Society of America Special Paper* 465:141-163, doi: 10.1130/2010.2465(10)

Raevsky F. B. and Potapova E. P. 1984. Geological map of the Anadyr region, sheet Q-59-III, IV. In *Official geological map of the USSR*, Moscow: Ministry of Geology, USSR. (In Russian).

Raikevich M. N. 1995. Magnetostratigraphic studies of Cretaceous volcanic rocks. In *Magnetostratigraphic studies of Phanerozoic rocks*, edited by Linkova T. I. and Izmailov L. I. Magadan: North East Interdisciplinary Research Institute, Russian Academy of Sciences Far East Branch. pp. 17-30. In Russian.

Raschke U., Reimold W. U., Zaag P. T., Pittarello L., and Koeberl C. 2013a. Lithostratigraphy of the impactite and bedrock section in ICDP drill core D1c from the El'gygytgyn impact crater, Russia. *Meteoritics and Planetary Science* 48:1143-1159, doi:10.1111/maps.12072.

Raschke U., Schmitt R. T., and Reimold W. U. 2013b. Petrography and geochemistry of impactites and volcanic bedrock in the ICDP drill core D1c from lake El'gygytgyn, NE Russia. *Meteoritics and Planetary Science* 48:1251-1286, doi:10.1111/maps.12087.

Raschke U., Zaag P. T., Schmitt R. T., and Reimold W. U. 2014. The 2011 expedition to the El'gygytgyn impact structure, Northeast Russia: Towards a new geological map for the crater area. *Meteoritics and Planetary Science* 49:978-1006, doi:10.1111/maps.12306.

Raschke U., Schmitt R. T., McDonald I., Reimold W. U., Mader D., and Koeberl C. 2015. Geochemical studies of impact breccias and country rocks from the El'gygytgyn impact structure, Russia. *Meteoritics and Planetary Science* 50:1071-1088, doi:10.1111/maps.12455.

Reimold W. U. 1995. Pseudotachylite in impact structures - generation by friction melting and shock brecciation?: A review and discussion. *Earth-Science Reviews* 39: 247-265. http://dx.doi.org/10.1016/0012-8252(95)00033-X.

Reimold W. U. and Koeberl C. 2014. Impact structures in Africa: A review. *Journal of African Earth Sciences* 93:57-175, doi: 10.1016/j.jafrearsci.2014.01.008.

Reimold W. U., Hansen B. K., Jacob J., Artemieva N. A., Wünnemann K., and Meyer C. 2011. Petrography of the impact breccias of the Enkingen (SUBO 18) drill core, southern Ries crater, Germany: New estimate of impact melt volume. *Geological Society of America Bulletin* 124:104-132, doi:10.1130/B30470.1.

Reimold W., U., McDonald I., Schmitt R., T., and Koeberl C. 2013. Geochemical studies of the SUBO 18 (Enkingen) drill core and other impact breccias from the Ries crater, Germany. *Meteoritics and Planetary Science* 48:1531-157, doi: 10.1111/maps.12175.

Reimold W. U., Ferrière L., Deutsch A. and Koeberl C. 2014. Impact controversies: Impact recognition criteria and related issues. *Meteoritics and Planetary Science* 49:723-731, doi: 10.1111/maps.12284.

Reimold W. U., Wannek D., Hoffmann M., Hansen B. T., Hauser N., Schulz T., Siegert S., Thirlwall M., Zaag P. T., and Mohr-Westheide T. 2015. Vredefort Pseudotachylitic Breccia and Granophyre (Impact Melt Rock): Clues to Their Genesis from New Field,

Chemical and Isotopic Investigations (abstract #1035). *Bridging the Gap III: Impact Cratering in Nature, Experiments, and Modeling*, Freiburg, Germany.

Reimold W. U., Hoffmann M., Hauser N., Schmitt R. T., Zaag P. T., and Mohr-Westheide T. 2016. A geochemical contribution to the discussion about the genesis of impact-related pseudotachylitic breccias: Studies of PTB in the Otavi and Kudu Quarries of the Vredefort Dome support the "In Situ Formation" hypothesis. *South African Journal of Geology* 119:453-472, doi: http://dx.doi.org/10.2113/gssajg.119.3.453.

Richards M. A., Alvarez A., Self S., Karlstrom L., Renne P. R., Manga M., Sprain C. J., Smit J., Vanderkluysen L., and Gibson S. 2015. Triggering of the largest Deccan eruptions by the Chicxulub impact. *Geological Society of America Bulletin* 127:1507-1520, doi:10.1130/B31167.1.

Roddy D. J. and Davis L. K. 1977. Shatter cones formed in large scale experimental explosion craters. In: *Impact and Explosion Cratering: Planetary and Terrestrial Implications.* Roddy D. J., Pepin R. O. and Merrill R. B. (Eds.) Pergamon Press, New York, pp. 715-750.

Schmid R. 1981. Descriptive nomenclature and classification of pyroclastic deposits and fragments: Recommendations of the IUGS Subcommission on the Systematics of Igneous Rock. *Geologische Rundschau* 70:794-799, doi: 10.1007/BF01822152.

Schulte P., Alegret L., Arenillas I., Arz J. A., Barton P. J., Bown P. R., Bralower T. J., Christeson G. L., Claeys P., Cockell C. S., Collins G. S., Deutsch A., Goldin T. J., Goto K., Grajales-Nishimura J. M., Grieve R. A. F., Gulick S. P. S., Johnson K. R., Kiessling W., Koeberl C., Kring D. A., MacLeod K. G., Matsui T., Melosh J., Montanari A., Morgan J. V., Neal C. R., Nichols D. J., Norris R. D., Pierazzo E., Ravizza G., Rebolledo-Vieyra M., Reimold, W. U., Robin E., Salge T., Speijer R. P., Sweet A. R., Urrutia-Fucugauchi J., Vajda V., Whalen M. T. and Willumsen P. S. 2010. The Chicxulub asteroid impact and mass extinction at the Cretaceous-Paleogene boundary. *Science* 327:1214-1218, doi: 10.1126/science.1177265.

Shand S. J. 1916. The Pseudotachylyte of Parijs (Orange Free State), and its Relation to 'Trap-Shotten Gneiss' and 'Flinty Crush-Rock'. *Geological Society of London Quarterly Journal* 72:198-221, doi: 10.1144/GSL.JGS.1916.072.01-04.12.

Sharpton V. L., Dressler B. O., Herrick R. R., Schnieders B., and Scott J. 1996. New constraints on the Slate Islands impact structure, Ontario, Canada. *Geology* 24:851-854.

Shilo N. A., Lozhkin A. V., Anderson P. M., Belaya B. V., Stetsenko T. V., Glushkova O. Y., Brigham-Grette J., Melles M., Minyuk P. S., Nowaczyk N., and Forman S. 2001. The

first continuous pollen record of climate and vegetation change during the last 300,000 years. *Proceedings of the National Academy of Sciences* 376:231-234. ISSN: 1028-334X. In Russian.

Smirnov V. N., Savva N. E., and Glushkova O. Yu. 2011. New data on spherules from the region of the El'gygytgyn crater. *Geochemistry International* 49:314-318, doi: 10.1134/S00167029 11030086.

Sparks R. S. J., Tait S. R., and Yanev Y. 1999. Dense welding caused volatile resorption. *Journal of Geological Society* 156:217-225, doi: 10.1144/gsjgs.156.2.0217.

Spudis P. D. 1994. The large impact process inferred from the geology of lunar multiring basins. In *Large Meteorite Impact and Planetary Evolution.* Edited by Dressler B. O., Grieve R. A. F. and Sharpton V. L. *Geological Society of America Special Paper* 293:1-10.

Stöffler D. 1971. Coesite and stishovite in shocked crystalline rocks. *Journal of. Geophysical Research* 76:5474-5488, doi: 10.1029/JB076i023p05474.

Stöffler D. 2015. The suevite conundrum: New concepts for the Ries crater – a retake (abstract #1002*). Bridging the Gap III: Impact Cratering in Nature, Experiments, and Modeling*, Freiburg, Germany.

Stöffler D. and Langenhorst F. 1994. Shock metamorphism of quartz in nature and experiment: 1. Basic observation and theory. *Meteoritics* 29:155-181, doi: 10.1111/j.1945-5100.1994. tb00670.x.

Stöffler D., and Grieve R. A. F. 2007. Impactites - A proposal on behalf of the IUGS Subcommission on the systematics of metamorphic rocks. In *Metamorphic Rocks - A Classification and Glossary of Terms*, edited by Fettes D. and Desmons J. Cambridge, UK: Cambridge University Press. pp. 82-92.

Stöffler D., Artemieva N.A., Ivanov B.A., Hecht L., Kenkmann T., Schmitt R.T., Tagle R.A., and Wittmann A., 2004, Origin and emplacement of the impact formations at Chicxulub, Mexico, as revealed by the ICDP deep drilling Yaxcopoil-1 and by numerical modeling: *Meteoritics and Planetary Science* 39:1035-1068, doi: 10.1111/j.1945-5100.2004.tb01128..x.

Stöffler D., Reimold W. U., Jacob J., Hansen B. K., Summerson I. A. T., Artemieva N. A., and Wünnemann K. 2013. Ries crater and suevite revisited - Observations and modeling Part I: Observations. *Meteoritics and Planetary Science* 48:515-589, doi: 10.1111/maps.12086.

Stone D. B., Layer P. W., and Raikevich M. I. 2009. Age and paleomagnetism of the Okhotsk-Chukotka Volcanic Belt (OCVB) near Lake El'gygytgyn, Chukotka, Russia. *Stephan Mueller Special Publication Series* 4:243-260. Published by Copernicus Publications on behalf of the European Geosciences Union.

Storzer D. and Wagner G. A. 1979. Fission track dating of Elgygytgyn, Popigai and Zhamanshin impact craters: No sources for Australasian or North-American Tektites. *Meteoritics* 14:541-542.

Symes S. K., Sears D. W. G., Akridge D. G., Huang S., and Benoit P. H. 1998. The crystalline lunar spherules: Their formation and implications for the origin of meteoric chondrules. *Meteoritics and Planetary Science* 33:13-29, doi: 10.1111/j. 1945-5100.1998.tb01604.x.

Tagle R. and Berlin J. 2008. A database of chondrite analyses including platinum group elements, Ni, Co., Au, and Cr: Implications for the identification of chondritic projectiles. *Meteoritics and Planetary Science* 43:541-559, doi: 10.1111/j.1945-5100.2008.tb00671.x.

Taylor S. R. and McLennan S. M. 1985. *The Continental Crust: Its Composition and Evolution.* Oxford: Blackwell Science Publishers. 312 p.

Therriault A. M., Fowler A. D. and Grieve R. A., 2002. The Sudbury Igneous Complex: A differentiated impact melt sheet. *Economic Geology*, 97:1521-1540, doi: 10.2113/gsecongeo.97.7.1521.

Tikhomirov P. L., Kalinina E. A., Kobayashi K. and Nakamura E. 2008. Late Mesozoic silicic magmatism of the North Chukotka area (NE Russia): Age, magma sources, and geodynamic implications. *Lithos* 105:329-346, doi:10.1016/j.lithos.2008.05.005.

Tredoux M. and McDonald I. 1996. Komatiite WITS-1: a low concentration noble metal standard for the analysis of non-mineralized samples. *Geostandards Newsletter* 20:267-276, doi: 10.1111/j.1751-908X.1996.tb00188.x.

Tredoux M., Lindsay N. M., Davies G., and McDonald L. 1995. The fractionation of platinum-group elements in magmatic systems with the suggestion of a novel causal mechanism. *South African Journal of Geology* 98:157-167.

U.S. Geological Survey 2005. *Selection of colors and patterns for geologic maps of the U.S.*. Reston, Virginia: Geological Survey. 19 p.

Val'ter A. A., Barchuk I. F., Bulkin V. S., Ogorodnik A. F., and Kotishevskaya E. Y. 1982. The El'gygytgyn meteorite-probable composition. *Soviet Astronomy Letters* 8:59-62.

Vasconcelos M. A. R., Wünnemann K., Crosta A. P., Molina E. C., Reimold W. U., and Yokoyama E. 2012. Insights into the morphology of the Serra da Cangalha impact structure from geophysical modeling. *Meteoritics and Planetary Science* 47:1659-1670, doi: 10.1111/maps.12001.

Vasconcelos M. A. R., Crósta A. P., Reimold W. U., Góes A. M., Kenkmann T. and Poelchau M. H. 2013. The Serra da Cangalha impact structure, Brazil: Geological, stratigraphic and petrographic aspects of a recently confirmed impact structure. *Journal of South American Earth Sciences* 45:316-330, doi:10.1016/j.jsames.2013.03.007.

Warren P. H., Ulff-Møller F., Huber H., and Kallemayn G. W. 2006. Siderophile geochemistry of ureilites: A record of early stages of planetesimal core formation. *Geochimica et Cosmochimica Acta* 70:2104-2126, doi:10.1016/j.gca.2005.12.026.

Weisberg M. K.; McCoy T. J.; Krot A. N. 2006. Systematics and Evaluation of Meteorite Classification. *Meteorites and the Early Solar System II*, D. S. Lauretta and H. Y. McSween Jr. (eds.), University of Arizona Press, Tucson, pp.19-52.

Wilk J. and Kenkmann T. 2015a. The surface of shatter cones in experimental impact craters (abstract #2637). *46th Lunar and Planetary Science Conference*. CD-ROM.

Wilk J. and Kenkmann T. 2015b. Shatter cones from the MEMIN impact experiments (abstract #1066). *Bridging the Gap III: Impact cratering in Nature, Experiments, and Modeling*. Freiburg, Germany.

Wilk J. and Kenkmann T. 2016. Formation of shatter cones in MEMIN impact experiments. *Meteoritics and Planetary Science* 51:1477-1496, doi: 10.1111/maps.12682

Wimmenauer W. 1985. *Petrographie der magmatischen und metamorphen Gesteine.* Stuttgart: Enke. 396 p.

Winchester, J. A. and Floyd, P. A. 1977. Geochemical discrimination of different magma series and their differentiation products using immobile elements. *Chemical Geology* 20:325-343, doi:10.1016/0009-2541(77)90057-2.

Wittmann A., Goderis S., Claeys P., Vanhaecke F., Deutsch A., and Adolph F. 2013. Petrology of impactites from El'gygytgyn crater: Breccias in the ICDP-drill core 1C, glassy impact melt rocks and spherules. *Meteoritics and Planetary Science* 48:1199-1235, doi: 10.1111/maps.12019.

Zaag P. T., Raschke U., Reimold W. U., and Schmitt R. T. 2011. Preliminary investigations of the ICDP Drill Core from El'gygytgyn Crater (Chukotka, Russia) and impressions from the 2011 Expedition. *Second Arab Impact and Astrogeology Conference (AICAC II)*, Casablanca, November, abstract volume, 2 p.

Zaag P., Reimold W. U., and Hipsley C. 2016. Microcomputed tomography and shock microdeformation studies on shatter cones. *Meteoritics and Planetary Science* 51:1435-1459 doi: 10.1111/maps.12673

Zhang J., Dauphas N., Davis A. M., Leya I. and A. Fedkin. 2012. The proto-Earth as a significant source of lunar material. *Nature Geoscience* 5:251-255, doi: 10.1038/ngeo1429.

Zheltovsky V. G. and Sosunov G. M. 1985. Geological map of the Anadyr region, sheet Q-59-V, IV. In: *Official Geological Map of the USSR*. Moscow: Ministry of Geology. In Russian.

Zotkin I. T. and Tsvetkov V. I. 1970. Search of meteorite craters on the Earth. *Astronomitcheskiy Vestnik* 4:55-65. In Russian.

Other source:

http://www.passc.net/EarthImpactDatabase/index.html